UC Santa Cruz
UC Santa Cruz Electronic Theses and Dissertations

Title

The Development Of Organic Reduction Reactions By Binary Hydrides And Binary Metal Catalysts

Permalink

https://escholarship.org/uc/item/1vd1d54t

Author

Amberchan, Gabriella

Publication Date

2020

Peer reviewed|Thesis/dissertation

eScholarship.org

Powered by the California Digital Library
University of California

UNIVERSITY OF CALIFORNIA

SANTA CRUZ

THE DEVELOPMENT OF ORGANIC REDUCTION REACTIONS BY BINARY HYDRIDES AND BINARY METAL CATALYSTS

A dissertation submitted in partial satisfaction
of the requirements for the degree of

DOCTOR OF PHILOSOPHY

in

CHEMISTRY

by

Gabriella A. Amberchan

December 2020

The Dissertation of Gabriella A. Amberchan
is approved:

Professor Bakthan Singaram, Chair

Professor Scott Lokey

Professor Scott Oliver

Quentin Williams
Interim Vice Provost and Dean of Graduate Studies

Copyright © by

Gabriella A. Amberchan

2020

Table of Contents

List of Figures vii

List of Schemes xvi

List of Tables xix

Abstract xxi

DEDICATION AND ACKNOWLEDGMENTS xxiv

CHAPTER 1. Metal Hydrides and Binary Hydrides in Organic Synthesis 1

1.1. Introduction 2

1.2. Metal hydrides 3

- 1.2.1. Borohydrides 4
- 1.2.2. Binary Hydrides 6

1.3. Metal Boron Composites 10

- 1.3.1. Hydrogenation of Alkenes and Dienes 11
- 1.3.2. Reduction of Nitriles 13
- 1.3.3. Reduction of Nitro Groups 18
- 1.3.4. Other Reductions with Metal Boron Composite Catalysts 21

1.4. Hydrogen Generation 23

- 1.4.1. Borohydride as a H_2 Source 24
- 1.4.2. Water Splitting to Produce H_2 28
  - 1.4.2.1. Reforming of Fossil Fuels to Produce H_2 28
  - 1.4.2.2. Water Splitting by Electrolysis 29
  - 1.4.2.3. Metal-Water Reactions 31

1.5. Conclusion 33

1.6. Thesis Outline 34

1.7. References 37

CHAPTER 2. Reaction of Diisobutylaluminum Borohydride, A Binary Hydride, with Selected Organic Compounds Containing Representative Functional Groups 45

2.1. Introduction 46
2.2. Results and Discussion 47
    2.2.1. Synthesis of Diisobutylaluminum Borohydride 47
    2.2.2. Reduction of Aldehydes & Ketones 51
    2.2.3. Reduction of Nitriles 56
    2.2.4. Reduction of Epoxides 60
    2.2.5. Reduction of Carboxylic Acids 67
    2.2.6. Reduction of Esters 69
    2.2.7. Reduction of Amides 73
    2.2.8. Chemoselective Reactions 79
2.3. Conclusion 83
2.4. References 84
CHAPTER 3. A Mesoporous Nanoparticle Supported Nickel Boron Composite Catalyst for the Catalytic Reduction of Nitroarenes 92
3.1. Introduction 93
    3.1.1. History of the Reduction of Nitroarenes 93
    3.1.2. History of Metal Boron Composites 97
3.2. Results and Discussion 105
    3.2.1. Metal Screening 105
    3.2.2. Catalyst Characterization 110
    3.2.3. Recycling Study 126
    3.2.4. Mechanistic Insights 130
    3.2.5. Nitroarene Substrate Scope 131
    3.2.6. Alternative Ni-based Catalyst 134
3.3. Conclusion 135
3.4. References 137
CHAPTER 4. Real-Time *Ex Situ* Monitoring of Organic Reduction Reactions in Aqueous Media Using Fiber Optic Raman Spectroscopy 146
4.1. Introduction 147

4.1.1. Background 147

4.1.2. History of the Reduction of Nitroarenes 148

4.1.3. History of Amine Boranes 148

4.1.4. Raman Spectroscopy in Organic Reactions 151

4.2. Results and Discussion 156

4.2.1. Reduction of Nitroarenes Monitored with Raman Spectroscopy 156

4.2.2. Reduction of Cyclohexanone by Aqueous Dimethylamine Borane (DMAB) 163

4.2.3. Reduction of 2-Cyclohexene-1-one by Aqueous Dimethylamine borane (DMAB) 167

4.2.4. Competitive Reactions 168

4.2.5. Mechanistic Insights 172

4.3. Conclusion 178

4.4. References 179

CHAPTER 5. On-Demand Hydrogen Generation using Commercial or Waste Aluminum, Water and Reusable Liquid Metal 189

5.1. Introduction 190

5.1.1. Background of water splitting 191

5.2. Results and Discussion 196

5.2.1. Synthesis of the Gallium Aluminum Alloy 196

5.2.2. Synthesis of Alloys Using Other Low Melting Point Metals 198

5.2.3. Hydrogen Generation *via* Water Splitting 199

5.2.4. Different Aluminum Sources 201

5.2.5. Recycling Gallium and Storage of the Alloy 202

5.2.6. Alloy Characterization 203

5.2.7. Proposed Mechanism for Hydrogen Evolution Reaction 205

5.2.8. Hydrogenation Reactions 207

5.3. Conclusion 209

5.4. References 210

6.1. Experimental Details and Characterization 215

6.1.1. Chapter 2 217

6.1.2. Chapter 3 248

6.1.3. Chapter 4 257

6.1.4. Chapter 5 268

APPENDIX A: ^{1}H and ^{13}C NMR Spectra 271

7. Bibliography 349

LIST OF FIGURES

Figure 1.1. Non-hydridic reduction methods of the early 20th century. 2

Figure 1.2. The partial and tandem reduction reactions 4-(bromomethyl)benzonitrile by $HInCl_2$ (**A**), and binary hydrides $HInCl_2$ and BH_3:THF (**B**), DIBAL and $HInCl_2$ (**C**). 8

Figure 1.3. The partial and tandem reduction reactions 4-(bromomethyl) benzoate by binary hydrides $HInCl_2$ and BH_3:THF (**D**), $HInCl_2$ (**E**), and $HInCl_2$ and MeLAB (**F**). 9

Figure 1.4. Proposed mechanism of the reduction of benzonitrile with CBC catalyst and $NaBH_4$. 15

Figure 1.5. Reduction of nitriles to the primary aldimine followed by addition of an amine to generate the secondary aldimine. Or the nitrile can undergo full reduction to the primary amine. 17

Figure 1.6. Co-catalyzed selective reduction of nitriles to primary amines (**J**) or secondary aldimines (**K**). 18

Figure 1.7. Tandem reduction and epoxide ring opening C-N coupling reaction. 21

Figure 1.8. Proposed mechanism for the cleavage of allyl esters. 23

Figure 1.9. Hydrolysis of various hydrides and complex hydrides. 24

Figure 1.10. Acidic accelerants (0.2-0.3 mol of compound/2.6 mol $NaBH_4$) to promote hydrogen evolution from the hydrolysis of $NaBH_4$ in 10 min. 25

Figure 1.11. The methanolysis products of $NaBH_4$ were recycled back into the starting borohydride. 27

Figure 1.12. Schematic of the HER and OER reactions in a simplified example of electrolysis. 30

Figure 2.1. ^{11}B NMR (coupled) of $(i\text{Bu})_2AlBH_4$. 48

Figure 2.2. ^{11}B NMR (coupled) spectra of $NaBH_4$ and DIBAL-Cl in a) NMP, b) THF:NMP (1:1), c) pyridine, d) THF: EtOH (1:1), 50

e) tetraglyme, f) addition of 1-hexene, and g) THF:tetraglyme (4:1).

Figure 2.3. Reduction of styrene oxide by hydrides produces either 2-phenylethanol (green) or 1-phenylethanol (blue), depending upon where the hydride reacts. 63

Figure 2.4. Brown's proposed pathway for the reduction of esters by BMS. 69

Figure 3.1. NBC supported on mesoporous silicate nanoparticles (NBC-MSN), showing large particles of NBC not bound to MSN. 109

Figure 3.2. Percent yield of *p*-toluidine after successive reuse cycles of NBC-MASN. Yields based on ^{1}H NMR ratios. 110

Figure 3.3. HAADF-STEM images of (a) as-synthesized MASN, (b) NBC-MASN imaged within 30 s of beam exposure, (c) NBC-MASN after EDS mapping for 5 min, with (d) the corresponding Ni EDS map. (e) HRTEM images of NBC-MASN after 5 min exposure to electron beam showing segregated regions of Ni, and (f) a magnified section (box in e) showing lattice fringes associated with these regions (arrows). 111

Figure 3.4. HAADF-STEM image of (a) unsupported NBC, and corresponding EDS elemental maps of (b) Ni and (c) O present in the composite. HRTEM of unsupported NBC, imaged within 2 min of beam exposure, progressively magnified (d-f) to show lattice fringes for Ni nanocrystals embedded within an amorphous matrix. 112

Figure 3.5. a) EDS spectrum for NBC-MASN. b) EDS spectrum for NBC. 112

Figure 3.6. Segregation/crystallization of Ni in NBC-MASN after electron beam exposure for 5 min. 113

Figure 3.7. The electron diffraction pattern from Ni in the unsupported NBC material (left) and the lattice spacing plot from the corresponding HRTEM (right). 114

Figure 3.8. a) PXRD of NBC-MASN after MeOH reflux followed by $N_{2(g)}$-calcination. b) ^{11}B NMR of the supernatant solution after NBC was refluxed in methanol for 3 h. 117

Figure 3.9. A comparison of PXRD profiles for as-synthesized (fresh) NBC-MASN and after calcination in air or flowing nitrogen. The inset shows the low angle diffraction pattern for the bare MASN compared to as-synthesized NBC-MASN before and after calcination. 119

Figure 3.10. A comparison of PXRD profiles for as-synthesized (fresh) unsupported NBC and after calcination in air or flowing nitrogen. All peaks in the N_2 calcined sample not assigned to Ni (asterisks) can be assigned to Ni_3B (ICDD 00-048-1223). The inset shows an enlargement of the profile for the air-calcined material, indicating the presence of NiO. 120

Figure 3.11. TGA data in air for NBC vs. NBC-MASN (top) and NBC vs $NaBH_4$ (bottom). 121

Figure 3.12. XPS data for NBC-MASN. 123

Figure 3.13. XPS data for unsupported NBC. 124

Figure 3.14. ICP-OES data for the Ni:B molar ratio in NBC-MASN after successive reuses in the catalytic hydrogenation of *p*-nitrotoluene. Two reaction conditions are compared: N_2H_4•H_2O as reducing agent (red diamonds), and N_2H_4•H_2O 128 with an equimolar addition of $NaBH_4$ (blue squares). The two red circular markers for reuse numbers 7 and 9 indicate the Ni:B ratio after ex-situ regeneration of NBC-MASN with $NaBH_4$ but before catalysis using $N_2H_4{\bullet}H_2O$.

Figure 3.15. Reuse study: The percent yield for the conversion of *p*-nitrotoluene to *p*-toluidine is plotted against reuse cycle number, using either $N_2H_4{\bullet}H_2O$ as the reducing agent or a combination of $N_2H_4{\bullet}H_2O$ and $NaBH_4$ as reducing and regenerating agents. The product yields were determined after 24 h reaction. Yield was determined by isolation and the purity was verified by ^1H NMR spectroscopy. 129

Figure 3.16. Percent yield of *p*-toluidine after 24 h. Yields are based on ^1H NMR ratios. 130

Figure 3.17. Left: ^1H NMR spectra of sample aliquots after 1 h, 2 h, and 3 h. Right: proposed reaction pathway for the reduction of nitroarenes. 131

Figure 3.18. Recycling and reuse study of the reduction of *p*-nitrotoluene with the catalyst formed from Ni and diisobutylaluminum hydride. 135

Figure 4.1. a) An example of the set up for an *in situ* reaction monitoring with Raman spectroscopy. b) An example of the set up for an *ex situ* reaction monitoring with Raman spectroscopy. 151

Figure 4.2. a) Condensation reaction between salicylaldehyde and ethyl acetoacetate to produce 3-acetylcoumarin and its significant Raman stretches. b) 3D profile of Raman spectra relating to 3-acetylcourmarin as a function of time and intensity from the region of 1500-1680 cm^{-1}. 155

Figure 4.3. *Ex situ* reaction monitoring with Raman spectroscopy for aqueous reduction reactions. 156

Figure 4.4. a) *Ex situ* Raman monitoring of the reduction of 4-nitrotoluene catalyzed with NBC catalyst and hydrazine hydrate in toluene at 25 °C. Red and green highlight the start and end of the reaction. b) A plot of the natural log of concentration vs. time to extract the rate constant of the nitro reduction reaction. 158

Figure 4.5. Photographs showing the reduction of 4-nitrotoluene at various time points. Overtime the reaction mixture transforms from clear and yellow to turbid and yellow/colorless to a clear and colorless solution. 159

Figure 4.6. a) Near-IR Raman spectra of 4-nitrotoluene in a series of dilutions in toluene from 0.01 M to 1.0 M. b) Calibration curve developed from taking the ratio of the nitro peak at 1343 cm^{-1} and the toluene peak at 1379 cm^{-1}. 160

Figure 4.7. Images of the reduction of 2,4-dinitrotoluene at the early stages and late stages of the experiment. Overtime the reaction mixture transforms from clear and yellow to turbid and colorless. 161

Figure 4.8. a) Full spectrum of *ex situ* Raman monitoring of the reduction of 2,4-dinitrotoluene using the NBC catalyst and hydrazine hydrate at 80 °C with continuous stirring where red and green highlight the start and end of the reaction. b) Expansion of the region associated with the nitro group. 162

Figure 4.9. a) Infrared Raman spectra of neat toluene (green), of a crystalline sample of 2,4-dinitrotoluene (red), and of 2,4-dinitroltoluene dissolved in toluene from 0.01 M to 1.0 M 162 (black). b) Calibration curve based on the ratio of the nitro peak at 1350 cm^{-1} and the toluene peak at 1379 cm^{-1}. c) A test of the goodness of fit of the calibration data.

Figure 4.10. a) Full spectrum *ex situ* Raman monitoring of the reduction of 2,4,6-trinitrotoluene using an NBC catalyst and hydrazine hydrate at 80 °C with continuous stirring. The red graph is the initial measurement, and the green graph is the final measurement. b) Expansion of the region associated with the nitro group. The red graph is the initial measurement, and the green graph is the final measurement. 163

Figure 4.11. Reduction of cyclohexanone by different amine boranes. This work, reported in this chapter, is in the blue box. The reductions on the right with cyclic amine boranes occurred in glacial acetic acid at 25 °C. 164

Figure 4.12. a) Full Raman spectra of the reduction of cyclohexanone using DMAB in water. The black spectrum shows starting material, and the green spectrum shows the product. b) and c) Expanded Raman spectra of the reduction of cyclohexanone using DMAB in water. The red spectrum shows starting material with the C=O stretch (carbonyl, 1707 cm^{-1}) and C-C ring stretch (753 cm^{-1}). The black spectra show the reaction progression. The green spectrum shows significant changes in the regions between 600 to 1800 cm^{-1}, attributed to the conversion of ketone to alcohol, including the appearance of the C-O (2° alcohol, 1450 cm^{-1}) and shifted C-C ring stretch (798 cm^{-1}). 166

Figure 4.13. a) Full Raman spectra of the reduction of 2-cyclohexen-1-one using DMAB in water. The red spectrum shows starting 168 material, the black spectra show the reaction progression, and the green spectrum shows the final reaction spectrum. b) and c) Expanded Raman spectra of the reduction of cyclohexen-1-one using DMAB in water. The red spectrum shows starting material with the C=O stretch (carbonyl, 1659 cm^{-1}), C=C (alkene, 1615 cm^{-1}), ring stretch (767 cm^{-1}). The black spectra show the reaction progression. The green spectrum shows significant changes indicative of reaction completion the appearance of the C-O (2° alcohol, 1442 cm^{-1}) and shifted C-C ring stretch (785 cm^{-1}).

Figure 4.14. a) Full Raman spectra of the reduction of a 1:1 mixture of cyclohexanone:cyclohexen-1-one using DMA in water. The selective reduction of the saturated ketone was complete within 5 min as shown by the disappearance of the carbonyl stretch (1707 cm^{-1}). The red and green spectra show the pure starting material and product in solution, respectively. b) Expanded view of the Raman spectra relating to the carbonyl stretch (1707 cm^{-1}). The red and green spectra show the pure starting material and product in solution, respectively. 170

Figure 4.15. Raman spectra of the reduction of a 1:1 mixture of cyclohexanone:cyclohexene oxide using DMAB in water. The reaction was monitored for 14 min total, but the selective reduction of the saturated ketone completed within 5 min as shown by the disappearance of the carbonyl stretch (1707 cm^{-1}) and the continued presence of the C-O stretch (1262 cm^{-1}). The red and green spectra show the starting material and product in solution. 171

Figure 4.16. ^{1}H NMR of dimethylamine in $CDCl_3$. 173

Figure 4.17. Three proposed interactions between DMAB, cyclohexanone, and water molecules. A) Basic conditions allow the hydroxide anion to displace the dimethylamine, forming a monohydroxy borohydride, $^{-}BH_3(OH)$, which would then react with the carbonyl. B) Water activates the carbonyl and DMAB reacts with the carbonyl. C) DMAB reacts with the unativated carbonyl. 174

Figure 4.18. ^{11}B NMR (decoupled) studies at 25 °C. a) BH_3:SMe_2 with 5% NaOH (solid) displayed peaks at δ -10 ppm [$NaBH_3(OH)$], δ -20 ppm (BH_3:SMe_2), and δ -29 ppm (NaB_2H_7). Insets b) and c) are expansions of the δ -10 ppm and -29 ppm signals, respectively. These peaks were quartets in the coupled spectra. d) DMAB with NaOH (aqueous) exhibiting a peak at δ -15 ppm (DMAB). 175

Figure 4.19. ^{11}B NMR (decoupled) of the reaction after DMAB reacts with cyclohexanone. 179

Figure 5.1. Metal cost per mol. 195

Figure 5.2. The gallium aluminum alloy was synthesized by two methods, with a heat gun or mechanically mixed on paper. Different alloys of atomic gallium aluminum ratios were made, and their hydrogen production was quantified. 198

Figure 5.3. Hydrogen generation from water splitting using 3:1 Ga:Al alloy and water from different sources. 201

Figure 5.4. Hydrogen generation from water splitting using Ga-Al alloy and aluminum from different sources. 202

Figure 5.5. (a) TEM imaging coupled with EELS spectroscopy shows dark areas are likely Al particles while the remaining area is Ga . (b) SEM-EDS map of the alloy’s surface shows the Al particles (red) well distributed in the Ga (green). 204

Figure 5.6. TEM of a Ga-Al sample: a) red arrows point to particles in the matrix; b) Diffraction for the selected area in a) showing rings that can be indexed for phase identification. 204

Figure 5.7. PXRD for varying Ga:Al ratio and the theoretical patterns for pure Al and Ga. 205

Figure 5.8. SEM image of 3:1 (Ga:Al) alloy. 206

LIST OF SCHEMES

Scheme 1.1. Reducing power of different metal borohydrides. 6

Scheme 1.2. Reduction of aliphatic (left) and aromatic (right) nitro groups to amines and azo compounds, respectively. 10

Scheme 1.3. Reduction of 2-cyclohexen-1-one by a nickel catalyst synthesized from washing with MeOH vs. refluxed in MeOH. 13

Scheme 1.4. Reaction of benzonitrile with CBC, synthesized from Vernekar's procedure, and $NaBH_4$ (**L**) or N_2H_4 (**M**). Reaction of 4-nitrobenzonitrile with CBC and N_2H_4 (**N**). 20

Scheme 1.5. Reduction of functional groups by diisobutylaluminum borohydride. 35

Scheme 2.1. Synthesis of Diisobutylaluminum Borohydride [$(i\text{Bu})_2AlBH_4$] from BMS and DIBAL (1:1) 48

Scheme 2.2. $NaBH_4$ reaction with DIBAL-Cl to produce $(i\text{Bu})_2AlBH_4$ 49

Scheme 2.3. Reduction of benzaldehyde *via* BMS, DIBAL, and $(i\text{Bu})_2AlBH_4$. 51

Scheme 2.4. Reduction of acetophenone *via* BMS, DIBAL, and $(i\text{Bu})_2AlBH_4$ 54

Scheme 2.5. Reduction of benzonitrile *via* BMS, DIBAL, and $(i\text{Bu})_2AlBH_4$. 57

Scheme 2.6. Possible Mechanism for the Reduction of Epoxides by $(i\text{Bu})_2AlBH_4$ 62

Scheme 2.7. Reduction of benzoic acid *via* BMS, DIBAL, and $(i\text{Bu})_2AlBH_4$ 67

Scheme 2.8. Reduction of various esters by BMS 71

Scheme 2.9. Proposed mechanism for the reduction of esters by DIBAL 72

Scheme 2.10. Chemoselective Reductions of Aldehydes and Ketones with $(i\text{Bu})_2AlBH_4$ 80

Scheme 2.11. Chemoselective Reduction of Aromatic Esters with $(i\mathrm{Bu})_2\mathrm{AlBH}_4$ 81

Scheme 2.12. Chemoselective Reduction of 4-tolunitrile with $(i\mathrm{Bu})_2\mathrm{AlBH}_4$ 82

Scheme 3.1. Two possible mechanisms for the reduction of nitroarenes to aniline 94

Scheme 3.2. Iron oxide hydroxide catalyst used to reduce nitroarenes in the presence of hydrazine hydrate 95

Scheme 3.3. Schematic illustration of (a) the synthesis and (b) use of NBC-MASN catalyst for the reduction of nitroarenes with hydrazine hydrate 105

Scheme 3.4. Synthesis of Ni catalyst with (left) $(i\mathrm{Bu})_2\mathrm{AlBH}_4$ and (right) DIBAL and the subsequent reductions of *p*-nitrotoluene 134

Scheme 4.1. Pechmann condensation reaction between resorcinol and ethyl acetoacetate to produce 7-hydroxy-4-methylcoumarin and their significant Raman stretches 153

Scheme 4.2. Production of solketal from the acetalization of acetone and glycerol with 3-mercaptopropyl)trimethoxy silane as the acidic catalyst 154

Scheme 4.3. Reduction of 4-nitrotoluene to 4-toluidine (90% isolated yield) using NBC catalyst and hydrazine hydrate 157

Scheme 4.4. Reduction of 2,4-dinitrotoluene to 2,4-diaminotoluene (55% isolated yield) using NBC catalyst and hydrazine hydrate 161

Scheme 4.5. The reduction of cyclohexen-1-one to cyclohexanol (95% isolated yield) in aqueous DMAB (pH 10) 167

Scheme 4.6. To elucidate the reaction kinetics of the mixture, a 1.5:1.5:3 mmol reaction of cyclohexanone:2-cyclohexen-1-one:DMAB was performed 170

Scheme 4.7. To elucidate the reaction kinetics of the mixture, a 1.5:1.5:3 mmol reaction of cyclohexanone:cyclohexene oxide:DMAB was performed 171

Scheme 4.8. DFT analysis of reaction pathway **C** 177

Scheme 5.1. Reduction of 4-phenyl-1-buten-4-ol (1.25 mmol) with Ni catalyst (1.25 mmol) in EtOH, followed by reaction with alloy-generated hydrogen (9.0 mmol) (2.6 g) in DI water (5 mL) 208

LIST OF TABLES

Table 1.1. Comparison of functional groups reduced by $NaBH_4$, $Al(BH_4)_3$, and $LiBH_4$ 5

Table 1.2. Selected dienes for the regioselective reduction 12

Table 1.3. Selection of examples for the Ni-catalyzed reduction nitriles to Boc-amines 16

Table 1.4. Reduction of nitrobenzene to aniline using various MBC catalysts 19

Table 2.1. Reduction of Aldehydes using $(i\text{Bu})_2AlBH_4$ 52

Table 2.2. Reduction of Ketones using $(i\text{Bu})_2AlBH_4$ 55

Table 2.3. Reduction of Aryl Nitriles by $(i\text{Bu})_2AlBH_4$ 58

Table 2.4. Reduction of benzylic nitriles to amines using $(i\text{Bu})_2AlBH_4$ 60

Table 2.5. Reduction of Epoxides by $(i\text{Bu})_2AlBH_4$ 61

Table 2.6. Reduction of *para*-substituted styrene oxide by $LiBH_4$ 64

Table 2.7. Reaction of various hydrides with styrene oxide 65

Table 2.8. Reaction of styrene oxide with $(i\text{Bu})_2AlBH_4$ 66

Table 2.9. Reduction of Carboxylic Acids by $(i\text{Bu})_2AlBH_4$ 68

Table 2.10. Reduction of Esters by $(i\text{Bu})_2AlBH_4$ 72

Table 2.11. Reduction of Primary Amides by Various Hydrides 74

Table 2.12. Reduction of Secondary and Tertiary Amides by Various Hydrides 75

Table 2.13. Reduction of aromatic tertiary amides using $i\text{Bu}_2AlBH_4$ 76

Table 2.14. Reduction of aliphatic amides and lactams using $i\text{Bu}_2AlBH_4$ 78

Table 2.15 Chemoselective Reduction Between an Aldehyde or Ketone and a Nitrile using $(i\text{Bu})_2AlBH_4$, DIBAL, and BMS 80

Table 3.1. Recyclability of Nickel Boron Composite Catalyst Supported on Nanocellulose 102

Table 3.2. Catalyst screening results 107

Table 3.3. Binding Energies of NBC-MASN and NBC 124

Table 3.4. Gas evolution analysis of NBC for differing ratios of $Ni:BH_4$ and NBC-MASN 125

Table 3.5. NBC-MASN vs NBC for selective nitro group reduction 132

Table 4.1. Solubilities of amine borane complexes at 25 °C 150

Table 4.2. Gas evolution analysis of the reaction between cyclohexanone and aqueous DMAB 172

Table 5.1. Binary, ternary, quaternary, and quinary alloys and their hydrogen 195

Table 5.2. Alternative metal alloys 199

Abstract

THE DEVELOPMENT OF ORGANIC REDUCTION REACTIONS BY BINARY HYDRIDES AND BINARY METAL CATALYSTS

Gabriella A. Amberchan

The synthesis of a binary hydride, diisobutylaluminum borohydride [(iBu)$_2$AlBH$_4$], was achieved from the equimolar addition of diisobutylaluminum hydride and borane dimethyl sulfide. Exploration into the reductive scope of (iBu)$_2$AlBH$_4$ showcased its versatility as a reducing agent. It was found that (iBu)$_2$AlBH$_4$ can convert aldehydes, ketones, and epoxides into alcohols (up to 98% yield), nitriles and tertiary amides to amines (up to 99% yield), and carboxylic acids and esters into alcohols (up to 93%). These reactions occurred at ambient conditions and the product was isolated with simple acid-base extractions, without the need for further purification via column chromatography. Further investigation showed that (iBu)$_2$AlBH$_4$ is effective as a selective hydride, as shown through a series of competitive reactions.

Borohydrides are not limited to reducing organic functional groups, as shown in the synthesis of an amorphous nickel and boron composite (NBC) catalyst. The NBC catalyst was synthesized from the reduction of a nickel salt by sodium borohydride and supported on mesoporous aluminosilicate nanoparticles (MASN). The NBC-MASN catalyst demonstrated excellent catalytic activity for the selective reduction of the nitro group on a variety of substituted nitroarenes, using hydrazine hydrate (N_2H_4•H_2O) as the H_2 source. Reuse and regeneration of NBC-MASN for the reduction of *para*-nitrotoluene demonstrated that the catalyst could be recycled up to nine times (67-99%

yield). The structure and composition of NBC-MASN were fully characterized by electron microscopy, various X-ray spectroscopy techniques, thermogravimetric analysis, and inductively coupled plasma optical emission spectroscopy.

By using Raman spectroscopy in a non-invasive, *ex situ* style, the reduction of nitroarenes in aqueous media was monitored. The catalytic reduction of nitroarenes was observed by the disappearance of the distinct nitro stretch (1350 cm^{-1}). Spectroscopic data determined that the aqueous reaction proceeded with pseudo first-order kinetics. Similarly, the reduction of cyclic ketones by dimethylamine borane (DMAB) in aqueous medium was also monitored using Raman spectroscopy. In this biphasic system, consisting of a carbonyl compound layer and an aqueous DMAB layer, the *ex situ* probe monitored the loss of the carbonyl stretch (1713 cm^{-1}). Density functional theory analysis established that the reaction occurred through a concerted hydride transfer.

As hydrogen cylinders are no longer available at UC Santa Cruz for academic research, it was of interest to develop a safe and efficient method of generating on-demand hydrogen gas. A binary gallium:aluminum (3:1) alloy was synthesized as a reagent to efficiently produce hydrogen gas from water. Gallium acts to remove the aluminum oxide coating. This allows pristine aluminum sites to be available for the water splitting reaction. Any source of water, including wastewater, commercial beverages, or ocean water were found to produce H_2. Similarly, commercial and waste aluminum were used to rapidly generate H_2. Gallium in the spent alloy was isolated and reused indefinitely. Characterization of the alloy showed aluminum particles within gallium were responsible for this room temperature water splitting activity, which likely proceeded through the Grotthuss mechanism. This work illustrates a possible method of generating H_2 without the need of fossil fuels and at ambient conditions.

This thesis is dedicated to my *Pao-Pao*, May, and to my mom, Judy.

My Dissertation Committee: Bakthan, I have learned so much from you. Your mentorship has helped me become a better researcher, a better presenter, and a better teacher. Thank you for understanding that graduate school is also about the activities outside the research lab and encouraging me to participate in different teaching and mentoring opportunities. I will continue to be guided by the Singaram two-thirds rule. Scott Lokey, thank you for always reminding me to ask the question “Why is this important?” and to relate my work back into a broader context. Scott Oliver, thank you for your research advice and knowledge. I have sincerely enjoyed collaborating with your group on different projects and learning techniques I had never heard of or envisioned I would learn as an organic chemist.

Dr. Beth Kochly, thank you for starting me on this journey into chemistry and teaching.

Labmates: Rachel, thank you for taking me under your wing and guiding me through the chemistry department, graduate school, and the best coffee shops in Santa Cruz. You became an immediate and lifelong friend. Your willingness to listen to all my practice talks, my ideas for orals, and whenever I needed advice was so generous of you. I will always remember our many hours studying and writing at Lulu Carpenters and our weekly Queer as Folk nights. I do not think graduate school could have gone as smoothly without your guidance and advice. Angel, thank you for always being willing to answer my very basic “how to” questions. I always admire your calm and easy going attitude towards research and I hope to someday have a similar mentality. And thank you for making me and Alice yummy breakfast burritos.

Undergraduates: I have learned to become a better teacher and mentor all because of the undergraduate students who have participated in the lab. Bella, as the first undergraduate student to work with me, you saw firsthand me trying to navigate our project and be just one step ahead of you, so thank you for your patience with me. Enrique, your love of learning helped me stay positive when we kept getting negative results. You asked questions that reminded me to keep reading and learning. Ryan, your energy to always do research and your excitement with the NBC-MASN project was infectious. Your love for science is so pure and it definitely made me excited to keep pushing forward in the project. Maddy, the lab would not have been as loud and full of laughter without you. You were so quick in learning the different techniques and understanding the project, in a way, this made it hard to wrap up the project because we kept having ideas to keep it going. Kyle, your constant presence each day made lab so much more fun and enjoyable. I loved having your come over to learn and play *mah joong* and going to see you kill it at volleyball. Isai, you grew so much during your time in the Singaram lab. You came out of your shell and it was wonderful to watch you share your wealth of knowledge with others. Roxy, I will not forget the day you taught me and Bakthan what "drip" meant, you lit up the lab. You always managed to find research articles on themes I would not have read and then educated the group.

Friends: Jocelyn, after our first meeting in PDP you became an immediate friend. I love being able to transition from talking about Disney movies to NMR spectra with you. You are one of the kindest souls I know, and your support has been so important when I was feeling lost or useless. A'Lester, from the first day we met as interviewees and bonding over being queer has formed such a strong friendship. I loved it when you would come into lab to talk about the Raman project and then segue into imposter syndrome. I still envision us working at the same or nearby institutions, collaborating on projects, and changing academia. Iris, cooking and laughing with you has been a highlight from these past few years. Thank you for always being game to try new things.

Family: Thank you to my family for being such an amazing support system. Thank you to my dad for driving me over the hill so I could be in lab on Monday mornings, when I had spent the weekend with you and mom. Thank you to my sister for taking on family responsibilities when I felt stressed or overwhelmed. Thank you to the Hewitt-Garrison family for reminding me how to relax (good food, company, and a cocktail makes everything fall away).

My Editors: I really cannot say enough thanks to the people who have read all the drafts of this work. Sam, you really went above and beyond editing my writing, even though you had no idea what I was talking about. Thank you for sprinkling in all the commas for me. You know I need all the help. Rachel, thank you for reading the documents before I was willing to send them to Bakthan. Ananya, thank you for taking the time to read my chapters and helping me clarify my thoughts.

Alice: Thank you for always calming me down when I went through moments of panic thinking I won’t be able to finish writing or when I have bouts of self-doubt. Thank you for being my sounding board. Thank you for reminding me that I can do this. Thank you for all the love and support you have provided me. I love you.

CHAPTER 1

Metal Hydrides and Binary Hydrides in Organic Reactions

1.1. Introduction

The reduction of organic functional groups is an integral chemical transformation. As there are a plethora of functional groups, so are the number of reducing reagents, each with their own set of abilities and limitations. Early 20th century reduction focused on reducing carbonyls. The methodologies included reacting the substrate with a metal in a highly acidic environment,[1] with either the use of the Meerwein-Ponndorf-Verley (MPV) reaction,[2-5] or the Bouveault-Blanc method for ester reduction (**Figure 1**). In addition to competing side reactions, many of these reactions suffered from high temperatures, extended reaction times, and excess reagents, none of which are sustainable reaction conditions for the modern era.[6, 7]

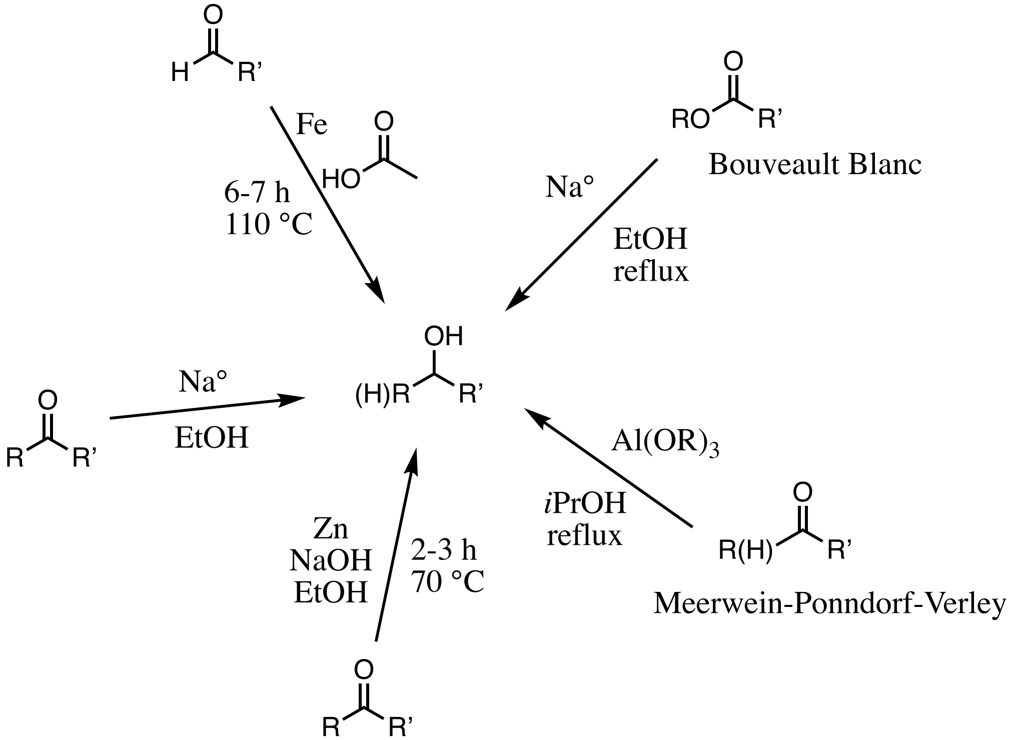
O
H R'
Fe
O
HO
6-7 h
110 °C
O
RO R'
Bouveault Blanc
Na°
EtOH
reflux
OH
(H)R R'
O
R R'
Na°
EtOH
Al(OR)3
iPrOH
reflux
O
R(H) R'
Meerwein-Ponndorf-Verley
Zn
NaOH
EtOH
2-3 h
70 °C
O
R R'

Figure 1.1. Non-hydridic reduction methods of the early 20th century.

Research has been done to alleviate some of these hurdles. The MPV reaction has seen renewed efforts in modernizing the reaction with the inclusion of additives,[8] and development of base-mediated reactions.[9] The Bouveault-Blanc method has been updated by using less pyrophoric sodium sources.[10, 11] Even with these changes these methods still suffer from excessive and costly reagents, limited functional group reactivity, and restricted solvent systems.

The development of hydrides was considered revolutionary for organic chemists because they were seen as relatively safer than sodium metal, tolerated wider solvents systems, and did not require extreme excess of reagents. More importantly, it was found that these hydride reagents could be tunable for the precise needs of the chemist, thus expanding the organic chemist's synthetic toolbox.

1.2. Metal Hydrides

Metal hydrides have become some of the most common reagents for reduction reactions, because they are easy to use and do not require extensive reagent preparation. Two most notable metal hydrides, lithium aluminum hydride ($LiAlH_4$) and sodium borohydride ($NaBH_4$), have remained as a constant presence in research, undergraduate, and industry laboratories. Lithium aluminum hydride and sodium borohydride represent two types of hydrides of aluminum and boron respectively, with wildly different reactivities. Known as the most powerful hydride, $LiAlH_4$ readily reduces aldehydes, ketones, nitriles, carboxylic acids and its derivatives, epoxides, and nitro groups.[12] Because of its high reactivity, it is not suitable as a selective reducing reagent for multifunctional compounds. Additionally, aluminum hydrides are notorious for being extremely flammable and are challenging to handle on a large scale.

1.2.1. Borohydrides

Since its discovery in the 1940s, $NaBH_4$ has become a popular reagent and its uses vary from reducing agent in organic synthesis to hydrogen storage material. The polarization of the $^{\delta+}$B-H$^{\delta-}$ bond is the reason it is considered a *hydride* and can react with electrophilic functional groups. The advent of ^{11}B NMR has allowed for facile identification of borohydride species, many of which display signals in the range of δ-26-45ppm. The variation in chemical shift derives from the corresponding cation, substituents on the boron atom, and solvent choice.

Two syntheses have been developed to produce $NaBH_4$, the Brown-Schlesinger method[13] (**equation 1**) and the Bayer process[14] (**equation 2**).

$$4\,NaH + B(OCH_3)_3 \xrightarrow{250\,^{\circ}\mathrm{C}} NaBH_4 + 3\,NaOCH_3 \qquad (1)$$

$$Na_2B_4O_7 + 16\,Na + 8\,H_2 + 7\,SiO_2 \rightarrow 4\,NaBH_4 + 7\,Na_2SiO_3 \qquad (2)$$

The Brown-Schlesinger method is frequently used in industrial production of $NaBH_4$, but work has been conducted to modernize the Bayer process. This has included using magnesium instead of sodium and hydrated borax, instead of the anhydrous version.[14] Once isolated, the white powder is soluble in water and alcohol solvents. In the presence of methanol, $NaBH_4$ evolves hydrogen gas, which is why it is considered a potential hydrogen source. Compared to $LiAlH_4$, $NaBH_4$ is categorized as a mild reducing reagent, readily reducing aldehydes, ketones, and acid chlorides.[12]

Interestingly, by changing the cation on the borohydride, the reactivity alters, which in turn causes differences in the reductive capabilities of the hydride. For instance, when aluminum chloride was mixed with sodium borohydride in diglyme, the new reagent produced was able to reduce a wider range of functionalities compared to $NaBH_4$ (**Table 1.1**).[15] Additionally, unlike $NaBH_4$, lithium borohydride ($LiBH_4$) has the advantage of being soluble in ethereal solvents[16] and was found to reduce aldehydes, ketones, and esters.[17] The reduction of esters proceeded slowly, but later work showed that when $LiBH_4$ was combined with catalysts, such as *B*-methoxy-9-BBN or methyl borate, then aliphatic and aromatic esters were reduced in 1-2 h.[18]

Table 1.1. Comparison of functional groups reduced by $NaBH_4$, $Al(BH_4)_3$, and $LiBH_4$

Functional Group	**$NaBH_4$**[a]	**$Al(BH_4)_3$**[b]	**$LiBH_4$**[c]
Aldehyde	Alcohol	Alcohol	Alcohol
Ketone	Alcohol	Alcohol	Alcohol
Ester	-	Alcohol	Alcohol[d]
Acid	-	Alcohol	Partial reduction[e]
Acid halide	Alcohol	Alcohol	Alcohol
Acid anhydride	-	Glycol	-
Epoxide	-	Alcohol	Alcohol
Lactone	-	Glycol	-
3° Amide	-	*t*-amine	-
Nitrile	-	Amine	-
Nitro	-	-	Partial reduction[f]
Disulfide	-	Thiol	-

[a] Ref:[12] [b]Ref:[15] [c]Ref:[17] [d] Reaction proceeded slowly (6 h) and required refluxing conditions. [e] Aromatic acids underwent no reaction, but aliphatic acids saw minor conversion to the alcohol. [f] Refluxing nitrobenzene with $LiBH_4$ in an ether:THF mixture of 16 h produced aniline (22%), starting material (30%), and unknown mixture of intermediates (30%).

A trend has been observed that might indicate why these borohydride species have different reactivities. The reducing strength of the borohydride increases as the size of the corresponding cation decreases (**Scheme 1.1**).[12, 19] Additionally, different metals exert slight variations in their polarization of the BH_4^- ion explaining the differences in their reactivity.

$$\underset{\text{Increasing reducing power}}{\xrightarrow{\mathrm{NaBH_4 > LiBH_4 > Al(BH_4)_3}}}$$

Scheme 1.1. Reducing power of different metal borohydrides.

The fact that cations influenced the reactivity, physical characteristics, and solvent compatibility of the corresponding borohydrides implies that hydrides can be tailor-made for specific reactions. Therefore, researchers have begun combining different hydrides together or reacting metal salts with hydrides to create new binary hydrides, all with the goal of developing unique reagents with different reactivities and applications.

1.2.2. Binary Hydrides

By combining two hydrides, the resulting mixture could contain two hydrides that can work synergistically with each other. Or the mixture affords an entirely new hydride that has its own reactivity profile. The advantage of binary hydrides is the potential for selective, partial, or tandem reductions. This is clearly observed in the reduction of 4-(bromomethyl)benzonitrile by a series of binary hydrides.[20] Dichloroindium hydride ($HInCl_2$) is a mild reagent that can be synthesized from a variety of sources. One method includes reacting indium trichloride ($InCl_3$) with diisobutylaluminum hydride (DIBAL), which produces the hydride along with a byproduct, diisobutylaluminum chloride (**Figure 1.2**, reaction **A**).

As we will see in the next section, $NaBH_4$ reacts with metal salts to create metal catalysts that can then be used to reduce a variety of functional groups. Interestingly, the reaction of $InCl_3$ and $NaBH_4$ does not produce In^0, but instead $HInCl_2$.[21] Furthermore, when the reaction occurs in THF, ^{11}B NMR analysis of the reaction mixture displayed a quartet (J = 105 Hz) at δ = -1 ppm, which is attributable to the borane-tetrahydrofuran adduct (BH_3:THF) (**Figure 1.2**, reaction **B**).[22] Therefore, both $HInCl_2$ and BH_3:THF were formed *in situ* and as each hydride source have unique reductive profiles it implied that the two hydrides could work cooperatively in a tandem reduction reaction.

Consequently, reduction of 4-(bromomethyl)benzonitrile with $HInCl_2$, prepared by various methods was studied. As expected, $HInCl_2$ synthesized by different methods afforded different reduced products (**Figure 1.2**). The $HInCl_2$ made by DIBAL/$InCl_3$ (route **A**) produced 4-cyanotoluene, suggesting that $HInCl_2$ can dehalogenate a benzyl bromide, but it is too mild to reduce a cyano group.[23] The reduction of the same compound, but with the binary hydride of $HInCl_2$ and BH_3:THF (**B**) tandemly reduced the substrate to give the primary amine. In this instance, both hydrides, $HInCl_2$ and BH_3:THF, are working cooperatively within the reaction to obtain the different substituents. The $HInCl_2$ acts to dehalogenate the benzyl bromide and the BH_3:THF reduces the cyano group to afford the primary amine.[24]

Interestingly, another tandem reduction can occur based on the order of addition of the hydrides. It was found that when DIBAL was allowed to react with 4-(bromomethyl)benzonitrile first (4 h) and then $HInCl_2$ was added to the mixture, 4-tolualdehyde was produced (**Figure 1.2**, reaction **C**).[23]

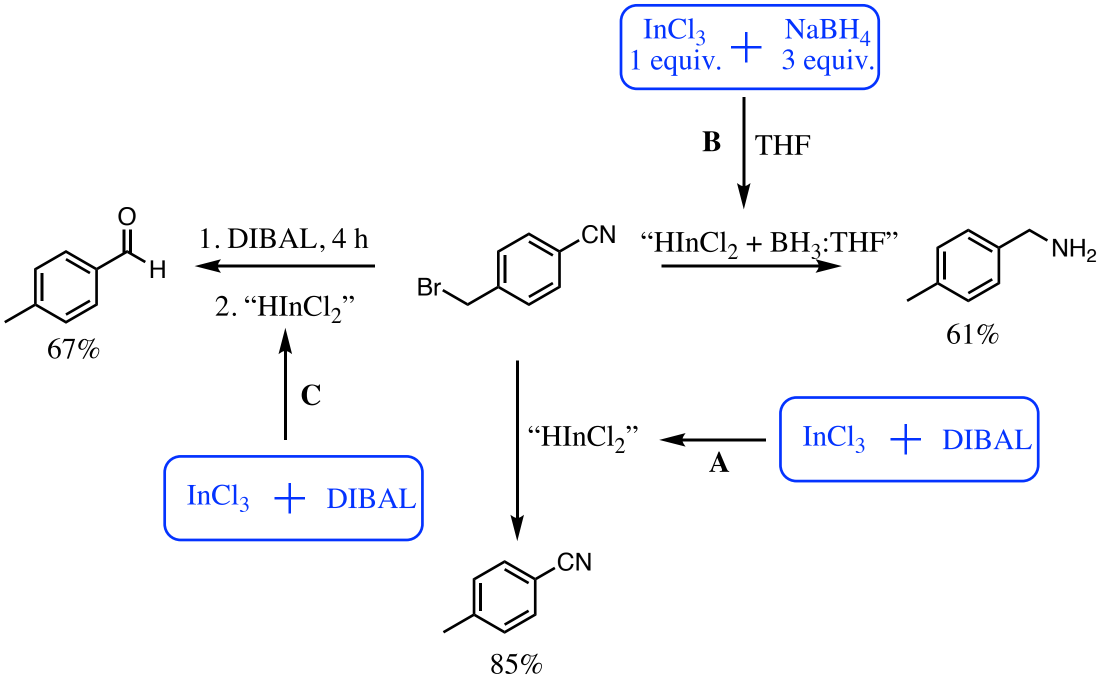

Figure 1.2. The partial and tandem reduction reactions 4-(bromomethyl)benzonitrile by $HInCl_2$ (**A**), and binary hydrides $HInCl_2$ and BH_3:THF (**B**), DIBAL and $HInCl_2$ (**C**).

In an additional demonstration, methyl 4-(bromomethyl) benzoate was chosen as another bifunctional compound to examine for reduction by binary hydrides.[23] As mentioned above, mixing $InCl_3$ and $NaBH_4$ in THF produces $HInCl_2$ and BH_3:THF. When this binary hydride was allowed to react with methyl 4-(bromomethyl) benzoate. Dehalogenation of the bromine occurred but the ester remained intact (**Figure 3**, reaction **D**). A separate experiment revealed that BH_3:THF showed no reaction with 4-(bromomethyl) benzoate. Thus, in the binary hydride reaction, the $HInCl_2$ is the reactive species and BH_3:THF is too weak to react with either functionality. To further corroborate and confirm that $HInCl_2$ cannot reduce the ester, the hydride was synthesized from DIBAL and $InCl_3$ (**Figure 1.3**, reaction **E**). Under these reaction parameters, methyl 4-toluate was produced in 78% yield.

If the goal was to reduce both functionalities of 4-(bromomethyl) benzoate, Snelling and colleagues were able to achieve it using a tandem reduction reaction system.[23] It is known that lithium aminoborohydrides (LABs) can reduce esters.[25] And as it has been established that $HInCl_2$ can dehalogenate this compound, it was predicted that both functionalities could be reduced by the two hydrides working synergistically. Consequently, reaction of 4-(bromomethyl) benzoate with $HInCl_2$ followed by addition of lithium dimethylaminoborohydride (MeLAB) showed that to be the case, affording 4-methylbenzyl alcohol in 90% yield (**Figure 1.3**, reaction **F**).

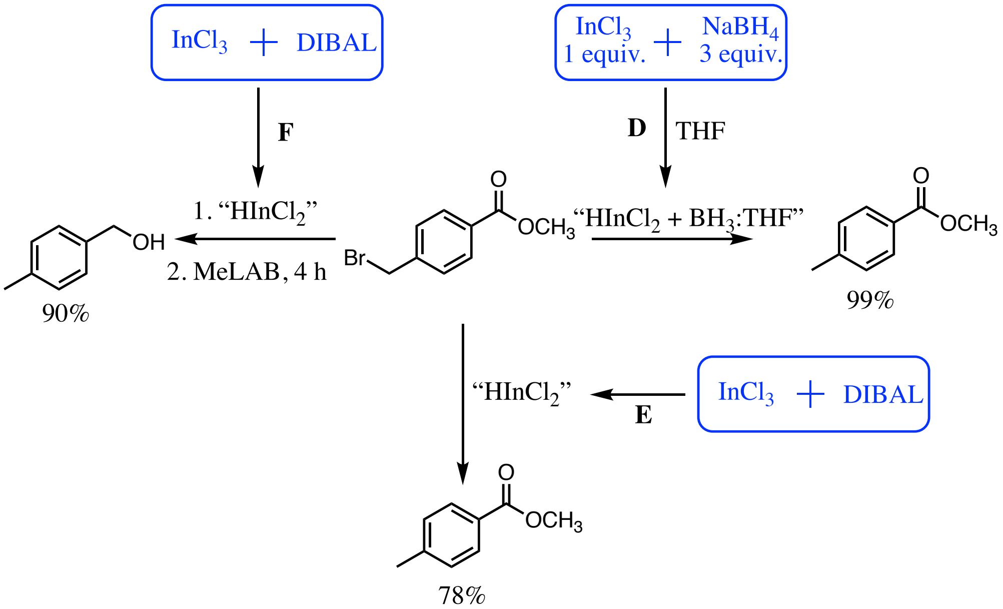

InCl3 + DIBAL
F
InCl3 1 equiv. + NaBH4 3 equiv.
D
THF
1. "HInCl2"
2. MeLAB, 4 h
OH
90%
Br
O
OCH3
"HInCl2 + BH3:THF"
O
OCH3
99%
"HInCl2"
E
InCl3 + DIBAL
O
OCH3
78%

Figure 1.3. The partial and tandem reduction reactions 4-(bromomethyl) benzoate by binary hydrides $HInCl_2$ and BH_3:THF (**D**), $HInCl_2$ (**E**), and $HInCl_2$ and MeLAB (**F**).

1.3. Metal Boron Composites

Many of the hydrides mentioned above do not reduce nitro groups, which are valuable sources to amines or aniline derivatives. As one of the more powerful hydrides, $LiAlH_4$ does react with nitro groups. Upon closer examination it was found that $LiAlH_4$ will reduce aromatic nitro compounds to the azo state and aliphatic nitro compounds to amines (**Scheme 1.2**).[26] Aniline compounds are highly useful and so developing a method to safely and efficiently obtain aniline derivatives from nitroarenes would be valuable.

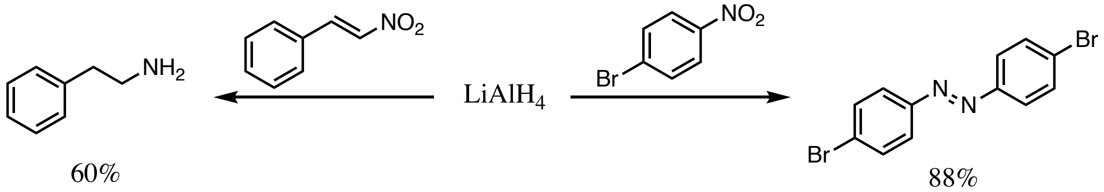

Scheme 1.2. Reduction of aliphatic (left) and aromatic (right) nitro groups to amines and azo compounds, respectively.

Sodium borohydride on its own cannot reduce a nitro group because the hydrogen is less polarized, thus inhibiting the reaction from even occurring.[27] Therefore, bond activation is required to promote reduction. Activation can be achieved from reaction with metal salts to create a heterogeneous catalyst, referred to here as a metal boron composite (MBC) catalyst. These amorphous catalysts, easily identifiable by the black color of the precipitate, have been shown to reduce more challenging functional groups. A more in-depth discussion on the composition of these types of MBC catalysts will be conducted in chapter 3. In these next few sections, application of MBC catalysts in organic synthesis will be discussed, including how they can be used to hydrogenate carbon double bonds and reduce nitriles and nitro groups.

1.3.1. Hydrogenation of Alkenes and Dienes

Initial application of the heterogeneous catalyst, synthesized from a metal salt and $NaBH_4$, was found in hydrogenation of alkenes. Expansion of that work examined if the catalyst was selective in the hydrogenation of dienes.[28] It is known that Ni^0 species will undergo oxidative addition to allyl substrates and form a π-allylnickel complex (**G**).[29, 30] Rather than using a nickel catalyst with expensive ligands, $NiCl_2$ and $NaBH_4$ were combined in methanol to make the catalyst *in situ*. A selection of dienes containing electron-donating groups at R^1 were tested to determine if regioselective hydrogenation (**H** or **I** alkenes) or if complete hydrogenation was obtained. It was found that the 3,4-double-bond underwent hydrogenation to produce **H**-type alkenes in high yields even when excess $NaBH_4$ was present (**Table 1.2**). Under these reaction conditions, alkylamino and alkyloxy groups were tolerated, as were protecting groups (entry 3). Bulky groups did not appear to deter the reaction, but if a nitro group was present it also underwent reduction to the amine (entry 4). Interestingly, the **I**-type of alkene was formed if the R^1-group was an alkyl substituent (entry 5). These observations led to the identification that if R^1 is an electron-donating group the hydride will react solely at carbon 3, affording **H**-type alkenes. Also, if the electron-donating group is on R^2 and R^1 is a phenyl group, **H**- type alkenes were formed. They rationalized that the sterics of the phenyl group influenced the hydride attack in these circumstances.

Table 1.2. Selected dienes for the regioselective reduction.[a,b]

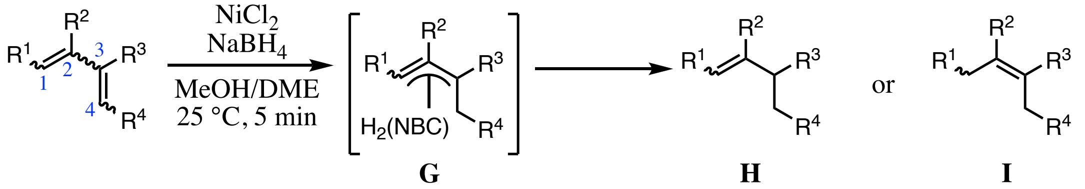

Entry	Diene	Product	Yield
1	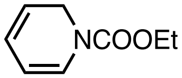	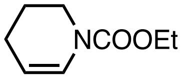	85
2	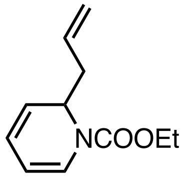	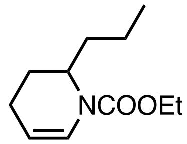	84
3	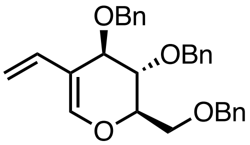	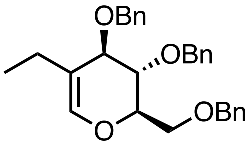	93
4	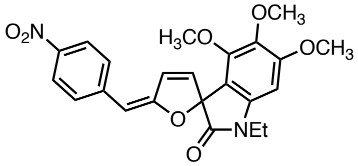	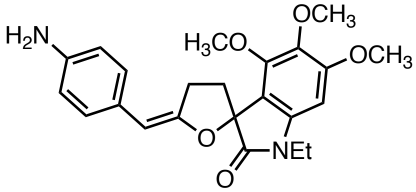	60
5	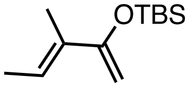	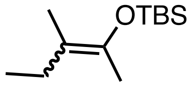	67

[a] Reactions were carried out on a 1 mmol scale: $NiCl_2$ (0.2 mmol), $NaBH_4$ (10 mmol), 5 mL MeOH/DME (1/1, v/v). [b] Ref: [28]

It has been shown that these heterogenous catalysts will reduce carbonyls and hydrogenate alkenes. Interestingly, one group found that their nickel catalyst was selective for 1,4-reduction of α,β-unsaturated aldehydes and ketones.[31] The key finding was how the catalyst was synthesized. When the nickel salt was allowed to react with excess $NaBH_4$ in methanol, the black precipitate forms. The catalyst was then subjected to either of two supplementary protocols, either a wash with methanol or a 3 h reflux in methanol. Catalysts synthesized from both methods were then used to reduce 2-cyclohexen-1-one, which afforded very different products (**Scheme 1.3**). When the catalyst was just washed with methanol, the saturated alcohol was produced. Oppositely, the refluxed catalyst produced cyclohexanone. It was hypothesized that the over-reduction of the α,β-unsaturated ketone was due to residual $NaBH_4$ present in the catalyst. When the catalyst was placed under refluxing conditions the excess borohydride was destroyed and only the 1,4-reduction occurred. This simple experimental change provides for catalysis selectivity.

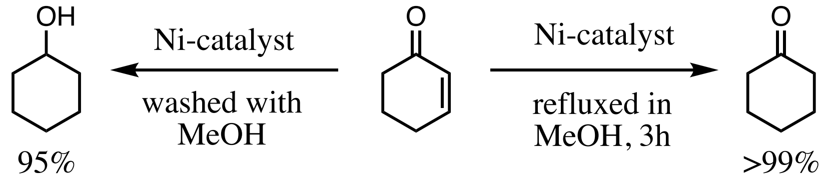

Scheme 1.3. Reduction of 2-cyclohexen-1-one by a nickel catalyst synthesized from washing with MeOH vs. refluxed in MeOH.

The black precipitate was also observed when a $Mn[N(SiMe_3)_2]_2$ was subjected to an equimolar amount of DIBAL.[32] The *in situ* formation of the Mn nanoparticles were successfully tested as a hydrogenation catalyst for alkenes, alkynes, and imines. This demonstrates that the hydride required to reduce a metal salt is not limited to $NaBH_4$ and that other hydrides can form the MBC catalysts. Sodium borohydride is more favorable because it is less expensive and more prevalent.

1.3.2. Reduction of Nitriles

Nitrile reductions are an efficient method to obtain primary amines. The discovery of MBC catalysts has allowed for expansive work in using these catalysts for the hydrogenation of nitriles. The addition of cobalt chloride with $NaBH_4$ led to the synthesis of a cobalt boron composite catalyst (CBC) that could effectively hydrogenate aromatic nitriles to the corresponding benzylic amines.[33, 34] Several mechanistic pathways were postulated for this hydrogenation: 1) complexation of the borohydride to the catalyst surface, which then acts as the “hydride donor”, 2) a cobalt hydride formed from the decomposition of the borohydride interacting with the catalyst surface, or 3) the nitrile complexes with the catalyst surface and then undergoes reduction by free borohydride. Subsequently, a series of experiments were conducted to elucidate the possible pathway. The researchers found that the rate of reduction was independent of the nitrile concentration and was more dependent upon the concentration of BH_4^- (calculated as first-order dependence). They also tested whether simply the supernatant solution above the catalyst could reduce benzonitrile and found that this was not the case. This suggested that the reduction was occurring on the catalyst surface and that the nitrile was coordinating to the metal. To test this theory, an equimolar amount of benzonitrile and CBC were combined, and it was found that the nitrile was strongly adsorbed upon the catalyst’s surface. Subsequent ammonolysis with NH_4OH released the substrate from the metal surface. Based on these findings it was rationalized that pathway 1 was not reasonable because it does not follow the observed kinetics data. The formation of a cobalt hydride, as predicted in pathway 2, could be possible with the kinetics. However, to form the cobalt hydride a resulting BH_3 species should also be present. In an effort to trap the possible BH_3, 2-aminopyridine was added but no formation of the borane was observed. As such, route 2 does not appear to be a likely pathway. This leaves route 3 as the possible mechanism, wherein the nitrile complexes with the catalyst's surface and is activated, thus allowing a borohydride species to undergo the hydride addition (**Figure 1.4**).

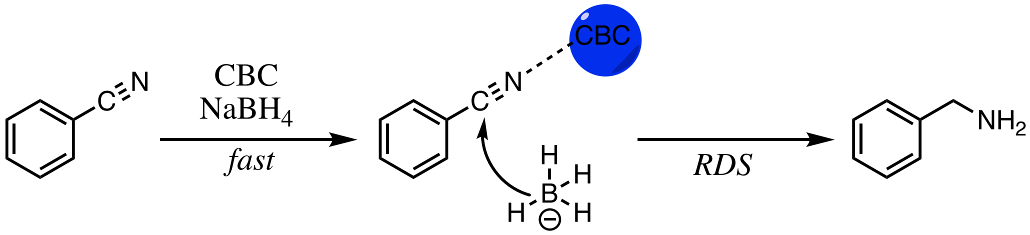

Figure 1.4. Proposed mechanism of the reduction of benzonitrile with CBC catalyst and $NaBH_4$.[33]

Further expansion of the reduction of nitriles led to the catalytic reduction of nitriles to Boc-amines, achieved using a nickel catalyst. This reaction occurred in a one-pot method.[35] It was contingent upon the reduction of the metal salt, nickel chloride hexahydrate, by $NaBH_4$. As soon as the catalyst was formed it was able *in situ* to react with the nitrile and di-tert-butyl dicarbonate. The protected amines were then isolated (21-96% yield). As shown in **Table 1.3**, this method was effective with aliphatic, aromatic, and heterocyclic nitriles. Halogens and esters were tolerated substituents, while amides were moderately accepted. They surmised that the reagent reacts with the amide substituent, but they were only able to isolate the protected amine from the nitrile (entry 2). Addition of the protecting group did occur when nitro groups or phenols were present (entries 4 and 5). Alkenes were also hydrogenated under these reaction conditions.

Table 1.3. Selection of examples for the Ni-catalyzed reduction nitriles to Boc-amines.[a]

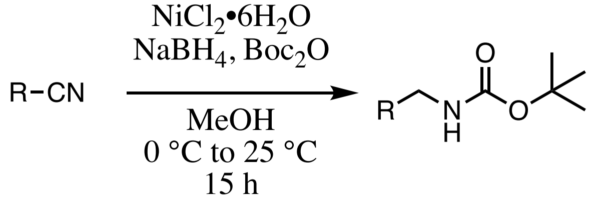

Entry	Starting Nitrile	Product	Yield (%)
1	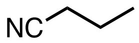	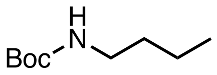	77
2	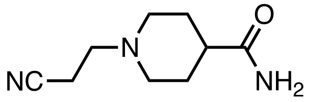	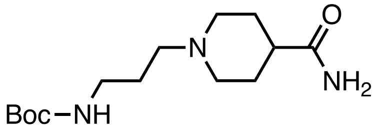	21
3	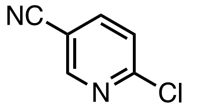	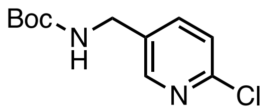	93[b]
4	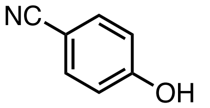	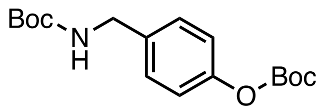	52
5	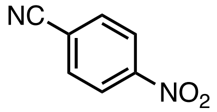	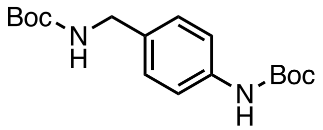	45

[a]Thirty nitriles were subjected to this methodology; reaction conditions: $NiCl_2$•$6H_2$ (0.1 equiv.), $NaBH_4$ (7 equiv.), Boc_2O (2 equiv.). [b]Reaction was complete in 1 h.

Moreover, the development of a selective cobalt-catalyzed nitrile reduction to afford either secondary aldimines or primary amines has been shown. It has been previously reported that phosphorous ligands were effective in transforming nitriles to secondary aldimines by self-condensation reactions.[36] Thus, it was hypothesized that the simultaneous addition of an amine could react immediately with the primary aldimine to give a secondary aldimine with unique substituents (**Figure 1.5**).

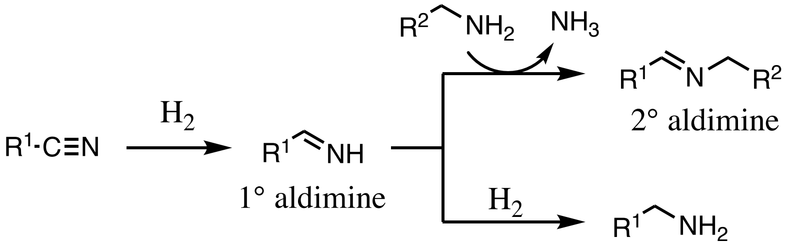

Figure 1.5. Reduction of nitriles to the primary aldimine followed by addition of an amine to generate the secondary aldimine. Or the nitrile can undergo full reduction to the primary amine.

Benzonitrile and cyclohexylamine were allowed to react with a cobalt catalyst, synthesized from $CoBr_2$ and sodium triethylborohydride ($NaHBEt_3$), as the reductant, and a tridentate ligand, $^{iPr}PN^{H}P$.[37] The order of reagent addition proved to be essential in predicting the selectivity. When $CoBr_2$ and $NaHBEt_3$ were combined first, a black precipitate was immediately formed indicating the formation of the cobalt boron composite (CBC) catalyst. Whether $^{iPr}PN^{H}P$ was absent from the reaction mixture in the beginning or was added afterwards did not affect the product distribution but gave the complete conversion of benzonitrile into the primary amine product **2** (**Figure 1.6**, reaction **J**). Some secondary aldimine **1** was observed (3%) and all of the cyclohexylamine was recovered, indicating it did not participate in this reaction under the above reaction condition. This method was effective in reducing aromatic and aliphatic nitriles to the corresponding primary amines. This methodology tolerated the presence of esters, amides, and alcohols, but did hydrogenate alkenes.

Interestingly, when $CoBr_2$ was combined with $^{iPr}PN^{H}P$ followed by $NaHBEt_3$ a homogeneous solution was obtained and this time only secondary aldimines were produced.[37] Under these reaction conditions it appeared that the primary aldimine underwent a nucleophilic addition with cyclohexylamine to generate **3** (87%) and a minute amount of **1** (**Figure 1.6**, reaction **K**). Overall, this suggests that the ligand affects the selectivity of the catalyst and offers a tunable catalytic system for chemists to synthesize either primary amines or secondary aldimines.

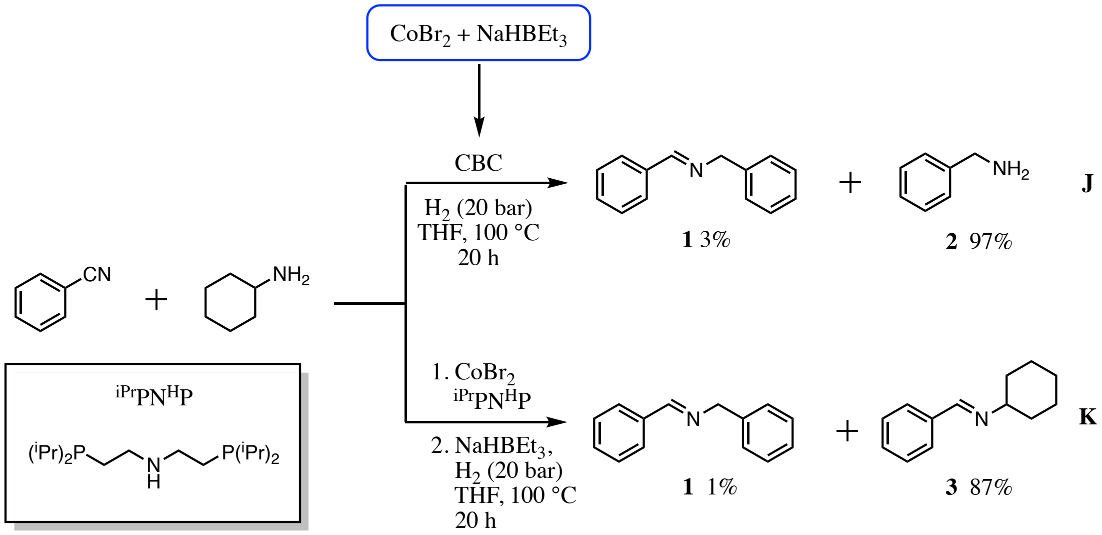

Figure 1.6. Co-catalyzed selective reduction of nitriles to primary amines (**J**) or secondary aldimines (**K**).

1.3.3. Reduction of Nitro Groups

As mentioned earlier, few hydride reagents can reduce nitro groups to amines in an efficient manner. However, activation of the hydride can be achieved in the presence of metal catalysts, which can then be used to effectively hydrogenate nitro groups. As shown in **Table 1.4**, MBC catalysts can transform nitrobenzene into aniline in high yields. The metal salts are typically first row transition metals (entries 1-7), such as cobalt and nickel, but other metals have been shown to produce effective catalysts (entry 8). The hydride used to reduce the metal salt is frequently $NaBH_4$ because it is inexpensive and easy to use. Other hydride sources, such as ammonia borane or other borohydrides, have been effective in reducing the metal cations to M^0 (entries 1-2).

Table 1.4. Reduction of nitrobenzene to aniline using various MBC catalysts.

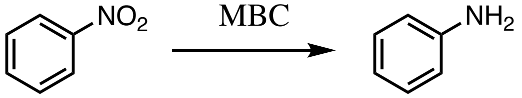

Entry	Metal Salt	Hydride[a]	Support/Additives	H_2 Source[b]	Yield (%)[c]	Ref
1	$CoCl_2$	$NH_3{:}BH_3$	--	$NaBH_4$	64	38
2	$CoCl_2$	$NH_3{:}BH_3$	--	N_2H_4	94	38
3	Co_3S_4	$NaBH_4$	--	$NaBH_4$	73	39
4	$CoCl_2•6H_2O$	$NaBH_4$	PVP	$N_2H_4•H_2O$	50	40
5	$NiCl_2•6H_2O$	$NaBH_4$	--	$NaBH_4$	76	41
6	$NiCl_2•6H_2O$	$NaBH_4$	PVP	$N_2H_4•H_2O$	99	40
7	$NiCl_2•6H_2O$ and $CoCl_2$	$NaBH_4$	PVP	$N_2H_4•H_2O$	96	42
8	$Au(en)_3Cl_3$	$NaBH_4$	Mesoporous TiO_2 nanoparticle assemblies (MTA)	$NaBH_4$	95	43

[a] Hydride used to reduce metal salt. [b] Compound used for the hydrogenation reaction. [c]Isolated yield.

For the reduction of nitroarenes, a hydrogen atmosphere is necessary, and it can be generated *in situ* from an excess of $NaBH_4$ (if the catalyst was made in an *in situ* style) or from hydrazine hydrate ($N_2H_4•H_2O$). For the reduction of nitroarenes both hydrogen sources are viable and effective in achieving complete reduction, unless other reducible functionalities are present. To explore potential chemo-selectivity, benzonitrile was tested using the same CBC catalyst but changed the H_2 source.[38] The nitrile was converted into the amine with $NaBH_4$, but no reaction occurred when N_2H_4 was used (**Scheme 1.4**, reactions **L** and **M**). This led to the possibility that the catalysis of CBC with N_2H_4 could be chemo-selective. To test this, 4-nitrobenzonitrile was subjected to the CBC catalyst and N_2H_4. This reaction afforded 4-aminobenzonitrile in 70% yield (**Scheme 1.4**, reactions **N**). Thus, demonstrating that this catalytic system can be chemo-selective.

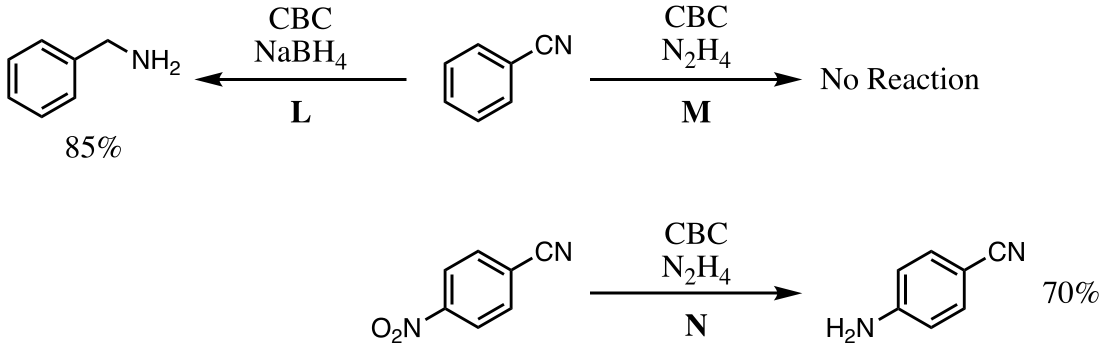

Scheme 1.4. Reaction of benzonitrile with CBC, synthesized from Vernekar's procedure,[38] and $NaBH_4$ (**L**) or N_2H_4 (**M**). Reaction of 4-nitrobenzonitrile with CBC and N_2H_4 (**N**).

An advantage of using alternative hydrogen sources like $NaBH_4$ or hydrazine is that the reduction can be carried out under one atmospheric pressure. Both $NaBH_4$ and hydrazine will degrade to provide the necessary hydrogen gas for the reductions, but how they liberate hydrogen is where they differ. Borohydrides in the presence of a metal salt and water/alcohol will reduce the metal, form borate species, and liberate hydrogen (**equation 3**).[44, 45]

$$BH_4^- + 2M^{2+} + 2H_2O \rightarrow 2M + BO_2^- + 4H^+ + 2H_2 \qquad (3)$$

Hydrazine when it interacts the MBC will decompose into hydrogen and a diimide intermediate (**equation 4**).[46-49] It has been reported that diimide on its own will not reduce a nitro or nitrile group, unless a metal catalyst is present to induce the reaction;

so both components are necessary to obtain the amine.[50] After the reaction, the diimide degrades into nontoxic N_2 and hydrogen (**equation 5**).

$$N_2H_4 \rightarrow N_2H_2 + e^- + 2H^+ \qquad (4)$$

$$N_2H_2 \rightarrow N_2 + 2e^- + 2H^+ \; (5)$$

1.3.4. Other Reductions with Metal Boron Composite Catalysts

Some groups have been able to take these reduction reactions a step further and trap the amine to undergo additional reactions. For example, nickel chloride was combined with TEMPO-oxidized nanocellulose, $NaBH_{4(aq)}$, and the nitro substrate for the conversion to the corresponding aniline.[51] The addition of the TEMPO-oxidized nanocellulose was to increase the catalyst's surface area, which lowered the reaction time and increase the product yields for the reduction of nitroarenes. It was predicted that the addition of an epoxide would synthesize β-amino alcohols in a one-pot reaction from the nitro compound (**Figure 1.7**). The metal salt would reduce first, it would then reduce the nitro group to the corresponding amine, and then the amine would act as a nucleophile and open the epoxide. This tandem reduction proved effective for both the aromatic and the aliphatic nitro and epoxide substrates.

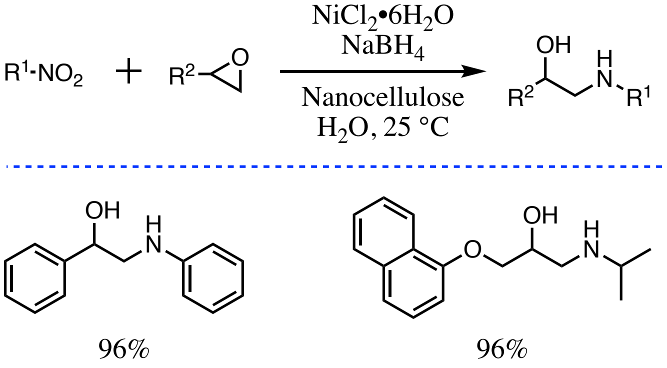

Figure 1.7. Tandem reduction and epoxide ring opening C-N coupling reaction.[51]

Similarly, a one-pot reaction was used to synthesize Boc-amines. Excess $NaBH_4$ was used to reduce both the nickel salt and the nitro group.[51] Once the amine was formed di-tert-butyl dicarbonate was present to react *in situ* with the product amine. The corresponding Boc-protected amines were isolated in high yields (up to 98%).

Further application of an MBC catalyst has been shown to facilitate reductive cleavage of allyl esters to glycals.[28] By using $NaBD_4$ and CD_3OD with $NiCl_2$ it was possible to examine the stereochemistry of the cleavage and to propose a possible mechanism. After the $NiCl_2$ and $NaBD_4$ were combined, the MBC catalyst underwent an oxidative addition with **4** to produce a π-allylnickel complex **5** (**Figure 1.8**). The hydride attack only occurred at carbon 3 on structure **5** to produce the final product and the researchers surmised that the π-allylnickel complex was the cause for the selectivity. After the hydride transfer, the MBC catalyst reacts with D_2 to restart the cycle. In addition to the deuterated compound, it was found that allyl esters containing a range of hydroxy protecting groups from acetyl to *t*-butyldiphenylsilyl groups were well tolerated and even the acyclic 3-phenylallyl acetate underwent cleavage. These examples illustrate that these heterogeneous catalysts can have wider reaching synthesis possibilities beyond use as reducing reagents.

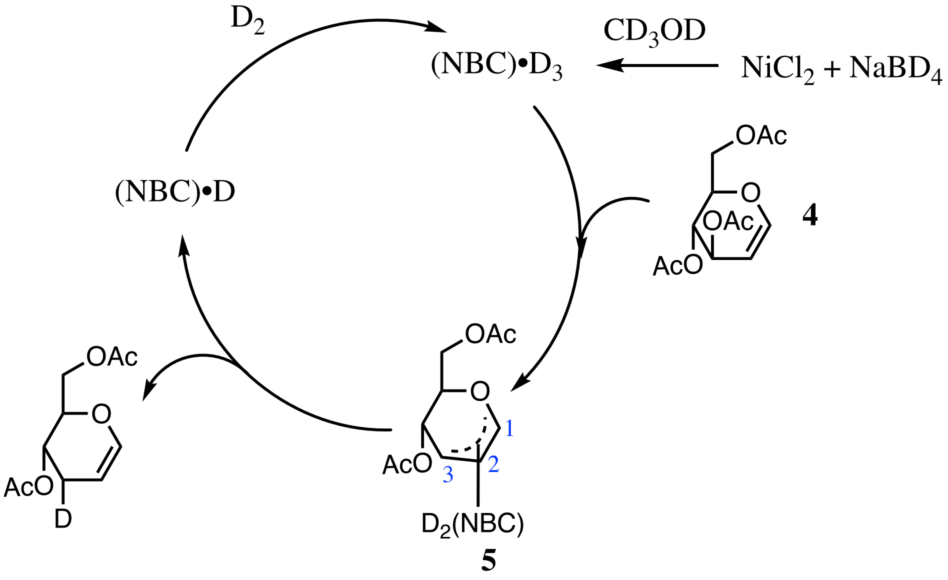

Figure 1.8. Proposed mechanism for the cleavage of allyl esters.

1.4. Hydrogen Generation

The discussion above focused primarily on how hydrogen can be used in the reduction of organic functional groups and in hydrogenation reactions. However, hydrogen has also been explored as an alternative fuel source, because it has a high gravimetric energy density (33.3 kWh/kg, in comparison, gasoline has a gravimetric energy density of 11.8 kWh/kg)[52, 53] and a nontoxic byproduct (water). The latter of which has led to its nickname as a "clean fuel." As the lightest gas, transporting it in theory would be less costly than fossil fuels, except that because of its low density it needs to be compressed. This is not ideal as hydrogen is flammable. Thus, storage of hydrogen is a widely and hotly discussed topic. In this section, focus will be on hydrogen sources and their effectiveness.

1.4.1. Borohydrides as a H_2 Source

Sodium borohydride has been considered as a potential source of hydrogen because it contains four hydrogen atoms that could be accessed and converted into hydrogen. Furthermore, the hydrolysis of $NaBH_4$ demonstrates that for one mol of borohydride, four moles of hydrogen are produced along with the nontoxic borate species (**equation 6**).

$$BH_4^- + 2H_2O \rightarrow BO_2^- + 4H_2 \qquad (6)$$

Sodium borohydride is not the only hydride that undergoes hydrolysis to produce hydrogen. As shown in **Figure 1.9**, a selection of hydrides have been tested for hydrogen production.[53, 54] In general, aluminum hydrides underperform compared to the metal borohydrides. Of the $M^+BH_4^-$ species, $LiBH_4$ ranks as the best hydrogen producer, however $LiBH_4$ and the Al and Mg analogs are not typically considered for hydrogen generation. That is because solid $NaBH_4$ is advantageous for being more stable and less pyrophoric, a desired quality when dealing with hydrogen generation.

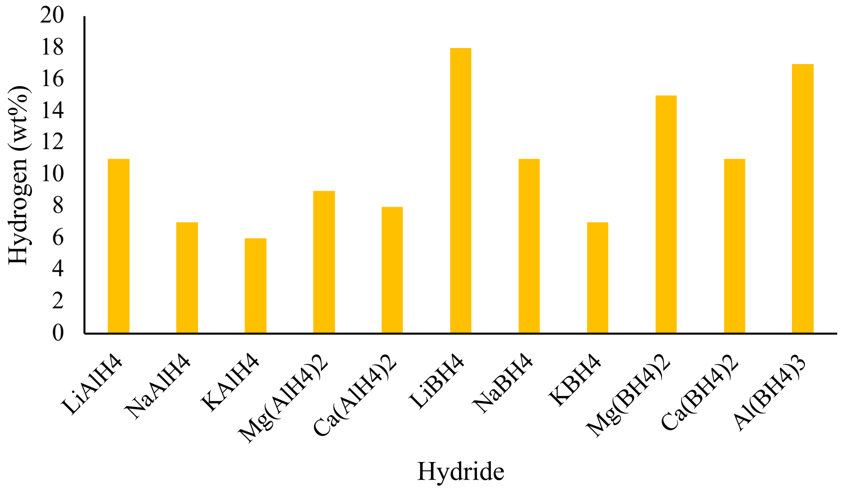

Figure 1.9. Hydrolysis of various hydrides and complex hydrides.

Brown and Schlesinger did notice that the rate of hydrogen evolution from $NaBH_4$ varied with the pH of the system.[45] Initial observations found that the more basic the solution the less hydrogen was produced. Therefore, it seemed reasonable to assume that the addition of acidic accelerators would increase the rate of hydrogen production. Eighteen acidic materials were tested, and it was found that all except one produced >50% H_2 (**Figure 1.10**). Oxalic, malonic, succinic, and malic acid all facilitated in producing ≥95% H_2 and only necessitated a 0.6:2.6 mol ratio of accelerant to $NaBH_4$.

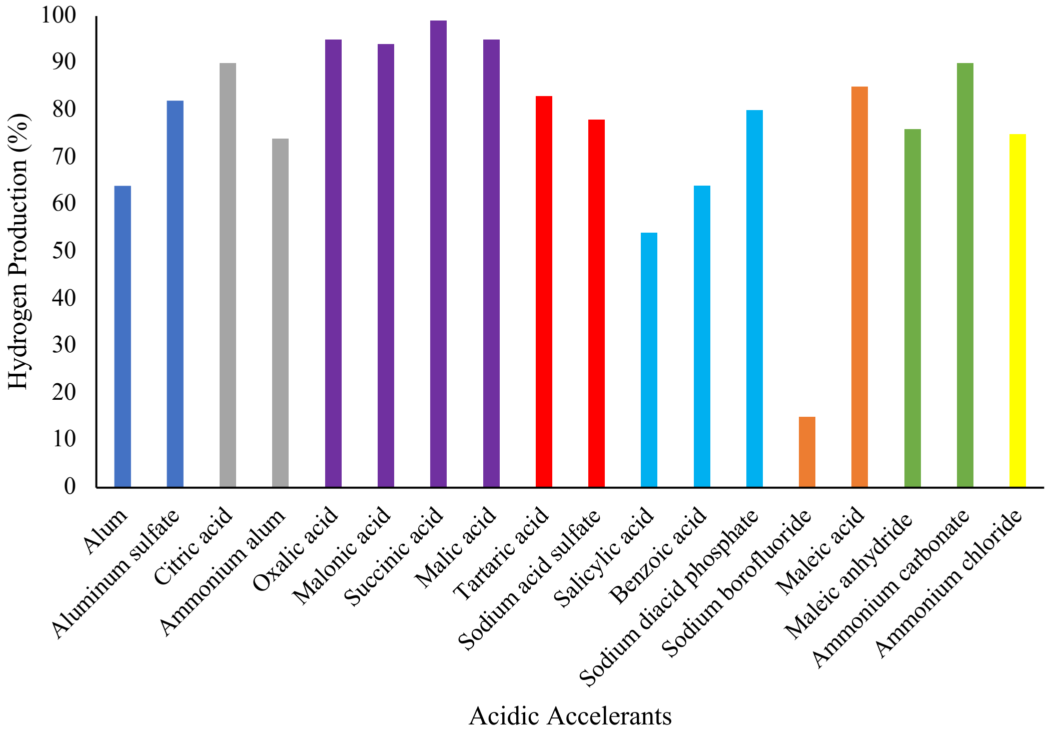

Figure 1.10. Acidic accelerants (0.2-0.3 mol of compound/2.6 mol $NaBH_4$) to promote hydrogen evolution from the hydrolysis of $NaBH_4$ in 10 min (blue bars). Acidic accelerants using 0.4 mol of accelerant to 2.6 mol $NaBH_4$ in 10 min (grey bars). Acidic accelerants using 0.6 mol of accelerant to 2.6 mol $NaBH_4$ in 10 min (purple bars). Acidic accelerants using 0.7 mol of accelerant to 2.6 mol $NaBH_4$ in 10 min (red bars).

Acidic accelerants using 0.8 mol of accelerant to 2.6 mol $NaBH_4$ in 10 min (light blue bars). Acidic accelerants using 0.9 mol of accelerant to 2.6 mol $NaBH_4$ in 10 min (orange bars). Acidic accelerants using 1.0 mol of compound to 2.6 mol $NaBH_4$ in 10 min (green bars). Acidic accelerants using 1.8 mol of compound/2.6 mol $NaBH_4$ in 10 min (yellow bars).

Although $NaBH_4$ can reasonably produce hydrogen from reaction with water or alcohol solvents it has not been considered for commercial use because research has yet to close the "hydrogen cycle." Even though the borate byproduct is environmentally benign, it would be more sustainable if the borate byproduct could be recycled into the synthesis of $NaBH_4$.

Recently, a method was reported for converting hydrated borax into $NaBH_4$.[14] Through the *in situ* formation of MgH_2 as the reductant, Zhu and colleagues were able to obtain $NaBH_4$ in 80% yield (**equation 7**). Through powder X-ray spectroscopy and ^{11}B NMR spectroscopy they were able to determine the reaction steps. They project that the first step of this reaction occurs between $Na_2B_4O_7{\bullet}5H_2O$, NaH, and Mg to generate $Na_2B_4O_5(OH)_4$. As this reaction is underway a simultaneous reaction takes place between Mg and H_2 to produce MgH_2. Once the MgH_2 is formed it can react with $Na_2B_4O_5(OH)_4$ and NaOH to produce $NaBH_4$, MgO and H_2. Although this method does repurpose the borate byproduct, this process necessitates 3.5 h of ball milling, which is not energetically favorable.

$$Na_2B_4O_7 \cdot 5H_2O + 2NaH + 12Mg + 2H_2 \rightarrow 4NaBH_4 + 12MgO \qquad (7)$$

Another group has done work to close the "hydrogen cycle" by developing an atom economical triangle of recycling (**Figure 1.11**).[55] In this system, $NaBH_4$ undergoes methanolysis to liberate hydrogen and $NaB(OCH_3)_4$. Addition of water then hydrolyzes $NaB(OCH_3)_4$ into $NaB(OH)_4$. At this point, to convert $NaB(OH)_4$ into $NaBH_4$ it has to go through the borate, $NaBO_2$. Through dehydration (calcination at 500 °C) $NaB(OH)_4$ can be converted into $NaBO_2$. Lastly, $NaBO_2$ is reduced to $NaBH_4$. Reduction by hydrogen keeps the process atom economical, but other reducing agents such as MgH_2 were found effective as well.

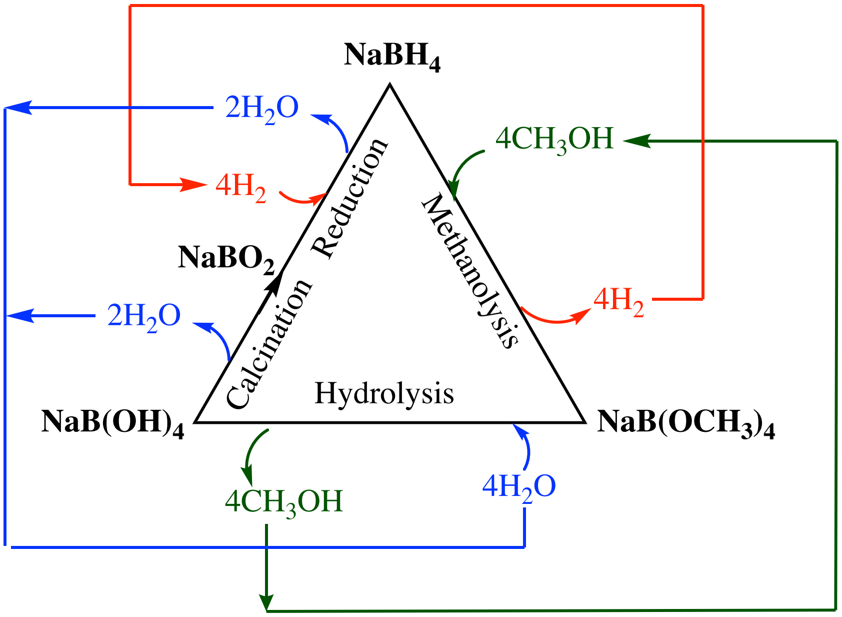

NaBH4
2H2O
4H2
4CH3OH
Reduction
Methanolysis
NaBO2
4H2
2H2O
Calcination
Hydrolysis
NaB(OH)4
NaB(OCH3)4
4CH3OH
4H2O

Figure 1.11. The methanolysis products of $NaBH_4$ were recycled back into the starting borohydride.[55]

As the previous two examples demonstrate, research have been conducted aiming to find sustainable and economical methods of synthesizing $NaBH_4$ and to recycling the byproducts into useful materials. Although imperfect at this point, these pathways are promising beginnings into developing more sustainable hydrogen fuel system from $NaBH_4$.

1.4.2. Water Splitting to Produce H_2

Additionally, energy researchers have worked to explore obtaining hydrogen from water. Water splitting is a sustainable option for hydrogen generation because water is readily available and, on its most basic level, it splits into hydrogen and oxygen (**equation 8**).

$$2H_2O \rightarrow O_2 + 2H_2 \qquad (8)$$

However, this reaction requires a large energy input of 286 kJ/mol (at ambient conditions).[56] Thus, finding an efficient method is a primary goal where maximum level of hydrogen is produced with minimum amount of energy input. In general, there are six types of methodologies that are currently in use for splitting water: 1) reforming of fossil fuels, 2) electrolysis, 3) photocatalysis, 4) nuclear hydrogen production, 5) biomass strategies, and 6) metal-water reactions. Each of the above water splitting technique suffers from unique challenges and the following sections will explore some of these methods.

1.4.2.1. Reforming of Fossil Fuels to Produce H_2

The vast majority (95%) of the hydrogen produced in the United States is from natural gas reforming.[57] In this method high-temperature steam (700-1,000 °C) is pressurized with a carbon source to generate hydrogen (**equation 9**). Methane is frequently used as the carbon source, but ethanol and propane can also be used as feedstocks.

$$CH_4 + H_2O \overset{\Delta}{\rightarrow} CO + 3H_2 \qquad (9)$$

Since excess steam is typically used in these plants, a second reaction occurs, known as a water-gas shift reaction (**equation 10**). In this reaction, the carbon monoxide that was produced in the initial water splitting reaction reacts with the steam again to form hydrogen and carbon dioxide.

$$CO + H_2O \rightarrow CO_2 + H_2 + \Delta \qquad (10)$$

A main criticism for this method is that it still uses fossil fuel sources as the primary feedstock. One group decided to test "trap grease" as possible carbon sources for the production of hydrogen.[58] Trap grease refers to the sewage lines present in restaurants and food processing plants. This oil does not have much of a commercial value and so finding a way to repurpose it seemed desirable. It was then subjected to the steam reforming conditions with a Ni-based catalyst at >800 °C for 120 h. Under those conditions 100 g of grease was able to produce 74% of the theoretical amount of hydrogen. A significant hurdle for this process was the aggregation of the Ni-based catalyst causing the gradual decline in hydrogen production over time.

Even if food waste could substitute the fossil fuels, generation of hydrogen by steam reforming requires extended reaction times, high temperatures and pressures, and they end up producing carbon monoxide and carbon dioxide as the byproduct. Thus, this method is not considered a true "clean fuel."

1.4.2.2. Water Splitting by Electrolysis

Electrolysis applies an electric current that causes water to split and produce hydrogen. Two reactions have to take place for this to occur, the oxygen evolution reaction (OER,) and the hydrogen evolution reaction (HER), one at the anode and the other at the cathode end (**equations 11** and **12**). **Figure 1.12** provides a basic schematic of the movement of electrons as they move from the OER anode side to the HER cathode end.

$$Acidic\ OER: 2H_2O \rightarrow O_2 + 4e^- + 4H^+ \qquad (11)$$

$$Acidic\ HER: 4e^- + 4H^+ \rightarrow 2H_2 \qquad (12)$$

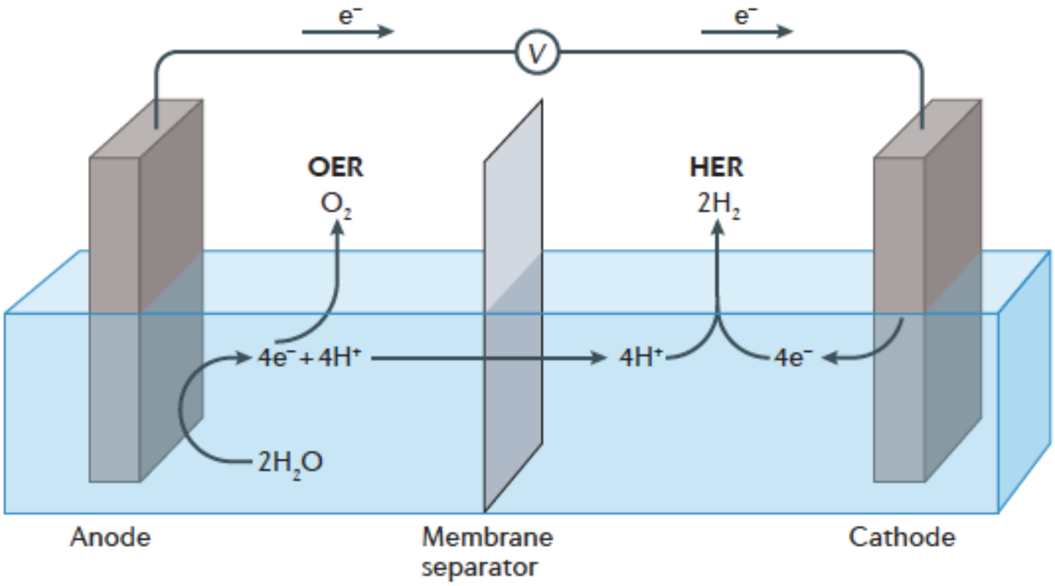

Figure 1.12. Schematic of the HER and OER reactions in a simplified example of electrolysis.[56]

For the HER and OER reactions to happen an input of at least 1.23 V is required. If the added energy is increased the rate of production increases, but the output has to be greater than the input, or else it is not a viable process. The use of metal catalysts aid in reducing the amount of extra energy needed and keep the system to the minimum amount of energy input. Precious metals, such as iridium, ruthenium, and rhodium,[59] are frequently chosen as the catalyst; but work has been conducted to show that first row transition metals can also split water.[60]

Since seawater makes up >95% of the water on Earth, the development of a water splitting protocol using seawater would be an innovative feat and a potential answer to the energy crisis. However, ocean water has salt ions that in the presence of an electric current can undergo a chlorine evolution reaction. Consequently, that reaction produces toxic chlorine gas that is not ideal, and the ions tend to degrade the anodes, which is unhelpful for continuous long-lasting energy production.

To circumvent this problem, different designs have been made to reduce or eliminate the chlorine evolution reaction. Some reports suggest that the metal catalysts react with the Cl_2 to produce the corresponding metal chlorides.[60, 61] Furthermore, a systematic study of pH found that a Ni catalyst performed well in splitting water and saw minimal chlorine production at high pH (pH 13).[62] These high alkaline environments may be conducive for chlorine suppression but they are highly corrosive and introduce other safety concerns. Thus, there remains challenges that impede commercial production of water splitting by electrolysis and electrocatalysis (and even photocatalysis).

1.4.2.3. Metal-Water Reactions

As previously mentioned, transition metal catalysts have been used to aid in hydrogen production for borohydride hydrolysis and in electrolysis reactions. These metals on their own will not readily react to split water. But there are some metals that are notorious for reacting extremely rapidly with water and produce hydrogen. Sodium and potassium are classic examples of violently reacting with water causing an explosion. Research has shown that when the water droplets land on the metal surface the morphology changes.[63] Pristine metal surfaces are then available for reaction with the next water molecule. Thus, a cyclic pattern emerges and as the exothermic reaction continues until an explosion occurs. In this instance, the production of hydrogen is extremely difficult to control, but by moving across the periodic table another element is able to split water in a more controlled manner.

In theory, one gram of aluminum can produce 1.24 L of hydrogen. An added benefit is that aluminum is highly abundant (8 wt%) making it much more cost-effective than some of the noble metals found in electrocatalysis. The limitation of aluminum is that it oxidizes readily. The constant coat of aluminum oxide that resides on the surface impedes any water splitting from happening. The oxide layer can be removed by ball milling, which grinds the metal into a fine powder. However, it then needs to be stored under an inert atmosphere to prevent oxidation.[64-66] The layer has also been shown to be removed under highly alkaline environments. Interestingly, once the layer is removed it has been shown that a high pH augments the water splitting reaction as displayed in the following chemical reactions:[67]

$$2Al + 6H_2O + 2NaOH \rightarrow 2NaAl(OH)_4 + 3H_2 \qquad (13)$$

$$NaAl(OH)_4 \rightarrow NaOH + Al(OH)_3 \qquad (14)$$

$$2Al + 6H_2O \rightarrow 2Al(OH)_3 + 3H_2 \qquad (15)$$

Another method of removing the aluminum oxide layer is dissolving it in a room temperature liquid metal like gallium to form an alloy.[68, 69] Gallium diffuses into the metal lattice, removes the oxide layer, and helps to create aluminum particles. Once the pristine aluminum surface is available, water molecules can be split, and hydrogen can be produced. Multi-metal alloys have been studied to enhance the hydrogen production. A more detailed discussion of these types of alloys will be conducted in chapter five. Overall, the advantage of the Ga-Al alloy is that hydrogen generation happens rapidly and at room temperature, unlike some of the previously mentioned water splitting methods.

1.5. Conclusions

Since their discovery, hydrides have shown their extreme value as reducing agents of organic functional groups, as participants in metal catalyzed reactions, and use in generating hydrogen. They have far reaching abilities in academic research, industrial applications, and pharmaceutical uses, making them highly versatile.

The versatility of metal hydrides, borohydrides, and boranes is an incredibly important characteristic as they can be easily tuned to achieve a high levels of functional group selectivity. Moreover, binary hydrides, the mixing of two hydrides, enables the creation of new reducing agents that have been shown to have unique characteristics, including functional group selectivity, varying solvent compatibility, and stability. Or by combining two hydrides they can work cooperatively to achieve partial or tandem reduction reactions.

Furthermore, hydrides have been shown to react with metal salts to create distinct black particulates. These heterogenous catalysts are highly catalytic and can reduce more challenging functionalities, such as nitro groups and nitriles to primary amines. Even in these catalysis systems some selectivity can be obtained, seemingly due to the hydrogen source, be it pressurized H_2, $NaBH_4$, or hydrazine. Expansion of this work has led to other uses of the catalysts in organic synthesis.

Lastly, hydrides have become part of the race to find renewable energy sources. Hydrogen's potential as a "clean fuel" has made identifying potential hydrogen sources automatic. The hydrolysis of $NaBH_4$ produces hydrogen in a facile manner and the addition of metal catalysts has increased its viability. However, it is in the area of water splitting where hydrogen generation has flourished and continues to offer potential as an alternative fuel. Liquid metals in particular are interesting compounds to better understand and determine their hydrogen production abilities.

1.6. Thesis Outline

In chapter two, the synthesis of diisobutylaluminum borohydride, a binary hydride, and its reduction profile towards various organic functional groups is described (**Scheme 1.5**). The hydride readily reduced aldehydes and ketones to the corresponding alcohols (up to 97% yield). Nitriles were reduced to the primary amines (up to 94% yield). Aliphatic epoxides afforded the more substituted alcohol (up to 70% yield). Esters produced the corresponding alcohols (up to 68% yield). Tertiary amides produced amines (up to 99% yield) and lactams were shown to retain their cyclic structure (up to 71% yield). Synthesis of this binary hydride can be obtained by reacting diisobutylaluminum hydride and borane dimethyl sulfide in a 1:1 ratio or by combining sodium borohydride and diisobutylaluminum chloride. A series of competitive reactions demonstrate that diisobutylaluminum borohydride shows some functional group selectivity.

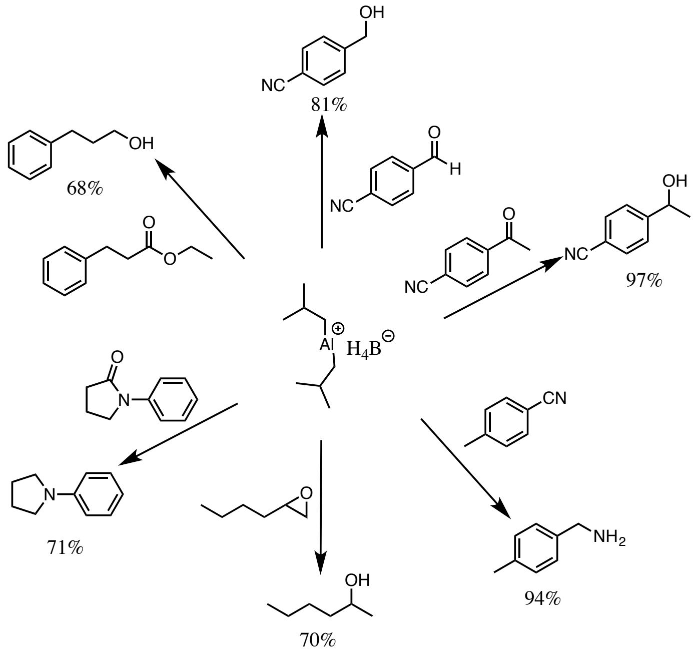

Scheme 1.5. Reduction of functional groups by diisobutylaluminum borohydride.

Chapter three deals with the reduction of nitroarenes using a nickel boron composite (NBC) catalyst. Synthesis of the catalyst came from reducing nickel chloride to Ni^0 with $NaBH_4$. Once formed the catalyst was placed onto a mesoporous aluminosilicate support to aid in catalyst distribution and increasing catalytic surface area. Interestingly, of the borohydride-synthesized catalysts mentioned earlier, they were frequently termed *borides*, implying a boron metal bond. An exploration of the catalyst structure and characterization found it was more likely a metal with borate species present. Even so, the catalyst was highly reactive, and the nitro reduction reaction occurred with hydrazine hydrate at ambient pressure and temperature. Conversion to the aniline derivatives occurred in high yields and the catalyst was able to be recycled and reused for multiple cycles.

In chapter four, reduction reactions in aqueous media are reported and are monitored *ex situ* using a portable Raman spectrometer. The non-invasive analytical tool provided precise monitoring of the reduction of nitroarenes with the NBC catalyst, such that the reaction kinetics could be calculated as pseudo first order kinetics. Further analysis of this *ex situ* technique led to the analysis of the reduction of cyclohexanone and 2-cyclohexen-1-one by dimethylamine borane in water. Through ^{11}B NMR analysis and density functional theory calculations it was determined that the carbonyl reduces once the amine dissociates.

In chapter five, a unique methodology of hydrogen generation by splitting neutral water, at ambient temperature with a gallium aluminum alloy, is elaborated. The alloy was synthesized in a 3:1 (Ga:Al) atomic ratio, which allowed for effective solvation of the aluminum and removal of the inhibiting oxide layer. Electron microscopy showed that the aluminum resides in a sea of gallium. The Al particles react with water to produce hydrogen. The generation of hydrogen could be formed from deionized water, ocean water, rainwater, and commercial beverages. The aluminum sources could also vary by using pristine commercial aluminum foil or waste aluminum foil. The used alloy was then separated into the aluminum oxide byproduct and gallium. The gallium was extracted, recycled, and reused for successive water splitting reactions. A hydrogenation reaction was conducted to demonstrate the utility of this hydrogen source in a chemical reaction. The hydrogen produced in this manner has also been shown to power a toy hydrogen fuel cell car.

1.7. References

1. Hill, A. J.; Nason, E. H., The Utilization of Cassia Oil for the Synthesis of Cinnamyl Alcohol. *J. Am. Chem. Soc* **1924,** *46*, 2236-2246.

2. Meerwein, H.; Schmidt, R., Ein neues Verfahren zur Reduktion von Aldehyden und Ketonen. *Liebigs Ann.* **1925,** *444*, 221-238.

3. Ponndorf, W. Z., The reversible exchange of oxygen between aldehydes or ketones on the one hand and primary or secondary alcohols on the other hand. *Angew. Chem.* **1926,** *39*, 138-143.

4. Verley, A., The exchange of functional groups between two molecules: The passage of ketones to alcohols and the reverse. *Bull. Soc. Chim. Fr.* **1925,** *37*, 871-874.

5. Lund, H., *Ber. Dtsh. Chem. Ges* **1937,** *70*, 1520.

6. Kreuder, A. D.; House-Knight, T.; Whitford, J.; Ponnusamy, E.; Miller, P.; Jesse, N.; Rodenborn, R.; Sayag, S.; Gebel, M.; Aped, I.; Sharfstein, I.; Manaster, E.; Ergaz, I.; Harris, A.; Grice, L. N., A Method for Assessing Greener Alternatives between Chemical Products Following the 12 Principles of Green Chemistry. *ACS Sustainable Chem. Eng.* **2017,** *5*, 2927-2935.

7. Sanderson, K., It's Not Easy Being Green. *Nature* **2011,** *469*, 18-20.

8. Leng, Y.; Shi, L.; Du, S.; Jiang, J.; Jiang, P., A tannin-derived zirconium-containing porous hybrid for efficient Meerwein-Ponndorf-Verley reduction under mild conditions. *Green Chem.* **2020,** *22*, 180-186.

9. Boit, T. B.; Mehta, M. M.; Garg, N. K., Base-Mediated Meerwein-Ponndorf-Verley Reduction of Aromatic and Heterocyclic Ketones. *Org. Lett.* **2019,** *21*, 6447-6451.

10. An, J.; Work, D. N.; Kenyon, C.; Procter, D. J., Evaluating a Sodium Dispersion Reagent for the Bouveault-Blanc Reduction of Esters. *J. Org. Chem.* **2014,** *79*, 6743-6747.

11. Han, M.; Ma, X.; Yao, S.; Ding, Y.; Yan, Z.; Adijiang, A.; Wu, Y.; Li, H.; Zhang, Y.; Lei, P.; Ling, Y.; An, J., Developement of a Modified Bouveault-Blanc Reduction for the Selective Synthesis of α,α-Dideuterio Alcohols. *J. Org. Chem.* **2017,** *82*, 1285-1290.

12. Brown, H. C.; Krishnamurthy, S., Forty Years of Hydride Reductions. *Tetrahedron* **1979,** *35*, 567-607.

13. Schlesinger, H. I.; Brown, H. C.; Finholt, A. E., The Preparation of Sodium Borohydride by the High Temperature Reaction of Sodium Hydride with Borate Esters. *J. Am. Chem. Soc* **1965,** *75*, 205-209.

14. Zhu, Y.; Ouyang, L.; Zhong, H.; Liu, J.; Wang, H.; Shao, H.; Huang, Z.; Zhu, M., Efficient Synthesis of Sodium Borohydride: Balancing Reducing Agents with Intrinsic Hydrogen Source in Hydrated Borax. *ACS Sustainable Chem. Eng.* **2020,** *8*, 13449-13458.

15. Brown, H. C.; Rao, B. C. S., A New Powerful Reducing Agent-Sodium Borohydride in the Presence of Aluminum Chloride and Other Polyvalent Metal Halides. *J. Am. Chem. Soc* **1956,** *78*, 2582-2588.

16. Brown, H. C.; Choi, Y. M.; Narasimhan, S., Convenient procedure for the conversion of sodium borohydride into lithium borohydride in simple ether solvents. *Inorg. Chem.* **1981,** *20*, 4454-4456.

17. Nystrom, R. F.; Chaikin, S. W.; Brown, W. G., Lithium Borohydride as a Reducing Agent. *J. Am. Chem. Soc.* **1949,** *71*, 3245-3246.

18. Brown, H. C.; Narasimhan, S., New powerful catalysts for the reduction of esters by lithium borohydride. *J. Org. Chem.* **1982,** *47*, 1604-1606.

19. Schlesinger, H. I.; Brown, H. C., Metallo Borohydrides. III. Lithium Borohydride. *J. Am. Chem. Soc.* **1940,** *62*, 3429-3435.

20. Baba, A.; Shibata, I., Dihaloindium Hydride as a Novel Reducing Agent. *Chem. Rec.* **2005,** *5*, 323-335.

21. Inoue, K.; Sawada, A.; Shibata, I.; Baba, A., Indium(III) Chloride — Sodium Borohydride System: A Convenient Radical Reagent for an Alternative to Tributyltin Hydride System. *J. Am. Chem. Soc.* **2002,** *124*, 906-907.

22. Saavedra, J. Z.; Resendez, A.; Rovira, A.; Eagon, S.; Haddenham, D.; Singaram, B., Reaction of $InCl_3$ with Various Reducing Agents: $InCl_3$-$NaBH_4$-Mediated Reduction of Aromatic and Aliphatic Nitriles to Primary Amines. *J. Org. Chem.* **2012,** *77*, 221-228.

23. Snelling, R.; Saavedra, J. Z.; Bayrasy, P.; Abdollahian, Y.; Singaram, B., Binary reducing agents containing dichloroindium hydride for the selective, partical, or tandem reductions of bifunctional compounds consisting of halo-nitriles, halo-esters and halo-carboxylic acids. *Org. Chem. Front.* **2015,** *2*, 133-140.

24. Brown, H. C.; Choi, Y. M.; Narasimhan, S., Selective Reductions. 29. A Simple Technique to Achieve an Enhanced Rate of Reduction of Representative Organic Compounds by Borane-Dimethyl Sulfide *J. Org. Chem.* **1982,** *47*, 3153-3163.

25. Pasumansky, L.; Goralski, C. T.; Singaram, B., Lithium Aminoborohydrides: Powerful, Selective, Air-Stable Reducing Agents. *Org. Process Res. Dev.* **2006,** *10*, 959-970.

26. Nystrom, R. F.; Brown, W. G., Reduction of Organic Compounds by Lithium Aluminum Hydride. III. Halides, Quinones, Miscellaneous Nitrogen Compounds. *J. Am. Chem. Soc* **1948,** *70*, 3738-3740.

27. Orlandi, M.; Brenna, D.; Harms, R.; Jost, S.; Benaglia, M., Recent Developments in the Reduction of Aromatic and Aliphatic Nitro Compounds to Amines. *Org. Process Res. Dev.* **2018,** *22*, 430-445.

28. Yin, B.-L.; Cai, C.-B.; Lai, J.-Q.; Zhang, Z.-R.; Huang, L.; Xu, L.-W.; Jiang, H.-F., Sodium Borohydride-Nickel Chloride-Methanol Catalytic System for Regioselctive Reduction of Electron-Rich Conjugated Dienes and Reductive Cleavage of Allyl Esters Involving π-Allylnickel Intermediate. *Adv. Synth. Catal.* **2011,** *353*, 3319-3324.

29. Shrestha, R.; Dorn, S. C. M.; Weix, D. J., Nickel-Catalyzed Reductive Conjugate Addition to Enones via Allylnickel Intermediates. *J. Am. Chem. Soc* **2013,** *135*, 751-762.

30. Birkenstock, U.; Bönnemann, H.; Bogdanović, B.; Walter, D.; Wilke, G., *π*-Allylnickel Compounds as Homogeneous Cataly. In *Homogeneous Catalysis*, 1974; pp 250-265.

31. Belisle, C. M.; Young, Y. M.; Singaram, B., Catalytic Reaction. 1. Catalytic 1,4-Hydrogenation of α,β-Unsaturated Aldehydes and Ketones Using SC-1 Nickel Boride. *Tetrahedron Lett.* **1994,** *35*, 5595-5598.

32. Chakraborty, U.; Reyes-Rodriguez, E.; Demeshko, S.; Meyer, F.; Wangelin, A. J. v., A Manganese Nanoseet: New Cluster Topology and Catalysis. *Angew. Chem. Int. Ed.* **2018,** *57*, 4970-4975.

33. Osby, J. O.; Heinzman, S. W.; Ganem, B., Studies on the Mechanism of Transition-Metal-Assisted Sodium Borohydride and Lithium Aluminum Hydride Reductions. *J. Am. Chem. Soc.* **1986,** *108*, 67-72.

34. Heinzman, S. W.; Ganem, B., The Mechanism of Sodium Borohydride-Cobaltous Chloride Reductions. *J. Am. Chem. Soc* **1982,** *104*, 6801-6802.

35. Caddick, S.; Judd, D. B.; Lewis, A. K.; Reich, M. T.; Williams, M. R., A Generic Approach for the Catalytic Reduction of Nitriles. *Tetrahedron* **2003,** *59*, 5417-5423.

36. Zerecero-Silva, P.; Jimenez-Solar, I.; Crestani, M. G.; Arévalo, A.; Barrios-Francisco, R.; García, J. J., Catalytic Hydrogenation of Aromatic Nitriles and Dinitriles with Nickel Compounds. *Appl. Catal., A* **2009,** *363*, 230-234.

37. Dai, H.; Guan, H., Switching the Selectivity of Cobalt-Catalyzed Hydrogenation of Nitriles. *ACS Catal.* **2018,** *8*, 9125-9130.

38. Vernekar, A. A.; Patil, S.; Bhat, C.; Tilve, S. G., Magnetically Recoverable Catalytic Co–Co2B Nanocomposites for the Chemoselective Reduction of Aromatic Nitro Compounds. *RSC Adv.* **2013,** *3*, 13243.

39. Piña, S.; Cedillo, D. M.; Tamez, C.; Izquierdo, N.; Parsons, J. G.; Gutierrez, J. J., Reduction of nitrobenzene derivatives using sodium borohydride and transistion metal sulfides *Tet. Lett.* **2014,** *55*, 5468-5470.

40. Rai, R. K.; Mahata, A.; Mukhopadhyay, S.; Gupta, S.; Li, P.-Z.; Nguyen, K. T.; Zhao, Y.; Pathak, B.; Singh, S. K., Room-Temperature Chemoselective Reduction of Nitro Groups Using Non-Noble Metal Nanocatalysts in Water. *Inorg. Chem.* **2014,** *53*, 2904-2909.

41. Nose, A.; Kudo, T., Reduction with Sodium Borohydride-Transition Metal Salt Systems. I. Reduction of Aromatic Nitro Compounds with the Sodium Borohydride-Nickelous Chloride System. *Chem. Pharm. Bull. (Tokyo)* **1981,** *29*, 1159-1161.

42. Zhang, J.; Lu, G.; Cai, C., Chemoselective Transfer Hydrogenation of Nitroarenes by Highly Dispersed Ni-Co BMNPs. *Catal. Commun.* **2016,** *84*, 25-29.

43. Fountoulaki, S.; Daikopoulou, V.; Gkizis, P. L.; Tamiolakis, I.; Armatas, G. S.; Lykakis, I. N., Mechanistic Studies of the Reduction of Nitroarenes by $NaBH_4$ or Hydrosilanes Catalyzed by Supported Gold Nanoparticles. *ACS Catal.* **2014,** *4*, 3504-3511.

44. Schaefer, Z. L.; Ke, X.; Schiffer, P.; Schaak, R. E., Direct Solution Synthesis, Reaction Pathway Studies, and Structural Characterization of Crystalline Ni_3B Nanoparticles. *J. Phys. Chem. C* **2008,** *112*, 19846-19851.

45. Schlesinger, H. I.; Brown, H. C.; Finholt, A. E.; Gilbreath, J. R.; Hoekstra, H. R.; Hyde, E. K., Sodium Borohydride, Its Hydrolysis and Its Use as a Reducing Agent and in the Generation of Hydrogen. *J. Am. Chem. Soc.* **1953,** *75*, 215-219.

46. Cantillo, D.; Moghaddam, M. M.; Kappe, C. O., Hydrazine-Mediated Reduction of Nitro and Azide Functionalities Catalyzed by Highly Active and Reusable Magnetic Iron Oxide Nanocrystals. *J. Org. Chem.* **2013,** *78*, 4530-4542.

47. Larsen, J. W.; Freund, M.; Kim, K. Y.; Sidovar, M.; Stuart, J. L., Mechanism of the Carbon Catalyzed Reduction of Nitrobenzene by Hydrazine. *Carbon* **2000,** *38*, 655-661.

48. Kumarraja, M., Simple and Efficient Reduction of Nitroarenes by Hydrazine in Faujasite Zeolites. *Appl. Catal. Gen.* **2004,** *265*, 135-139.

49. Zhao, Z.; Yang, H.; Li, Y.; Guo, X., Cobalt-Modified Molybdenum Carbide as an Efficient Catalyst for Chemoselective Reduction of Aromatic Nitro Compounds. *Green Chem.* **2014,** *16*, 1274-1281.

50. Tamelen, E. E. V.; Dewey, R. S.; Lease, M. F.; Pirkle, W. H., Selectivity and Mechanism of Diimide Reductions. *J. Am. Chem. Soc* **1961,** *83*, 4302.

51. Prathap, K. J.; Wu, Q.; Olsson, R. T.; Dinér, P., Catalytic Reductions and Tandem Reactions of Nitro Compounds Using in Situ Prepared Nickel Boride Catalyst in Nanocellulose Solution. *Org. Lett.* **2017,** *19*, 4746-4749.

52. Eppinger, J.; Huang, K.-W., Formic Acid as a Hydrogen Energy Carrier. *ACS Energy Lett.* **2017,** *2*, 188-195.

53. Marrero-Alfonso, E. Y.; Beaird, A. M.; Davis, T. A.; Matthews, M. A., Hydrogen Generation from Chemical Hydrides. *Ind. Eng. Chem. Rres.* **2009,** *48*, 3703-3712.

54. Orimo, S.-i.; Nakamori, Y.; Eliseo, J. R.; Züttel, A.; Jensen, C. M., Complex Hydrides for Hydrogen Storage. *Chem. Rev.* **2007,** *107*, 4111-4132.

55. Aydin, K.; Kulakli, B. N.; Filiz, B. C.; Alligier, D.; Demirci, U. B.; Figen, A. K., Closing the hydrogen cycle with the couple sodium borohydride-methanol, via the formation of sodium tetramethoxyborate and sodium metaborate. *Int. J. Energy. Res.* **2020,** *44*, 11405-11416.

56. Roger, I.; Shipman, M. A.; Symes, M. D., Earth-abundant catalysts for electrochemical and photochemical water splitting. *Nature* **2017,** *1*, 1-13.

57. Hydrogen Production: Natural Gas Reforming https://www.energy.gov/eere/fuelcells/hydrogen-production-natural-gas-reforming (accessed November 16, 2020).

58. Czernik, S.; French, R. J.; Magrini-Bair, K. A.; Chornet, E., The Production of Hydrogen by Steam Reforming of Trap Grease — Progress in Catalyst Performance *Energy & Fuels* **2004,** *18*, 1738-1743.

59. Liu, Y.; Hu, X.; Huang, B.; Xie, Z., Surface Engineering of Rh Catalysts with N/S-Codoped Carbon Nanosheets toward High-Performance Hydrogen Evolution from Seawater. *ACS Sustainable Chem. Eng.* **2019,** *7*, 18835-18843.

60. Yu, L.; Zhu, Q.; Song, S.; McElhenny, B.; Wang, D.; Wu, C.; Qin, Z.; Bao, J.; Yu, Y.; Chen, S.; Ren, Z., Non-noble metal-nitride based electrocatalysts for high-performance alkaline seawater electrolysis. *Nat. Commun.* **2019,** *10*, 1-10.

61. Zheng, J.; Zhao, Y.; Xi, H.; Li, C., Seawater splitting for hydrogen evolution by robust electrocatalysts from secondary M (M = Cr, Fe, Co, Ni, Mo) incorporated Pt. *RSC Adv.* **2018,** *8*, 9423-9429.

62. Dionigi, F.; Reier, T.; Pawolek, Z.; Gliech, M.; Strasser, P., Design Criteria, Operating Conditions, and Nickel-Iron Hydroxide Catalyst Materials for Selective Seawater Electrolysis. *ChemSusChem* **2016,** *9*, 962-972.

63. Mason, P. E.; Uhlig, F.; Vaněk, V.; Buttersack, T.; Bauerecker, S.; Jungwirth, P., Coulomb explosion during the early stages of the reaction of alkali metals with water. *Nature Chemistry* **2015,** *7*, 250-254.

64. Fan, M.-Q.; Xu, F.; Sun, L.-X., Studies on hydrogen generation characteristics of hydrolysis of te ball milling Al-based materials in pure water. *Int. J. Hydrogen Energy* **2007,** *32*, 2809-2815.

65. Ying, C.; Bei, L.; Huihu, W.; Shijie, D., Effect of preparation parameters and alloy elements on HER performance at 0 °C in water. *Rare Metal Materials and Engineering* **2017,** *46*, 2428-2432.

66. Ilyukhina, A. V.; Kravchenko, O. V.; Bulychev, B. M.; Shkolnikov, E. I., Mechanochemical activation of aluminum with gallams for hydrogen evolution from water. *Int. J. Hydrogen Energy* **2010,** *35*, 1905-1910.

67. Xu, S.; Zhao, X.; Liu, J., Liquid metal activated aluminum-water reaction for direct hydrogen generation at room temperature. *Renewable and Sustainable Energy Reviews* **2018,** *92*, 17-37.

68. Choi, G.; Ziebarth, J. T.; Woodall, J. M.; Sherman, D.; Allen, C. R.; Kramer, R., Mechanism of Hydrogen Generation via Water Reaction with Aluminum Alloys. In *18th Biennial University/Government/Industry Micro/Nano Symposium*, IEEE: West Lafayette, IN, USA, 2010; pp 1-3.

69. Ziebarth, J. T.; Woodall, J. M.; Kramer, R. A.; Choi, G., Liquid phase-enabled reactions of Al-Ga and Al-Ga-In-Sn alloys wtih water. *Int. J. Hydrogen Energy* **2011,** *36*, 5271-5279.

CHAPTER 2

Reaction of Diisobutylaluminum Borohydride, A Binary Hydride, with Selected Organic Compounds Containing Representative Functional Groups

2.1. Introduction

The reduction of functional groups is an integral synthetic operation. As such, a variety of reducing reagents exist, such as hydrides,[1-8] bimetallic hydrogenation catalyses,[9-13] boranes,[14-16] and silanes.[17, 18] Metal hydrides, such as lithium aluminum hydride ($LiAlH_4$), sodium borohydride ($NaBH_4$), and diisobutylaluminum hydride (DIBAL) are conventional reagents used to reduce a variety of functional groups.[19] Sodium borohydride efficiently reduces aldehydes and ketones,[20-22] anhydrides, esters and lactones,[23] as well as, acid chlorides[19] to the corresponding alcohols. However, the poor solubility of $NaBH_4$ in ether and hydrocarbon solvents restricts its reduction capabilities. In addition to the functional groups capable of being reduced by $NaBH_4$, DIBAL reduction profile include epoxides, carboxylic acids, nitriles, and tertiary amides.[2] Unlike $NaBH_4$, DIBAL is soluble in both ethereal and hydrocarbon solvents, making it a more versatile reagent.[24]

Seminal work on hydroboration reactions and reductions with borane tetrahydrofuran (BH_3:THF) and other alkylboranes established them as significant reagents in organic chemistry.[25, 26] Unfortunately, commercial BH_3:THF is temperature sensitive and easily degrades into dialkoxyborane and trialkoxyborane, and therefore cannot be shipped due to quality control concerns.[27-30] Later, borane dimethyl sulfide (BMS, $BH_3:S(CH_3)_2$) was developed as a more stable alternative to BH_3:THF, which is capable of carrying out almost the same organic functional group reductions.[15, 19] A limitation, however, with BMS is that the dimethyl sulfide needs to be distilled off as the reduction reaction is going.

Versatile boranes and borohydrides can be developed by fine tuning the stereo-electronic nature of the ligands on the B-atom.[19] Binary hydride reagents are implicated in the hydrogenation of functional groups using bimetallic catalysts.[31, 32] Alternatively, binary hydride reagents can be generated from $NaBH_4$ and metal halides. Thus, a binary hydride system containing dichloroindium hydride ($HInCl_2$) and BH_3:THF was generated from indium trichloride ($InCl_3$) and $NaBH_4$ in THF.[33, 34] This result prompted the investigation of the synthesis of other binary hydride systems, by mixing BH_3:THF and BMS with metal hydrides, such as $HInCl_2$ and DIBAL. Unfortunately, both BH_3:THF and BMS did not generate a binary hydride system with $HInCl_2$ as evidenced by ^{11}B NMR spectral analysis. However, the reaction of BMS with DIBAL showed the formation of a single binary hydride. This hydride displayed a quintet at δ -36 ppm (J = 83 Hz) in the ^{11}B NMR spectrum and has been attributed as a new binary hydride, diisobutylaluminum borohydride [$(i\text{Bu})_2AlBH_4$]. Since this new binary hydride is stable at room temperature, examination of its reducing characteristics toward representative organic functional groups at 25 °C was conducted. Herein, we report the scope and limitations of $(i\text{Bu})_2AlBH_4$ as an effective reducing agent.

2.2. Results and Discussion

2.2.1. Synthesis of Diisobutylaluminum Borohydride

Even through both borane dimethyl sulfide (BMS) and diisobutylaluminum hydride (DIBAL) are Lewis acids, they are not equivalent in their Lewis acid strength. DIBAL behaves like a metal hydride and transfers its hydride completely to BMS upon mixing the two reactants in a 1:1 ratio (**Scheme 2.1**). As shown below, ^{11}B NMR analysis was used to monitor the disappearance of the BMS quartet (δ -20 ppm, J = 103 Hz) and the appearance of a quintet at δ -36 ppm (J = 83 Hz), indicative of a borohydride species, known as diisobutylaluminum borohydride [(*i*Bu)$_2$AlBH$_4$] (**Figure 2.1**).

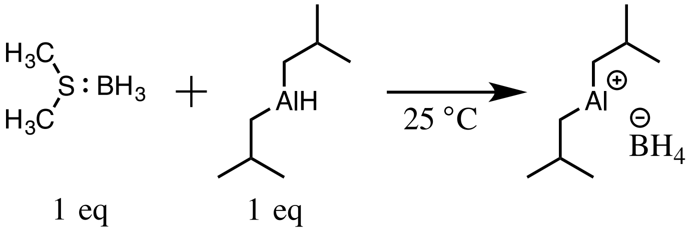

Scheme 2.1. Synthesis of Diisobutylaluminum Borohydride [(*i*Bu)$_2$AlBH$_4$] from BMS and DIBAL (1:1)

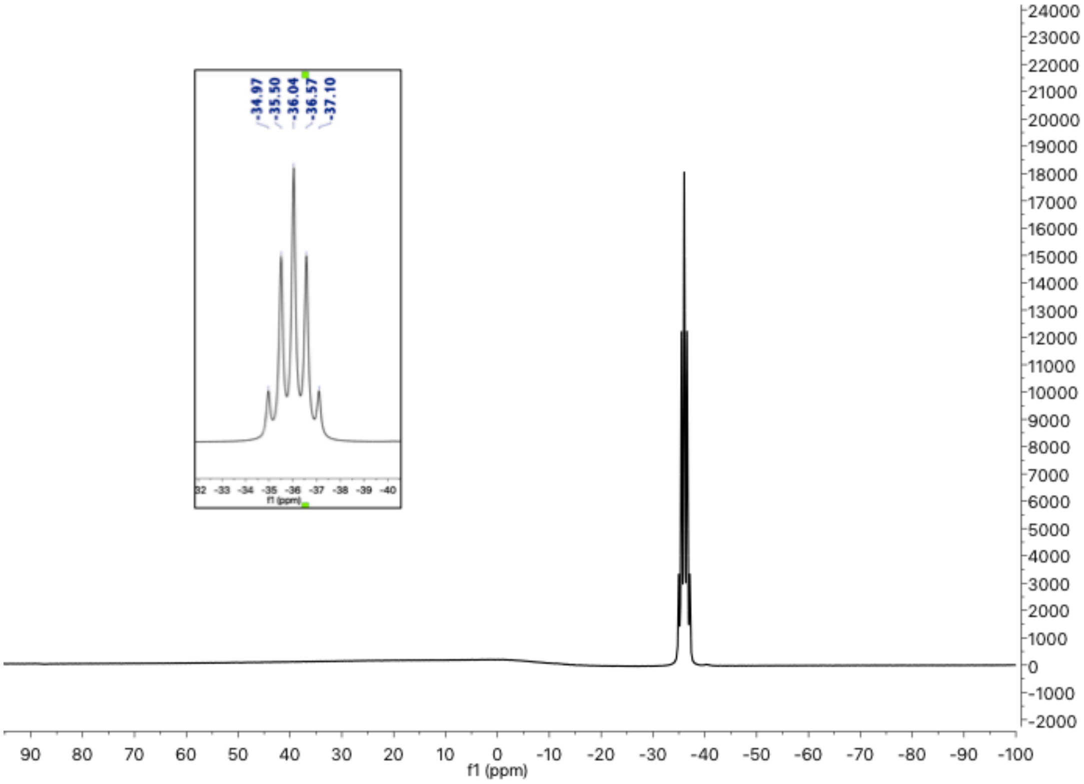

Figure 2.1. ^{11}B NMR (coupled) of (*i*Bu)$_2$AlBH$_4$

Ready access to reagents like BMS or DIBAL may be challenging and so exploration into other methods to synthesize $(i\text{Bu})_2\text{AlBH}_4$ from readily available starting materials were carried out. Sodium borohydride (NaBH_4) is a prevalent reagent, and in theory, combining it with diisobutylaluminum chloride (DIBAL-Cl) should produce $(i\text{Bu})_2\text{AlBH}_4$ (**Scheme 2.2**).

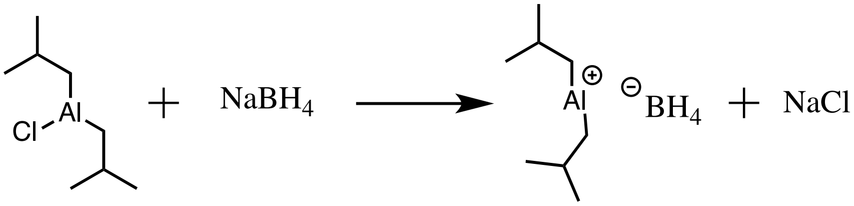

Scheme 2.2. NaBH_4 reaction with DIBAL-Cl to produce $(i\text{Bu})_2\text{AlBH}_4$

The first hurdle to carry out this reaction is the solubility of NaBH_4. It is soluble in water and alcohol solvents, but insoluble in ethereal and hydrocarbon solvents. On the other hand, DIBAL-Cl is water reactive and is commercially available as a hydrocarbon solution. Fortunately, NaBH_4 is also soluble in pyridine, tetraglyme, N-methyl pyrrolidone (NMP), and in a mixed solvent of THF:NMP (1:1). Accordingly, NaBH_4 and DIBAL-Cl were combined in a 1:1 ratio in each of the above solvents, stirred at 25 °C for one hour and the reaction mixtures analyzed via ^{11}B NMR (**Figure 2.2**).

In NMP and THF:NMP (1:1) solvent media, unreacted NaBH_4 was present (quartet, δ -41 ppm) along with a quartet at δ -10 ppm (**Figure 2.2a**, **Figure 2.2b**). The quartet at δ -10ppm is close to that of pyrrolidine:BH_3, arising from the reduction of NMP.[35] Similarly, the reaction in pyridine displayed a quartet at δ -10 ppm, indicating that NaBH_4 liberates borane with DIBAL-Cl and is trapped by pyridine to give pyridine:BH_3 (**Figure 2.2c**).[35, 36] When $NaBH_4$ and DIBAL-Cl were in the mixed solvent of THF:EtOH (1:1) there was an incomplete reaction, with $NaBH_4$ remaining, as well as, a borate species (singlet at δ +3 ppm), (**Figure 2.2d**). Finally, addition of DIBAL-Cl to a tetraglyme solution of $NaBH_4$ successfully afforded $(i\mathrm{Bu})_2AlBH_4$ as the major product [quintet at δ -37ppm (J = 81 Hz)] along with a quartet at δ -20ppm (**Figure 2.2e**). This quartet at δ -20 ppm disappeared when 1-hexene was added to the reaction mixture, indicating that the quartet at δ -20ppm may be due to a tetraglyme:BH_3 complex (**Figure 2.2f**). In order to minimize the amount of tetraglyme, THF was added as a co-solvent (1:4). Using this mixed solvent system, successful synthesis of $(i\mathrm{Bu})_2AlBH_4$ was achieved from $NaBH_4$ and DIBAL-Cl. However, for the reduction of selected organic functional group reported in this chapter, $(i\mathrm{Bu})_2AlBH_4$ was made from the method using BMS and DIBAL.

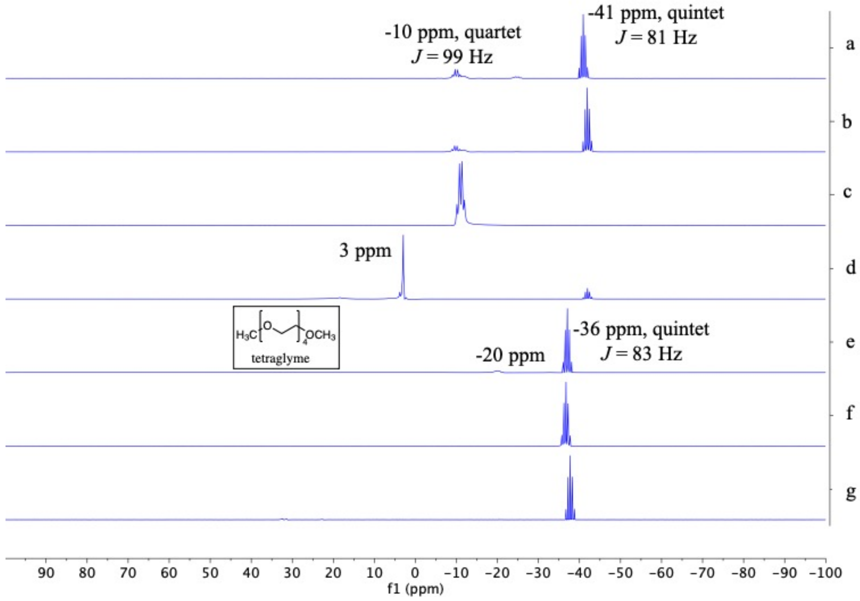

Figure 2.2. ^{11}B NMR (coupled) spectra of $NaBH_4$ and DIBAL-Cl in a) NMP, b) THF:NMP (1:1), c) pyridine, d) THF: EtOH (1:1), e) tetraglyme, f) addition of 1-hexene, and g) THF:tetraglyme (4:1).

2.2.2. Reduction of Aldehydes & Ketones

Reduction optimization of benzaldehyde with (iBu)$_2$AlBH$_4$ demonstrated that the aldehyde is efficiently converted to the corresponding alcohol at ambient conditions and in one hour. Because the conversion of an aldehyde to an alcohol requires the addition of one hydride, only 0.5 equivalence of (iBu)$_2$AlBH$_4$ was necessary to complete the reduction (**Scheme 2.3**). Since (iBu)$_2$AlBH$_4$ is synthesized from BMS and DIBAL, it was necessary to compare (iBu)$_2$AlBH$_4$ to its parent reagents. Both BMS and DIBAL require excess hydride for the complete reduction of benzaldehyde to benzyl alcohol at 0 °C (**Scheme 2.3**).[2, 37] Even though (iBu)$_2$AlBH$_4$ reacts similarly to BMS and DIBAL, the binary hydride is required to achieve complete conversion.

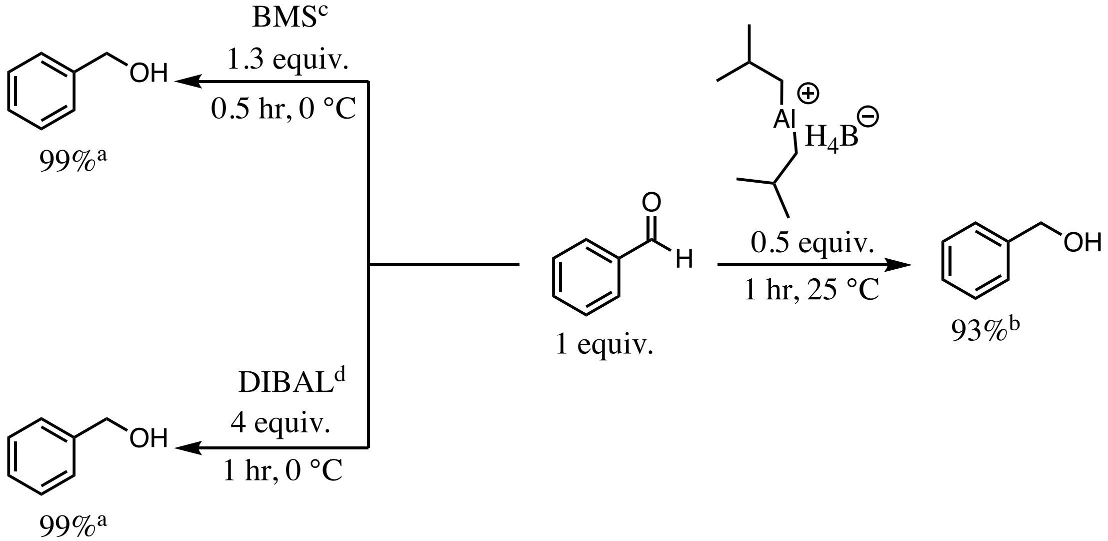

Scheme 2.3. Reduction of benzaldehyde *via* BMS, DIBAL, and (iBu)$_2$AlBH$_4$. [a] Conversion yields. [b] Isolated yields. [c] Ref [37]. [d] Ref [2].

A wider scope of aldehyde substrates illustrates the ease which (iBu)$_2$AlBH$_4$ can reduce the carbonyl at ambient conditions (**Table 2.1**). Aliphatic aldehydes, such as cyclohexanecarboxaldehyde, reacted with $(i\text{Bu})_2\text{AlBH}_4$ to produce the corresponding alcohol in good yields (Table 2.1, entry 1). A variety of aromatic aldehydes were tested producing the corresponding benzyl alcohol in high yields (Table 2.1, entries 2-9). 2-Phenylpropionaldehyde was reduced to the alcohol in 81% yield (Table 2.1, entry 10). Halides and nitro groups were well tolerated by $(i\text{Bu})_2\text{AlBH}_4$, reducing solely the carbonyl group (Table 2.1, entries 5-9). The lack of reactivity towards the nitro group is similar to BMS[15] but is different from DIBAL, which produces the corresponding hydroxylamine.[2] An aldehyde containing a furan substituent was also reduced efficiently (Table 2.1, entry 10). In general, aliphatic and aromatic aldehydes can be reduced by $(i\text{Bu})_2\text{AlBH}_4$, regardless of the type or position of the substituents present, at ambient conditions and in an hour.

Table 2.1. Reduction of Aldehydes using $(i\text{Bu})_2\text{AlBH}_4$[a]

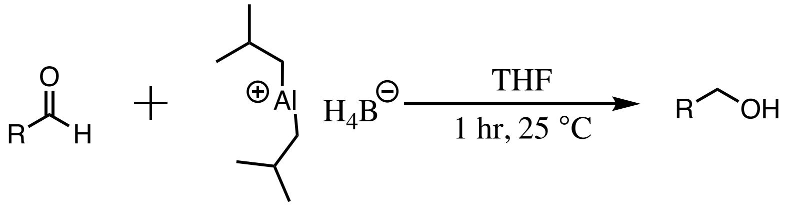

Entry	Substrate	Product (Yield %)[b]
1	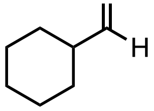	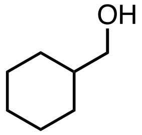 71%
2	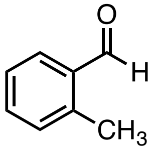	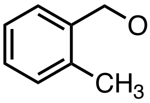 98%

3	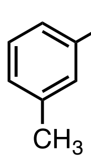	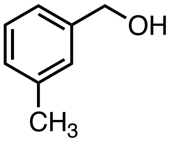 98%
4	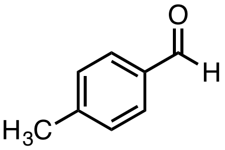	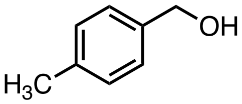 82%
5	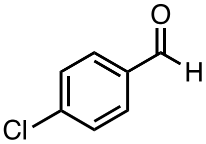	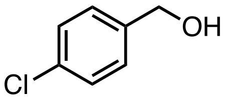 92%
6	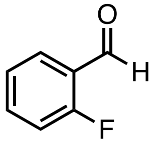	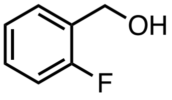 76%
7	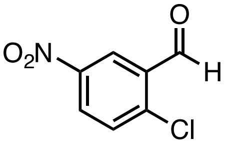	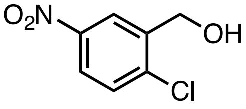 79%
8	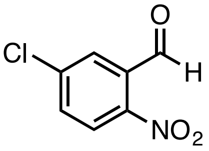	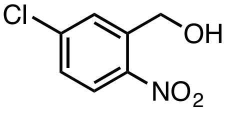 88%
9	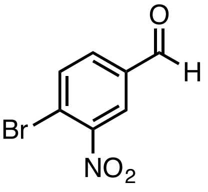	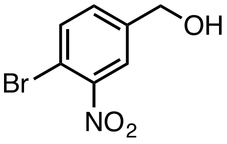 90%
10	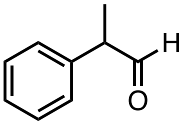	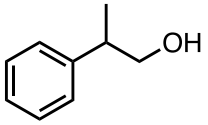 81%
11	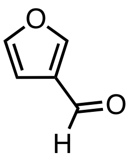	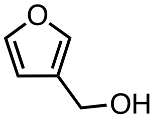 74%

[a]Reaction conditions with (iBu)$_2$AlBH$_4$: aldehyde substrate (5 mmol, 1 equiv.), (iBu)$_2$AlBH$_4$ (2.5 mmol, 0.5 equiv.), anhydrous THF (5mL), 25 °C, 1 h, under argon atmosphere. [b]Isolated yield.

Similar to aldehydes, the transformation of ketones to secondary alcohols is efficiently completed with (iBu)$_2$AlBH$_4$. Acetophenone was used to optimize the reaction conditions. Only half an equivalence of (iBu)$_2$AlBH$_4$ was necessary to achieve essentially quantitative conversion to the corresponding secondary benzylic alcohol (**Scheme 2.4**). In comparison, both BMS and DIBAL require excess hydride for the complete reduction of ketones.[2, 37]

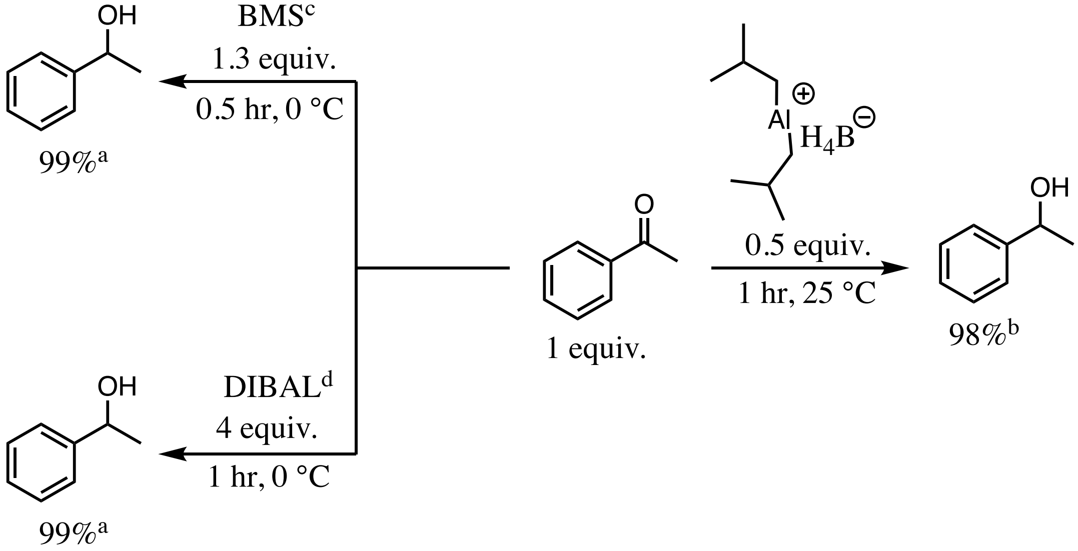

Scheme 2.4. Reduction of acetophenone *via* BMS, DIBAL, and (iBu)$_2$AlBH$_4$. [a] Conversion yields. [b] Isolated yields. [c] Ref [37]. [d] Ref [2].

A variety of ketones were examined showing the generality of (iBu)$_2$AlBH$_4$'s ability to reduce ketones to the corresponding alcohol (**Table 2.2**). Initial work began with the quantifiable reduction of aliphatic ketones (**Table 2.2**, entries 1 and 2). Acetophenone analogues, containing halide and methoxy substituents gave good yields

(**Table 2.2**, entries 3 and 4). Both naphthalene and thiophene-based ketones react efficiently to form the corresponding secondary alcohol (**Table 2.2**, entries 5 and 6). Interestingly, having acidic protons did not impede the reaction nor did the hydride undergo a dehalogenation (**Table 2.2**, entries 7-8).

Table 2.2. Reduction of Ketones using (*i*Bu)$_2$AlBH$_4$^{a}

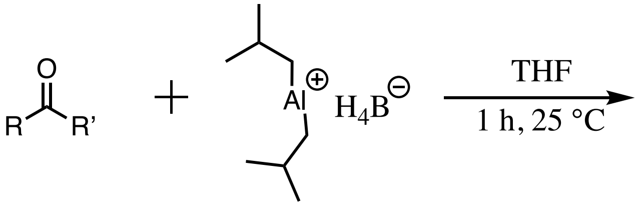

Entry	Substrate	Yield (%)^{b}
1	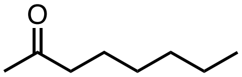	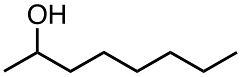 99%
2	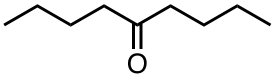	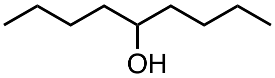 89%
3	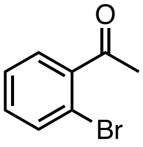	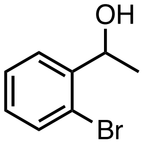 86%
4	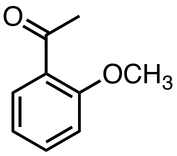	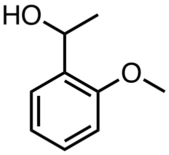 69%
5	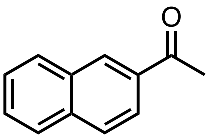	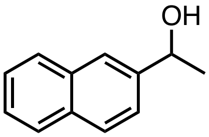 99%

6	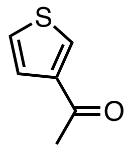	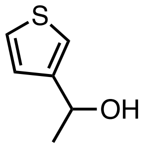 86%[c]
7	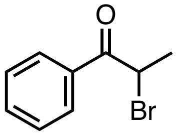	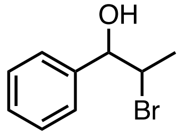 60%
8	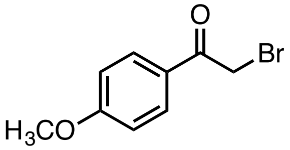	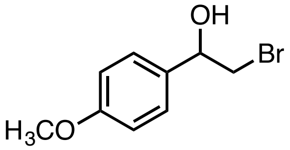 84%[d]

[a]Reaction conditions: ketone substrate (5 mmol, 1 equiv), $(i\text{Bu})_2\text{AlBH}_4$ (2.5 mmol, 0.5 equiv), anhydrous THF (5mL), 25 °C, 1 h, under argon atmosphere. [b]Isolated Yield. [c]Reaction ran for 5 h. [d]Reaction ran for 7 h.

2.2.3. Reduction of Nitriles

The reduction of nitriles using $(i\text{Bu})_2\text{AlBH}_4$ is an important transformation to understand the reduction profile of this binary hydride. Amines are chemical motifs frequently found in natural products, fine chemicals, and biomolecules[38,39, 40] and have been accessed from nitriles using silanes,[41] samarium diiodide,[10] and metal hydrides.[42-44] Metal hydrides, such as lithium aluminum hydride (LiAlH_4),[42, 43] aluminum hydride (AlH_3),[44] dichloroindium hydride (HInCl_2),[34] and even NaBH_4, when in the presence of a ruthenium catalyst,[9] can reduce nitriles to primary amines. Milder reagents, including aminoborohydrides[6] and boranes,[14, 45] will reduce nitriles, albeit slowly. Interestingly, bulky aluminum hydride reagents, like DIBAL can provide the aldehyde upon hydrolysis of the imine intermediate.[24, 46]

When mapping the reductive profile of (iBu)$_2$AlBH$_4$, it could act like BMS and give a primary amine or behave like the bulky DIBAL and afford the corresponding imine, which could undergo further reduction with BMS to give the primary amine. Borane dimethyl sulfide has been shown to reduce benzonitrile to the amine, but excess hydride was necessary due to the formation of a borazine intermediate.[15] Additionally, the reaction was sluggish at room temperature and requires heating and continuous removal of methyl sulfide to achieve a complete reaction (**Scheme 2.5**).[15] In comparison, the reduction of benzonitrile with DIBAL formed the benzaldehyde imine at 0 °C, which afforded benzaldehyde following hydrolysis.[3, 5] With (iBu)$_2$AlBH$_4$, benzonitrile reacted within one hour at room temperature to cleanly generate the primary amine.

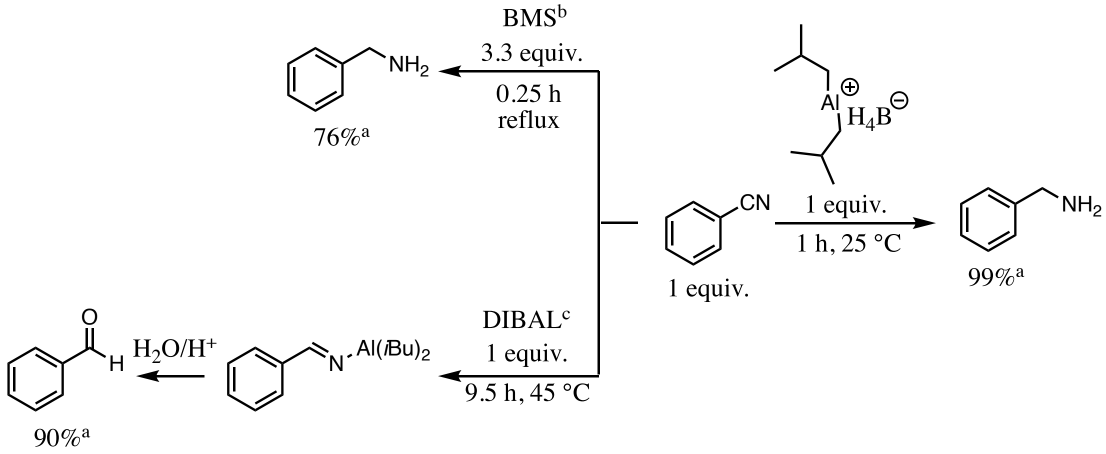

Scheme 2.5. Reduction of benzonitrile *via* BMS, DIBAL, and (iBu)$_2$AlBH$_4$. [a]Isolated yield. [b] Ref [15]. [c] Ref [3, 5].

As shown in **Table 2.3**, (iBu)$_2$AlBH$_4$ can reduce aromatic nitriles containing a variety of substituents. Halogens were tolerated to generate the amine in good yields (**Table 2.3**, entries 1-4). **Table 2.3**, entry 5, demonstrates that (iBu)$_2$AlBH$_4$ is a selective reagent and is capable of reducing nitriles in the presence of nitro groups. Trisubstituted aryl nitriles can be reduced to the corresponding benzyl amine (**Table 2.3**, entries 6-8). It was found that sterics do cause a decrease in the product yield as demonstrated in **Table 2.3**, entries 7 and 8. A more complex nitrile, such as 4-(4-methyl-5-thiazolyl)benzonitrile, was reduced using $(i\text{Bu})_2\text{AlBH}_4$ and the product was isolated in high yields, demonstrating the capability of the reagent (**Table 2.3**, entry 9).

Table 2.3. Reduction of Aryl Nitriles by $(i\text{Bu})_2\text{AlBH}_4$[a]

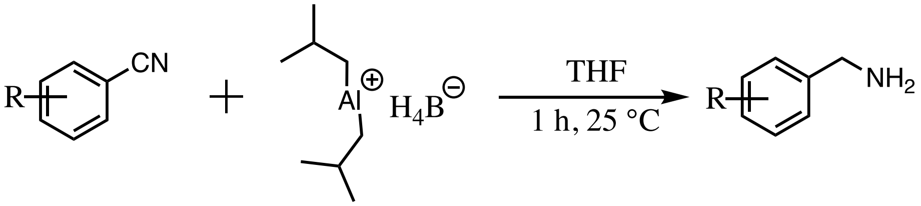

Entry	Substrate	Product Yield (%)[b]
1	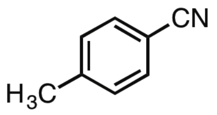	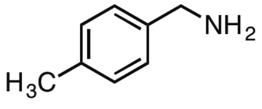 94%
2	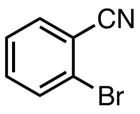	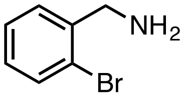 37%
3	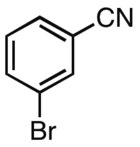	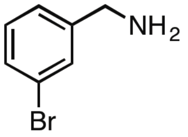 72%
4	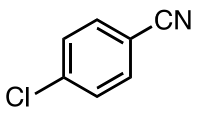	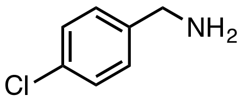 85%
5	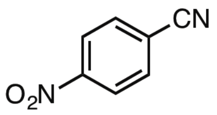	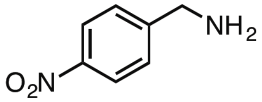 98%

6	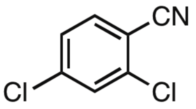	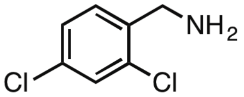 94%
7	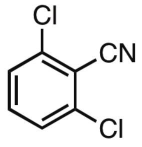	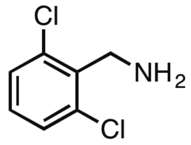 27%
8	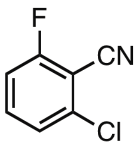	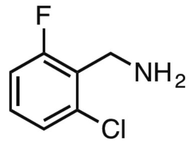 16%
9	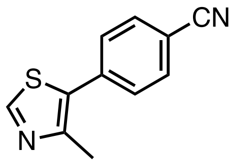	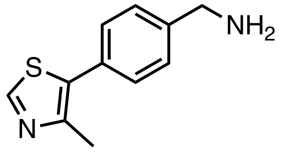 90%

[a]Reaction conditions with $(i\text{Bu})_2\text{AlBH}_4$: nitrile substrate (5 mmol, 1 equiv), $(i\text{Bu})_2\text{AlBH}_4$ (5 mmol, 1 equiv), anhydrous THF (5mL), 25 °C, 1 h, under argon atmosphere. [b]Isolated yield.

Benzylic nitriles were also included in this study to determine whether the acidic benzylic protons would inhibit the reduction (**Table 2.4**). Nevertheless, the conversion to the amine was efficient and clean, demonstrating that the acidic protons do not significantly hinder the hydride from reduction of the nitrile. The examples chosen contained both electron donating and withdrawing substituents, which were well tolerated for these reduction reactions (**Table 2.4**, entries 1-3). Similarly, heterocycles, like thiophene, could produce the corresponding amine in good yields (**Table 2.4**, entry 4).

Table 2.4. Reduction of benzylic nitriles to amines using $(i\mathrm{Bu})_2\mathrm{AlBH}_4$[a,b]

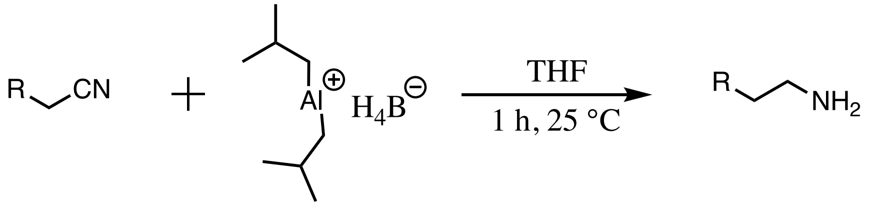

Entry	Substrate	Product Yield (%)
1	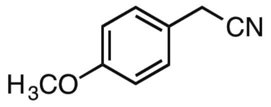	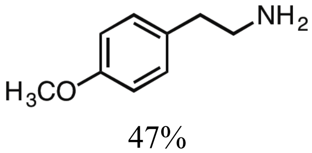 47%
2	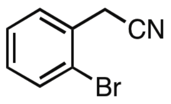	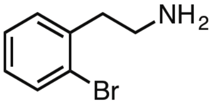 74%
3	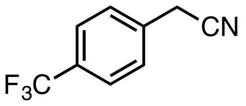	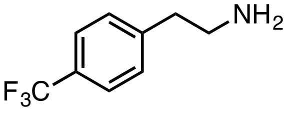 74%
4	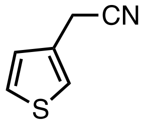	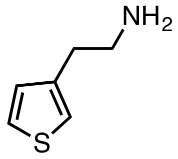 71%

[a]Reaction conditions with $(i\mathrm{Bu})_2\mathrm{AlBH}_4$: nitrile substrate (5 mmol, 1 equiv), $(i\mathrm{Bu})_2\mathrm{AlBH}_4$ (5 mmol, 1 equiv), anhydrous THF (5mL), 25 °C, 1 h, under argon atmosphere. [b]Isolated yield.

2.2.4. Reduction of Epoxides

Hydridic ring opening reactions of epoxides affords the corresponding alcohol products.[1, 24, 47] Since epoxides require one hydride to react completely, 0.5 equivalents of $(i\mathrm{Bu})_2\mathrm{AlBH}_4$ was employed. As expected, when cyclohexene oxide was reduced with $(i\mathrm{Bu})_2\mathrm{AlBH}_4$, cyclohexanol was produced as the sole product (**Table 2.5**, entry 1). Unsymmetric epoxides afforded a more interesting product distribution due to the presence of regioselectivity at different reactive sites. Reduction of 1,2-epoxy-hexane at 25 °C gave a mixture 2-hexanol and 1-hexanol in a 77:23 ratio, respectively (**Table 2.5**, entry 2). However, at 0 °C only 2-hexanol was obtained and isolated in a 70% yield (**Table 2.5**, entry 3). The regioselectivity exhibited by $(i\text{Bu})_2\text{AlBH}_4$ is similar to that of DIBAL[2] implying that $(i\text{Bu})_2\text{AlBH}_4$, again, is influenced by its parent hydrides. Another unsymmetric epoxide, 2-biphenylyl glycidyl ether, was reduced regioselective to the secondary alcohol in high yields (**Table 2.5**, entry 4). This reaction further demonstrated that $(i\text{Bu})_2\text{AlBH}_4$ most likely attacks the least hindered carbon atom in a $\text{S}_\text{N}2$-like pathway.

Table 2.5. Reduction of Epoxides by $(i\text{Bu})_2\text{AlBH}_4$[a]

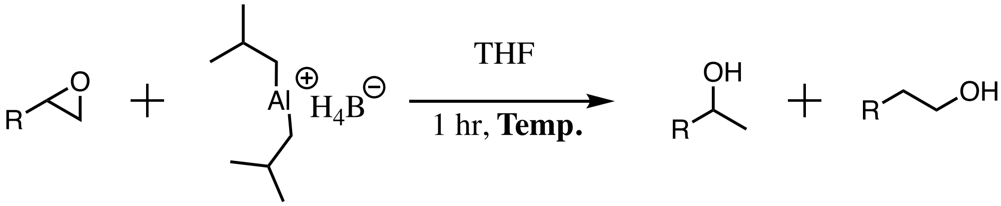

1 equiv. 0.5 equiv.

Entry	Epoxide	Temperature	Yield (%)	
1	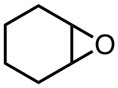	0°C	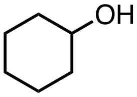 84%[c]	
2	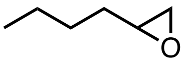	25°C	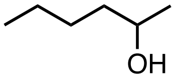 77%[b]	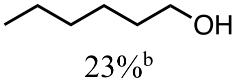 23%[b]
3	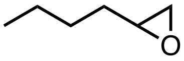	0°C	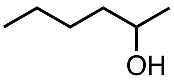 70%[c]	

4	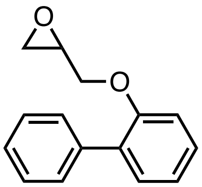	0°C	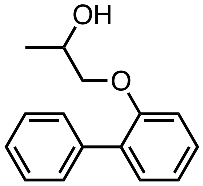 90%[c]

[a] Reaction conditions: epoxide substrate (5 mmol, 1 equiv), (*i*Bu)$_2$AlBH$_4$ (0.5 equiv.), anhydrous THF (5mL), 1 h, under argon atmosphere. [b] Ratio based on ^{1}H NMR. [c] Isolated yield.

The S_N2-pathway could occur when the bulky aluminum atom coordinates to the epoxide oxygen and directs the hydride to the sterically less hindered carbon atom, providing the more substituted alcohol product (**Scheme 2.6**).[2]

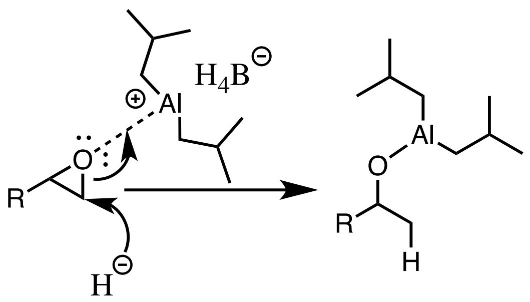

Scheme 2.6. Possible Mechanism for the Reduction of Epoxides by (*i*Bu)$_2$AlBH$_4$

Styrene oxide is an interesting substrate as the stereo-electronic effects can influence the site of the hydridic attack. If the hydride undergoes a primary attack (S_N2-like) the more substituted alcohol, 1-phenylethanol, is formed (**Figure 2.3**, blue route). Should the hydride react at the secondary carbon, the less substituted alcohol, 2-phenylethanol, is generated (**Figure 2.3**, green route). A selection of hydrides and their corresponding products after reaction with styrene oxide are displayed in **Table 2.7**.

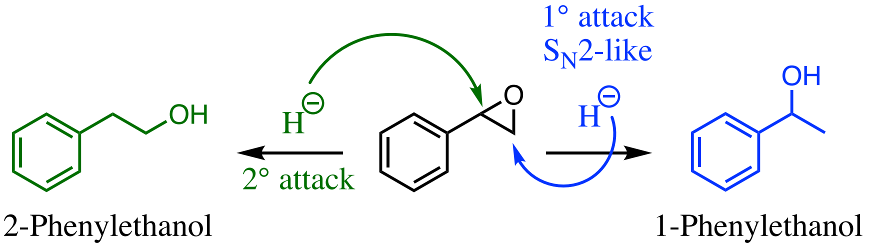

Figure 2.3. Reduction of styrene oxide by hydrides produces either 2-phenylethanol (green) or 1-phenylethanol (blue), depending upon where the hydride reacts.

Aluminum-based hydrides have complex reactivities when reacting with styrene oxide. Reaction of the epoxide with $LiAlH_4$ generates primarily 1-phenylethanol (**Table 2.7**, 99-93%) with minimal quantities of 2-phenylethanol (1-7%).[48] The reverse selectivity is shown when $LiAlH_4$ was combined with $AlCl_3$, producing 2-phenylethanol as the major product (**Table 2.7**, 99%).[48, 49] It has been reported that the combination of $LiAlH_4$ with excess $AlCl_3$ forms a mixed metal hydride, $HAlCl_2$.[49] As a strong Lewis acid, $HAlCl_2$ favors an attack at the benzylic carbon. This is in contrast to the weaker Lewis acid, AlH_3, which favors the production of 1-phenylethanol (76%),[2, 44, 50] as does many of the other alkoxyaluminum hydrides.[50]

Diisobutylaluminum hydride differs from the alkoxyaluminum hydrides, producing a roughly 70:30 mixture of 2-phenylethanol to 1-phenylethanol in toluene at 0 °C.[2] However, through the course of this work, it was found that DIBAL reacts with styrene oxide at 25 °C, to produce 2-phenylethanol as the sole product. Other reports describe the reduction of styrene oxide by combining DIBAL with *n*-butyl lithium and LiCl, respectively.[2, 51] The reaction with *n*-butyl lithium displayed a dramatic preference for 1-phenylethanol (96%).[51] Similarly, the reaction with LiCl appeared to favor the secondary alcohol (86%), although not to the same degree.[2]

It has been reported that lithium borohydride ($LiBH_4$) will react with aliphatic epoxides to afford the more substituted alcohol (S_N2-like attack) as the single product.[52] Reaction of $LiBH_4$ with styrene oxide generated a mixture of products, with 1-phenylethanol as the major product (74%) (**Table 2.6**). This result is in agreement with the fact that borohydrides act as Lewis bases and so it would prefer to react with areas of low electron density.[53] Interestingly, when different *para*-substituted styrene oxides were reduced with $LiBH_4$, it was observed that the substituents greatly influenced the product ratios (**Table 2.6**).[52] A trend was observed that as electron-donating abilities increased, the S_N2-like products decreased. For instance, when methoxy was present in the *para*-position the major product was the primary alcohol (**Table 2.6**, entry 4, 95%). It was rationalized that strong electron-donating groups aid in stabilizing the slight positive charge on the benzylic carbon. An exception was when a strong electron-withdrawing group, such as a nitro group, was present as the *para*-substituent on the styrene ring. In which case, a mixture of the primary alcohol (62%) and the secondary alcohol (38%) was observed.

Table 2.6. Reduction of *para*-substituted styrene oxide by $LiBH_4$[a]

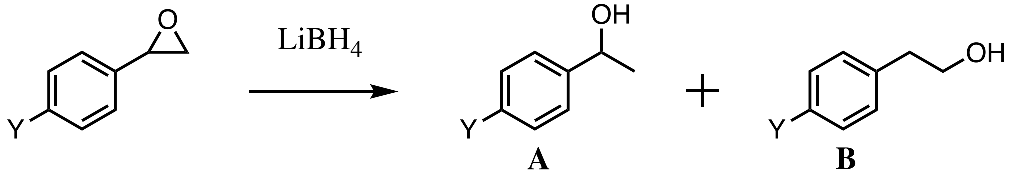

Entry	Substituent (Y)	Relative Yield of **2** (%)	Relative Yield of **3** (%)
1	NO_2	38	62

2	Br	84	16
3	H	74	26
4	OCH_3	5	95

[a]Ref [52]

The reduction of styrene oxide with BH_3:THF occurred more slowly, but there was a clear preference for the formation of 2-phenylethanol (**Table 2.7**). [37, 54] The yields were improved when boron trifluoride was added.[55]

Table 2.7. Reaction of various hydrides with styrene oxide.

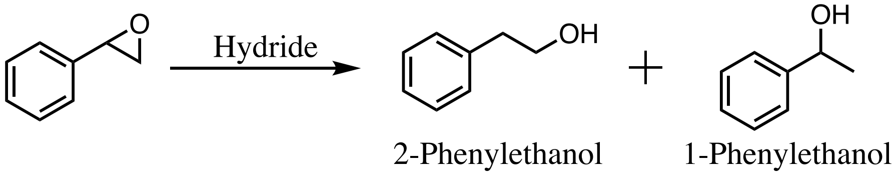

Hydride	2-Phenylethanol	1-Phenylethanol	References
$LiAlH_4$	1-7%	99-93%	[48, 50]
"$HAlCl_2$" $LiAlH_4$ + $AlCl_3$[a]	98%	2%	[48, 49]
AlH_3	24%	76%	[2, 44, 50]
AlH_2O-*t*-Bu	21%	79%	[50]
AlH(O-*t*-Bu)$_2$	20%	80%	[50]
AlH_2O-*i*-Pr	15%	85%	[50]
DIBAL[e]	73%	27%	[2]
DIBAL[f]	99%	--	This work
DIBAL+*n*-BuLi[b]	4%	96%	[51]
DIBAL+LiCl	14%	86%	[2]
$LiBH_4$	26%	74%	[52]
$LiEt_3BH$	-	97%	[47]
$NaBH_4$+BF_3	52%	19%	[53]
BH_3:THF[c]	41%	1%	[54]
BH_3:THF[d]	28%	--	[37]
BH_3-BF_3[e]	98%	Trace	[55]

[a] $LiAlH_4$ and $AlCl_3$ mixed in a 1:3 and 1:4 ratios produced similar results. [b] Reaction conditions: 0 °C, 1.5 h. [c] Reaction was occurred over 12 days, analysis of which also

detected: styrene oxide (8%), 2-*n*-butoxy-2-phenylethanol (~24%), and unknown products (~5%). [d] Reaction took place over 6 h at 25 °C.[e] Reaction conditions: 0 °C, 30 min. [f] Reaction conditions: Styrene oxide (1 equiv), DIBAL (2 equiv), reaction occurred at 25 °C for 1 h.

Therefore, it was important to determine how well (iBu)$_2$AlBH$_4$ reduced styrene oxide and if it would generate a mixture of products or a single product. Unfortunately, (iBu)$_2$AlBH$_4$ consistently produced a mixture of products (**Table 2.8**). There was a slight favorability for 2-phenylethanol, but not a substantial amount to indicate selectivity. Consequently, reduction of styrene oxide using (iBu)$_2$AlBH$_4$ is synthetically not useful.

Table 2.8. Reaction of styrene oxide with (iBu)$_2$AlBH$_4$.[a,b]

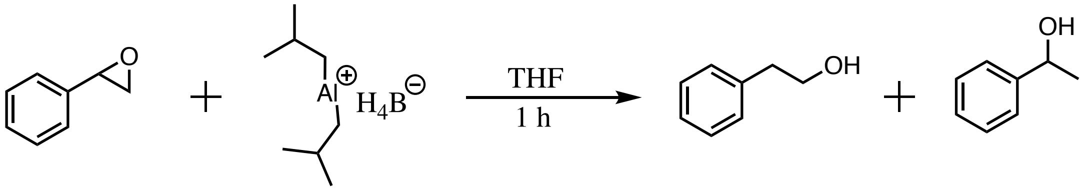

Entry	Temperature	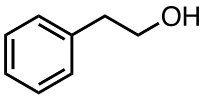 Yield (%)	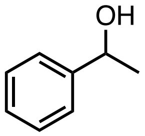 Yield (%)
1	25 °C	55	45
2	0 °C	52	48
3	-4 °C	54	46
4	-78 °C	61	39
5	reflux	65	35
6[c]	25 °C	66	34

[a] Reaction conditions: styrene oxide (5 mmol, 1 equiv), (iBu)$_2$AlBH$_4$ (5 mmol, 1 equiv.), anhydrous THF (5mL), 1 h, under argon atmosphere. [b] Yield based upon ^{1}H NMR analysis. [c] (iBu)$_2$AlBH$_4$ (7.5 mmol, 1.5 equiv.)

2.2.5. Reduction of Carboxylic Acids

Benzoic acid was used as the representative substrate for the reduction of carboxylic acids with the binary hydride. Borane dimethyl sulfide is known to reduce aliphatic carboxylic acids rapidly (30 min) and reduce aromatic carboxylic acids more slowly (4 h) while having a significantly lower yield.[56] Addition of trimethyl borate as an additive showed an increase in yields of the primary alcohols in this reduction.[56] Similarly, reduction of benzoic acid with DIBAL affords benzyl alcohol after 12 h (**Scheme 2.7**).[2, 3, 56, 57] Earlier work with DIBAL has also implicated partial reduction of the acid to the aldehyde.[57] It should be noted that an excess of BMS or DIBAL were required because of the hydride reaction with the acidic proton.[2, 56] For the optimized reaction conditions with $(i\mathrm{Bu})_2\mathrm{AlBH}_4$, a slight excess (1.5 equivalents) of the hydride was necessary, due to the reaction with the acidic proton present on the carboxylic acid group. Complete reduction to the corresponding alcohol products were achieved in high yields, at room temperature, in one hour.

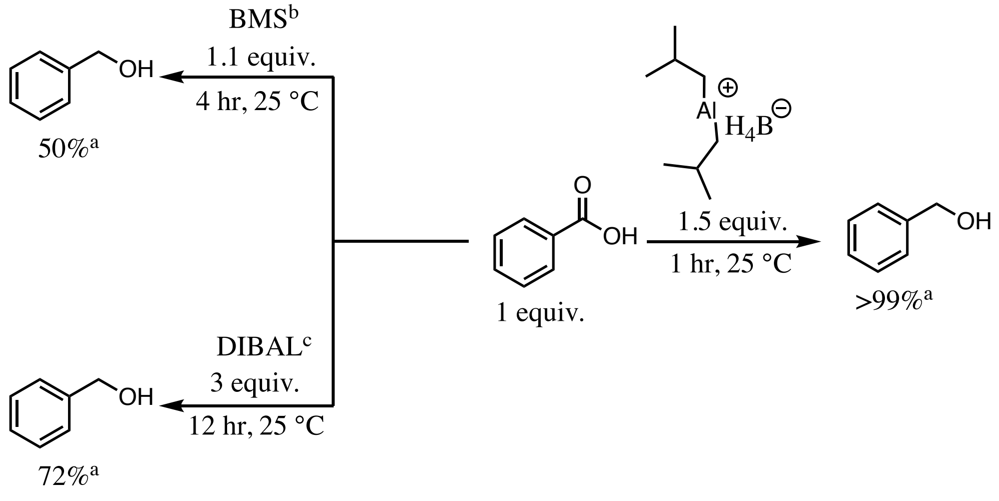

Scheme 2.7. Reduction of benzoic acid *via* BMS, DIBAL, and $(i\mathrm{Bu})_2\mathrm{AlBH}_4$. [a]Isolated yield. [b]Ref [56]. [c]Ref [2, 3].

Several carboxylic acids were investigated to establish the generality of the reduction of carboxylic acids using $(i\mathrm{Bu})_2\mathrm{AlBH}_4$ (**Table 2.9**). Aromatic acid derivatives were reduced efficiently, under ambient conditions (Table 2.9, entries 1-4). Neither the acidic benzylic protons nor the benzylic chloride in 4-(chloromethyl)benzoic acid interfered with the hydride reduction producing the corresponding alcohol in 95% isolated yield (**Table 2.9**, entry 2). An aryl carboxylic acid with an electron donating group, such as a methoxy group, was reduced successfully (**Table 2.9**, entry 3). Aryl bromides were tolerated in the reduction of 2-bromophenylacetic acid. However, this reduction required longer reaction time (3 h) to achieve complete reduction, possibly due to the steric inhibition of the ortho substituent (**Table 2.9**, entry 4). Overall, $(i\mathrm{Bu})_2\mathrm{AlBH}_4$ readily reduced carboxylic acids to the corresponding alcohols in good yields and at ambient conditions.

Table 2.9. Reduction of Carboxylic Acids by $(i\mathrm{Bu})_2\mathrm{AlBH}_4$[a]

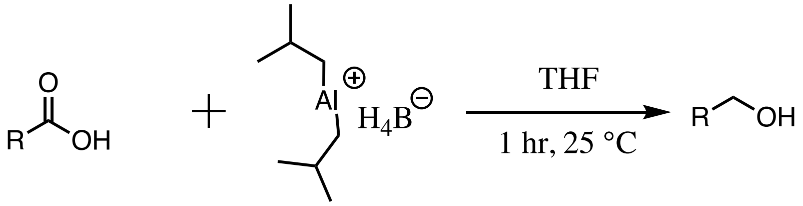

Entry	Carboxylic Acid	Yield (%)[b]
1	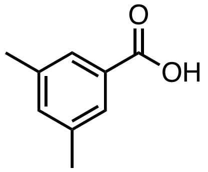	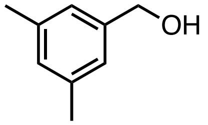 44%
2	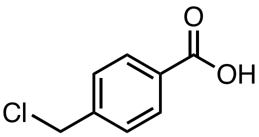	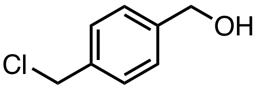 95%

3	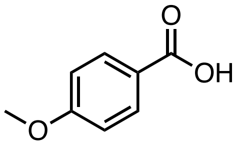	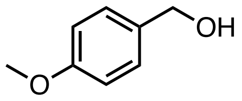 98%
4[c]	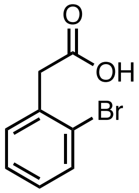	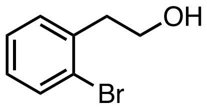 79%

[a] Reaction conditions: carboxylic acid (5 mmol, 1 equiv), $(i\mathrm{Bu})_2\mathrm{AlBH}_4$ (5.5 mmol, 1.1 equiv.), anhydrous THF (5mL), 1 h, under argon atmosphere. [b] Isolated yield. [c] Reaction ran for 3 h.

2.2.6. Reduction of Esters

The reduction of esters generated the alcohol products but are typically slower reactions. H. C. Brown found that to achieve the reduction of esters by BMS, the mixture required refluxing conditions and constant distilling off of the methyl sulfide.[15] He hypothesized that the accumulation of methyl sulfide was the cause of the decrease in reaction rates and yields for two reasons. First, the proposed mechanism for the reduction implicated a transfer reaction, to form structures **C** or **D** (**Figure 2.4**); any accumulation of the methyl sulfide would suppress the formation of these intermediates. Second, if dimethyl sulfide accrues in the reaction flask it would decrease the temperature of the reaction mixture, leading to lowering the reaction rate.

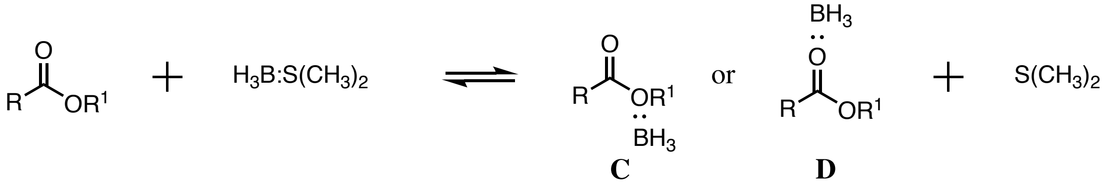

Figure 2.4. Brown’s proposed pathway for the reduction of esters by BMS.

Ethyl benzoate was subjected to the two reaction parameters, no distillation versus distillation. It was found that the rate of the reactions were different.[15] The experiment that removed the methyl sulfide was able to achieve 100% reaction after 1 h, compared to the 8 h required to achieve a 98% reaction when no distillation was used. After determining the optimum conditions, a more detailed study on the different types of esters were examined. The data showed that BMS reduced aliphatic esters more quickly than aromatic esters and that nitro, halides, and ether groups were well tolerated (**Scheme 2.8**). Diethyl succinate and $\boldsymbol{\gamma}$-butyrolactone were chosen as representative examples for the reduction of lactones and diesters. Both afforded 1,4-butanediol in similar yields. However, the reduction of the aromatic lactone, phthalide, using BMS produced a mixture of products.

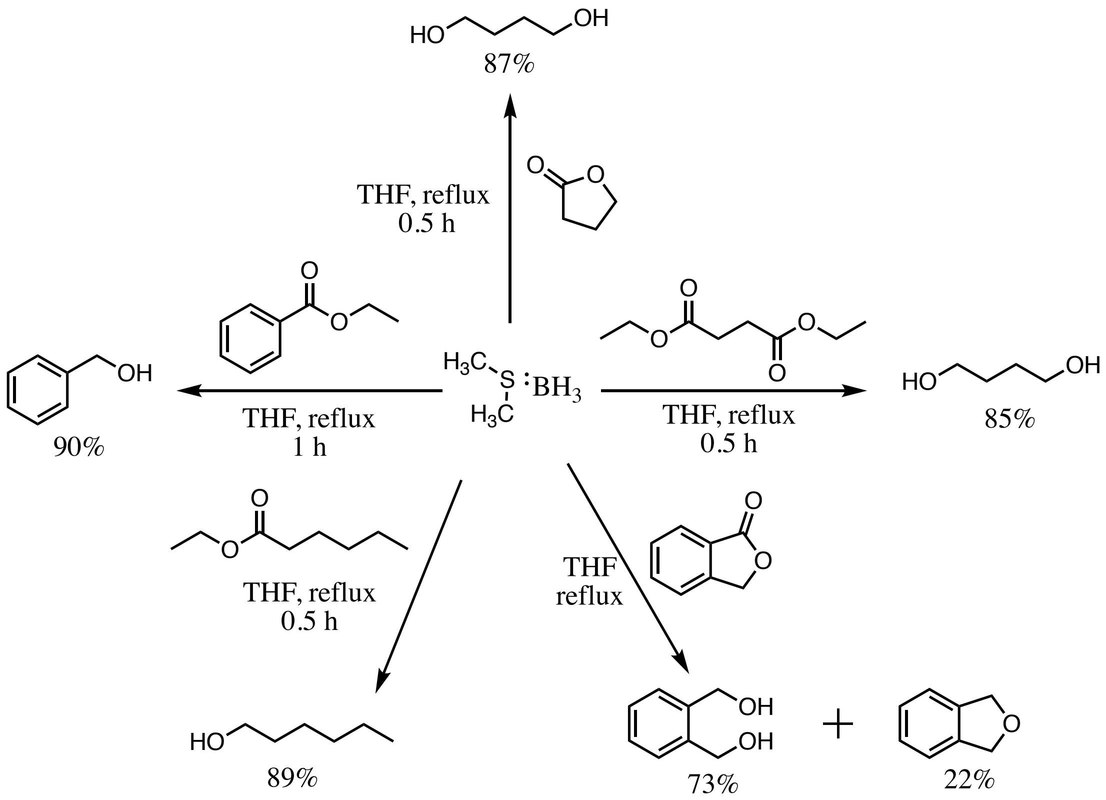
HO OH
87%
THF, reflux
0.5 h
O
O
OH
90%
THF, reflux
1 h
H_3C
S
BH_3
H_3C
THF, reflux
0.5 h
HO OH
85%
O
THF, reflux
0.5 h
THF
reflux
HO
89%
OH
OH
73%
+
O
22%

Scheme 2.8. Reduction of various esters by BMS.

The reduction of esters using DIBAL requires excess hydride, otherwise poor yields were observed. Two equivalents of DIBAL achieved the highest results to convert esters into the corresponding alcohols.[2, 3] It has been proposed that the reaction intermediate is an alkoxy aluminum compound that generates an aldehyde, and then subsequently undergoes a hydride attack to afford the alcohol (**Scheme 2.9**).[2, 58] Some research groups have tried to stop the reaction at the aldehyde by drastically lowering the reaction temperature (-78 °C) or use microreactors at a slightly higher temperature (-20 °C).[58]

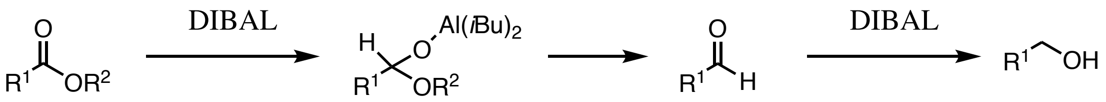

Scheme 2.9. Proposed mechanism for the reduction of esters by DIBAL.

Using (*i*Bu)$_2$AlBH$_4$, methyl benzoate was reduced completely to benzyl alcohol using a 1:1 ratio of the binary hydride to ester (**Table 2.10**, entry 1). Both aryl and benzylic halides were well tolerated by (*i*Bu)$_2$AlBH$_4$ and no dehalogenation was observed (**Table 2.10**, entries 2-4). Full conversion of methyl-4-hydroxybenzoate and the pyridine analogue were not seen, but it demonstrates that some transformation does occur and that (*i*Bu)$_2$AlBH$_4$ can reduce these esters (**Table 2.10**, entries 5 and 6). Additionally, the propionate derivative was cleanly reduced to the primary alcohol (**Table 2.10**, entry 7).

Table 2.10. Reduction of Esters by (*i*Bu)$_2$AlBH$_4$^{a}

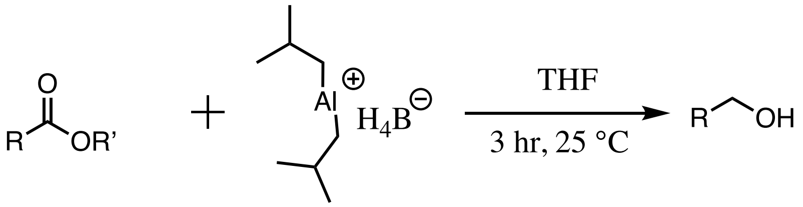

Entry	**Substrate**	**Yield (%)^{b}**
1	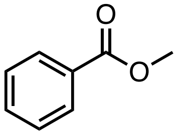	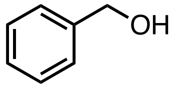 74%
2	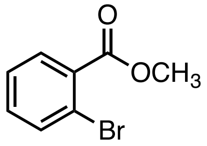	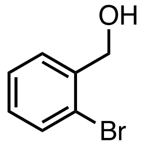 93%
3	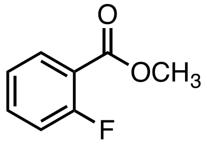	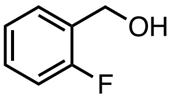 89%

4	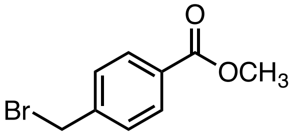	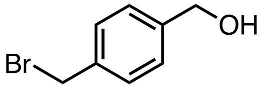	84%
5	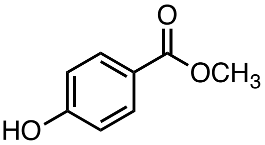	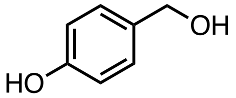	70%[c,d]
6	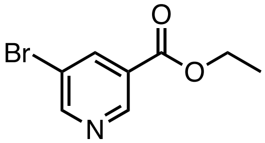	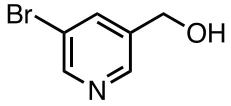	20%[c]
7	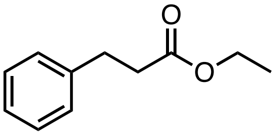	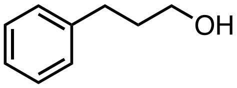	91%

[a] Reaction conditions: ester (3 mmol, 1 equiv), (iBu)$_2$AlBH$_4$ (3 mmol, 1 equiv.), anhydrous THF (3mL), 3 h, under argon atmosphere. [b] Isolated yield. [c] Yield based on ^{1}H NMR.[d] Reaction ran for 24 h.

2.2.7. Reduction of Amides

Finally, we studied the reductions of amides as they are a more difficult functional group to reduce at ambient temperatures, due to the low electrophilicity at the carbonyl position. In general, the reduction of amides can produce aldehydes or alcohols, when the reaction undergoes a C-N bond cleavage or provide an amine when there is a C-O bond cleavage.[59] Amides are classified as either primary, secondary, or tertiary depending on the substitution of the nitrogen atom. This distinction is important because there are varying reactivities in the substituted amides and also produce unique products when reduced.

For instance, reduction of primary amides by LiAlH$_4$ appeared contingent upon the stoichiometry (**Table 2.11**). If 0.5 equivalents of LiAlH$_4$ was used, then the nitrile was produced in greater quantities.[60] A 1:1 ratio of hydride to amide generated the corresponding amine.[61] Similarly, the reduction of primary amides by $NaBH_4$ produced conflicting products. In one report, benzamide (1 equiv) was converted into benzonitrile by $NaBH_4$ (1.1 equiv) when refluxed in diglyme.[62] Yet another group reported that reacting benzamide (1 equiv) with excess $NaBH_4$ (4 equiv) converted the primary amide into benzylamine in 1.5 h, also in diglyme and refluxing conditions.[63]

Reaction of primary amides with boranes produced the amine, however it required heating the reaction. A detailed rate study revealed that aliphatic primary amides reduce more rapidly than aromatic amides.[64] Borane dimethyl sulfide reduced amides, but it required concurrent removal of dimethyl sulfide by distillation.[15]

Table 2.11. Reduction of Primary Amides by Various Hydrides

Primary Amide Reduction		
Hydride	**Product**	**Reference**
BH_3:THF[a]	amine	64
$LiAlH_4$	amine[b]	61
	nitrile [c]	60
$NaBH_4$[d]	nitrile	62
$NaBH_4$[d]	amine	63
$NaBH_4$ + $AlCl_3$[e]	No reduction	65
DIBAL[f]	amine	2
BMS	amine	15, 16

[a] Reflux in THF. [b] Requires 1:1 (amide:hydride). [c] Requires 1:<0.5 (amide:hydride). [d] Reaction conditions: reflux in diglyme (162 °C). [e] Used 3:1 ($NaBH_4$:$AlCl_3$) in diglyme. [f] Slow reduction

Secondary and tertiary amides produced amines more readily, as seen in **Table 2.12**. Lithium aluminum hydride reduced secondary and tertiary amides to the corresponding amines.[61] Sodium borohydride, under refluxing conditions, also afforded the tertiary amines from tertiary amides.[61] Interestingly, DIBAL could successfully reduce tertiary amides but not secondary amides.[2]

Borane tetrahydrofuran and BMS reduced secondary and tertiary amides at higher temperatures and required excess of the hydride.[64] For BMS, constant removal of the dimethyl sulfide by distillation was found to facilitate the reduction reaction.[15]

Table 2.12. Reduction of Secondary and Tertiary Amides by Various Hydrides.

	Secondary Amide Reduction	
Hydride	**Product**	**Reference**
$LiAlH_4$	amine	[61]
BH_3:THF	amine	[64]
BMS[a]	amine	[15]
	Tertiary Amide Reduction	
$LiAlH_4$	amine	[61]
BH_3:THF	amine	[64]
BMS	amine	[15]
$NaBH_4$[b]	amine	[61]
$NaBH_4 + AlCl_3$	amine	[65]
DIBAL	Amine	[2]

[a] Reaction conditions: 1:2.2 (amide:BMS), reflux in THF [b] Reaction conditions: reflux in pyridine.

Thus, examining how $(i\text{Bu})_2AlBH_4$ reacted with amides was of interest. It was found that aromatic primary and secondary amides were not reduced with $(i\text{Bu})_2AlBH_4$. When benzamide, N-methylbenzamide, and unsubstituted acetanilide were reacted with the binary hydride, the starting material was recovered. Even increasing the amount of hydride (2 equivalents) and employing a longer reaction time (24 h) the reductions were unsuccessful. These results indicate that $(i\text{Bu})_2AlBH_4$, just like DIBAL, is unsuitable for the reduction of primary or secondary amides.

Satisfactorily, tertiary amides were reduced using (iBu)$_2$AlBH$_4$ at ambient temperature to the corresponding tertiary amines in under an hour (**Table 2.13**). These reductions were followed by IR spectral analysis of aliquots withdrawn periodically from the reaction mixture; the reduction was considered complete when the carbonyl stretch was no longer visible in the IR spectrum analysis. An exception to this was the reduction of *N,N*-dimethylbenzamide which underwent C-N bond cleavage to produce benzyl alcohol in 98% yield (**Table 2.13**, entry 1). *N*,*N*-Diethylbenzamide and *N*,*N*-diethyl-*m*-toluamide afforded the corresponding benzyl amines in 80% and 99% isolated yields, respectively (**Table 2.13**, entries 2 and 3). Even sterically hindered amides, such as *N*,*N*-diisopropylbenzamide, were reduced to *N*,*N*-diisopropylbenzyl amine in 99% isolated yield (**Table 2.13**, entry 4). Unsymmetrical *N*-methyl-*N*-propylbenzylamine was isolated from the reduction of *N*-methyl-*N*-propylbenzamide in 92% yield (**Table 2.13**, entry 5). Benzamides with electron-withdrawing groups, such as bromo or trifluoromethyl substituents, were successfully reduced (**Table 2.13**, entries 6 and 7).

Table 2.13. Reduction of aromatic tertiary amides using iBu$_2$AlBH$_4$^{a}

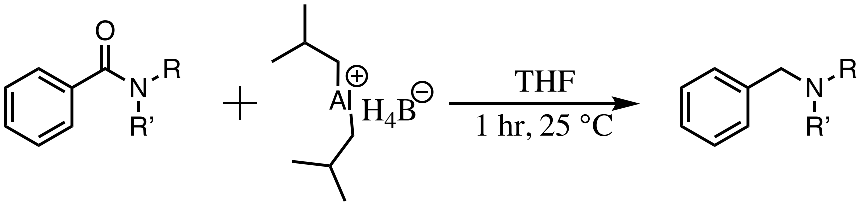

Entry	Amide	Yield (%)^b
1	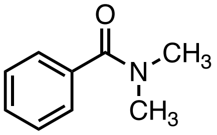	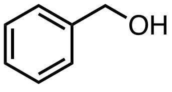 98%

2	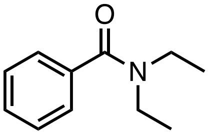	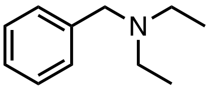 80%
3	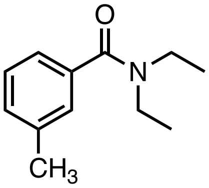	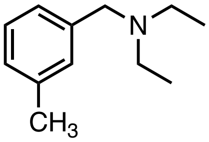 99%
4	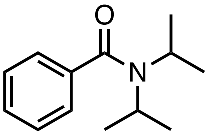	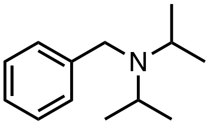 99%
5	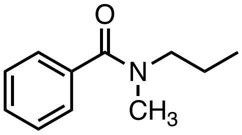	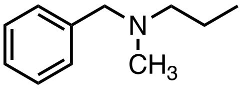 92%
6	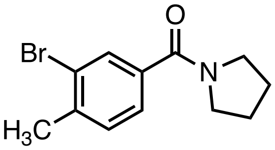	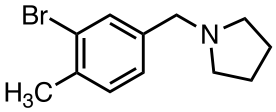 89%
7	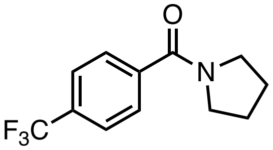	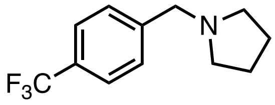 84%

[a] Reaction conditions: amide (5 mmol, 1 equiv), (iBu)$_2$AlBH$_4$ (5.5 mmol, 1.1 equiv.), anhydrous THF (5mL) were combined at 0 ºC. Once all the hydride was added the ice bath was removed and the reaction mixture continued to stir for 1 h, under argon atmosphere. [b] Isolated yield.

Aliphatic tertiary amides and lactams were also reduced efficiently by (iBu)$_2$AlBH$_4$ to the corresponding amines in very good yields (**Table 2.14**, entries 1-3). Lactams can be reduced either to acyclic amino alcohols or cyclic amines.[66] Reduction of lactams by either BMS[15] or DIBAL[67] afforded the cyclic amine. Similar to the parent hydrides, (iBu)$_2$AlBH$_4$ reduced 1-octyl-2-pyrrolidone to 1-octylpyrrolidine in 87% isolated yield (**Table 2.14**, entry 4). Most notably, 1-phenyl-

2-pyrrolidone was reduced to 1-phenylpyrrolidine in a 71% isolated yield (**Table 2.14**, entry 5). Reduction of this lactam with other reducing agents typically gives the amino-alcohol product, 4-(phenylamino)butan-1-ol.[66] Apparently, reductions using (iBu)$_2$AlBH$_4$ go through an imine intermediate leading to the cyclic amine product. *N*-methyl-2-piperidone and *N*-methylcaprolactam were reduced to give the 1-methylpiperidine-borane complex and 1-methylazepane-borane complex, respectively (**Table 2.14**, entries 6 and 7).

Table 2.14. Reduction of aliphatic amides and lactams using iBu$_2$AlBH$_4$^{a}

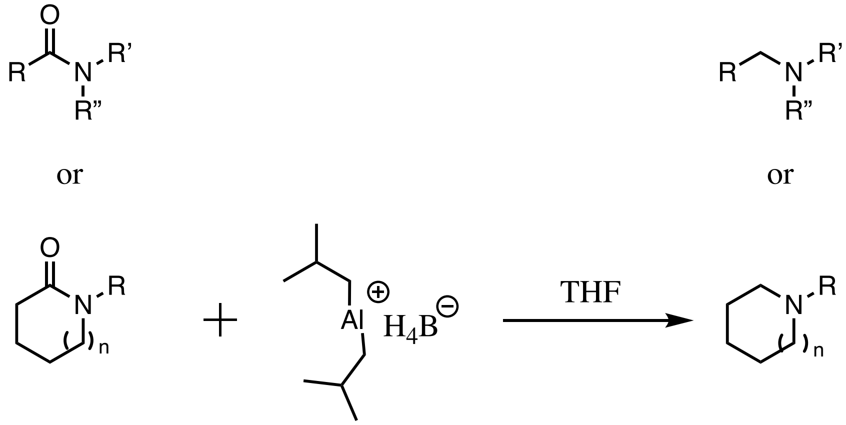

Entry	Amide	Product (Yield %)^b
1	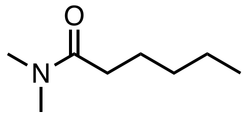	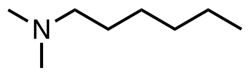 84%
2	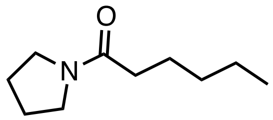	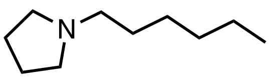 88%
3	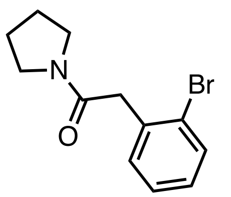	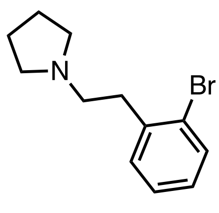 83%

4	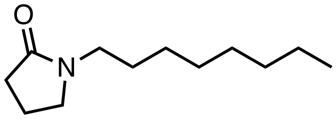	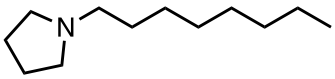 87%
5	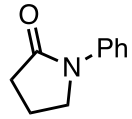	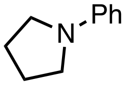 71%
6	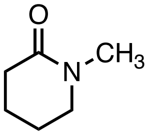	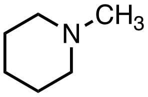 X
7	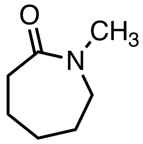	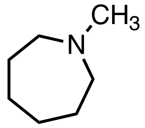 X

[a] Reaction conditions: amide (5 mmol, 1 equiv.), $(i\text{Bu})_2\text{AlBH}_4$ (5.5 mmol, 1.1 equiv.), anhydrous THF (5mL) were combined at 0 ºC. Once all the hydride was added the ice bath was removed and the reaction mixture continued to stir for 1 h, under argon atmosphere. [b] Isolated yield.

2.2.8. Chemoselective Reactions

As described above, $(i\text{Bu})_2\text{AlBH}_4$ is capable of reducing a wide range of functionalities, but the hallmark of a useful reducing agent is its ability to reduce a specific functional group in a multifunctional compound. Consequently, we examined whether $(i\text{Bu})_2\text{AlBH}_4$ would selectively reduce an aldehyde or ketone in the presence of a nitrile or ester. The reaction of $(i\text{Bu})_2\text{AlBH}_4$ and 4-cyanobeznaldehyde **1** illustrated the selective reduction of the aldehyde in the presence of a cyano group (**Scheme 2.10**). It is important to note that this selectivity occurs at 0 °C. When the reaction was performed at room temperature the nitrile was partially reduced (**Table 2.15**, entry 1). When BMS was subjected to **1** it reduced the carbonyl and retained the cyano group, but the reaction was much slower (**Table 2.15**, entry 3). With DIBAL, both functionalities reduced, thus offering no functional group selectivity (**Table 2.15**, entry 2). Similar results were observed for 4-cyanoacetophenone **2** and 4-cyanobenzophenone **3** with (*i*Bu)$_2$AlBH$_4$. Reaction of **2** and **3** at 0 ° C illustrate that the ketones were reduced preferentially over the nitrile to generate a single product, whereas a mixture of products was observed with DIBAL and BMS.

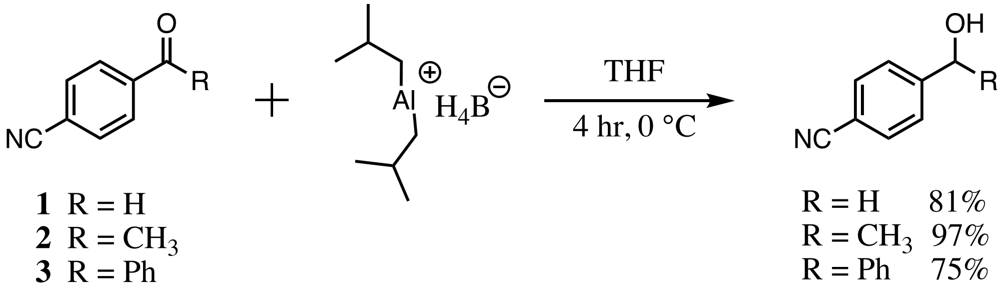

Scheme 2.10. Chemoselective Reductions of Aldehydes and Ketones with (*i*Bu)$_2$AlBH$_4$

Table 2.15. Chemoselective Reduction Between an Aldehyde or Ketone and a Nitrile using (*i*Bu)$_2$AlBH$_4$,[a] DIBAL,[b] and BMS[c]

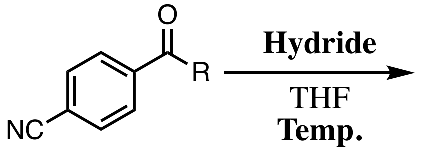

R = H
R = CH$_3$
R = Ph

Entry	Hydride	Temperature	Product (%)[d]	
1	*i*Bu)$_2$AlBH$_4$	25 °C	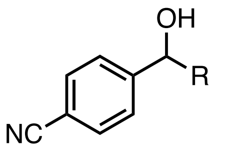 R = H 88% R = CH$_3$ 87% R = Ph 84%	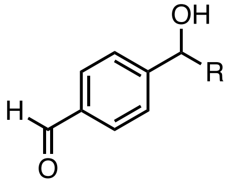 R = H 12% R = CH$_3$ 13% R = Ph 16%

2	DIBAL	0 °C	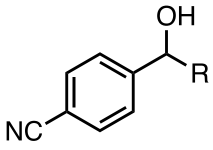 R = H 79% R = CH_3 18% R = Ph 17%	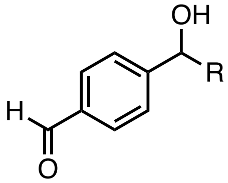 R = H 0% R = CH_3 82% R = Ph 83%
3	BMS	0 °C	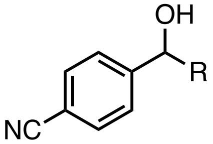 R = H 66%[e] R = CH_3 33%[e] R = Ph 42%[e]	

[a] Reaction conditions: substrate (1 equiv), $(i\text{Bu})_2AlBH_4$ (1 equiv.), anhydrous THF, 4 h, under argon atmosphere. [b] Reaction conditions: substrate (1 mmol, 1 equiv), DIBAL (4 equiv.), anhydrous THF, 5 h, under argon atmosphere. [c] Reaction conditions: substrate (1 equiv), BMS (1.33 equiv.), anhydrous THF, 3.5 h, under argon atmosphere. [d] Yield based on ^1H NMR. [e] Isolated yields

Further exploration into the selectivity of $(i\text{Bu})_2AlBH_4$ with bifunctional compounds led to a substrate containing an ester and an aldehyde or ketone substituent (**Scheme 2.11**). These reactions have to be conducted at -78 °C to in order to selectively reduce the carbonyl group of an aldehyde or ketone.

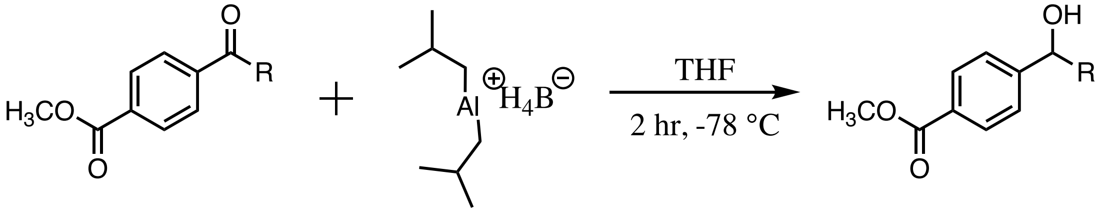

4 R = H
5 R = CH_3

R = H 55%
R = CH_3 77%

Scheme 2.11. Chemoselective Reduction of Aromatic Esters with $(i\text{Bu})_2AlBH_4$

For many of these multifunctional compound reductions, $NaBH_4$ can be used to achieve similar selectivity as that of $(i\text{Bu})_2AlBH_4$. However, $NaBH_4$ is soluble only in alcohol solvents and undergo solvolysis decomposition to produce H_2 gas. Diisobutylaluminum borohydride is more advantageous, because it has a wider solvent compatibility as it is soluble in both ethereal and hydrocarbons. Overall, the mixed metal hydride can be selective for aldehydes and ketones when in the presence of nitriles or esters.

One of the benefits of $(i\text{Bu})_2AlBH_4$ is its ability to reduce tertiary amides and nitriles in an efficient manner. However, the question remains if $(i\text{Bu})_2AlBH_4$ has a preference to react with one of these nitrogen compounds over the other. The results of the competitive reaction between 4-tolunitrile and N,N-diethyl-*m*-toluamide with $(i\text{Bu})_2AlBH_4$ are reported in **Scheme 2.12**. At room temperature, the nitrile and amide were both reduced. However, when the reaction mixture was cooled to -78 °C, clear selectivity for the reduction of the nitrile was achieved, producing the primary amine in good yields.

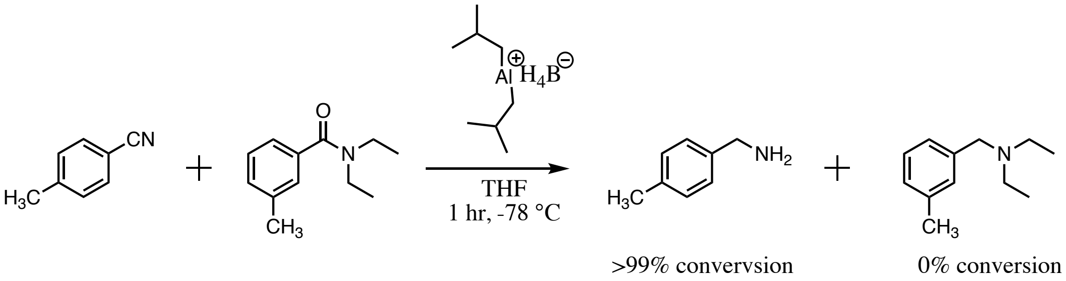

Scheme 2.12. Chemoselective Reduction of 4-tolunitrile with $(i\text{Bu})_2AlBH_4$

2.3. Conclusions

In summary, the work described in this chapter explored the reductive scope of diisobutylaluminum borohydride [$i(\mathrm{Bu})_2\mathrm{AlBH}_4$]. In a 1:1 ratio of borane dimethyl sulfide and diisobutylaluminum hydride (DIBAL), $i(\mathrm{Bu})_2\mathrm{AlBH}_4$ is generated and it is stable at ambient conditions. To make the binary hydride more accessible it is possible to synthesize $i(\mathrm{Bu})_2\mathrm{AlBH}_4$ from sodium borohydride and diisobutylaluminum chloride in a THF:tetraglyme mixture. Under ambient conditions, $i(\mathrm{Bu})_2\mathrm{AlBH}_4$ effectively and efficiently reduced aldehydes, ketones, carboxylic acids, and esters to the corresponding alcohols. It was found that the reduction of unsymmetric epoxides produced the more substituted alcohol. The binary hydride system can also reduce tertiary amides and nitriles to the corresponding amines. It should be noted that DIBAL is known to reduce tertiary amides to the corresponding aldehyde at low temperatures. Borane dimethyl sulfide is not a sufficiently strong reducing agent for the reduction of tertiary amides because the reaction requires long reaction times along with concurrent distillation of dimethyl sulfide. Additionally, $i(\mathrm{Bu})_2\mathrm{AlBH}_4$ showed to be selective towards aldehydes and ketones when in the presence of nitriles or esters. In a competitive reaction between a nitrile or a tertiary amide, the nitrile was reduced first. This new reducing agent is an attractive alternative to lithium aluminum hydride or borane tetrahydrofuran. Overall, $i(\mathrm{Bu})_2\mathrm{AlBH}_4$ is a relatively safe reducing agent that can reduce a wide variety of functionalities, and product isolation did not require column chromatography.

2.4. References

1. Brown, H. C.; Kim, S. C.; Krishnamurthy, S., Lithium Triethylborohydride as an Exceptionally Powerful and Selective Reducing Agent in Organic Synthesis. Exploration of the Reactions with Selected Organic Compounds Containgin Representative Functional Groups. *J. Org. Chem.* **1980,** *45*, 1-12.

2. Yoon, N. M.; Gyoung, Y. S., Reaction of Diisobutylaluminum Hydride with Selected Organic Compounds Containing Representative Functional Groups. *J. Org. Chem.* **1985,** *50*, 2443-2450.

3. Miller, A. E. G.; Biss, J. W.; Schwartzman, L. H., Reductions with Dialkylaluminum Hydrides. *J. Org. Chem.* **1959,** *24*, 627-630.

4. Choi, Y. M.; Yoo, M.; An, D. K., A New Method of Partial and Chemoselective Reduction of Nitriles to Aldehydes by Lithium Diisobutyl-*iso*-propoxyaluminum Hydride (LDBIPA). *Bull. Korean Chem. Soc* **2010,** *31*, 473-474.

5. Muñoz, J. d. M.; Alcázar, J.; Hoz, A. d. l.; Díaz-Ortiz, A., Application of flow chemistry to the reduction of nitriles to aldehdyes. *Tetrahedron Letters* **2011,** *52*, 6058-6060.

6. Thomas, S.; Collins, C. J.; Cuzens, J. R.; Spiciarich, D.; Goralski, C. T.; Singaram, B., Aminoborohydrides. 12. Novel Tandem S_nAr Amination-Reduction Reactions of 2-Halobenzonitriels with Lithium *N*,*N*-Dialkylaminoborohydrides. *J. Org. Chem.* **2001,** *66*, 1999-2004.

7. Bedi, D.; Brar, A.; Findlater, M., Transition metal- and solvent-free double hydroboration of nitriles. *Green Chem.* **2020,** *22*, 1125-1128.

8. Yao, W.; He, L.; Han, D.; Zhong, A., Sodium Triethylborohydride-Catalyzed Controlled Reduction of Unactivated Amides to Secondary or Tertiary Amines. *J. Org. Chem.* **2019,** *84*, 14627-14635.

9. Lu, Z.; Williams, T. J., A dual site catalyst for mild, selective nitrile reduction. *Chem. Commun.* **2014,** *50*, 5391-5393.

10. Szostak, M.; Sautier, B.; Spain, M.; Procter, D. J., Electron Transfer Reduction of Nitriles Using SmI_2-Et_3N-H_2O: Synthetic Utility and Mechanism. *Org. Lett.* **2014,** *16*, 1092-1095.

11. Rao, C. N.; Hoz, S., Photostimulated Reduction of Nitriles by SmI_2. *J. Org. Chem.* **2012,** *77*, 4029-4034.

12. Ding, Y.; Luo, S.; Weng, C.; An, J., Reductive Deuteration of Nitriles Using D_2O as a Deuterium Source. *J. Org. Chem.* **2019,** *84*, 15098-15105.

13. Simmons, B. J.; Hoffmann, M.; Hwang, J.; Jackl, M. K.; Garg, N. K., Nickel-Catalyzed Reduction of Secondary and Tertiary Amides. *Org. Lett.* **2017,** *19*, 1910-1913.

14. Haddenham, D.; Pasumanksy, L.; DeSoto, J.; Eagon, S.; Singaram, B., Reductions of Aliphatic and Aromatic Nitriles to Primary Amines with Diisopropylaminoborane. *J. Org. Chem.* **2009,** *74*, 1964-1970.

15. Brown, H. C.; Choi, Y. M.; Narasimhan, S., A Simple Technique to Achieve an Enhanced Rate of Reduction of Representative Organic Compounds by Borane-Dimethyl Sulfide. *J. Org. Chem.* **1982,** *47*, 3153-3163.

16. Brown, H. C.; Narasimhan, S.; Choi, Y. M., Improved Procedure for Borane-Dimethyl Sulfide Reduction of Primary Amides to Amines. *Synthesis* **1981,** *6*, 441-442.

17. Cabrita, I.; Fernandes, A. C., A novel efficient and chemoselective method for the reduction of nitriles using the system silane/oxo-rhenium complexes. *Tetrahedron* **2011,** *67*, 8183-8186.

18. Gandhamsetty, N.; Jeong, J.; Park, J.; Park, S.; Chang, S., Boron-Catalyzed Silylative Reduction of Nitriles in Accessing Primary Amines and Imines. *J. Org. Chem.* **2015,** *80*, 7281-7287.

19. Brown, H. C.; Krishnamurthy, S., Forty Years of Hydride Reductions. *Tetrahedron* **1979,** *35*, 567-607.

20. Gilmore, K.; Vukelić, S.; McQuade, D. T.; Koksch, B.; Seeberger, P. H., Continuous Reductions and Reductive Aminations Using Solid $NaBH_4$. *Org. Process Res. Dev.* **2014,** *18*, 1771-1776.

21. Fleck, T. J.; William W. McWhorter, J.; Dekam, R. N.; Pearlman, B. A., Synthesis of N-Methyl-N-{(1S)-1-[(3R)-pyrrolidin-3-yl]ethyl}amine. *J. Org. Chem.* **2003,** *68*, 9612-9617.

22. Magano, J.; Dunetz, J. R., Large-Scale Carbonyl Reductions in the Pharmaceutical Industry. *Org. Process Res. Dev.* **2012,** *16*, 1156-1184.

23. Prasanth, C. P.; Joseph, E.; Abhijith, A.; Nair, D. S.; Ibnusaud, I.; Raskatov, J.; Singaram, B., Stablization of $NaBH_4$ in Methanol Using a Catalytic Amount of NaOMe. Reduction of Esters and Lactones at Room Temperature without Solvent-Induced Loss of Hydride. *J. Org. Chem.* **2018,** *83*, 1431-1440.

24. Galatis, P.; Sollogoub, M.; Sinaÿ, P., *Encyclopedia of Reagents for Organic Synthesis*. John Wiley & SOns: New York, 2001.

25. Brown, H. C.; Subba Rao, B. C. J., A New Technique for the Conversion of Olefins into Organoboranes and Related Alcohols. *J. Am. Chem. Soc* **1956,** *78*.

26. Brown, H. C.; Subba Rao, B. C. J., Hydroboration of Olefins. A Remarkably Fast Room-Temperature Addition of Diborane to Olefins. *J. Org. Chem.* **1957,** *22*, 1136-1136.

27. Potyen, M.; Josyula, K. V. B.; Schuck, M.; Lu, S.; Gao, P.; Hewitt, C., Borane-THF: New Solutions with Improved Thermal Properties and Stability. *Org. Process Res. Dev.* **2007,** *11*, 210-214.

28. Lane, C. F., Reduction of Organic Compounds with Diborane. *Chem. Rev.* **1976,** *76*, 773-799.

29. Kollonitsch, J., Reductive Ring-Cleavage of Tetrahydrofurans by Diborane. *J. Am. Chem. Soc* **1961,** *83*, 1515.

30. Fujiwara, K.; Yasuda, S.; Mizuta, T., Reduction of CO_2 to Trimethoxyboroxine with BH_3 in THF. *Organometallics* **2014,** *33*, 6692-6695.

31. Patelli, N.; Calizzi, M.; Migliori, A.; Morandi, V.; Pasquini, L., Hydrogen Desorption Below 150 °C in MgH_2-TiH_2 Composite Nanoparticles: Equilibrium and Kinetic Properties. *J. Phys. Chem. C.* **2017,** *121*, 11166-11177.

32. Schouwink, P.; D'Anna, V.; Ley, M. B.; Daku, L. M. L.; Richter, B.; Jensen, T. R.; Hagemann, H.; Černy, R., Bimetallic Borohydrides in the System $M(BH_4)_2$-KBH_4 (M=Mg, Mn): On the Structural Diversity. *J. Phys. Chem. C.* **2012,** *116*, 10829-10840.

33. Snelling, R.; Saavedra, J. Z.; Bayrasy, P.; Abdollahian, Y.; Singaram, B., Binary reducing agents containing dichloroindium hydride for the selective, partial, or tandem reductions of bifunctional compounds consisting of halo-nitriles, halo-esters and halo-carboxylic acids. *Org. Chem. Front* **2015,** *2*, 133-140.

34. Saavedra, J. Z.; Resendez, A.; Rovira, A.; Eagon, S.; Haddenham, D.; Singaram, B., Reaction of $InCl_3$ with Various Reducing Agents: $InCl_3$-$NaBH_4$-Mediated Reduction of Aromatic and Aliphatic Nitriles to Primary Amines. *J. Org. Chem.* **2012,** *77*, 221-228.

35. Ramachandran, P. V.; Kulkarni, A. S.; Zhao, Y.; Mei, J., Amine-boranes bearing borane-incompatible functionalities: application to selective amine protection and surface functionalization. *Chem. Commun.* **2016,** *52*, 11885-11888.

36. Taylor, M. D.; Grant, L. R.; Sands, C. A., A Convenient Preparation of Pyridine-Borane. *J. Am. Chem. Soc* **1955,** *77*, 1506-1507.

37. Brown, H. C.; Heim, P.; Yoon, N. M., Selective Reductions. XV. Reaction of diborane in tetrahydrofuran with selected organic compounds containing representative functional groups. *J. Am. Chem. Soc* **1970,** *92*, 1637-1646.

38. Lawrence, S. A., *Amines: Synthesis, Properties, and Application*. Cambridge University: Cambridge, 2004.

39. Lemoine, D.; Jiang, R.; Taly, A.; Chataigneau, T.; Specht, A.; Grutter, T., Ligand-Gated Ion Channels: New Insights into Neurological Disorders and Ligand Recognition *Chem. Rev.* **2012,** *112*, 6285-6318.

40. Heiss, J. D.; Argersinger, D. P.; Theodore, W. H.; Butman, J. A.; Sato, S.; Khan, O. I., Convection-Enhanced Delivery of Muscimol in Patients with Drug-Resistatn Epilepsy *Neurosurgery* **2019,** *85*, E3-E15.

41. Wübbolt, S.; Oestreich, M., Exhaustive Chemoselective Reduction of Nitriles by Catalytic Hydrosilylation Involving Cooperative Si-H Bond Activation. *Synlett* **2017,** *28*, 2411-2414.

42. Nystrom, R. F.; Brown, W. G., Reduction of Organic Compounds by Lithium Aluminum Hydride. III. Halides, Quinones, Miscellaneous Nitrogen Compounds. *J. Am. Chem. Soc* **1948,** *70*, 3738-3740.

43. Brown, W. G., Reductions by Lithium Aluminum Hydride In *Organic Reactions*, John Wiley and Sons, Inc. : 2011; pp 469-509.

44. Brown, H. C.; Yoon, N. M., Reaction of Aluminum Hydride with Selected Organic Compounds Containing Representative Functional Groups. Comparison of the Reducing Characteristics of Lithium Aluminum Hydride and Its Derivatives. *J. Am. Chem. Soc* **1966,** *88*, 1464-1472.

45. Jaganyi, D.; Mzinyati, A., An ^{11}B NMR spectrscopy investigation of the mechanism of the reduction of nitriles by BH_3SMe_2. *Polyhedron* **2006,** *25*, 2730-2736.

46. Crimmins, M. T.; Jung, D. K.; Gray, J. L., Synthetic Studies on the Ginkgolides: Total Synthesis of (+/-)-Bilobalide. *Journal of American Chemical Society* **1993,** *115*, 3146-3155.

47. Brown, H. C.; Narasimhan, S.; Somayaji, V., Selective Reductions. 32. Structural Effects on the Reduction of Epoxides by Lithium Triethylborohydride. A Kinetic Study. *J. Org. Chem.* **1983,** *48*, 3091-3096.

48. Eliel, E. L.; Delmonte, D. W., The Mechanism of Halide Reductons with Lithium Aluminum Hydride. VI. Reduction of Certain Bromohydrins and Epoxides. *J. Am. Chem. Soc* **1958,** *80*, 1744-1752.

49. Ashby, E. C.; Cooke, B., The Mechanism of Mixed Hydride Reductions. Effects of Reagent Composition, Nature of Halogen, and Solvating Ligand on the Mechansim of Epoxide Reduction. *J. Am. Chem. Soc* **1969,** *90*, 1625-1630.

50. Cooke, B.; Ashby, E. C.; Lott, J., Reductions Using Alkoxyaluminum Hydrides. I. Reduction of Epoxides. *J. Org. Chem.* **1968,** *33*, 1132-1136.

51. Kim, S.; Ahn, K. H., Ate Complex from Diisobutylaluminum Hydride and *n*-Butyllithium as a Powerful and Selective Reducing Agent for the Reduction of Selected Organic Compounds Containing Various Functional Gropus. *J. Org. Chem.* **1984,** *49*, 1717-1724.

52. Fuchs, R.; VanderWef, C. A., Direction of Ring Opening in the Reduction of p-Substituted Styrene Oxides with Lithium Borohydride. *J. Am. Chem. Soc* **1954,** *76*, 1631-1634.

53. Brown, H. C.; Rao, B. C. S., Hydroboration. III. The Reduction of Organic Compounds by Diborane, an Acid-type Reducing Agent. *J. Am. Chem. Soc* **1960,** *82*, 681-686.

54. Pasto, D. J.; Cumbo, C. C.; Hickman, J., Transfer Reactions Involving Boron. VIII. The Stereochemistry and Mechanism of the Reduction of Epoxides with Borane-d_3-Tetrahydrofuran. *J. Am. Chem. Soc* **1966,** *88*, 2201-2207.

55. Brown, H. C.; Yoon, N. M., Reaction of Diborane in Tetrahydrofuran with Styrene Oxide and Related Epoxides in the Presence of Boron Trifuloride. A Convenient Anti-Markovnikov Reductive Opening of Such Epoxides. *Chem. Commun.* **1968**, 1549-1550.

56. Lane, C. F.; Myatt, H. L.; Daniels, J.; Hopps, H. B., Reduction of Aromatic Carboxylic Acids in the Presence of Trimethyl Borate. *J. Org. Chem.* **1974,** *39*, 3052-3054.

57. Zakharkin, L. I.; Khorlina, I. M., *Zh. Obshch. Khim.* **1964,** *34*, 1029.

58. Ducry, L.; Roberge, D. M., Dibal-H Reduction of Methyl Butyrate into Butyraldehyde using Microreactors. *Org. Process Res. Dev.* **2008,** *12*, 163-167.

59. Ong, D. Y.; Yen, Z.; Yoshii, A.; Imbernon, J. R.; Takita, R.; Chiba, S., Controlled Reduction of Carboxamides to Alcohols or Amines by Zinc Hydrides. *Angew. Chem. Int. Ed.* **2019,** *58*, 4992-4997.

60. Newman, M. S.; Fukunaga, T., The Reduction of Amides to Amines via Nitriles by Lithium Aluminum Hydride. *J. Am. Chem. Soc* **1960,** *82*, 693-696.

61. Smith, A. M.; Whyman, R., Review of Methods for the Catalytic Hydrogenation of Carboxamides. *Chem. Rev.* **2014,** *114*, 5477-5510.

62. Jr., S. E. E.; Mack, C. H.; Jr., W. J. C., Dehydration of primary amides with sodium borohydride. *J. Org. Chem.* **1967,** *32*, 846-847.

63. Yang, C.; Jr., C. U. P., Reductions of Organic Functional Groups Using $NaBH_4$ or $NaBH_4$/LiCl in Diglyme at 125 to 162 °C. *Synthetic Communications* **1998,** *28*, 2027-2041.

64. Brown, H. C.; Heim, P., Selective reductions. XVIII. Fast reaction of primary, secondary, and tertiary amides with diborane. Simple, convenient procedure for the conversion of amides to the corresponding amines. *J. Org. Chem.* **1973,** *38*, 912-916.

65. Brown, H. C.; Rao, B. C. S., A New Powerful Reducing Agent-Sodium Borohydride in the Presence of Aluminum Chloride and Other Polyvalent Metal Halides. *J. Am. Chem. Soc* **1956,** *78*, 2582-2588.

66. Flaniken, J. M.; Colins, C. J.; Lanz, M.; Singaram, B., Aminoborohydrides. 11. Facile Reduction of *N*-Alkyl Lactams to the Corresponding Amines Using Lithium Aminoborohydrides. *Org. Lett.* **1999,** *1*, 799-801.

67. Winterfeldt, E., Applications of Diisobutylaluminum Hydride (DIBAH) and Triisobutylaluminum (TIBA) as Reducing Agents in Organic Synthesis. *Synthesis* **1975**, 617-630.

CHAPTER 3

A Mesoporous Nanoparticle Supported Nickel Boron Composite for the Catalytic Reduction of Nitroarenes

3.1. Introduction

3.1.1 History of the Reduction of Nitroarenes

Anilines are essential compounds as they are found in the production of dyes, pharmaceuticals, fertilizers, pesticides, and numerous polymers.[1] Synthesis of aniline and its analogues can come from the reduction of nitroarenes, a process that largely requires a metal catalyst and a hydrogen source. Various metal catalysts can be used and will be discussed further in this chapter. The source of hydrogen is equally as varied but one of the most common is a pressurized H_2 cylinder, which involves specific safety precautions. Alternatively, hydrogen made *in situ* from the hydrolysis of sodium borohydride ($NaBH_4$) or degradation of hydrazine hydrate ($N_2H_4 \bullet H_2O$) are seen as safer and more stable chemical sources of the gas.[2-7]

The accepted mechanism for the reduction of nitroarenes was first modeled in the 19th century using electrochemical experiments. This pathway has persisted regardless of metal catalyst and follows two possible routes: direct reduction or condensation followed by reduction (**Scheme 3.1**).[8] In both pathways the first step is the formation of the nitroso (**A**) and hydroxylamine (**B**) species. At that point, aniline can be formed directly from the hydroxylamine intermediate. The second possible pathway has the nitroso and hydroxylamine condense to form a series of azoxy (**C**), azo (**D**), and hydrazo (**E**) species before reducing to aniline. Depending upon the catalyst and hydrogen source used, some of these intermediates can be observed through gas chromatography (GC) or nuclear magnetic resonance (NMR) spectroscopy thus revealing that specific catalysis mechanism.

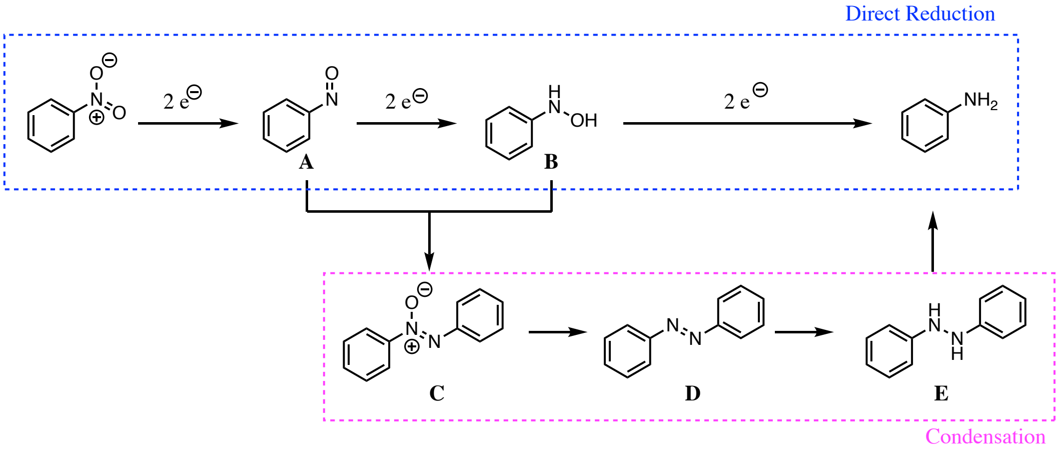

Scheme 3.1. Two possible mechanisms for the reduction of nitroarenes to aniline.

One of the oldest industrial methods of reducing nitroarenes was discovered by Béchamp (1854).[9] Iron in aqueous acid was refluxed with the nitroarene to produce aniline. Derivations of his original methodology have included using zinc and tin; however, shortcomings of this process, included stoichiometric amounts of metal, the generation of vast amounts of waste, and slow reaction rates. Consequently, this process is not useful in modern practice. Focus has since shifted to catalytic hydrogenation and hydrogen from non-acidic sources.

Metal catalyzed reductions have become more popular, as they do not require stoichiometric quantities of the catalyst, which is an economic necessity when some of these methodologies use expensive noble metals, including platinum,[10] palladium,[11] or ruthenium.[12] Other drawbacks associated with these heterogeneous catalysis systems can include large energy consumption and safety hazards associated with the use of compressed hydrogen gas at elevated temperatures and pressures. First row transition metals, like iron, cobalt, and nickel, are earth abundant, making them cheaper and easier reagents to obtain and use.[8]

While iron-mediated reduction of nitroarenes has been known for over a century, modern methodologies have found a way to use it catalytically. Iron oxide catalysts have found success in reducing nitroarenes with the aid of hydrazine hydrate. In one example, iron(III) chloride when reduced by sodium hydroxide (2M) forms an iron oxide hydroxide catalyst that has been shown to reduce nitroarenes in the presence of nitriles, azo groups, and carboxylic acids (**Scheme 3.2**).[13] However, the methodology is susceptible to a competitive condensation reaction if an aldehyde is present, causing the production of benzylidene-amines or dibenzylidine-hydrazines. Through Hammett plot analysis, it was found that the reaction rate increased when an electron-withdrawing group was present but decreased with electron-donating substituents.

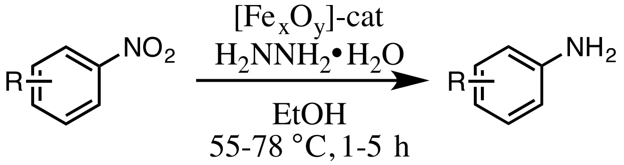

Scheme 3.2. Iron oxide hydroxide catalyst used to reduce nitroarenes in the presence of hydrazine hydrate.

In a one-pot method, Cantillo and colleagues were able to reduce a variety of nitro-containing substrates with their *in situ* generated iron oxide nanocrystals.[14] A brief chemoselective study was conducted and saw that no dehalogenation nor amide reduction occurred, therefore generating the corresponding aniline products in excellent yields (92-84% yield). Aliphatic nitro-substrates and aromatic azides were rapidly reduced in 2-3 min when under microwave conditions (150 °C) (96-99% yield). One of the major intentions for using iron oxide nanocrystals was to utilize their magnetic nature for ease of collection followed by subsequent catalyst reuse. The group found that the catalyst could be used up to three times before seeing a decline in conversion. Inductively coupled plasma-mass spectrometry (ICP-MS) revealed continued loss of iron (~5%) each time the catalyst was recycling, which was likely a cause of the gradual decline in catalytic efficiency.

It has been reported that several of these iron oxide catalysts undergo an Fe^{2+}/Fe^{3+} redox pathway with hydrazine hydrate to form the necessary six electrons required of a direct reduction pathway (**Scheme 3.1**).[14, 15] Evidence of this pathway has included observing the hydroxylamine with GC-MS analysis.[16] It was reasoned that if the hydroxylamine is observed then the nitroso species forms rapidly thus cannot be detected.

In addition to iron, nickel-based catalysts have been well used in the reduction of nitroarenes, notably the catalyst Raney Nickel (Raney Ni). Commercial Raney Ni can be used as a hydrogenation catalyst for many functionalities, including nitriles, olefins, aldehydes, ketones, and nitro groups.[17, 18] Originally developed at the University of Wisconsin, Raney Ni is a bimetallic catalyst of nickel and aluminum. It was developed as an alternative to the high-pressure Pt and Pd catalysts that were in use at that time. Almost comparable to that of the noble metals, Raney Ni gained in popularity in part because it can hydrogenate nitroarenes at low pressures. However, due to the fine Ni and Al particles present, the catalyst can ignite if dried in air.[19]

It is then advantageous to develop catalysts that does not share similar pyrophoric qualities. A nickel-catalyzed hydrosilylative process was developed and found great utility in reducing analogues of nitro-containing 3,4-dihydropyrimidin-2(1H)-one.[20] Cyano, ester, and azide substituents were well tolerated, affording only reduction of the nitroarene. Interestingly, a trimetallic catalyst was created combining nickel, cobalt, and iron to create Ni-doped cobalt ferrite nanoparticles.[21] These nanoparticles combined with sodium borohydride ($NaBH_4$) reduced 4-nitrophenol to 4-aminophenol. Although this catalyst was not subjected to a wide substrate scope of nitroarenes, it is interesting to note the use of $NaBH_4$. In their report, $NaBH_4$ was used as the hydrogen source; however, a large excess was used in the reaction. It was also noted that once all the reagents were combined, the solution turned from yellow to black, which they took as indicative as a complete reduction of the nitro group. However, there is a class of amorphous catalysts where the black precipitate is an iconic feature when metal salts are reduced by borohydrides.

3.1.2. History of Metal Boron Composites

Amorphous heterogeneous catalysts composed of mixtures of transition metal and various boron species, have a long history of success in a wide variety of reduction reaction schemes.[22-25] These catalysts are formed from reacting metal salts (typically those of Ni or Co) with $NaBH_4$. In protic solvents at ambient pressure and temperature, most salts of the first row transition metals, to the left of copper, generate precipitates containing various boron species when reacted with excess $NaBH_4$, whereas copper and noble metal salts with more favorable reduction potentials tend to give pure metallic phases.[26] In the case of nickel (and similarly for cobalt), these precipitates have historically been referred to as amorphous nickel borides (Ni_3B, Ni_2B, etc.), a designation initially based on a combination of elemental analysis and powder X-ray diffraction studies of the crystalline structures evolved upon heating in inert atmosphere.[27-29] These amorphous precipitates are now known to be more structurally complex. They possess a variety of possible compositions and morphologies, depending on the choice of synthetic parameters (solvent system, pH, temperature, mixing rate and the presence of oxygen in solution), the ratio of borohydride to nickel reacted, and the choice of nickel salt precursor.[26, 30]

One of the first reports describing the combination of metal salts with $NaBH_4$ was focused on hydrogen generation. Schlesinger's group found that metal salts could act as catalytic accelerators to promote H_2 generation.[3] In aqueous media, $NaBH_4$ reduced the metal salts (such as $NiCl_2$ and $CoBr_2$) to their corresponding metallic (M^0) phase, while undergoing hydrolysis to form borate species and liberate hydrogen gas (**equation 1**).[3, 31]

$$BH_4^- + 2M^{2+} + 2H_2O \rightarrow 2M + BO_2^- + 4H^+ + 2H_2 \qquad (1)$$

To explain the characteristically high activity of amorphous catalysts such as nickel boron and cobalt boron composites (NBC and CBC, respectively), earlier works in this field suggested the presence of a direct metal-boron interaction based on X-ray photoelectron spectroscopy (XPS) data. One scenario put forward is that electron donation occurs from boron to symmetry related transition metal d-orbitals, and therefore increases catalytic activity through electron enrichment of the metal surface, while also sacrificially protecting the metal from oxidation.[30, 32-38] However, a review of the previously published XPS data reveals a certain amount of ambiguity in assigning both the B 1s and Ni or Co 2p binding energy shifts to that of the corresponding borides, as well as debate about the direction of electron donation between the metal and boron, in both the amorphous and crystalline compounds.[39]

With careful use of electron microscopy and elemental analysis, some authors have shown that bulk NBC and CBC powders are nanocomposites comprising single-nanometer sized crystalline metal particles imbedded in an amorphous matrix containing boron oxides (transition or alkali metal borates, (poly)borates, etc.).[40-45] Although many of these authors invoke the presence of borides, they presume that the main function of the amorphous matrix is to physically prevent sintering and rapid oxidation of the catalytically active metal particles during synthesis, thereby preserving the large catalytic surface area claimed to be responsible for high activity.

While the exact nature of the metal-boron interaction in these amorphous materials remains uncertain, it is known that crystalline borides of transition metals are routinely formed under much more energetically demanding conditions than those of protic solvent synthesis at near-ambient conditions. Traditional nickel borides are synthesized in solid state reactions such as laser ablation or melt quenching of elemental Ni and B,[46] or in non-protic solvent systems at elevated temperatures (~90 °C).[26] Given that borohydrides are known to decompose readily in protic solvents[39] to produce H_2 and various borates ($B(OH)_4^-$, BO_2^-, B_2O_3, polyborates, etc.), and given that this process is autocatalyzed *in situ* by the very same precipitates formed during the reaction of borohydrides with certain transition metal salts, particularly Ni^{2+} and Co^{2+},[3] it seems self-evident that protic solvent synthesis routes cannot produce true transition metal borides. It is much more plausible that such reactions primarily produce oxides of boron, which may then interact strongly with metallic precipitates to form amorphous transition metal and borate composites.[47]

Regardless of the specific bonding and composition of these NBC or CBC catalysts, they have shown themselves to be valuable catalysts. After Schlesinger's initial foray into the synthesis of borohydride reduced metal salts, Brown expanded upon the work by taking the resultant black precipitate and using it as a hydrogenation catalyst.[48] The synthesis of the black solid in aqueous media, termed P-1 Ni catalyst, displayed good reactivity in hydrogenating alkenes and suffered less double bond migration compared to Raney Ni. An even more significant advantage to the P-1 Ni catalyst was that it was not pyrophoric, a trait Raney Ni suffers from. A second generation of this nickel-based catalyst was synthesized again from a nickel salt and $NaBH_4$, but this time in ethanol. Named P-2 Ni catalyst, it exhibited greater selectivity as it underwent partial reduction of conjugated dienes and reduced alkynes to cis alkenes.[22]

The reductive abilities of the amorphous catalysts have been particularly successful at reducing nitroarene compounds to their corresponding aniline derivatives.[4, 49] In a one-pot method, Nose combined nickel chloride hexahydrate ($NiCl_2 \bullet 6H_2O$) with $NaBH_4$ and a nitroarene (*in situ* catalyst formation).[49] The reaction mixture was stirred at room temperature to afford the corresponding aniline analogues (76-95%). Under this catalytic system halides and carboxylic acids were tolerated, solely reducing the nitro group. They were pleasantly surprised to discover that nitroso, azoxy, azo, and hydroxylaminobenzenes were rapidly reduced to aniline as well. These last few reactions suggest that the reduction occurs through the condensation pathway mentioned earlier (**Scheme 3.1**).

Three decades later, the reduction of nitroarenes by these amorphous catalysts are still being studied. In one report, Ni-Co bimetallic nanoparticles were synthesized by combining $NiCl_2•6H_2O$ and $CoCl_2$ with an ethanolic solution of $NaBH_4$, producing a black precipitate.[4] These nanoparticles were shown to have a smaller particle size, average diameter of 2.5 nm, than the individual Ni and Co nanoparticles. This would then indicate that there were more active sites for interaction with the nitroarene. It would then be advantageous if these highly active nanoparticles could be recycled and reused for multiple reactions. However, the catalyst showed only moderate performance when reused, with 56% aniline isolated compared to the 96% isolated yield when fresh catalyst was used. Through transmission electron microscopy (TEM) imaging and XPS data, it was concluded that particle aggregation and oxidation were the causes for the product depletion.

The reusability of these metal boron catalysts is typically limited due to particle sintering, agglomeration, and surface oxidation. More recently it has been shown that supporting these composites on inert scaffolds (such as titania, silica gel or mesoporous silica nanoparticles) can enhance activity and reusability, compared to the bulk powders, by increasing catalyst surface area and stabilizing against particle agglomeration. In one example, a Ni boron composite catalyst was synthesized within nanocellulose to aid in reducing particle agglomeration.[7] The hypothesis was that the positively charged Ni ions would associate with the negatively charged carboxylates on the nanocellulose and thus allow for even particle dispersion and prevent particle agglomeration. In addition to reducing a variety of nitroarenes and conducting a tandem reduction and epoxide ring opening reaction to produce β-amino alcohols, the nanocellulose nickel boron catalyst was reused for multiple reaction cycles. As shown in **Table 3.1**, high isolated yields were obtained when 4-nitrobenzoic acid was reduced with the catalyst even after the 5th cycle. Longer reaction times were required, indicating that the surface morphology was changing and likely lessening the catalyst's overall reactivity. It is important to note that after each cycle, additional $NaBH_4$ was added to maintain the metallic Ni and likely to remove any oxide layer potentially forming.

Table 3.1. Recyclability of Nickel Boron Composite Catalyst Supported on Nanocellulose[a]

Cycle	**Time (min)**	**Yield (%)**[b]
1st	12	96
2nd	15	95
3rd	19	96
4th	50	96
5th	120	83

[a] Reaction conditions: nanocellulose (4.0 mL, 0.01 wt%), $NiCl_2$ (0.0015 mmol), and $NaBH_4$ (1.5 mmol) were combined and allowed to react at 25 °C. After 1 min, 4-nitrobenzoic acid (0.6 mmol) was added. [b] Isolated yield.

Further illustrating the usefulness of placing the metal catalysts on a support, Petal and coworkers compared the morphology of bulk cobalt boron nanoparticles to the nanoparticles embedded into nonporous silica and mesoporous silica particles.[50] When examining the electron microscopy images, the bulk nanoparticles appeared as spheres (diameter 30-40 nm) crowding together. The addition of the nonporous silica to the catalyst allowed the nanoparticles to disperse but the nanoparticle size remained similar to that of the bulk catalyst. When the cobalt boron catalyst was loaded onto the mesoporous silica, the nanoparticle size decreased (~10 nm) and greater particle dispersion was observed. This led the authors to conclude that because of the many mesopore channels present, the catalyst can grow without agglomerating. The varying particle morphology appeared to dictate the reactivity of the catalyst, with the mesoporous silica being the most reactive, followed by the nonporous, and lastly the bulk.

Several of these catalysis schemes have also benefited from the use of safer sources of hydrogen, such as $N_2H_4{\bullet}H_2O$.[2, 4-7] Hydrazine itself is toxic but the hydrated form is less harmful. Advantageously, $N_2H_4{\bullet}H_2O$ does not require pressure or heat to form H_2 and will generate it *in situ*, only producing N_2 as the byproduct. These qualities have made $N_2H_4{\bullet}H_2O$ a more attractive source of hydrogen. Additionally, a pattern has emerged that, of the catalysis research that use $N_2H_4{\bullet}H_2O$, more functional groups are tolerated. In particular, nitroarenes containing reducible functionalities like nitriles,[6, 51] aldehydes and ketones,[6, 51, 52] alkenes,[4, 51] and alkynes[4] remained untouched after the reaction, a trait that is not seen when pressurized hydrogen or hydrogen from $NaBH_4$ is used.[7, 24, 51, 53, 54]

Hydrazine's selectivity is likely due to how it degrades. The catalytic decomposition of hydrazine has been well known to produce a diimide intermediate, which then undergoes further degradation into nontoxic $N_{2(g)}$ (**equations 2** and **3**).[14, 16, [52, 55] The diimide then reacts preferentially with the nitro substituent before decomposing into N_2.

$$N_2H_4 \rightarrow N_2H_2 + e^- + 2H^+ \qquad (2)$$

$$N_2H_2 \rightarrow N_2 + 2e^- + 2H^+ \ (3)$$

The motivation for this project was to investigate the safe and economically efficient reduction of nitroarenes using $N_2H_4 \bullet H_2O$ and a reusable amorphous nickel boron composite (NBC) catalyst, derived from the reaction of Ni^{2+} salts with $NaBH_4$, and supported on mesoporous aluminosilicate nanoparticles (MASN) (**Scheme 3.3**). In the course of this work, fundamental questions arose concerning the difference in physical character between supported and unsupported versions of NBC. Therefore, the bulk NBC and supported NBC-MASN catalysts studied here are not referred to as *nickel boride*, in recognition that the exact identities of the boron species present in such composites are still not entirely known. Additionally, NBC-MASN was found to be an efficient, recyclable, and selective catalyst for the reduction of nitroarene compounds.

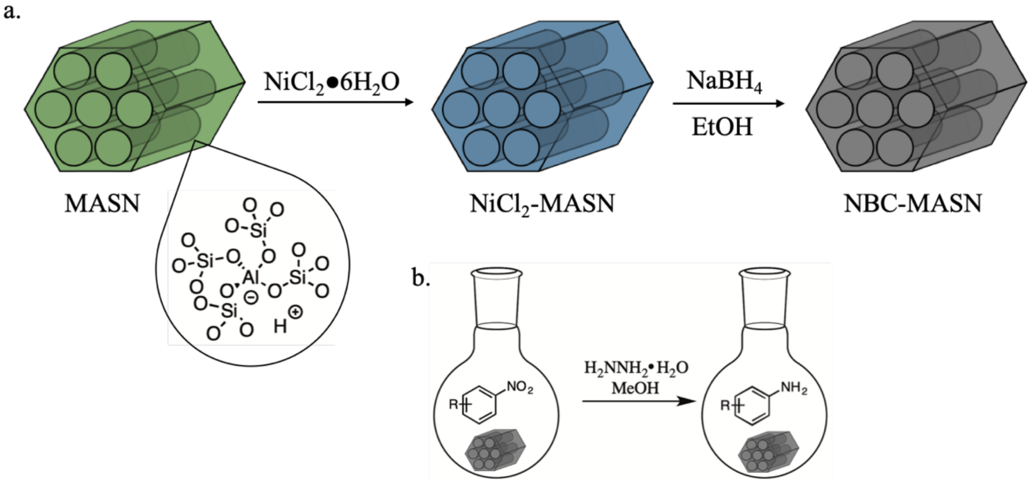

Scheme 3.3. Schematic illustration of (a) the synthesis and (b) use of NBC-MASN catalyst for the reduction of nitroarenes with hydrazine hydrate.[56]

3.2. Results and Discussion

3.2.1 Metal Screening

This work began by screening a number of catalysts made from different transition metal salts reacted with sodium borohydride ($NaBH_4$) in ethanol, for the reduction of *p*-nitrotoluene to *p*-toluidine using hydrazine hydrate ($N_2H_4 \cdot H_2O$) (**Table 3.2**). Zinc, indium, and copper salts did not perform the reduction as only starting material was observed after 24 h of reaction time (entries 1-4). It was found that $NiCl_2 \cdot 6H_2O$ was the most suitable precursor in forming a catalyst to this effect (entry 5). Control experiments were also conducted and show that both the metal catalyst and $NaBH_4$ are required for the reduction reaction to occur (entries 8-10). When the hydrogen source was changed from $N_2H_4 \cdot H_2O$ to hydrazine acetate minimal amounts of *p*-toluidine was produced, indicating that $N_2H_4 \cdot H_2O$ was the superior hydrogen source (entries 12 and 13). Supporting the catalyst, which we have termed nickel boron composite (NBC), on an inert scaffold made of mesoporous aluminosilicate nanoparticles (MASN) improved catalytic activity (entry 11).

Table 3.2. Catalyst screening results.[a]

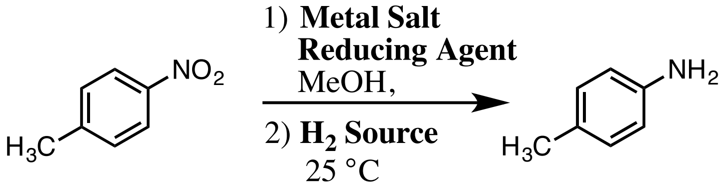

Entry	Metal Salt	Reducing Agent	Support	H_2 Source	Yield (%)[b]
1	$ZnBr_2$	$NaBH_4$	--	N_2H_4•H_2O	0%
2	$InCl_3$	$NaBH_4$	--	N_2H_4•H_2O	0%
3	$CuCl_2$	$NaBH_4$	--	N_2H_4•H_2O	0%
4	$InBr_3$	$NaBH_4$	--	N_2H_4•H_2O	0%
5	$NiCl_2$•$6H_2O$	$NaBH_4$	--	N_2H_4•H_2O	85%
8	$NiCl_2$•$6H_2O$	--	--	N_2H_4•H_2O	0%
9	--	$NaBH_4$	--	N_2H_4•H_2O	0%
10	--	$NaBH_4$	MASN	N_2H_4•H_2O	0%
11	$NiCl_2$•$6H_2O$	$NaBH_4$	MASN	N_2H_4•H_2O	94%
12	$NiCl_2$•$6H_2O$	$NaBH_4$	--	N_2H_4•Acetate	0%
13	$NiCl_2$•$6H_2O$	$NaBH_4$	MASN	N_2H_4•Acetate	15%[c]

[a] Reaction conditions: nitroarene (2 mmol), metal salt (10 mol%), reducing agent (20 mol%), hydrazine hydrate (10 mmol), MeOH (8 mL), 25 °C, 24 h, under argon atmosphere. [b] Isolated yield. [c] Ratio based on NMR.

In their work to remove organosulfur compounds from fossil fuels, the Oliver research group developed MASN as an appropriate support for their silver-based adsorbent.[57] They found that the addition of aluminum allowed their silver nanoparticles to adhere more effectively to the mesoporous silica nanoparticles (MSN). The aluminum ions create mildly negative surface charges that would electrostatically attract the silver ions into the mesochannels much better than the neutral MSN. Confirmation through inductively coupled plasma optical emission spectroscopy (ICP-OES) showed that negligible amounts of the silver nanoparticles appeared after the desulfurization reaction, suggesting tight coordination to the MASN. Subsequent electron microscopy imaging showed the presence of the silver ions within the MASN mesochannels further demonstrating the interaction between the silver nanoparticles to the support. Therefore, in an effort to improve the NBC catalyst, MASN was chosen as the support owing to the material's robust aluminosilicate structure, high surface area (~100 nm average diameter, ~1000 $m^2 \cdot g^{-1}$), and coordination with metal nanoparticles.

It was hypothesized that these features would allow for good incorporation of Ni^{2+} into the support during impregnation with $NiCl_2 \bullet 6H_2O$, and also slow diffusion of Ni^{2+} out of MASN during reaction of dried $NiCl_2$-MASN with $NaBH_4$ in absolute ethanol. Attempts to support NBC on non-aluminum MSN resulted in a greater quantity of large, detached NBC particles formed separate from the MSN support, as observed by electron microscopy (**Figure 3.1**). The better retention and slowed diffusion of Ni^{2+} from MASN appears to allow for even distribution of the resulting composite material formed close to the MASN surface, and possibly anchored within its mesochannels.

Low temperature (0 °C) synthesis was likewise chosen to allow for slower and more complete reaction of Ni^{2+} with BH_4^-. Indeed, the synthesis of NBC-MASN was found to take approximately 2 h to complete, compared to approximately 20 min for the synthesis of unsupported NBC.

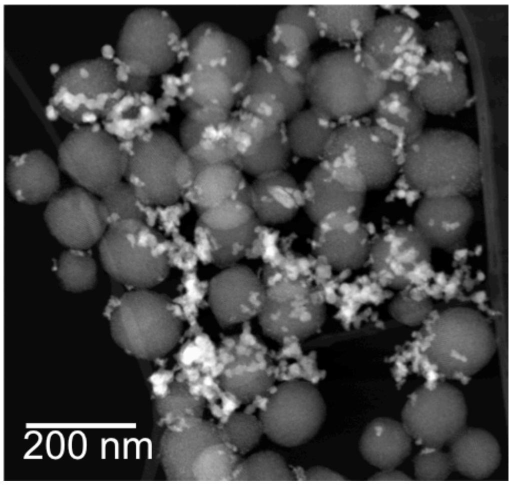

Figure 3.1. NBC supported on mesoporous silicate nanoparticles (NBC-MSN), showing large particles of NBC not bound to MSN.

The initial catalysis reaction using fresh NBC-MASN in the reduction of *p*-nitrotoluene to *p*-toluidine reached completion after 2 h. Subsequent reuse cycles of the catalyst, however, showed progressively longer incubation periods to achieve full conversion of *p*-toluidine (**Figure 3.2**).

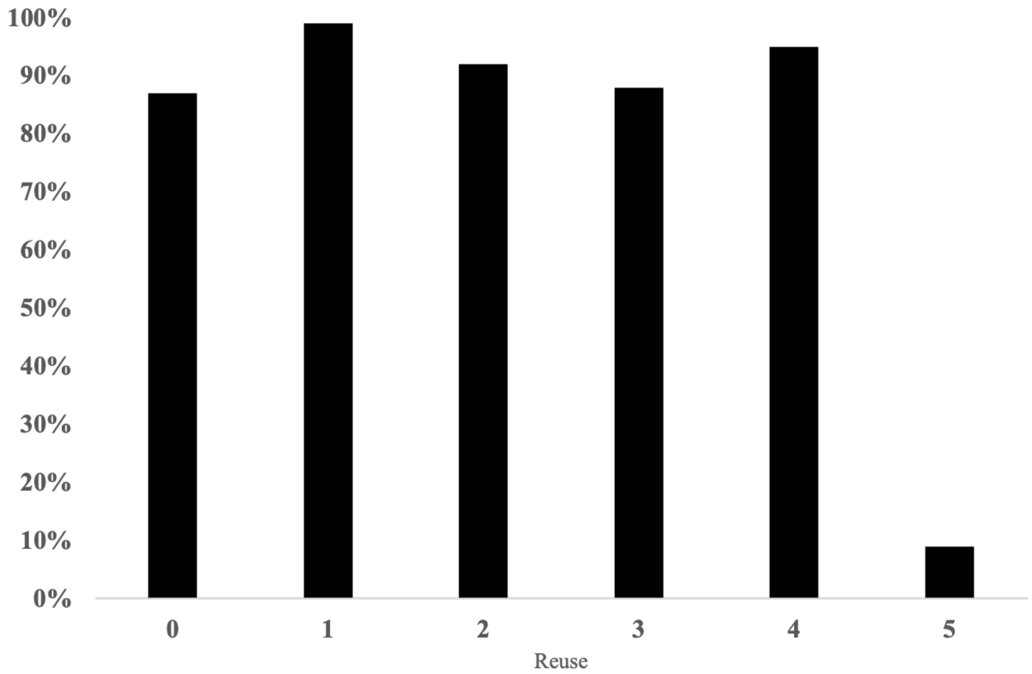

Figure 3.2. Percent yield of *p*-toluidine after successive reuse cycles of NBC-MASN. Yields based on ^{1}H NMR ratios.

It was speculated the cause of this increasing incubation period might be due to a loss of catalytic surface area, from the agglomeration of active Ni, and/or passivation of the catalytic surface by NiO formation during successive catalysis reactions. This prompted us to characterize the catalytic surface of NBC-MASN using various techniques. For structural comparison the characterization of unsupported NBC was included.

3.2.2. Catalyst Characterization

High angle annular dark field scanning transmission electron microscopy (HAADF-STEM) imaging of NBC-MASN revealed a very thin (< 10 nm) amorphous coating of material covering the honeycombed MASN particles (**Figure 3.3a**) after synthesis (**Figure 3.3b**). Synthesis of unsupported NBC typically gave particles in the hundreds of nanometers size regime (**Figure 3.4a**). Energy-dispersive X-ray spectroscopy (EDS) confirmed the presence of nickel in both NBC-MASN and unsupported NBC (**Figure 3.4b**), but detection of boron could not be confirmed due to its low signal intensity and overlap from the adjacent carbon signal (**Figure 3.5**). Given the more positive reduction potential of nickel, the majority of oxygen present in NBC (**Figure 3.4c**) is likely from borate species, rather than NiO, since freshly synthesized and carefully handled NBC should contain mostly reduced nickel. No information from EDS mapping of oxygen in NBC-MASN can be gained since the signal from SiO_2 overwhelms any contribution from borates.

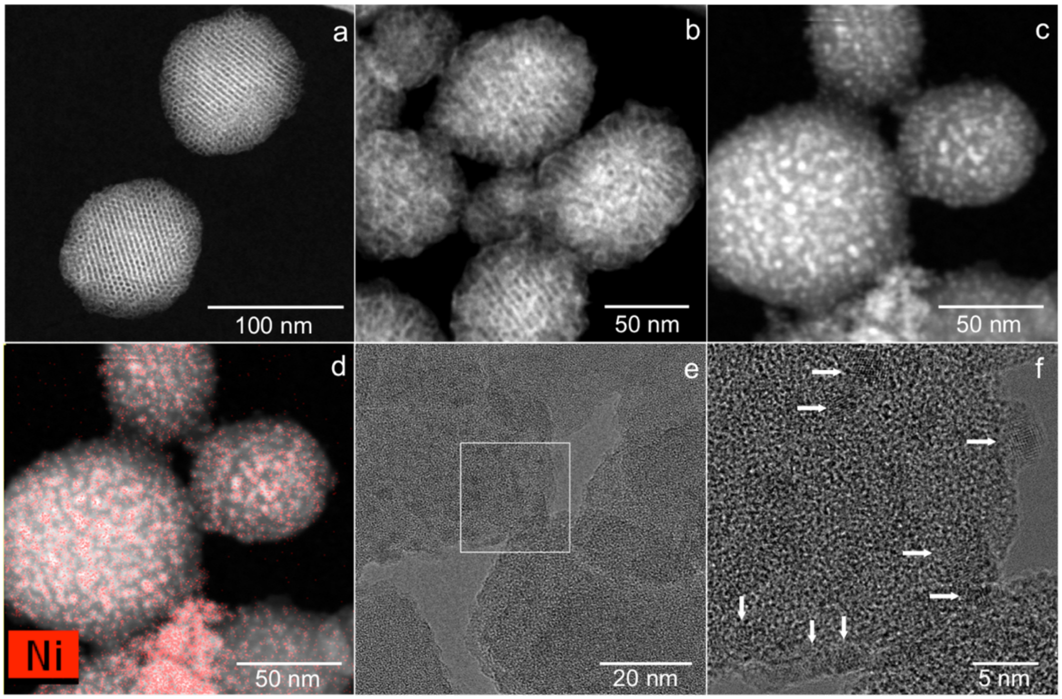

Figure 3.3. HAADF-STEM images of (a) as-synthesized MASN, (b) NBC-MASN imaged within 30 s of beam exposure, (c) NBC-MASN after EDS mapping for 5 min, with (d) the corresponding Ni EDS map. (e) HRTEM images of NBC-MASN after 5 min exposure to electron beam showing segregated regions of Ni, and (f) a magnified section (box in e) showing lattice fringes associated with these regions (arrows).

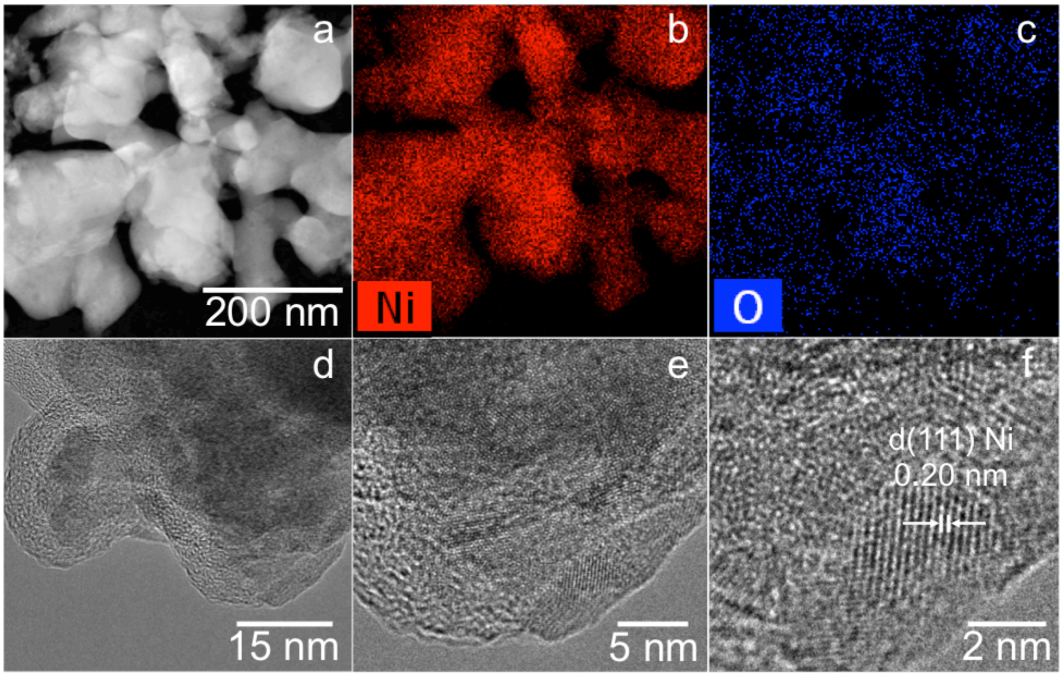

Figure 3.4. HAADF-STEM image of (a) unsupported NBC, and corresponding EDS elemental maps of (b) Ni and (c) O present in the composite. HRTEM of unsupported NBC, imaged within 2 min of beam exposure, progressively magnified (d-f) to show lattice fringes for Ni nanocrystals embedded within an amorphous matrix.

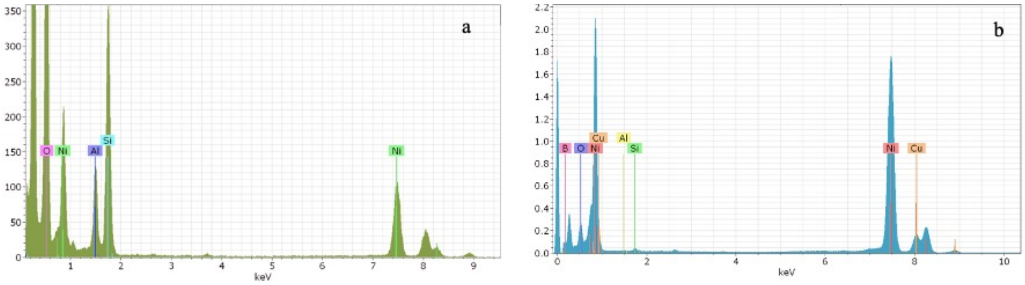

Figure 3.5. a) EDS spectrum for NBC-MASN. b) EDS spectrum for NBC.

Both HAADF-STEM and high-resolution transmission electron microscopy (HRTEM) imaging of fresh NBC-MASN indicated the NBC coating was amorphous. If NBC-MASN particles were subjected to several minutes of continuous electron flux, however, it was observed that small spots of high contrast material developed on or within NBC-MASN (**Figure 3.3c**). EDS mapping revealed that these spots appear to correspond with higher concentrations of Ni compared to the bulk of the composite (**Figure 3.3d**). HRTEM shows these tiny regions have crystallinity (**Figure 3.3e,f**), indicating the amorphous nickel in the composite segregated into larger particles and partially crystallized under the electron beam. The segregation/crystallization was particularly difficult to avoid during EDS mapping, wherein the samples were necessarily subjected to long exposures and higher beam current (**Figure 3.3c, d**). **Figure 3.6** shows the progression of this segregation starting at 30 s and after 5 min.

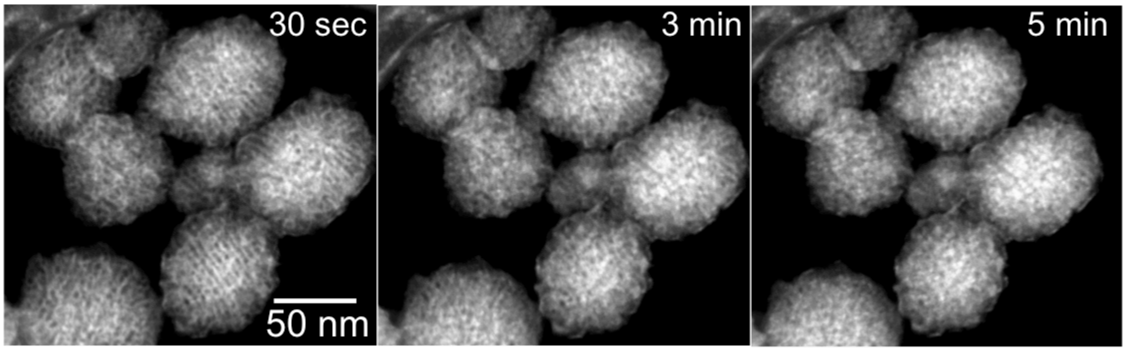

Figure 3.6. Segregation/crystallization of Ni in NBC-MASN after electron beam exposure for 5 min.

By comparison, HRTEM imaging of fresh unsupported NBC immediately revealed the presence of approximately 1-3 nm nanocrystalline domains of metallic Ni deposited within a surrounding amorphous matrix (**Figure 3.4d-f, and 3.7**), an observation consistent with previous reports of a similarly formed composite.[39] The unsupported NBC appeared much more stable under the electron beam than the amorphous surface of NBC-MASN, and additional segregation/crystallization of Ni was more difficult to observe during longer beam exposures in the case of unsupported NBC. This suggests that much of the metallic nickel resides as these pre-formed nanocrystals in unsupported NBC, whereas nickel in NBC-MASN is more homogenously amorphous and evenly distributed within the NBC structure that coats the MASN.

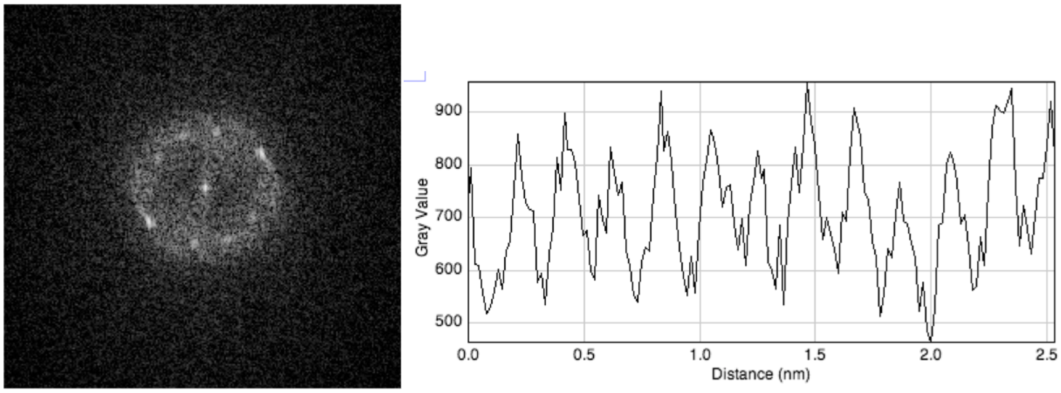

Figure 3.7. The electron diffraction pattern from Ni in the unsupported NBC material (left) and the lattice spacing plot from the corresponding HRTEM (right).

To confirm the amorphous quality of the catalyst, powder X-ray diffraction (PXRD) was conducted to identify the level of crystallinity within the catalyst. Hofer and researchers found that their similarly synthesized NBC catalysts displayed amorphous PXRD profiles when at room temperature. But when the catalysts were heated to 250 °C crystallization and the presence of metallic nickel appeared. Increasing the temperature to 750 °C caused similar effects in the PXRD profiles.[27]

Further characterization of these transition metal boron composite catalysts demonstrated similar findings. Corrias examined both two boron composite catalysts, one containing nickel and a second with cobalt.[29] He too found that at low temperatures the samples are amorphous but as the catalysts are heated the morphology changes. The Ni-based catalyst showed diffraction signals for metallic Ni and Ni_3B at 350 °C. As the temperature increased the peak for metallic Ni increased and by 600 °C it was the only pattern visible. A similar trend was seen with the cobalt-based catalyst.

A separate research group studied whether the Ni:B ratio of these NBC catalysts would affect the formation of the observed crystallization.[28] Two ratios were examined, a 1:4 (Ni:B) mmol ratio compared to a 1:2 (Ni:B) mmol ratio. PXRD analysis of the catalysts prepared in either method showed amorphous patterns when at room temperature (303K). Increased heating of the samples from 303K to 803K showed that the catalyst with more boron had better thermal stability. This catalyst did not display the strong metallic nickel diffraction signals until 803K compared to the reduced boron catalyst which showed the signals at 603K. The researchers concluded that the greater thermal stability was caused by the higher metalloid content and that the increased boron content could cause the decrease in the aggregation of the nickel nanoparticles.

Therefore, heating these amorphous composites in inert atmospheres allowed for identification of the mixture of crystalline nickel and nickel boron species present in bulk materials such as NBC.[27-29] **Figures 3.9** and **3.10** show the PXRD profiles for NBC-MASN and NBC, respectively, in their as-synthesized (or fresh) form, and after calcination in air or flowing nitrogen at 550 °C for 2 h. The high angle diffraction data for as-synthesized NBC-MASN displays an amorphous profile, while that of unsupported NBC gives only a broad peak occurring near the (111) reflection for fcc Ni (44.5° 2θ). This lack of appreciable diffraction from the nanocrystalline nickel present in fresh unsupported NBC can be explained by their small size, below the ~5 nm domain cut-off necessary to produce X-ray diffraction in metallic nanoparticles.[58,

[59] Calcining NBC and NBC-MASN in either air or $N_{2(g)}$ gave crystalline diffraction profiles in both cases, likely due in part to the same segregation/crystallization phenomena observed by electron microscopy. Interestingly, the air-calcined NBC-MASN diffraction profile shows only peaks indexed to NiO, whereas the unsupported NBC calcined in air gave a profile showing predominantly metallic Ni, with relatively low intensity peaks for NiO. The $N_{2(g)}$-calcined NBC-MASN gave a profile for metallic Ni, whereas similar calcination of unsupported NBC yielded a mixture of crystalline Ni and Ni_3B (ICDD 00-048-1223).

In an attempt to explain this commonly reported formation of Ni_3B upon calcination of NBC in an inert atmosphere, we offer preliminary evidence to suggest there may be residual boron hydrides within the amorphous matrix of NBC. It has been previously shown that various alkali earth and transition metal borohydrides and boranes [$Mg(BH_4)$, $Ti(BH_4)_3$, $Zr(BH_4)_4$, $Hf(BH_4)_4$, and $Cr(B_3H_8)_2$] can undergo thermal decomposition to form the corresponding metal borides at high temperatures (> 400 °C).[60-65] In particular, it has been shown that Ni_3B can be formed at 530 °C from the precursors $NiCl_2$ and various boranes (B_5H_9 or $B_{10}H_{14}$).[66] Thermal decomposition of residual boron hydrides during calcination of NBC would explain why crystalline nickel boride phases were observed in NBC catalyst (**equation 4**).

$$NiCl_2 + 2NaBH_4 \rightarrow Ni(BH_4)_2 + NaCl \xrightarrow{\Delta} "Ni_2B" \xrightarrow{Ni^\circ} Ni_3B \qquad (4)$$

When unsupported NBC was first refluxed in methanol for several hours prior to $N_{2(g)}$-calcination, then only crystalline Ni was observed (**Figure 3.8a**). Refluxing in methanol has been previously shown to remove residual boron hydrides from similar materials,[24] which was presuming to be trapped within the composite during the rapid reaction of Ni^{2+} and BH_4^-. ^{11}B NMR analysis of the supernatant solution of the refluxed material provided a singlet at 18 ppm, suggesting that a borate formed from hydrolysis of borohydride (**Figure 3.8b**). Trapped boron hydride [possibly $Ni(BH_4)_2$][26] or hydrogen adducts[67] in the matrix of unsupported NBC may then decompose during heating, explaining the formation of Ni_3B upon $N_{2(g)}$-calcination (**equation 4**), as well as the predominance of Ni over NiO upon air-calcination of unsupported NBC. The slow formation of the thin NBC layer in NBC-MASN may prevent this entrapment of boron hydrides and would explain the formation of both Ni upon $N_{2(g)}$-calcination and NiO upon air-calcination of NBC-MASN.

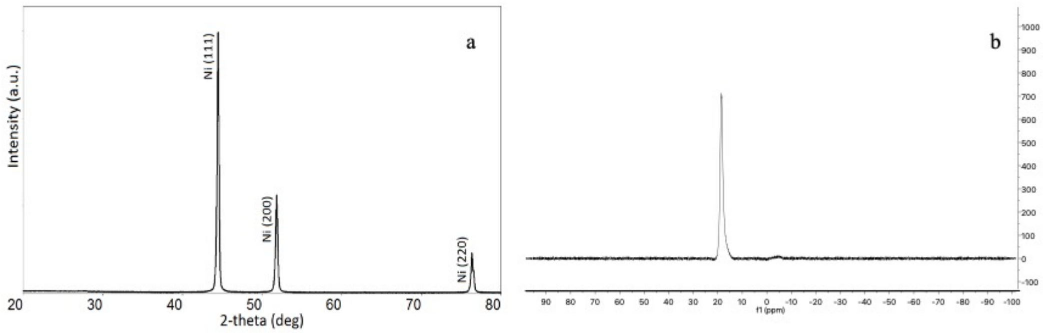

Figure 3.8. a) PXRD of NBC-MASN after MeOH reflux followed by $N_{2(g)}$-calcination. b) ^{11}B NMR of the supernatant solution after NBC was refluxed in methanol for 3 h.

The predominance of Ni compared to NiO in the PXRD profile of air-calcined NBC may also be attributed to the sintering and surface passivation of the Ni nanocrystals during heating. These agglomerated Ni nanocrystals may retain interior particle domains of Ni sufficiently large to diffract X-rays, while being protected from further oxidation by an exterior layer composed of NiO and borate, as previously shown for similarly formed cobalt boron composites.[34] In the case of air-calcined NBC-MASN, where only NiO was present in the PXRD profile, it may be that the very thin layer of homogenously amorphous NBC coating the MASN was more extensively oxidized than in bulk unsupported NBC. Finally, in the case of $N_{2(g)}$-calcination of NBC-MASN, amorphous Ni present in the NBC-MASN simply segregates and crystalizes in domains large enough to diffract X-rays.

Calcining NBC or NBC-MASN in either air or $N_{2(g)}$ atmosphere diminished the catalytic activity toward the reduction of aromatic nitro groups, likely due to nickel segregation/crystallization and a subsequent loss of catalytic surface area, as well as catalytically inactive surface NiO in the case of air-calcination.

The location of NBC on the external surface of MASN is apparent in **Figure 3.3**, but whether this material extends into the mesochannels of the support is less apparent due to the low contrast between NBC and SiO_2. Some information can be determined, however, from low angle PXRD of the material. The inset in **Figure 3.9** shows the change in the (100) peak position and intensity for the MASN support, before and after NBC formation and subsequent calcination in air or nitrogen. This peak corresponds to the distance between the walls of the ~3 nm diameter channels that run through the MASN spheres. The reduction of intensity and slight shift to lower 2-theta angles may be attributed, respectively, to inclusion of NBC material within the channels, and a subtle expansion of the pores as a result of their partial degradation during calcination.[46] This degradation was not typically seen upon template extraction during MASN synthesis, which occurred at the same temperature of 550 °C, so it may result here in part from the growth of a crystalline nickel phase within the mesochannels upon calcination of NBC-MASN. Inclusion of the NBC coating within the channels of MASN may indicate that the composite is partially anchored in the pores of the MASN, allowing it to remain highly dispersed and catalytically active over multiple reuse cycles (vide infra).

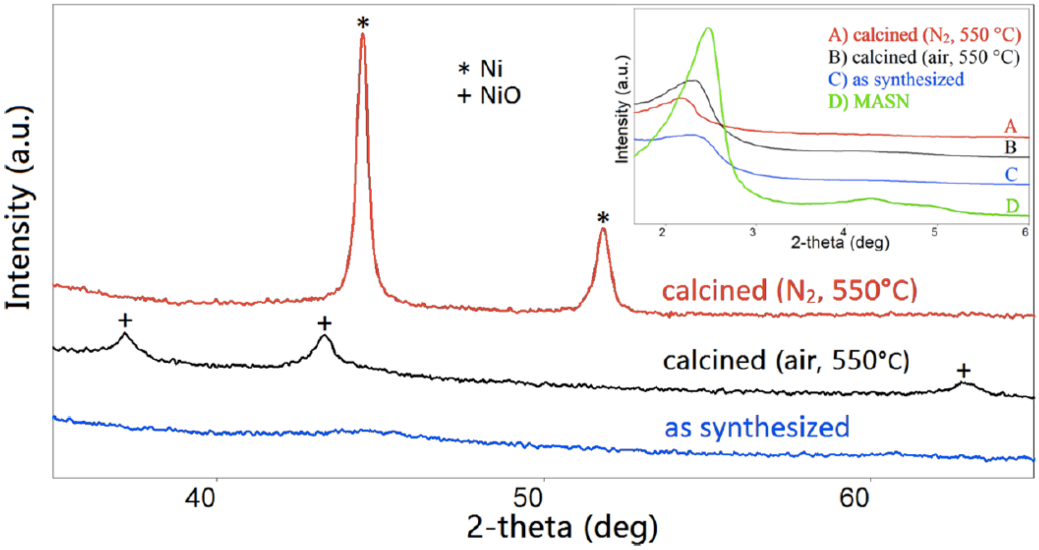

Figure 3.9. A comparison of PXRD profiles for as-synthesized (fresh) NBC-MASN and after calcination in air or flowing nitrogen. The inset shows the low angle diffraction pattern for the bare MASN compared to as-synthesized NBC-MASN before and after calcination.

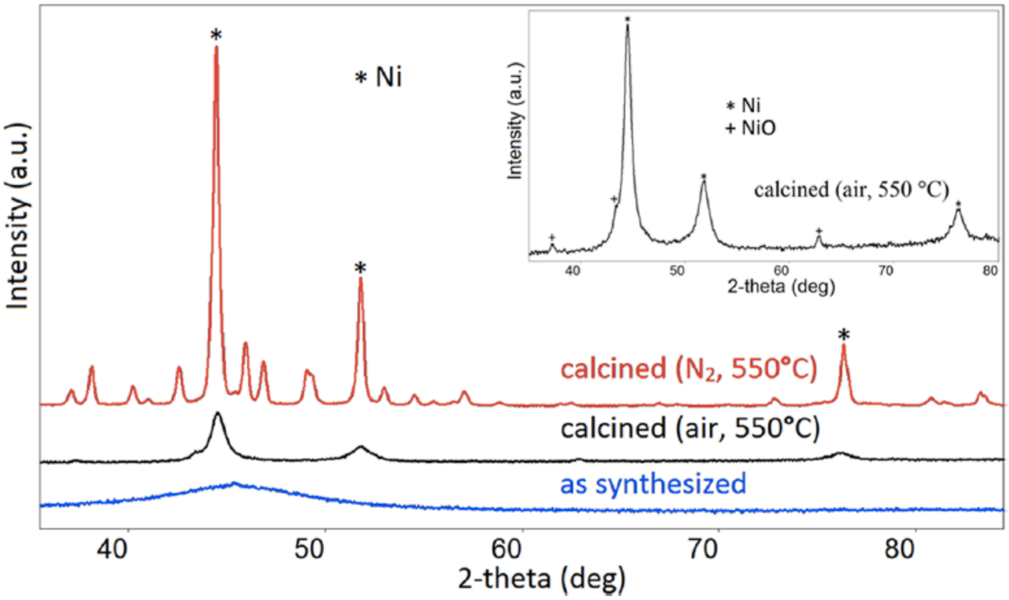

Figure 3.10. A comparison of PXRD profiles for as-synthesized (fresh) unsupported NBC and after calcination in air or flowing nitrogen. All peaks in the N_2 calcined sample not assigned to Ni (asterisks) can be assigned to Ni_3B (ICDD 00-048-1223). The inset shows an enlargement of the profile for the air-calcined material, indicating the presence of NiO.

Thermogravimetric analysis (TGA) of both unsupported NBC and NBC-MASN was performed to investigate the possible decomposition of trapped borohydride in NBC in general, as well as the oxidation of metallic nickel in both materials (**Figure 3.11**). Upon heating to 800 °C in air, NBC-MASN shows only the expected mass loss associated with removal of physically adsorbed water, with no appreciable mass gain that would indicate oxidation of boron or nickel. Considering that PXRD clearly shows the formation of NiO at 550 °C in air-calcined NBC-MASN, this TGA result is not easily explained. However, a similar TGA of unsupported NBC demonstrated two increases in mass initiating at approximately 350 °C and 650 °C. The first mass gain initiates very close to that observed for $NaBH_4$ similarly heated in air, which initiates at a temperature of ~360 °C and may indicate the presence of residual borohydride in unsupported NBC, while the second mass increase starting at ~650 °C is consistent with the oxidation of Ni nanoparticles in the nanometer size regime.[68]

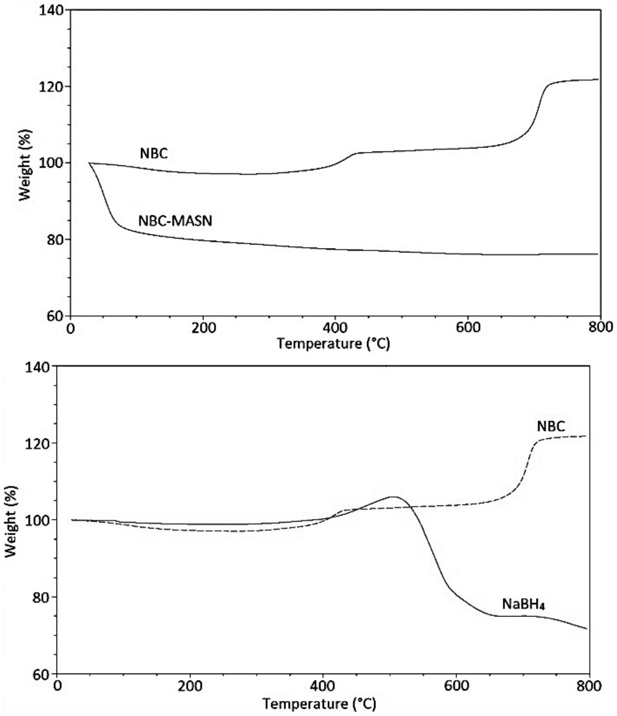

Figure 3.11. TGA data in air for NBC vs. NBC-MASN (top) and NBC vs $NaBH_4$ (bottom).

Because the surface of a catalytic material is of particular interest, X-ray photoelectron spectroscopy (XPS) was used in an attempt to identify the surface species present in both NBC-MASN and unsupported NBC. **Figures 3.12** and **3.13** show the wide-scans and core-level scans for freshly prepared samples of both NBC-MASN and NBC, respectively. **Table 3.3** gives the relevant electron binding energies for Ni, B and O in each material. It is evident from the Ni 2p core-level scans that the catalyst surface in both cases contains a mixture of metallic and oxidized nickel. The B 1s core-level scans show the presence of oxidized boron as well as a peak occurring at 187.7 eV for both materials, which is within the region typically assigned to nickel boride in the literature.[30, 32, 3330–32] The interpretation of this B 1s peak and its assignment to nickel boride is difficult to make, considering the very slight shifts in binding energy observed between elemental boron, borohydride, and the relevant borides.[39] As for the B 1s shifts in these materials, the assigned shifts for Ni 2p binding energies are also typically less than 1 eV from that of metallic Ni.[30, 33, 69] There is also considerable and longstanding disagreement as to whether electron donation occurs from boron to metal or vice versa in amorphous nickel borides.[39] Evidence has been given of residual hydrides or hydrogen adducts in both nickel and cobalt composites, particularly when synthesized in ethanol, though the specific identity of these purported hydrides (M-H or B-H) has not been resolved.[67] Considering the interpretation of PXRD and TGA data in this work, we reason that the B 1s binding energy previously reported by others as evidence of amorphous nickel boride, may actually be indicative of residual borohydride sequestered in the composite upon formation. Indeed, the presence of residual borohydride in similar nickel based composites has been previously reported.[24] In comparing the spectra for NBC-MASN and unsupported NBC, the greatly diminished intensity of this B 1s peak at 187.7 eV relative to the adjacent borate peak implies a much lower surface concentration of this boron species in NBC-MASN. Considering the NBC layer on MASN appears by HAADF-STEM to be quite thin (perhaps only a few nanometers on average), the XPS analysis, with a reliable surface penetration depth of 5 to 10 nm, may largely account for the entire composition of the

NBC layer in NBC-MASN. Assuming the B 1s peak at 187.7 eV arises from sequestered borohydride, then its lower concentration in NBC-MASN could account for the lack of any Ni_3B phase observed by PXRD after calcining in $N_{2(g)}$. Of course, some portion of the initial $NaBH_4$ will fully react and become borate in the composite matrix (or rinse away as boric acid), which explains why a mixture of metallic nickel and nickel boride are typically seen after calcination.

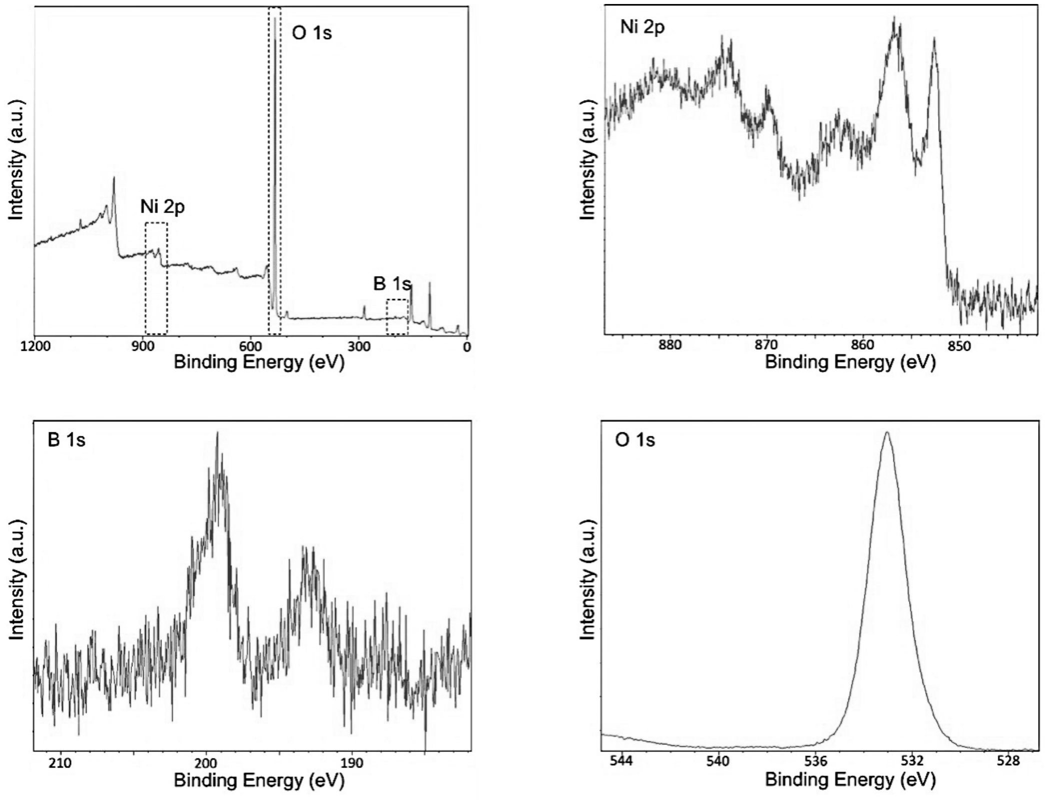

Figure 3.12. XPS data for NBC-MASN.

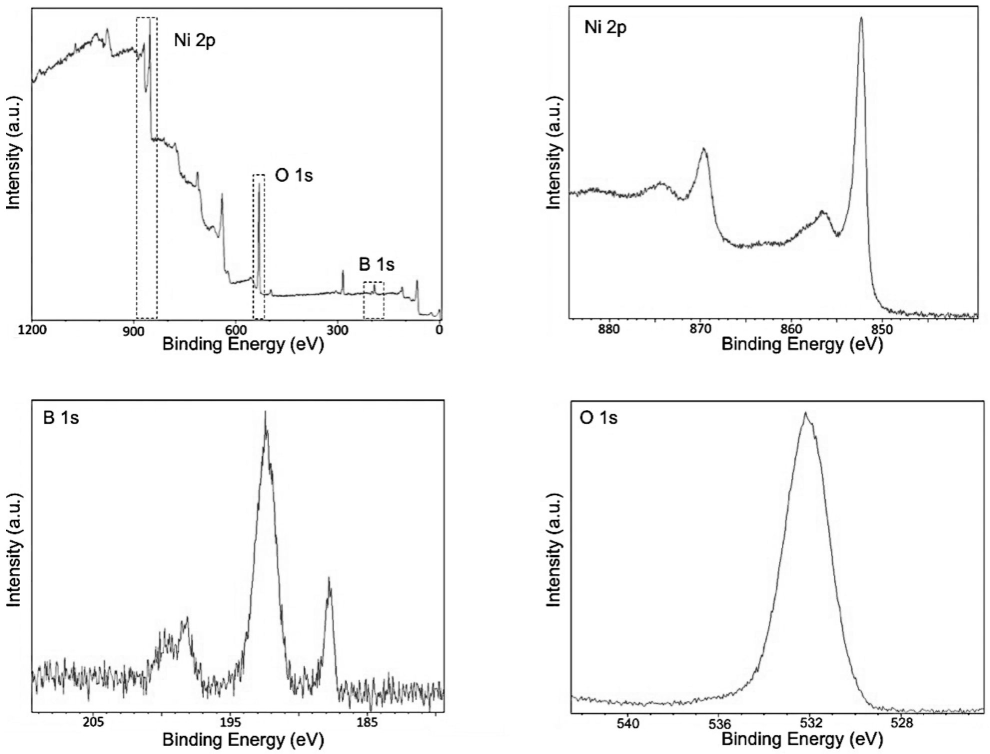

Figure 3.13. XPS data for unsupported NBC.

Table 3.3. Binding Energies of NBC-MASN and NBC

Element	NBC-MASN (eV)	NBC (eV)	Possible Compounds
Ni 2p	852.6	852.3	Ni
	856.8	856.6	NiO, $Ni(OH)_2$, $Ni(BO_2)_2$
B 1s	187.7	187.7	B_xH_y
	193.0	192.4	BO_2^-, B_2O_3
O 1s	532.8	532.3	NiO, BO_2^-, B_2O_3

Further evidence for the presence of borohydride trapped within the matrix of NBC was given by examining the quantity of hydrogen evolved during synthesis of both unsupported and supported NBC (**Table 3.4**). For unsupported NBC, only 51% of the theoretical amount of hydrogen was released when $NiCl_2$:$NaBH_4$ (1:2) were allowed to react at 0 °C in ethanol. Even when varying the ratio of $NiCl_2$:$NaBH_4$ from 1:1 to 1:0.5, the amount of hydrogen evolved were 43% and 54%, respectively. Similar results were obtained for $NiCl_2$-MASN:$NaBH_4$ (1:2), which liberated 56% of the theoretical amount of hydrogen, indicating that some B-H compound remains unreacted, possibly sequestered within the interstitial spaces of the material.

Table 3.4. Gas evolution analysis of NBC for differing ratios of Ni:BH_4 and NBC-MASN[a]

$NiCl_2$:$NaBH_4$	$NiCl_2$	$NaBH_4$	H_2 Evolved	Theoretical Amount of H_2	Percentage of H_2 Evolved
1:2	0.5 mmol	1 mmol	2.05 mmol	4 mmol	51%
1:1	0.5 mmol	0.5 mmol	0.85 mmol	2 mmol	43%
1:0.5	0.5 mmol	0.25 mmol	0.54 mmol	1 mmol	54%
Ni:$NaBH_4$	**Ni-MASN**	**$NaBH_4$**	**H_2 Evolved**	**Theoretical Amount of H_2**	**Percentage of H_2 Evolved**
1:2	0.15 mmol	0.3 mmol	0.71 mmol	1.256 mmol	56%

[a]Anhydrous $NiCl_2$ and solid $NaBH_4$ were added and the flask cooled to 0 °C. A cannula connected the round bottom flask to the gas burette reservoir. The system was allowed to equilibrate before the addition of 4 mL of 0 °C ethanol via syringe. By the controlled relief of pressure in the closed system into a graduated cylinder, the volume of gas generated, plus total volume injected, was measured by water displacement. The temperature of the displaced water and barometric pressure was also measured, and the temperature dependent vapor pressure of water. The quantity of hydrogen produced was then determined by the following method published before.[70]

The bulk nickel and boron content in both NBC-MASN and unsupported NBC were determined by ICP-OES. Throughout this work, the content of Ni initially present in fresh NBC-MASN averaged 9.0_w%, while the calculated loading of Ni^{2+} into MASN via impregnation with $NiCl_2$•$6H_2O$ was $10._w$%. However, no significant amount of Ni was observed by ICP-OES in the ethanol/water supernatant collected after the syntheses of either NBC or NBC-MASN. Therefore, additional moisture adsorbed in the hydrated nickel salt and instrumental error inherent during ICP-OES may account for the discrepancy. The initial ratio of Ni:B was approximately 2 in both NBC and NBC-MASN and remained unchanged for both catalysts after calcination in either nitrogen or air.

3.2.3. Recycling Study

ICP-OES was further used to track changes in the nickel and boron content after successive reuses of NBC-MASN in the reduction of *p*-nitrotoluene to *p*-toluidine. **Figures 3.14 and 3.15** show, respectively, the Ni:B ratio NBC-MASN and the percent yield of *p*-toluidine determined after 24 h by ^{1}H NMR for two different reuse studies. In both studies, 5 mmol of $N_2H_4 \bullet H_2O$ was used as the reducing agent for 1 mmol of *p*-nitrotoluene, in the presence of NBC-MASN containing approximately 0.1 mmol of nickel. Sodium borohydride was used either *ex situ* or *in situ* with $N_2H_4 \bullet H_2O$, in an attempt to prolong the catalyst's reusable lifetime. In the *ex situ*-$NaBH_4$ study, when the percent yield of *p*-toluidine was observed to decrease significantly (below 80%) upon cycling, the used NBC-MASN catalyst was cleaned, dried, and regeneration attempted by reacting it with a quantity of $NaBH_4$ equivalent to twice the molar amount of Ni assumed to be present in the catalyst. In the *in situ*-$NaBH_4$ reuse study, a combination of $N_2H_4 \bullet H_2O$ and equimolar $NaBH_4$ were used, with the intention of affecting continuous *in situ* regeneration of the catalyst by reaction with $NaBH_4$. As can be seen in **Figure 3.14**, a progressive loss of boron from NBC-MASN is observed upon each cycle in both study but is more dramatic in the study where only $N_2H_4 \bullet H_2O$ is present, compared to *in situ* regeneration by $NaBH_4$. As can be seen in **Figure 3.15**, the use of $NaBH_4$ along with $N_2H_4 \bullet H_2O$ extends the lifetime of the catalyst up to nine reuse cycles, compared to only four cycles when regeneration is performed *ex situ*. No significant loss of nickel from NBC-MASN was observed during either reuse study, indicating that all of the Ni^{2+} initially loaded onto MASN was reacted during the synthesis of the catalyst.

It must be pointed out that $N_2H_4•H_2O$ will not reduce NiO to Ni^0 at 25°C, and oxidation from continuous reaction with the substrate nitro group during catalysis makes oxidation of the catalyst inevitable.[71] The sustained catalytic activity of NBC-MASN observed when both $NaBH_4$ and $N_2H_4•H_2O$ were present during each catalysis cycle (**Figure 3.15**) is attributed to the ability of borohydride to reduce passivating surface NiO. It is also possible, given the higher average boron content compared to the ex-situ study, that *in situ* $NaBH_4$ may replenish some protective borate species that physically prevent agglomeration of the active nickel or its more rapid oxidation. In contrast, it was found that exposing the catalyst to additional borohydride *ex situ*, as soon as catalytic activity was observed to decrease, did not improve catalytic performance upon subsequent reuse. As can be seen in **Figure 3.14**, the boron content in NBC-MASN did increase after these *ex situ* borohydride treatments prior to reuse 7 and 9, but sharply decreased again upon further cycling. We interpret this as evidence that $NaBH_4$ is reducing oxides formed on the catalytically active nickel surface, so long as the oxidation is not too extensive—as may be the case in the *ex situ* regeneration study. Severe oxidation of the amorphous nickel, along with loss of the surrounding borate matrix, may leave the nickel constituent vulnerable to agglomeration, and loss of surface area, during subsequent reduction by borohydride. Further XPS and electron microscopy studies examining the surface oxidation and agglomeration/crystallization of nickel at each reuse cycle, would likely elucidate the point at which surface oxidation and/or segregation/crystallization deactivates the catalyst, and either *in situ* or *ex situ* borohydride regeneration is no longer possible for NBC-MASN.

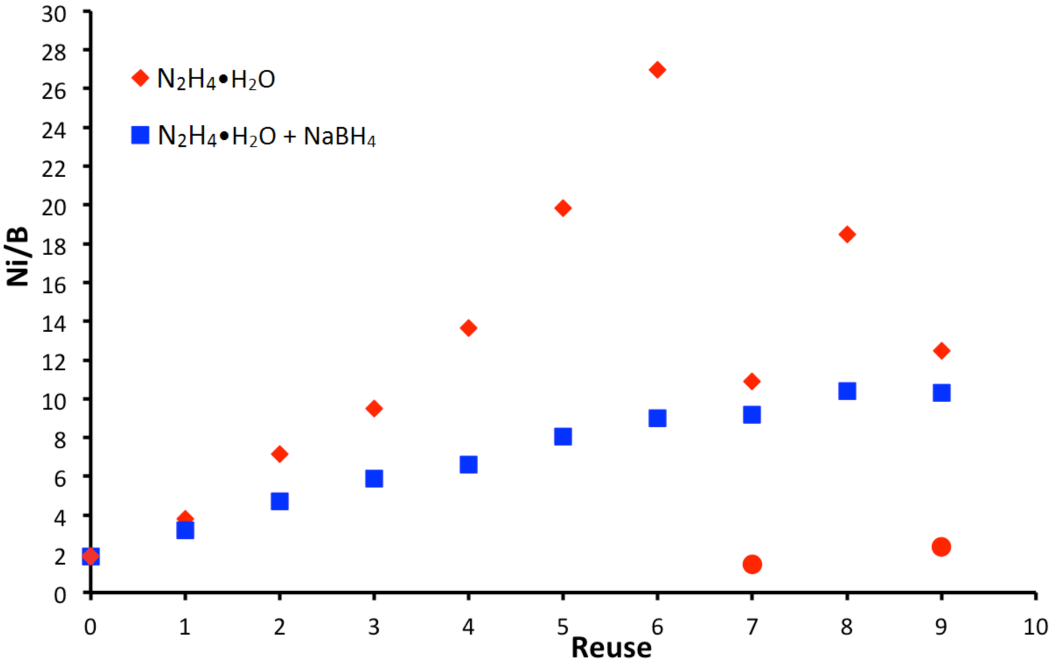

Figure 3.14. ICP-OES data for the Ni:B molar ratio in NBC-MASN after successive reuses in the catalytic hydrogenation of *p*-nitrotoluene. Two reaction conditions are compared: $N_2H_4 \bullet H_2O$ as reducing agent (red diamonds), and $N_2H_4 \bullet H_2O$ with an equimolar addition of $NaBH_4$ (blue squares). The two red circular markers for reuse numbers 7 and 9 indicate the Ni:B ratio after ex-situ regeneration of NBC-MASN with $NaBH_4$ but before catalysis using $N_2H_4 \bullet H_2O$.

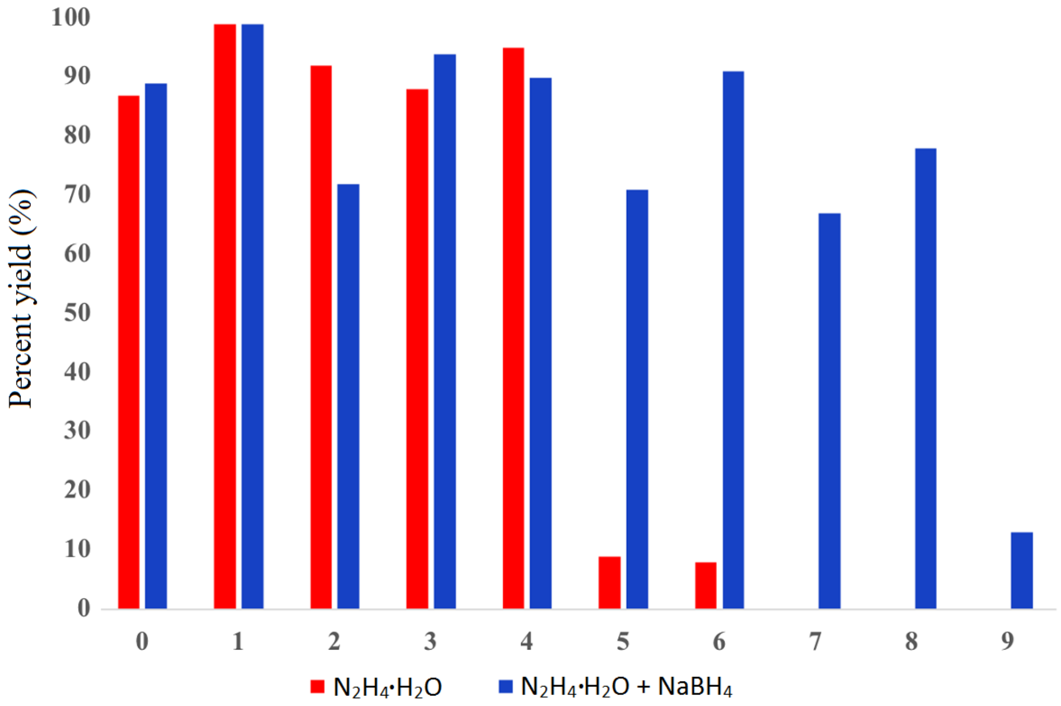

Figure 3.15. Reuse study: The percent yield for the conversion of *p*-nitrotoluene to *p*-toluidine is plotted against reuse cycle number, using either N_2H_4•H_2O as the reducing agent or a combination of N_2H_4•H_2O and $NaBH_4$ as reducing and regenerating agents. The product yields were determined after 24 h reaction. Yield was determined by isolation and the purity was verified by ^{1}H NMR spectroscopy.

A tandem ^{1}H NMR spectroscopy study was performed during the reuse study where NBC-MASN was regenerated with $NaBH_4$ *ex situ* (**Figure 3.16**). The first catalysis reaction using fresh NBC-MASN to reduce *p*-nitrotoluene to *p*-toluidine reached completion after 2 h. However, subsequent reuses of the catalyst showed progressively longer incubation periods to achieve full conversion of *p*-toluidine. This may be evidence of the formation of an oxide layer on the catalytic nickel surface, which inhibits the interaction of hydrazine.[72] Although full conversion to *p*-toluidine was not achieved in the 5th cycle, all of the starting material was consumed and several intermediates were identified that did not fully react with the catalyst to finish conversion into *p*-toluidine.

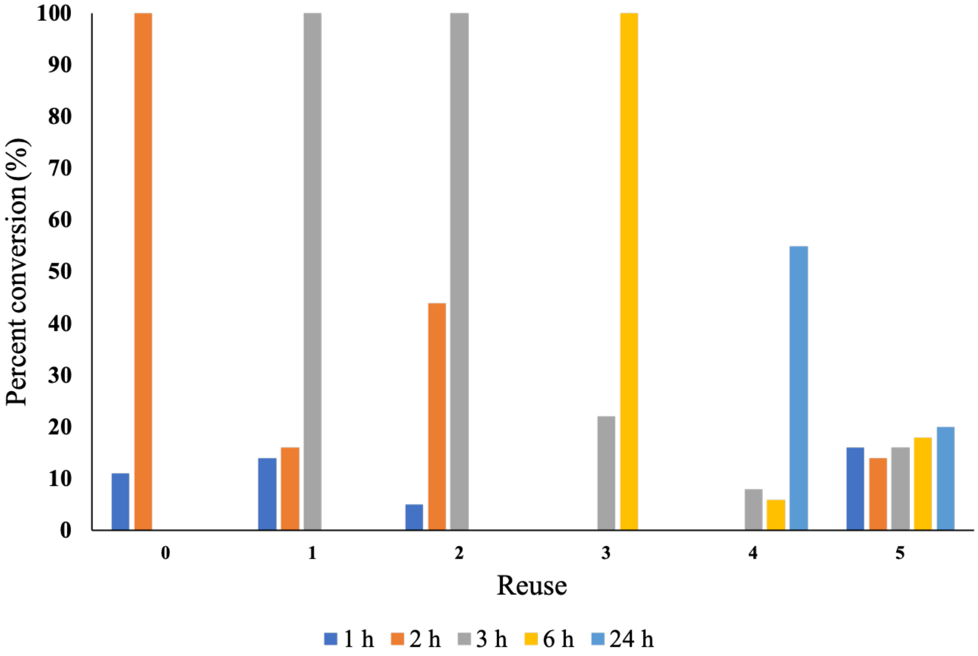

Figure 3.16. Percent yield of *p*-toluidine after 24 h. Yields are based on ^{1}H NMR ratios.

3.2.4. Mechanistic Insights

As mentioned earlier, the reduction of nitroarenes to anilines can progress by one of two proposed pathways, direct reduction or condensation. ^{1}H NMR analysis was used to monitor the reaction progress to better understand how the reduction occurs with NBC-MASN and hydrazine hydrate (**Figure 3.17**). In the first hour, *p*-nitrotoluene was present and some initial conversion into *p*-toluidine was seen. Additional signals corresponding to two reaction intermediates 4,4-dimethylazoxybenzene (**B**) and 4,4-dimethylhydrazobenzene (**D**) were also present. After 2 h, a steep decline in *p*-nitrotoluene can be seen as product intensity increased. Intermediate **B** remained but **D** was no longer as prominent suggesting a rapid transformation into the product. After 3 h, the reaction was complete as only signals corresponding to *p*-toluidine were present. The presence of the azoxy and hydrazo reaction intermediates suggests that the reduction of *p*-nitrotoluene using this methodology occurs through the condensation pathway. The condensation pathway appears to be the preferred route for many of these metal boron composite catalysts.[4, 51, 54]

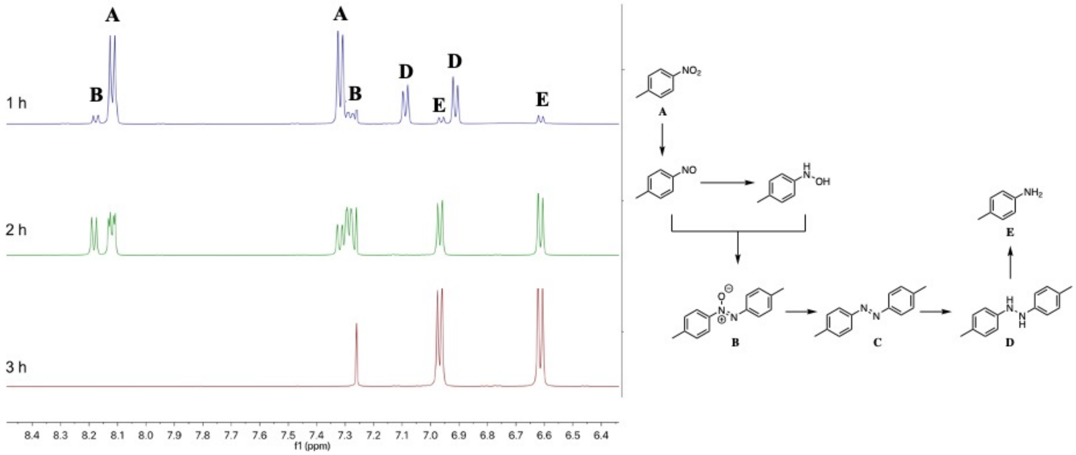

Figure 3.17. Left: ^{1}H NMR spectra of sample aliquots after 1 h, 2 h, and 3 h. Right: proposed reaction pathway for the reduction of nitroarenes.

3.2.5. Nitroarene Substrate Scope

In order to verify the catalytic ability of NBC-MASN for the reduction of other nitroarenes, a preliminary substrate scope was investigated (**Table 3.5**). Simple nitroarenes, such as *p*-nitrotoluene and nitrobenzene easily produced the aniline products (entries 1 and 2). Halogenated nitroarenes were reduced in excellent yields to the corresponding aniline derivatives and no dehalogenated product was observed (entry 3). Both trisubstituted and pyrene nitroarene derivatives were tolerated as well (entries 4 and 5).

Interestingly, 4-nitro-benzonitrile was selectively reduced to 4-cyano-benzylamine (entry 6) while the nitrile in 4-cyanotoluene remained unreacted during the catalysis (entry 7). This selectivity differs from previously published catalyst systems, which reduced both nitro and nitrile groups simultaneously.[73-75] In those methodologies, the reducing agent was H_2 generated from $NaBH_4$, as opposed to $N_2H_4 \bullet H_2O$.

Table 3.5. NBC-MASN vs NBC for selective nitro group reduction

Entry	Substrate	Product	Catalyst[a]	
			NBC-MASN[b]	NBC[c]
1	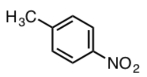	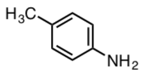	94%	85%
2	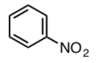	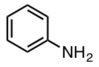	99%	58%
3	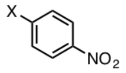 X = Br, Cl, I	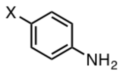 X = Br, Cl, I	99% X= Br, Cl, I	X = Br 83% X = Cl 96% X = I 87%
4	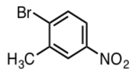	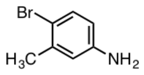	99%	99%
5	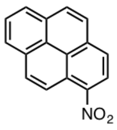	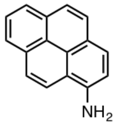	99%	89%
6	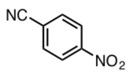	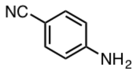	48%	19%
7	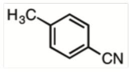	--	0%	--

[a]Isolated yield; [b] Reaction conditions for supported catalyst: nitroarene (4 mmol), NBC-MASN (10 mol%), MeOH (8 mL), hydrazine hydrate (20 mmol), 25 °C, 24 h, under argon atmosphere; [c] Reaction conditions for unsupported catalyst: nitroarene (4 mmol), NBC (10 mol%), MeOH (8 mL), hydrazine hydrate (20 mmol), 25 °C, 24 h, under argon atmosphere.

These results propose that the hydrogen source can dictate functional group selectivity. To further demonstrate this fact, Vernekar's group compared how their Co-Co_2B catalyst performed in the presence of different functionalities and substituents when mediated with $NaBH_4$ or with hydrazine hydrate.[51] Both hydrogen sources did not reduce carboxylic acids, oximes, or esters and they tolerated the presence of halides, alcohols, and ethers. If a nitrile or alkene was present, $NaBH_4$ would react to produce the amine or saturated compound, respectively. Interestingly, hydrazine would not react with either of those functional groups. The hydrogenation with $NaBH_4$ converted aldehydes and ketones to the corresponding alcohols, while when hydrazine was used partial conversion was achieved. More specifically, hydrazine and the catalyst would react with aldehydes to produce the hydrazine adduct and with ketones the alcohol and hydrazo product would form (2:1). These observations follow a similar trend found by other researchers.[4, 6, 54]

Overall, the initial arylamine product yield was higher for a variety of substrates when using supported NBC-MASN catalyst, compared with the unsupported NBC catalyst. This is likely due to the more amorphous character of NBC grown on MASN, potentially possessing a larger proportion of minimally coordinated nickel sites for catalysis, compared to the more crystalline character of NBC.[7, 76] Similar arguments have been made for the enhanced activity of Co-B when dispersed on mesoporous silica nanoparticles versus solid silica beads or bulk Co-B, where larger domains of metallic Co tend to aggregate.[50]

3.2.6. Alternative Ni-based Catalyst

Most of the discussion surrounding these amorphous metal catalysts involves reducing a metal salt with $NaBH_4$, to obtain the active catalyst. But as described above the borohydride species is there to reduce Ni^{2+} to Ni^0 and so it should be possible for other hydrides to reduce a metal salt and achieve similar results. This query was tested by reacting $NiCl_2$ with diisobutylaluminum borohydride [$(i\text{Bu})_2AlBH_4$] and diisobutylaluminum hydride (DIBAL), both reactions produced a black precipitate. The catalysts were then subjected to the optimized reduction reaction conditions to reduce *p*-nitrotoluene (**Scheme 3.4**). The reduction reaction with $(i\text{Bu})_2AlBH_4$ did not achieve complete reduction. Even after 24 h the product was a mixture of intermediates in addition to the final product. Interestingly, catalyst synthesized from DIBAL performed well, accomplishing a complete reduction to *p*-toluidine in 78% isolated yield. It should be noted that DIBAL on its own will not reduce nitroarenes to aniline but instead stops at the hydroxylamine stage.[77]

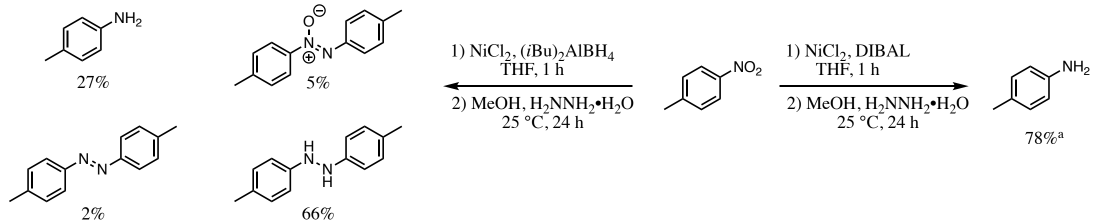

Scheme 3.4. Synthesis of Ni catalyst with (left) $(i\text{Bu})_2AlBH_4$ and (right) DIBAL and the subsequent reductions of *p*-nitrotoluene. Yields based on NMR ratios. [a]Isolated yield.

The Ni catalyst made from DIBAL was then cleaned and reused for multiple cycles. The isolated yield of *p*-toluidine remained steady and did not see a dramatic decrease even after the 5th recycle (**Figure 3.18**). Unlike NBC-MASN, which benefited from *in situ* addition of $NaBH_4$ to reduce the oxide layer, the DIBAL synthesized catalyst did not require additional quantities of the hydride. This suggests that the catalyst was less susceptible to agglomeration or oxide formation. Although a full characterization profile was not conducted it seems that the aluminum from DIBAL is interacting with Ni to maintain a highly active catalyst.

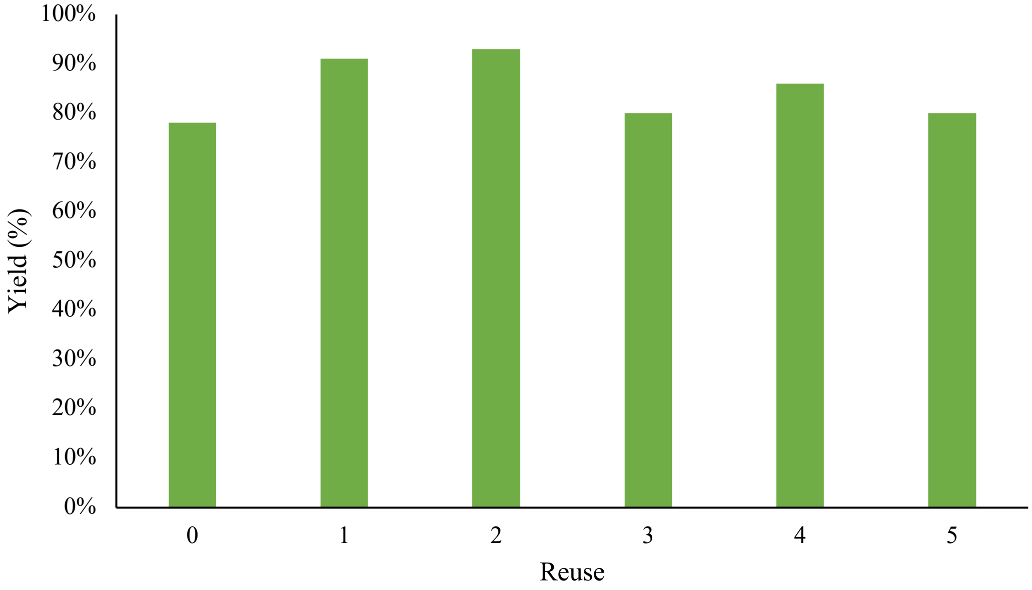

Figure 3.18. Recycling and reuse study of the reduction of *p*-nitrotoluene with the catalyst formed from Ni and diisobutylaluminum hydride.

3.3. Conclusions

In summary, a nickel boron composite (NBC) supported on mesoporous aluminosilicate nanoparticles (NBC-MASN) was synthesized for the purpose of reducing nitroarenes. The supported catalyst showed increased catalytic activity compared to unsupported NBC for the selective reduction of several different nitroarenes to their corresponding aniline derivatives. The catalytically active amorphous nickel in NBC-MASN may be deactivated by oxidation and/or agglomeration/crystallization of nickel during catalysis, leading to an average reusable lifetime of four cycles. The reusable lifetime of the catalyst could be prolonged up to nine cycles (for the reduction of *p*-nitrotoluene) when equimolar $NaBH_4$ was used with N_2H_4•H_2O during catalysis, but not when $NaBH_4$ was used *ex situ* to attempt regeneration of the exhausted catalyst. Introducing $NaBH_4$ *in situ* during catalysis likely reduces surface NiO back to Ni and may help to fortify the borate content believed responsible for preventing agglomeration and rapid oxidation of the amorphous nickel present in NBC.

The structural character and negative surface charge of the MASN support appears to aid in forming a thin, highly dispersed amorphous coating of NBC on MASN during synthesis. Comparatively, unsupported NBC consists of much larger particles containing 1-3 nm metallic nickel nanocrystals embedded in an amorphous matrix. We attribute the boron content in NBC-MASN, observed by ICP-OES and XPS, largely to the presence of unknown borate species rather than amorphous nickel boride, since the degradation of borohydrides in protic solvents prohibits the formation of elemental boron or true borides. The XPS, TGA, and PXRD analyses, along with the results of methanol refluxing, indicate the possible entrapment of borohydrides within the rapidly formed precipitate of unsupported NBC. This residual borohydride may explain the formation of Ni_3B upon $N_{2(g}$-calcining of unsupported NBC. The slower formation of the thin NBC layer grown on MASN may allow for a more complete reaction of $NaBH_4$ and would explain why only crystalline Ni is observed by PXRD upon $N_{2(g)}$-calcining of NBC-MASN, as well as the greatly reduced intensity of the B 1s peak at 187.7 eV in the case of NBC-MASN compared to that of unsupported NBC. The same 2:1 Ni:B ratio observed by ICP-OES for both NBC-MASN and unsupported NBC may be explained if the majority of boron present in the supported catalyst is oxidized, while some portion of the boron in NBC is residual boron hydride trapped within the amorphous matrix.

3.4. References

1. Vogt, P. F.; Gerulis, J. J., Amines, Aromatic. In *Ullmann's Encyclopedia of Industrial Chemistry*, Wiley-VCH Verlag GmbH & Co.: Weinheim, Germany, 2000.

2. Ramya, K.; Dhathathreyan, K. S.; Sreenivas, J.; Kumar, S.; Narasimhan, S., Hydrogen production by alcoholysis of sodium borohydride. *Int. J. Energy Res.* **2013,** *37*, 1889-1895.

3. Schlesinger, H. I.; Brown, H. C.; Finholt, A. E.; Gilbreath, J. R.; Hoekstra, H. R.; Hyde, E. K., Sodium Borohydride, Its Hydrolysis and Its Use as a Reducing Agent and in the Generation of Hydrogen. *J. Am. Chem. Soc.* **1953,** *75*, 215-219.

4. Zhang, J.; Lu, G.; Cai, C., Chemoselective Transfer Hydrogenation of Nitroarenes by Highly Dispersed Ni-Co BMNPs. *Catal. Commun.* **2016,** *84*, 25-29.

5. Rahman, A.; Jonnalagadda, S. B., Swift and Selective Reduction of Nitroaromatics to Aromatic Amines with Ni–Boride–Silica Catalysts System at Low Temperature. *Catal. Lett.* **2008,** *123*, 264-268.

6. Rai, R. K.; Mahata, A.; Mukhopadhyay, S.; Gupta, S.; Li, P.-Z.; Nguyen, K. T.; Zhao, Y.; Pathak, B.; Singh, S. K., Room-Temperature Chemoselective Reduction of Nitro Groups Using Non-Noble Metal Nanocatalysts in Water. *Inorg. Chem.* **2014,** *53*, 2904-2909.

7. Prathap, K. J.; Wu, Q.; Olsson, R. T.; Dinér, P., Catalytic Reductions and Tandem Reactions of Nitro Compounds Using in Situ Prepared Nickel Boride Catalyst in Nanocellulose Solution. *Org. Lett.* **2017,** *19*, 4746-4749.

8. Formenti, D.; Ferretti, F.; Scharnagl, F. K.; Beller, M., Reduction of Nitro Compounds Using 3d-Non-Noble Metal Catalysts. *Chem. Rev.* **2019,** *119*, 2611-2680.

9. Wang, Z., Béchamp Reduction. In *Comprehensive Organic Name Reactions and Reagents*, Wang, Z., Ed. 2010.

10. Climent, M. J.; Corma, A.; Iborra, S.; Martí, L., Process Instensification with Bifunctional Heterogeneous Catalysts: Selective One-Pot Synthesis of 2'-Aminochalcones. *ACS Catal.* **2015,** *5*, 157-166.

11. Pan, X.; Xu, Y.-J., Efficient Thermal-and Photocatalyst of Pd Nanoparticles on TiO_2 Achieved by an Oxygen Vacancies Promoted Synthesis Strategy. *ACS Appl. Mater. Interfaces* **2014,** *6*, 1879-1886.

12. Tomkins, P.; Gebauer-Henke, E.; Leitner, W.; Müller, T. E., Concurrent Hydrogenation of Aromatic and Nitro Groups over Carbon-Supported Ruthenium Catalysts. *ACS Catal.* **2015,** *5*, 203-209.

13. Lauwiner, M.; Rys, P.; Wissmann, J., Reduction of aromatic nitro compounds with hydrazine hydrate in the presence of an iron oxide hydroxide catalyst. I. The reduction of monosubstituted nitrobenzenes with hydrazine hydrate in the presence of ferrihydrite. *Appl. Catal. A: Gen.* **1998,** *172*, 141-148.

14. Cantillo, D.; Moghaddam, M. M.; Kappe, C. O., Hydrazine-Mediated Reduction of Nitro and Azide Functionalities Catalyzed by Highly Active and Reusable Magnetic Iron Oxide Nanocrystals. *J. Org. Chem.* **2013,** *78*, 4530-4542.

15. Benz, M.; Kraan, A. M. v. d.; Prins, R., Reduction of aromatic nitrocompounds with hdyrazine hydrate in the presence of an iron oxide hydroxide catalyst: II. Activity, X-ray diffraction and Mössbauer study of the iron oxide hydroxide catalyst. *Appl. Catal. A: Gen.* **1998,** *172*, 149-157.

16. Kumarraja, M., Simple and Efficient Reduction of Nitroarenes by Hydrazine in Faujasite Zeolites. *Appl. Catal. Gen.* **2004,** *265*, 135-139.

17. Pavlic, A. A.; Adkins, H., Preparation of a Raney Nickel Catalyst. *J. Am. Chem. Soc.* **1946,** *68*, 1471-1471.

18. Adkins, H.; Billica, H. R., The Preparaton of Raney Nickel Catalysts and their Use Under Conditions with Those for Platinum and Palladium Catalysts. *J. Am. Chem. Soc.* **1948,** *70*, 695-698.

19. Raney Nickel. https://cameochemicals.noaa.gov/chemical/4024 (accessed September 30, 2020).

20. Sun, S.; Quan, Z.; Wang, X., Selective reduction of nitro-compounds to primary amines by nickel-catalyzed hydrosilylative reduction. *RSC Adv.* **2015,** *5*, 84574-84577.

21. Singh, C.; Goyal, A.; Singhal, S., Nickel-doped cobalt ferrite nanoparticles: efficient catalysts for the reduction of nitroaromatic compounds and photo-oxidative degredation of toxic dyes. *Nanoscale* **2014,** *6*, 7959-7970.

22. Brown, C. A.; Ahuja, V. K., Catalytic hydrogenation. VI. Reaction of sodium borohydride with nickel salts in ethanol solution. P-2 Nickel, a highly convenient, new, selective hydrogenation catalyst with great sensitivity to substrate structure. *J. Org. Chem.* **1973,** *38*, 2226-2230.

23. Paul, R.; Buisson, P.; Joseph, N., Catalytic Activity of Nickel Borides. *Ind. Eng. Chem.* **1952,** *44*, 1006-1010.

24. Belisle, C. M.; Young, Y. M.; Singaram, B., Catalytic Reaction. 1. Catalytic 1,4-Hydrogenation of α,β-Unsaturated Aldehydes and Ketones Using SC-1 Nickel Boride. *Tetrahedron Lett.* **1994,** *35*, 5595-5598.

25. Leggans, E. K.; Barker, T. J.; Duncan, K. K.; Boger, D. L., Iron(III)/$NaBH_4$-Mediated Additions to Unactivated Alkenes: Synthesis of Novel 20′-Vinblastine Analogues. *Org. Lett.* **2012,** *14*, 1428-1431.

26. Glavee, G. N.; Klabunde, K. J.; Sorensen, C. M.; Hadjipanayis, G. C., Borohydride Reduction of Nickel and Copper Ions in Aqueous and Nonaqueous Media. Controllable Chemistry Leading to Nanoscale Metal and Metal Boride Particles. *Langmuir* **1994,** *10*, 4726-4730.

27. Hofer, L. J. E.; Shultz, J. F.; Panson, R. D.; Anderson, R. B., The Nature of the Nickel Boride Formed by the Action of Sodium Borohydride on Nickel Salts. *Inorg. Chem.* **1964,** *3*, 1783-1785.

28. He, Y.; Qiao, M.; Hu, H.; Pei, Y.; Li, H.; Deng, J.; Fan, K., Preparation of Amorphous Ni–B Alloy: The Effect of Feeding Order, Precursor Salt, PH and Adding Rate. *Mater. Lett.* **2002,** *56*, 952-957.

29. Corrias, A.; Ennas, G.; Licheri, G.; Marongiu, G.; Paschina, G., Amorphous Metallic Powders Prepared by Chemical Reduction of Metal Ions with Potassium Borohydride in Aqueous Solution. *Chem. Mater.* **1990,** *2*, 363-366.

30. Okamoto, Y.; Nitta, Y.; Imanaka, T.; Teranishi, S., Surface characterisation of nickel boride and nickel phosphide catalysts by X-ray photoelectron spectropscopy *J. Chem. Soc., Faraday Trans. 1* **1979,** *75*, 2027-2039.

31. Schaefer, Z. L.; Ke, X.; Schiffer, P.; Schaak, R. E., Direct Solution Synthesis, Reaction Pathway Studies, and Structural Characterization of Crystalline Ni_3B Nanoparticles. *J. Phys. Chem. C* **2008,** *112*, 19846-19851.

32. Legrand, J.; Taleb, A.; Gota, S.; Guittet, M.-J.; Petit, C., Synthesis and XPS Characterization of Nickel Boride Nanoparticles. *Langmuir* **2002,** *18*, 4131-4137.

33. Schreifels, J., X-Ray Photoelectron Spectroscopy of Nickel Boride Catalysts: Correlation of Surface States with Reaction Products in the Hydrogenation of Acrylonitrile. *J. Catal.* **1980,** *65*, 195-206.

34. Yoshida, S.; Yamashita, H.; Funabiki, T.; Yonezawa, T., Catalysis by Amorphous Metal Alloys. Part 1.—Hydrogenation of Olefins over Amorphous Ni–P and Ni–B Alloys. *J. Chem. Soc. Faraday Trans. 1 Phys. Chem. Condens. Phases* **1984,** *80*, 1435.

35. Deng, J., The Study of Ultrafine Ni-B and Ni-P Amorphous Alloy Powders as Catalysts. *J. Catal.* **1994,** *150*, 434-438.

36. Li, H., Liquid Phase Hydrogenation of Acetonitrile to Ethylamine over the Co_B Amorphous Alloy Catalyst. *J. Catal.* **2003,** *214*, 15-25.

37. Fernandes, R.; Patel, N.; Miotello, A.; Filippi, M., Studies on Catalytic Behavior of Co–Ni–B in Hydrogen Production by Hydrolysis of $NaBH_4$. *J. Mol. Catal. Chem.* **2009,** *298*, 1-6.

38. Liu, Y.-C.; Huang, C.-Y.; CHen, Y.-W., Hydrogenation of P-Chloronitrobenzene on Ni–B Nanometal Catalysts. *J. Nanopartical Res.* **2006,** *8*, 223-234.

39. Carenco, S.; Portehault, D.; Boissière, C.; Mézailles, N.; Sanchez, C., Nanoscaled Metal Borides and Phosphides: Recent Developments and Perspectives. *Chem. Rev.* **2013,** *113*, 7981-8065.

40. Arzac, G. M.; Rojas, T. C.; Fernández, A., Boron Compounds as Stabilizers of a Complex Microstructure in a Co-B-Based Catalyst for $NaBH_4$ Hydrolysis. *ChemCatChem* **2011,** *3*, 1305-1313.

41. Cavaliere, S.; Hannauer, J.; Demirci, U. B.; Akdim, O.; Miele, P., Ex Situ Characterization of N_2H_4-, $NaBH_4$- and NH_3BH_3-Reduced Cobalt Catalysts Used in $NaBH_4$ Hydrolysis. *Catal. Today* **2011,** *170*, 3-12.

42. Kalidindi, S. B.; Vernekar, A. A.; Jagirdar, B. R., Co–Co_2B, Ni–Ni_3B and Co–Ni–B Nanocomposites Catalyzed Ammonia–Borane Methanolysis for Hydrogen Generation. *Phys. Chem. Chem. Phys.* **2009,** *11*, 770-775.

43. Demirci, U. B.; Miele, P., Cobalt-Based Catalysts for the Hydrolysis of $NaBH_4$ and NH_3BH_3. *Phys. Chem. Chem. Phys.* **2014,** *16*, 6872.

44. Ozerova, A. M.; Bulavchenko, O. A.; Komova, O. V.; Netskina, O. B.; Zaikovskii, V. I.; Odegova, G. B.; Simagina, V. I., Cobalt Boride Catalysts for Hydrogen Storage Systems Based on NH_3BH_3 and $NaBH_4$. *Kinet. Catal.* **2012,** *53*, 511-520.

45. Geng, J.; Jefferson, D. A.; Johnson, B. F. G., The Unusual Nanostructure of Nickel–Boron Catalyst. *Chem. Commun.* **2007**, 969-971.

46. Akopov, G.; Yeung, M. T.; Kaner, R. B., Rediscovering the Crystal Chemistry of Borides. *Adv. Mater.* **2017,** *29*, 1604506.

47. Prasanth, C. P.; Joseph, E.; D. S., N.; Ibnusaud, I.; Raskatov, J.; Singaram, B., Stabilization of $NaBH_4$ in Methanol Using a Catalytic Amount of NaOMe. Reduction of Esters and Lactones at Room Temperature without Solvent-Induced Loss of Hydride. *J. Org. Chem.* **2018,** *83*, 1431-1440.

48. Brown, C. A., Catalytic Hydrogenation. V. The Reaction of Sodium Borohydride with Aqueous Nickel Salts. P-1 Nickel Boride, a Convenient, Highly Active Nickel Hydrogenation Catalyst. *J. Org. Chem.* **1970,** *35*, 1900-1904.

49. Nose, A.; Kudo, T., Reduction with Sodium Borohydride-Transition Metal Salt Systems. I. Reduction of Aromatic Nitro Compounds with the Sodium Borohydride-Nickelous Chloride System. *Chem. Pharm. Bull. (Tokyo)* **1981,** *29*, 1159-1161.

50. Patel, N.; Fernandes, R.; Edla, R.; Lihitkar, P. B.; Kothari, D. C.; Miotello, A., Superior Hydrogen Production Rate by Catalytic Hydrolysis of Ammonia Borane Using Co-B Nanoparticles Supported over Mesoporous Silica Particles. *Catal. Commun.* **2012,** *23*, 39-42.

51. Vernekar, A. A.; Patil, S.; Bhat, C.; Tilve, S. G., Magnetically Recoverable Catalytic Co–Co_2B Nanocomposites for the Chemoselective Reduction of Aromatic Nitro Compounds. *RSC Adv.* **2013,** *3*, 13243.

52. Zhao, Z.; Yang, H.; Li, Y.; Guo, X., Cobalt-Modified Molybdenum Carbide as an Efficient Catalyst for Chemoselective Reduction of Aromatic Nitro Compounds. *Green Chem.* **2014,** *16*, 1274-1281.

53. Khurana, J. M.; Kukreja, G., Rapid Reduction of Nitriles to Primary Amines with Nickel Boride at Ambient Temperature. *Synth. Commun.* **2002,** *32*, 1265-1269.

54. Pogorelić, I.; Filipan-Litvić, M.; Merkaš, S.; Ljubić, G.; Cepanec, I.; Litvić, M., Rapid, Efficient and Selective Reduction of Aromatic Nitro Compounds with Sodium Borohydride and Raney Nickel. *J. Mol. Catal. Chem.* **2007,** *274*, 2020-207.

55. Larsen, J. W.; Freund, M.; Kim, K. Y.; Sidovar, M.; Stuart, J. L., Mechanism of the Carbon Catalyzed Reduction of Nitrobenzene by Hydrazine. *Carbon* **2000,** *38*, 655-661.

56. Hauser, J. L.; Amberchan, G.; Tso, M.; Manley, R.; Bustillo, K.; Cooper, J.; Golden, J. H.; Singaram, B.; Oliver, S. R. J., A Mesoporous Aluminosilicate Nanoparticle-Supported Nickel–Boron Composite for the Catalytic Reduction of Nitroarenes. *ACS Applied Nano Materials* **2019,** *2*, 1472-1483.

57. Hauser, J. L.; Tran, D. T.; Conley, E. T.; Saunders, J. M.; Bustillo, K. C.; Oliver, S. R. J., Plasma Treatment of Silver Impregnated Mesoporous Aluminosilicate Nanoparticles for Adsorptive Desulfurization. *Chem. Mater.* **2016,** *28*, 474-479.

58. Kondrat, S. A.; Shaw, G.; Freakley, S. J.; He, Q.; Hampton, J.; Edwards, J. K.; Miedziak, P. J.; Davies, T. E.; Carley, A. F.; Taylor, S. H., Physical Mixing of Metal Acetates: A Simple, Scalable Method to Produce Active Chloride Free Bimetallic Catalysts. *Chem. Sci.* **2012,** *3*, 2965.

59. Yan, W.; Chen, B.; Mahurin, S. M.; Schwartz, V.; Mullins, D. R.; Lupini, A. R.; Pennycook, S. J.; Dai, S.; Overbury, S. H., Preparation and Comparison of Supported Gold Nanocatalysts on Anatase, Brookite, Rutile, and P25 Polymorphs of TiO_2 for Catalytic Oxidation of CO. *J. Phys. Chem. B* **2005,** *109*, 10676-10685.

60. Saldan, I., Decomposition and Formation of Magnesium Borohydride. *Int. J. Hydrog. Energy* **2016,** *41*, 11201-11224.

61. Crociani, L.; Rossetto, G.; Kaciulis, S.; Mezzi, A.; El-Habra, N.; Palmieri, V., Study of Magnesium Boride Films Obtained From $Mg(BH_4)_2$ by CVD. *Chem. Vap. Depos.* **2007,** *13*, 414-419.

62. Jensen, J. A.; Gozum, J. E.; Pollina, D. M.; Girolami, G. S., Titanium, Zirconium, and Hafnium Tetrahydroborates as “Tailored” CVD Precursors for Metal Diboride Thin Films. *J. Am. Chem. Soc.* **1988,** *110*, 1643-1644.

63. Jayaraman, S.; Yang, Y.; Kim, D. Y.; Girolami, G. S.; Abelson, J. R., Hafnium Diboride Thin Films by Chemical Vapor Deposition from a Single Source Precursor. *J. Vac. Sci. Technol. Vac. Surf. Films* **2005,** *23*, 1619-1625.

64. Rice, G. W.; Woodin, R. L., Zirconium Borohydride as a Zirconium Boride Precursor. *J. Am. Ceram. Soc.* **1988,** *71*, C-1818-C-183.

65. Goedde, D. M.; Girolami, G. S., A New Class of CVD Precursors to Metal Borides: $Cr(B_3H_8)_2$ and Related Octahydrotriborate Complexes. *J. Am. Chem. Soc.* **2004,** *126*, 12230-12231.

66. Kher, S. S.; Spencer, J. T., Chemical Vapor Deposition Precursor Chemistry. 3. Formation and Characterization of Crystalline Nickel Boride Thin Films from the Cluster-Assisted Deposition of Polyhedral Borane Compounds. *Chem. Mater.* **1992,** *4*, 538-544.

67. Maybury, P. C.; Mitchell, R. W.; Hawthorne, M. F., Hydrogen Adducts of Cobalt and Nickel Boride. *J. Chem. Soc. Chem. Commun.* **1974,** *14*, 534.

68. Beygi, H.; Sajjadi, S. A., Magnetic Properties of Crystalline Nickel and Low Phosphorus Amorphous Ni 1-X P x Nanoparticles. *Mater. Chem. Phys.* **2018,** *204*, 403-409.

69. Hendrickson, D. N.; Hollander, J. M.; Jolly, W. L., Core-Electron Binding Energies for Compounds of Boron, Carbon, and Chromium. *Inorg. Chem.* **1970,** *9*, 612-615.

70. Clary, J. W.; Rettenmaier, T. J.; Snelling, R.; Bryks, W.; Banwell, J.; Wipke, W. T.; Singaram, B., Hydride as a Leaving Group in the Reaction of Pinacolborane with Halides under Ambient Grignard and Barbier Conditions. One-Pot Synthesis of Alkyl, Aryl, Heteroaryl, Vinyl, and Allyl Pinacolboronic Esters. *J. Org. Chem.* **2011,** *76*, 9602-9610.

71. Chekin, F.; Sadeghi, S., Room Temperature Decomposition of Hydrazine Catalyzed by Nickel Oxide Nanoparticles. *Bulgarian Chemical Communications* **2015,** *47*, 714-719.

72. Petkar, D. R.; Kadu, B. S.; Chikate, R. C., Highly Efficient and Chemoselective Transfer Hydrogenation of Nitroarenes at Room Temperature over Magnetically Separable Fe–Ni Bimetallic Nanoparticles. *RSC Adv.* **2014,** *4*, 8004.

73. Schreifels, J. A.; Maybury, P. C.; Swartz, W. E., Comparison of the Activity and Lifetime of Raney Nickel and Nickel Boride in the Hydrogenation of Various Functional Groups. *J. Org. Chem.* **1981,** *46*, 1263-1269.

74. Caddick, S.; Judd, D. B.; Lewis, A. K.; Reich, M. T.; Williams, M. R., A Generic Approach for the Catalytic Reduction of Nitriles. *Tetrahedron* **2003,** *59*, 5417-5423.

75. Osby, J. O.; Heinzman, S. W.; Ganem, B., Studies on the Mechanism of Transition-Metal-Assisted Sodium Borohydride and Lithium Aluminum Hydride Reductions. *J. Am. Chem. Soc.* **1986,** *108*, 67-72.

76. Zhang, J.; Cai, Y.; Lu, G.; Cai, C., Facile and Selective Hydrogenolysis of β-O-4 Linkages in Lignin Catalyzed by Pd–Ni Bimetallic Nanoparticles Supported on ZrO_2. *Green Chem.* **2016,** *18*, 6229-6235.

77. Yoon, N. M.; Gyoung, Y. S., Reaction of Diisobutylaluminum Hydride with Selected Organic Compounds Containing Representative Functional Groups. *J. Org. Chem.* **1985,** *50*, 2443-2450.

CHAPTER 4

Real-Time Monitoring of Aqueous Organic Reduction Reactions Using Fiber Optic *Ex Situ* Raman Spectroscopy

4.1. Introduction

4.1.1. Background

Chemists have worked diligently to develop methods that reduce pollution by designing more sustainable methodologies and minimizing waste.[1-3] Many organic solvents have been singled out for being toxic, environmentally hazardous, and contributing to unnecessary waste. Designer solvents, including ionic liquids, supercritical fluids, and liquid polymers, have found use as reaction media for a variety of chemical reactions; nonetheless, many are too expensive for high volume industrial use.[4, 5] Consequently, the focus has shifted towards conducting organic reactions in aqueous medium because water is non-toxic, economically viable, and readily accessible.[6-12] However, one significant drawback in the use of water-based reaction media has been that most traditional reaction-monitoring spectroscopic techniques are not compatible with an aqueous environment. One exception is Raman spectroscopy, wherein the bands associated with water vibrational modes are mostly located in a spectral range (above 3000cm^{-1}) away from the bands associated with many organic species.[13, 14] This unique aspect of Raman spectroscopy has led to a wide realm of medical research centered on using Raman for detection of biomolecules,[15, 16] probes,[17-19] and even in aiding in understanding protein function.[20] The application of using this analytical tool to monitor aqueous organic reactions, such as the reduction of nitroarenes and carbonyl compounds, is highly desirable.

4.1.2. History of the Reduction of Nitroarenes

The reduction of nitroarenes suffers from various unsustainable reaction conditions, such as toxic metal catalysts, pressurized hydrogen, and extreme temperatures (see chapter 3 introduction).[21-23] Mitigation of these unsafe practices have included using earth abundant metals, safer hydrogen sources, and atmospheric conditions.[24-28] Specifically, a nickel boron composite (NBC) catalyst combined with a more stable hydrogen source, hydrazine hydrate, has been shown to reduce nitroarenes at ambient conditions.[26] A step further in developing more sustainable reactions would be to conduct it in an aqueous system. By using Raman spectroscopy, the reduction of nitroarenes to aniline derivatives could be easily monitored without interference from the solvent. This reaction monitoring technique could then be applied to the neutralization of more energetic compounds, such as trinitrotoluene (TNT).

4.1.3. History of Amine Boranes

As a more sustainable solvent, water-based reactions aid in conducting experiments with greener practices in mind. However, many hydrides are not soluble in water or are highly reactive in water. Amine boranes are good sources of diborane, as they are more stable than other borane adducts (such as borane-tetrahydrofuran, BH_3:THF),[29] less sensitive to moisture and air (such as borane dimethyl sulfide, BH_3SMe_2),[30] and more soluble in more diverse solvents.[31] By combining trimethylamine and diborane, Schlesinger and Burg synthesized the trimethylamine borane (**equation 1**).[32] Subsequent exchange reactions have since been found to form amine boranes including combining the amine of choice with either BH_3:THF or

BH_3SMe_2 (**equation 2**).[33] If starting from an amine salt, then a metal borohydride can be used to generate the amine borane; however, this method also produces hydrogen gas and thus, is less ideal (**equation 3**).[34-37]

$$2(\mathrm{CH_3})_3\mathrm{N} + \mathrm{B_2H_6} \longrightarrow 2(\mathrm{CH_3})_3\mathrm{N{:}BH_3} \qquad (1)$$

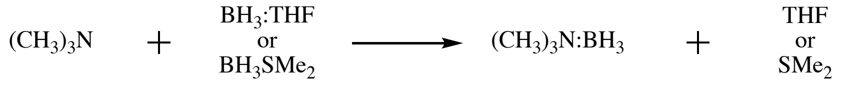

$$(\mathrm{CH_3})_3\mathrm{N} + \begin{matrix}\mathrm{BH_3{:}THF}\\ \text{or}\\ \mathrm{BH_3SMe_2}\end{matrix} \longrightarrow (\mathrm{CH_3})_3\mathrm{N{:}BH_3} + \begin{matrix}\mathrm{THF}\\ \text{or}\\ \mathrm{SMe_2}\end{matrix} \qquad (2)$$

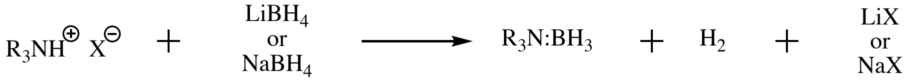

$$\mathrm{R_3NH}^{\oplus}\ \mathrm{X}^{\ominus} + \begin{matrix}\mathrm{LiBH_4}\\ \text{or}\\ \mathrm{NaBH_4}\end{matrix} \longrightarrow \mathrm{R_3N{:}BH_3} + \mathrm{H_2} + \begin{matrix}\mathrm{LiX}\\ \text{or}\\ \mathrm{NaX}\end{matrix} \qquad (3)$$

Traditionally, the reduction of carbonyl compounds requires the use of metal hydrides or reactive boranes in organic solvents, but they may also be achieved using amine boranes in a water-alcohol mixture.[38-40] Amine boranes have found wide utility in the reduction of a variety of functional groups because they can tolerate protic and aprotic solvents.[33, 41, 42] **Table 4.1** illustrates a selection of amine boranes and their solubilities in different solvents. All of the selected amine boranes are soluble in the ethereal solvents, THF and diethyl ether. The use of benzene and dichloromethane showed reasonable solubility across the amine boranes; however, use of these solvents is not ideal from a green chemistry perspective. It is the protic solvents, ethanol and water, that make amine boranes differ from other reducing agents, which would react with the solvent. Even within this selection of amine boranes, few are soluble in water. Ammonia borane, dimethylamine borane (DMAB), and morpholine borane are the most soluble in water.

Table 4.1. Solubilities of amine borane complexes at 25 °C [a,b]

Borane Complex	H_2O	CH_3OH	Et_2O	THF	Hexane	Benzene	CH_2Cl_2
Ammonia	VS	VS	VS	VS	SS	S	VS
t-butylamine	S	VS	S	VS	I	S	S
dimethylamine	VS	VS	VS	VS	I	VS	VS
trimethylamine	SS	VS	VS	VS	I	VS	VS
triethylamine	SS	VS	VS	VS	VS	VS	VS
morpholine	VS	VS	S	VS	I	S	VS
N,N-diethylaniline	R	R	VS	VS	VS	VS	VS
pyridine	SS	VS	VS	VS	I	VS	VS
2,6-lutidine	SS	VS	S	VS	I	VS	VS

[a] R = reacts; I = insoluble, <0.1g/100mL; SS = slightly soluble, 0.1-1.0g/100mL; S = soluble, 1.0-3.0g/100mL; VS = very soluble, >3.0g/100mL. [b] Refs: [41, 42]

Nonetheless, the precise reducing ability of amine borane complexes is specific to the amine. For instance, a trend has been observed in which the reducing ability of an aliphatic amine borane decreases as the sterics surrounding the nitrogen atom increases: $H_3N{:}BH_3 > RNH_2{:}BH_3 > R_2NH{:}BH_3 > R_3N{:}BH_3$.[37, 42] Thus, DMAB should be a desirable reducing agent as it is both soluble in water and not too sterically demanding. Various reports have illustrated DMAB as an effective reductant in electroless plating,[43-45] as a hydrogen source for catalytic hydrogenation reactions,[46-48] and in reductive amination reactions.[48, 49] As a reducing reagent for organic transformations, DMAB has been shown to reduce Schiff bases,[50] imines,[42] and α,β-unsaturated hydrazones.[51] Based on its reductive abilities and its solubility in water, DMAB was chosen to demonstrate the aqueous reduction of carbonyls and how Raman spectroscopy can be used to monitor the aqueous reaction.

4.1.4. Raman Spectroscopy in Organic Reactions

A Raman spectrometer can be outfitted with a fiber optic probe that may be immersed into the reaction vessel (*in situ*) or placed outside of the reaction vessel (*ex situ*) to perform "real-time" monitoring and analysis of any reaction (**Figure 4.1**). The *ex situ* probe allows for fast monitoring that is easy to use, non-invasive, and requires little to no sample preparation. Utilization of this *ex situ*[52] analytical tool ranges in disciplines from art conservation analysis[53, 54] to forensic science.[55, 56] In spite of these uses, Raman spectroscopy has been used sparingly as a tool to monitor reactions in an aqueous medium, especially in terms of *ex situ* real-time reaction monitoring.

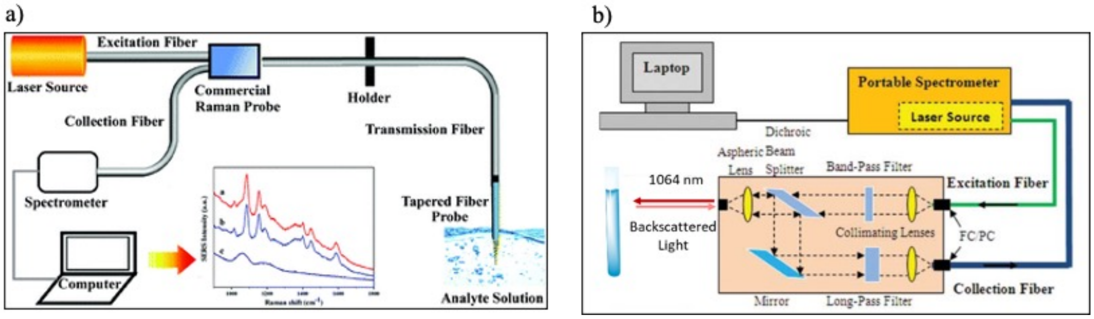
a)
Excitation Fiber
Laser Source
Commercial Raman Probe
Holder
Collection Fiber
Transmission Fiber
Spectrometer
Tapered Fiber Probe
Computer
Analyte Solution
b)
Laptop
Portable Spectrometer
Laser Source
Dichroic
Aspheric Beam Lens Splitter
Band-Pass Filter
1064 nm
Excitation Fiber
Backscattered Light
Collimating Lenses
FC/PC
Mirror
Long-Pass Filter
Collection Fiber

Figure 4.1. a) An example of the set up for an *in situ* reaction monitoring with Raman spectroscopy. b) An example of the set up for an *ex situ* reaction monitoring with Raman spectroscopy.

Raman spectroscopy has been used to monitor some organic reactions. Many of them involve the *in situ* method,[57-60] or the reactions occur under neat or organic solvents, which have distinct signals that may obscure the signal of interest.[57-61] For instance, the synthesis of substituted imidazoles and epoxides were two reactions where *in situ* Raman spectroscopy was used to monitor the reaction mixtures' progress.[57, 58] In both reactions, an immersible probe was dipped into the reaction flask and as the reaction progressed, scans were taken to monitor the decrease of the reactant signals and the increase of the product signals. After normalizing the Raman signals and isolating distinct signals relating to starting materials and products, the Raman data could be plotted against time. By doing this, researchers were able to identify a clear moment when the reactions reached completion.

Additionally, the synthesis of coumarins were shown to be easily monitored by Raman spectroscopy, and by careful analysis of the data, some mechanistic information could be obtained, expanding Raman's utility.[59] The Pechmann condensation reaction, between resorcinol and ethyl acetoacetate, was chosen as the model reaction for this chemical transformation (**Scheme 4.1**). The Raman probe was immersed into the reaction mixture and scans were taken every 10 minutes. The Raman stretches associated with the starting materials and the products were distinct enough to allow for clear real-time reaction monitoring. The reaction progressed as anticipated, with the resorcinol and ester signals decreasing in intensity over time and the signals for the coumarin product increasing in intensity. To show more clearly the transformation, the intensities from the 998 cm^{-1} stretch for resorcinol and the two stretches indicative for the coumarin product (the 1570 cm^{-1} associated with the C-O stretch and 1200 cm^{-1} correlated to the trisubstituted arene) were normalized and plotted against reaction time. Interestingly, the resorcinol stretch at 998 cm^{-1} showed two sharp declines, after

0.5 h and 1.5 h, yet the product plots do not increase as sharply until after the 2 h reaction mark. This data indicated that, within the first two hours, the reaction was undergoing a series of intermediate steps. The researchers predicted an electrophilic aromatic substitution and transesterification steps followed by dehydration. This has since been corroborated with NMR studies of some isolated intermediates.[62] Even though the intermediates themselves were not observed in Raman spectroscopy, this work highlights how Raman spectroscopy could be used to monitor a reaction, and through subtle tuning, mechanistic insights can be obtained.

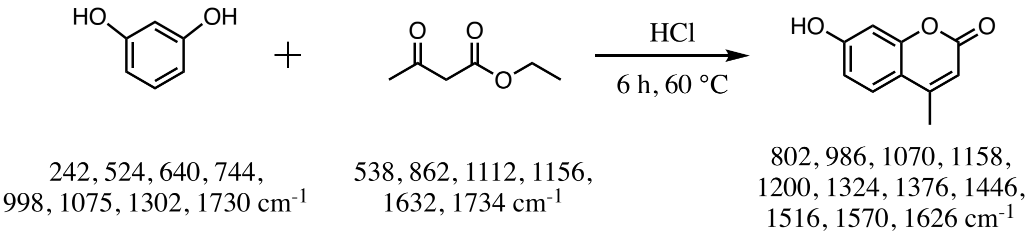
HO
OH
O
O
O
HCl
6 h, 60 °C
HO
O
O
242, 524, 640, 744, 998, 1075, 1302, 1730 cm-1
538, 862, 1112, 1156, 1632, 1734 cm-1
802, 986, 1070, 1158, 1200, 1324, 1376, 1446, 1516, 1570, 1626 cm-1

Scheme 4.1. Pechmann condensation reaction between resorcinol and ethyl acetoacetate to produce 7-hydroxy-4-methylcoumarin and their significant Raman stretches.

Similarly, mechanistic observations were obtained from the real-time monitoring of the acetalization of acetone with glycerol to afford solketal (**Scheme 4.2**).[60] In addition to the stretches corresponding to starting materials and product, Raman spectroscopy was able to detect glycerol-glycerol interactions (3324 cm^{-1}) and glycerol-acetone interactions (732 cm^{-1}). It was interesting to observe that the glycerol-glycerol interactions appeared 30 min after the acidic catalyst, (3-mercaptopropyl)trimethoxy silane, was added. However, since solketal stretches were present within the first several minutes, it was reasoned that the glycerol-glycerol interactions were not important for the formation of solketal. Oppositely, the glycerol-acetone stretch emerged as soon as the acidic catalyst was added, and soon afterwards the bands relating to solketal appeared. This trend indicates that the glycerol-acetone interaction was a necessary occurrence for the formation of the product. These results demonstrate that Raman spectroscopy is a subtle analytical tool that can be used to monitor a reaction, in real-time, and be used to better under a reaction's mechanism.

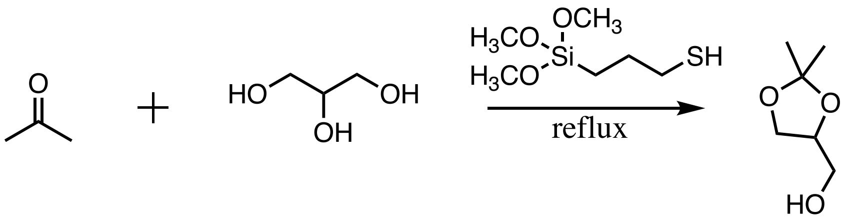

Scheme 4.2. Production of solketal from the acetalization of acetone and glycerol with 3-mercaptopropyl)trimethoxy silane as the acidic catalyst.

Limited reports describe using Raman spectroscopy in an *ex situ* manner to monitor a reaction.[63, 64] Work conducted by Leadbeater and Smith demonstrate how a Suzuki coupling reaction can be monitored with Raman spectroscopy.[63] By setting up the Raman probe outside the reaction vessel, they were able to observe the coupling reaction occur through a non-invasive manner.

Similarly, when salicylaldehyde and ethyl acetoacetate were combined with piperidine as the catalyst, and ethyl acetate as the solvent, 3-acetylcoumarin was formed (**Figure 4.2a**).[64] This reaction took place in a microwave unit containing a cavity where the Raman probe could be inserted and positioned against the reaction vessel. The reaction mixture was monitored in real time using the *ex situ* method. Of the Raman stretches associated with 3-acetylcoumarin, the signals at 1563 cm^{-1} and

1608 cm^{-1} were closely monitored as they do not overlap with any of the starting materials or reagents. Closer examination of the 1500-1680 cm^{-1} region showed a local maximum at 1630 cm^{-1} that formed and then disappeared once the reaction was complete (**Figure 4.2b**). The researchers theorized that this peak was an intermediate of the reaction, thus demonstrating that Raman spectroscopy can aid in providing mechanistic insights. Because of the non-invasive monitoring approach, kinetic data was easily obtained and calculated to be first order rate laws.

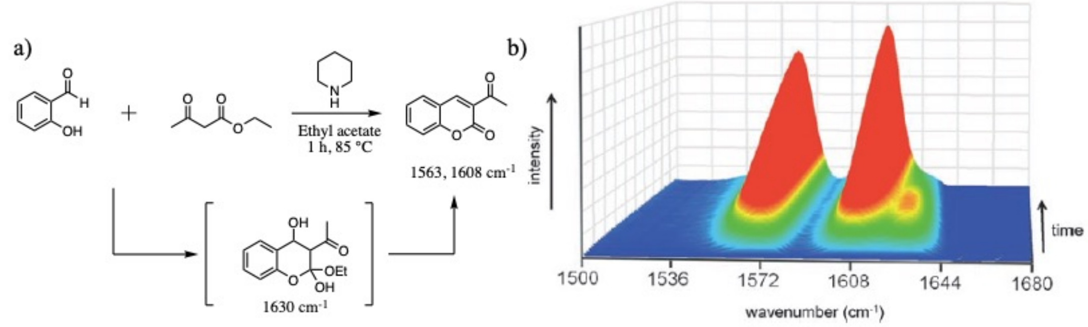

Figure 4.2. a) Condensation reaction between salicylaldehyde and ethyl acetoacetate to produce 3-acetylcoumarin and its significant Raman stretches. b) 3D profile of Raman spectra relating to 3-acetylcourmarin as a function of time and intensity from the region of 1500-1680 cm^{-1}.[64]

In both of these examples of *ex situ* reaction monitoring, additional data manipulation was required due to their selection of solvent systems, water/ethanol, and ethyl acetate, respectively.[63, 64] The organic solvents contain Raman stretches that mask the reactant and product signals. The researchers overcame this problem by subtracting out the solvent signals. However, a more efficient method would be to use a more water-based reaction system, as the water signal is less apparent in the region for many organic compounds.

Accordingly, aqueous reductions of nitroarenes and ketones, using a nickel boron composite catalyst and dimethylamine borane respectively, were undertaken to evaluate the utility of *ex situ* Raman spectroscopy (**Figure 4.3**). The instrument's sensitivity in calculating reaction kinetics and substrate selectivity demonstrate the efficacy and practicality of this analytical tool. Herein, we report the viability of using Raman spectroscopy as an *ex situ*, real-time, and non-invasive reaction monitoring technique for reactions in aqueous medium.

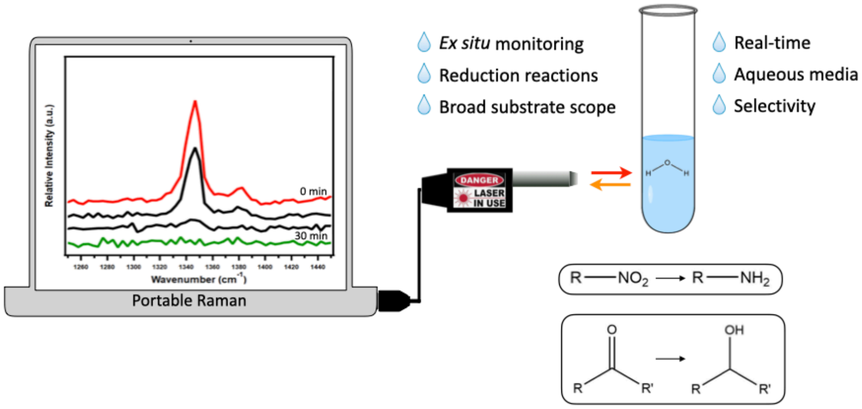
Relative Intensity (a.u.)
0 min
30 min
Wavenumber (cm^{-1})
1260
1280
1300
1320
1340
1360
1380
1400
1420
1440
Portable Raman
DANGER
LASER IN USE
Ex situ monitoring
Reduction reactions
Broad substrate scope
Real-time
Aqueous media
Selectivity
R—NO$_2$ → R—NH$_2$
O
R
R'
OH
R
R'

Figure 4.3. *Ex situ* reaction monitoring with Raman spectroscopy for aqueous reduction reactions.

4.2. Results and Discussion

4.2.1. Reduction of Nitroarenes Monitored with Raman Spectroscopy

Tri-nitroarenes are explosive compounds which may be neutralized by chemical reduction in aqueous media before safe disposal.[65] Advantageously, the aromatic nitro groups exhibit Raman signals (1330 – 1370 cm^{-1}) and thus enable the safe real-time monitoring of the transformation to more innocuous amines. The facile reduction of 4-nitrotoluene to the amine was achieved using a catalysis procedure, as reported in Chapter 3, in which the nitro group is reduced to the amine using a nickel boron composite (NBC) catalyst (**Scheme 4.3**).[26]

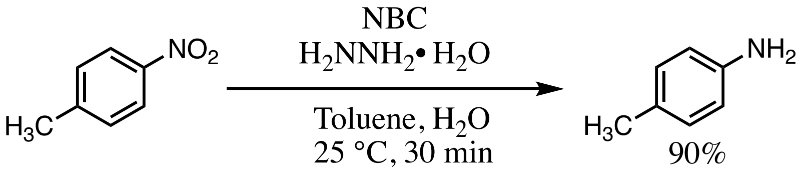

Scheme 4.3. Reduction of 4-nitrotoluene to 4-toluidine (90% isolated yield) using NBC catalyst and hydrazine hydrate.

We were able to continuously monitor the nitro group reduction by positioning the fiber optic probe against the test tube, and wherein the laser focal point was focused just inside the vial glass wall so as to just impinge on the reaction mixture on the other side of the glass wall. This *ex situ* technique is convenient in that it avoids the need for an immersion probe or for the need to remove aliquots for analysis. The reduction of 4-nitrotoluene was considered complete when the nitro group signal (1350 cm^{-1}) was no longer observed, or was undifferentiated from the baseline noise, (ca. 30 min.) (**Figure 4.4**).

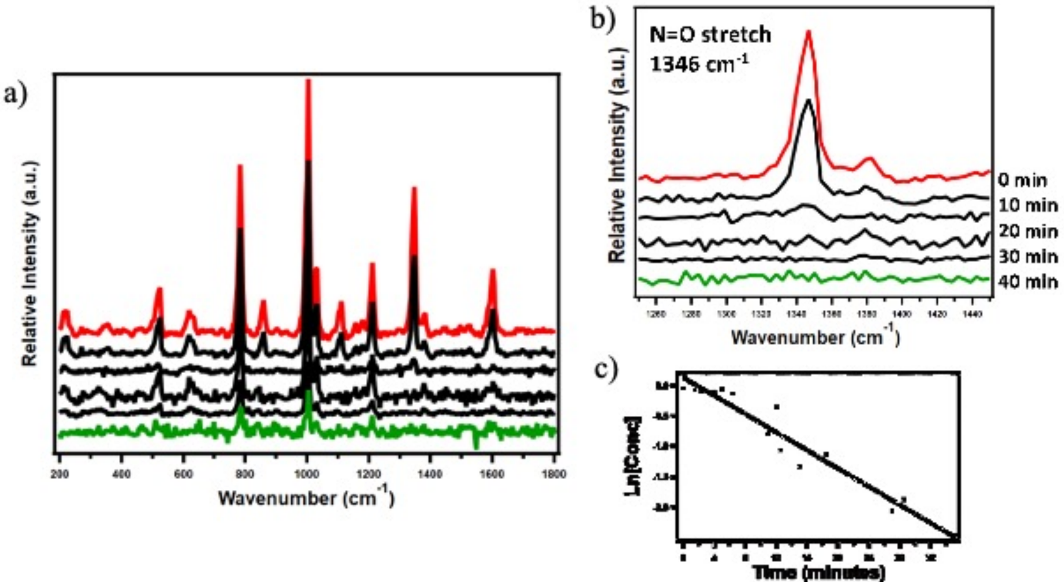

Figure 4.4. a) *Ex situ* Raman monitoring of the reduction of 4-nitrotoluene catalyzed with NBC catalyst and hydrazine hydrate in toluene at 25 °C. Red and green highlight the start and end of the reaction. b) A plot of the natural log of concentration vs. time to extract the rate constant of the nitro reduction reaction.

Visually, the reaction mixture transformed from a yellow solution to a yellow turbid mixture, and then finally to a clear colorless solution (**Figure 4.5**). Quantitative product formation was confirmed by determining ^{1}H NMR spectrum of the isolated product, which showed signals corresponding to the complete conversion of 4-nitrotoluene to 4-toluidine.

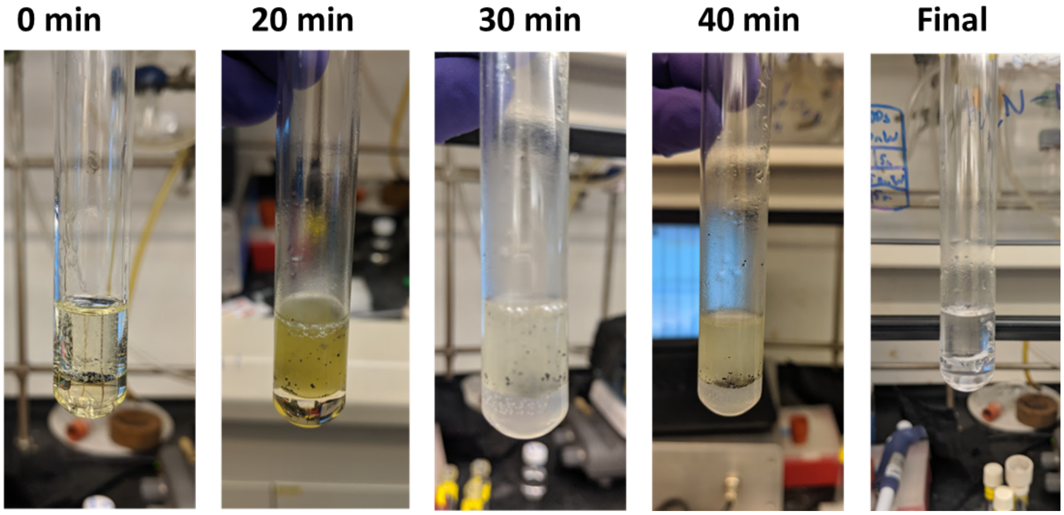

Figure 4.5. Photographs showing the reduction of 4-nitrotoluene at various time points. Overtime the reaction mixture transforms from clear and yellow to turbid and yellow/colorless to a clear and colorless solution.

A calibration curve of 4-nitrotoluene was used to determine the concentration of the reactant as the reaction proceeded. Prior to initiating the reaction or reagent addition, the intensity of the nitro stretch at 10 concentrations between 1.0 M and 0.01 M were measured and normalized to a toluene co-solvent peak at 1379 cm^{-1} (**Figure 4.6**). The rate of reaction could then be determined. By comparing the normalized peak intensity of 4-nitrotoluene as the reaction progressed over time, Raman spectroscopy provided a straightforward method to calculate that the reduction follows a pseudo first order rate law (**equation 4**).[66, 67]

$$Ln[C(t)] = kt + Ln[C(0)]; k = -0.018 \pm 0.003; C(0) = 1.0\ M \qquad (4)$$

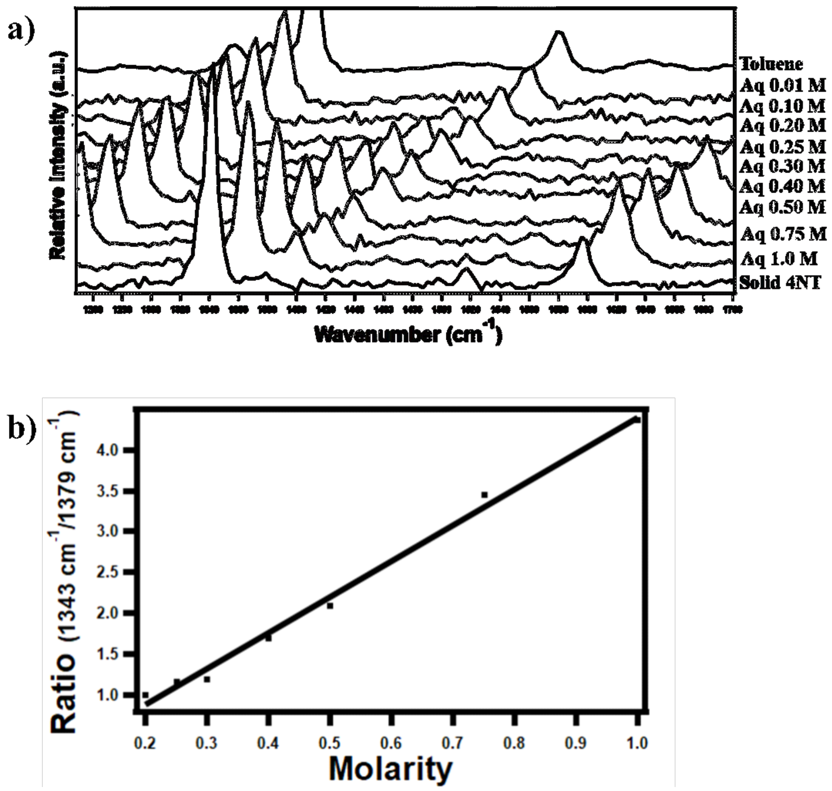

Figure 4.6. a) Near-IR Raman spectra of 4-nitrotoluene in a series of dilutions in toluene from 0.01 M to 1.0 M. b) Calibration curve developed from taking the ratio of the nitro peak at 1343 cm^{-1} and the toluene peak at 1379 cm^{-1}.

As mentioned earlier, the reduction and neutralization of nitroarenes comprising of multiple nitro groups are of interest as they are higher energy compounds and are more challenging to neutralize and/or to dispose of. The reduction of di-nitroarenes are less explored and typically require elevated temperatures to obtain either partial or complete reduction of the dinitro compounds.[25] The compound 2,4-dinitrotoluene was selected to undergo reduction with NBC catalyst and hydrazine hydrate (**Scheme 4.4**).

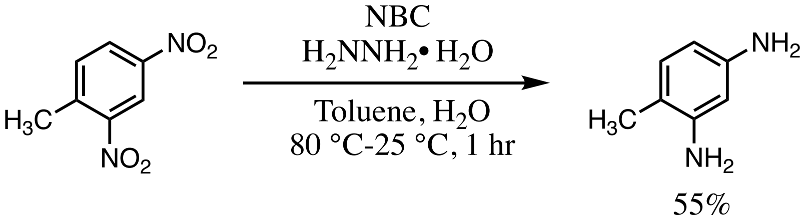

Scheme 4.4. Reduction of 2,4-dinitrotoluene to 2,4-diaminotoluene (55% isolated yield) using NBC catalyst and hydrazine hydrate.

Under our reaction conditions, no reduction was observed at 25 °C, but initiated at 80 °C. Interestingly, as soon as hydrazine was introduced to the reaction mixture the solution turned red, possibly due to a Meisenheimer complex formation between the nucleophilic hydrazine and the electron-poor aromatic ring (**Figure 4.7**).[68] Over time, the red color disappeared and the reaction mixture returned to a colorless solution.

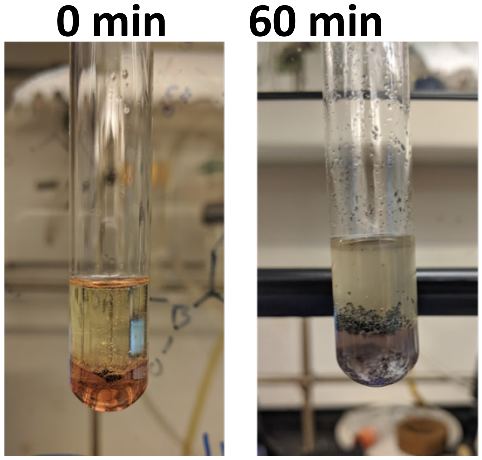

Figure 4.7. Images of the reduction of 2,4-dinitrotoluene at the early stages and late stages of the experiment. Overtime the reaction mixture transforms from clear and yellow to turbid and colorless.

Real-time monitoring of the reduction of 2,4-dinitrotoluene with the *ex situ* Raman probe showed that the nitro signal (1350cm^{-1}) disappeared after a 60 min (**Figure 4.8**). Using the spectral data and the calibration curve (**Figure 4.9**), we were able to calculate the kinetics of the reduction reaction follows a pseudo first order rate law (**equation 5**).

$$Ln[C(t)] = kx + LN[C(0)]; k = -0.049 \pm 0.029; C(0) = 1.0\ M \qquad (5)$$

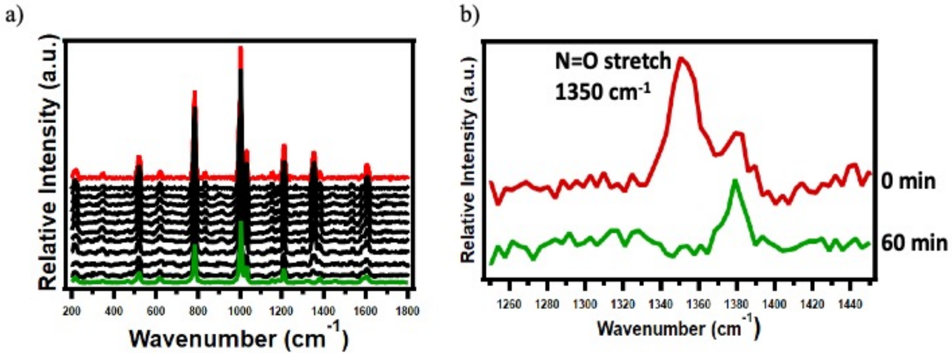

Figure 4.8. a) Full spectrum of *ex situ* Raman monitoring of the reduction of 2,4-dinitrotoluene using the NBC catalyst and hydrazine hydrate at 80 °C with continuous stirring where red and green highlight the start and end of the reaction. b) Expansion of the region associated with the nitro group.

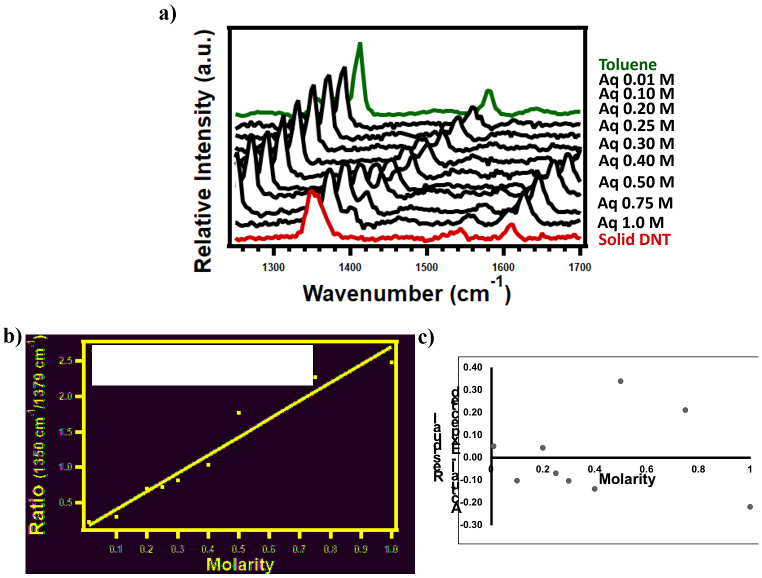

Figure 4.9. a) Infrared Raman spectra of neat toluene (green), of a crystalline sample of 2,4-dinitrotoluene (red), and of 2,4-dinitroltoluene dissolved in toluene from 0.01 M to 1.0 M (black). b) Calibration curve based on the ratio of the nitro peak at 1350 cm^{-1} and the toluene peak at 1379 cm^{-1}. c) A test of the goodness of fit of the calibration data.

We also probed the reduction of 2,4,6-trinitrotoluene (TNT) using an *ex situ* Raman spectroscopy. In this reduction we also observed a color changed from pale yellow to purple, suggesting the formation of a Meisenheimer complex. As before, the *ex situ* Raman probe enabled us to monitor the disappearance of the nitro signal at 1360 cm^{-1} over a 3 h period (**Figure 4.10**). Although the amine was not isolated, these data demonstrate that TNT can be reduced using this method and the utility of *ex situ* Raman spectroscopy to monitor the reduction of hazardous materials in real-time.

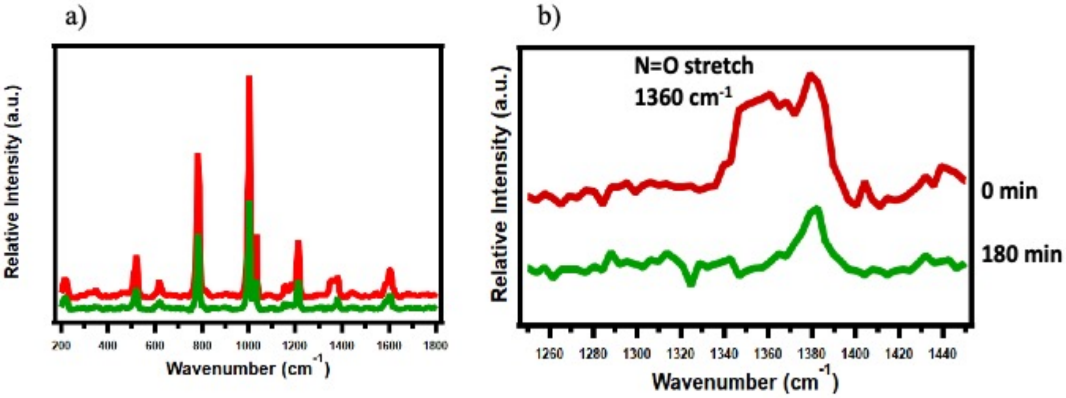

Figure 4.10. a) Full spectrum *ex situ* Raman monitoring of the reduction of 2,4,6-trinitrotoluene using an NBC catalyst and hydrazine hydrate at 80 °C with continuous stirring. The red graph is the initial measurement, and the green graph is the final measurement. b) Expansion of the region associated with the nitro group. The red graph is the initial measurement, and the green graph is the final measurement.

4.2.2. Reduction of Cyclohexanone by Aqueous Dimethylamine Borane (DMAB).

We monitored in real-time the reduction reactions of ketones by DMAB in aqueous media using *ex situ* Raman spectroscopy. The relatively high solubility of DMAB in water (8 M) and immiscibility with most carbonyl compounds produced two phases (organic-water) after mixing. The biphasic system allows for the Raman probe to be focused *ex situ* in or about on each separate phase, thereby lessening any signal overlap or interference that would be present in a homogenous system.

Cyclohexanone was initially chosen for this study due to its ease of reduction and immiscibility in water. Previous amine boranes have been shown to reduce the cyclic ketone, but many require extended reaction times or acidic environments to achieve high product yields (**Figure 4.11**).[41] Conversely, reduction by DMAB occurs at in water, under basic conditions, and complete reduction is achieved in under 5 min (**Figure 4.11**, blue box). Because DMAB contains three hydrides and cyclohexanone only needs one hydride to form the alcohol, a 3:1 stoichiometric ratio (cyclohexanone:DMAB) was employed. Overall, complete reduction of cyclohexanone to cyclohexanol was rapidly achieved at ambient conditions and without the aid of an acidic catalyst.

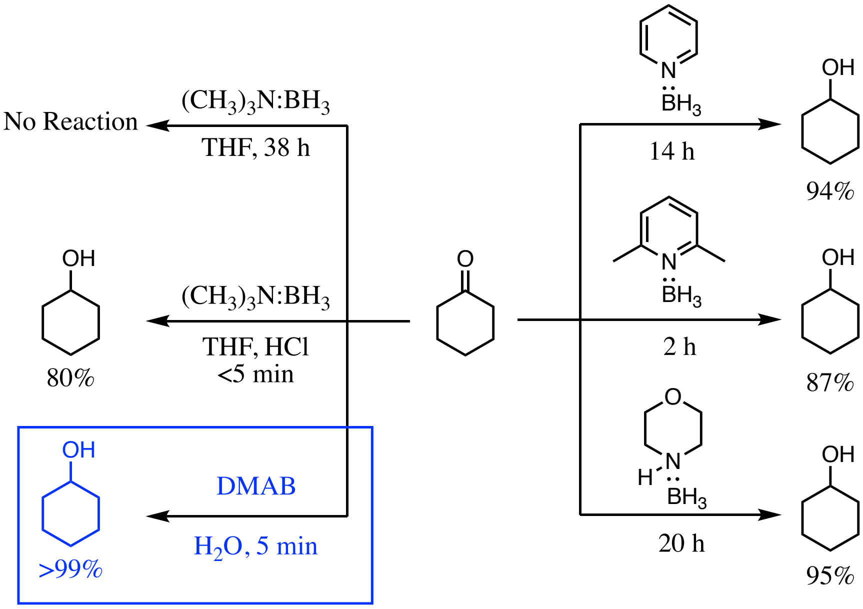

Figure 4.11. Reduction of cyclohexanone by different amine boranes. This work, reported in this chapter, is in the blue box. The reductions on the right with cyclic amine boranes occurred in glacial acetic acid at 25 °C.

The real-time *ex situ* monitoring of the carbonyl reduction by aqueous DMAB captured the rapid conversion of the carbonyl to the secondary alcohol (**Figure 4.12**). As the reaction progressed, three distinct signal shifts were observed. The most prominent feature was the disappearance of the carbonyl signal (C=O stretch at 1707 cm^{-1}) after 5 min. Additionally, as the reaction proceeded, the ring stretch position shifted from 753 cm^{-1} to 789 cm^{-1}. The ring stretch is the in-phase extension of the C-C and C-H bond lengths.[69] The shift occurs due to the decreased bond stiffness of the C-O bond allowing the C-C and C-H bonds to vibrate at a higher frequency.[70] Lastly, the secondary alcohol (C-O stretch at 1450 cm^{-1}) appeared and grew as the carbonyl stretch decreased.[69, 71]

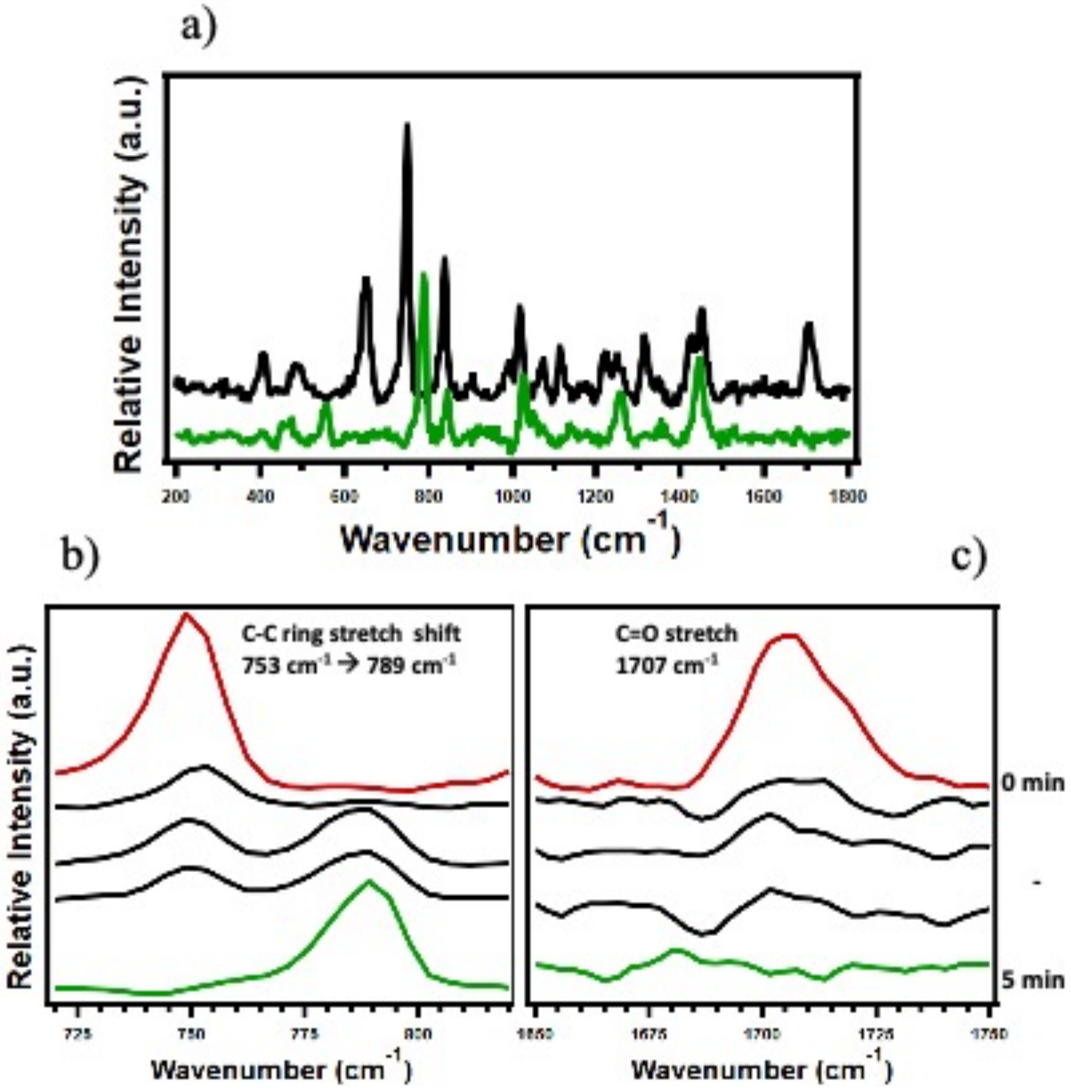

Figure 4.12. a) Full Raman spectra of the reduction of cyclohexanone using DMAB in water. The black spectrum shows starting material, and the green spectrum shows the product. b) and c) Expanded Raman spectra of the reduction of cyclohexanone using DMAB in water. The red spectrum shows starting material with the C=O stretch (carbonyl, 1707 cm^{-1}) and C-C ring stretch (753 cm^{-1}). The black spectra show the reaction progression. The green spectrum shows significant changes in the regions between 600 to 1800 cm^{-1}, attributed to the conversion of ketone to alcohol, including the appearance of the C-O (2° alcohol, 1450 cm^{-1}) and shifted C-C ring stretch (798 cm^{-1}).

4.2.3. Reduction of Cyclohexene-1-one by Aqueous Dimethylamine borane (DMAB).

The reduction by DMAB of a less reactive ketone was studied to explore the utility of aqueous DMAB and to monitor the reaction by placing the Raman probe outside the reaction vessel.[38] Indeed, this reduction required a significantly longer reaction time of 4 h compared to cyclohexanone reduction in 5 min (**Scheme 4.5**). When using a 3:1 ratio of *α,β*-unsaturated ketone to DMAB, cyclohexanol was isolated as a singular product. Interestingly, when ketone:DMAB was used in 3:2 ratio, a mixture of products containing 2-cyclohexen-1-ol (60%) and cyclohexanol (40%) was obtained. This product distribution suggests that 1,2-reduction is more facile than 1,4-reduction.

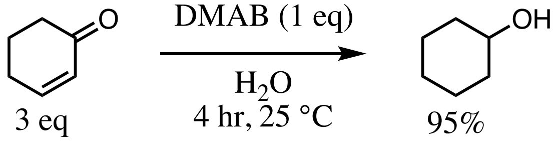

Scheme 4.5. The reduction of cyclohexen-1-one to cyclohexanol (95% isolated yield) in aqueous DMAB (pH 10).

By placing the fiber optic probe against the reaction vial, clear observation of the carbonyl stretch (1659 cm^{-1}) and the alkene stretch (1615 cm^{-1}) were seen to diminish in intensity over the course of 4 h (**Figure 4.13**). The reaction was considered complete after 4 h when no distinct carbonyl stretch was observed. Much like the saturated ketone, there was an observed peak shift from 767 cm^{-1} to 785 cm^{-1} associated with the in-phase ring stretch of alkyl ring.

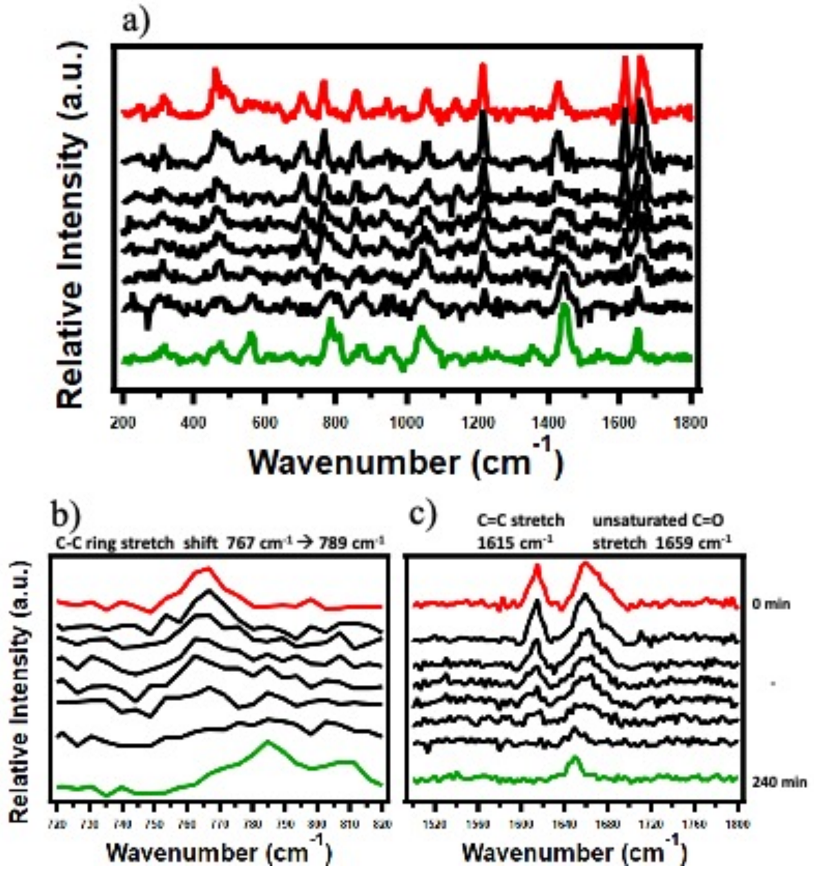

Figure 4.13. a) Full Raman spectra of the reduction of 2-cyclohexen-1-one using DMAB in water. The red spectrum shows starting material, the black spectra show the reaction progression, and the green spectrum shows the final reaction spectrum. b) and c) Expanded Raman spectra of the reduction of cyclohexen-1-one using DMAB in water. The red spectrum shows starting material with the C=O stretch (carbonyl, 1659 cm^{-1}), C=C (alkene, 1615 cm^{-1}), ring stretch (767 cm^{-1}). The black spectra show the reaction progression. The green spectrum shows significant changes indicative of reaction completion the appearance of the C-O (2° alcohol, 1442 cm^{-1}) and shifted C-C ring stretch (785 cm^{-1}).

4.2.4. Competitive Reductions by Aqueous Dimethylamine borane (DMAB).

As mild reducing reagents, amine boranes have the advantage of being chemo-selective, for instance they can reduce aldehydes or ketones in the presence of esters.[39] However it would be fruitful to further understand if there is reliable selectivity between aldehydes and ketones or even between higher and lower reactive ketones.

Andrews found that aldehydes were selectively reduced over cyclohexanone by *t*-butylamine borane. Additionally, *t*-butylamine borane preferentially reduced cyclohexanone when in the presence of aliphatic or aromatic ketones. When comparing cyclohexanone to 2-cyclohexen-1-one, *t*-butylamine converted cyclohexanone in 95% yield. His results demonstrate that when an amine borane is in the presence of two carbonyls it will selectively reduce the more reactive one.[38]

Since aqueous DMAB reacts more slowly with the α,β-unsaturated carbonyl compound, it seemed possible that it could be used as a selective reducing agent for saturated carbonyl compounds. Accordingly, a competitive reaction between 2-cyclohexen-1-one and cyclohexanone was conducted to demonstrate this selectivity of aqueous DMAB (**Scheme 4.6**). A sub-stoichiometric amount of DMAB (0.33 equiv) was used in the competitive reactions so that only the faster reacting carbonyl compound might be reduced selectively. By positioning the Raman probe outside the reaction vessel, it was possible to observe in real-time the competitive reduction reaction of the two carbonyl compounds. In the presence of aqueous DMAB, the Raman spectral analysis exhibited the saturated carbonyl stretch (1707 cm^{-1}) disappeared in 5 min while the α,β-unsaturated carbonyl signal (1659 cm^{-1}) remained unchanged (**Figure 4.14**). Product analysis through ^{1}H NMR spectroscopy confirmed the presence of unreacted 2-cyclohexen-1-one while cyclohexanone was fully converted into the corresponding alcohol.

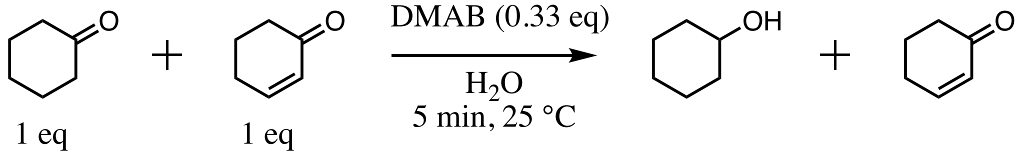

Scheme 4.6. To elucidate the reaction kinetics of the mixture, a 1.5:1.5:3 mmol reaction of cyclohexanone:2-cyclohexen-1-one:DMAB was performed.

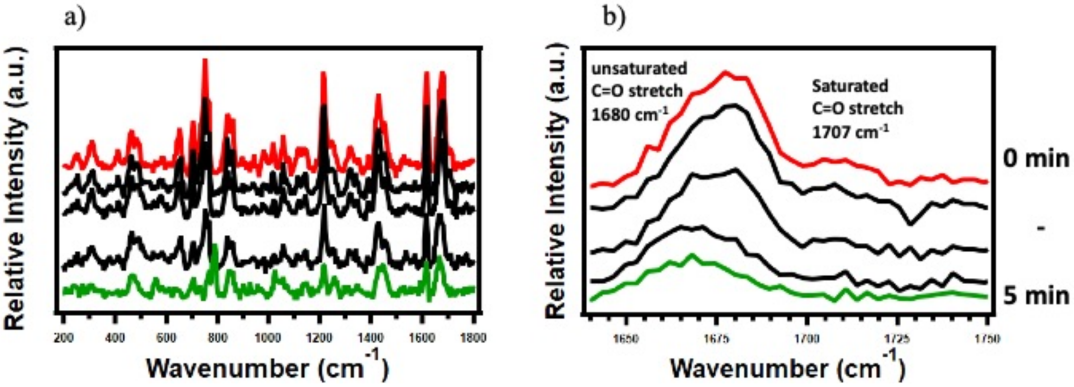

Figure 4.14. a) Full Raman spectra of the reduction of a 1:1 mixture of cyclohexanone:cyclohexen-1-one using DMAB in water. The selective reduction of the saturated ketone was complete within 5 min as shown by the disappearance of the carbonyl stretch (1707 cm^{-1}). The red and green spectra show the pure starting material and product in solution, respectively. b) Expanded view of the Raman spectra relating to the carbonyl stretch (1707 cm^{-1}). The red and green spectra show the pure starting material and product in solution, respectively.

Further exploration of aqueous DMAB as a selective reducing agent warranted us to compare the relative rate of the cyclohexanone reduction with the reduction of an epoxide, such as cyclohexene oxide (**Scheme 4.7**). Similar to the results for 2-cyclohex-1-one reported above, the saturated ketone was reduced in less than 5 min, as evidenced by the fiber optic Raman spectral data, and the epoxide remained unreactive under the same reaction condition and was recovered in essentially pure form when 0.33 equivalence of DMAB was used (**Figure 4.15**). The reaction of cyclohexanone and cyclohexene oxide was reacted for 15 minutes; however, the selective reduction of the cyclohexanone was complete within 5 min. as evidenced by the disappearance of the carbonyl stretch (1707 cm^{-1}). The epoxide remained unreacted as demonstrated by the presence of the C-O stretch (1262 cm^{-1}).[58, 72, 73,74] It is evident from these experimental results, that aqueous DMAB can be used as a selective reducing agent for saturated carbonyl compounds in presence of conjugated carbonyl compounds and simple epoxides.

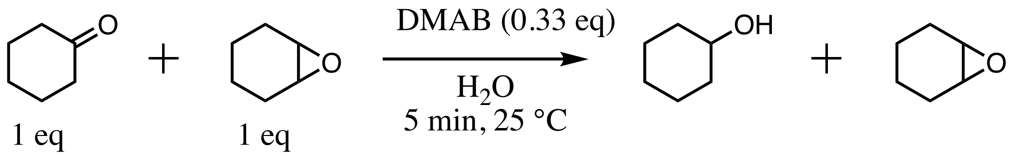

Scheme 4.7. To elucidate the reaction kinetics of the mixture, a 1.5:1.5:3 mmol reaction of cyclohexanone:cyclohexene oxide:DMAB was performed.

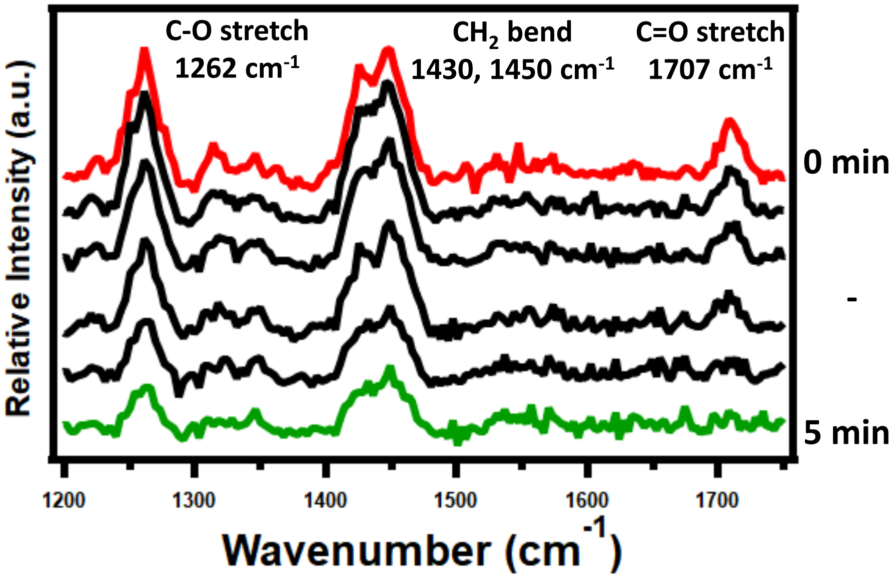

Figure 4.15. Raman spectra of the reduction of a 1:1 mixture of cyclohexanone:cyclohexene oxide using DMAB in water. The reaction was monitored for 14 min total, but the selective reduction of the saturated ketone completed within 5 min as shown by the disappearance of the carbonyl stretch (1707 cm^{-1}) and the continued presence of the C-O stretch (1262 cm^{-1}). The red and green spectra show the starting material and product in solution.

4.2.5. Mechanistic Insights for the Reduction of DMAB and Cyclohexanone.

During the reactions with cyclohexanone, some interesting observations were made that led to the exploration into the mechanism of DMAB's hydride transfer. When neat cyclohexanone was mixed with aqueous DMAB (8M, pH 10), an opaque-amber emulsion was formed, with heat generation and gas evolution observed. The Raman data that was collected after mixing indicated that the reaction was essentially complete in 5 min. Although, gas evolution was observed, hydrogen gas meter measurements[75] showed only a small amount of hydrogen evolution (<9%), due to hydrolysis of DMAB (**Table 4.2).**

Table 4.2. Gas evolution analysis of the reaction between cyclohexanone and aqueous DMAB[a]

Trial	Cyclohexanone	DMAB	H_2 Evolved	Theoretical Amount of H_2	Percentage of H_2 Evolved
1	3 mmol	1 mmol	0.233 mmol	3 mmol	7%
2	3 mmol	1 mmol	0.273 mmol	3 mmol	9%

[a]Cyclohexanone was added to a round-bottom flask containing a side-arm, which was then attached to the hydrogen meter. Once the system had equilibrized, aqueous DMAB was injected and the H_2 was quantified.

We subsequently found that the gas evolution and bubbling was due to gaseous dimethylamine, as shown by a gas trapping experiment and ^{1}H NMR analysis (**Figure 4.16**). However, when a more dilute aqueous DMAB (2 M) was used, we did not observe the gas evolution or bubbling.

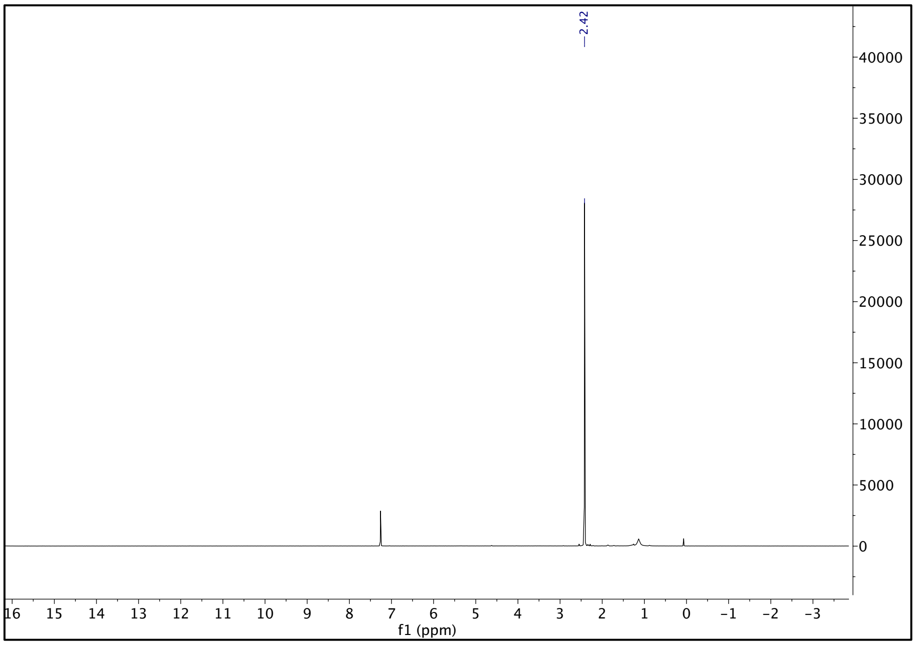

Figure 4.16. ^{1}H NMR of dimethylamine in $CDCl_3$.

Based on these observations, three scenarios may be mechanistically plausible: A) at high pH, the hydroxide anions in the reaction mixture may activate the DMAB to form a monohydroxy borohydride species (**Figure 4.17A**), B) DMAB reacts with the protonated carbonyl group at the organic-water interface (**Figure 4.17B**), or C) the undissociated DMAB molecule in the aqueous phase undergoes phase transfer into the cyclohexanone organic phase, and reacts with cyclohexanone in the organic phase in a concerted fashion (**Figure 4.17C**).[76, 77]

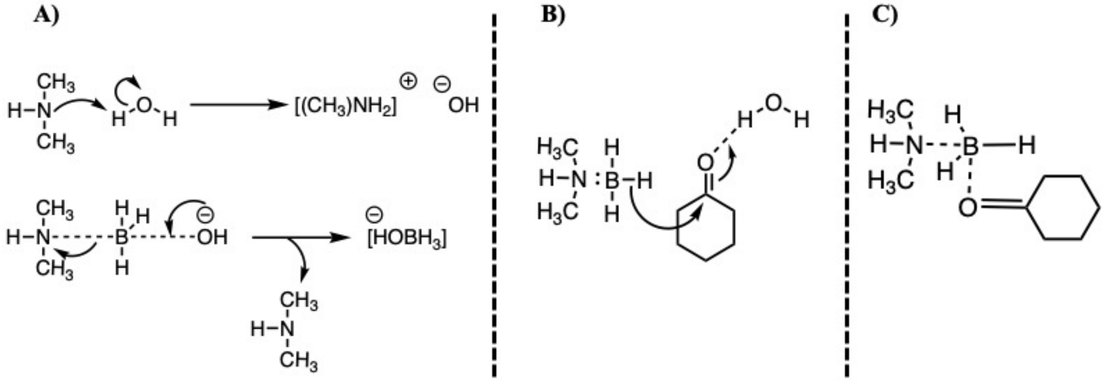

Figure 4.17. Three proposed interactions between DMAB, cyclohexanone, and water molecules. A) Basic conditions allow the hydroxide anion to displace the dimethylamine, forming a monohydroxy borohydride, $^-BH_3(OH)$, which would then react with the carbonyl. B) Water activates the carbonyl and DMAB reacts with the carbonyl. C) DMAB reacts with the unativated carbonyl.

In mechanism (**A**), a reactive monohydroxy borohydride species, $^-BH_3(OH)$, with anionic character, is proposed to form from DMAB and hydroxide anion by displacement of dimethylamine from DMAB. The carbonyl reduction is therefore speculated to occur via the hydridic $^-BH_3(OH)$ species rather than with BH_3. Other boranes, such as BH_3:SMe_2, in the presence of hydroxide anions are expected to form an adduct with hydroxide anions to form a reactive monohydroxy borohydride species, $NaBH_3(OH)$.[75] In an analogous fashion, it was anticipated that DMAB will form Me_2NH^+ $^-BH_3OH$ under basic conditions, which may transfer its hydride to the carbonyl group. To probe this hypothesis, BH_3:SMe_2 and DMAB were mixed separately with sodium hydroxide and subsequently analyzed by ^{11}B NMR spectroscopy for the $NaBH_3(OH)$ signal (-10 ppm).[78] The ^{11}B NMR spectrum of a mixture of BH_3:SMe_2 and solid NaOH displayed three signals attributable to $NaBH_3(OH)$ (-10 ppm),[78] unreacted BH_3:SMe_2, and NaB_2H_7 (δ -29 ppm)[79] (**Figure**

4.18). The $NaBH_3(OH)$ was absent in the ^{11}B NMR spectrum of the mixture of DMAB and aqueous NaOH, displaying solely the unreacted amine borane (δ -15 ppm). The unchanging ^{11}B NMR spectrum of DMAB indicated the stability of DMAB, even under high pH environments, and confirmed that no monohydroxy borohydride was formed in aqueous DMAB over a period of 12 h at 25 °C. Consequently, we suggest that $Me_2NH^+ \ ^-BH_3OH$ is not the source of hydride for the exothermic reduction reaction, thus pathway **A** is ruled out.

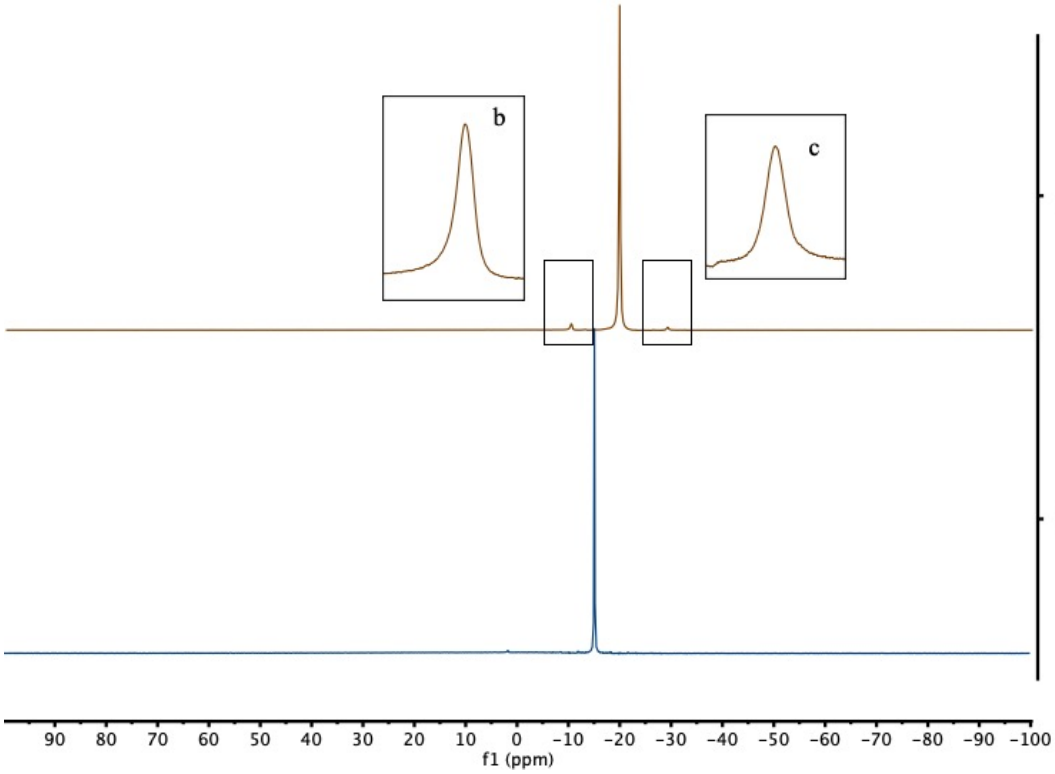

Figure 4.18. ^{11}B NMR (decoupled) studies at 25 °C. a) BH_3:SMe_2 with 5% NaOH (solid) displayed peaks at δ -10 ppm [$NaBH_3(OH)$], δ -20 ppm (BH_3:SMe_2), and δ -29 ppm (NaB_2H_7). Insets b) and c) are expansions of the δ -10 ppm and -29 ppm signals, respectively. These peaks were quartets in the coupled spectra. d) DMAB with NaOH (aqueous) exhibiting a peak at δ -15 ppm (DMAB).

Alternatively, the reaction pathway may involve the activation of the carbonyl group by a hydrogen bonded water molecule followed by a hydride transfer (**Figure 4.17B**).[38-40, 80] Density functional theory (DFT) was used to calculate the energy of the optimized geometry of different molecular conformations during the hydride transfer. However, we could not discover or find a transition state for this pathway. Consequently, we omitted pathway **B** from our mechanistic consideration.

Pathway **C** involves a concerted transfer of a hydride from DMAB to the carbonyl carbon atom.[76] Theoretical calculations, for the hydroboration of carbonyls with ammonia borane in THF and methanol, predicted a concerted double hydrogen atom transfer.[81, 82] If this double hydrogen atom transfer were to occur with aqueous DMAB, we would expect to observe the cyclic dimer of dimethylamino-borane ($(Me_2N\text{-}BH_2)_2$) in the ^{11}B NMR spectrum (δ 5, t, $J = 114$ Hz).[46, 83] Additionally, this cyclic dimer has been shown to be an inactive reducing agent in the absence of a catalyst.[84] Since the reduction of cyclohexanone with DMAB in 3:1 stoichiometry afforded cyclohexanol essentially quantitatively and no $(Me_2N\text{-}BH_2)_2$ signal was observed in the ^{11}B NMR spectrum, it was concluded that the double hydrogen atom transfer was not a viable pathway for this aqueous reduction reaction.

Previous reports suggested a four-membered transition state for pathway **C**, that eventually afforded borate esters.[76, 77, 85] To arrive at the cyclic transition state, the amine needs to dissociate first through two possible routes: first, the amine could dissociate from the BH_3 which is then captured by the carbonyl O-atom or the amine is displaced from DMAB as the carbonyl coordinates to the boron center.[77] DFT analysis found that, for the rate determining dissociation of BH_3 followed by formation of adduct with carbonyl O-atom, the activation barrier is 20 kcal/mol (**Scheme 4.8**). Following that coordination, the BH_3:carbonyl adduct (**2**) undergoes a rapid hydride transfer to the carbonyl carbon, structure **3**, which then gives way the reduced product (**4**). As previously reported, after the first hydride transfer, two more cyclohexanones would add to **4** leading to borate esters.[77] Borate ester formation was confirmed by ^{11}B NMR analysis (broad singlet at δ 19 ppm) of the reaction mixture (**Figure 4.19**).[77] Since water is not involved in pathway **C**, we can assume that this reaction is occurring in the organic phase explaining the lack of significant H_2 evolution during this reduction.

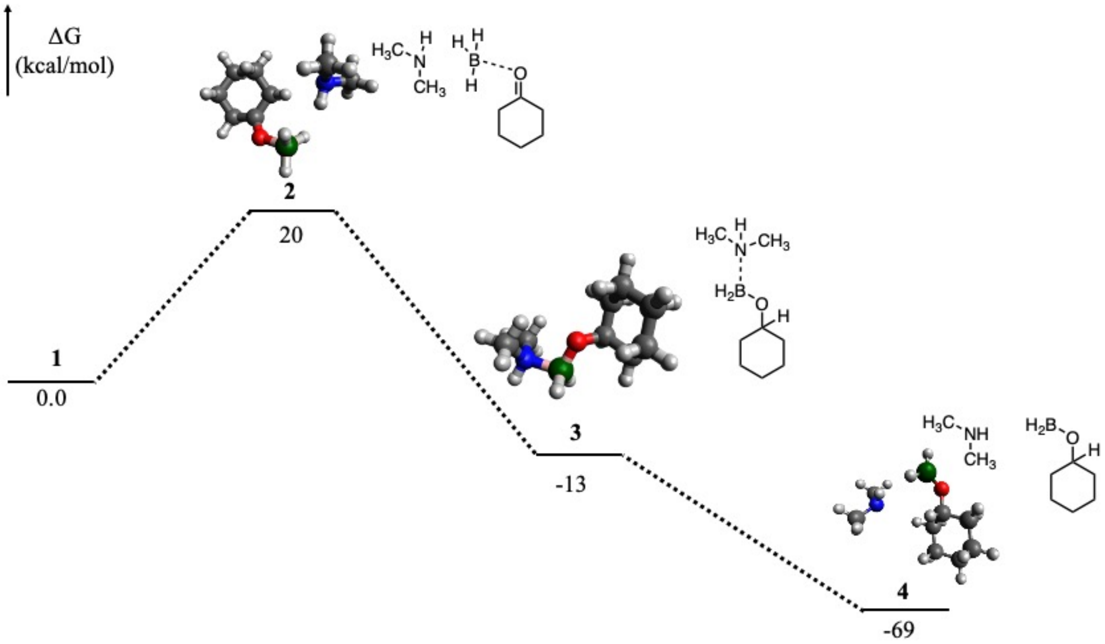

Scheme 4.8. DFT analysis of reaction pathway **C**.

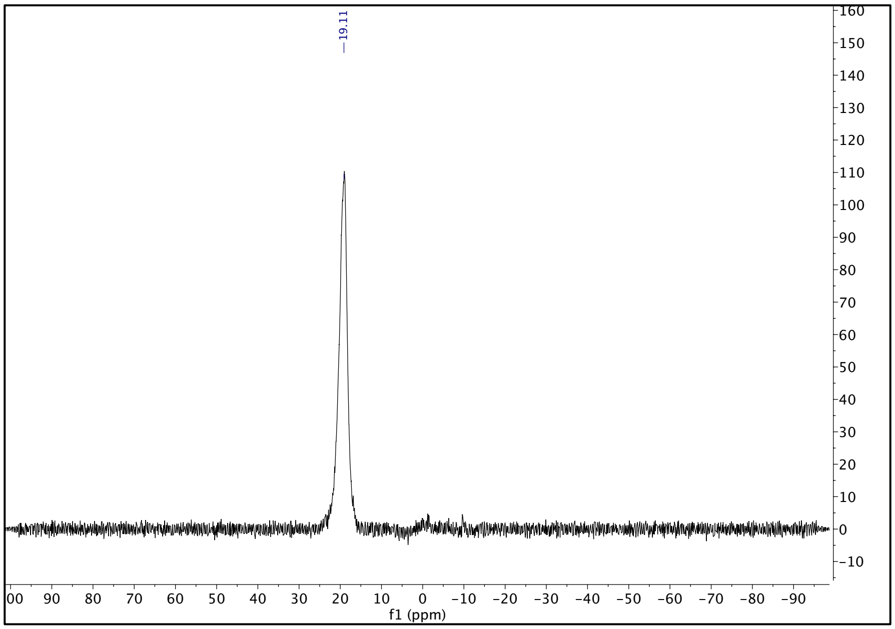

Figure 4.19. ^{11}B NMR (decoupled) of the reaction after DMAB reacts with cyclohexanone.

4.3. Conclusion

In conclusion, we have demonstrated that portable fiber optic Raman spectroscopy can be used as a real-time tool to monitor various reduction reactions in aqueous medium. The *ex situ* probe configuration was convenient as the reaction mixture can be monitored easily without the need for an immersion probe or the removal of aliquots. Two types of reduction reactions were conducted to demonstrate the applicability of Raman spectroscopy in organic reactions, the reduction of nitroarenes and the reductions of ketones. The reduction of mono- and di- nitroarenes to the corresponding aniline derivatives were easily observed by following the disappearance of the nitro stretch (1350 cm^{-1}). Additional information calculated from the Raman data determined that the reaction progresses under pseudo first-order kinetics. The reduction of ketones with aqueous DMAB in a biphasic system was also followed in real-time by monitoring the two separate phases. Aqueous DMAB efficiently reduced saturated carbonyls, such as cyclohexanone, to the corresponding alcohol within a 5 min period. Using both ^{11}B NMR and DFT analysis, we determined that the reduction of cyclohexanone by DMAB, likely occurs by a hydride transfer in a cyclic transition state. When a less reactive α,β-unsaturated ketone was used as the substrate, the corresponding saturated alcohol was obtained as well, albeit at a slower rate. This discovery revealed that aqueous DMAB can be used as a selective reducing reagent for saturated carbonyls in the presence of either conjugated carbonyl compounds. Aside from these specific organic transformations, we envision using the probe to monitor any reaction in an *ex situ* fashion and we have shown the proof of principle of the utility of this monitoring tool when there are sensitive reactants or a water-based reaction environment.

4.4. References

1. Anastas, P. T.; Warner, J. C., *Green Chemistry: Theory and Practice*. Oxford University Press: UK, 1998.

2. Kreuder, A. D.; House-Knight, T.; Whitford, J.; Ponnusamy, E.; Miller, P.; Jesse, N.; Rodenborn, R.; Sayag, S.; Gebel, M.; Aped, I.; Sharfstein, I.; Manaster, E.; Ergaz, I.; Harris, A.; Grice, L. N., A Method for Assessing Greener Alternatives between Chemical Products Following the 12 Principles of Green Chemistry. *ACS Sustainable Chem. Eng.* **2017,** *5*, 2927-2935.

3. Sheldon, R. A., Metrics of Green Chemistry and Sustainability: Past, Present, and Future. *ACS Sustainable Chem. Eng.* **2018,** *6*, 32-48.

4. Clarke, C. J.; Tu, W. C.; Levers, O.; Brohl, A.; Hallett, J. P., Green and Sustainable Solvents in Chemical Processes. *Chem. Rev.* **2018,** *118*, 747-800.

5. López-Porfiri, P.; Gorgojo, P.; Gonzalez-Miquel, M., Green Solvent Selection Guide for Biobased Organic Acid Recovery. *ACS Sustainable Chem. Eng.* **2020,** *8*, 8958-8969.

6. Yang, L.; Dong, T.; Revankar, H. M.; Zhang, C.-P., Recent progress on fluorination in aqueous media. *Green Chem.* **2017,** *19*, 3951-3992.

7. Bi, H. Y.; Du, M.; Pan, C. X.; Xiao, Y.; Su, G. F.; Mo, D. L., Nickel(II)-Catalyzed [5 + 1] Annulation of 2-Carbonyl-1-propargylindoles with Hydroxylamine To Synthesize Pyrazino[1,2-a]indole-2-oxides in Water. *J. Org. Chem.* **2019,** *84*, 9859-9868.

8. Filimonov, V. O.; Dianova, L. N.; Beryozkina, T. V.; Mazur, D.; Beliaev, N. A.; Volkova, N. N.; Ilkin, V. G.; Dehaen, W.; Lebedev, A. T.; Bakulev, V. A., Water/Alkali-Catalyzed Reactions of Azides with 2-Cyanothioacetamides. Eco-Friendly Synthesis of Monocyclic and Bicyclic 1,2,3-Thiadiazole-4-carbimidamides and 5-Amino-1,2,3-triazole-4-carbothioamides. *J. Org. Chem.* **2019,** *84*, 13430-13446.

9. Xie, L.-Y.; Peng, S.; Liu, F.; Liu, Y.-F.; Sun, M.; Tang, Z.-L.; Jiang, S.; Cao, Z.; He, W.-m., Clean Preparation of Quinolin-2-yl Substituted Ureas in Water. *ACS Sustainable Chem. Eng.* **2019,** *7*, 7193-7199.

10. Zeng, H.; Wang, Z.; Li, C.-J., Two-in-One Strategy for Palladium-Catalyzed C-H Functionalization in Water. *Angew. Chem., Int. Ed.* **2019,** *58*, 2859-2863.

11. Muhammad, M. H.; Chen, X.-L.; Liu, Y.; Shi, T.; Peng, Y.; Qu, L.; Yu, B., Recyclable Cu@C_3N_4-Catalyzed Hydroxylation of Aryl Boronic Acids in Water under Visible Light: Synthesis of Phenols under Ambient Conditions and Room Temperature *ACS Sustainable Chem. Eng.* **2020,** *8*, 2682-2687.

12. Duval, M.; Navarre, S.; Sagorin, G.; Denicourt-Nowicki, A.; Roucoux, A., Multigram Scale-up of the Selective Hydrogenation of alpha-Pinene with Ruthenium Nanoparticles in Water. *ACS Sustainable Chem. Eng.* **2020,** *8*, 5985-5993.

13. Walrafen, G.; Pugh, E., Raman combinations and stretching overtones from water, heavy water, and NaCl in water at shifts to ca. 7000 cm^{-1}. *Journal of solution chemistry* **2004,** *33*, 81-97.

14. Medders, G. R.; Paesani, F., Infrared and Raman spectroscopy of liquid water through "first-principles" many-body molecular dynamics. *Journal of chemical theory and computation* **2015,** *11*, 1145-1154.

15. Zong, C.; Xu, M.; Xu, L. J.; Wei, T.; Ma, X.; Zheng, X. S.; Hu, R.; Ren, B., Surface-Enhanced Raman Spectroscopy for Bioanalysis: Reliability and Challenges. *Chem. Rev.* **2018,** *118*, 4946-4980.

16. Singh, S. P.; Mukherjee, S.; Galindo, L. H.; So, P. T. C.; Dasari, R. R.; Khan, U. Z.; Kannan, R.; Upendran, A.; Kang, J. W., Evaluation of accuracy dependence of Raman spectroscopic models on the ratio of calibration and validation points for non-invasive glucose sensing. *Anal. Bioanal. Chem.* **2018,** *410*, 6469-6475.

17. Wang, Z.; Zong, S.; Wu, L.; Zhu, D.; Cui, Y., SERS-Activated Platforms for Immunoassay: Probes, Encoding Methods, and Applications. *Chem. Rev.* **2017,** *117*, 7910-7963.

18. Lane, L. A.; Qian, X.; Nie, S., SERS Nanoparticles in Medicine: From Label-Free Detection to Spectroscopic Tagging. *Chem. Rev.* **2015,** *115*, 10489-529.

19. Wang, Y.; Yan, B.; Chen, L., SERS tags: novel optical nanoprobes for bioanalysis. *Chem. Rev.* **2013,** *113*, 1391-428.

20. Buhrke, D.; Hildebrandt, P., Probing Structure and Reaction Dynamics of Proteins Using Time-Resolved Resonance Raman Spectroscopy. *Chem. Rev.* **2020,** *120*, 3577-3630.

21. Béchamp, A., De l'action des protosels de fer sur la nitronaphtaline et la nitrobenzine. nouvelle méthode de formation des bases organiques artificielles de Zinin. *Ann. Chim. Phys.* **1854,** *42*, 186.

22. Tomkins, P.; Gebauer-Henke, E.; Leitner, W.; Müller, T. E., Concurrent Hydrogenation of Aromatic and Nitro Groups over Carbon-Supported Ruthenium Catalysts. *ACS Catalysis* **2014,** *5*, 203-209.

23. Climent, M. J.; Corma, A.; Iborra, S.; Martí, L., Process Intensification with Bifunctional Heterogeneous Catalysts: Selective One-Pot Synthesis of 2′-Aminochalcones. *ACS Catalysis* **2014,** *5*, 157-166.

24. Vernekar, A. A.; Patil, S.; Bhat, C.; Tilve, S. G., Magnetically recoverable catalytic Co–Co_2B nanocomposites for the chemoselective reduction of aromatic nitro compounds. *RSC Advances* **2013,** *3* (32).

25. Zhang, J.-W.; Lu, G.-P.; Cai, C., Chemoselective transfer hydrogenation of nitroarenes by highly dispersed Ni-Co BMNPs. *Catal. Commun.* **2016,** *84*, 25-29.

26. Hauser, J. L.; Amberchan, G.; Tso, M.; Manley, R.; Bustillo, K.; Cooper, J.; Golden, J. H.; Singaram, B.; Oliver, S. R. J., A Mesoporous Aluminosilicate Nanoparticle-Supported Nickel–Boron Composite for the Catalytic Reduction of Nitroarenes. *ACS Applied Nano Materials* **2019,** *2*, 1472-1483.

27. Yao, K.; Li, T.; Zhao, C.; Lu, W.; Zhao, S.; Wang, J., Au_3Pd_1 Nanodendrites with Hyperbranched Architectures: Green Synthesis at Room Temperature and Highly Selective Hydrogenation for 4-Nitrophenylacetylene. *ACS Sustainable Chem. Eng.* **2020,** *8*, 14914-14925.

28. Zhang, C.; Lu, J.; Li, M.; Wang, Y.; Zhang, Z.; Chen, H.; Wang, F., Transfer hydrogenation of nitroarenes with hdyrazine at near-room temperature catalyzed by a MoO_2 catalyst. *Green Chem.* **2016,** *18*, 2435-2442.

29. Borane-tetrahydrofuran degrades into alkoxyborates if stored improperly.

30. Borane dimethyl suflide reacts with air and moisture.

31. Kanth, J. V. B., Borane-Amine Complexes for Hydroboration. *Aldrichimica Acta* **2002,** *35*, 57-66.

32. Burg, A. B.; Schlesinger, H. I., Hydrides of Boron. VII. Evidence of the Transitory Existence of Borine (BH_3): Borine Carbonyl and Borine Trimethylammine. *J. Am. Chem. Soc.* **1938,** *59*, 780-787.

33. Carboni, B.; Monnier, L., Recent Developments in the Chemistry of Amine and Phosphine Boranes. *Tetrahedron* **1999,** *55*, 1197-1248.

34. Schaeffer, G. W.; Anderson, E. R., The Preparation of Trimethylamine-borine, N-Trimethylborazole and N-Dimethylaminoborine. *J. Am. Chem. Soc.* **1949,** *71*, 2143-2145.

35. Nainan, K. C.; Ryschkewitsch, G. E., New synthesis of amine- and phosphine-boranes. *Inorg. Chem.* **1969,** *8*, 2671-2674.

36. Kikugawa, Y., Chemsitry of Amine-Boranes. XI. A Convenient Synthesis of Dimethylamine-Borane. *Chem. Pharm. Bull.* **1987,** *35*, 4988-4989.

37. Staubitz, A.; Robertson, A. P. M.; Sloan, M. E.; Manners, I., Amine- and Phosphine- Borane Adducts: New Interest in Old Molecules. *Chem. Rev.* **2010,** *110*, 4023-4078.

38. Andrews, G. C., Chemoselectivity in the Reduction of Aldehydes and Ketones with Amine Boranes. *Tetrahedron Letters* **1980,** *21*, 697-700.

39. Andrews, G. C.; Crawford, T. C., The Synthetic Utility of Amine Borane Reagents in the Reduction of Aldehydes and Ketones. *Tetrahedron Letters* **1980,** *21*, 693-696.

40. Salunkhe, A. M.; Burkhardt, E. R., N,N-Diethylaniline Borane, an Efficient Reducing Agent for Reduction of Representative Functional Groups. *Tetrahedron Letters* **1997,** *38*, 1519-1522.

41. Lane, C. F., Borane Amine Complexes *Aldrichimica Acta* **1973,** *6*, 51-59.

42. Hutchins, R. O.; Learn, K.; Nazer, B.; Pytlewski, D.; Pelter, A., Amine Boranes as Selective Reducing and Hydroborating Agents. A Review. *Organic Preparations and Procedures International* **1984,** *16*, 335-372.

43. Lelental, M., Dimethylamine Borane as the Reducing Agent in Electroless Plating Systems. *J. Electrochem. Soc.* **1973,** *120*, 1650-1654.

44. Lelental, M., Effect of Amine Borane Structure on Activity in Electroless Plating. *J. Catal.* **1974,** *32*, 429-433.

45. Homma, T.; Tamaki, A.; Nakai, H.; Osaka, T., Molecular orbital study on the reaction process of dimetylamine borane as a reductant for electroless deposition. *J. Electroanalytical Chem.* **2003,** *559*, 131-136.

46. Yurderi, M.; Bulut, A.; Zahmakiran, M.; Gülcan, M.; Özkar, S., Ruthenium(0) nanoparticles stabilized by metal-organic framework (ZIF-8): Highly efficient catalyst for the dehydrogenation of dimethylamine-borane and transfer hydrogenation of unsaturated hydrocarbons using dimethylamine-borane as hydrogen source. *Applied Catal. B: Environ.* **2014,** *160-161*, 534-541.

47. Patil, N. M.; Sasaki, T.; Bhanage, B. M., Immobilized ruthenium metal-containing ionic liquid-catalyzed dehydrogenation of dimethylamine borane complex for the reduction of olefins and nitroarenes. *RSC Adv.* **2016,** *6*, 52347-52352.

48. Waals, D. v. d.; Pettman, A.; Williams, J. M. J., Copper-catalysed reductive amination of nitriles and organic-group reductions using dimethylamine borane. *RSC Adv.* **2014,** *4*, 51845-51849.

49. Cabacungan, J. C.; Ahmed, A. I.; Feeney, R. E., Amine Boranes as Alternative Reducing Agents for Reductive Alklylation of Proteins. *Anal. Biochem.* **1982,** *124*, 272-278.

50. Billman, J. H.; McDowell, J. W., Reduction of Schiff Bases. III. Reduction with Dimethylamine Borane. *J. Org. Chem.* **1961,** *26*, 1437-1440.

51. Casarini, M. E.; Ghelfi, F.; Libertini, E.; Pagoni, U. M.; Parsons, A. F., 1,2-Reduction of α,β-unsaturated hydrazones using dimethylamine-borane/p-toluenesulfonic acid: an easy route to allyl hydrazine. *Tetrahedron* **2002,** *58*, 7925-7932.

52. For the purposes of this work, ex situ refers to placing the Raman probe outside the reaction vial and in situ refers to immersing the Raman probe inside the reaction mixture.

53. Vandenabeele, P.; H.G.M., W.; Moens, L., A Decade of Raman Spectroscopy in Art and Archeology. *Chem. Rev.* **2007,** *107*, 675-686.

54. Dallongeville, S.; Garnier, N.; Rolando, C.; Tokarski, C., Proteins in Art, Archaeology, and Paleontology: From Detection to Identification. *Chem. Rev.* **2016,** *116*, 2-79.

55. Sikirzhytskaya, A.; Sikirzhytski, V.; Lednev, I. K., Determining Gender by Raman Spectroscopy of a Bloodstain. *Anal. Chem.* **2017,** *89*, 1486-1492.

56. Pereira de Oliveira, L.; Rocha, D. P.; Reis de Araujo, W.; Abarza Muñoz, R. A.; Longo Cesar Paixão, T. R.; Oliveira Salles, M., Forensics in hand: new trends in forensic devices (2013–2017). *Analytical Methods* **2018,** *10*, 5135-5163.

57. Calvino-Casilda, V.; Bañares, M. A., In situ Raman monitoring of Michael addition for the synthesis of 1-substituted imidazoles intermediates with antiviral properties. *Catalysis Today* **2012,** *187*, 191-194.

58. Mikolajska, E.; Calvino-Casilda, V.; Bañares, M. A., Real-time Raman monitoring of liquid-phase cyclohexene epoxidation over alumina-supported vanadium and phosphorous catalysts. *Applied Catalysis A: General* **2012,** *421-422*, 164-171.

59. Calvino-Casilda, V.; Bañares, M. A.; LozanoDiz, E., Real-time Raman monitoring during coumarins synthesis via Pechmann condensation: A tool for controlling the preparation of pharmaceuticals. *Catalysis Today* **2010,** *155*, 279-281.

60. Calvino-Casilda, V.; Stawicka, K.; Trejda, M.; Ziolek, M.; Bañares, M. A., Real-Time Raman Monitoring and Control of the Catalytic Acetalization of Glycerol with Acetone over Modified Mesoporous Cellular Foams. *The Journal of Physical Chemistry C* **2014,** *118*, 10780-10791.

61. Kumaravel, S.; Thiruvengetam, P.; Karthick, K.; Sankar, S. S.; Kundu, S., Detection of Lignin Motifs with RuO2-DNA as an Active Catalyst via Surface-Enhanced Raman Scattering Studies. *ACS Sustainable Chem. Eng.* **2019,** *7*, 18463-18475.

62. Tyndall, S.; Wong, K. F.; VanAlstine-Parris, M. A., Insight into the Mechanism of the Pechmann Condensation Reaction Using NMR. *J. Org. Chem.* **2015,** *80*, 8951-8953.

63. Leadbeater, N. E.; Smith, R. J., Real-Time Monitoring of Microwave-Promoted Suzuki Coupling Reactions Using in Situ Raman Spectroscopy. *Organic Letters* **2006,** *8*, 4589-4591.

64. Schmink, J. R.; Holcomb, J. L.; Leadbeater, N. E., Use of Raman spectroscopy as an in situ tool to obtain kinetic data for organic transformations. *Chemistry* **2008,** *14*, 9943-50.

65. Vogt, P. F.; Gerulis, J. J., Amines, Aromatic. In *Ullmann's Encyclopedia of Industrial Chemistry*, Wiley-VCH Verlag GmbH & Co. : Weinheim, Germany 2000.

66. Fountoulaki, S.; Daikopoulou, V.; Gkizis, P. L.; Tamiolakis, I.; Armatas, G. S.; Lykakis, I. N., Mechanistic Studies of the Reduction of Nitroarenes by $NaBH_4$ or Hydrosilanes Catalyzed by Supported Gold Nanoparticles. *ACS Catal.* **2014,** *4*, 3504-3511.

67. Strachan, J.; Barnett, C.; Masters, A. F.; Maschmeyer, T., 4-Nitrophenol Reduction: Probing the Putative Mechanism of the Model Reaction. *ACS Catalysis* **2020**, 5516-5521.

68. Terrier, F., Rate and Equilibrium Studies in Jackson-Meisenheimer Complexes. *Chem. Rev.* **1982,** *82*, 77-152.

69. Colthup, N. B.; Daly, L. H.; Wiberly, S. E., *Introduction to Infrared and Raman Spectroscopy*. Academic Press: San Diego, 1990.

70. Stone, P.; Thompson, H., Vibrational band intensity of the hydroxyl group in phenols. *Spectrochimica Acta* **1957,** *10*, 17-20.

71. Lin-Vien, D.; Colthup, N. B.; Fateley, W. B.; Graselli, J. G., *The Handbook of Infrared and Raman Characteristic Frequencies of Organic Molecules*. Academic Press: Boston, 1991.

72. Fräulin, C.; Rinke, G.; Dittmeyer, R., In-Situ Laser Raman Spectroscopy Adapted to Process Conditions for Studying Cyclohexane Oxidation. *Journal of Flow Chemistry* **2013,** *3*, 87-91.

73. Yu, H.; Peng, F.; Tan, J.; Hu, X.; Wang, H.; Yang, J.; Zheng, W., Selective catalysis of the aerobic oxidation of cyclohexane in the liquid phase by carbon nanotubes. *Angewandte Chemie* **2011,** *123*, 4064-4068.

74. Chan, H.-Y.; Nguyen, V.-H.; Wu, J.; Calvino-Casilda, V.; Bañares, M. A.; Bai, H., Real-time Raman monitoring during photocatalytic epoxidation of cyclohexene over V-Ti/MCM-41 catalysts. *Catalysts* **2015,** *5*, 518-533.

75. Clary, J. W.; Rettenaier, T. J.; Snelling, R.; Byrks, W.; Banwell, J.; Wipke, W. T.; Singaram, B., Hydride as a Leaving Group in the Reaction of Pinacolborane with Halides under Ambient Grignard and Barbier Conditions. One-Pot Synthesis of Alkyl, Aryl, Heteroaryl, Vinyl, and Allyl Pinacolboronic Esters. *J. Org. Chem.* **2011,** *76*, 9602-9610.

76. White, S. S.; Kelly, H. C., Kinetics and Mechanism of the Morpholine-Borane Reduction of Methyl Alkyl Ketones. *J. Am. Chem. Soc.* **1970,** *92*, 4203-4209.

77. Yang, X.; Fox, T.; Berke, H., Ammonia borane as a metal free reductant for ketones and aldehydes: a mechanistic study. *Tetrahedron* **2011,** *67*, 7121-7127.

78. Prasanth, C. P.; Joseph, E.; Abhijith, A.; Nair, D. S.; Ibnusaud, I.; Raskatov, J.; Singaram, B., Stabilization of $NaBH_4$ in Methanol Using a Catalytic Amount of NaOMe. Reduction of Esters and Lactones at Room Temperature without Solvent-Induced Loss of Hydride. *J. Org. Chem.* **2018,** *83*, 1441-1440.

79. Chen, X.-M.; Ma, N.; Zhang, Q.-F.; Wang, J.; Feng, X.; Wei, C.; Wang, L.-S.; Zhang, J.; Chen, X., Elucidation of the Formation Mechanisms of the Octahydrotriborate Anion ($B_3H_8^-$) through the Nucleophilicity of the B-H Bond. *J. Am. Chem. Soc.* **2018,** *140*, 6718-6726.

80. White, S. S.; Kelly, H. C., On the Morpholine Borane Reduction of Acetone. *J. Am. Chem. Soc.* **1968,** *90*, 2009-2011.

81. Ma, N.; Song, M.; Meng, Q.; Wei, C.; Zhang, G., Theoretical insight into the solvent effect on the stoichiometric reduction of carbonyl compounds by ammonia borane and N-methyl amine borane. *Int. J. Quantum Chem.* **2020,** *120*, 1-8.

82. Wang, X.; Yao, W.; Zhou, D.; Fan, H., Theoretical study on the mechanism for NH_3BH_3 reduction of ketones and imines. *Molecular Physics* **2013,** *111*, 3014-3024.

83. Pal, S.; Kusumoto, S.; Nozaki, K., Dehydrogenation of Dimethylamine-Borane Catalyzed by Half-Sandwich Ir and Rh Complexes: Mechanism and the Role of Cp* Noninnocence. *Organometallics* **2018,** *37*, 906-914.

84. Pasumanksy, L.; Haddenham, D.; Clary, J. W.; Fisher, G. B.; Goralski, C. T.; Singaram, B., Lithium Aminoborohydrides 16. Synthesis and Reactions of Monomeric and Dimeric Aminoboranes. *J. Org. Chem.* **2008,** *73*, 1898-1905.

85. Brown, H. C.; Wang, K. K.; Chandrasekharan, J., Hydroboration Kinetics. 7. Kinetics and Mechanism of the Reduction of Aldehydes and Ketones with 9-Borabicyclo[3.3.1]nonane Diemr. *J. Am. Chem. Soc.* **1983,** *105*, 2340-2343.

Chapter 5

On-Demand Hydrogen Generation using Commercial or Waste Aluminum, Water and a Reusable Liquid Metal

5.1 Introduction

The generation of sustainable, renewable energy with new or existing materials has long been sought, even before the correlation between fossil fuel emissions and the changing climate was proposed.[1] Hydrogen fuel is an appealing option because of its substantial energy density and its nontoxic water byproduct, leading to its designation as a "clean fuel." Hydrogen evolution reactions through water splitting is well established *via* electrocatalysis,[2, 3] photocatalysis,[4] and electrolysis.[5-12] These methods, however, require expensive catalysts (e.g. Pt/C, Ru/C or Ir/C) or an applied potential and are thus not feasible as a continuous, affordable source of chemical energy. They also produce minimal amounts of hydrogen and require extended periods of time to generate the gas (2-9 mL of H_2 in 50-180 min, depending on the catalyst).[3, 6-12]

Aluminum is ideal for hydrogen generation because it is economically viable and in high abundance (approximately 8 wt.% in the earth's crust).[13] One gram of pure aluminum can in principle produce 1.24 L of hydrogen while generating aluminum oxide as the only byproduct (Equation 1).[14]

$$2Al + 3H_2O \rightarrow Al_2O_3 + 3H_2 \qquad (1)$$

To access aluminum's potential, however, the passivating aluminum oxide layer present on the surface must be removed. Eradication of the layer can occur through mechanical manipulation, extreme pH, or room temperature liquid metals. Ball milling is a technique to synthesize a powder from two or more materials.[15] Those materials are subjected to a pressurized environment for extended periods of time to achieve a fine particle structure. The fine particle morphology allows for more surface area but there is greater susceptibility for the oxide coating to return. The powders must therefore be kept under an inert environment, such as an argon-purged glove box.[16-18] Concentrated acidic or alkaline solution is effective at removing the oxide layer, but the reagents are highly corrosive and costly.[19, 20]

5.1.1. Background of Water Splitting

A room temperature liquid metal mixed with aluminum creates a eutectic system that simultaneously prevents the passivation layer from forming and liquifies the aluminum, allowing for efficient production of hydrogen. Woodall discovered in 1968, that when aluminum dissolved in gallium the resultant material can split water. This opened the possibility that aluminum could be a viable hydrogen production material. His choice of gallium is clever as he utilizes the metal's inherent characteristics to his advantage. Gallium has a low melting point (29 °C) and a high boiling point (~2204°C).[21] Due to these properties, it has been used in high temperature thermometers and in the 1960s it was used in some semiconductors. Woodall's mixing with aluminum takes advantage of gallium's low melting point to dissolve the aluminum (melting point of 660 °C) and form an alloy.

In Woodall's work, he compared different gallium aluminum ratios and how well they split water to produce hydrogen. He focused on binary Al-Ga alloys composed of 28wt%Al-72wt%Ga and 50wt%Al-50wt%Ga.[22] However, the use of weight precents is misleading as the former would imply that the alloy was Ga-rich, but when the atomic ratio was calculated it is actually a 1:1 (Ga:Al) alloy. Similarly, the 50:50wt% corresponds to a 1:2.6 (Ga:Al) ratio, or in other words, aluminum-rich alloys. Since gallium is costly, Woodall wanted to use the minimum amount of gallium necessary to dissolve the aluminum. When the binary alloy was in a 1:1 ratio the maximum production of H_2 occurred after 5 min but only 8% was obtained. The Al-rich suffered even more, only generating 3% of H_2 in 6 min (**Table 5.1**, entry 1).

Further research expanded into ternary,[23] quaternary,[22] and quinary[24] alloys that included mixing Al with Ga, In, Sn, and Bi in various ratios. The motivation for producing some of these alloys was to generate hydrogen at less elevated temperatures and to reduce the formation of the aluminum oxide layer.

In one example, Al was mixed with Ga and Sn to create a ternary alloy.[25] Using a mass ratio of Ga:Sn (1.7:1) the researchers then varied the alloys' composition by adding in, by weight percent, different amounts of the Ga:Sn mixture to the Al (3wt%-15wt% of the Ga-Sn mixture). Hydrogen generation from the ternary alloy was quantified using those samples as well as testing the water splitting reaction at a range of temperatures (10-70 °C) (**Table 5.1**, entry 2). A trend was observed that as the Ga and Sn content increased so did the H_2 production. Similarly, when the reaction temperature increased the H_2 increased too. The best H_2 production was obtained at 70 °C using a 15wt% Al-Ga-Sn alloy (90% of H_2). Using the same 1.7:1 (Ga:In) mass ratio, Al-Ga-In alloys (3wt% and 15wt% of the Ga-In mixture) were synthesized, which performed similarly to the Sn version. The exception was that the 15wt% Al-Ga-In alloy performed well across all of the temperatures, seeing hydrogen yields ranging from 85-98% (entry 3). The addition of Sn and In were chosen because they could alloy with the Al and disrupt the oxide layer to create active sites for the water splitting to occur at.

The addition of Sn and In into the Al-Ga alloy was also predicted to produce H_2 at lower temperatures because the Ga-In-Sn eutectic melting point (10 °C)[26, 27] is lower than pure Ga.[22] Consequently, the hydrogen production of the Al-Ga-In-Sn alloy (50 wt% Al-34 wt% Ga-11 wt% In-5 wt% Sn, or 44:12:2:1 mol ratio) was compared across four temperatures. At the highest temperature, 55 °C, the Al-rich alloy rapidly produced 83% of hydrogen in under 1.5 min (**Table 5.1**, entry 4). The lowest temperature, 24 °C, took longer to achieve the maximum amount of hydrogen (78% of H_2 in 5 min). The researchers observed that at higher temperatures, 45 °C and 55 °C, the maximum amount of hydrogen was achieved early (in under 2 min) and stops evolving gas after 3 min. The two lower temperatures, 24 °C and 35 °C, took longer to achieve the maximum amounts of hydrogen, 5 min (78% of H_2) and 3 min (84% of H_2), respectively, and the gas production stopped after 7 min. Characterization of the alloy illustrated the inhomogeneity of the material. Based on scanning electron microscopy (SEM) and energy-dispersive X-ray spectroscopy (EDX) it appears that the aluminum is concentrated on the outermost edges of the alloy while the inner areas are mostly comprised of In and Sn. The higher concentration of Al on the surface allows for higher contact with water to perform the water splitting reaction. Powder x-ray diffraction (PXRD) analysis of the spent alloy found $Al(OH)_3$ and In_3Sn patterns, which is consistent with the data presented in the SEM and EDX that the alloy is not homogeneous and that there are In-Sn rich domains.

A quinary alloy, synthesized from Ga, Sn, In, Zn, and Al was formed, and its ability to split water was tested.[16] The composition of the Al-rich alloy (5.3wt% Ga, 5.4wt% Sn, 7.3wt% Zn, and 80 wt% Al, or mol ratio of 4:3:1:6:171) remained the same when the two preparation methods were tested. Two methods for the alloy synthesis were compared, one had the metals melted together and the second through mechanical milling. The mechanical milling method applied a ball miller to mix the metals together at 0.2-0.3 MPa for 5 h to create a powder. Each produced hydrogen, however, the milling method produced greater amounts of H_2 (77%) compared to the melting method (**Table 5.1**, entry 5). Through thermal analysis it was concluded that the milling method was more effective because there were more distinct Al sites for the water splitting to react with.

Further expansion into different additives included a quinary alloy composed of Al-Ga-$InSn_4$-InBi.[24] The alloy composition consisted of 80 wt% Al, 5 wt% Ga, 3.77 wt% In, 7.80wt% Sn, and 3.43 wt% Bi, which translates to a mol ratio of 186:5:2:4:1, therefore an Al-rich alloy. The addition of In and Sn have been frequent partners with Al and Ga, and this group wanted to reduce the amount of In by supplementing the alloy with Bi, another low melting metal and less expensive than In. With this quinary alloy, water splitting typically yielded >90% production of H_2 (**Table 5.1**, entry 6). The alloy produced hydrogen rapidly (in under 10 min) at 50 °C and 60 °C. At 30 °C and 40 °C, longer reaction times were needed to achieve maximum H_2 gas evolution, 48 and 26 min, respectively. Differential scanning calorimetry (DSC) curves showed peaks at 26 °C, 63 °C, and 85 °C. The latter two temperatures have been correlated with the melting point between Al and $InSn_4$ and Al with In-Bi. The 26 °C peak in DSC corresponds to the Al-Ga binary eutectic, which was not observed when Al-Ga-$InSn_4$

alloys were made as controls. This led the researchers to conclude that the Bi aids in the Al-Ga interaction. However, once used the metals in the spent alloy could not be separated for reuse, making it limited in application.

Table 5.1. Binary, ternary, quaternary, and quinary alloys and their hydrogen production.

Entry	Alloy	Hydrogen Production (%)	References
1	Al-Ga[a]	3-8%	22
2	Al-Ga-Sn[b]	90%	25
3	Al-Ga-In[b]	90%	25
4	Al-Ga-In-Sn[a]	78-83%	22
5	Ga-Sn-In-Zn-Al[c]	48% (melting) 77% (milling)	16
6	Al-Ga-InS_4-InBi[d]	90-99%	24

[a] The alloys were prepared by heating the components to 700 °C for 10 h in an N_2 environment. [b] The alloys were synthesized using an arc melting method under an inert atmosphere. [c] A ball miller combined the metals under 0.2-0.3 MPa for 5 h in an inert atmosphere. [d] The metals were combined and heated to 800 °C for 1 h in an N_2 environment.

Many of these multicomponent alloys suffer from being unable to extract the metals for reuse. And as many of them are costly or rare, being able to reuse each metal is an economic necessity (**Figure 5.1**). Therefore, further alloy generations need to be recyclable and relatively nontoxic if they are to find application outside of academia.

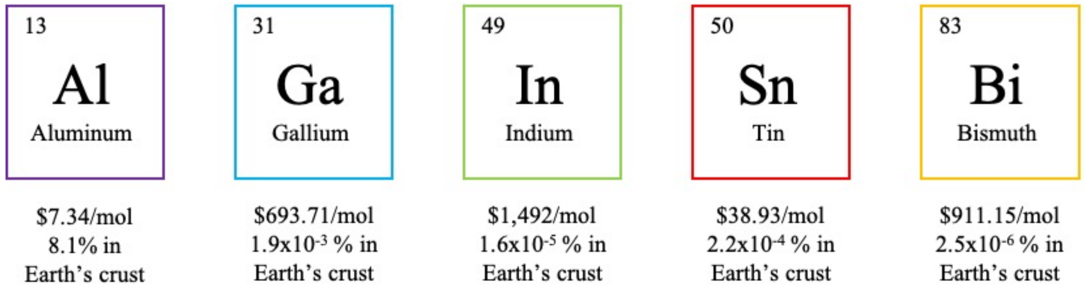
13
Al
Aluminum
$7.34/mol
8.1% in
Earth's crust
31
Ga
Gallium
$693.71/mol
1.9x10-3 % in
Earth's crust
49
In
Indium
$1,492/mol
1.6x10-5 % in
Earth's crust
50
Sn
Tin
$38.93/mol
2.2x10-4 % in
Earth's crust
83
Bi
Bismuth
$911.15/mol
2.5x10-6 % in
Earth's crust

Figure 5.1. Metal cost per mol.[28]

Consequently, the goal of this project was to develop a method to generate hydrogen that was efficient, recyclable, and stable. While previous work focused on Al-rich alloys,[22, 24] it was found that the Ga-rich compositions produce hydrogen in far greater yield and rate. Additionally, different sources of water and aluminum were found effective at producing hydrogen from the binary alloy. An added discovery was the finding that the gallium fully regenerates, allowing it to be reused for multiple hydrogen generation cycles. Characterization of the alloy found that aluminum particles in the gallium are responsible for this room temperature water splitting activity, as previously predicted by theoretical calculations.[29, 30] As an initial example of the application of the evolved H_2, a hydrogenation reaction was conducted to demonstrate its ease of use.

5.2 Results and Discussion

5.2.1. Synthesis of the Gallium Aluminum Alloy

Two methods were developed to synthesize the gallium aluminum alloy. In the first method, samples of solid gallium and commercial aluminum foil were placed into a reaction flask and melted together with a heat gun. As the flask was swirled, the melted gallium appeared to dissolve the aluminum. The second method consisted of weighing out the aluminum foil on weigh paper then adding the liquified gallium to it. The sample was then manually combined to ensure all the aluminum was dissolved into gallium. Once no solid aluminum remained, the sample was solidified (by cooling it with dry ice), peeled off the paper, placed into a reaction vessel, and remelted to create what appears to be a uniform nugget. These alloys were then attached to the hydrogen meter for hydrogen quantification. The two methods were then compared based on how much hydrogen they each produced.

Even though most of the literature uses Al-rich alloys, it was important to test samples using a variety of molar compositions of the binary alloy. Samples were made using the two synthetic methods in each of the three ratio categories: 1:1 (Ga:Al), 2:1 (Ga:Al), and 1:2 (Ga:Al). Then the percent of hydrogen produced was calculated for each alloy sample's reaction with water (**Figure 5.2**). Across all ratios tested, the manual mixing method consistently produced more hydrogen than the heat gun method. It is likely that the heat gun method does not allow the aluminum to fully dissolve in gallium and so aluminum's full potential is not harnessed. This is in contrast to the mechanical mixing, which can produce >70% of the theoretical amount of hydrogen. Therefore, it can be surmised that using this manual mixing method ensures that the gallium has contact with the aluminum and can fully dissolve to create micro-aluminum domains.

Of the different ratios examined the gallium-rich alloys performed better than the aluminum-rich alloy (**Figure 5.2**). The 2:1 (Ga:Al) ratio produced the largest quantity of hydrogen for either synthetic method. The 1:1 (Ga:Al) alloy produced 50% H_2 versus the aluminum-rich alloy, which generated 17% H_2. Increasing the amount of gallium further in a 3:1 (Ga:Al) ratio saw a corresponding increase in H_2 production, 77% of H_2 on average. This suggests that having a slight excess of gallium present increases the hydrogen efficacy, likely due to it more effectively removing the aluminum oxide layer and potentially creating aluminum particles. A large excess of gallium does not appear to drastically increase the hydrogen production as seen in the 4:1 and 6:1 (Ga:Al) samples, which produced 66% and 74%, respectively. Based on these results the 3:1 (Ga:Al) alloys became the optimized alloy ratio.

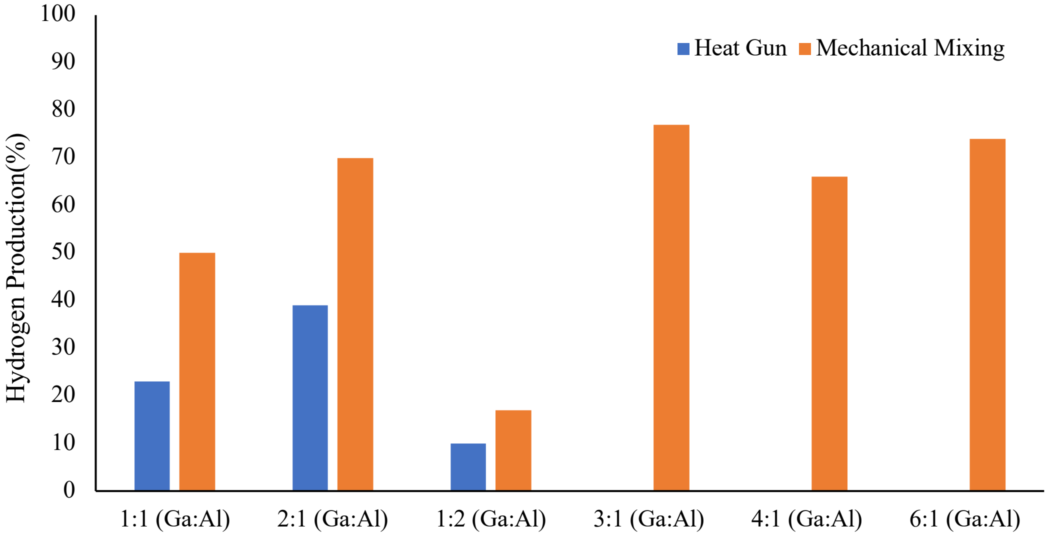

Figure 5.2. The gallium aluminum alloy was synthesized by two methods, with a heat gun or mechanically mixed on paper. Different alloys of atomic gallium aluminum ratios were made, and their hydrogen production was quantified.

5.2.2. Synthesis of Alloys Using Other Low Melting Point Metals

Other reports have described using other low melting point metals as additives to aid in hydrogen production. As a control, an alloy of gallium and bismuth was made to show that aluminum was the hydrogen source and that the dissolving metals do not undergo their own water splitting reaction. The 1:1 (Ga:Bi) alloy did not produce any hydrogen as expected (**Table 5.2**, entry 1). When aluminum was added to the mixture, 16% H_2 was produced (entry 2). Two ternary alloys were synthesized out of gallium, aluminum, and indium. Both were gallium-rich, which was reported earlier to enhance the production of hydrogen. However, for these alloys, <20% of H_2 was obtained (entries 3 and 4). A third quaternary aluminum alloy was made using a commercially available eutectic alloy known as Galinstan (Gs). Galinstan consists of Ga (68.5%), In (21.5%), and Sn (10%). It was developed as a nontoxic liquid metal to replace mercury in thermometers and other devices. Three ratios were tested, 1:1, 2:1, and 3:1 (Gs:Al), with the largest production of hydrogen coming from the 3:1 (Gs:Al) ratio (entries 5-7). The Gs-Al alloy performed better than the Bi or the Ga-Al-In alloys, but its hydrogen production with water remained lower than the binary alloy of gallium and aluminum (3:1).

Table 5.2. Alternative metal alloys[a]

Entry	Alloy Ratio	Hydrogen Production (%)
1	1:1 (Ga:Bi)	0
2	1:2:4 (Bi:Ga:Al)	16
3	2:1:1 (Ga:Al:In)	17
4	4:1:1 (Ga:Al:In)	13
5	1:1 (Gs:Al)	49
6	2:1 (Gs:Al)	35
7	3:1 (Gs:Al)	56

[a] Alloys synthesized using the mechanical mixing method. Each alloy reacted with deionized water (10 mL) to produce hydrogen. See experimental for hydrogen meter set up.

5.2.3. Hydrogen Generation *via* Splitting Other Sources of Water

In addition to deionized water (DI water), other water sources proved successful in generating hydrogen using the 3:1 (Ga:Al) alloy. Tap water produced substantial amounts of hydrogen, much like DI water (89%, **Figure 5.3**). Rainwater, collected from a rainstorm, was tested producing 86% H_2, almost equivalent to that of tap water. Ocean water or simulated sea water produced ~30% H_2. Gas chromatography mass spectrometry confirmed that no chlorine gas was formed, a pervasive problem that prevents the use of electrode-based water splitting.[5, 31] Visual comparison showed a much less vigorous reaction for the alloy in ocean water than in DI water. The slower production of hydrogen could be due to the presence of sodium chloride passivating the alloy. A NaCl solution (0.33M) was made to emulate the salt content of ocean water to confirm that the salt was the inhibiting factor. The water splitting reaction with the NaCl solution produced 25% H_2 indicating that the salt was the likely culprit for the decreased hydrogen yield in ocean water splitting using Ga:Al alloy.

Inductively coupled plasma optical emission spectroscopy (ICP-OES) analysis of the residual water showed that Ga was present at a concentration of 12.77 ppm and Al was present at 9.212 ppm. The concentration of Al was slightly higher than the normal range of Al^{3+} known to exist in groundwater (0.1-8.0 ppm).[32] And the concentration of Ga found in the residual water was much greater than that found in the water supply, indicating that this water should not be introduced into the water supply.[33] However, it was possible to collect and reuse that water in subsequent water splitting reactions, producing good amounts of hydrogen (72%). This demonstrated that the concentration of Al or Ga present due to previous reactions did not greatly effect subsequent water splitting reactions. Lastly, a degassed commercial soda (Coca Cola) yielded 86% H_2, showing that the sweetener does not impede the reaction. On average, the 3:1 (Ga:Al) alloy generates 109 mL of H_2 within 15 min at room temperature, demonstrating that the alloy maintains excellent hydrogen production, regardless of water source.

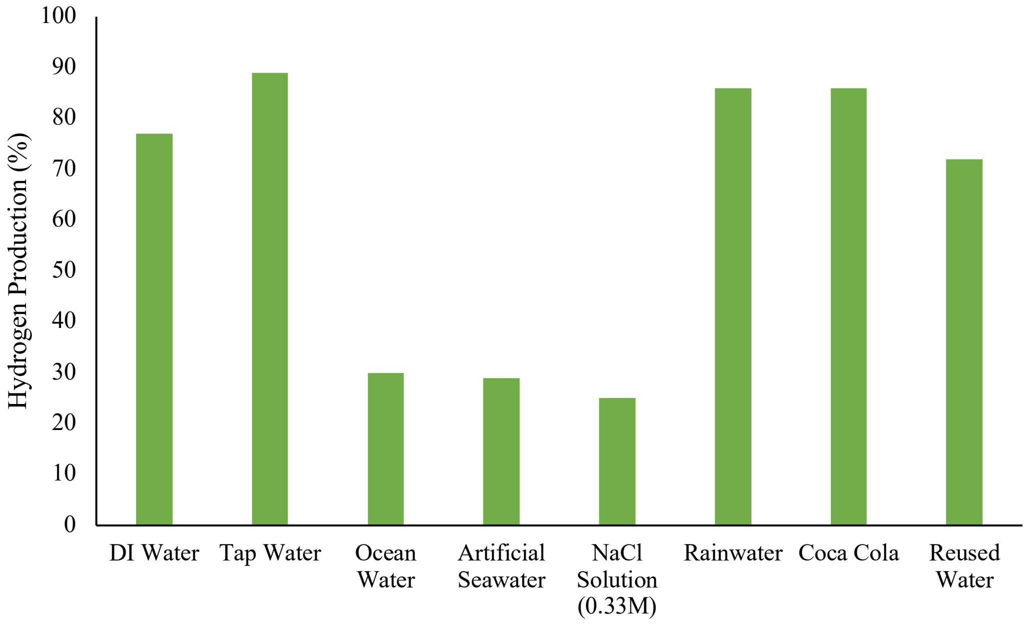

Figure 5.3. Hydrogen generation from water splitting using 3:1 Ga:Al alloy and water from different sources.

5.2.4. Different Aluminum Sources

Pristine aluminum foil was initially used to optimize the Ga:Al alloy ratio that produced high yields of hydrogen from water. Further expansion into waste aluminum, such as used commercial baking trays and food wrappers, demonstrated that hydrogen was efficiently generated even when using waste aluminum (**Figure 5.4**).

In the United States, the most recycled source of aluminum is beverage cans. Since such an abundant aluminum source is widely accessible, it was deemed necessary to demonstrate that hydrogen can be produced from an alloy comprised of this ubiquitous aluminum source.[34] The top and bottom of a standard soda can contains over 90% of the aluminum and far less paint and polymer coating resides in those areas. Therefore, the can was segmented into three sections: the top of the can, bottom of the can, and the wall of the can, and each were tested individually for the synthesis of Ga:Al alloy and was tested in the hydrogen generation from water. When testing the soda can, it was discovered that a higher ratio of gallium was necessary to dissolve the aluminum completely due to its greater thickness (Ga:Al of 6:1) (**Figure 5.4**). Subsequent hydrogen studies revealed that the Ga-Al alloy made from a soda can lid produced 80% of the theoretical amount of H_2, while the bottom and can walls produced <50% H_2. The polymer present on the aluminum can likely interferes with the aluminum interacting with water, causing the decrease in hydrogen yield.

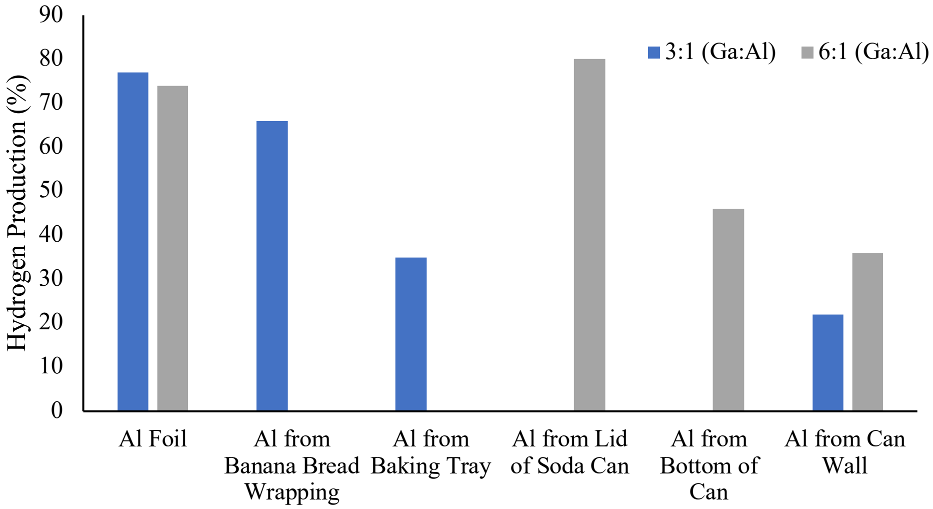

Figure 5.4. Hydrogen generation from water splitting using Ga-Al alloy and aluminum from different sources.

5.2.5. Recycling Gallium and Storage of the Alloy

As stated earlier, gallium is expensive and since gallium-rich alloys generate more hydrogen, development of a method to recycle and reuse gallium metal was desirable. Fortunately, an efficient method to recycle gallium was developed. By a simple filtration and aqueous rinse, gallium (unoptimized recovery ~ 98%) can be separated from the aluminum byproduct, Al_2O_3. The recovered gallium was then reused for subsequent Ga:Al alloy synthesis and H_2 generation showing no depreciating effect for the ability of recycled Ga to produce hydrogen (84%). The fact that both the gallium and water can be reused and recycled for subsequent water splitting reactions illustrates the versatility of this hydrogen generation method.

Hydrogen storage is a major challenge for practical use of hydrogen as an energy source. Initially, storage of the Ga:Al alloy was a challenge because moisture from the atmosphere degrades the efficacy of the material. However, it was discovered that the Ga-Al alloys can be stored as pre-made pellets under cyclohexane and used as needed. Samples of the Ga-Al alloy nuggets under cyclohexane were tested periodically over three months of storage for their hydrogen production and it maintained an average yield of 82%. The alloy pellets can therefore be stored and used as and when needed without any oxidative or hydrolytic decomposition.

5.2.6. Gallium Aluminum Alloy Characterization

It was speculated that the hydrogen evolution reaction occurs through micro-aluminum sites present within the gallium and that after the water splitting occurs gallium regenerates along with aluminum oxide, Al_2O_3. This hypothesis prompted the characterization of the (Ga:Al) alloy through various electron microscopy techniques. Transmission electron microscopy (TEM) coupled with electron energy loss spectroscopy (EELS) analysis of the optimal 3:1 (Ga:Al) alloy revealed particles of aluminum in the ~ 8-27 nm diameter range (**Figure 5.5a**). Furthermore, scanning electron microscopy-energy dispersive X-ray spectroscopy (SEM-EDS) showed an even distribution of Al particles in the Ga (**Figure 5.5b**). Electron diffraction confirmed the dark areas are aluminum and the lighter areas in between are gallium (**Figure 5.6b**).

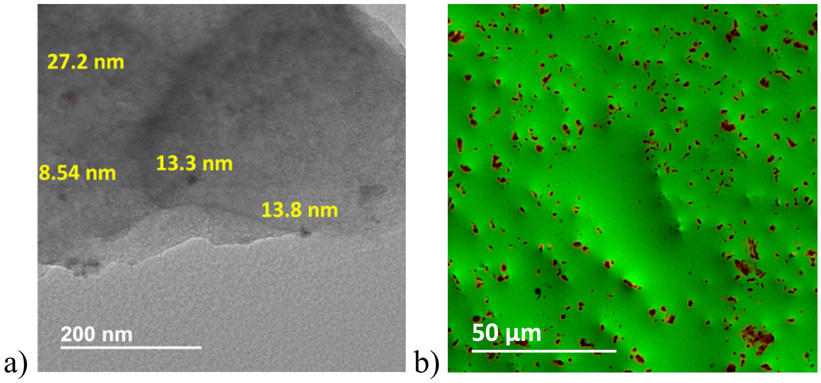

Figure 5.5. (a) TEM imaging coupled with EELS spectroscopy shows dark areas are likely Al particles while the remaining area is Ga . (b) SEM-EDS map of the alloy's surface shows the Al particles (red) well distributed in the Ga (green).

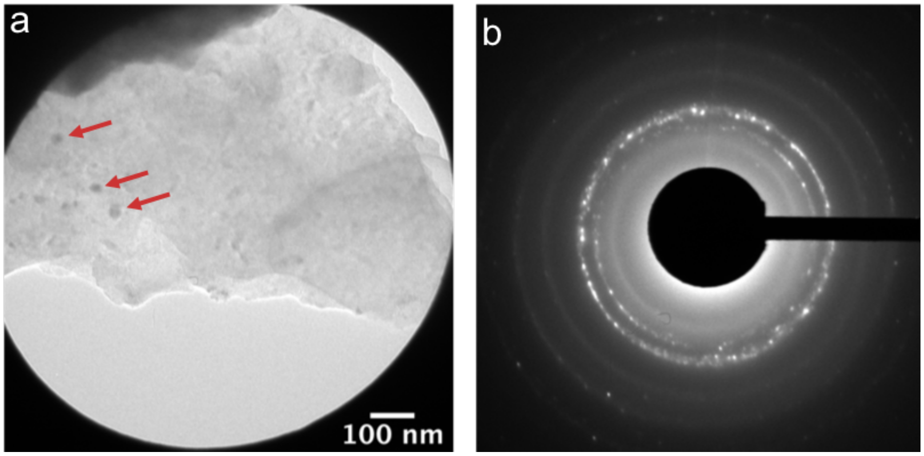

Figure 5.6. TEM of a Ga-Al sample: a) red arrows point to particles in the matrix; b) Diffraction for the selected area in a) showing rings that can be indexed for phase identification.

Structural analysis of the alloys at various Ga:Al ratios were performed using powder X-ray diffraction (PXRD) (**Figure 5.7**). Aluminum-rich samples contained stronger signals characteristic for cubic aluminum (Fm3m: 38.5, 44.7, 65.1 and 75.3°

(2q)) while the Ga-rich samples displayed patterns indicative of orthorhombic gallium (Cmca: 30.3, 30.6, 45.4, 46.4, 57.6, 63.6, 76.3 and 77.0° (2q).[35]

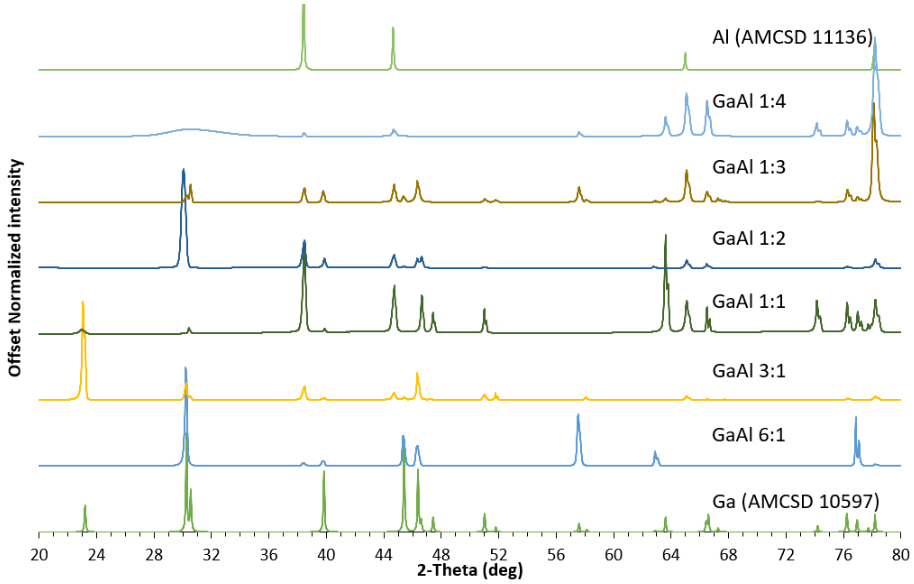

Figure 5.7. PXRD for varying Ga:Al ratio and the theoretical patterns for pure Al and Ga.

5.2.7. Proposed Mechanism for Hydrogen Evolution Reaction

It is generally believed that hydrogen generation occurs at the interface between the particles of aluminum and water, thus requiring a pristine micro-aluminum surface.[29, 30] Bulk commercial aluminum foil will not generate hydrogen gas, as a passivating oxide layer prevents any reaction from occurring with water. According to the data presented above, it was proposed that gallium dissolves aluminum, removing any passivating aluminum oxide film and forming aluminum particles that can split water and form aluminum oxide and hydrogen gas.

Scanning emission microscopy clearly indicates aluminum particles form within a sea of gallium by simple mechanical mixing in 3:1 (Ga:Al) ratio (**Figure 5.8**).

Additionally, each element maintains their individual crystal structures as seen in PXRD data (**Figure 5.7**). Therefore, at these micro-aluminum sites, a series of hydrogen bond exchanges occur to liberate hydrogen.[29, 30, 36, 37] The Al_2O_3 byproduct is porous and gets swept away by the agitation of bubble formation, exposing a new surface of pristine aluminum on the particles for further reaction.

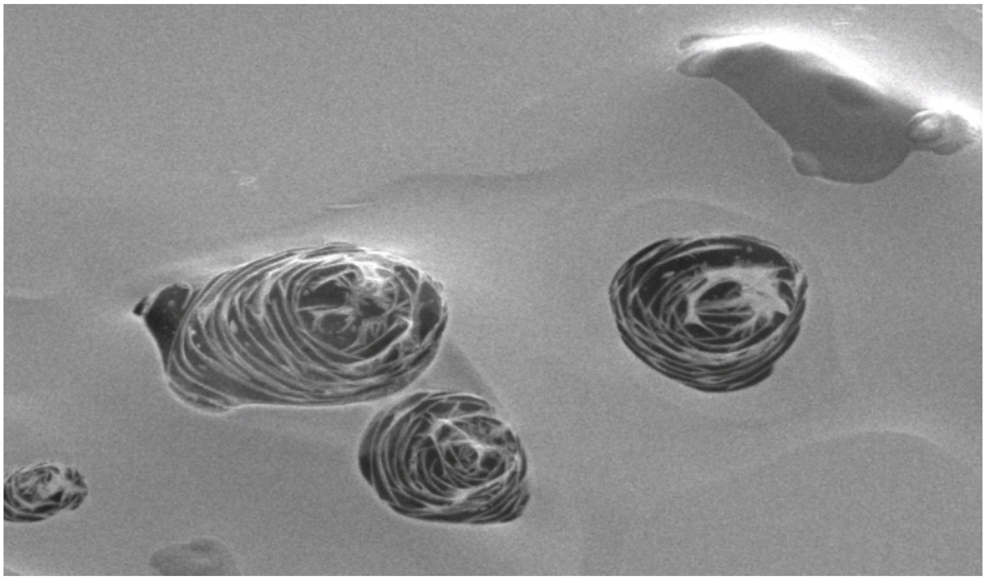

Figure 5.8. SEM image of 3:1 (Ga:Al) alloy.

These observations are in qualitative agreement with the theoretical calculations previously reported that aluminum particles can split water by the Grotthuss mechanism.[29, 30, 36] The Grotthuss mechanism is the movement of protons through the hydrogen bonds of water. It typically involves the transfer of a proton from a hydronium ion to a water molecule and this hopping of protons continues until solvation of the hydronium ion is achieved.[38, 39] Theoretical calculations of water splitting reactions using aluminum have shown that the hydrogens transfer in a similar manner.

Simulations of aluminum clusters (Al_n, n = 16, 17, and 18) for water splitting were conducted to better understand the interaction between aluminum and water.[29, 30, 36, 40] It was reasoned that a water molecule bonds to Lewis acidic sites on the aluminum cluster, which then creates a Lewis basic site at the opposite end of the cluster. Then through a series of proton transfers, in a Grotthuss mechanism-like fashion, a hydrogen atom attaches to the Lewis basic end of the metal cluster. A molecule of H_2 is then released and the process can continue again.

Similar results were obtained when density functional theory calculations were conducted on 13-atom clusters of Al_{13}, Ga_{13}, and $GaAl_{12}$.[37] An in-depth analysis of complementary Lewis acid/base pairs of these metal clusters facilitates the production of hydrogen. Further calculations revealed that H_2 forms through two possible pathways, either from the simultaneous breaking of O-H and Al-H bonds or from the cleavage of two neighboring Al-H bonds. It is important to note that when the aluminum clusters were doped with gallium there was a decrease in the transition state barrier for water splitting. This is encouraging as this is another reason for gallium's importance as part of the binary alloy.

5.2.8. Hydrogenation Reactions

To demonstrate the utility of the alloy for use in a research setting, a hydrogenation reaction was conducted. These reactions traditionally use a metal catalyst under pressurized hydrogen and heat to induce the transformation. The substrate, 4-phenyl-1-buten-4-ol, was chosen as a representative substrate. Previous hydrogenation reactions of this olefin have been reported.[41-43] Ghosh described a procedure using Lindlar's catalyst (10 wt%) to produce the benzyl alcohol in high yields.[41] A Parr hydrogenation apparatus was required to introduce the H_2 (20 psi), which is not ideal for industrial use. Two ruthenium catalysis methods were developed to undergo the same transformation. One used a H_2 cylinder to achieve hydrogenation[42] while the second used 1,4-butanediol as the *in situ* H_2 source for a transfer hydrogenation reaction.[43] Both were able to produce 1-phenyl-butanol in high yields although heightened temperatures were necessary (110 °C).

With the Ga-Al alloy, hydrogen generation occurred under atmospheric pressure and room temperature conditions. Hydrogen was generated *ex situ* and then transferred *via* cannula into the flask containing the substrate and a nickel catalyst. The alkene was hydrogenated in an hour and the product was isolated in very high yields and purity (**Scheme 5.1**). This hydrogenation reaction can be completed with methanol instead of water as the hydrogen source, which reacts more vigorously and quickly with the alloy to produce hydrogen.

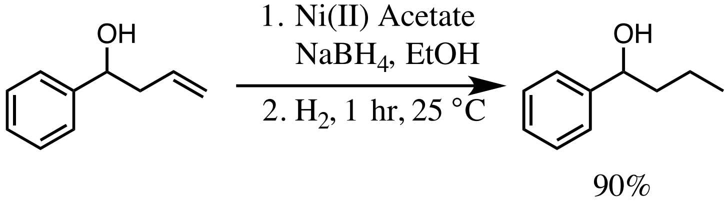

Scheme 5.1. Reduction of 4-phenyl-1-buten-4-ol (1.25 mmol) with Ni catalyst (1.25 mmol) in EtOH, followed by reaction with alloy-generated hydrogen (9.0 mmol) (2.6 g) in DI water (5 mL).

5.3. Conclusions

Previous reports of Ga-Al alloys used primarily Al-rich alloys to generate hydrogen and required special milling techniques and higher temperatures.[22, 24] As the data presented in this chapter showed, Ga-rich alloys are far more effective at producing hydrogen from water and can be used under ambient conditions. The gallium dissolves the aluminum, removes the passivating oxide layer, and allows the pristine micro-aluminum surface to split water into hydrogen gas. Because the gallium selectively dissolves the aluminum, waste aluminum such as soda cans generate equivalent amounts of hydrogen as pure aluminum, without needing to expend energy into cleaning the surface. Different types of water ranging from DI H_2O to rainwater were all comparable in generating stoichiometric amounts of hydrogen in under 15 min and at room temperature. Characterization and theoretical predictions verified that the hydrogen evolution reaction occurs at micro-aluminum sites in a sea of gallium. Application of the alloy in a simple hydrogenation reaction demonstrated that the hydrogen can be used without needing to pressurize the system. The used alloy can be separated and recovered into aluminum oxide and its original gallium components. The aluminum oxide could act as an aluminum source for smelting plants. The gallium can be recycled into subsequent alloys with no depletion in its ability to generate hydrogen. Overall, the Ga-rich Ga-Al alloy can produce substantial amounts of hydrogen at room temperature, no energy input and without excessive material manipulation or pH modification.

5.4. References

1. Pachauri, R. K.; Meyer, L. A., Climate Change 2014: Synthesis Report. Contribution of Working Groups, I, II, and III, to the Fifth Assessment Report of the Intergovernmental Panel on Climate Change. IPCC: 2014; pp 1-151.

2. Zhang, Y.; Luo, M.; Yang, Y.; Li, Y.; Guo, S., Advanced multifunctional electrocatalyst for energy conversion. *ACS Energy Lett.* **2019,** *4*, 1672-1680.

3. Tran, P. D.; Chiam, S. Y.; Boix, P. P.; Ren, Y.; Pramana, S. S.; Fize, J.; Artero, V.; J., B., Novel cobalt/nickel-tungsten-sulfide catalysts for electrocatalytic hydrogen generation from water. *Energy Environ. Sci.* **2013,** *6*, 2452-2459.

4. Wang, Q.; Domen, K., Particulate photocatalysts for light-driven water spilitting: mechansim, challenges, and design strategies. *Chem. Rev.* **2020,** *120*, 919-985.

5. Dresp, S.; Dionigi, F.; Klingenhof, M.; Strasser, P., Direct electrolytic splitting of seawater: opportunities and challenges. *ACS Energy Lett.* **2019,** *4*, 933-942.

6. Liu, R.; Gu, S.; Du, H.; Li, C. M., Controlled syntehsis of FeP nanorod arrays as highly efficient hydrogen evolution cathode. *J. Mater. Chem. A* **2014,** *2*, 17263-17267.

7. Merki, D.; Fierro, S.; Vrubel, H.; Hu, X., Amorphous molybdenum sulfide films as catalysts for electrochemical hydrogen production in water. *Chem. Sci* **2011,** *2*, 1262-1267.

8. Sun, Y.; Liu, C.; Grauer, D. C.; Yano, J.; Long, J. R.; Yang, P.; Chang, C. J., Electrodeposited cobalt-sulfide catalyst for electrochemical and photoelectrochemical hydrogen generation from water. *J. Am. Chem. Soc.* **2013,** *135*, 17699-17702.

9. Kiran, V.; Mukherjee, J.; Jenjeti, R. N.; Sampath, S., Active guests in the MoS_2/$MsSe_2$ host lasttice: efficient hydrogen evolution using few-layer alloys of $MoS_{2(1-x)}Se_{2x}$. *Nanoscale* **2014,** *6*, 12856-12863.

10. Fan, L.; Liu, P. F.; Yan, X.; Gu, L.; Yang, Z. Z.; Yang, H. G.; Qiu, S.; Yao, X., Atomically isolated nickel species anchored on graphitized carbon for efficient hydrogen evolution electrocatalysis. *Nat. Commun.* **2016,** *7*, 10667.

11. Vrubel, H.; Hu, X., Molybdenum boride and carbide catalyze hydrogen evolution in both acidic and basic solutions. *Angew. Chem. Int. Ed.* **2012,** *51*, 12703-12706.

12. Cao, B.; Veith, G. M.; Neuefeind, J. C.; Adzic, R. R.; Khalifah, P. G., Mixed closed-packed cobalt molybdenum nitrides as non-noble metal electrocatalysts for the hydrogen evolution reaction. *J. Am. Chem. Soc.* **2013,** *135*, 19186-19192.

13. Aluminum. In *Encyclopedia Britannica*.

14. Xu, S.; Zhao, X.; Liu, J., Liquid metal activated aluminum-water reaction for direct hydrogen generation at room temperature. *Renewable and Sustainable Energy Rev.* **2018,** *92*, 17-37.

15. Sherif El-Eskandarany, M., The history and necessity of mechanical alloying. In *Mechanical Alloying*, William Andrew: Oxford, UK, 2015; pp 13-47.

16. Fan, M.-Q.; Xu, F.; Sun, L.-X., Studies on hydrogen generation characteristics of hydrolysis of te ball milling Al-based materials in pure water. *Int. J. Hydrogen Energy* **2007,** *32*, 2809-2815.

17. Ilyukhina, A. V.; Kravchenko, O. V.; Bulychev, B. M.; Shkolnikov, E. I., Mechanochemical activation of aluminum with gallams for hydrogen evolution from water. *Int. J. Hydrogen Energy* **2010,** *35*, 1905-1910.

18. Ying, C.; Bei, L.; Huihu, W.; Shijie, D., Effect of preparation parameters and alloy elements on HER performance at 0 °C in water. *Rare Metal Materials and Engineering* **2017,** *46*, 2428-2432.

19. Ma, G.-L.; Dai, H.-B.; Zhuang, D.-W.; Xia, H.-J.; Wang, P., Controlled hydrogen generation by reaction of aluminum/sodium hydroxide/sodium stannate solid mixture with water. *J. Hydrogen Energy* **2012,** *37*, 5811-5816.

20. Huang, X.; Gao, T.; Pan, X.; Wei, D.; Ly, C.; Quin, L.; Huang, Y., A review: Feasibility of hydrogen generation from the reaction between aluminum and water for fuel cell applications. *J. Power Sources* **2013,** *229*, 133-140.

21. Foley, N.; Jaskula, B. W. Gallium — A Smart Metal. https://pubs.usgs.gov/fs/2013/3006/pdf/fs2013-3006.pdf (accessed October 22, 2020).

22. Ziebarth, J. T.; Woodall, J. M.; Kramer, R. A.; Choi, G., Liquid phase-enabled reactions of Al-Ga and Al-Ga-In-Sn alloys wtih water. *Int. J. Hydrogen Energy* **2011,** *36*, 5271-5279.

23. Wang, W.; Chen, D. M.; Yang, K., Investigation on microstructure and hydrogen generation performance of Al-rich alloys. *Int. J. Hydrogen Energy* **2010,** *35*, 12011-12019.

24. Huang, T.; Gao, Q.; Liu, D.; Xu, S.; Guo, C.; Zou, J.; Wei, C., Preparation of Al-Ga-In-Sn-Bi quinary alloy and its hydrogen production via water splitting. *Int. J. Hydrogen Energy* **2015,** *40*, 2354-2362.

25. He, T.; Wang, W.; Chen, W.; Chen, D.; Yang, K., Reactivity of Al-rich Alloys with Water Promoted by Liquid Al Grain Boundary Phases. *J. Mater. Science & Technology* **2017,** *33*, 397-403.

26. Evans, D. S.; Prince, A., Thermal analysis of Ga-In-Sn system. *Metal Science* **1978,** *12*, 411-414.

27. Plevachuk, Y.; Sklyarchuk, V.; Eckert, S.; Gerbeth, G.; Novakovic, R., Thermophysical Properties of the Liquid Ga-In-Sn Eutectic Alloy. *J. Chem. Eng. Data* **2014,** *59*, 757-763.

28. As sold by Sigma Aldrich, accessed Oct. 25, 2020.

29. Vashishta, P.; Shimojo, F.; Ohmura, S.; Shimamura, K.; Mou, W.; Kalia, R. K.; Nakano, A., Rapid hydrogen production from water using aluminum nanoclusters: A quantum molecular dynamics simulation study. *Solid State Ionics* **2014,** *262*, 908-910.

30. Reber, A. R.; Khanna, S. N.; Roach, P. J.; Woodward, W. H.; Castleman, A. W., Reactivity of aluminum cluster anions with water: Origins of reactivity and mechanisms for H_2 release. *J. Phys. Chem. A* **2010,** *114*, 6071-6081.

31. Zheng, J.; Zhao, Y.; Xi, H.; Li, C., Seawater splitting for hydrogen evolution by robust electrocatalysts from secondary M (M= Cr, Fe, Co, Ni, Mo) incorporated Pt. *RSC Adv.* **2018,** *8*, 9423-9429.

32. Patil, A.; Hatch, G.; Michaud, C.; Brotman, M.; Regunathan, P.; Tallon, R.; Andrew, R.; Murphy, S.; Murphy, S.; Undesser, P.; Redden, K. *Aluminum Fact Sheet*; Water Quality Association: Illinois, USA, 2013.

33. Foley, N. K.; Jaskula, B. W.; Kimball, B. E.; Schulte, R. F., Gallium. In *Critical Mineral Resources of the United States — Ecomic and Environmental Geology and Prospects for Future Supply*, Schulz, K. J.; John H. DeYoung, J.; II, R. R. S.; Bradley, D. C., Eds. U.S. Geological Survey 2017; pp H1-H35.

34. United States Environmental Protection Agency. Facts and figures about materials, waste and recycling. https://www.epa.gov/facts-and-figures-about-materials-waste-and-recycling/aluminum-material-specific-data (accessed March 30, 2020).

35. American Mineralogist Crystal Structure Database (AMCSD)

36. Shimojo, F.; Ohmura, S.; Kalia, R. K.; Nakano, A.; Vashishta, P., Molecular dynamics and simulations of rapid hydrogen production from water using aluminum clusters as catalyzsers. *Phys. Rev. Lett.* **2010,** *104*, 126102.

37. Chen, J.; Luo, Z., Single-point attack of two H_2O molecules towards a Lewis Acid site on the $GaAl_{12}$ clusters for hydrogen evolution. *ChemPhysChem* **2019,** *20*, 499-505.

38. Agmon, N., The Grotthuss mechanism. *Chem. Phys. Lett.* **1995,** *244*, 456-462.

39. Fischer, S. A.; Gunlycke, D., Anaylsis of Correlated Dynamics in the Grotthuss Mechanism of Proton Diffusion. *J. Phys. Chem. B* **2019,** *123*, 5536-5544.

40. Roach, P. J.; Woodward, W. H.; Castleman, A. W.; Reber, A. C.; Khanna, S. N., Complementary Active sites cause size-selective reactivity of aluminum cluster anions with water. *Science* **2009,** *323*, 492-495.

41. Ghosh, A. K.; Krishnan, K., Chemoselective catalystic hydrogenation of alkenes by Lindlar Catalyst. *Tett. Lett.* **1998,** *39*, 947-948.

42. Adair, G. R. A.; Williams, J. M. J., A catalytic deracemisation of alcohols. *Chem. Commun.* **2007**, 2608-2609.

43. Maytum, H. C.; Francos, J.; Whatrup, D. J.; Williams, J. M. J., 1,4-Butanediol as a reducing agent in transfer hydrogenation reactions. *Chem. Asian J.* **2010,** *5*, 538-542.

EXPERIMENTAL DETAILS

AND

CHARACTERIZATION

General Methods

All materials were commercially available unless otherwise notes. All products were analyzed by nuclear magnetic resonance (NMR) spectroscopy measured in ppm and recorded on a Bruker 500 MHz spectrometer at 297 K using $CDCl_3$ ($\delta = 7.26$) as an internal standard for ^1H NMR and 125.7 MHz using $CDCl_3$ ($\delta = 77.0$) as an internal standard for ^{13}C NMR. Using a different probe, ^{11}B NMR analysis occurred on a 160 MHZ spectrometer using $BF_3 \bullet Et_2O$ ($\delta = 0$) as an external standard. Coupling constants (*J*) are given in Hertz (Hz) and signal multiplicities are abbreviated as s = singlet, d = doublet, t = triplet, m = multiplet, and br = broad. Spectra of compounds were consistent with literature data.

6.1.1. Chapter 2

Synthesis of Diisobutylaluminum Borohydride [*i*(Bu)$_2$AlBH$_4$]. In an argon-purged 100mL round bottom flask, DIBAL (1M in toluene, 5 mL, 5 mmol, 1 equiv.) was added. BMS (0.474mL, 5 mmol, 1 equiv.) was added dropwise. The reaction mixture was allowed to stir for 1 h at room temperature. The *i*(Bu)$_2$AlBH$_4$ (1M) was used without purification or stored under Ar in an ampule. ^{11}B NMR (500 MHz) δ -36 (quintet, *J* = 83Hz).

Alternative Synthesis of Diisobutylaluminum Borohydride. In an Ar-purged 100mL round bottom flask, NaBH$_4$ (0.078g, 2 mmol, 1 equiv.) and tetraglyme (2mL) were allowed to stir until a homogenous solution formed. To that solution diisobutylaluminum chloride (1M in hexanes, 0.49 mL, 2 mmol, 1 equiv.) was added. The reaction mixture was allowed to stir for 1 h at room temperature. Anhydrous THF (7.96mL) was added to make a 0.25M solution. The *i*(Bu)$_2$AlBH$_4$ (0.25M) was used without purification. ^{11}B NMR (500 MHz) δ -36 (quintet, *J* = 83Hz).

Representative Procedure for the Reduction of Aldehydes Using *i*(Bu)$_2$AlBH$_4$. In an Ar-purged 100mL round bottom flask fitted with a rubber septum, aldehyde (1 equiv.) and anhydrous THF were combined. The *i*(Bu)$_2$AlBH$_4$ (0.5 equiv.) was added dropwise. Once all the *i*(Bu)$_2$AlBH$_4$ was added the reaction mixture was allowed to stir for 1 h at room temperature. The reaction mixture was quenched with methanol (5 mL) and deionized H$_2$O (5 mL) (*caution: H_2 evolution!*). A gel formed with the addition of methanol. The resulting reaction mixture was filtered, and the filtrate was acidified with concentrated HCl (12 M, 1 mL). The product was extracted with diethyl ether (3x10 mL) and the combined organic extracts were dried ($MgSO_4$) and concentrated to afford the alcohol.

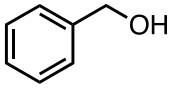

Benzyl alcohol. Benzaldehyde (0.5 mL, 5 mmol) was reacted with *i*$(Bu)_2AlBH_4$ (3.3 mL, 2.5 mmol) in THF (5 mL) for 1 h. The product was isolated via the above procedure (0.494g, 93%): ^{1}H NMR (500 MHz, Chloroform-*d*) δ 7.38 – 7.30 (m, 5H), 4.63 (s, 2H), 2.64 (bs, 1H). ^{13}C NMR (126 MHz, Chloroform-*d*) δ 140.91, 128.55, 127.61, 127.04, 65.12.

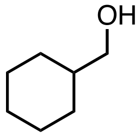

Cyclohexanemethanol. Cyclohexanecarboxaldehyde (0.61 mL, 5 mmol) was reacted with *i*$(Bu)_2AlBH_4$ (4.55 mL, 2.5 mmol) in THF (5 mL) for 1 h. The product was isolated via the above procedure (0.406g, 71%): ^{1}H NMR (500 MHz, Chloroform-*d*) δ 4.72 (s, 1H), 3.41 (s, 2H), 1.72 (s, 5H), 1.45 (s, 1H), 1.20 (d, *J* = 46.3 Hz, 3H), 0.91 (d, *J* = 9.8 Hz, 2H); ^{13}C NMR (126 MHz, Chloroform-*d*) δ 68.81, 40.58, 29.69, 26.71, 25.96.

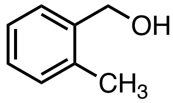

2-Methylbenzyl alcohol. 2-Tolualdehyde (0.35 mL, 3 mmol) was reacted with $i(\mathrm{Bu})_2\mathrm{AlBH}_4$ (2.11 mL, 1.5 mmol) in THF (3 mL) for 1 h. The product was isolated via the above procedure (0.483g, 98%): ^{1}H NMR (500 MHz, Chloroform-*d*) δ 7.38 (d, *J* = 9.0 Hz, 1H), 7.26 (d, *J* = 11.8 Hz, 2H), 7.23 (d, *J* = 2.9 Hz, 1H), 4.66 (s, 2H), 2.75 (s, 1H), 2.38 (s, 3H); ^{13}C NMR (126 MHz, Chloroform-*d*) δ 138.78, 136.05, 130.28, 127.69, 127.53, 126.04, 63.19, 18.64.

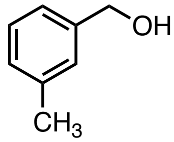

3-Methylbenzyl alcohol. 3-Tolualdehyde (0.35 mL, 3 mmol) was reacted with $i(\mathrm{Bu})_2\mathrm{AlBH}_4$ (2.11 mL, 1.5 mmol) in THF (3 mL) for 1 h. The product was isolated via the above procedure (0.358g, 98%): ^{1}H NMR (500 MHz, Chloroform-*d*) δ 7.13 (t, *J* = 7.5 Hz, 1H), 7.04 (s, 1H), 7.00 (dd, *J* = 14.5, 7.7 Hz, 2H), 4.48 (s, 2H), 2.77 (s, 1H), 2.24 (s, 3H); ^{13}C NMR (126 MHz, Chloroform-*d*) δ 140.88, 138.18, 128.46, 128.33, 127.80, 124.09, 65.17, 21.41.

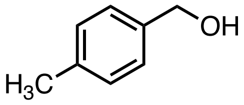

4-Methylbenzyl alcohol. 4-Tolualdehyde (0.24 mL, 2 mmol) was reacted with $i(\mathrm{Bu})_2\mathrm{AlBH}_4$ (1.09 mL, 1 mmol) in THF (2 mL) for 1 h. The product was isolated via the above procedure (0.201g, 82%): ^{1}H NMR (500 MHz, Chloroform-*d*) δ

7.27 (d, 2H), 7.18 (d, 2H), 4.65 (s, 2H), 2.35 (s, 3H), 1.56 (bs, 1H); ^{13}C NMR (500 MHz, Chloroform-*d*) δ 137.9, 137.4, 129.3, 127.1, 65.3, 21.2

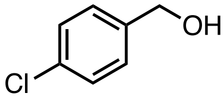

4-Chlorobenzyl alcohol. 4-Chlorobenzaldehyde (0.420 g, 3 mmol) was reacted with *i*(Bu)$_2$AlBH$_4$ (2.11 mL, 1.5 mmol) in THF (3 mL) for 1 h. The product was isolated via the above procedure (0.396g, 93%): ^{1}H NMR (500 MHz, Chloroform-*d*) δ 7.33 (d, *J* = 8.6 Hz, 2H), 7.30 (d, *J* = 8.5 Hz, 2H), 4.67 (s, 2H), 1.72 (s, 1H); ^{13}C NMR (126 MHz, Chloroform-*d*) δ 139.25, 133.38, 128.69, 128.27, 64.58.

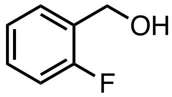

2-Fluorobenzyl alcohol. 2-Fluorobenzaldehyde (0.3 mL, 3 mmol) was reacted with *i*(Bu)$_2$AlBH$_4$ (3.75 mL, 3 mmol) in THF (3 mL) for 1 h. The product was isolated via the above procedure (0.288g, 76%): ^{1}H NMR (500 MHz, Chloroform-*d*) δ 7.32 (t, *J* = 7.6 Hz, 1H), 7.18 (q, *J* = 7.0, 6.6 Hz, 1H), 7.05 (t, *J* = 7.5 Hz, 1H), 6.98 – 6.92 (m, 1H), 4.65 (s, 2H), 2.23 (s, 1H); ^{13}C NMR (126 MHz, Chloroform-*d*) δ 161.59, 159.63, 129.30, 127.87, 127.76, 124.21 (d, *J* = 3.6 Hz), 115.32, 115.15, 59.26 (d, *J* = 4.4 Hz).

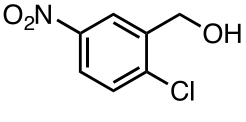

2-Chloro-5-nitrobenzyl alcohol. 2-Chloro-5-nitrobenzaldehyde (0.47 g, 2.5 mmol) was reacted with *i*(Bu)$_2$AlBH$_4$ (1.4 mL, 1.26 mmol) in THF (2.5

mL) for 1 h. The product was isolated via the above procedure (0.37g, 79%): ^{1}H NMR (500 MHz, Chloroform-*d*) δ 8.46 (d, *J* = 2.7 Hz, 1H), 8.11 (dd, *J* = 8.7, 2.7 Hz, 1H), 7.52 (d, *J* = 8.7 Hz, 1H), 4.87 (d, *J* = 4.5 Hz, 2H), 1.56 (s, 1H); ^{13}C NMR (126 MHz, Chloroform-*d*) δ 140.42, 138.82, 130.16, 128.59, 126.62, 123.43, 123.09, 61.89.

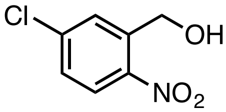

5-Chloro-2-nitrobenzyl alcohol. 5-Chloro-2-nitrobenzaldehyde (0.557 g, 3 mmol) was reacted with *i*(Bu)$_2$AlBH$_4$ (2.11 mL, 1.5 mmol) in THF (3 mL) for 1 h. The product was isolated via the above procedure (0.496g, 88%): ^{1}H NMR (500 MHz, Chloroform-*d*) δ 8.09 (d, *J* = 8.7 Hz, 1H), 7.82 (s, 1H), 7.43 (d, *J* = 9.5 Hz, 1H), 5.02 (s, 2H), 2.17 (s, 1H); ^{13}C NMR (126 MHz, Chloroform-*d*) δ 140.93, 139.13, 129.45, 128.35, 126.53, 62.00.

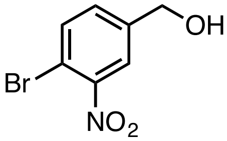

4-Bromo-3-nitrobenzyl alcohol. 4-Bromo-3-nitrobenzaldehyde (0.400 g, 1.74 mmol) was reacted with *i*(Bu)$_2$AlBH$_4$ (1.2 mL, 0.87 mmol) in THF (2 mL) for 1 h. The product was isolated via the above procedure (0.363 g, 90%): ^{1}H NMR (500 MHz, Chloroform-*d*) δ 7.86 (d, *J* = 2.2 Hz, 1H), 7.71 (d, *J* = 8.2 Hz, 1H), 7.43 (dd, *J* = 8.3, 1.9 Hz, 1H), 4.76 (s, 2H); ^{13}C NMR (126 MHz, Chloroform-*d*) δ 142.03, 135.04, 131.03, 123.49, 112.96, 63.31.

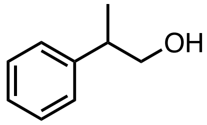

2-Phenyl-1-propanol. 2-Phenylpropionaldehyde (0.66 mL, 5 mmol) was reacted with *i*(Bu)$_2$AlBH$_4$ (3.42 mL, 2.5 mmol) in THF (5 mL) for 1 h. The product was isolated via the above procedure (0.552g, 81%): ^{1}H NMR (500 MHz, Chloroform-*d*) δ 7.39 (d, *J* = 7.5 Hz, 2H), 7.31 – 7.27 (m, 3H), 3.73 (d, *J* = 7.5 Hz, 2H), 2.98 (h, *J* = 7.0 Hz, 1H), 1.89 (s, 1H), 1.33 (d, *J* = 7.1 Hz, 3H). ^{13}C NMR (126 MHz, Chloroform-*d*) δ 143.94, 128.66, 127.58, 126.67, 68.66, 42.49, 17.72.

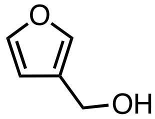

Furan-3-methanol. 3-Furancarboxaldehyde (0.418 mL, 5 mmol) was reacted with *i*(Bu)$_2$AlBH$_4$ (3.42 mL, 2.5 mmol) in THF (5 mL) for 1 h. The product was isolated via the above procedure (0.361g, 74%): ^{1}H NMR (500 MHz, Chloroform-*d*) δ 7.37 (s, 2H), 6.39 (s, 1H), 4.48 (s, 2H), 2.70 (s, 1H); ^{13}C NMR (126 MHz, Chloroform-*d*) δ 143.39, 139.87, 125.16, 109.82, 56.37.

Representative Procedure for the Reduction of Ketones Using *i*(Bu)$_2$AlBH$_4$. In an Ar-purged 100mL round bottom flask, ketone (1 equiv.) and anhydrous THF were combined. The *i*(Bu)$_2$AlBH$_4$ (0.5 equiv.) was added dropwise. Once all the *i*(Bu)$_2$AlBH$_4$ was added the reaction mixture was allowed to stir for 1 h at room temperature. The reaction mixture was quenched with methanol (7mL) and deionized H$_2$O (5 mL) (*Caution! Hydrogen evolution*). A gel formed with the addition of methanol. The resulting reaction mixture was filtered, and the filtrate was acidified with concentrated HCl (12M, 1mL). The product was extracted with diethyl ether (3x10mL) and the combined organic extracts were dried ($MgSO_4$) and concentrated to afford an alcohol.

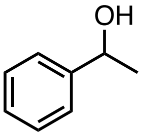

1-Phenylethanol. Acetophenone (0.585 mL, 5 mmol) was reacted with *i*$(Bu)_2AlBH_4$ (2.5 mL, 2.5 mmol) in THF (5 mL) for 1 h. The product was isolated via the above procedure (0.598g, 98%): ^{1}H NMR (500 MHz, Chloroform-*d*) δ 7.33 (s, 4H), 7.28 – 7.24 (m, 1H), 4.83 (q, J = 6.5 Hz, 1H), 2.72 (s, 1H), 1.46 (d, J = 5.0 Hz, 3H). ^{13}C NMR (126 MHz, Chloroform-*d*) δ 145.82, 128.51, 127.48, 125.39, 70.43, 25.17.

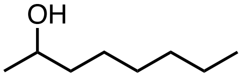

2-Octanol. 2-Octanone (0.785 mL, 5 mmol) was reacted with *i*$(Bu)_2AlBH_4$ (2.75 mL, 2.5 mmol) in THF (5 mL) for 1 h. The product was isolated via the above procedure (0.683g, 99%): ^{1}H NMR (500 MHz, Chloroform-*d*) δ 3.77 (sextet, J = 6.2 Hz, 1H), 2.69 (bs, 1H), 1.49 – 1.35 (m, 3H), 1.26 (s, 7H), 1.16 (d, J = 6.2 Hz, 3H), 0.87 – 0.84 (m, 3H). ^{13}C NMR (126 MHz, Chloroform-*d*) δ 68.19, 39.38, 31.83, 29.31, 25.73, 23.47, 22.60, 14.06.

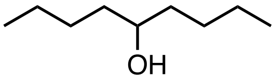

5-Nonanol. 5-nonanone (0.711 g, 5 mmol) was reacted with *i*$(Bu)_2AlBH_4$ (2.75 mL, 2.5 mmol) in THF (5 mL) for 1 h. The product was isolated via the above procedure (0.640g, 89%): ^{1}H NMR (500 MHz, Chloroform-*d*) δ 3.59 (s, 1H), 1.42 (m, 13H), 0.91 (s, 6H). ^{13}C NMR (126 MHz, Chloroform-*d*) δ 71.86, 37.14, 27.83, 22.75, 14.00.

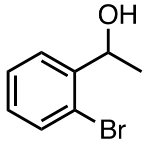
1-(2-Bromophenyl)ethanol. 2-Bromo-acetophenone (0.67 mL, 5 mmol) was reacted with *i*(Bu)$_2$AlBH$_4$ (2.5 mL, 3.3 mmol) in THF (5 mL) for 1 h. The product was isolated via the above procedure (0.858g, 86%): ^{1}H NMR (500 MHz, Chloroform-*d*) δ 7.56 (d, *J* = 7.7 Hz, 1H), 7.49 (d, *J* = 7.9 Hz, 1H), 7.32 (t, *J* = 7.3 Hz, 1H), 7.10 (t, *J* = 7.6 Hz, 1H), 5.20 (q, *J* = 6.4 Hz, 1H), 1.45 (d, *J* = 6.5 Hz, 3H). ^{13}C NMR (126 MHz, Chloroform-*d*) δ 144.72, 132.63, 128.73, 127.85, 126.71, 121.67, 69.12, 23.61.

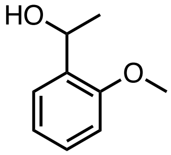
1-(2-Methoxyphenyl)ethanol. 2-Methoxy-acetophenone (0.413 mL, 3 mmol) was reacted with *i*(Bu)$_2$AlBH$_4$ (2.68 mL, 1.5 mmol) in THF (3 mL) for 1 h. The product was isolated via the above procedure (0.239g, 69%): ^{1}H NMR (500 MHz, Chloroform-*d*) δ 7.35 (d, *J* = 7.5 Hz, 1H), 7.27 – 7.23 (m, 1H), 6.97 (t, *J* = 7.5 Hz, 1H), 6.88 (d, *J* = 8.2 Hz, 1H), 5.10 (q, *J* = 6.5 Hz, 1H), 3.86 (s, 3H), 2.54 (s, 1H), 1.51 (d, *J* = 6.5 Hz, 3H). ^{13}C NMR (126 MHz, Chloroform-*d*) δ 156.58, 133.48, 128.31, 126.12, 120.82, 110.46, 66.56, 55.28, 22.87.

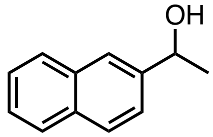

1-(2-Naphthyl)ethanol. 2-Acetonaphthone (0.851 mL, 5 mmol) was reacted with *i*(Bu)$_2$AlBH$_4$ (2.75 mL, 2.5 mmol) in THF (5 mL) for 1 h. The product was isolated via the above procedure (0.879g, 99%): ^{1}H NMR (500 MHz, Chloroform-*d*) δ 7.86 – 7.80 (m, 4H), 7.52 – 7.46 (m, 3H), 5.06 (q, *J* = 6.5 Hz, 1H), 2.09 (bs, 1H), 1.59 (d, *J* = 6.5 Hz, 3H). ^{13}C NMR (126 MHz, Chloroform-*d*) δ 143.19, 133.34, 132.94, 128.33, 127.94, 127.68, 126.16, 125.81, 123.81, 70.56, 25.16.

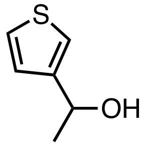

1-(3-Thienyl)ethanol. 3-Acetylthiophene (0.25 g, 2 mmol) was reacted with *i*(Bu)$_2$AlBH$_4$ (1.25 mL, 1 mmol) in THF (2 mL) for 5 h. The product was isolated via the above procedure (0.219g, 86%) ^{1}H NMR (500 MHz, Chloroform-*d*) δ 7.29 (d, *J* = 8.1 Hz, 1H), 7.17 (s, 1H), 7.09 (d, *J* = 5.0 Hz, 1H), 4.94 (q, *J* = 6.5 Hz, 1H), 2.29 (s, 1H), 1.51 (d, *J* = 6.5 Hz, 3H). ^{13}C NMR (126 MHz, Chloroform-*d*) δ 147.34, 126.14, 125.65, 120.17, 66.54, 24.47.

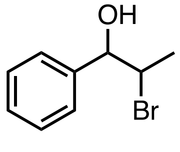

2-Bromo-1-phenyl-1-propan-1-ol. 2-Bromopropiophenone (0.45 mL, 3 mmol) was reacted with *i*(Bu)$_2$AlBH$_4$ (2.68 mL, 1.5 mmol) in THF (3 mL) for 1 h. The product was isolated via the above procedure (0.385g, 60%) ^{1}H NMR (500 MHz, Chloroform-*d*) δ 7.37 (d, *J* = 8.1 Hz, 5H), 4.62 (d, *J* = 7.6 Hz, 1H), 4.37 – 4.32 (quintet, 1H), 1.57 (d, *J* = 6.8 Hz, 3H). ^{13}C NMR (126 MHz, Chloroform-*d*) δ 139.64, 128.62, 128.53, 126.73, 79.20, 58.47, 22.73.

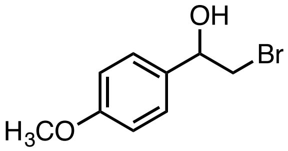

2-Bromo-1-(4-methoxyphenyl)ethanol. 2-Bromo-4-methoxyacetophenone (0.043 mL, 0.188 mmol) was reacted with *i*(Bu)$_2$AlBH$_4$ (0.23 mL, 0.188 mmol) in THF (0.2 mL) for 7 h. The product was isolated via the above procedure (0.036g, 84%) ^{1}H NMR (500 MHz, Chloroform-*d*) δ 7.30 (d, *J* = 8.7 Hz, 2H), 6.90 (d, *J* = 8.7 Hz, 2H), 4.87 (dd, *J* = 8.9, 3.5 Hz, 1H), 3.81 (s, 3H), 3.61 – 3.50 (m, 2H), 2.65 (s, 1H). ^{13}C NMR (126 MHz, Chloroform-*d*) δ 159.69, 132.47, 127.25, 114.09, 73.48, 55.32, 40.24.

Representative Procedure for the Reduction of Nitriles Using *i*(Bu)$_2$AlBH$_4$. In an Ar-purged 100mL round bottom flask, the nitrile (1 equiv.) and anhydrous THF were combined. The *i*(Bu)$_2$AlBH$_4$ (1 equiv.) was added dropwise. Once all the *i*(Bu)$_2$AlBH$_4$ was added the reaction mixture was allowed to stir for 1 h at room temperature. The reaction mixture was quenched with methanol (5mL) and deionized H$_2$O (5 mL) (*Caution! Hydrogen evolution*). A gel formed with the addition of methanol. The resulting reaction mixture was filtered, and the filtrate was acidified with concentrated HCl (12M, 1mL). The reaction mixture was refluxed for 1 h. The reaction mixture was extracted with diethyl ether (3x10mL) and the combined aqueous extracts were basified with $NaOH_{(s)}$ (pH ~12). The product was then extracted with diethyl ether (3x10mL). The product was extracted with diethyl ether (3x10mL) and the combined organic extracts were dried ($MgSO_4$) and concentrated to afford the amine.

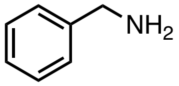

Benzylamine. Benzonitrile (0.408 mL, 4 mmol) was reacted with $i(Bu)_2AlBH_4$ (4.37 mL, 4 mmol) in THF (4 mL) for 1 h. The product was isolated via the above procedure (0.425 g, 99%) ^{1}H NMR (500 MHz, Chloroform-*d*) δ 7.20 (d, *J* = 19.8 Hz, 4H), 7.12 (s, 1H), 3.72 (s, 2H), 1.45 (s, 2H). ^{13}C NMR (126 MHz, Chloroform-*d*) δ 143.42, 128.53, 127.08, 126.77, 46.54.

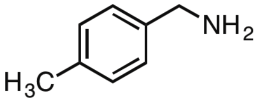

4-Methylbenzyl amine. 4-Methylbenzonitrile (0.470 g, 4 mmol) was reacted with $i(Bu)_2AlBH_4$ (4.4 mL, 4 mmol) in THF (5 mL) for 1 h. The product was isolated via the above procedure (0.459 g, 94%). ^{1}H NMR (500 MHz, Chloroform-*d*) δ 7.21 (d, *J* = 7.8 Hz, 2H), 7.15 (d, *J* = 7.9 Hz, 2H), 3.83 (s, 2H), 2.35 (s, 3H), 1.36 (s, 2H). ^{13}C NMR (126 MHz, Chloroform-*d*) δ 140.42, 136.34, 129.21, 127.03, 46.27, 21.06.

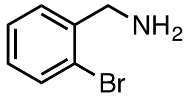
2-Bromobenzyl amine. 2-Bromobenzonitrile (0.548 g, 3 mmol) was reacted with *i*(Bu)$_2$AlBH$_4$ (2.5 mL, 3 mmol) in THF (3 mL) for 1 h. The product was isolated via the above procedure (0.207 g, 37%). ^{1}H NMR (500 MHz, Chloroform-*d*) δ 7.50 (d, *J* = 4.3 Hz, 1H), 7.34 (d, *J* = 7.4 Hz, 1H), 7.23 (s, 1H), 7.12 – 7.03 (m, 1H), 3.87 (s, 2H). ^{13}C NMR (126 MHz, Chloroform-*d*) δ 142.18, 132.78, 129.03, 128.43, 127.71, 123.51, 46.78.

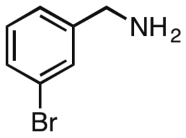
3-Bromobenzyl amine. 3-Bromobenzonitrile (0.546 g, 3 mmol) was reacted with *i*(Bu)$_2$AlBH$_4$ (3.3 mL, 3 mmol) in THF (3 mL) for 1 h. The product was isolated via the above procedure (0.399 g, 72%). ^{1}H NMR (500 MHz, Chloroform-*d*) δ 7.46 (s, 1H), 7.35 (d, *J* = 7.8 Hz, 1H), 7.22 (d, *J* = 7.6 Hz, 1H), 7.18 (d, *J* = 7.7 Hz, 1H), 3.83 (s, 2H), 1.42 (s, 2H). ^{13}C NMR (126 MHz, Chloroform-*d*) δ 145.61, 130.15, 130.08, 129.81, 125.66, 122.61, 45.91.

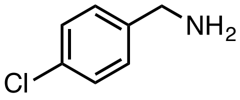
4-Chlorobenzylamine. 4-Chlorobenzonitrile (0.691 g, 5 mmol) was reacted with *i*(Bu)$_2$AlBH$_4$ (5.49 mL, 5 mmol) in THF (5 mL) for 1 h. The product was isolated via the above procedure (0.604 g, 85%) ^{1}H NMR (500 MHz, Chloroform-*d*) δ 7.29 (d, *J* = 8.5 Hz, 2H), 7.24 (d, *J* = 8.4 Hz, 2H), 3.83 (s, 2H), 1.51 (s, 2H). ^{13}C NMR (126 MHz, Chloroform-*d*) δ 141.66, 132.44, 128.60, 128.45, 45.79.

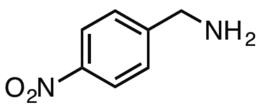

4-Nitrobenzyl amine. 4-Nitrobenzonitrile (0.086 g, 0.58 mmol) was reacted with *i*(Bu)$_2$AlBH$_4$ (0.623 mL, 0.58 mmol) in THF (1 mL) for 1 h. The product was isolated via the above procedure (0.87 g, 98%). ^{1}H NMR (500 MHz, Chloroform-*d*) δ 8.20 (d, *J* = 8.7 Hz, 2H), 7.50 (d, *J* = 8.6 Hz, 2H), 3.49 (s, 2H), 1.59 (s, 2H).^{13}C NMR (126 MHz, Chloroform-*d*) δ 147.46, 128.63, 123.73, 115.06, 52.45.

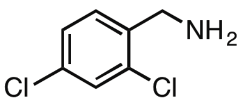

2,4-Dichlorobenzyl amine. 2,4-Dichlorobenzonitrile (0.860 g, 5 mmol) was reacted with *i*(Bu)$_2$AlBH$_4$ (5.5 mL, 5 mmol) in THF (5 mL) for 1 h. The product was isolated via the above procedure (0.833 g, 94%). ^{1}H NMR (500 MHz, Chloroform-*d*) δ 7.26 – 7.22 (m, 2H), 7.13 (dd, *J* = 8.3, 2.1 Hz, 1H), 3.80 (s, 2H), 1.40 (s, 2H). ^{13}C NMR (126 MHz, Chloroform-*d*) δ 137.06, 135.73, 131.77, 129.59, 129.49 (d, *J* = 6.8 Hz), 129.37, 129.15, 127.47, 43.75.

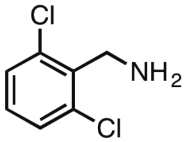

2,6-Dichlorobenzyl amine. 2,6-Dichlorobenzonitrile (0.860 g, 5 mmol) was reacted with *i*(Bu)$_2$AlBH$_4$ (5.5 mL, 5 mmol) in THF (5 mL) for 1 h. The product was isolated via the above procedure (0.236, 27%). ^{1}H NMR (500 MHz, Chloroform-*d*) δ 7.21 (d, *J* = 8.0 Hz, 2H), 7.04 (t, *J* = 7.9 Hz, 1H), 4.02 (s, 2H), 1.75 (s, 2H). ^{13}C NMR (126 MHz, Chloroform-*d*) δ 138.54, 135.91, 133.80, 130.96, 128.83, 128.15, 47.90.

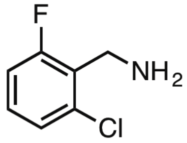

2-Chloro-6-fluorobenzyl amine. 2-Chloro-6-fluorobenzonitrile (0.780 g, 5 mmol) was reacted with *i*(Bu)$_2$AlBH$_4$ (5.5 mL, 5 mmol) in THF (5 mL) for 1 h. The product was isolated via the above procedure (0.129 g, 16%). ^{1}H NMR (500 MHz, Chloroform-*d*) δ 7.16 (m, *J* = 2.8, 2.4 Hz, 2H), 7.00 – 6.96 (m, 1H), 3.99 (d, *J* = 1.9 Hz, 2H), 1.55 (s, 2H). ^{13}C NMR (126 MHz, Chloroform-*d*) δ 162.06, 129.03, 128.89, 125.43, 114.39, 114.21, 37.29.

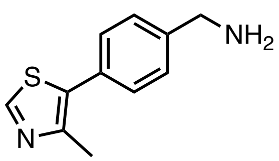

4-(4-Methyl-5-thiazolyl)benzenemethanamine. 4-(4-Methyl-5-thiazolyl)benzonitrile (0.111 g, 0.554 mmol) in THF (1 mL) for 1 h. The product was isolated via the above procedure (0.11 g, 90%). ^{1}H NMR (500 MHz, Chloroform-d) δ 8.67 (s, 1H), 7.42 (s, 4H), 3.88 (s, 2H), 2.54 (s, 3H), 1.70 (s, 2H). ^{13}C NMR (126 MHz, Chloroform-d) δ 161.46, 150.23, 148.48, 130.92, 129.39, 128.69, 52.47, 16.13.

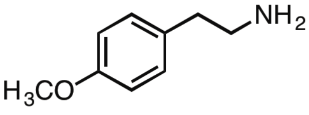

2-(4-Methoxyphenyl)ethanamine. 4-Methoxyphenylacetonitrile (0.4 mL, 3 mmol) was reacted with *i*(Bu)$_2$AlBH$_4$ (3.3 mL, 3 mmol) in THF (3 mL) for 1 h. The product was isolated via the above procedure (0.214 g, 47%). ^{1}H NMR (500 MHz, Chloroform-*d*) δ 7.11 (d, *J* = 8.6 Hz, 2H), 6.84 (d, *J* = 8.7 Hz, 2H), 3.78 (s, 3H), 2.92 (t, *J* = 6.9 Hz, 2H), 2.68 (t, *J* = 6.9 Hz, 2H), 1.41

(bs, 2H). ^{13}C NMR (126 MHz, Chloroform-*d*) δ 158.05, 131.89, 129.72, 113.88, 55.23, 43.68, 39.18.

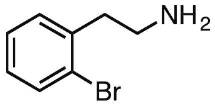

2-Bromophenethylamine. 2-Bromophenylacetonitrile (0.39 mL, 3 mmol) was reacted with *i*(Bu)$_2$AlBH$_4$ (4 mL, 3 mmol) in THF (3 mL) for 1 h. The product was isolated via the above procedure (0.446 g, 74%). ^{1}H NMR (500 MHz, Chloroform-d) δ 7.51 (d, J = 8.0 Hz, 1H), 7.20 (s, 2H), 7.05 (s, 1H), 2.94 (t, J = 7.0 Hz, 2H), 2.87 (t, J = 6.9 Hz, 2H), 1.77 (s, 2H). ^{13}C NMR (126 MHz, Chloroform-*d*) δ 139.14, 132.92, 130.88, 127.91, 127.41, 124.69, 42.07, 40.36.

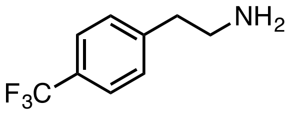

4-Trifluoromethylphenethylamine. 4-(Trifluoromethyl)phenylacetonitrile (0.377 g, 2 mmol) was reacted with *i*(Bu)$_2$AlBH$_4$ (2.22 mL, 2 mmol) in THF (2 mL) for 1 h. The product was isolated via the above procedure (0.283 g, 74%). ^{1}H NMR (500 MHz, Chloroform-*d*) δ 7.54 (d, *J* = 8.0 Hz, 2H), 7.30 (d, *J* = 7.9 Hz, 2H), 2.97 (t, *J* = 6.9 Hz, 2H), 2.79 (t, *J* = 6.9 Hz, 2H).

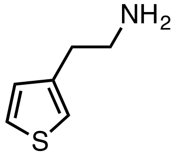

2-Thiophen-3-ylethanamine. 3-Thiopheneacetonitrile (0.570 mL, 5 mmol) was reacted with *i*(Bu)$_2$AlBH$_4$ (4.5 mL, 5 mmol) in THF (5 mL) for 1 h. The product was isolated via the above procedure (0.451 g, 71%). ^{1}H NMR (500 MHz, Chloroform-*d*) δ 7.19 – 7.16 (m, 1H), 6.91 (s, 1H), 6.86 (d, *J* = 5.1 Hz, 1H), 2.87 (t, *J* = 6.9 Hz, 2H), 2.71 (t, *J* = 6.9 Hz, 2H), 2.14 (s, 2H). ^{13}C NMR (126 MHz, Chloroform-*d*) δ 140.09, 128.16, 125.63, 121.07, 42.69, 34.36.

Representative Procedure for the Reduction of Epoxides Using *i*(Bu)$_2$AlBH$_4$. In an Ar-purged 100mL round bottom flask, the epoxide (1 equiv.) and anhydrous THF were combined. The flask was placed in an ice bath and cooled to 0 °C before *i*(Bu)$_2$AlBH$_4$ (0.5 equiv.) was added dropwise. Once all the *i*(Bu)$_2$AlBH$_4$] was added the reaction mixture was allowed to stir for 1 h under the ice bath. The reaction mixture was quenched with methanol (7mL) and deionized H_2O (5 mL) (*Caution! Hydrogen evolution*). A gel formed with the addition of methanol. The resulting reaction mixture was filtered, and the filtrate was acidified with concentrated HCl (12M, 1mL). The product was then extracted with diethyl ether (3x10mL). The product was extracted with diethyl ether (3x10mL) and the combined organic extracts were dried ($MgSO_4$) and concentrated to afford the alcohol.

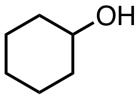

Cyclohexanol. Cyclohexene oxide (0.5 mL, 5 mmol) was reacted with *i*(Bu)$_2$AlBH$_4$ (3.13 mL, 2.5 mmol) in THF (5 mL) for 1 h. The product was isolated via the above procedure (0.42 g, 84%). ^{1}H NMR (500 MHz, Chloroform-*d*) δ 3.57 (dp, *J* = 8.6, 4.2 Hz, 1H), 1.89 (d, *J* = 23.7 Hz, 3H), 1.70 (s, 2H), 1.51 (d, *J* = 12.3 Hz, 1H), 1.24

(d, J = 8.1 Hz, 4H), 1.14 (d, J = 2.9 Hz, 1H). ^{13}C NMR (126 MHz, Chloroform-d) δ 70.32, 35.56, 25.54, 24.24.

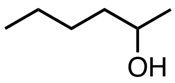
2-Hexanol. 1,2-Epoxy hexane (0.6 mL, 5 mmol) was reacted with i(Bu)$_2$AlBH$_4$ (2.5 mL, 2.5 mmol) in THF (5 mL) for 1 h. The product was isolated via the above procedure (0.356 g, 70%). ^{1}H NMR (500 MHz, Chloroform-d) δ 3.74 (dq, J = 11.8, 6.2 Hz, 1H), 2.23 (bs, 1H), 1.43 (m, 6H), 1.14 (d, J = 6.2 Hz, 3H), 0.86 (d, J = 7.2 Hz, 3H). ^{13}C NMR (126 MHz, Chloroform-d) δ 68.20, 39.07, 27.96, 23.49, 22.71, 14.06.

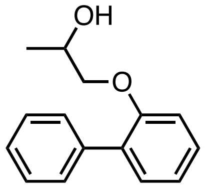
1-biphenyl2-yloxypropan-2-ol. 2-Biphenylyl glycidyl ether (0.452 g, 2 mmol) was reacted with i(Bu)$_2$AlBH$_4$ (1.36 mL, 1 mmol) in THF (2 mL) for 1 h. The product was isolated via the above procedure (0.41 g, 90%). ^{1}H NMR (500 MHz, Chloroform-d) δ 7.55 (d, J = 6.9 Hz, 2H), 7.44 (t, J = 7.6 Hz, 2H), 7.38 – 7.32 (m, 3H), 7.10 (t, J = 7.5 Hz, 1H), 7.01 (d, J = 8.2 Hz, 1H), 4.10 – 4.04 (m, 1H), 3.98 (d, J = 9.2 Hz, 1H), 3.78 (dd, J = 9.2, 7.6 Hz, 1H), 2.21 (d, J = 3.7 Hz, 1H), 1.21 (d, J = 6.4 Hz, 3H). ^{13}C NMR (126 MHz, Chloroform-d) δ 155.44, 138.45, 131.48, 130.92, 129.46, 128.74, 128.12, 127.09, 121.65, 113.38, 74.31, 66.20, 18.65.

Reduction of Styrene Oxide Using DIBAL. In an Ar-purged 100mL round bottom flask, styrene oxide (0.230 mL, 2 mmol, 1 equiv.) and anhydrous THF (2.43 mL) were combined. Diisobutylaluminum hydride (1M, 4 mL, 4 mmol, 2 equiv.) was added dropwise and once all the DIBAL was added the reaction mixture was allowed to stir for 1 h at room temperature. The reaction mixture was quenched with 3M HCl (2mL) (*Caution! Hydrogen evolution*). The product was extracted with diethyl ether (3x10mL) and the combined organic extracts were dried ($MgSO_4$) and concentrated to afford the alcohol (0.562g, >99%).

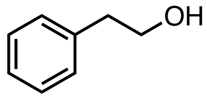

2-Phenylethanol. ^{1}H NMR (500 MHz, Chloroform-*d*) δ 7.24 – 7.20 (m, 2H), 7.13 (d, *J* = 7.5 Hz, 3H), 3.74 (t, *J* = 6.6 Hz, 2H), 2.76 (t, *J* = 6.6 Hz, 2H), 2.02 (s, 1H). ^{13}C NMR (126 MHz, Chloroform-*d*) δ 138.64, 129.08, 128.59, 126.46, 63.62, 39.22.

Representative Procedure for the Reduction of Carboxylic Acids Using *i*(Bu)$_2$AlBH$_4$. In an Ar-purged 100mL round bottom flask, the carboxylic acid (1 equiv.) and anhydrous THF were combined. The *i*(Bu)$_2$AlBH$_4$ (1.1 equiv.) was added dropwise and once all the *i*(Bu)$_2$AlBH$_4$ was added the reaction mixture was allowed to stir for 1 h at room temperature. The reaction mixture was quenched with methanol (7mL) and deionized H_2O (5 mL) (*Caution! Hydrogen evolution*). A gel formed with the addition of methanol. The resulting reaction mixture was filtered, and the filtrate was acidified with concentrated HCl (12M, 1mL). The product was extracted with diethyl ether (3x10mL) and the combined organic extracts were dried ($MgSO_4$) and concentrated to afford the alcohol.

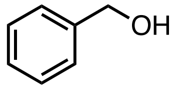

Benzyl alcohol. Benzoic acid (0.491 g, 4 mmol) was reacted with *i*$(Bu)_2AlBH_4$ (6 mL, 4 mmol) in THF (4 mL) for 1 h. The product was isolated via the above procedure (0.43 g, 99%). ^{1}H NMR (500 MHz, $CDCl_3$) δ 7.37-7.36 (m, 5H, *J* = 4.4 Hz), 4.68 (s, 2H), 1.85 (s, 1H). ^{13}C NMR (151 MHz, $CDCl_3$) δ 140.88, 128.47, 127.49, 127.01, 64.73.

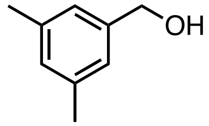

3,5-Dimethylbenzene methanol. 3,5-Dimethylbenzoic acid (0.303 g, 2 mmol) was reacted with *i*$(Bu)_2AlBH_4$ (2.82 mL, 2 mmol) in THF (2 mL) for 1 h. The product was isolated via the above procedure (0.122 g, 44%). ^{1}H NMR (500 MHz, Chloroform-*d*) δ 6.82 (s, 2H), 6.80 (s, 1H), 4.42 (s, 2H), 2.83 (s, 1H), 2.19 (s, 6H). ^{13}C NMR (126 MHz, Chloroform-*d*) δ 140.84, 138.17, 129.25, 124.86, 65.37, 21.26.

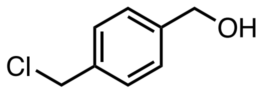

4-(Chloromethyl)-benzene methanol. 4-(Chloromethyl)benzoic acid (0.689 g, 4 mmol) was reacted with *i*$(Bu)_2AlBH_4$ (6.03 mL, 4.4 mmol) in THF (4 mL) for 1 h. The product was isolated via the above procedure (0.597 g, 95%). ^{1}H NMR

(500 MHz, Chloroform-*d*) δ 7.36 (d, *J* = 8.2 Hz, 2H), 7.31 (d, *J* = 8.0 Hz, 2H), 4.62 (s, 2H), 4.57 (s, 2H), 2.64 (s, 1H). ^{13}C NMR (126 MHz, Chloroform-*d*) δ 141.21, 136.81, 128.83, 127.29, 64.71, 46.08.

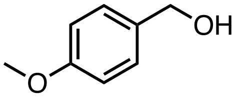

4-Methoxybeznene methanol. 4-Methoxybenzoic acid (0.610 g, 4 mmol) was reacted with *i*(Bu)$_2$AlBH$_4$ (4.84 mL, 4.4 mmol) in THF (4 mL) for 1 h. The product was isolated via the above procedure (0.657 g, 98%). ^{1}H NMR (500 MHz, Chloroform-*d*) δ 7.31 (d, *J* = 8.1 Hz, 2H), 6.92 (d, *J* = 8.5 Hz, 2H), 4.91 (s, 1H), 4.63 (s, 1H), 3.83 (d, *J* = 1.7 Hz, 3H). ^{13}C NMR (126 MHz, Chloroform-*d*) δ 159.21, 128.67, 113.96, 64.99, 55.30.

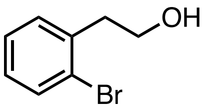

2-Bromobenzene ethanol. 2-Bromophenylacetic acid (0.862 g, 4 mmol) was reacted with *i*(Bu)$_2$AlBH$_4$ (6 mL, 4.4 mmol) in THF (4 mL) for 1 h. The product was isolated via the above procedure (0.639 g, 79%). ^{1}H NMR (500 MHz, Chloroform-*d*) δ 7.56 (d, *J* = 7.9 Hz, 1H), 7.28 – 7.25 (m, 2H), 7.12 – 7.08 (m, 1H), 3.89 (t, *J* = 6.7 Hz, 2H), 3.03 (t, *J* = 6.7 Hz, 2H), 1.62 (s, 1H). ^{13}C NMR (126 MHz, Chloroform-*d*) δ 137.81, 132.98, 131.27, 128.22, 127.47, 124.70, 62.09, 39.34.

Representative Procedure for the Reduction of Esters Using *i*(Bu)$_2$AlBH$_4$. In an Ar-purged 100mL round bottom flask, the ester (1 equiv.) and anhydrous THF were combined. The *i*(Bu)$_2$AlBH$_4$ (1 equiv.) was added dropwise and once all the *i*(Bu)$_2$AlBH$_4$ was added the reaction mixture was allowed to stir for 3 h at room temperature. The reaction mixture was quenched with methanol (7mL) and deionized H_2O (5 mL) (*Caution! Hydrogen evolution*). A gel formed with the addition of methanol. The resulting reaction mixture was filtered, and the filtrate was acidified with concentrated HCl (12M, 1mL). The product was extracted with diethyl ether (3x10mL) and the combined organic extracts were dried ($MgSO_4$) and concentrated to afford the alcohol.

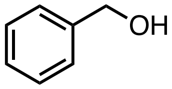

Benzyl alcohol. Methyl benzoate (0.328 mL, 3 mmol) was reacted with *i*(Bu)$_2$AlBH$_4$ (4.3 mL, 3 mmol) in THF (3 mL) for 1 h. The product was isolated via the above procedure (0.239 g, 74%). ^{1}H NMR (500 MHz, Chloroform-*d*) δ 7.40 – 7.29 (m, 5H), 4.60 (s, 2H), 3.17 (s, 1H). ^{13}C NMR (126 MHz, Chloroform-*d*) δ 140.98, 128.52, 127.55, 127.05, 64.97.

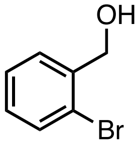

2-Bromobenzyl methanol. Methyl 2-bromobenzoate (0.42 mL, 3 mmol) was reacted with *i*(Bu)$_2$AlBH$_4$ (4.29 mL, 3 mmol) in THF (3 mL) for 1 h. The product was isolated via the above procedure (0.52 g, 93%). ^{1}H NMR (500 MHz, Chloroform-*d*) δ 7.55 (d, *J* = 7.9 Hz, 1H), 7.49 (d, *J* = 7.6 Hz, 1H), 7.34 (t, *J* = 7.5 Hz, 1H), 7.17 (t, *J* =

7.7 Hz, 1H), 4.76 (s, 2H), 1.69 (bs, 1H). ^{13}C NMR (126 MHz, Chloroform-*d*) δ 139.73, 132.61, 129.14, 128.94, 127.66, 122.60, 65.13.

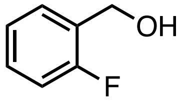

2-Fluorobenzyl alcohol. Methyl 2-fluorobenzoate (0.637 mL, 5 mmol) was reacted with *i*(Bu)$_2$AlBH$_4$ (6.94 mL, 5 mmol) in THF (5 mL) for 1 h. The product was isolated via the above procedure (0.563 g, 89%). ^{1}H NMR (500 MHz, Chloroform-*d*) δ 7.45 (s, 1H), 7.31 – 7.28 (m, 1H), 7.17 (t, *J* = 7.8 Hz, 1H), 7.07 (s, 1H), 5.08 (s, 1H), 4.78 (s, 2H). ^{13}C NMR (126 MHz, Chloroform-*d*) δ 161.63, 129.30 (d, *J* = 4.5 Hz), 127.78, 124.23, 115.36, 59.37.

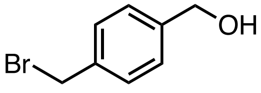

4-(Bromomethyl)benzene methanol. Methyl 4-(bromomethyl)benzoate (0.688 g, 3 mmol) was reacted with *i*(Bu)$_2$AlBH$_4$ (4.29 mL, 3 mmol) in THF (3 mL) for 1 h. The product was isolated via the above procedure (0.505 g, 84%). ^{1}H NMR (500 MHz, Chloroform-*d*) δ 7.39 (d, *J* = 8.0 Hz, 2H), 7.35 (d, *J* = 8.2 Hz, 2H), 4.70 (s, 2H), 4.50 (s, 2H), 1.67 (s, 1H). ^{13}C NMR (126 MHz, Chloroform-*d*) δ 141.18, 137.20, 129.27, 127.33, 64.93, 33.22.

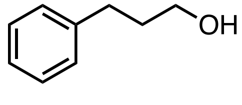

3-Phenyl-1-propanol. Ethyl 3-phenylpropionate (0.479 mL, 4.5 mmol) was reacted with *i*(Bu)$_2$AlBH$_4$ (6.78 mL, 4.95 mmol) in THF (4.5 mL) for 1 h.

The product was isolated via the above procedure (0.558 g, 91%). ^{1}H NMR (500 MHz, Chloroform-*d*) δ 7.25 (t, *J* = 7.6 Hz, 2H), 7.17 (d, *J* = 7.7 Hz, 3H), 3.60 (t, *J* = 6.5 Hz, 2H), 2.66 (t, *J* = 7.8 Hz, 2H), 2.41 (bs, 1H), 1.87 – 1.82 (m, 2H). ^{13}C NMR (126 MHz, Chloroform-*d*) δ 141.85, 128.43, 125.88, 62.26, 34.24, 32.11.

General Procedure for the Reduction of Amides Using *i*(Bu)$_2$AlBH$_4$. The following procedure for the reduction of *N,N*-diethylbenzamide by i(Bu)$_2$AlBH$_4$ is representative of the amide reductions. An oven-dried 50-mL round-bottom flask equipped with a magnetic stir bar and cooled under Argon atmosphere. *N*,*N*-diethylbenzamide (0.886 g, 5 mmol, 1 equiv) was added to the flask. The flask was fitted with a rubber septum and cooled to 0 °C. Anhydrous THF (5 mL) was added to the flask via a syringe. Diisobutylaluminum borohydride (6.0 mL, 5.5 mmol, 1.1 equiv) was added dropwise over 15 minutes with stirring. Upon the completion of the addition of i(Bu)$_2$AlBH$_4$, the ice-bath was removed, and the reaction mixture was allowed to stir at 25 °C for 1 h. The reaction mixture was then concentrated under reduced pressure and the reaction flask was recapped with a septum. Methanol (15 mL) was added slowly to the residue (*Caution! Hydrogen evolution*) and was and stirred for 1 h at 25 °C. The reaction mixture was concentrated under reduced pressure to give a white solid. Methanol (15 mL) followed by conc. HCl (12M, 1 mL) was added and the reaction refluxed for 1 h. The reaction was filtered and concentrated. Pentane (10 mL) and deionized water (5 mL) were added to the filtrate. The layers were separated, and the aqueous layer was neutralized using NaOH$_{(s)}$ until the pH of the aqueous layer becomes 10. The aqueous layer was then extracted with diethyl ether (3 x 10 mL). The combined organic layers were dried with anhydrous $MgSO_4$, filtered, and concentrated to afford the amine (0.653g, 80%).

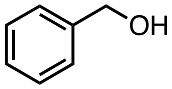

Benzyl alcohol. Colorless oil. ^{1}H NMR (500 MHz, $CDCl_3$): δ 7.37-7.36 (m, 5H, *J* = 4.4 Hz), 4.68 (s, 2H), 1.85 (s, 1H); ^{13}C NMR (151 MHz, $CDCl_3$): δ 140.88, 128.47, 127.49, 127.01, 64.73.

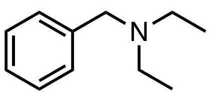

N,N-Diethylbenzylamine. Colorless oil. ^{1}H NMR (500 MHz, $CDCl_3$): δ 7.35-7.31 (m, 5H), 3.58 (s, 2H), 2.53 (q, 4H, *J* = 5 Hz), 1.05 (t, 6H, *J* = 5 Hz); ^{13}C NMR (126 MHz, $CDCl_3$): δ 139.80, 129.01, 128.15, 126.73, 57.55, 46.70, 11.70.

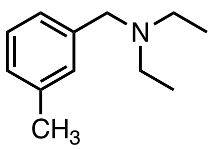

N,N-Diethyl-(3-methylbenzyl)amine. Colorless oil. ^{1}H NMR (500 MHz, $CDCl_3$): δ 7.21 (s, 1H), 7.17 (d, 1H, *J* = 7.4 Hz), 7.09 (d, 2H, *J* = 7.4 Hz), 3.58 (s, 2H), 2.57 (q, 4H, *J* = 7.1 Hz), 2.38 (s, 3H), 1.09 (q, 6H, *J* = 7.1 Hz); ^{13}C NMR (151 MHz, $CDCl_3$): δ 139.58, 137.92, 130.01, 128.27, 127.80, 126.40, 57.67, 46.87, 21.64, 11.76.

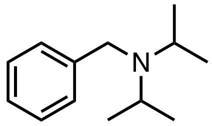

N,N-Diisopropylbenzylamine. Colorless oil. ^{1}H NMR (500 MHz, CDCl$_3$): δ 7.44 (d, 2H, *J* = 7.4 Hz), 7.34 (d, 2H, *J* = 7.4 Hz), 7.24 (t, 1H, *J* = 7.4 Hz), 3.70 (s, 2H), 3.08 (dt, 2H, *J* = 12.9, 6.5 Hz), 1.09 (d, 12H, *J* = 6.5 Hz); ^{13}C NMR (151 MHz, CDCl$_3$): δ 143.25, 128.00, 127.92, 126.18, 48.97, 47.81.

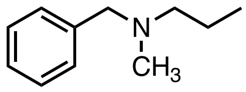

N-Benzyl-N-methylpropan-1-amine. Colorless oil. ^{1}H NMR (600 MHz, CDCl$_3$): δ 7.32-7.30 (m, 4H), 7.25-7.21 (m, 1H) 3.47 (s, 2H), 2.32 (d, 2H, *J* = 7.6 Hz), 2.18 (s, 3H), 1.53 (h, 2H, *J* = 7.4 Hz), 0.90 (t, 3H, *J* = 7.4 Hz); ^{13}C NMR (151 MHz, CDCl$_3$): δ 139.47, 129.27, 128.38, 127.06, 62.53, 59.75, 42.45, 20.76, 12.10.

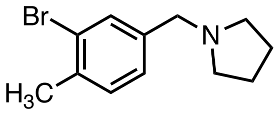

1-(3-bromo-4-methylbenzyl)pyrrolidine. Colorless oil. ^{1}H NMR (500 MHz, CDCl$_3$): δ 7.49 (s, 1H), 7.14 (app. s, 2H), 3.52 (s, 2H), 2.47 (app. s, 4H), 2.35 (s, 3H), 1.76-1.74 (m, 4H); ^{13}C NMR (151 MHz, CDCl$_3$): δ 139.06, 136.45, 132.76, 130.74, 127.98, 124.92, 59.92, 54.30, 23.66, 22.74.

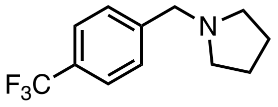

1-(4-(trifluoromethyl)benzyl)pyrrolidine. Colorless oil. ^{1}H NMR (500 MHz, CDCl$_3$): δ 7.49 (d, 2H, *J* = 8 Hz), 7.39 (d, 2H, *J* = 8 Hz), 3.61 (s, 2H), 2.47-2.44 (app. T, 4H, *J* = 6.6 Hz), 1.75-1.72 (m, 4H); ^{13}C NMR (126 MHz, CDCl$_3$): δ

143.43, 129.01, 127.47, 125.17, 123.22, 60.15, 54.20, 23.50; ^{19}F NMR (470 MHz, $CDCl_3$): δ -64.45.

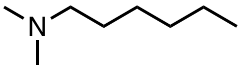

N,N-Dimethylhexan-1-amine. Colorless oil. ^{1}H NMR (500 MHz, $CDCl_3$): δ 2.21-2.17 (m, 2H), 2.15 (s, 6H), 1.42-1.36 (m, 2H), 1.26-1.21 (m, 6H), 0.82 (t, 3H, *J* = 6.8 Hz); ^{13}C NMR (126 MHz, $CDCl_3$): δ 59.73, 45.13, 31.70, 27.37, 27.07, 22.49, 13.89.

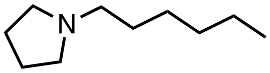

1-Hexylpyrrolidine. Colorless oil. ^{1}H NMR (500 MHz, $CDCl_3$): δ 2.42 (app. t, 4H, *J* = 5.6 Hz), 2.35 -2.32 (m, 2H), 1.70 (q, 4H, *J* = 3.1 Hz), 1.47-1.40 (m, 2H), 1.22 (s, 6H), 0.85-0.79 (m, 3H); ^{13}C NMR (126 MHz, $CDCl_3$): δ 68.27, 62.24, 56.68, 54.11, 31.77, 28.94, 27.39, 23.29, 22.55, 13.97.

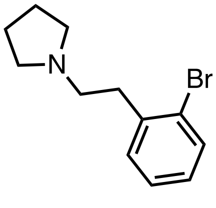

1-(2-bromophenethyl)pyrrolidine. Colorless oil. ^{1}H NMR (500 MHz, $CDCl_3$): δ 7.47 (d, 1H, *J* = 8 Hz), 7.22-7.16 (m, 2H, *J* = 7.4 Hz), 7.00 (app. t, 1H, J = 8.4 Hz), 2.93 (dd, 2H, J = 9.8, 6.8 Hz), 2.66-2.62 (m, 2H), 2.57 (app. s, 4H), 1.77 (app. s, 4H); ^{13}C NMR (151 MHz, $CDCl_3$): δ 139.94, 132.95, 130.86, 127.97, 127.66, 124.68, 56.54, 54.27, 36.03, 23.70.

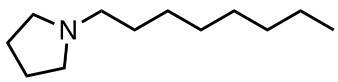

1-Octylpyrrolidine. Colorless oil. ^{1}H NMR (500 MHz, CDCl$_3$): δ 2.40 (app. t, 4H, *J* = 5.2 Hz), 2.34-2.31 (m, 2H), 1.68 (app. s, 4H), 1.20-1.19 (m, 12H), 0.79 (t, 3H, *J* = 7.0 Hz); ^{13}C NMR (126 MHz, CDCl$_3$): δ 56.70, 54.17, 31.81, 29.54, 29.22, 29.06, 27.73, 23.33, 22.61, 14.02.

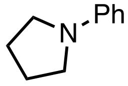

1-Phenylpyrrolidine. Colorless oil. ^{1}H NMR (500 MHz, CDCl$_3$): δ 7.15-7.11 (m, 2H), 6.58-6.55 (m, 1H), 6.48 (d, 2H, *J* = 8.6 Hz), 3.18 (app. t, 4H, 6.2 Hz), 1.91-1.88 (m, 4H); ^{13}C NMR (126 MHz, CDCl$_3$): δ 148.06, 129.20, 115.45, 111.73, 47.66, 25.56.

Reduction of 4-formyl-benzonitrile with *i*(Bu)$_2$AlBH$_4$. In an Ar-purged 100mL round bottom flask, 4-formyl-benzonitrile (0.1g, 0.76 mmol, 1 equiv.) and anhydrous THF (1mL) were combined. The *i*(Bu)$_2$AlBH$_4$ (0.8M, 0.95 mL, 0.76 mmol, 1 equiv.) was added dropwise and once all the *i*(Bu)$_2$AlBH$_4$ was added the reaction mixture was allowed to stir for 4 h at 0 °C. The reaction mixture was quenched with methanol (5mL) (*Caution! Hydrogen evolution*). A gel formed with the addition of methanol, which was filtered off and rinsed with DI H$_2$O (5mL). The filtrate was acidified with HCl (1M) to achieve pH ~2. The product was extracted with diethyl ether (3x10mL) and the combined organic extracts were dried (MgSO$_4$) and concentrated to afford the alcohol (0.082g, 81%).

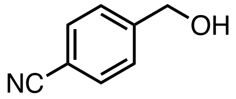

4-(Hydroxymethyl)-benzonitrile. ^{1}H NMR (500 MHz, Chloroform-*d*) δ 7.64 (d, *J* = 7.9 Hz, 2H), 7.47 (d, *J* = 7.9 Hz, 2H), 4.77 (s, 2H), 2.09 (s, 1H); ^{13}C NMR (126 MHz, Chloroform-*d*) δ 146.22, 132.32, 127.02, 118.83, 111.17, 64.21.

Reduction of 4-acetyl-benzonitrile with *i*(Bu)$_2$AlBH$_4$. In an Ar-purged 100mL round bottom flask, 4-acetyl-benzonitrile (0.729g, 5 mmol, 1 equiv.) and anhydrous THF (5mL) were combined. The *i*(Bu)$_2$AlBH$_4$ (0.8M, 6.25 mL, 5 mmol, 1 equiv.) was added dropwise and once all the *i*(Bu)$_2$AlBH$_4$ was added the reaction mixture was allowed to stir for 4 h at 0 °C. The reaction mixture was quenched with methanol (5mL). A gel formed with the addition of methanol, which was filtered off and rinsed with DI H_2O (5mL) (*Caution! Hydrogen evolution*). The filtrate was acidified with HCl (1M) to achieve pH ~2. The product was extracted with diethyl ether (3x10mL) and the combined organic extracts were dried ($MgSO_4$) and concentrated to afford the alcohol (0.726g, 97%).

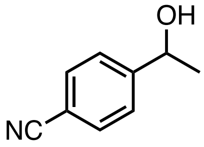

4-(1-Hydroxyethyl)-benzonitrile. ^{1}H NMR (500 MHz, Chloroform-*d*) δ 7.59-7.54 (d, 2H), 7.44 (d, *J* = 7.9 Hz, 2H), 4.89 (q, *J* = 6.5 Hz, 1H) 2.98 (bs, 1H), 1.44 (dd, *J* = 6.6, 1.4 Hz, 3H); ^{13}C NMR (126 MHz, Chloroform-*d*) δ 151.35, 132.28, 126.10, 118.89, 110.81, 69.50, 25.35.

Reduction of 4-benzoyl-benzonitrile with *i*(Bu)$_2$AlBH$_4$. In an Ar-purged 100mL round bottom flask, 4-benzoyl-benzonitrile (0.623g, 3 mmol, 1 equiv.) and anhydrous THF (3mL) were combined. The *i*(Bu)$_2$AlBH$_4$ (0.7M, 4.29 mL, 5 mmol, 1 equiv.) was added dropwise and once all the *i*(Bu)$_2$AlBH$_4$ was added the reaction mixture was allowed to stir for 4 h at 0 °C. The reaction mixture was quenched with methanol (5mL). A gel formed with the addition of methanol, which was filtered off and rinsed with DI H$_2$O (5mL) (*Caution! Hydrogen evolution*). The filtrate was acidified with HCl (1M) to achieve pH ~2. The product was extracted with diethyl ether (3x10mL) and the combined organic extracts were dried (MgSO$_4$) and concentrated to afford the alcohol (0.468g, 75%).

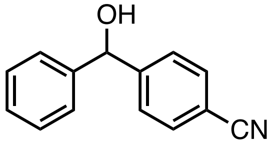

4-(Hydroxyphenylmethyl)-benzonitrile. ^{1}H NMR (500 MHz, Chloroform-*d*) δ 7.51 (d, *J* = 8.3 Hz, 2H), 7.44 (d, *J* = 8.2 Hz, 2H), 7.31 (m, 5H), 5.75 (s, 1H), 3.48 (bs, 1H); ^{13}C NMR (126 MHz, Chloroform-*d*) δ 149.33, 142.95, 132.24, 128.81, 128.14, 127.11, 126.75, 118.97, 110.72, 75.39.

Reduction of methyl-4-formylbenzoate with *i*(Bu)$_2$AlBH$_4$. In an Ar-purged 100mL round bottom flask, methyl-4-formylbenzoate (0.492g, 3 mmol, 1 equiv.) and anhydrous THF (3mL) were combined. The *i*(Bu)$_2$AlBH$_4$ (0.7M, 4.23 mL, 3 mmol, 1 equiv.) was added dropwise and once all the *i*(Bu)$_2$AlBH$_4$ was added, the reaction mixture was allowed to stir for 5 h at -78 °C. The reaction mixture was quenched with methanol (5mL) (*Caution! Hydrogen evolution*). The reaction mixture was evaporated followed by the addition of pentanes (5 mL) and DI H_2O (5mL). The reaction mixture was filtered, and the filtrate was acidified with HCl (1M) to achieve pH ~2. The product was extracted with diethyl ether (3x10mL). The combined organic extracts were dried ($MgSO_4$) and concentrated to afford the alcohol (0.272g, 55%).

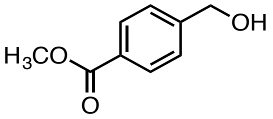

Methyl 4-(hydroxymethyl)benzoate. ^{1}H NMR (500 MHz, Chloroform-*d*) δ 8.02 (d, *J* = 8.4 Hz, 2H), 7.43 (d, *J* = 8.0 Hz, 2H), 4.76 (s, 2H), 3.91 (s, 3H), 1.79 (s, 1H). ^{13}C NMR (126 MHz, Chloroform-*d*) δ 166.97, 145.97, 129.85, 129.33, 126.46, 64.69, 52.11.

Reduction of methyl-4-acetylbenzoate with *i*(Bu)$_2$AlBH$_4$. In an Ar-purged 100mL round bottom flask, methyl-4-acetylbenzoate (0.530g, 3 mmol, 1 equiv.) and anhydrous THF (3mL) were combined. The *i*(Bu)$_2$AlBH$_4$ (0.7M, 4.23 mL, 3 mmol, 1 equiv.) was added dropwise and once all the *i*(Bu)$_2$AlBH$_4$ was added, the reaction mixture was allowed to stir for 5 h at -78 °C. The reaction mixture was quenched with methanol (5mL) (*Caution! Hydrogen evolution*). The reaction mixture was evaporated followed by the addition of pentanes (5 mL) and DI H_2O (5mL). The reaction mixture was filtered, and the filtrate was acidified with HCl (1M) to achieve pH ~2. The product was extracted with diethyl ether (3x10mL). The combined organic extracts were dried ($MgSO_4$) and concentrated to afford the alcohol (0.417g, 77%).

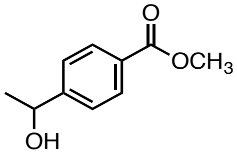

Methyl-4-(1-hydroxyethyl)benzoate. ^{1}H NMR (500 MHz, Chloroform-*d*) δ 7.91 (d, *J* = 8.3 Hz, 2H), 7.36 (d, *J* = 8.4 Hz, 2H), 4.86 (q, *J* = 6.5 Hz, 1H), 3.84 (s, 3H), 2.96 (s, 1H), 1.43 (d, *J* = 6.6 Hz, 3H). ^{13}C NMR (126 MHz, Chloroform-*d*) δ 167.08, 151.26, 129.70, 128.85, 125.28, 69.68, 52.04, 25.19.

Competitive reduction between 4-cyanotoluene and *N,N*-diethyl-3-methylbenzamide with *i*(Bu)$_2$AlBH$_4$. In an Ar-purged 100mL round bottom flask, 4-cyanotoluene (0.175g, 1.5 mmol, 1 equiv.), *N,N*-diethyl-3-methylbenzamide (0.290 mL, 1.5 mmol, 1 equiv.), and anhydrous THF (1.5 mL) were combined. The *i*(Bu)$_2$AlBH$_4$ (0.7M, 2.1 mL, 1.5 mmol, 1 equiv.) was added dropwise and once all the *i*(Bu)$_2$AlBH$_4$ was added, the reaction mixture was allowed to stir for 24 h at -78 °C. The reaction mixture was then concentrated under reduced pressure and the reaction flask was recapped with a septum. Methanol (5 mL) was added slowly to the residue (*Caution! Hydrogen evolution*) followed by conc. HCl (12M, 1 mL) and the reaction refluxed for 1 h. The reaction was filtered and concentrated. Pentane (5 mL) and deionized water (5 mL) were added to the filtrate. The layers were separated, and the aqueous layer was neutralized using NaOH$_{(s)}$ until the pH~10. The aqueous layer was then extracted with diethyl ether (3 x 10 mL). The combined organic layers were dried with anhydrous MgSO$_4$, filtered, and concentrated to afford 4-methylbenzyl amine (0.500g, >99%).

6.1.2. Chapter 3

Synthesis of MASN. Mesoporous aluminosilicate nanoparticles (MASN) were synthesized by adding a mixture of TEOS (4.58 g, 21.98 mmol) and $Al(O\text{-}i\text{-}Pr)_3$ (0.244 g, 1.19 mmol) (briefly sonicated) to a previously prepared solution consisting of water (485 g), CTAB (1.0 g, 2.74 mmol) and solid NaOH (2.80 g, 70.01 mmol). The CTAB and NaOH solution was first stirred for 15 minutes at 80 °C to homogenize, before adding the alkoxide mixture drop wise over 5 minutes. The combined solution was stirred at 80 °C for 2 h, then allowed to cool to room temperature while stirring for an additional hour. The cooled precipitate was filtered and washed with 1.0 L of Milli-Q water and then dried in vacuo overnight at 100 °C. The dried material was then ground to a fine powder and calcined in air at 550 °C for 5 h (at a heating rate of 1 °C per minute) to remove the organic template.

Synthesis of NBC-MASN Catalyst. In a typical synthesis of NBC-MASN catalyst, MASN support (0.65 g) was dried in a vacuum oven overnight at 100 °C, cooled to room temperature, and then soaked in a solution of $NiCl_2{\bullet}6H_2O$ (0.26 g, 1.09 mmol) dissolved in 50/50 v/v EtOH and water. A minimal amount (~3 mL) of solvent was used to create a thick slurry with the MASN. This slurry was sonicated in a tightly sealed 20 mL scintillation vial for 90 minutes and then allowed to soak for 5 d before drying overnight in a thoroughly $Ar_{(g)}$ purged vacuum oven at 100°C. Dried $NiCl_2$-MASN was mechanically ground with $NaBH_4$ (0.084 g, 2.20 mmol) until thoroughly mixed together as a fine powder. The powder mixture was then gently purged with

$Ar_{(g)}$ while cooling in a 0 °C water bath for 20 min, before rapidly introducing 19 mL of 0 °C absolute EtOH (200 proof) with vigorous magnetic stirring. The synthesis was carried out in a semi-sealed scintillation vial with two small ports in the cap, one to allow for the introduction of a glass cannula into the reaction solution to deliver $Ar_{(g)}$, and the other for gas ventilation. The synthesis proceeded with continuous argon purging of the solution and rapid stirring for approximately 2 h, or until no more effervescent bubbling from $H_{2(g)}$ production could be observed. The solution was then diluted with 30 mL of room temperature water to help remove excess salts, centrifuged to isolate the solid, and the solid was dried overnight in a $Ar_{(g)}$ purged vacuum oven at 100 °C. The dry NBC-MASN catalyst was then stored under $Ar_{(g)}$ until use in catalysis or characterization.

Synthesis of NBC Catalyst. Unsupported, bulk NBC catalyst powder was synthesized by adding a solution of $NiCl_2 \cdot 6H_2O$ (0.26 g, 1.09 mmol) dissolved in 8.5 mL of absolute EtOH to a solution of $NaBH_4$ (0.084 g, 2.20 mmol) suspended in 8.5 mL of absolute EtOH, with rapid stirring at 0 °C under continuous $Ar_{(g)}$ purging as described above. Synthesis proceeded for approximately 20 min or until no more $H_{2(g)}$ production could be observed, at which point the material was rinsed, retrieved and dried as described above.

Calcination of as-synthesized catalysts. A custom-made calcination furnace with a quartz tube was used to heat the catalyst materials in either flowing nitrogen or air at 550 °C for 2 h, at a heating rate of 10 °C·min^{-1}.

General Procedure for the Reduction of Nitroarenes. To an argon-purged 50-mL round bottom flask the NBC-MASN catalyst (0.235 g, 0.4 mmol of Ni), nitroarene (4 mmol), MeOH (8 mL), and either $N_2H_4 \cdot H_2O$ (20 mmol) or a combination of $N_2H_4 \cdot H_2O$ (20 mmol) and $NaBH_4$ (20 mmol) were added and allowed to stir at room temperature for 24 h. The reaction mixture was then centrifuged, and the supernatant decanted into a pre-weighed 100 mL round bottom flask. The solid catalyst was rinsed with 15 mL of MeOH under brief sonication, followed by centrifugation and the supernatant was decanted into the same 100 mL flask. This rinse step was repeated, and the combined supernatants were then concentrated by rotary evaporation and analyzed via ^{1}H and ^{13}C NMR.

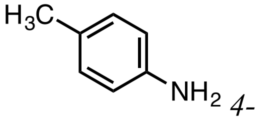

4-Toluidine. ^{1}H NMR (500 MHz, Chloroform-*d*): δ 7.00 (d, *J* = 7.5 Hz, 2H), 6.63 (d, *J* = 8.2 Hz, 2H), 3.46 (s, 2H), 2.27 (s, 3H). ^{13}C NMR ($CDCl_3$, 500 MHz): δ 143.8, 129.8, 127.8, 115.3, 20.5

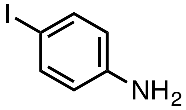

4-Iodo-aniline.^{1}H NMR (500 MHz, Chloroform-*d*): δ 7.41 (d, *J* = 8.6 Hz, 2H), 6.47 (d, *J* = 8.7 Hz, 2H), 3.49 (s, 2H). ^{13}C NMR (CDCl$_3$, 500 MHz): δ 137.9, 117.3.

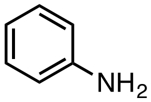

Aniline.^{1}H NMR (500 MHz, Chloroform-*d*): δ 7.19 (t, 2H), 6.77 (t, *J* = 7.4 Hz, 1H), 6.69 (d, *J* = 7.5 Hz, 2H), 3.66 (s, 2H). ^{13}C NMR (CDCl$_3$, 500 MHz): δ 143.4, 129.3, 118.6, 115.2.

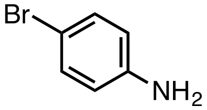

4-Bromo-aniline.^{1}H NMR (500 MHz, Chloroform-*d*): δ 7.24 (d, *J* = 8.5 Hz, 2H), 6.57 (d, *J* = 8.6 Hz, 2H), 3.65 (s, 2H). ^{13}C NMR (CDCl$_3$, 500 MHz): δ 145.4, 132.0, 116.7, 110.2.

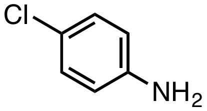

4-Chloro-aniline. ^{1}H NMR (500 MHz, Chloroform-*d*): δ 7.10 (d, *J* = 8.7Hz, 2H), 6.60 (d, *J* = 8.7 Hz, 2H), 3.60 (s, 2H). ^{13}C NMR (CDCl$_3$, 500 MHz): δ 144.9, 129.1, 123.1, 116.3.

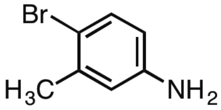

4-Bromo-3-methylaniline. ^{1}H NMR (500 MHz, Chloroform-*d*): δ 7.25 (d, *J* = 8.0 Hz, 1H), 6.57 (s, 1H), 6.39 (d, *J* = 8.1 Hz, 1H), 3.59 (bs, 2H), 2.30 (s, 3H). ^{13}C NMR ($CDCl_3$, 500 MHz): δ 145.7, 138.4, 132.7, 117.5, 114.3, 112.9, 22.9.

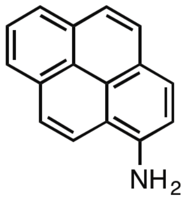

1-Aminopyrene. ^{1}H NMR (500 MHz, Chloroform-*d*): δ 8.05 (d, *J* = 6.2 Hz, 2H), 7.98 (s, 3H), 7.91 (d, *J* = 8.5 Hz, 2H), 7.82 (s, 1H), 7.39 (s, 1H), 4.52 (bs, 2H). ^{13}C NMR ($CDCl_3$, 500 MHz): δ 140.9, 132.2, 131.6, 127.6, 126.1, 125.5, 124.3, 124.1, 123.8, 123.6, 120.2, 116.9, 113.9.

General Procedure for Cleaning NBC-MASN. The used NBC-MASN catalyst and methanol (2 × 15 mL) were combined in an argon-purged Falcon tube, the mixture was sonicated for 10 min, then centrifuged and the supernatant decanted. Ethanol (2 × 15 mL) was added to the catalyst and sonicated for 10 min, centrifuged, and the supernatant decanted. Methanol (10 mL) was added to the catalyst before sonication for 10 min, centrifuged, and the supernatant decanted. The catalyst was then immediately reused.

General Procedure for the Regeneration of NBC-MASN. Cleaned (as above) and dried NBC-MASN and $NaBH_4$ (2 mol equivalent to Ni, assuming Ni was 10_w% of NBC-MASN) were added to an argon-purged Falcon tube capped with a rubber septum. The tube was cooled to 0 °C before adding 5 mL of 0 °C ethanol. The cold mixture was rapidly stirred for approximately 1 h or until no more $H_{2(g)}$ production was observed. The mixture was then centrifuged, the supernatant decanted, and the recovered solid was rinsed as described above and dried in an argon-purged vacuum oven until further use.

Characterization. Powder X-ray diffraction (PXRD) was performed on a Rigaku SmartLab X-ray diffractometer with Cu-Kα (1.54 Å) radiation (40 kV, 44 mA). All samples were prepared fresh and handled with minimal exposure to atmosphere prior to scanning. All samples were ground under $Ar_{(g)}$ and evenly dispersed on an amorphous SiO_2 sample holder and scanned with a step size of 0.01° and scan rate of $1°\cdot min^{-1}$. High angle annular dark field scanning transmission electron microscopy (HAADF-STEM) imaging was performed on an FEI Titan TEM operated at 300 kV. The STEM probe had a convergence semiangle, α, of 10 mrad and a beam current of 25 pA (300 kV). HAADF-STEM images were acquired using a Fischione annular dark-field (ADF) detector with an inner semiangle, β, of 45 mrad. EDS data was simultaneously collected along with HAADF-STEM data on four silicon drift detectors with a solid angle of 0.7 steradians (SuperX) and analyzed using Bruker's Espirit software. HRTEM images were acquired using an FEI ThemIS microscope operated at 300kV with a FEI Ceta Camera. All electron microscopy and EDS data collection were carried out on fresh samples suspended by brief sonication in absolute ethanol and deposited on 400 mesh copper TEM grids with lacey carbon support. Inductively coupled plasma optical emission spectroscopy (ICP-OES) data were collected on a PerkinElmer Optima 7000 DV. Samples for ICP-OES were prepared by digestion in an aqueous solution comprised of $50_v\%$ concentrated HNO_3 and $5_v\%$ H_2O_2 (30% stock solution) at 85 °C, rapidly stirring in a sealed polypropylene container for 2 h prior to dilution with Milli-Q water. Thermogravimetric analysis (TGA) was performed on a TA Q500 Thermoanalyzer, using a platinum weighing boat and flowing air during heating fresh samples at a rate of 10 $°C \cdot min^{-1}$. X-ray photoelectron spectroscopy was performed on a Kratos Axis Ultra spectrometer using an Al-K_α source ($h\nu = 1486.69$ eV) operated at 150 W and a hemispherical electron energy analyzer. Spectral positions were calibrated using adventitious alkyl carbon signals by shifting the C 1*s* peak to 284.8 eV. For samples which exhibited charging, a flood gun was used to neutralize the sample.

General Procedure for Hydrogen Evolution by Gas Burette. To the gas burette reservoir, outfitted with a rubber septum, 1 M HCl (15mL), methanol (15mL), and tetrahydrofuran (15mL) were added and allowed to stir. A few trials of sacrificial hydride sources were used for the purpose of equilibrating the system. In a separate Ar-purged round bottom flask, anhydrous $NiCl_2$ (0.065 g, 0.5 mmol) and solid $NaBH_4$ (0.038 g, 1 mmol) were added and the flask cooled to 0 °C. A cannula connected the round bottom flask to the gas burette reservoir. The system was allowed to equilibrate before the addition of 4 mL of 0 °C ethanol via syringe. By the controlled relief of pressure in the closed system into a graduated cylinder, the volume of gas generated, plus total volume injected, was measured by water displacement. The temperature of the displaced water and barometric pressure was also measured, and the temperature dependent vapor pressure of water.

Synthesis of Nickel Catalyst with Diisobutylaluminum Borohydride [(*i*Bu)$_2$AlBH$_4$]. Unsupported, bulk catalyst powder was synthesized by adding $NiCl_2$ (0.066 g, 0.5 mmol), anhydrous THF (5 mL), and (*i*Bu)$_2$AlBH$_4$ (0.549 mL, 0.5 mmol) together at 25 °C for 1 h. The THF was decanted off and the catalyst was immediately used.

Reduction of 4-Nitrotoluene by (*i*Bu)$_2$AlBH$_4$ Synthesized Catalyst. 4-Nitrotoluene (0.689 g, 5 mmol), methanol (11 mL), and hydrazine hydrate (1.22 mL, 25 mmol) were added to the catalyst. The reaction mixture was allowed to stir at room temperature for 24 h. Additional methanol (2 × 15 mL) was added followed by sonication (10 min). The reaction mixture was centrifuged (6 min, 4200 RPM) and the supernatant decanted. The process was repeated once more. The combined supernatant layers were dried with $MgSO_4$, filtered, and concentrated under vacuum to afford a mixture of products (0.523 g).

Synthesis of Nickel Catalyst with Diisobutylaluminum Hydride (DIBAL). Unsupported, bulk catalyst powder was synthesized by adding $NiCl_2$ (0.074 g, 0.5 mmol), anhydrous THF (5 mL), and DIBAL (2 mL, 2 mmol, 0.4 equiv) together at 25 °C for 1 h. The catalyst was used as is.

Reduction of 4-Nitrotoluene by DIBAL Synthesized Catalyst. 4-Nitrotoluene (0.694 g, 5 mmol), methanol (8 mL), and hydrazine hydrate (1.22 mL, 25 mmol) were added to the catalyst. The reaction mixture was allowed to stir at room temperature for 24 h. Additional methanol (2 × 15 mL) was added followed by sonication (10 min). The reaction mixture was centrifuged (6 min, 4200 RPM) and the supernatant decanted. The process was repeated once more. The combined supernatant layers were concentrated under vacuum to afford 4-toluidine (0.424 g, 78%). ^{1}H NMR (500 MHz, Chloroform-*d*): δ 6.98 (d, *J* = 7.5 Hz, 2H), 6.63 (d, *J* = 8.2 Hz, 2H), 3.56 (bs, 2H), 2.24 (s, 3H). ^{13}C NMR ($CDCl_3$, 500 MHz): δ 143.7, 129.8, 127.9, 115.3, 20.4.

Procedure for Cleaning DIBAL synthesized Nickel Catalyst. The used catalyst and methanol (2 × 15 mL) were combined in an argon-purged Falcon tube, the mixture was sonicated for 10 min, then centrifuged and the supernatant decanted. Ethanol (2 × 15 mL) was added to the catalyst and sonicated for 10 min, centrifuged, and the supernatant decanted. Methanol (10 mL) was added to the catalyst before sonication for 10 min, centrifuged, and the supernatant decanted. The catalyst was then immediately reused.

6.1.3. Chapter 4

Measurements. All reactions were monitored using a 1064 nm BaySpec BRAM Raman System (BaySpec Inc., San Jose, CA). The system features a fiber optic probe with a working distance of 4.5 mm. The 80 mW diode laser system was adjusted so that the incident beam focal point was located just within the wall of the reaction vessels as to maximize the signal intensity.

Synthesis of Nickel Boron Composite (NBC) Catalyst. Bulk NBC catalyst powder was synthesized by adding a solution of $NiCl_2$•$6H_2O$ (0.26 g, 2 mmol) dissolved in ethanol (10 mL) to a solution of $NaBH_4$ (0.076 g, 2 mmol) suspended in ethanol (8.5 mL), with rapid stirring at 0 °C under a moisture-free Ar environment. After the initial H_2 bubbling subsided, the solution was diluted with water (30 mL) and centrifuged to isolate the solid. The solid catalyst was then dried in an Ar-purged vacuum oven at 100 °C.

Procedure for the Reduction of 4-Nitrotoluene. NBC catalyst (0.0117 g, 0.2 mmol of Ni), 4-nitrotoluene (0.274 g, 2 mmol), toluene (0.5 mL), and water (0.5 mL) were combined. The Raman fiber optic probe was positioned outside of the reaction vial so that laser beam spot was focused so as to impinge upon the liquid just inside the vial. The probe was then secured and fixed in place when the signal was maximized. Prior to initiating the reaction or reagent addition, the intensity of the nitro stretch at 10 concentrations between 1.0 M and 0.01 M were measured and normalized using a toluene co-solvent peak at 1379 cm^{-1}. The reaction progress was determined by correlating the normalized intensity of the symmetric nitro stretch (1350 cm^{-1}) of the sample to a calibration curve. For each measurement, a single 5000 millisecond accumulation at 350 mW laser power was collected. The reaction was considered complete as determined by monitoring the loss or complete disappearance of the nitro stretch. Once deemed complete, the reaction mixture was centrifuged, and the supernatant was decanted and concentrated to isolate 4-toluidine (0.192 g, 90% yield).

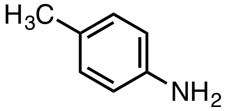

4-Toluidine. ^{1}H NMR (500 MHz, Chloroform-*d*) δ 7.02 (d, J = 7.9 Hz, 2H), 6.65 (d, J = 8.1 Hz, 2H), 3.56 (s, 2H), 2.30 (s, 3H). ^{13}C NMR (126 MHz, Chloroform-*d*) δ 143.95, 129.82, 127.76, 115.32, 20.52.

Procedure for the Reduction of 2,4-dinitrotoluene. NBC catalyst (0.0117 g, 0.2 mmol of Ni) was added to an Ar-purged test tube, followed by 2,4-dinitrotoluene (0.366 g, 2 mmol), toluene (2 mL), and water (2 mL). The substrate was allowed to dissolve before adding $N_2H_4 \cdot H_2O$ (0.94 mL, 10 mmol). The reaction vial was then placed in a water bath at 80 °C for 20 min and then the hot water bath was removed, and the reaction continued at 25 °C until the reaction was deemed complete by Raman spectroscopy. The reaction mixture was monitored, and the product was isolated, using the same procedure as described above. (0.132 g, 55% yield).

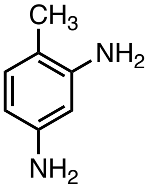

2,4-Diaminotoluene. ^{1}H NMR (500 MHz, Chloroform-*d*) δ 6.85 (d, *J* = 7.8 Hz, 1H), 6.11 (d, *J* = 7.9 Hz, 1H), 6.05 (s, 1H), 3.54 (s, 4H), 2.10 (s, 3H). ^{13}C NMR (126 MHz, Chloroform-*d*) δ 145.61, 145.36, 131.10, 112.87, 106.02, 102.28, 16.49.

Procedure for the Reduction of Cyclohexanone or 2-Cyclohexen-1-one by DMAB. The ketone (5 mmol) was added to a test tube containing a stir bar. To that vessel, DMAB (0.101 g, 1.7 mmol) and DI water (100 μL) were added. For each measurement, a single 5000 millisecond accumulation at 350 mW laser power was collected. After the reaction was complete as determined by the Raman peak intensity data, the reaction mixture was acidified with HCl (1M) to pH 2, after which the organic layer was extracted with diethyl ether (3x10 mL), dried over $MgSO_4$, and then filtered and concentrated to obtain the product.

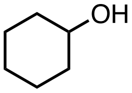

Cyclohexanol. ^{1}H NMR (500 MHz, Chloroform-*d*) δ 3.55 (s, 1H), 2.35 (s, 1H), 1.85 (d, *J* = 3.8 Hz, 2H), 1.68 (s, 2H), 1.50 (d, *J* = 12.1 Hz, 1H), 1.22 (s, 5H). ^{13}C NMR (126 MHz, Chloroform-*d*) δ 70.19, 35.45, 25.45, 24.15.

Procedure for Measuring Hydrogen Evolution by Gas Buret. To a gas buret reservoir, outfitted with a rubber septum, 1 M HCl (15 mL), methanol (15 mL), and tetrahydrofuran (15 mL) were added and allowed to stir. A few trials of sacrificial hydride sources, such as $NaBH_4$ and BH_3SMe_2, were used for the purpose of system equilibration. In a separate round-bottom flask containing a side-arm, cyclohexanone (0.3 mL, 3 mmol) was added. A solution of DMAB (0.125 mL, 1 mmol, 8 M) was then injected via syringe through the side-arm of the flask. By the controlled relief of pressure in the closed system into a graduated cylinder, the volume of gas generated, plus total volume injected, was measured by water displacement. The temperature of the displaced water and barometric pressure were also measured, in addition to the temperature-dependent vapor pressure of water. The quantity of hydrogen ultimately produced was determined by following a previously published method.

Computational Details. Density functional theory (DFT) for several steps along the hydride transfer in the reduction of cyclohexanone were performed using Gaussian 09. The B3LYP/6-311G (d,p) basis set was utilized to perform a geometry optimization along with a frequency calculation. The energies of the optimized geometry were used to construct the proposed reaction pathway. A series of geometry optimization were performed to find the steps along the reaction pathway. The structures contained no imaginary frequencies. The $\epsilon + G_{corr}$ energy for each structure were extracted from the log file, converted to kcal/mol, and used for constructing the reaction pathway. Listed below are the Cartesian coordinates for the structures in pathway C.

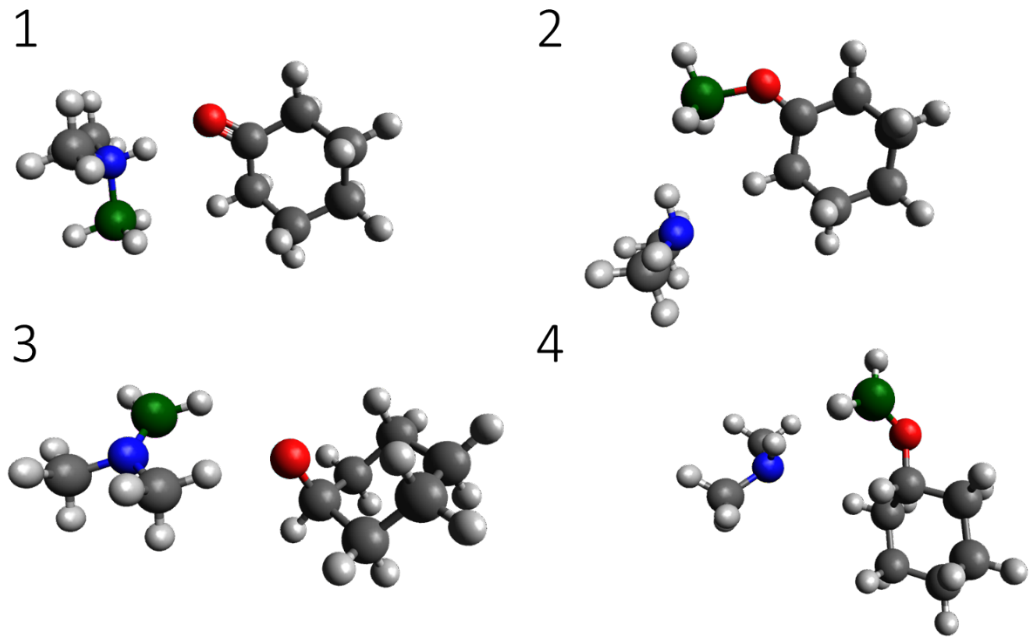

DFT calculated optimized structures where white, grey, green, blue, and red represent hydrogen, carbon, boron, nitrogen, and oxygen respectively.

Cartesian Coordinates Structure 1

C	3.2625330000	-0.5032260000	1.3789110000
N	2.7840550000	0.0366460000	0.0847210000
C	3.6396840000	-0.4180550000	-1.0357760000
H	1.8434910000	-0.3455980000	-0.0722840000
B	2.6213150000	1.6613870000	0.1182320000
H	1.8479290000	1.9027870000	1.0215380000
H	3.7276550000	2.1138950000	0.3178940000
H	2.1792600000	1.9772950000	-0.9670120000
H	3.2174060000	-0.0499710000	-1.9691890000
H	4.6361650000	0.0067020000	-0.9110520000

H	3.7015450000	-1.5096650000	-1.0604390000
H	2.5745290000	-0.1905720000	2.1623030000
H	3.3186250000	-1.5948630000	1.3479170000
H	4.2475670000	-0.0861460000	1.5898100000
C	-2.1911190000	1.5134570000	0.1564310000
C	-1.1321280000	0.8259230000	-0.7322660000
C	-0.9765070000	-0.6405760000	-0.3872570000
C	-2.2663180000	-1.4320650000	-0.2699620000
C	-3.3014900000	-0.7123390000	0.6198670000
C	-3.5149590000	0.7395610000	0.1745480000
O	0.1066190000	-1.1718080000	-0.2117300000
H	-2.3441820000	2.5368250000	-0.1959020000
H	-1.7991220000	1.5930220000	1.1766390000
H	-0.1635140000	1.3234220000	-0.6663950000
H	-1.4639750000	0.8715140000	-1.7791260000
H	-2.0277890000	-2.4316540000	0.0969170000
H	-2.6774160000	-1.5356130000	-1.2833410000
H	-2.9497960000	-0.7252170000	1.6581030000
H	-4.2437720000	-1.2671270000	0.6026550000
H	-3.9624120000	0.7525950000	-0.8276120000
H	-4.2282870000	1.2332950000	0.8412360000

Cartesian Coordinates Structure 2

C	0.9891710000	-1.5972120000	0.0152500000
C	0.5059720000	-0.2559350000	-0.5807520000
C	1.3654260000	0.8928540000	-0.1497440000
C	2.8585490000	0.6992690000	-0.1598500000
C	3.2865820000	-0.6502300000	0.4516720000
C	2.4959650000	-1.8137430000	-0.1566160000
O	0.9325990000	2.0006500000	0.1880130000
H	0.4200780000	-2.4053250000	-0.4498610000
H	0.7370930000	-1.6170970000	1.0813010000
H	-0.5455130000	-0.0806460000	-0.3529110000
H	0.5954550000	-0.2961860000	-1.6768790000
H	3.3245800000	1.5525140000	0.3346970000
H	3.1630670000	0.7240950000	-1.2158640000
H	3.1210030000	-0.6215600000	1.5345900000
H	4.3611280000	-0.7844470000	0.3029710000
H	2.7383580000	-1.9049570000	-1.2230160000
H	2.7948390000	-2.7549230000	0.3138220000
C	-3.8520600000	-0.3053010000	-1.1242280000
N	-2.9673170000	-0.2672480000	0.0337680000
C	-3.5729110000	-0.8287070000	1.2349590000

H	-3.3771120000	0.2043350000	-1.9654610000
H	-4.8359620000	0.1639860000	-0.9490780000
H	-4.0310250000	-1.3448260000	-1.4188100000
H	-2.6766050000	0.6890810000	0.2119520000
H	-4.5457030000	-0.3768930000	1.4969260000
H	-2.8972090000	-0.6965610000	2.0830270000
H	-3.7350010000	-1.9032930000	1.0997230000
B	-0.6131140000	2.5224050000	0.2277760000
H	-0.4963150000	3.7018870000	0.4101590000
H	-1.1085930000	1.9319880000	1.1612010000
H	-1.0907380000	2.2263650000	-0.8419980000

Cartesian Coordinates Structure 3

C	-3.1026960000	0.6371800000	-0.9492980000
N	-2.8478740000	-0.3197700000	0.1550890000
C	-2.8811580000	0.3488500000	1.4807190000
H	-3.5746610000	-1.0326320000	0.1386150000
B	-1.4146360000	-1.1656200000	-0.0595330000
H	-1.5379320000	-1.6950940000	-1.1490050000
H	0.2301520000	-0.2783140000	-1.9508260000
H	-1.4374870000	-1.9623290000	0.8624210000

H	-2.7847730000	-0.4097130000	2.2558990000
H	-2.0243010000	1.0178350000	1.5350040000
H	-3.8100640000	0.9093150000	1.6141330000
H	-3.1514200000	0.0847200000	-1.8864500000
H	-4.0336200000	1.1866530000	-0.7873170000
H	-2.2626780000	1.3284170000	-0.9882790000
C	2.4169050000	-1.0770100000	0.6396210000
C	1.6737020000	-1.2682150000	-0.6896830000
C	0.6596790000	-0.1383150000	-0.9464820000
C	1.3539020000	1.2291950000	-0.8795010000
C	2.1005930000	1.4322160000	0.4471810000
C	3.1019710000	0.2962650000	0.7043790000
O	-0.3848110000	-0.1554400000	0.0146930000
H	3.1532470000	-1.8759870000	0.7772810000
H	1.6975070000	-1.1620640000	1.4605920000
H	1.1506810000	-2.2290660000	-0.7050340000
H	2.3943630000	-1.2840340000	-1.5182270000
H	0.6082790000	2.0181910000	-1.0247560000
H	2.0620500000	1.3009440000	-1.7148440000
H	1.3693780000	1.4591100000	1.2615900000
H	2.6140330000	2.3998910000	0.4453330000
H	3.8995540000	0.3397680000	-0.0501260000

H	3.5870770000	0.4334040000	1.6768790000

Cartesian Coordinates Structure 4

C	1.3764880000	-1.7200790000	-0.3496750000
C	0.6495080000	-0.4242310000	-0.7427400000
C	1.0517210000	0.7309940000	0.1732990000
C	2.5652790000	0.9325490000	0.2152520000
C	3.2876640000	-0.3637640000	0.6128380000
C	2.8990890000	-1.5294150000	-0.3074880000
O	0.4436940000	1.9495610000	-0.3105590000
H	1.1097520000	-2.5170370000	-1.0502050000
H	1.0264370000	-2.0489040000	0.6374370000
H	-0.4356500000	-0.5579760000	-0.6980390000
H	0.9080600000	-0.1478910000	-1.7720460000
H	2.8082160000	1.7425490000	0.9100330000
H	2.8934500000	1.2557410000	-0.7794580000
H	3.0316240000	-0.6208980000	1.6488450000
H	4.3699450000	-0.2040620000	0.5934230000
H	3.2667380000	-1.3264470000	-1.3213880000
H	3.3880120000	-2.4510610000	0.0238950000
C	-3.9633840000	0.0662660000	-0.9113100000
N	-3.0305590000	-0.3118810000	0.1432160000
C	-3.5633200000	-1.3300210000	1.0400950000

H	-3.5435070000	0.8886350000	-1.4947360000
H	-4.9541660000	0.3799610000	-0.5386020000
H	-4.1193450000	-0.7804990000	-1.5881350000
H	-2.7652600000	0.5098380000	0.6772800000
H	-4.5386050000	-1.0660250000	1.4853070000
H	-2.8560230000	-1.5098920000	1.8528930000
H	-3.6942520000	-2.2709120000	0.4952440000
B	-0.5514230000	2.5760870000	0.3282240000
H	-0.9866710000	3.5670620000	-0.1755250000
H	0.6757200000	0.5407250000	1.1871930000
H	-0.9812610000	2.1495410000	1.3657940000

6.1.4. Chapter 5

General Procedure to Prepare the Gallium Aluminum Alloy. On a piece of weighing paper, shape aluminum foil (0.108 g, 4 mmol) into a cup and into the center add 65 °C gallium (0.837 g, 12 mmol). Fold the weighing paper in fourths, pressing the aluminum and gallium together. Continue pressing the gallium into the aluminum until the alloy appears homogenous and shiny in color. Once all the aluminum has been dissolved by the gallium, fold the paper in half and press a dry ice pellet over the paper, solidifying the alloy. The Ga-Al alloy will appear dull grey when it hardens. Using a razor blade, delicately peel the alloy off the paper and place into desired vessel or store under cyclohexane for future use.

General Procedure for Measuring Hydrogen Evolution by Gas Buret. An alloy nugget was placed into a round-bottom flask containing a 65 °C magnetic stir bar, the heat from which "melted" the alloy in ~1 min. The flask was connected to a gas buret reservoir *via* a cannula. DI water (10 mL) was added to the flask containing the alloy causing hydrogen gas to evolve immediately. Measurements were taken after it appeared all of the material had reacted, 15 min. By the controlled release of pressure in the closed system into a graduated cylinder, the volume of gas generated was measured by water displacement. The temperature of the displaced water and barometric pressure were also measured. The quantity of hydrogen produced was determined by following a previously published method.

Procedure to Recycle Ga. The used alloy reaction mixture was vacuum filtered, and the residue was collected. The Ga appears in the residue as shiny nuggets and were collected in a vial.

Characterization. ICP-OES data were obtained on a Thermo Scientific iCAP 7000 Series ICP spectrometer using scandium and yttrium as internal standards. Calibration curves for aluminum and gallium were prepared using external standards.

Procedure for the Hydrogenation of 4-Phenyl-1-butene-4-ol Using Nickel Catalyst. In a 100-mL round-bottom flask, $NaBH_4$ (1 g, 26.43 mmol) was suspended in EtOH (24 mL) and 2 M NaOH (1.25 mL, 2.5 mmol) with stirring. In a separate 100-mL round-bottom flask, nickel(II) acetate tetrahydrate (0.314 g, 1.25 mmol) was dissolved in EtOH (12.5 mL). To the nickel solution, the $NaBH_4$ solution (1.25 mL, 1.38 mmol) was added slowly *via* syringe. (CAUTION: H_2 evolution!). Once the hydrogen evolution abates, the stirring was stopped and the alkene, 4-phenyl-1-butene-4-ol (0.187 mL, 1.25 mmol), was added to the reaction flask and a balloon was then connected to the reaction flask. An Ga:Al alloy nugget (0.945 g, 4 mmol of theoretical H_2) was placed into a separate round-bottom flask and melted with a warm stir bar, then connected *via* cannula to the reaction flask containing the nickel catalyst and the alkene. With both flasks stirring, DI water (5 mL) was added to the alloy flask to generate hydrogen that is then led into the reaction flask. After 15 min the two flasks were disconnected and a second flask containing another alloy nugget (0.945 g, 4 mmol of theoretical H_2) was attached and the same procedure as above was conducted to generate hydrogen gas. After the hydrogen had evolved, the reaction mixture was allowed to stir for 1 h. The reaction mixture was then centrifuged and the supernatant decanted. The solid catalyst was rinsed with diethyl ether (2×10 mL), centrifuged and the supernatant decanted. The combined supernatants were then concentrated by rotary evaporation to afford essentially pure product, 1-phenyl-1-butanol, (yield 90%).

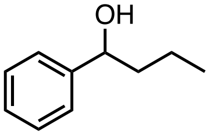

1-Phenyl-1-butanol. ^{1}H NMR (500 MHz, Chloroform-*d*) δ 7.35 (d, *J* = 5.5 Hz, 4H), 7.30 – 7.26 (m, 1H), 4.66 (dd, *J* = 7.5, 5.8 Hz, 1H), 2.12 (s, 1H), 1.83 – 1.76 (m, 1H), 1.72 – 1.65 (m, 1H), 1.47 – 1.40 (m, 1H), 1.35 – 1.28 (m, 1H), 0.94 (t, *J* = 7.4 Hz, 3H). ^{13}C NMR (126 MHz, Chloroform-*d*) δ 144.99, 128.41, 127.45, 125.93, 74.40, 41.26, 19.05, 13.99.

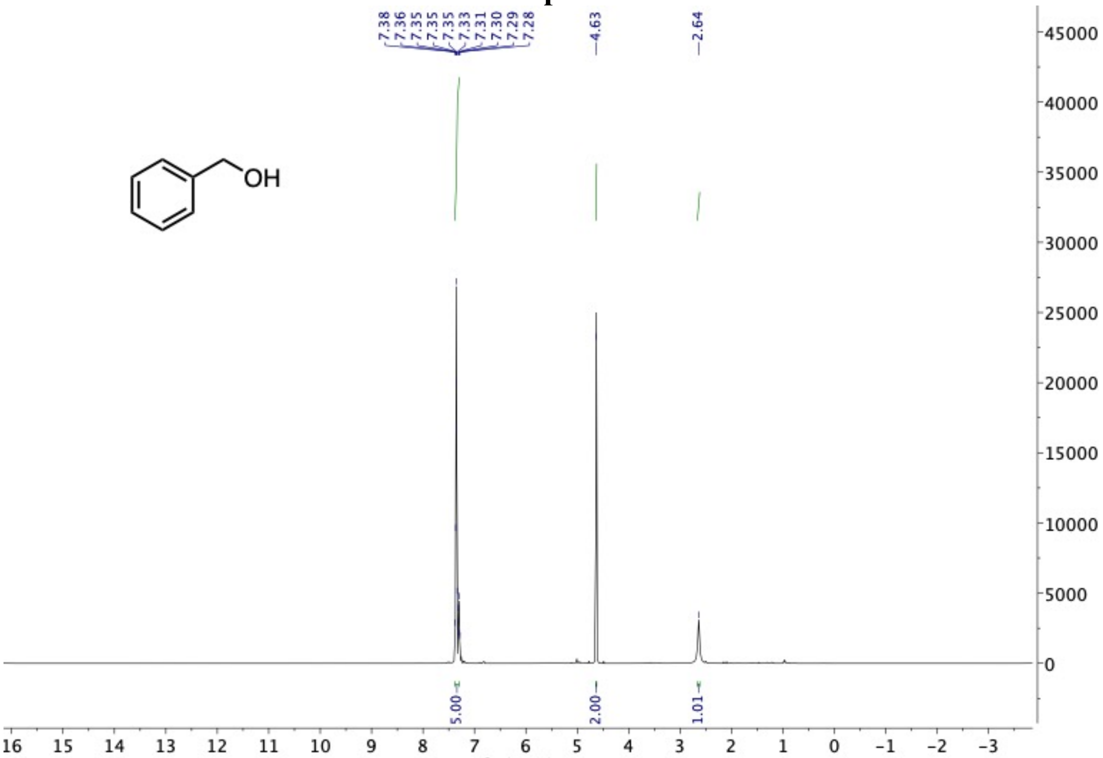
7.38
7.36
7.35
7.35
7.35
7.33
7.31
7.30
7.29
7.28
4.63
2.64
OH
5.00
2.00
1.01
45000
40000
35000
30000
25000
20000
15000
10000
5000
0
16 15 14 13 12 11 10 9 8 7 6 5 4 3 2 1 0 −1 −2 −3
f1 (ppm)

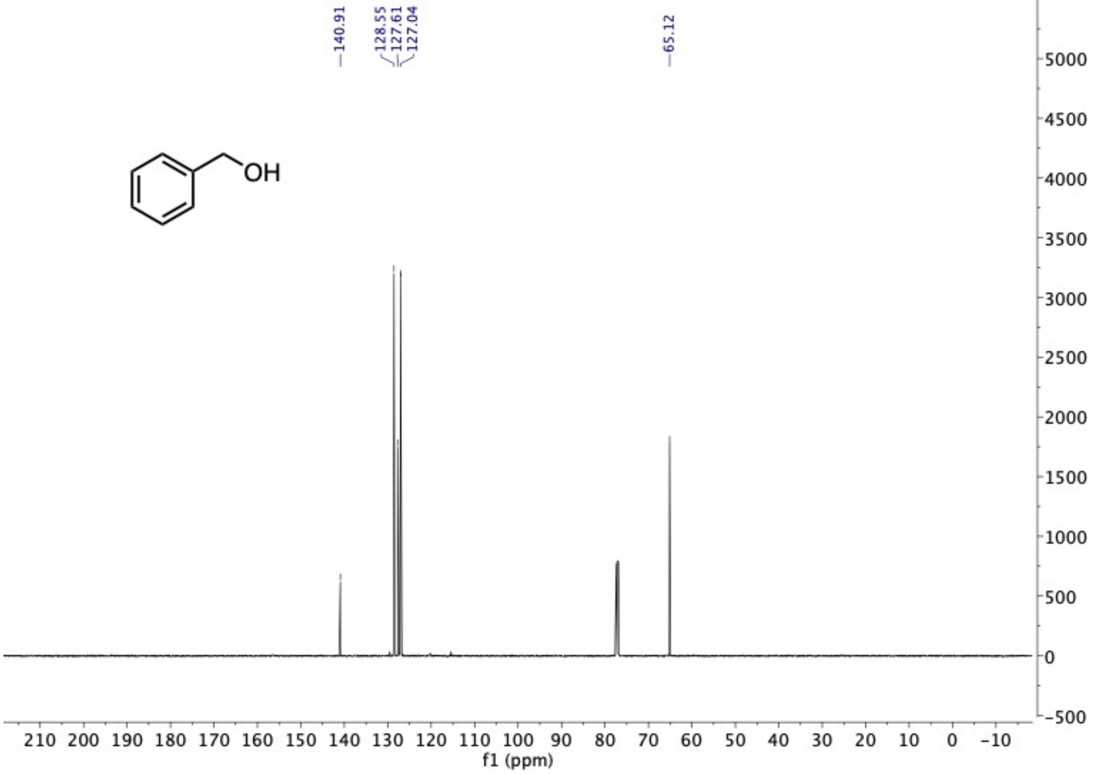
140.91
128.55
127.61
127.04
65.12
OH
5000
4500
4000
3500
3000
2500
2000
1500
1000
500
0
−500
210 200 190 180 170 160 150 140 130 120 110 100 90 80 70 60 50 40 30 20 10 0 −10
f1 (ppm)

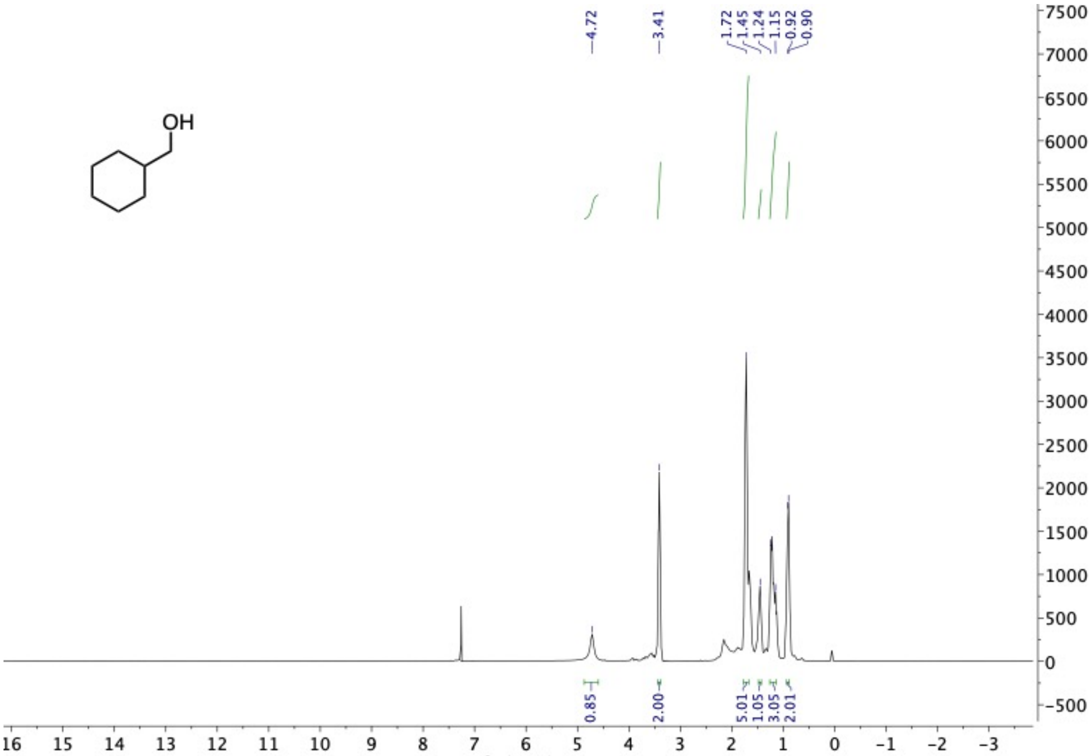
OH
4.72
3.41
1.72
1.45
1.24
1.15
0.92
0.90
0.85
2.00
5.01
1.05
3.05
2.01
7500
7000
6500
6000
5500
5000
4500
4000
3500
3000
2500
2000
1500
1000
500
0
-500
16 15 14 13 12 11 10 9 8 7 6 5 4 3 2 1 0 -1 -2 -3
f1 (ppm)

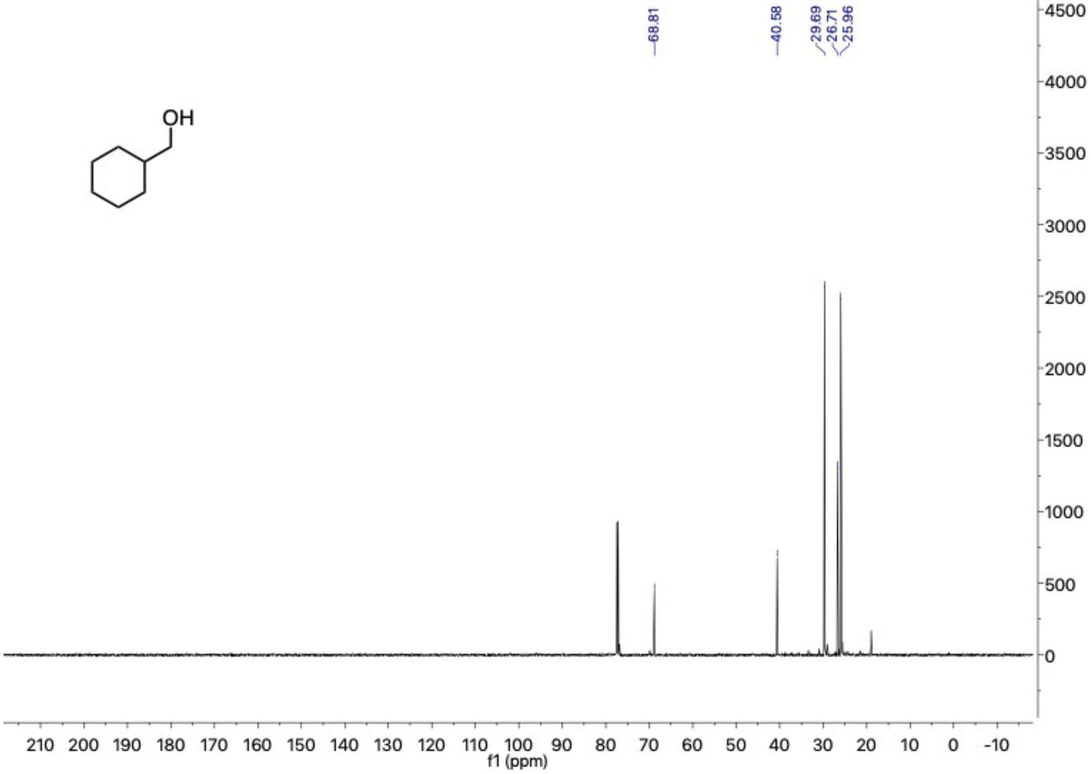
OH
68.81
40.58
29.69
26.71
25.96
4500
4000
3500
3000
2500
2000
1500
1000
500
0
210 200 190 180 170 160 150 140 130 120 110 100 90 80 70 60 50 40 30 20 10 0 -10
f1 (ppm)

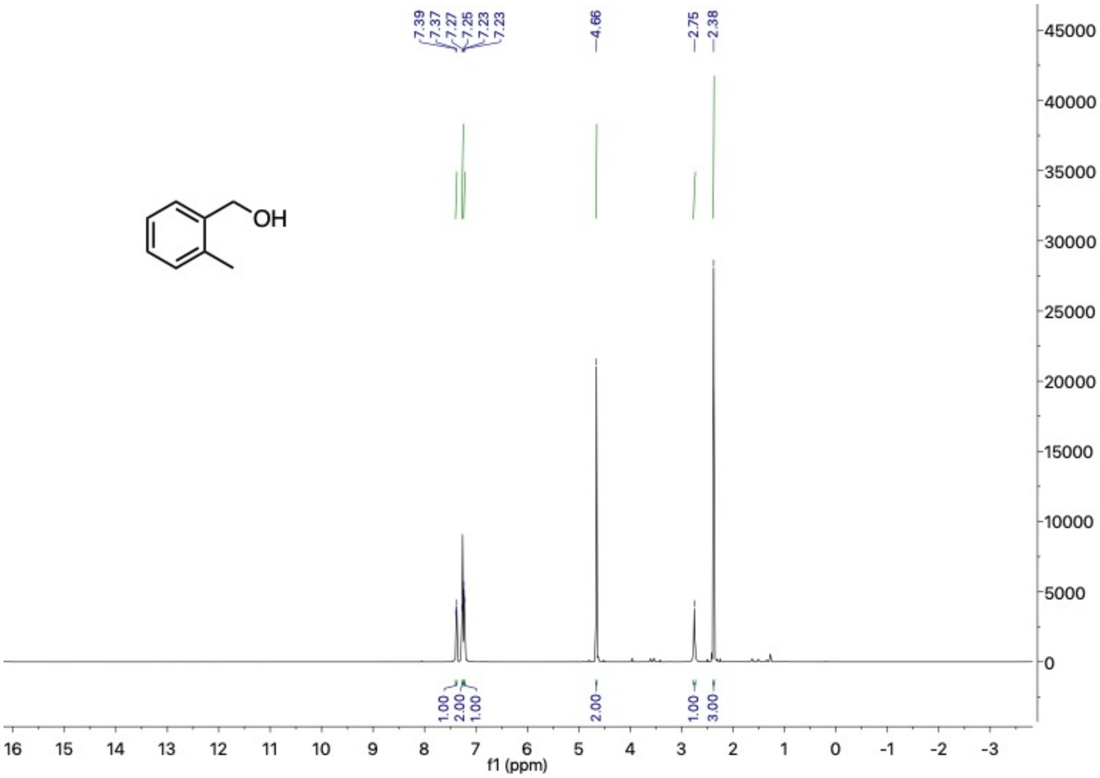
7.39
7.37
7.27
7.25
7.23
7.23
4.66
2.75
2.38
OH
1.00
2.00
1.00
2.00
1.00
3.00
45000
40000
35000
30000
25000
20000
15000
10000
5000
0
16 15 14 13 12 11 10 9 8 7 6 5 4 3 2 1 0 -1 -2 -3
f1 (ppm)

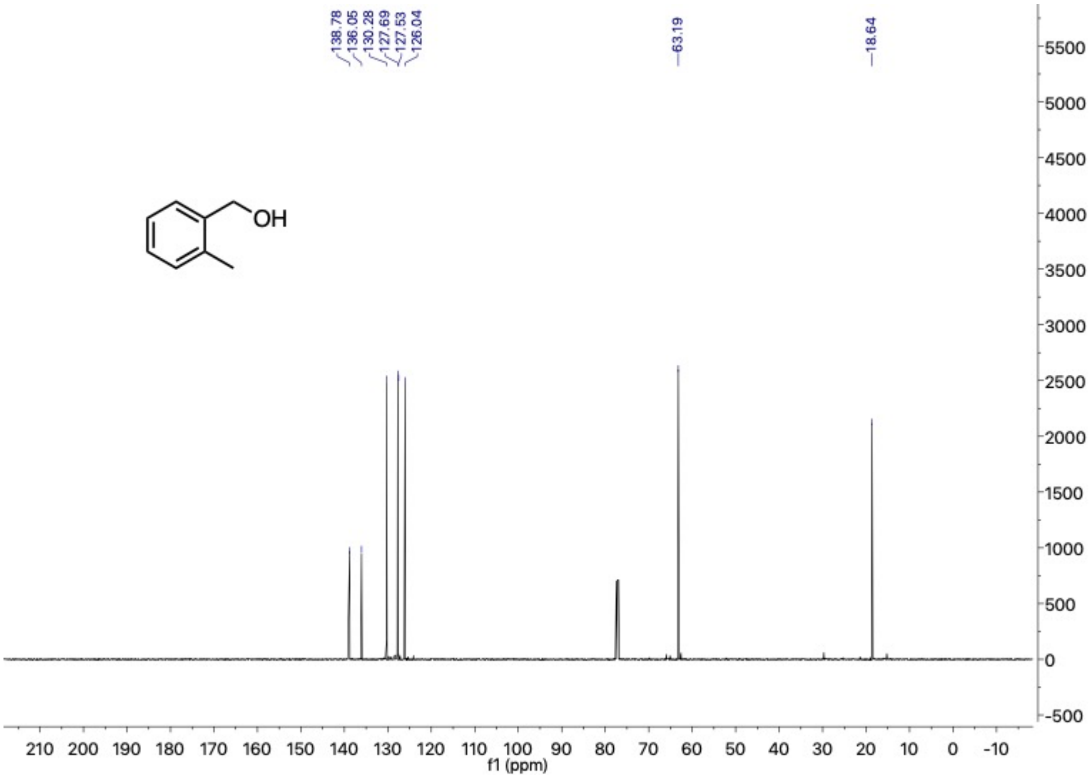
138.78
136.05
130.28
127.69
127.53
126.04
63.19
18.64
OH
5500
5000
4500
4000
3500
3000
2500
2000
1500
1000
500
0
-500
210 200 190 180 170 160 150 140 130 120 110 100 90 80 70 60 50 40 30 20 10 0 -10
f1 (ppm)

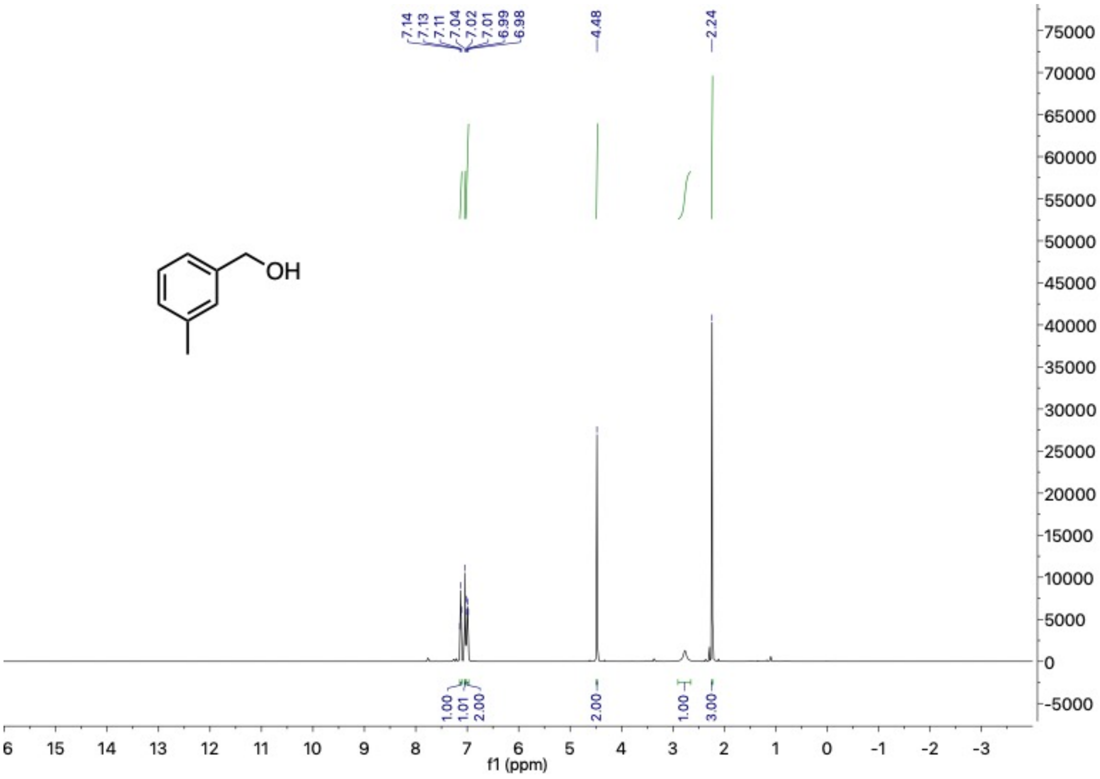
7.14
7.13
7.11
7.04
7.02
7.01
6.99
6.98
4.48
2.24
OH
1.00
1.01
2.00
2.00
1.00
3.00
f1 (ppm)

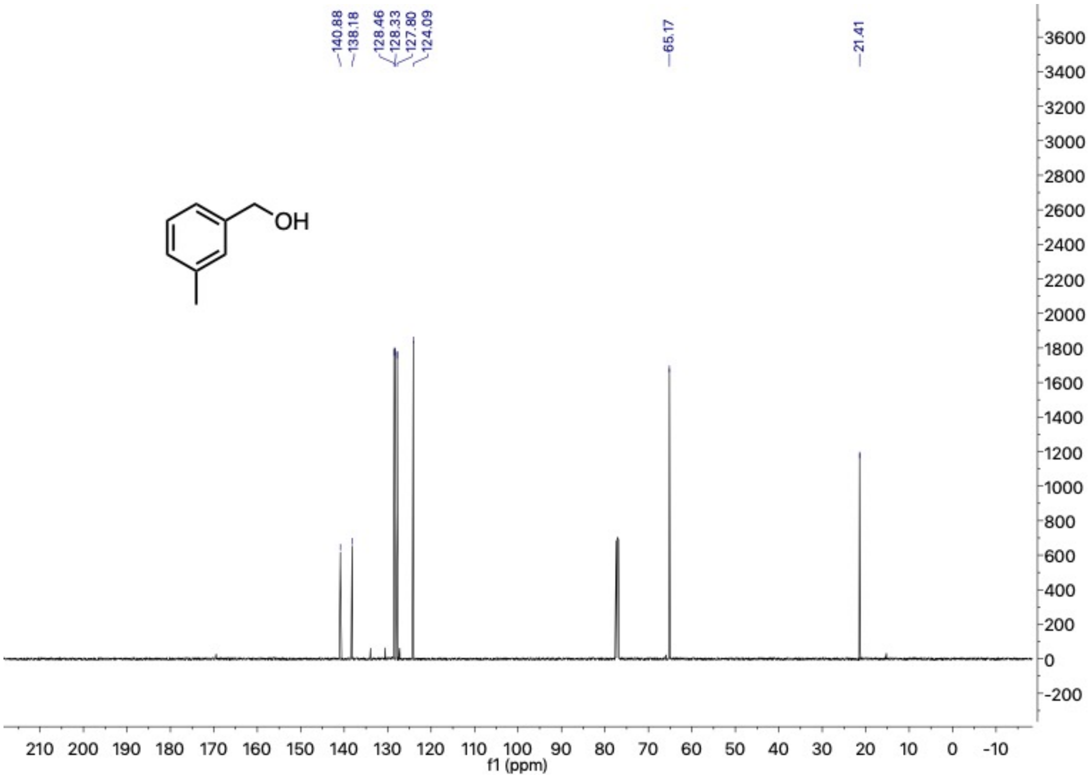
140.88
138.18
128.46
128.33
127.80
124.09
65.17
21.41
OH
f1 (ppm)

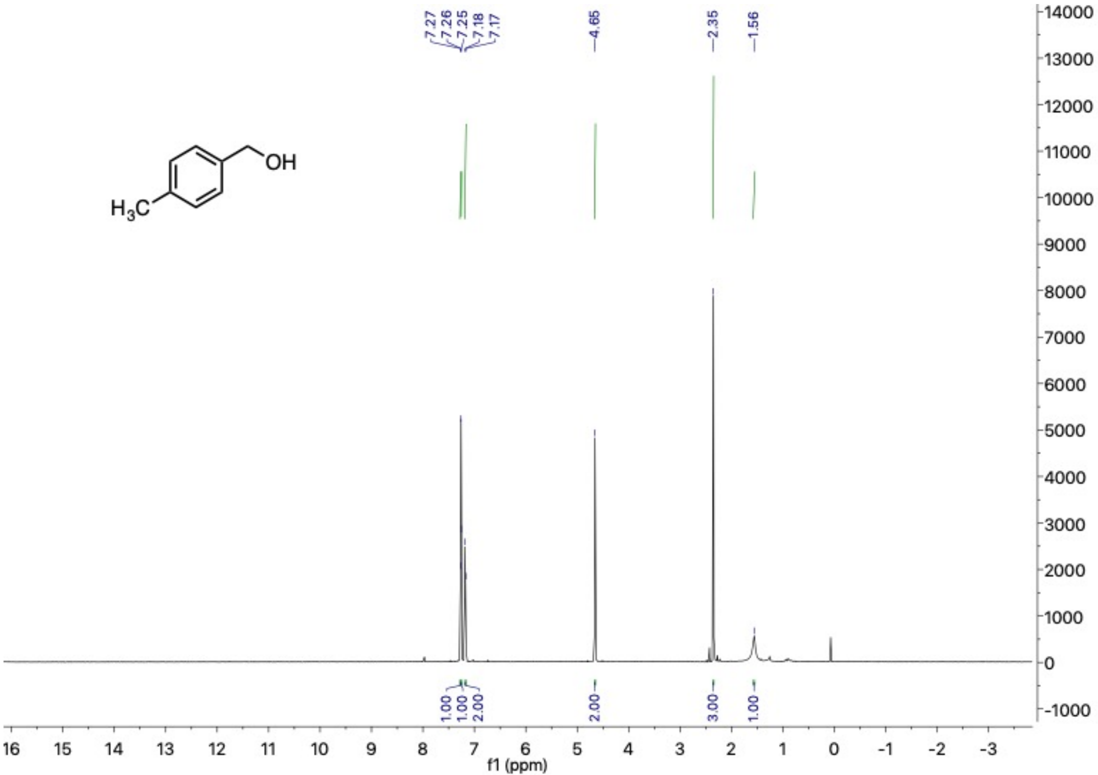
7.27
7.26
7.25
7.18
7.17
4.65
2.35
1.56
OH
H3C
1.00
1.00
2.00
2.00
3.00
1.00
16 15 14 13 12 11 10 9 8 7 6 5 4 3 2 1 0 -1 -2 -3
f1 (ppm)
14000 13000 12000 11000 10000 9000 8000 7000 6000 5000 4000 3000 2000 1000 0 -1000

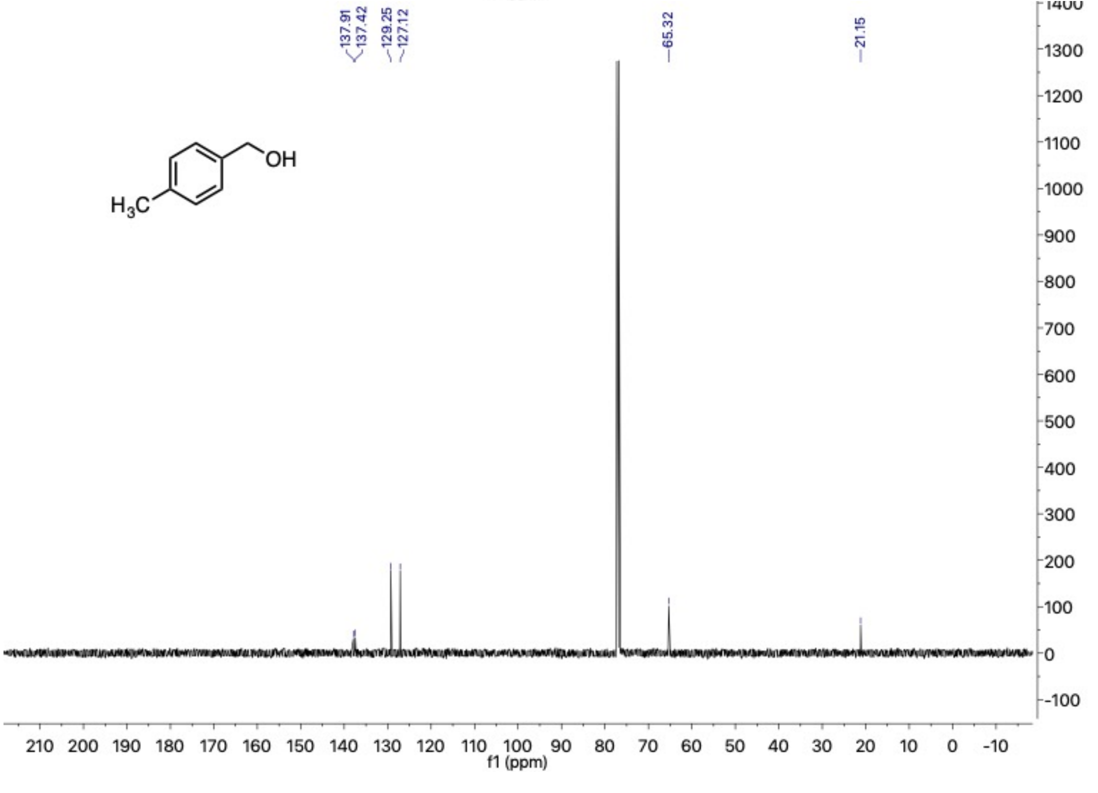
137.91
137.42
129.25
127.12
65.32
21.15
OH
H3C
210 200 190 180 170 160 150 140 130 120 110 100 90 80 70 60 50 40 30 20 10 0 -10
f1 (ppm)
1400 1300 1200 1100 1000 900 800 700 600 500 400 300 200 100 0 -100

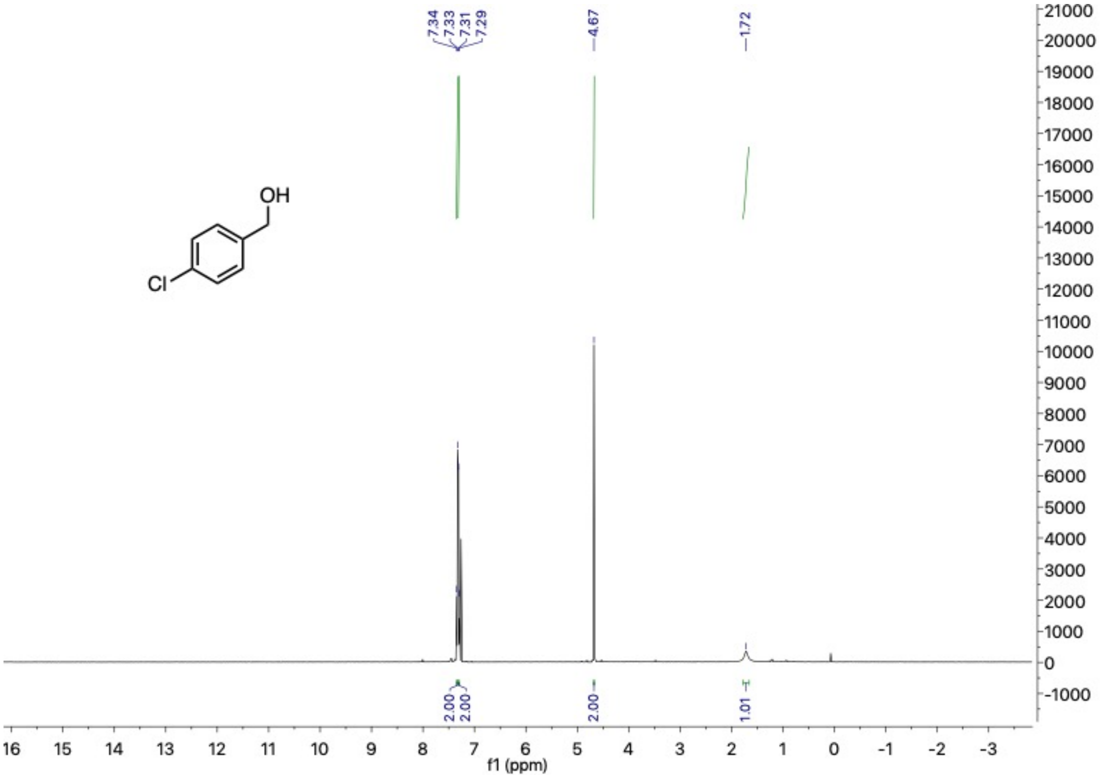
7.34
7.33
7.31
7.29
4.67
1.72
OH
Cl
2.00
2.00
2.00
1.01
f1 (ppm)

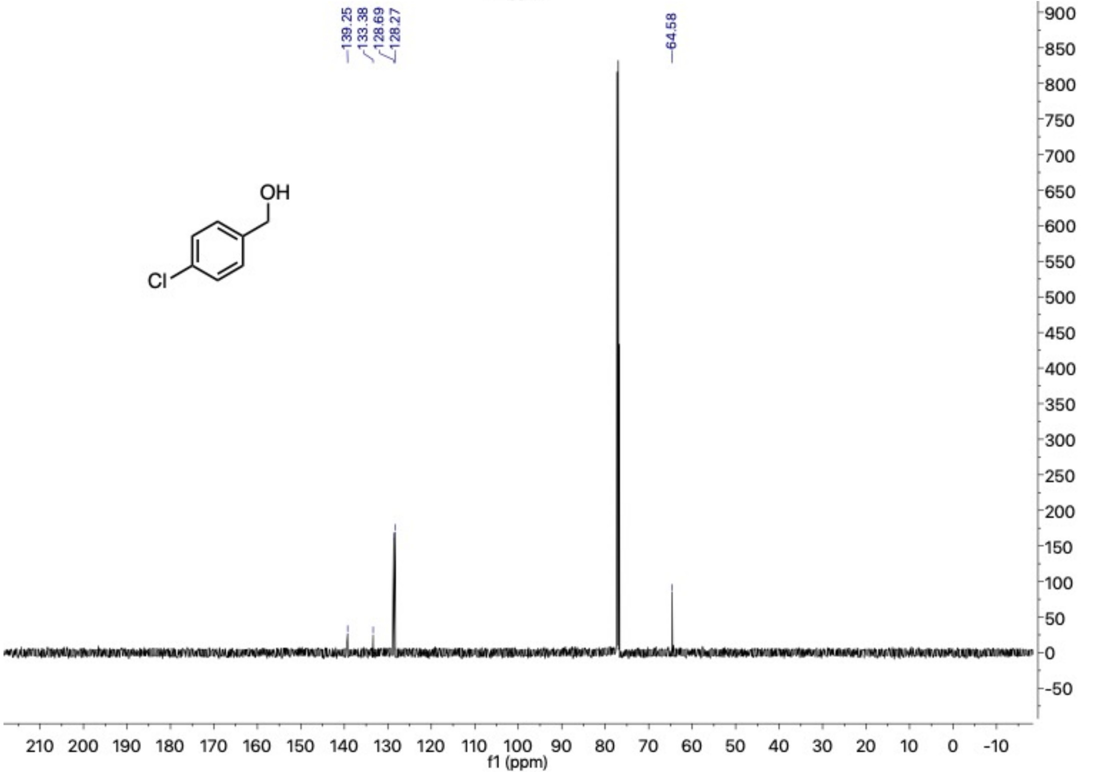
139.25
133.38
128.69
128.27
64.58
OH
Cl
f1 (ppm)

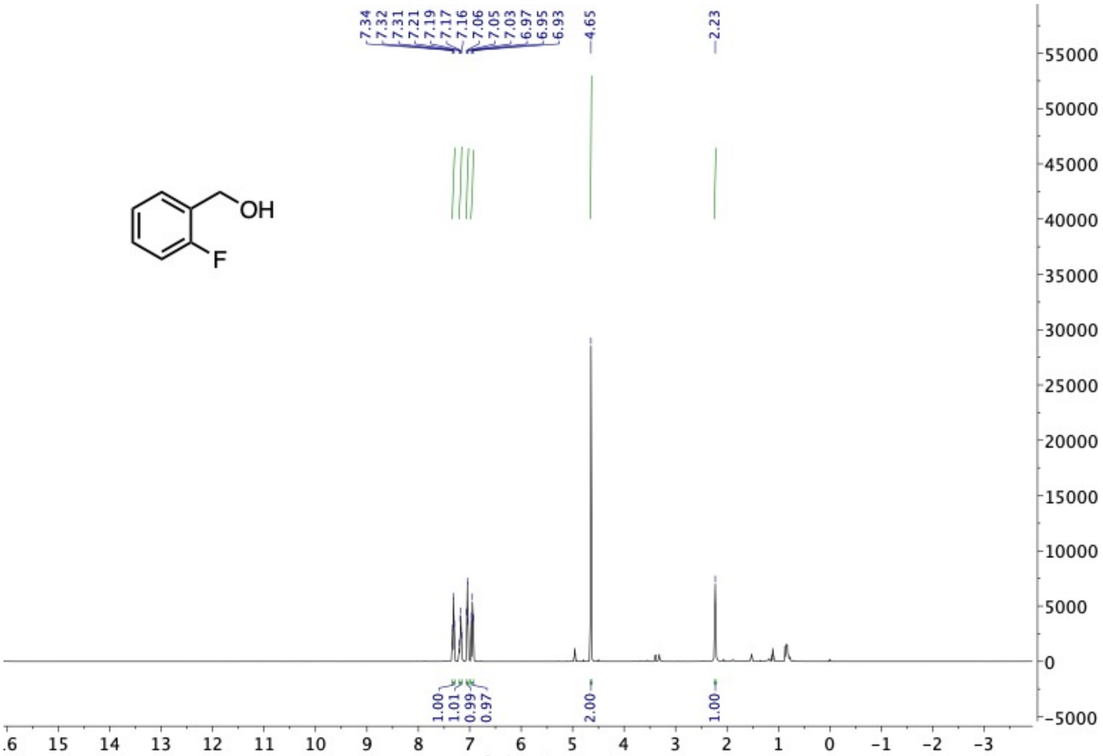
7.34
7.32
7.31
7.21
7.19
7.17
7.16
7.06
7.05
7.03
6.97
6.95
6.93
4.65
2.23
OH
F
1.00
1.01
0.99
0.97
2.00
1.00
55000
50000
45000
40000
35000
30000
25000
20000
15000
10000
5000
0
−5000
.6 15 14 13 12 11 10 9 8 7 6 5 4 3 2 1 0 −1 −2 −3
f1 (ppm)

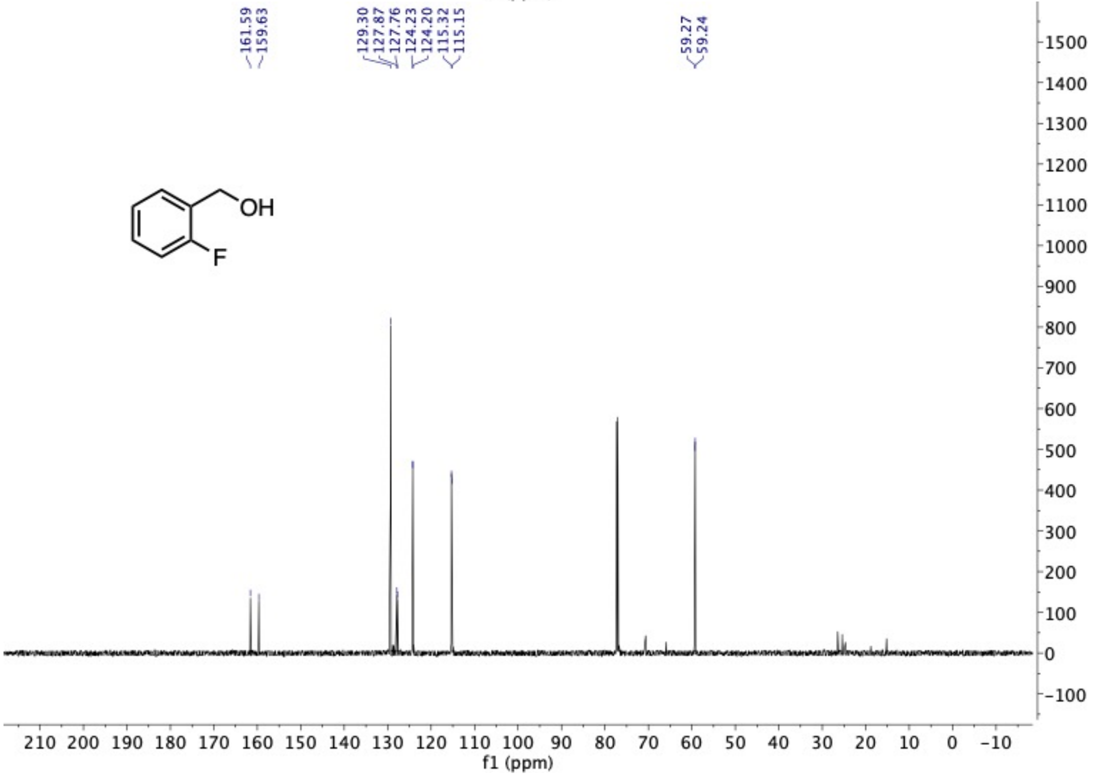
161.59
159.63
129.30
127.87
127.76
124.23
124.20
115.32
115.15
59.27
59.24
OH
F
1500
1400
1300
1200
1100
1000
900
800
700
600
500
400
300
200
100
0
−100
210 200 190 180 170 160 150 140 130 120 110 100 90 80 70 60 50 40 30 20 10 0 −10
f1 (ppm)

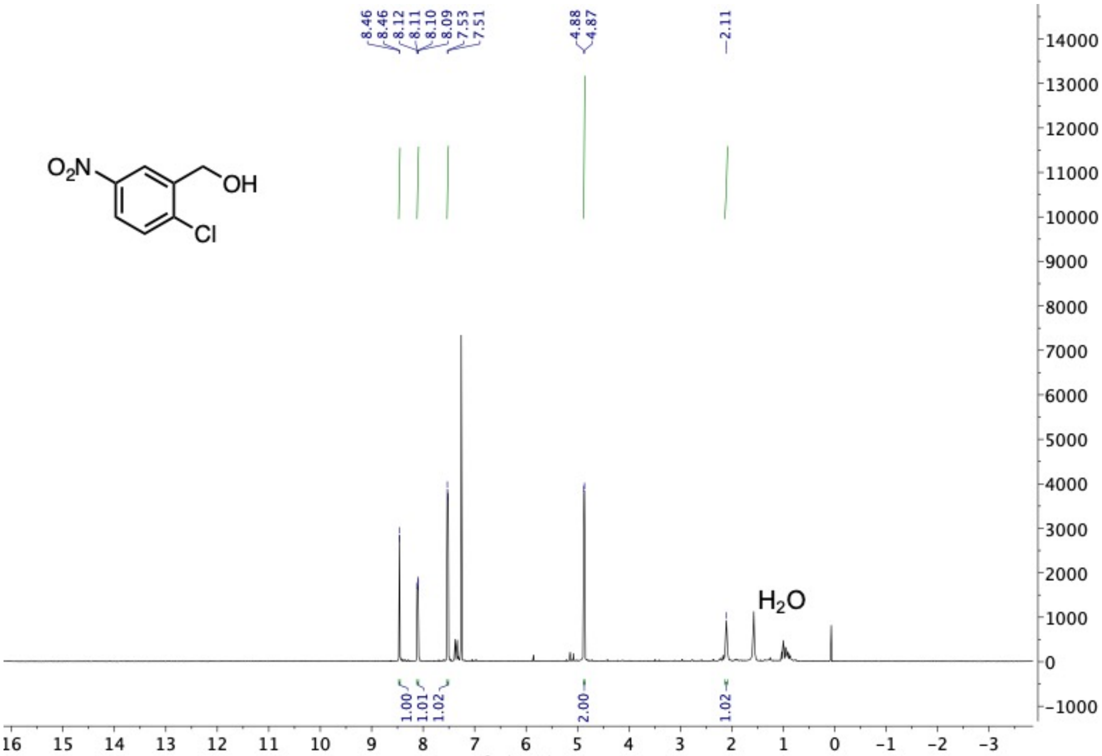
8.46
8.46
8.12
8.11
8.10
8.09
7.53
7.51
4.88
4.87
2.11
O₂N
OH
Cl
H₂O
1.00
1.01
1.02
2.00
1.02
14000
13000
12000
11000
10000
9000
8000
7000
6000
5000
4000
3000
2000
1000
0
−1000
16 15 14 13 12 11 10 9 8 7 6 5 4 3 2 1 0 −1 −2 −3
f1 (ppm)

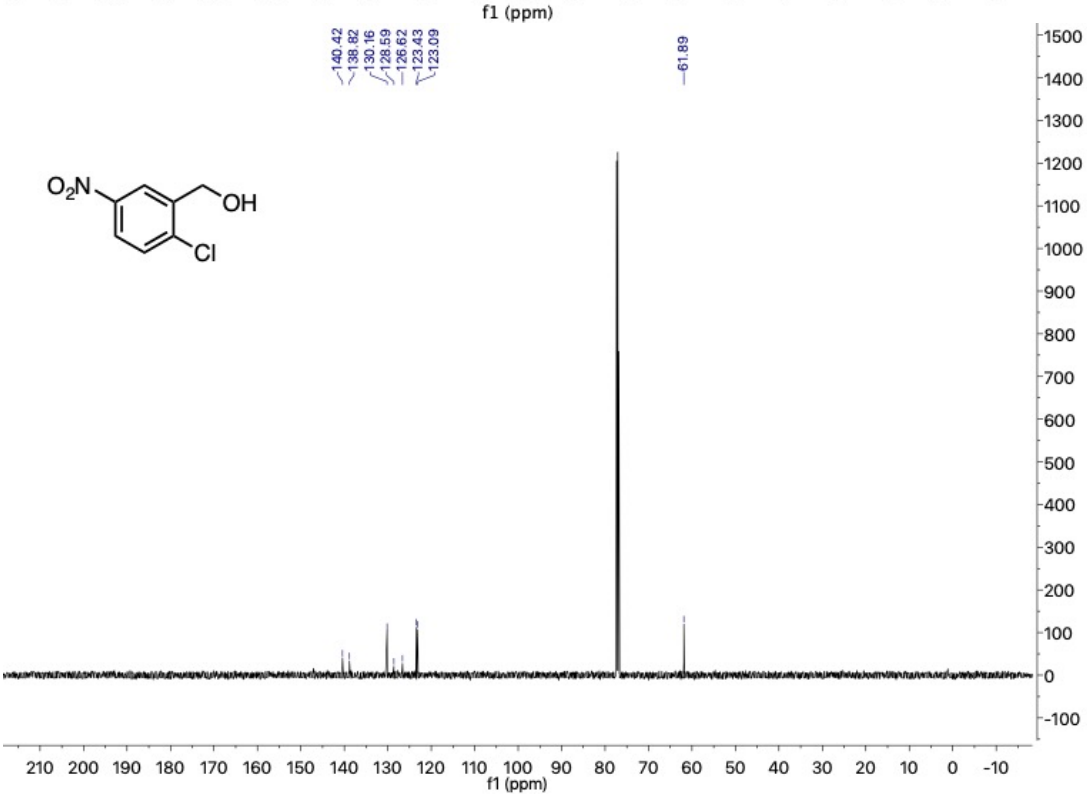
140.42
138.82
130.16
128.59
126.62
123.43
123.09
61.89
O₂N
OH
Cl
1500
1400
1300
1200
1100
1000
900
800
700
600
500
400
300
200
100
0
−100
210 200 190 180 170 160 150 140 130 120 110 100 90 80 70 60 50 40 30 20 10 0 −10
f1 (ppm)

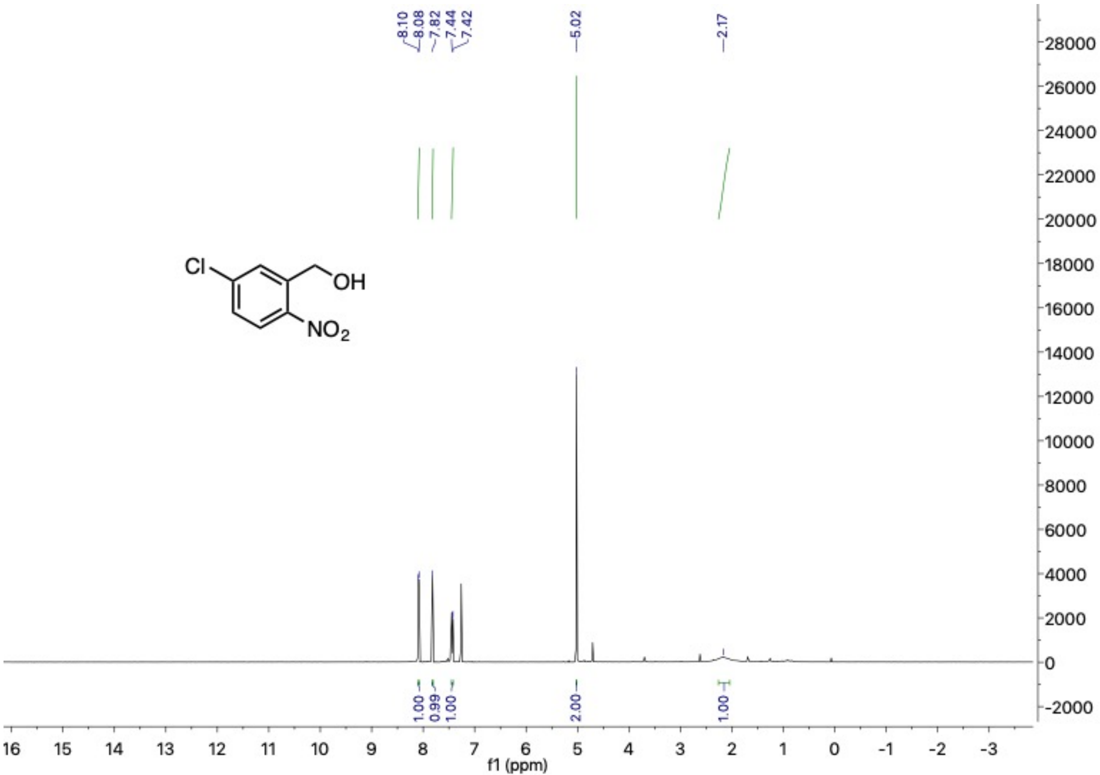
8.10
8.08
7.82
7.44
7.42
5.02
2.17
Cl
OH
NO2
1.00
0.99
1.00
2.00
1.00
28000
26000
24000
22000
20000
18000
16000
14000
12000
10000
8000
6000
4000
2000
0
-2000
16 15 14 13 12 11 10 9 8 7 6 5 4 3 2 1 0 -1 -2 -3
f1 (ppm)

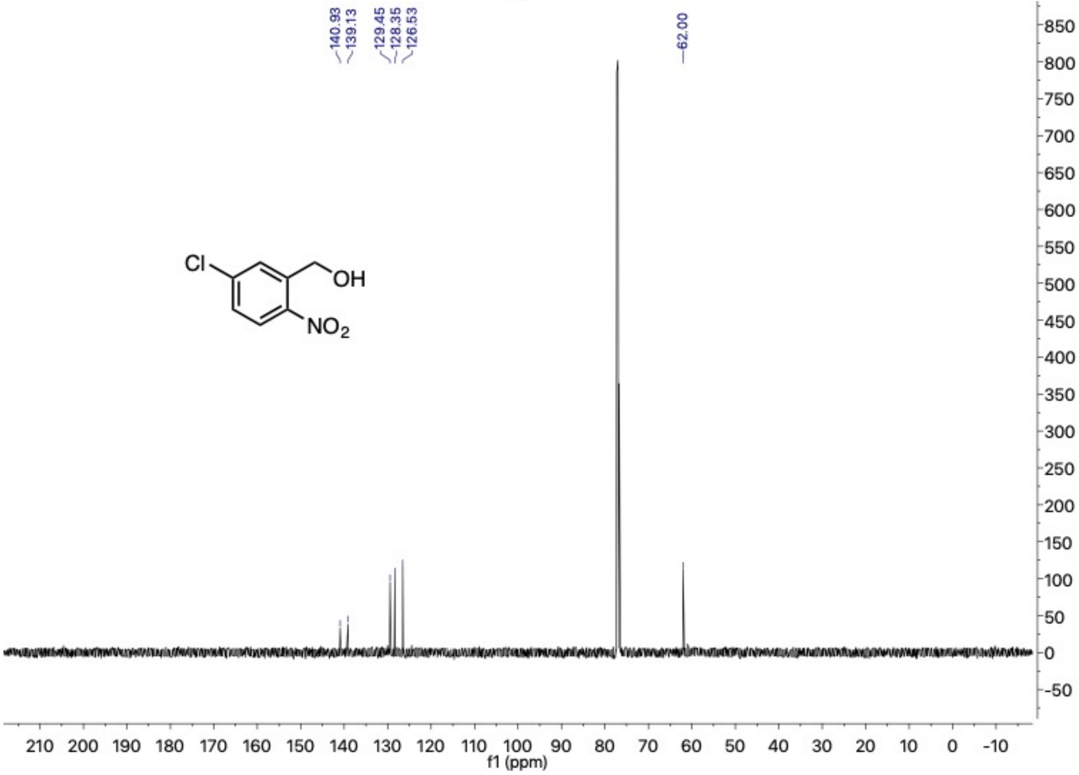
140.93
139.13
129.45
128.35
126.53
62.00
Cl
OH
NO2
850
800
750
700
650
600
550
500
450
400
350
300
250
200
150
100
50
0
-50
210 200 190 180 170 160 150 140 130 120 110 100 90 80 70 60 50 40 30 20 10 0 -10
f1 (ppm)

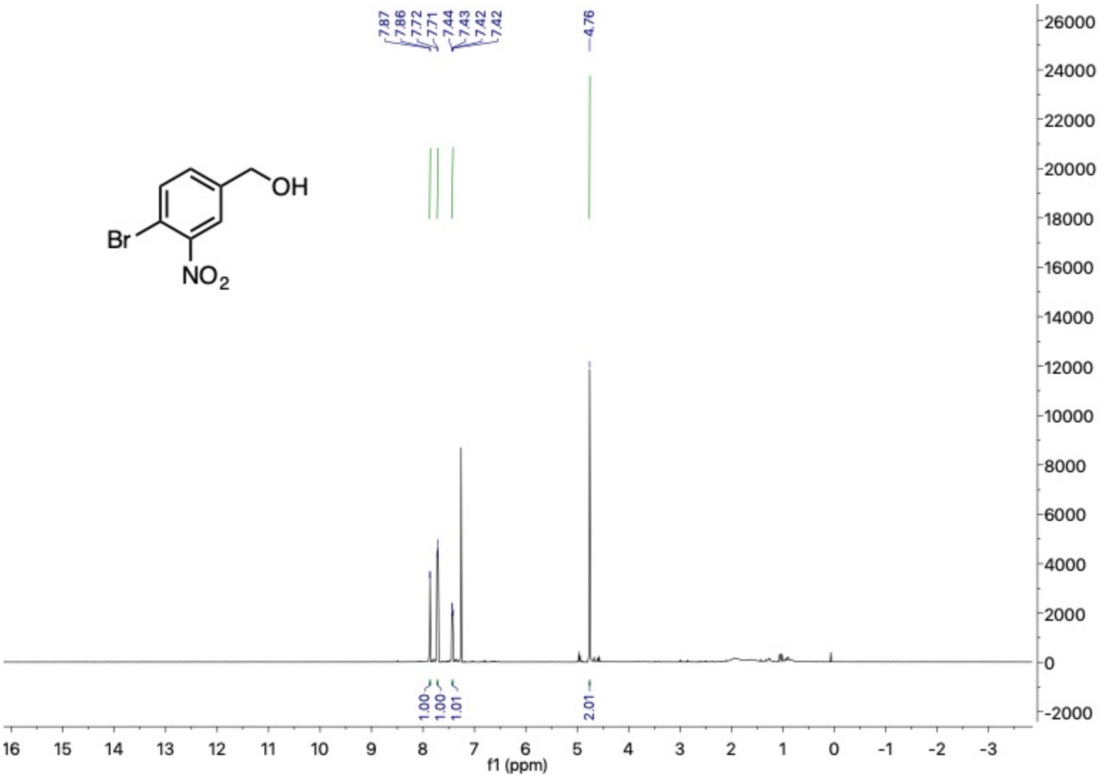
7.87
7.86
7.72
7.71
7.44
7.43
7.42
7.42
4.76
OH
Br
NO2
1.00
1.00
1.01
2.01
26000
24000
22000
20000
18000
16000
14000
12000
10000
8000
6000
4000
2000
0
-2000
16 15 14 13 12 11 10 9 8 7 6 5 4 3 2 1 0 -1 -2 -3
f1 (ppm)

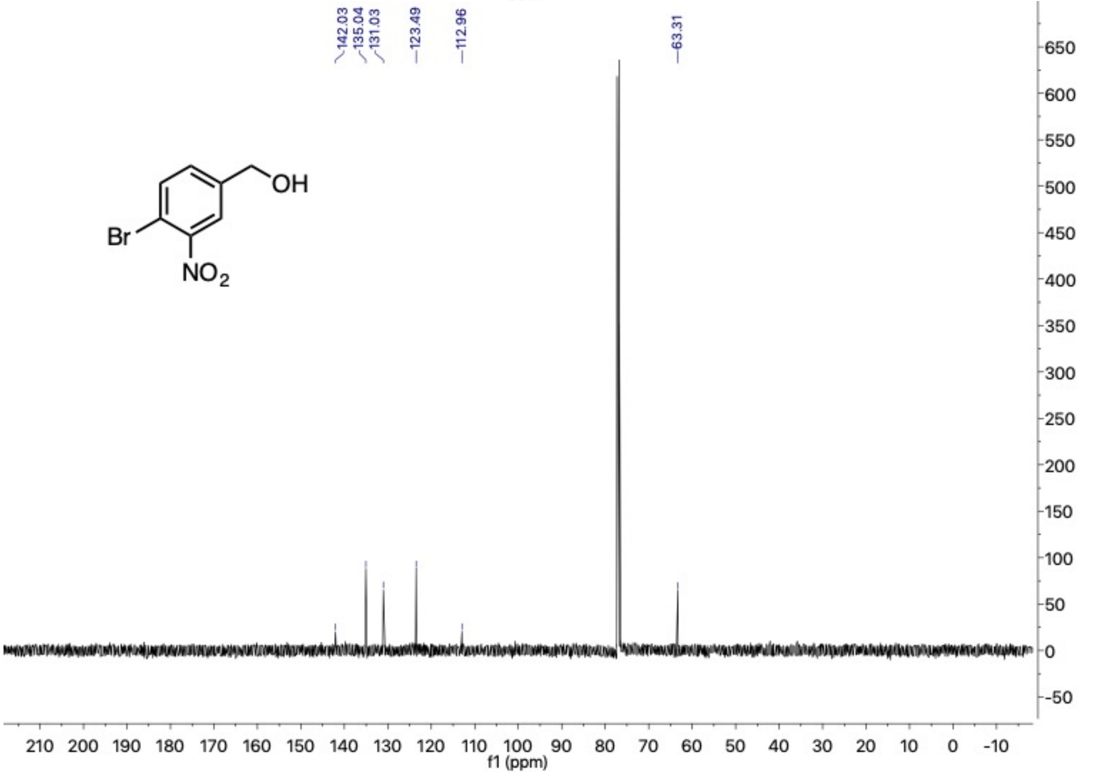
142.03
135.04
131.03
123.49
112.96
63.31
OH
Br
NO2
650
600
550
500
450
400
350
300
250
200
150
100
50
0
-50
210 200 190 180 170 160 150 140 130 120 110 100 90 80 70 60 50 40 30 20 10 0 -10
f1 (ppm)

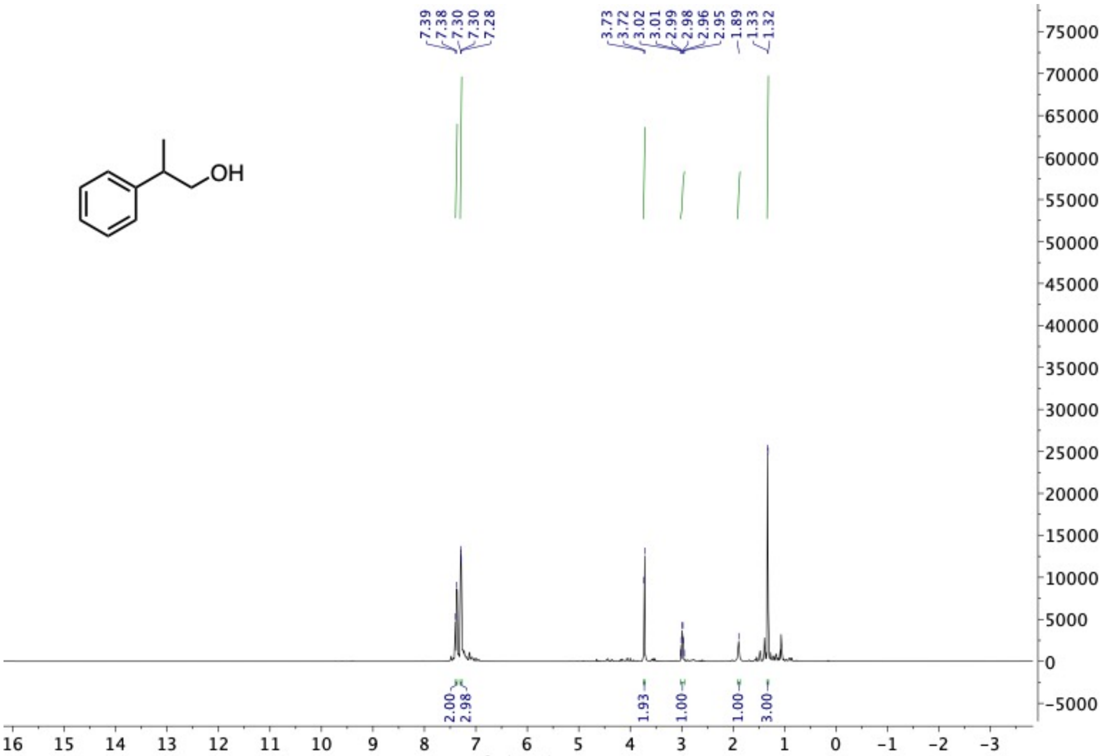
7.39
7.38
7.30
7.30
7.30
7.28
3.73
3.72
3.02
3.01
2.99
2.98
2.96
2.95
1.89
1.33
1.32
OH
2.00
2.98
1.93
1.00
1.00
3.00
75000
70000
65000
60000
55000
50000
45000
40000
35000
30000
25000
20000
15000
10000
5000
0
−5000
16 15 14 13 12 11 10 9 8 7 6 5 4 3 2 1 0 −1 −2 −3
f1 (ppm)

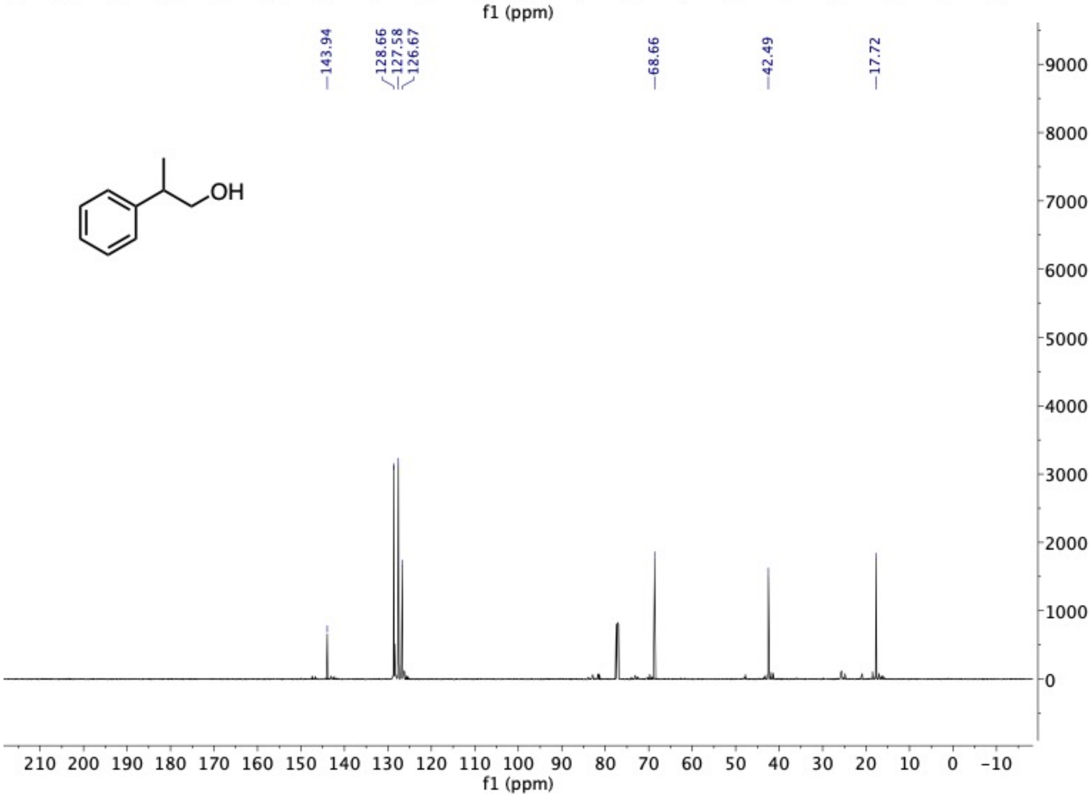
143.94
128.66
127.58
126.67
68.66
42.49
17.72
OH
9000
8000
7000
6000
5000
4000
3000
2000
1000
0
210 200 190 180 170 160 150 140 130 120 110 100 90 80 70 60 50 40 30 20 10 0 −10
f1 (ppm)

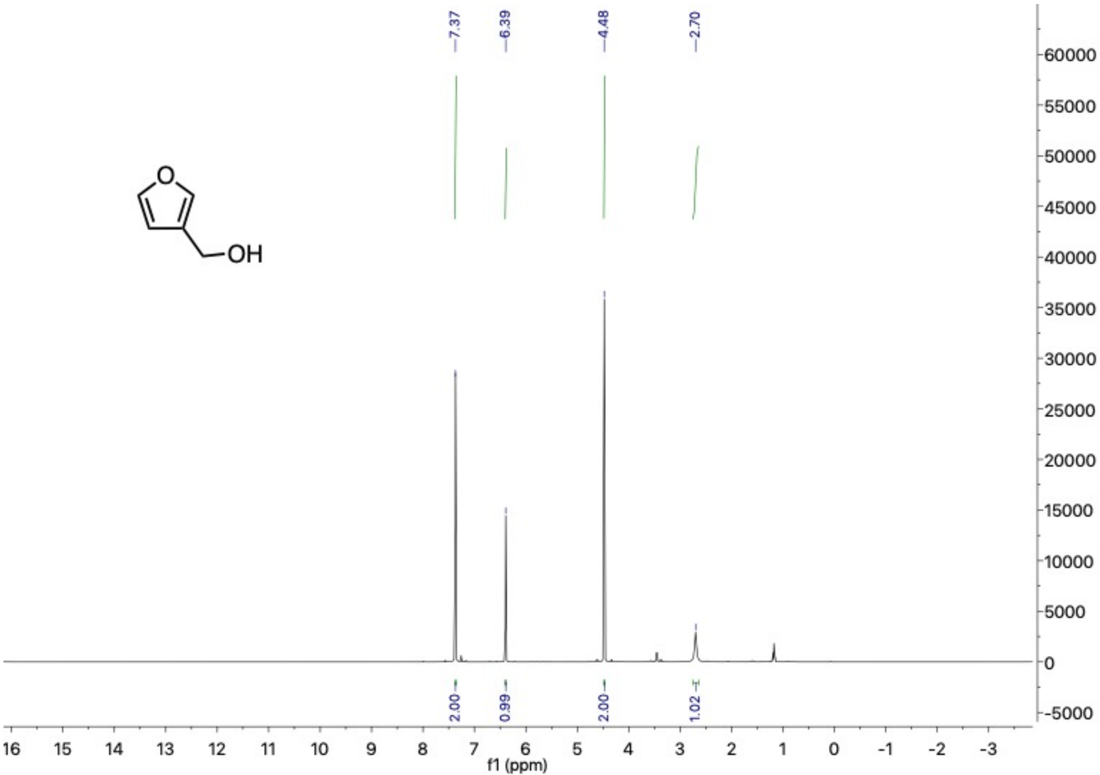

7.37
6.39
4.48
2.70
OH
2.00
0.99
2.00
1.02
60000
55000
50000
45000
40000
35000
30000
25000
20000
15000
10000
5000
0
-5000
16 15 14 13 12 11 10 9 8 7 6 5 4 3 2 1 0 -1 -2 -3
f1 (ppm)

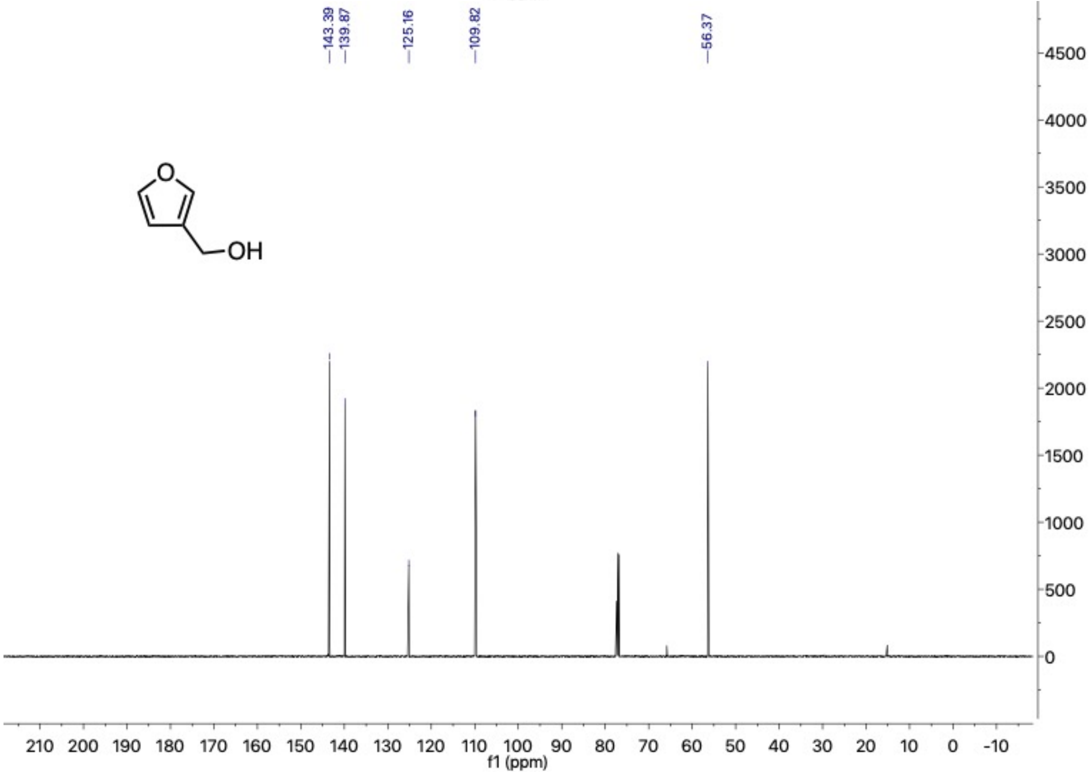

143.39
139.87
125.16
109.82
56.37
OH
4500
4000
3500
3000
2500
2000
1500
1000
500
0
210 200 190 180 170 160 150 140 130 120 110 100 90 80 70 60 50 40 30 20 10 0 -10
f1 (ppm)

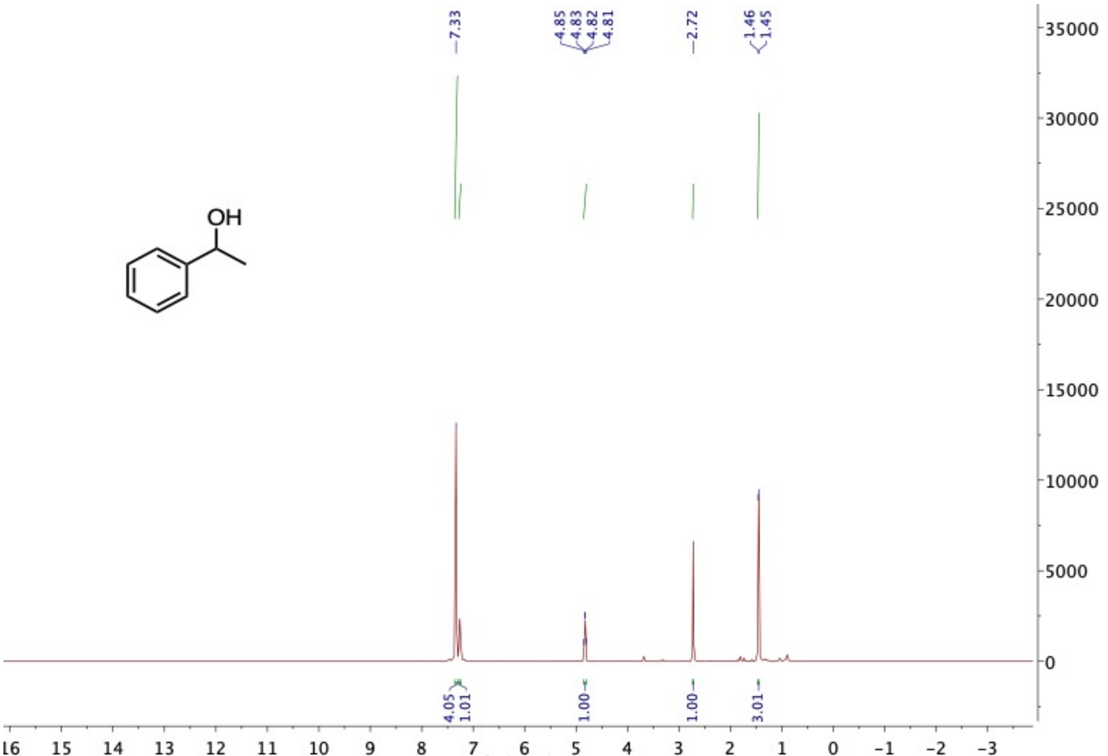
7.33
4.85
4.83
4.82
4.81
2.72
1.46
1.45
OH
4.05
1.01
1.00
1.00
3.01
35000
30000
25000
20000
15000
10000
5000
0
16 15 14 13 12 11 10 9 8 7 6 5 4 3 2 1 0 −1 −2 −3
f1 (ppm)

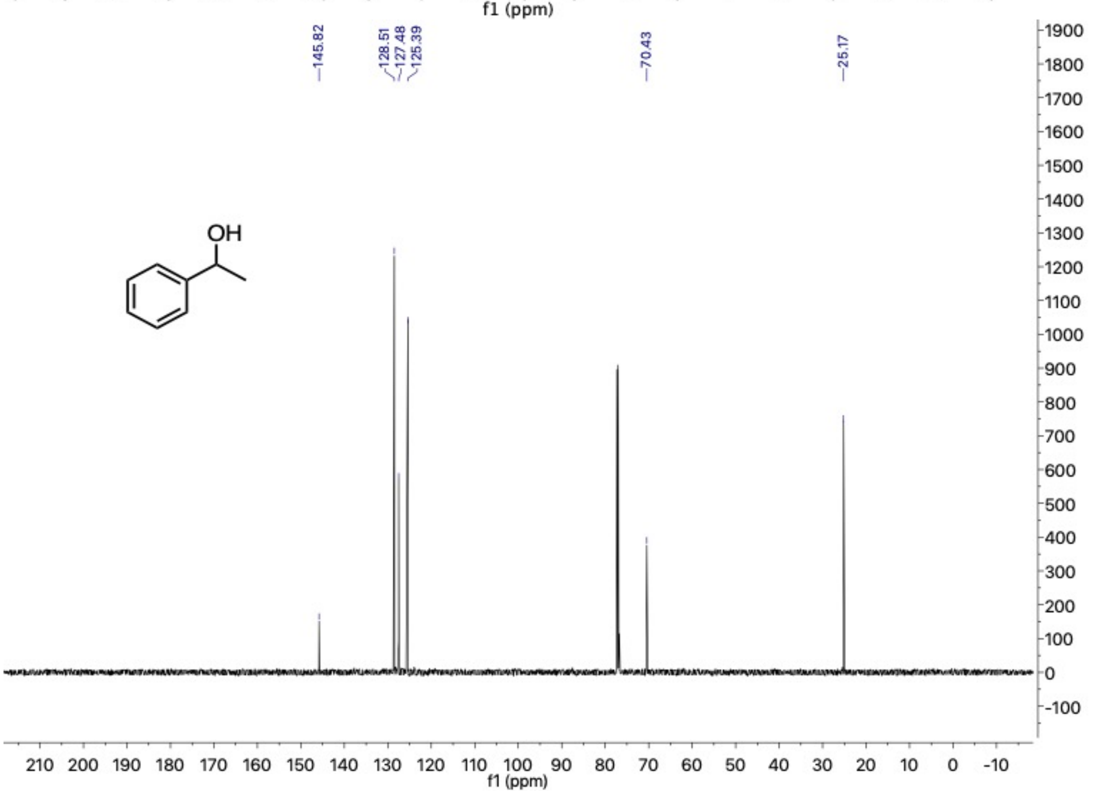
145.82
128.51
127.48
125.39
70.43
25.17
OH
1900
1800
1700
1600
1500
1400
1300
1200
1100
1000
900
800
700
600
500
400
300
200
100
0
-100
210 200 190 180 170 160 150 140 130 120 110 100 90 80 70 60 50 40 30 20 10 0 -10
f1 (ppm)

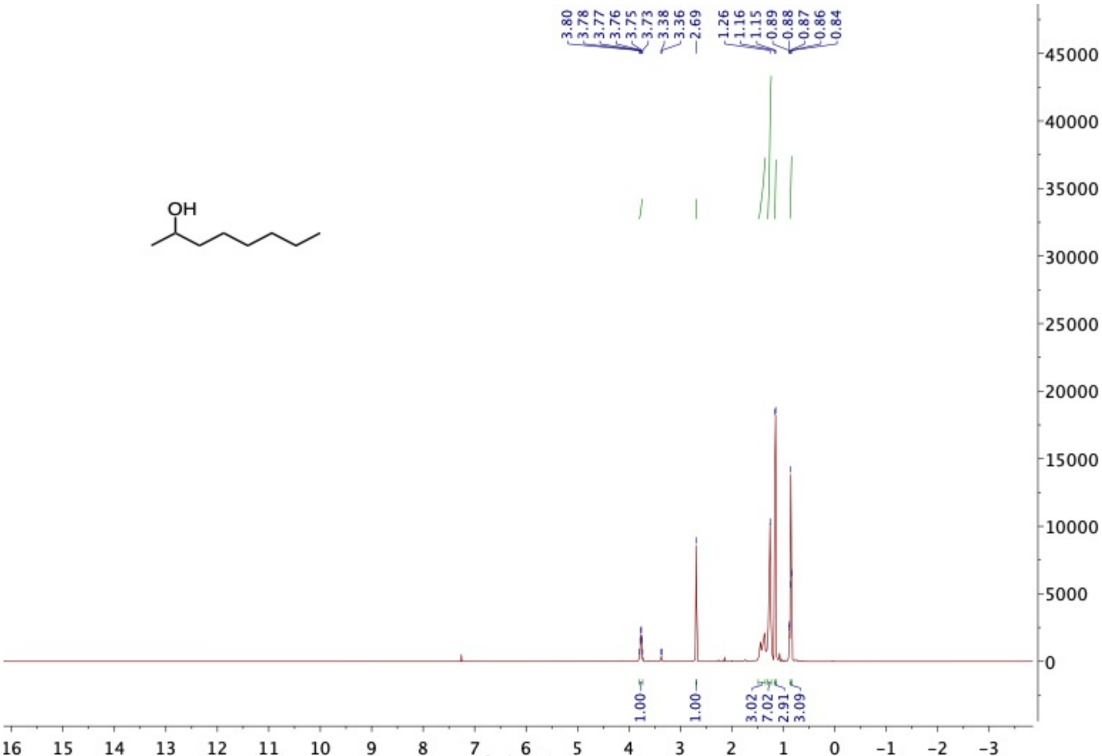
OH
3.80
3.78
3.77
3.76
3.75
3.73
3.38
3.36
2.69
1.26
1.16
1.15
0.89
0.88
0.87
0.86
0.84
1.00
1.00
3.02
7.02
2.91
3.09
45000
40000
35000
30000
25000
20000
15000
10000
5000
0
16 15 14 13 12 11 10 9 8 7 6 5 4 3 2 1 0 −1 −2 −3
f1 (ppm)

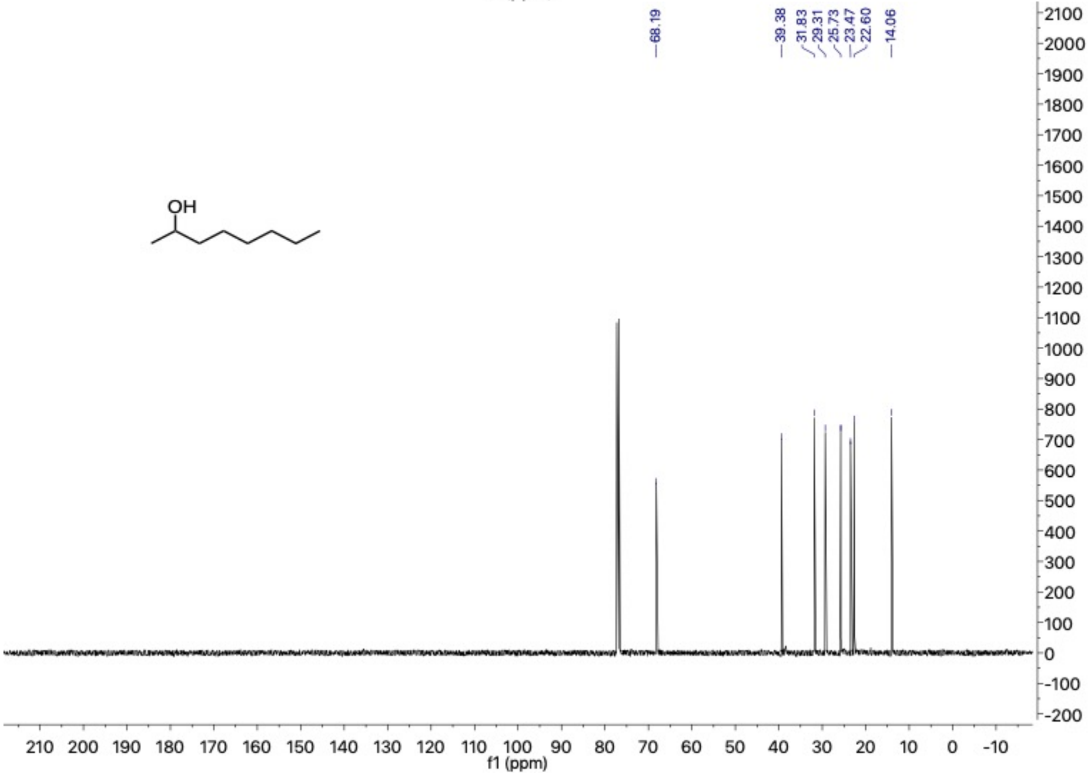
OH
68.19
39.38
31.83
29.31
25.73
23.47
22.60
14.06
2100
2000
1900
1800
1700
1600
1500
1400
1300
1200
1100
1000
900
800
700
600
500
400
300
200
100
0
−100
−200
210 200 190 180 170 160 150 140 130 120 110 100 90 80 70 60 50 40 30 20 10 0 −10
f1 (ppm)

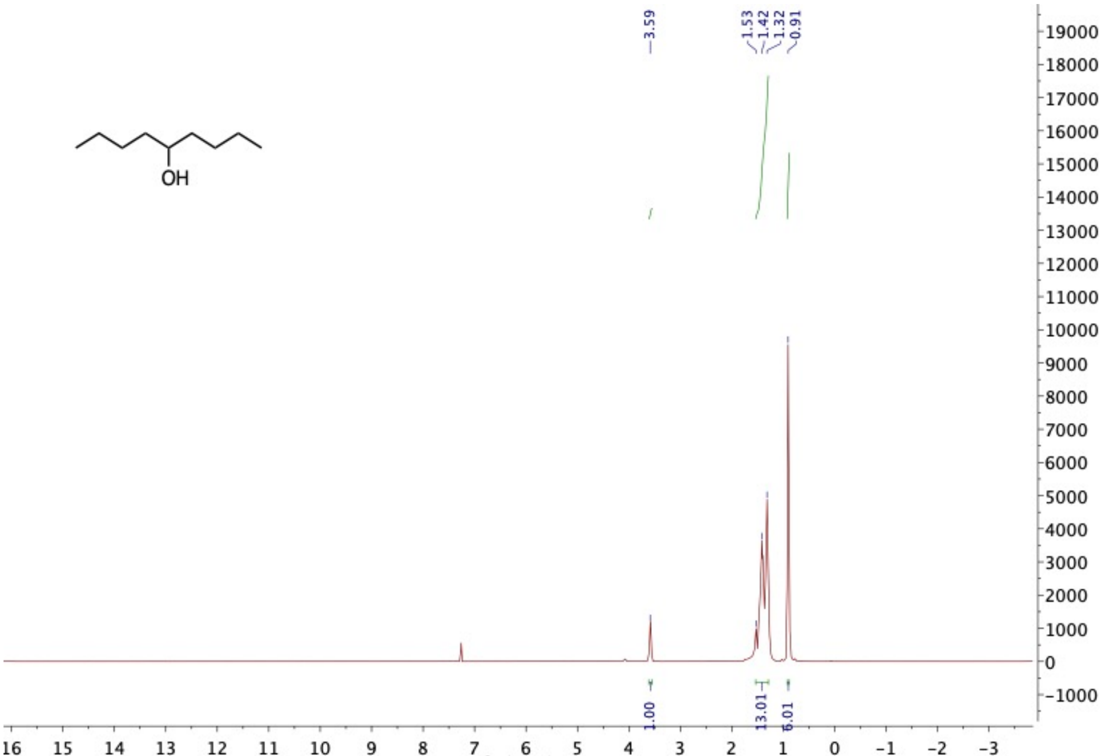
OH
3.59
1.53
1.42
1.32
0.91
1.00
13.01
6.01
19000
18000
17000
16000
15000
14000
13000
12000
11000
10000
9000
8000
7000
6000
5000
4000
3000
2000
1000
0
−1000
16 15 14 13 12 11 10 9 8 7 6 5 4 3 2 1 0 −1 −2 −3
f1 (ppm)

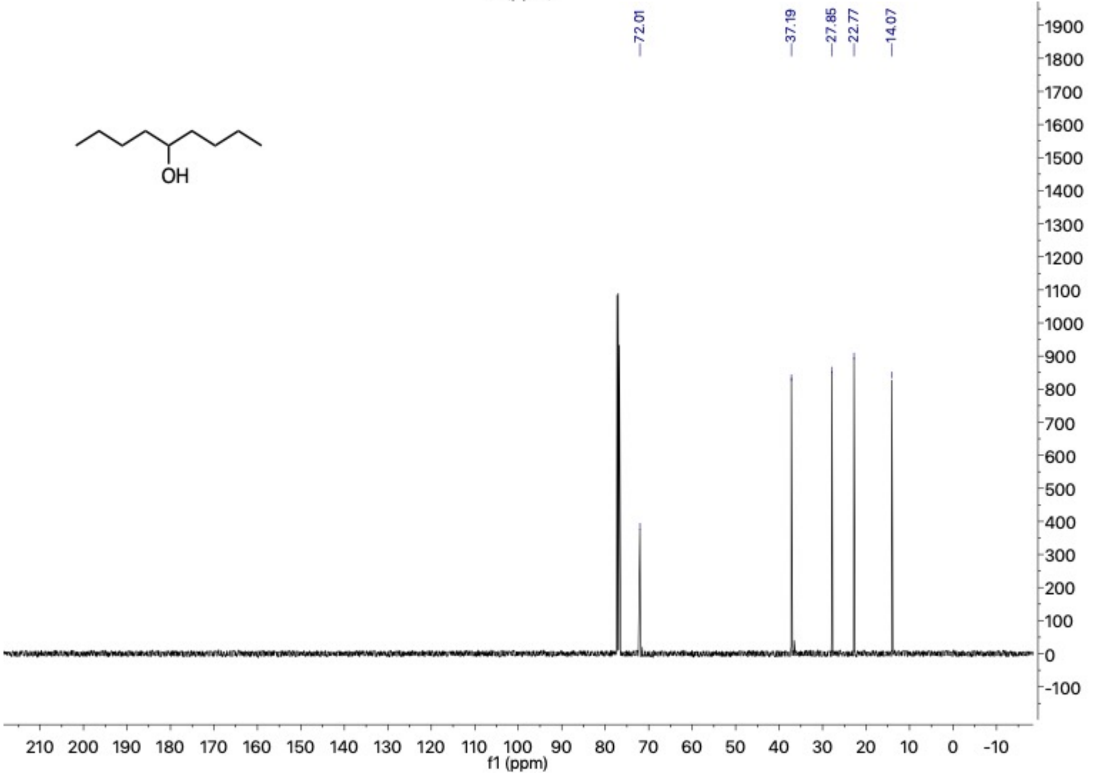
OH
72.01
37.19
27.85
22.77
14.07
1900
1800
1700
1600
1500
1400
1300
1200
1100
1000
900
800
700
600
500
400
300
200
100
0
−100
210 200 190 180 170 160 150 140 130 120 110 100 90 80 70 60 50 40 30 20 10 0 −10
f1 (ppm)

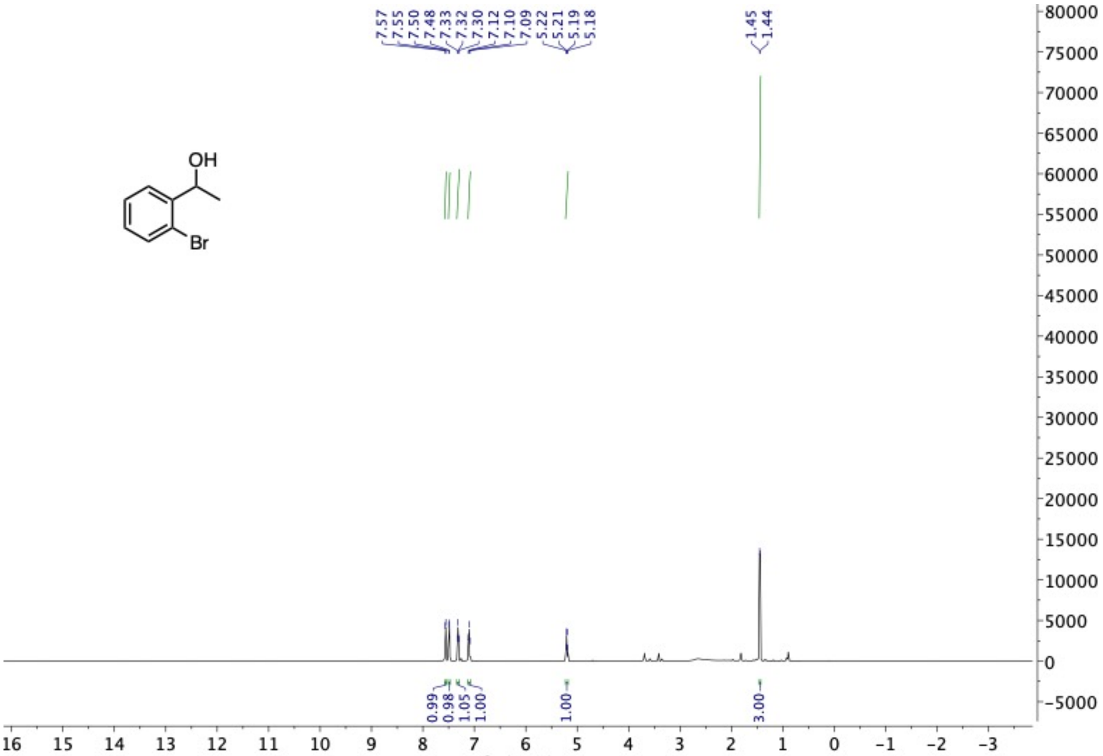
7.57
7.55
7.50
7.48
7.33
7.32
7.30
7.12
7.10
7.09
5.22
5.21
5.19
5.18
1.45
1.44
OH
Br
0.99
0.98
1.05
1.00
1.00
3.00
f1 (ppm)

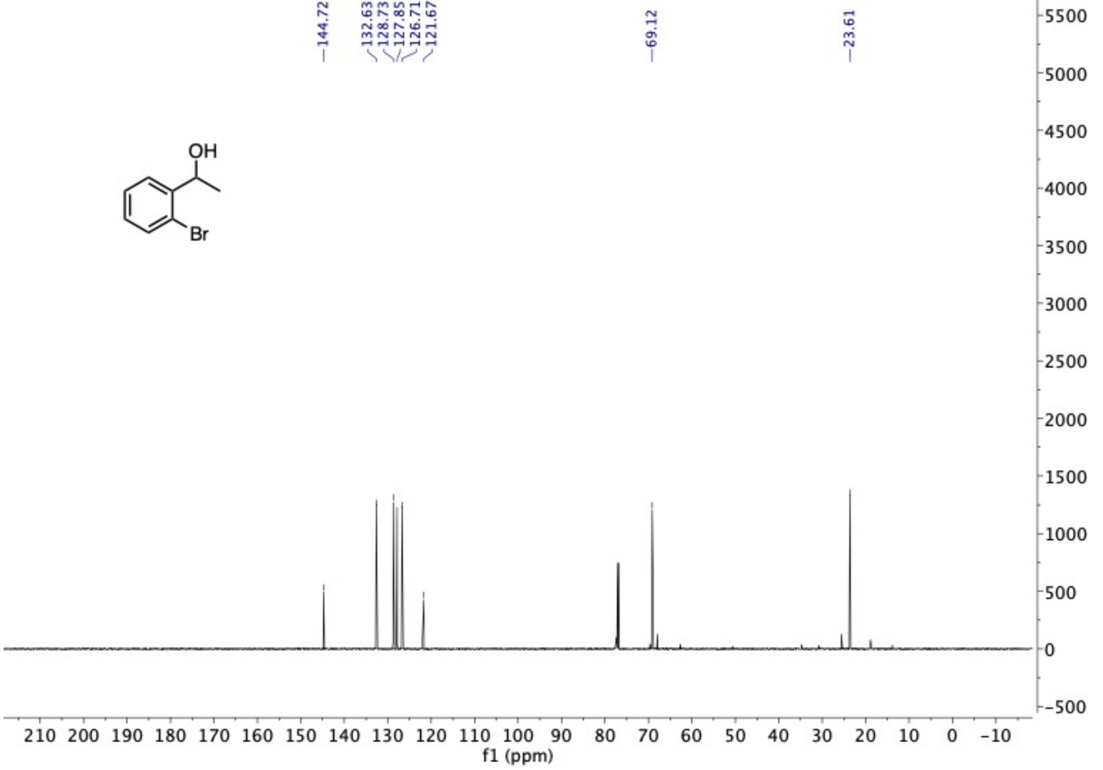
144.72
132.63
128.73
127.85
126.71
121.67
69.12
23.61
OH
Br
f1 (ppm)

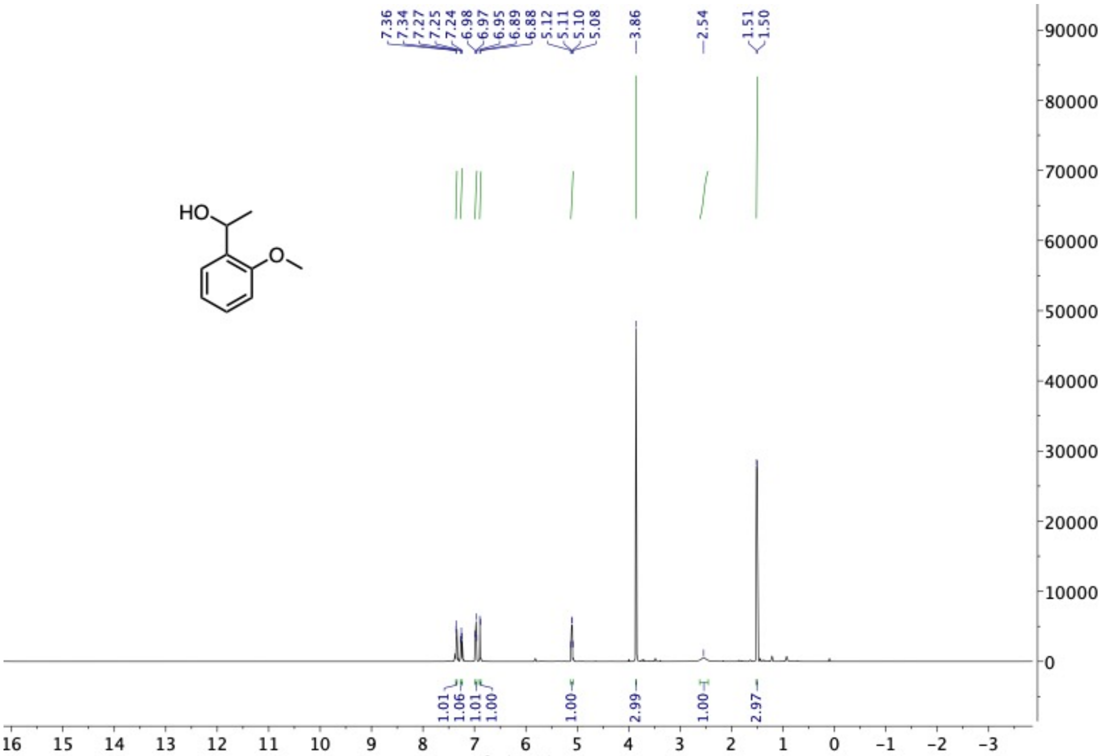
7.36
7.34
7.27
7.25
7.24
6.98
6.97
6.95
6.89
6.88
5.12
5.11
5.10
5.08
3.86
2.54
1.51
1.50
HO
O
1.01
1.06
1.01
1.00
1.00
2.99
1.00
2.97
90000
80000
70000
60000
50000
40000
30000
20000
10000
0
16 15 14 13 12 11 10 9 8 7 6 5 4 3 2 1 0 −1 −2 −3
f1 (ppm)

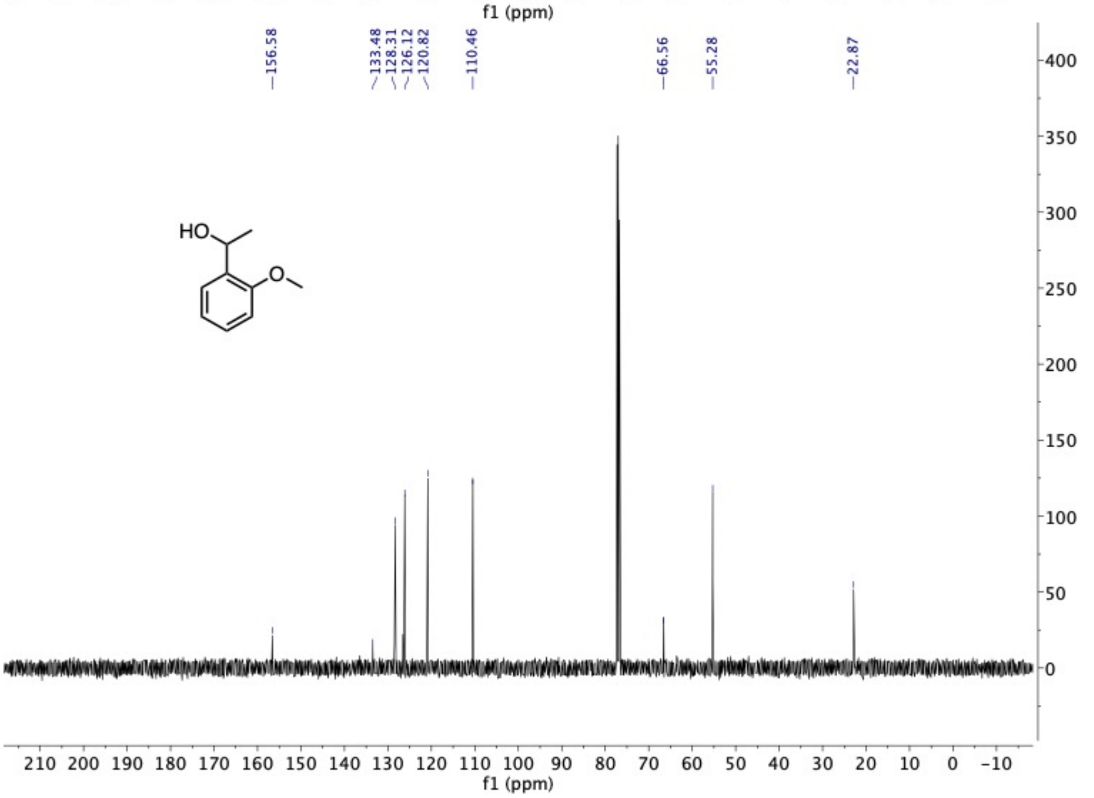
156.58
133.48
128.31
126.12
120.82
110.46
66.56
55.28
22.87
HO
O
400
350
300
250
200
150
100
50
0
210 200 190 180 170 160 150 140 130 120 110 100 90 80 70 60 50 40 30 20 10 0 −10
f1 (ppm)

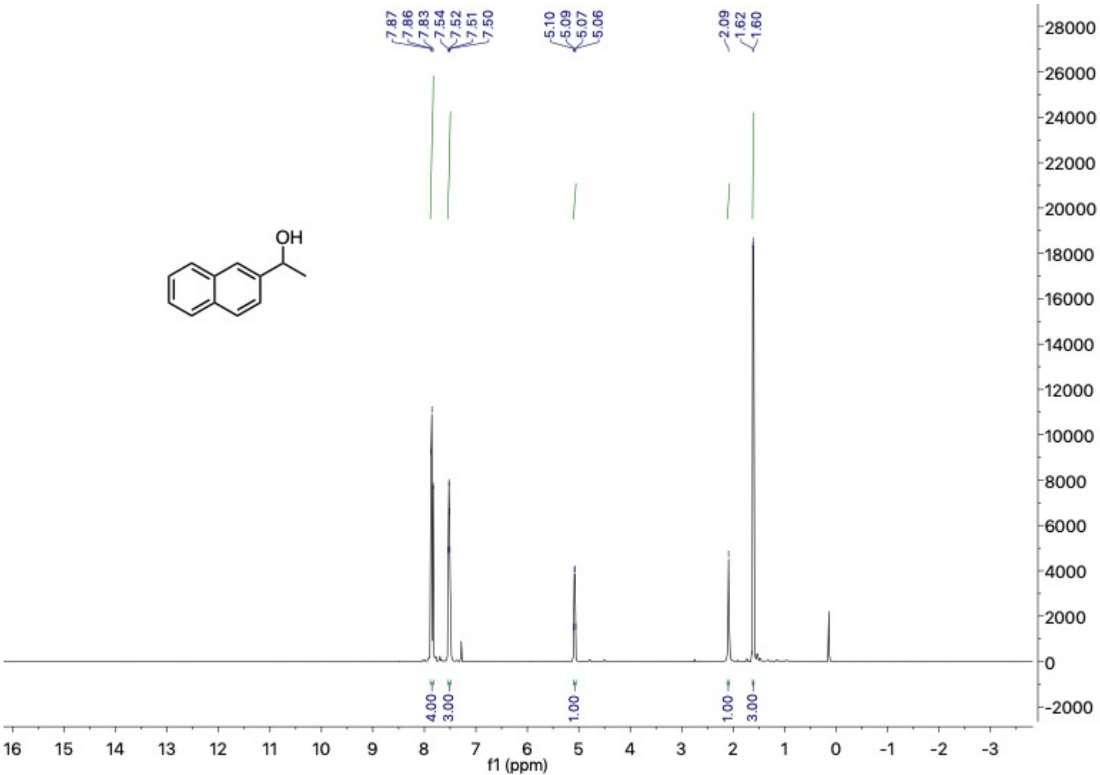
7.87
7.86
7.83
7.54
7.52
7.51
7.50
5.10
5.09
5.07
5.06
2.09
1.62
1.60
OH
4.00
3.00
1.00
1.00
3.00
28000
26000
24000
22000
20000
18000
16000
14000
12000
10000
8000
6000
4000
2000
0
-2000
16 15 14 13 12 11 10 9 8 7 6 5 4 3 2 1 0 -1 -2 -3
f1 (ppm)

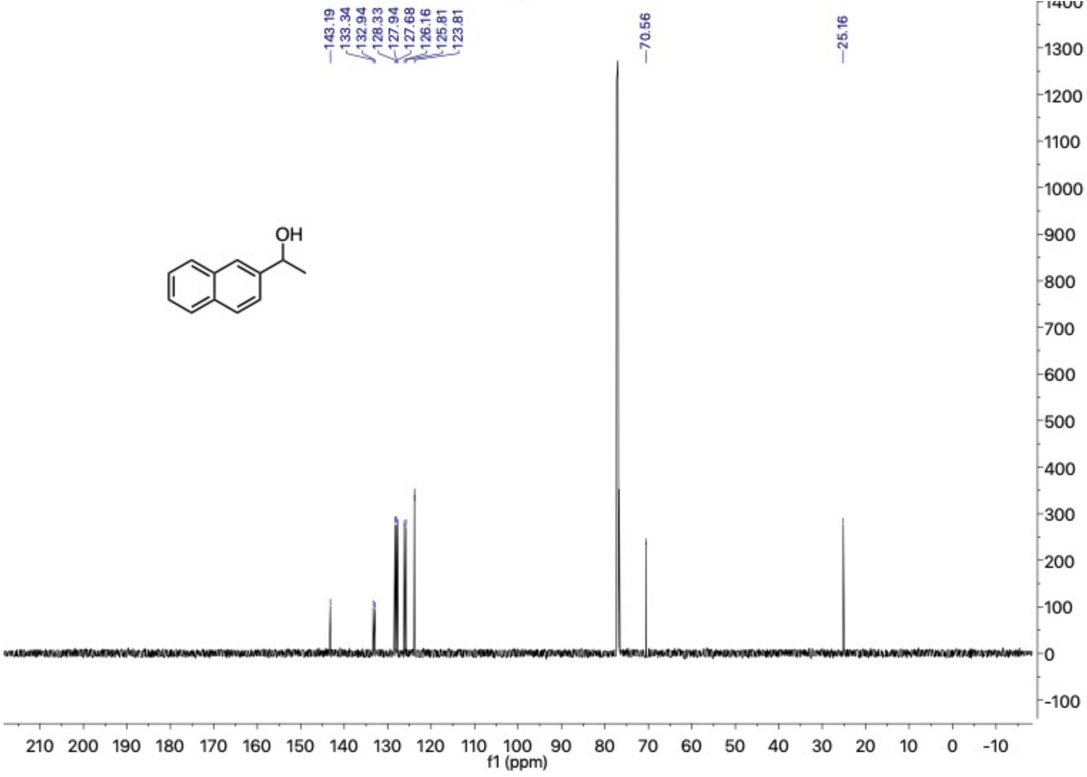
143.19
133.34
132.94
128.33
127.94
127.68
126.16
125.81
123.81
70.56
25.16
OH
1400
1300
1200
1100
1000
900
800
700
600
500
400
300
200
100
0
-100
210 200 190 180 170 160 150 140 130 120 110 100 90 80 70 60 50 40 30 20 10 0 -10
f1 (ppm)

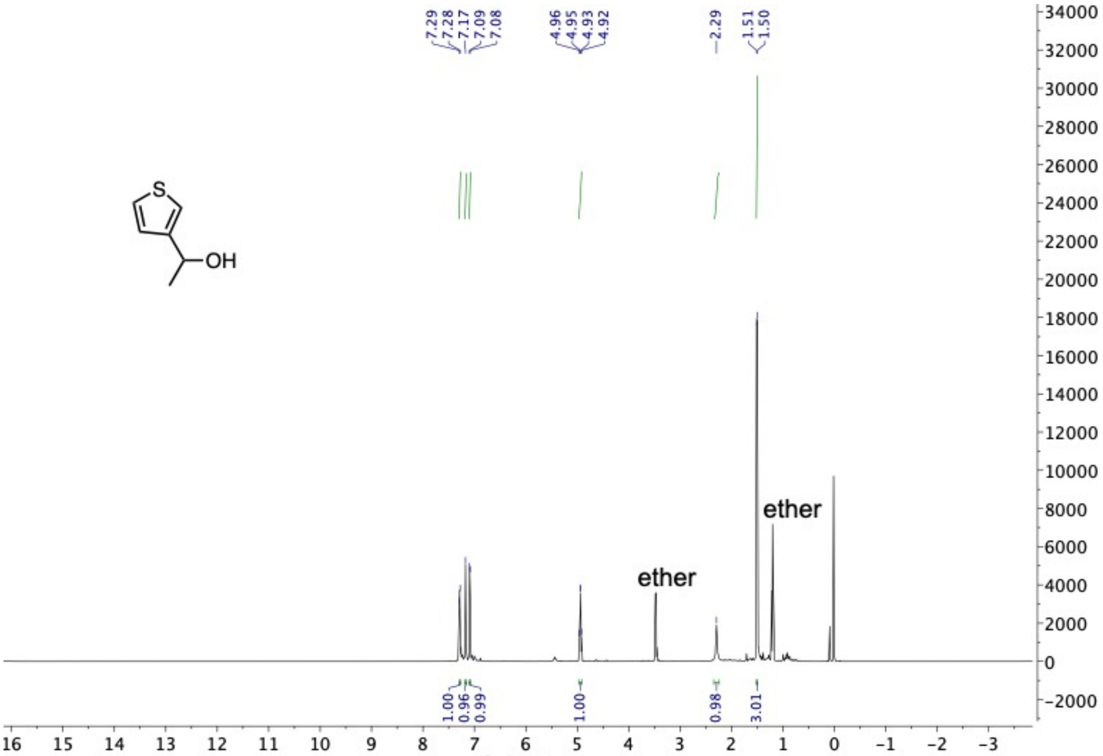
7.29
7.28
7.17
7.09
7.08
4.96
4.95
4.93
4.92
2.29
1.51
1.50
S
OH
ether
ether
1.00
0.96
0.99
1.00
0.98
3.01
34000
32000
30000
28000
26000
24000
22000
20000
18000
16000
14000
12000
10000
8000
6000
4000
2000
0
−2000
16 15 14 13 12 11 10 9 8 7 6 5 4 3 2 1 0 −1 −2 −3
f1 (ppm)

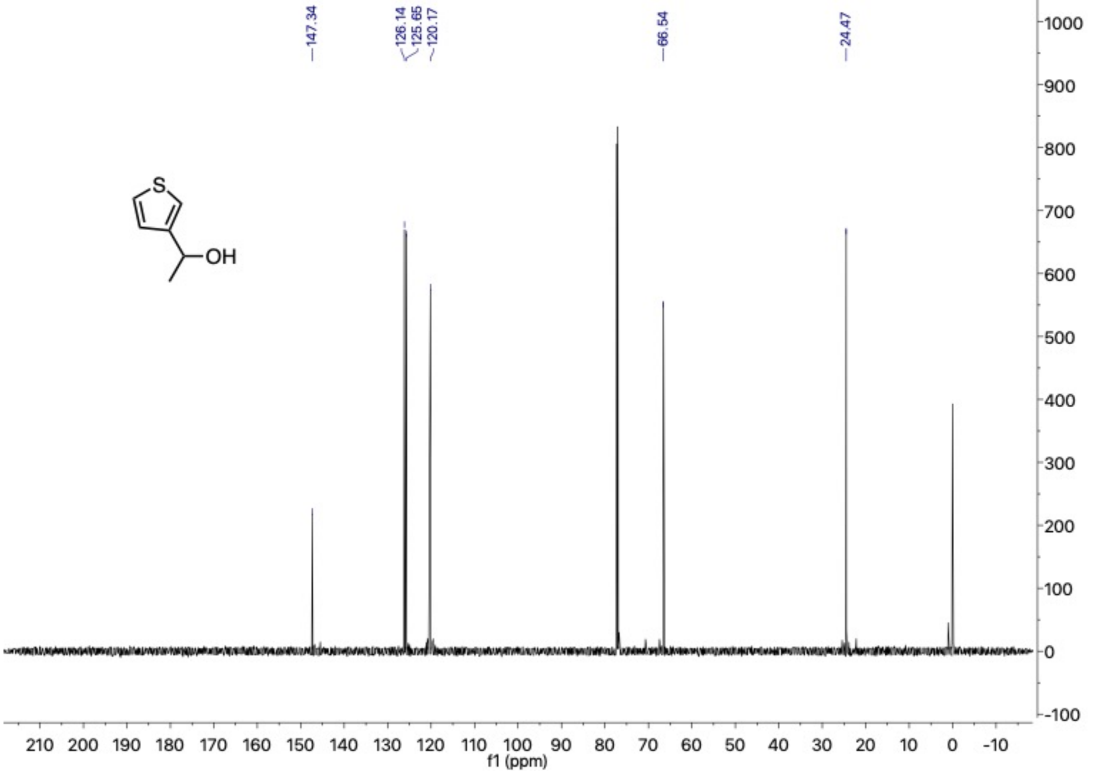
147.34
126.14
125.65
120.17
66.54
24.47
S
OH
1000
900
800
700
600
500
400
300
200
100
0
−100
210 200 190 180 170 160 150 140 130 120 110 100 90 80 70 60 50 40 30 20 10 0 −10
f1 (ppm)

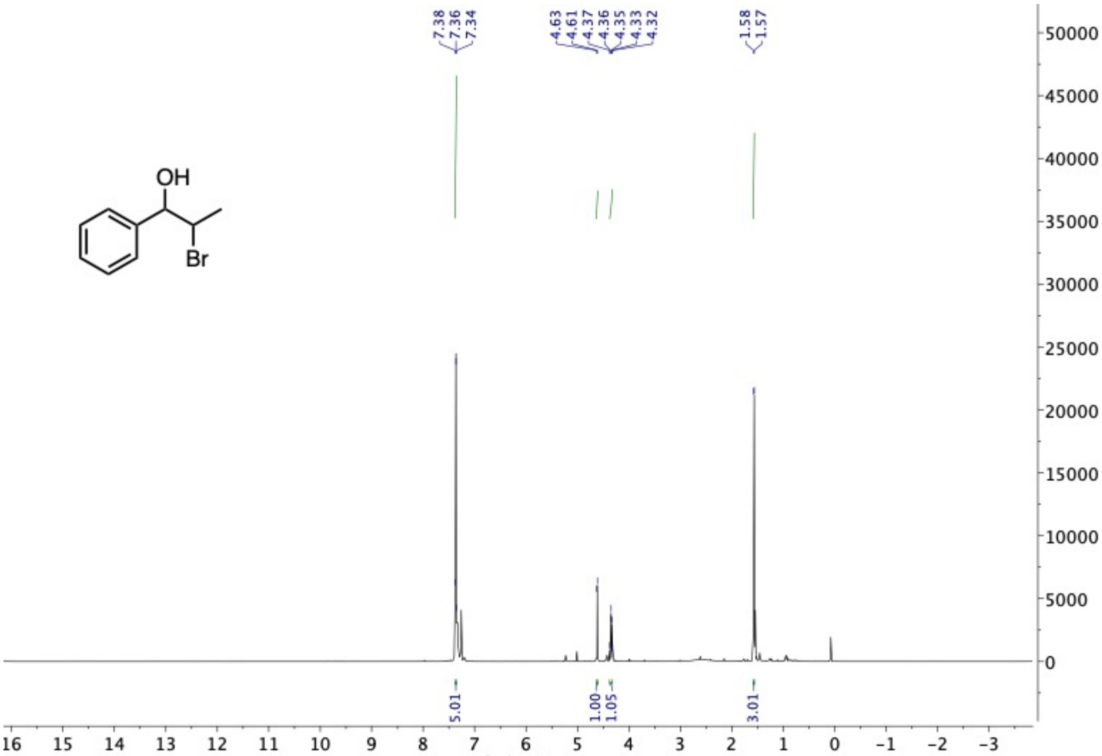
7.38
7.36
7.34
4.63
4.61
4.37
4.36
4.35
4.33
4.32
1.58
1.57
OH
Br
5.01
1.00
1.05
3.01
50000
45000
40000
35000
30000
25000
20000
15000
10000
5000
0
16 15 14 13 12 11 10 9 8 7 6 5 4 3 2 1 0 −1 −2 −3
f1 (ppm)

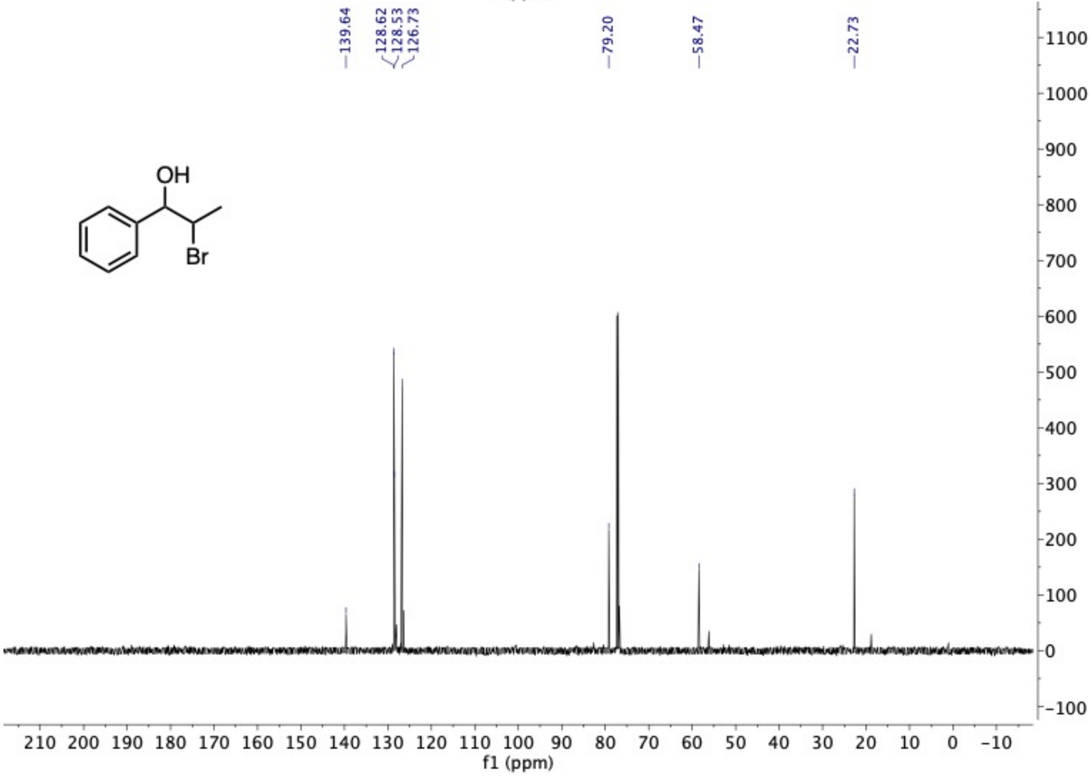
139.64
128.62
128.53
126.73
79.20
58.47
22.73
OH
Br
1100
1000
900
800
700
600
500
400
300
200
100
0
−100
210 200 190 180 170 160 150 140 130 120 110 100 90 80 70 60 50 40 30 20 10 0 −10
f1 (ppm)

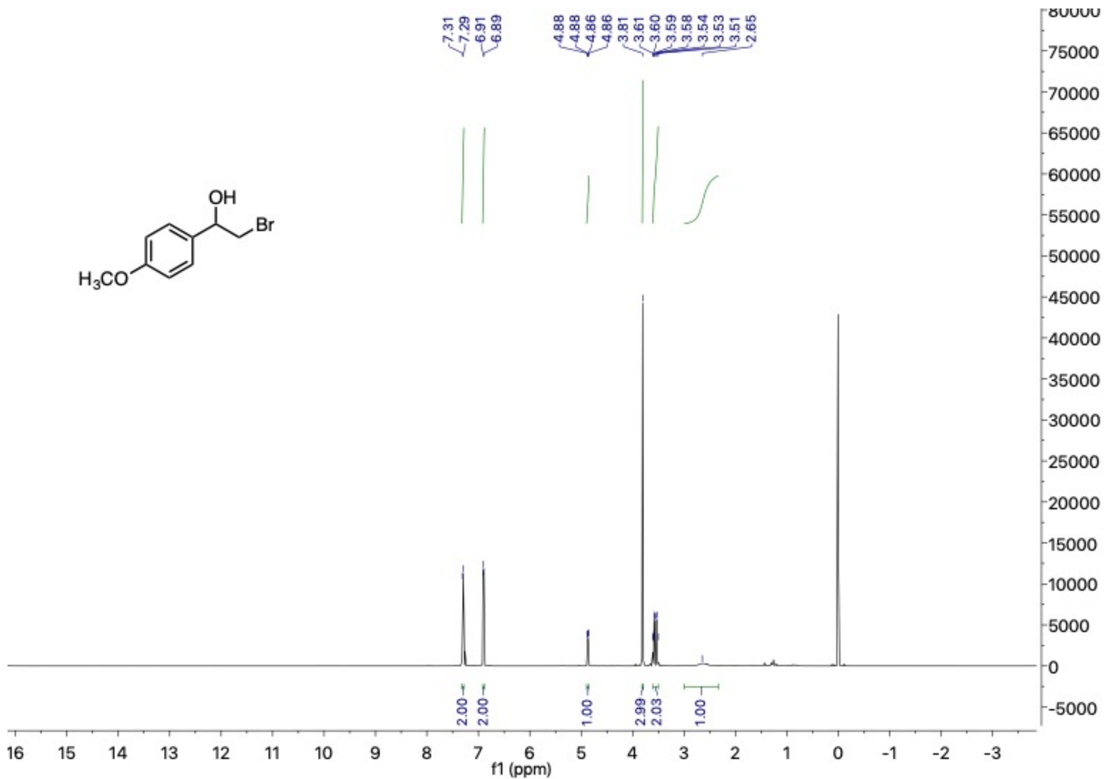
7.31
7.29
6.91
6.89
4.88
4.88
4.86
4.86
3.81
3.61
3.60
3.59
3.58
3.54
3.53
3.51
2.65
OH
Br
H3CO
2.00
2.00
1.00
2.99
2.03
1.00
f1 (ppm)
16 15 14 13 12 11 10 9 8 7 6 5 4 3 2 1 0 -1 -2 -3
80000 75000 70000 65000 60000 55000 50000 45000 40000 35000 30000 25000 20000 15000 10000 5000 0 -5000

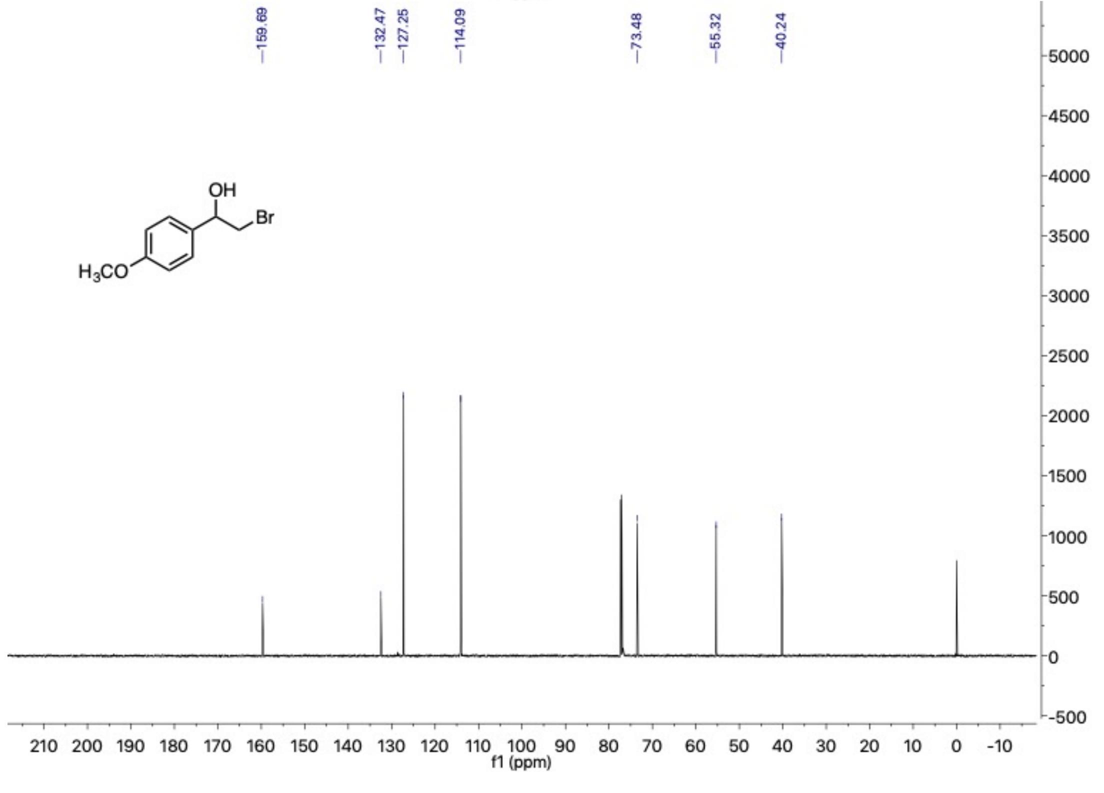
159.69
132.47
127.25
114.09
73.48
55.32
40.24
OH
Br
H3CO
f1 (ppm)
210 200 190 180 170 160 150 140 130 120 110 100 90 80 70 60 50 40 30 20 10 0 -10
5000 4500 4000 3500 3000 2500 2000 1500 1000 500 0 -500

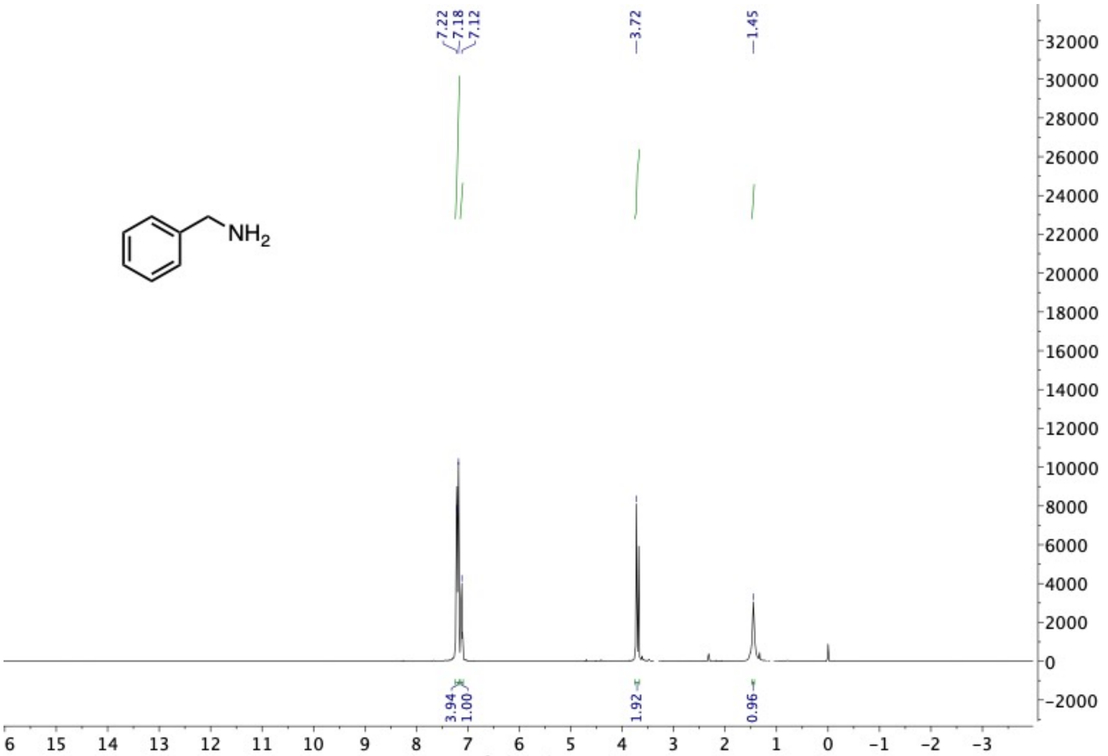
7.22
7.18
7.12
3.72
1.45
NH2
3.94
1.00
1.92
0.96
32000
30000
28000
26000
24000
22000
20000
18000
16000
14000
12000
10000
8000
6000
4000
2000
0
−2000
6 15 14 13 12 11 10 9 8 7 6 5 4 3 2 1 0 −1 −2 −3
f1 (ppm)

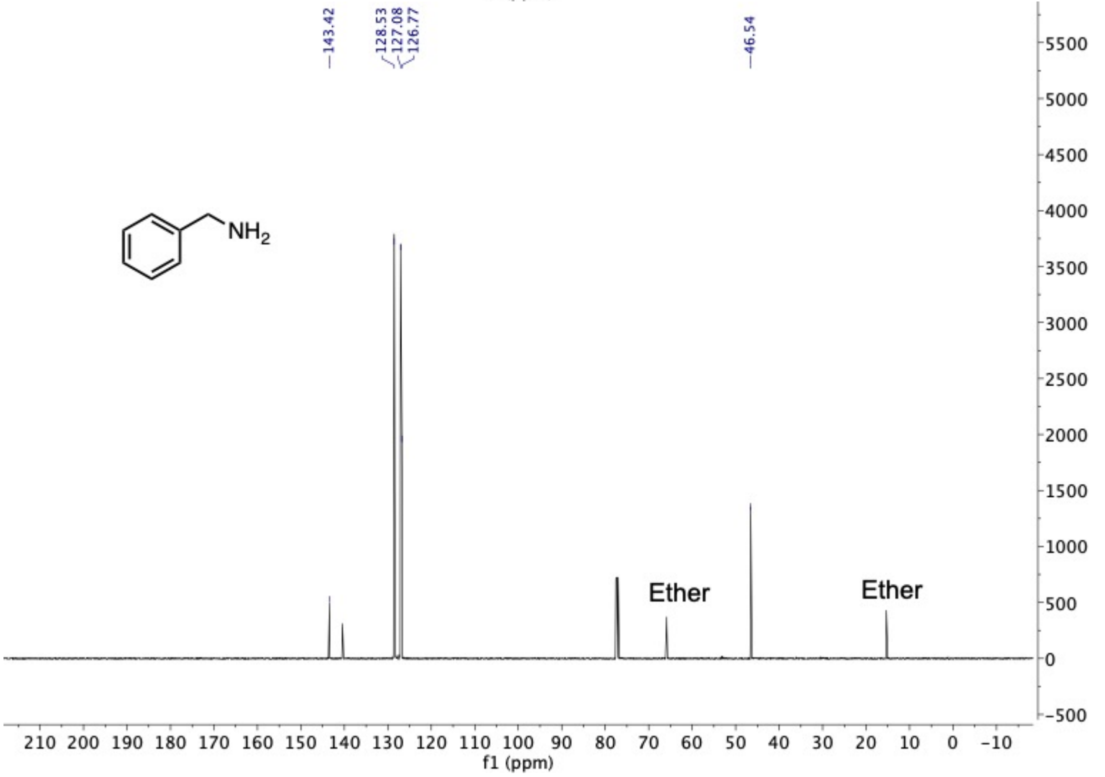
143.42
128.53
127.08
126.77
46.54
NH2
Ether
Ether
5500
5000
4500
4000
3500
3000
2500
2000
1500
1000
500
0
−500
210 200 190 180 170 160 150 140 130 120 110 100 90 80 70 60 50 40 30 20 10 0 −10
f1 (ppm)

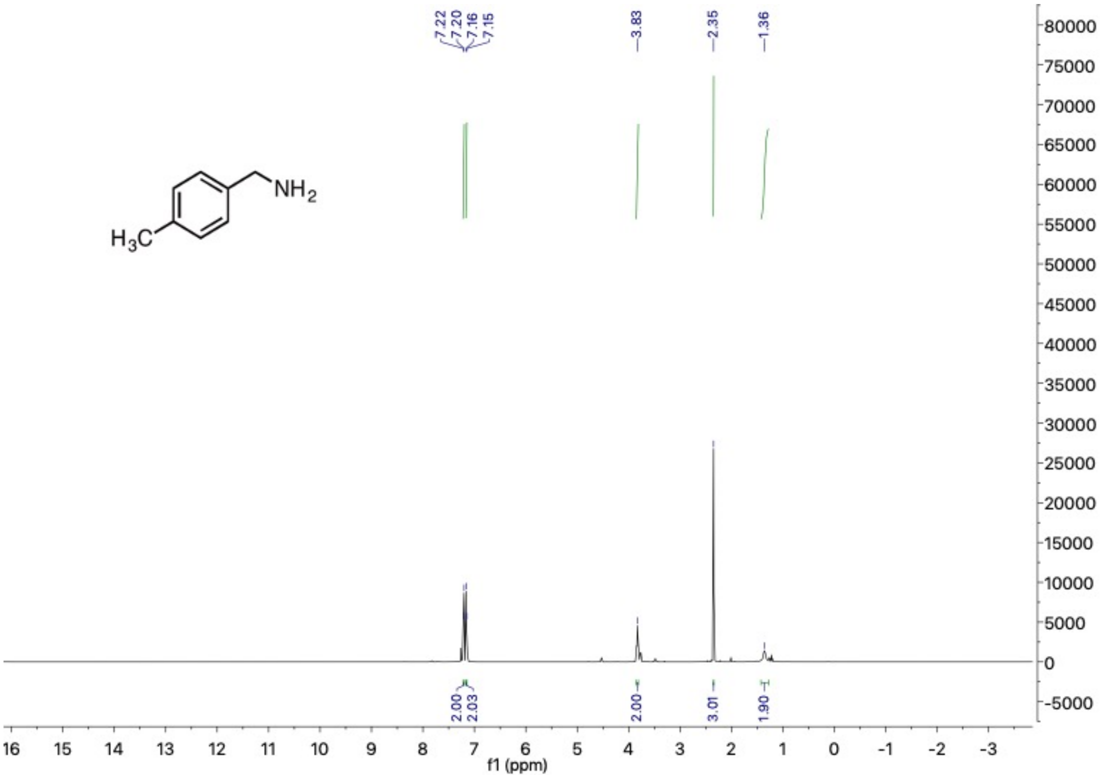
7.22
7.20
7.16
7.15
3.83
2.35
1.36
NH2
H3C
2.00
2.03
2.00
3.01
1.90
80000
75000
70000
65000
60000
55000
50000
45000
40000
35000
30000
25000
20000
15000
10000
5000
0
-5000
16 15 14 13 12 11 10 9 8 7 6 5 4 3 2 1 0 -1 -2 -3
f1 (ppm)

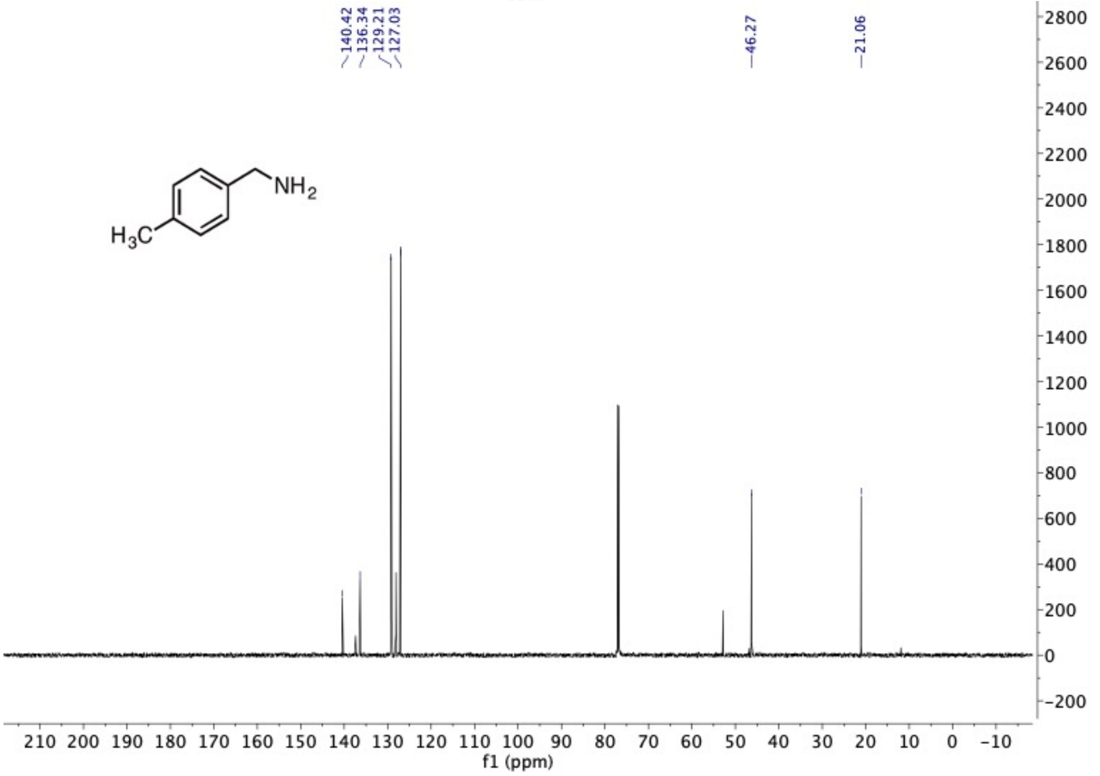
140.42
136.34
129.21
127.03
46.27
21.06
NH2
H3C
2800
2600
2400
2200
2000
1800
1600
1400
1200
1000
800
600
400
200
0
-200
210 200 190 180 170 160 150 140 130 120 110 100 90 80 70 60 50 40 30 20 10 0 -10
f1 (ppm)

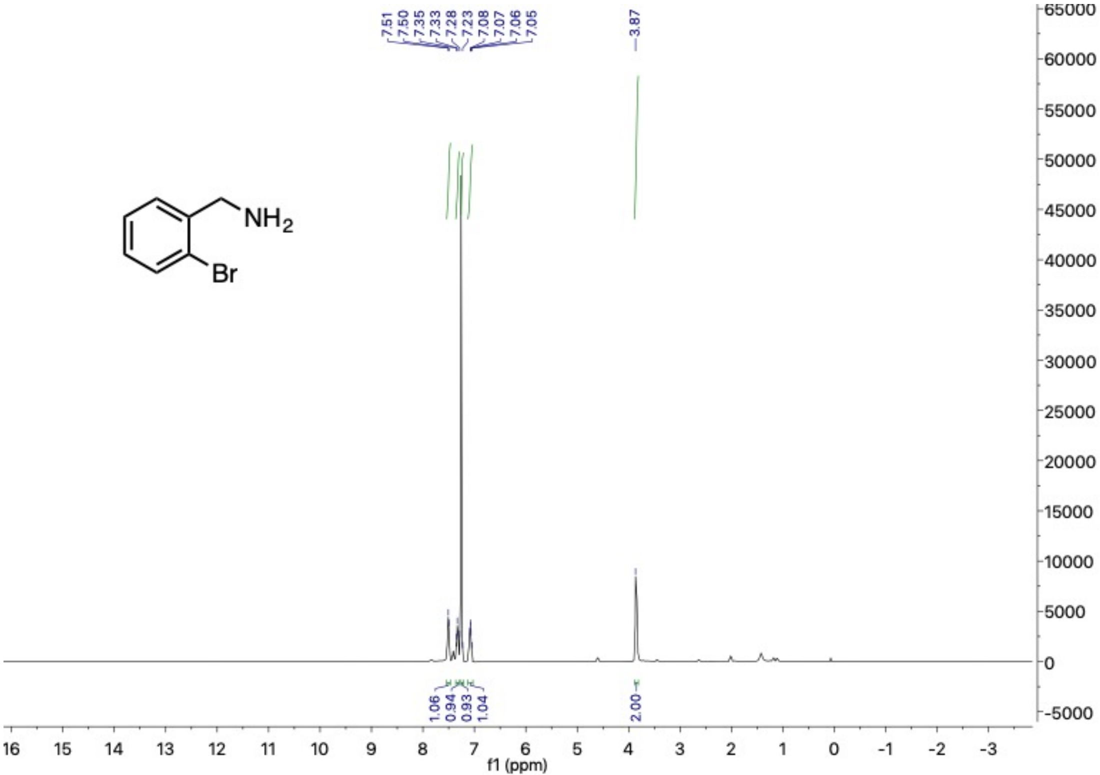
7.51
7.50
7.35
7.33
7.28
7.23
7.08
7.07
7.06
7.05
3.87
NH2
Br
1.06
0.94
0.93
1.04
2.00
65000
60000
55000
50000
45000
40000
35000
30000
25000
20000
15000
10000
5000
0
-5000
16 15 14 13 12 11 10 9 8 7 6 5 4 3 2 1 0 -1 -2 -3
f1 (ppm)

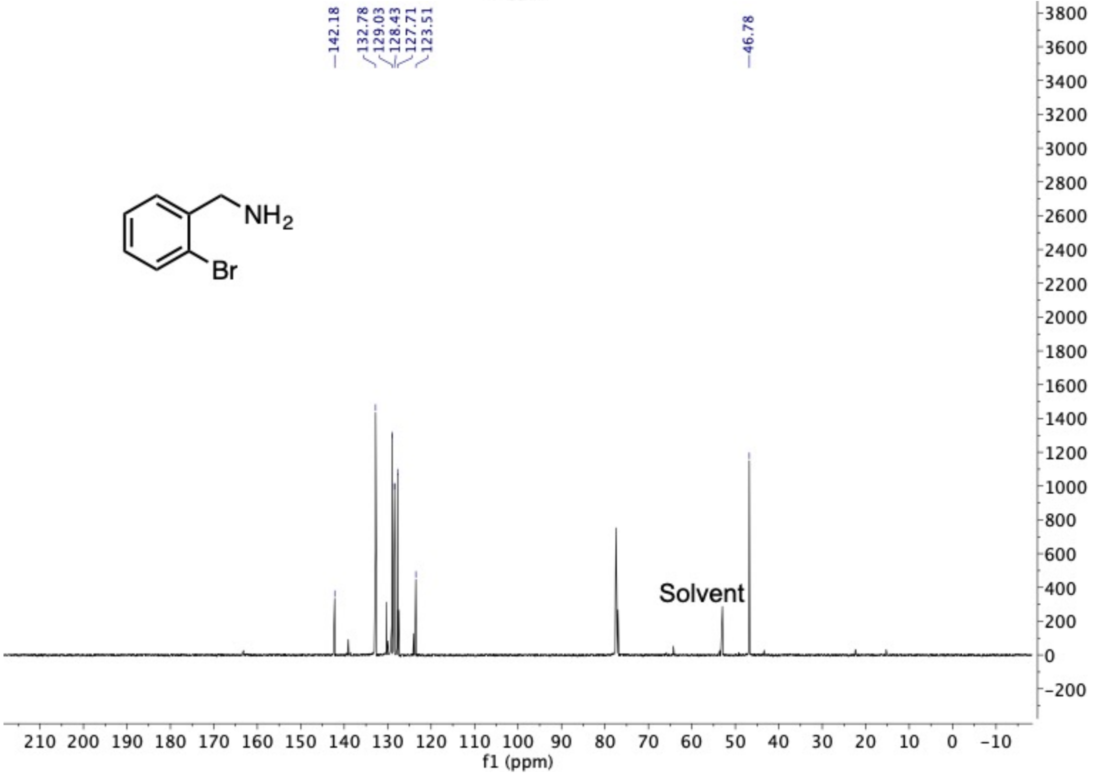
142.18
132.78
129.03
128.43
127.71
123.51
46.78
NH2
Br
Solvent
3800
3600
3400
3200
3000
2800
2600
2400
2200
2000
1800
1600
1400
1200
1000
800
600
400
200
0
−200
210 200 190 180 170 160 150 140 130 120 110 100 90 80 70 60 50 40 30 20 10 0 −10
f1 (ppm)

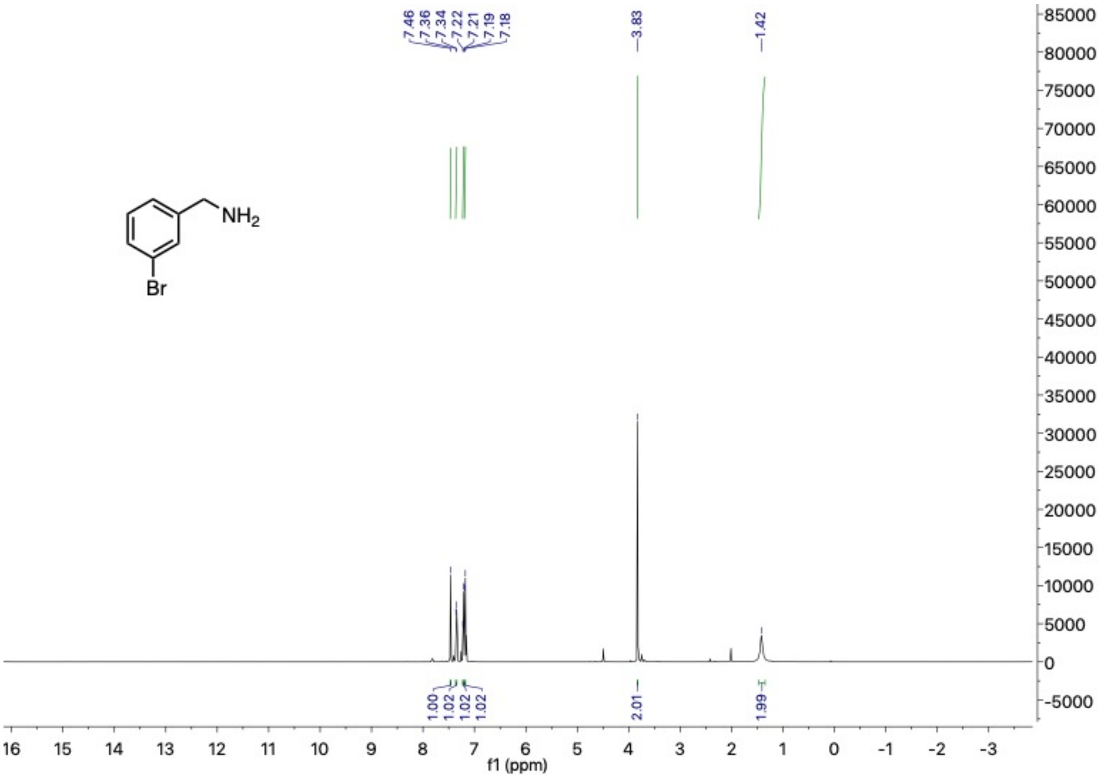
7.46
7.36
7.34
7.22
7.21
7.19
7.18
3.83
1.42
NH2
Br
1.00
1.02
1.02
1.02
2.01
1.99
85000
80000
75000
70000
65000
60000
55000
50000
45000
40000
35000
30000
25000
20000
15000
10000
5000
0
-5000
16 15 14 13 12 11 10 9 8 7 6 5 4 3 2 1 0 -1 -2 -3
f1 (ppm)

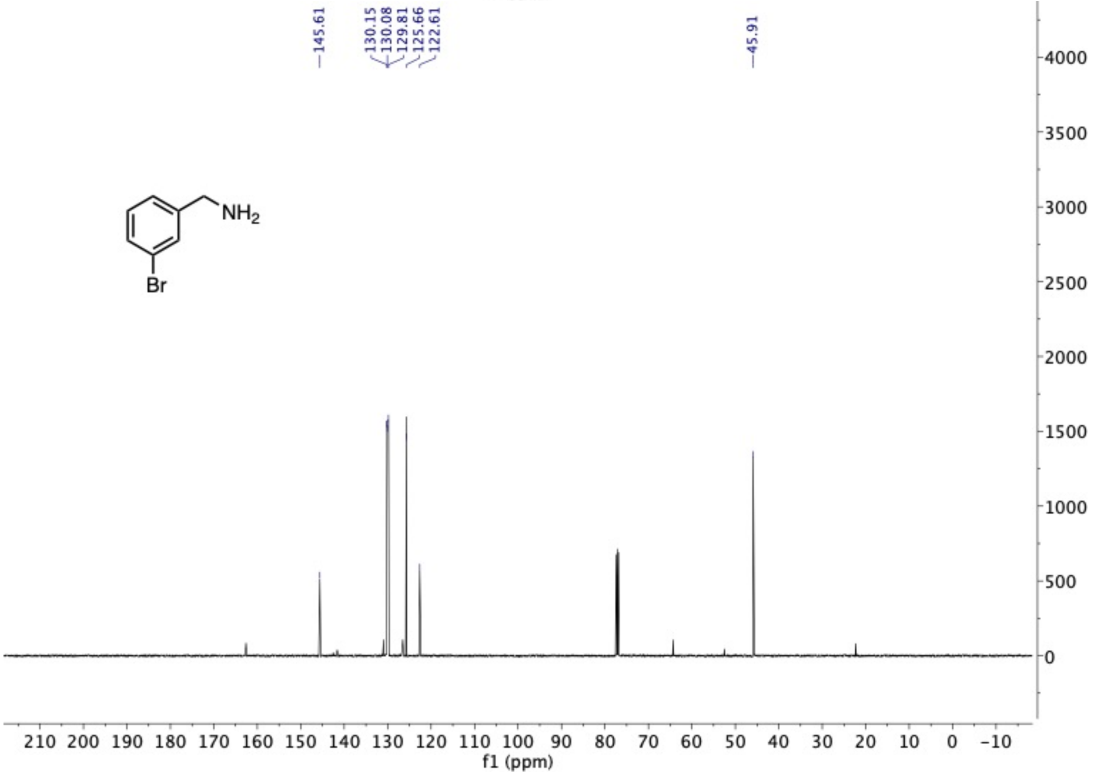
145.61
130.15
130.08
129.81
125.66
122.61
45.91
NH2
Br
4000
3500
3000
2500
2000
1500
1000
500
0
210 200 190 180 170 160 150 140 130 120 110 100 90 80 70 60 50 40 30 20 10 0 −10
f1 (ppm)

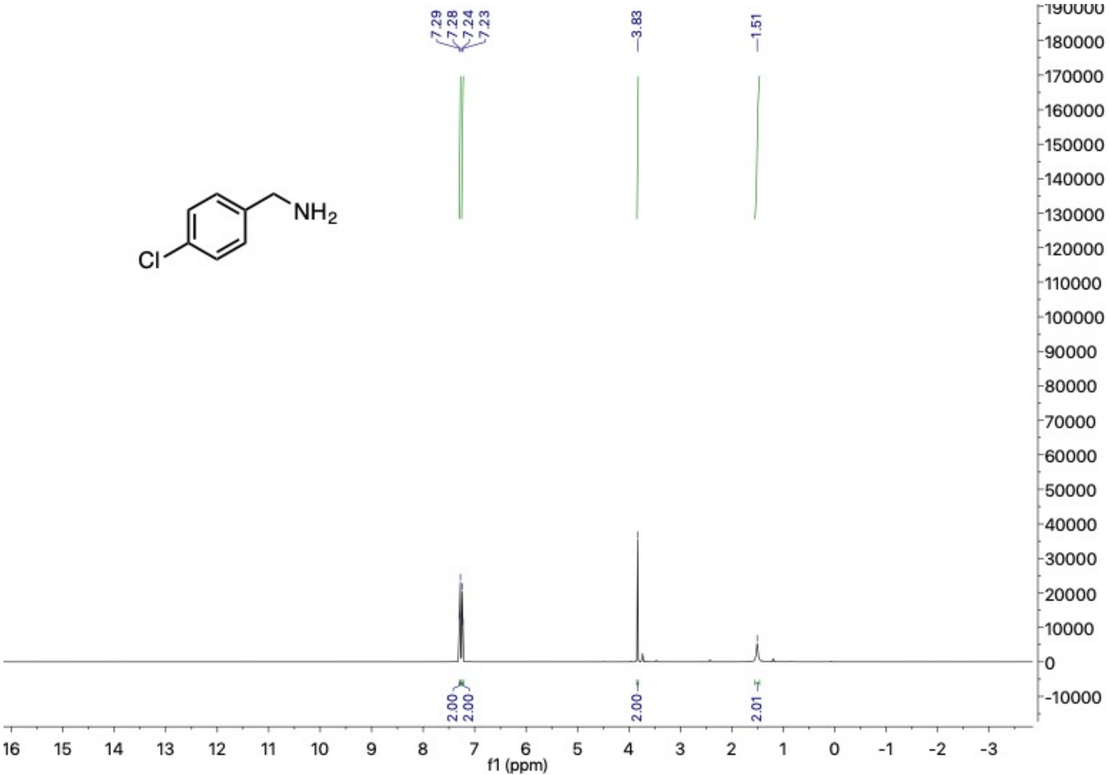

7.29
7.28
7.24
7.23
3.83
1.51
NH2
Cl
2.00
2.00
2.00
2.01
16 15 14 13 12 11 10 9 8 7 6 5 4 3 2 1 0 -1 -2 -3
f1 (ppm)
190000
180000
170000
160000
150000
140000
130000
120000
110000
100000
90000
80000
70000
60000
50000
40000
30000
20000
10000
0
-10000

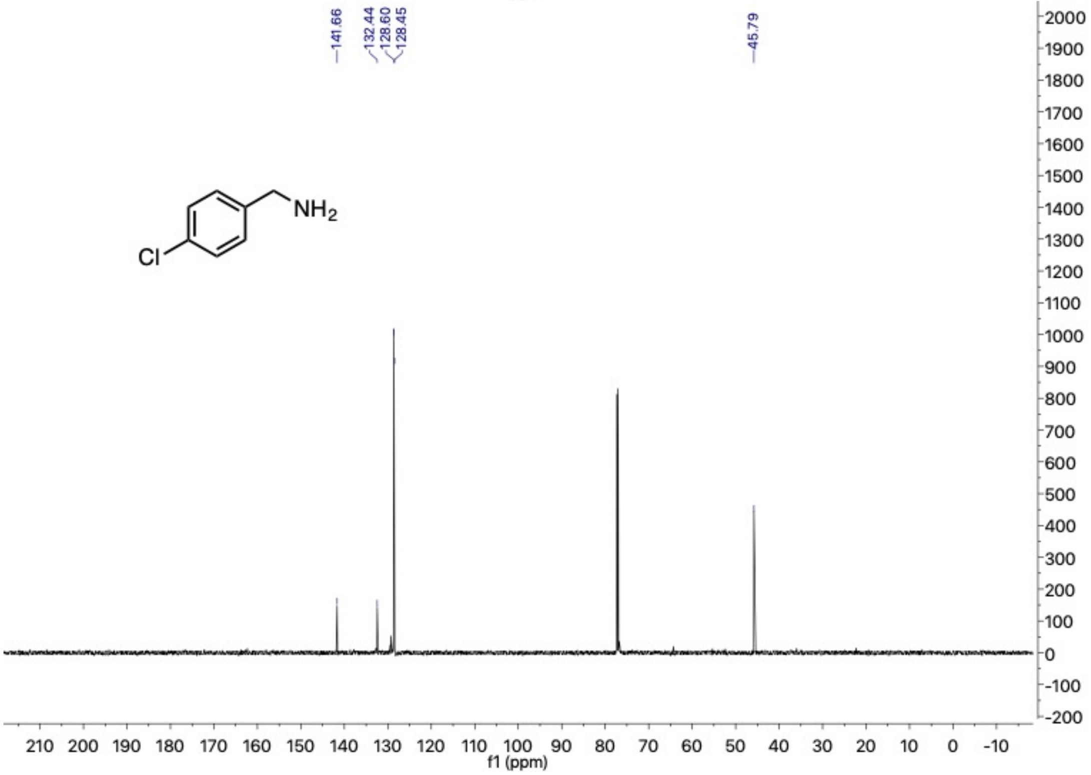

141.66
132.44
128.60
128.45
45.79
NH2
Cl
210 200 190 180 170 160 150 140 130 120 110 100 90 80 70 60 50 40 30 20 10 0 -10
f1 (ppm)
2000
1900
1800
1700
1600
1500
1400
1300
1200
1100
1000
900
800
700
600
500
400
300
200
100
0
-100
-200

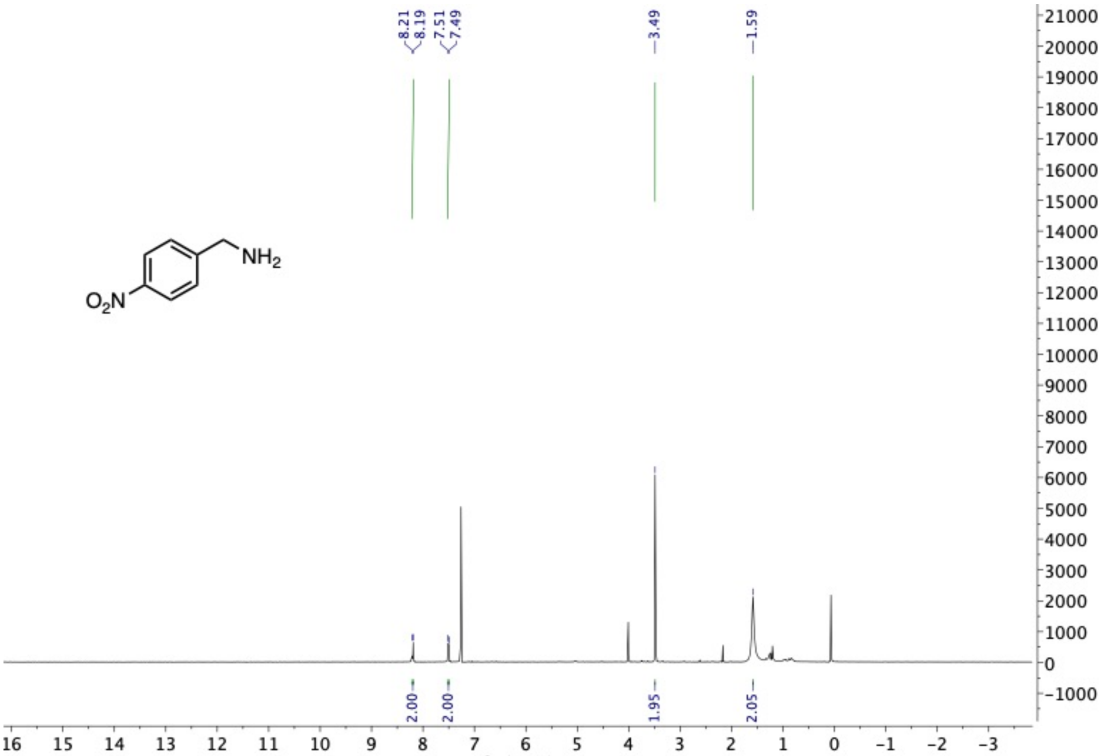

8.21
8.19
7.51
7.49
3.49
1.59
NH2
O2N
2.00
2.00
1.95
2.05
21000
20000
19000
18000
17000
16000
15000
14000
13000
12000
11000
10000
9000
8000
7000
6000
5000
4000
3000
2000
1000
0
−1000
16 15 14 13 12 11 10 9 8 7 6 5 4 3 2 1 0 −1 −2 −3
f1 (ppm)

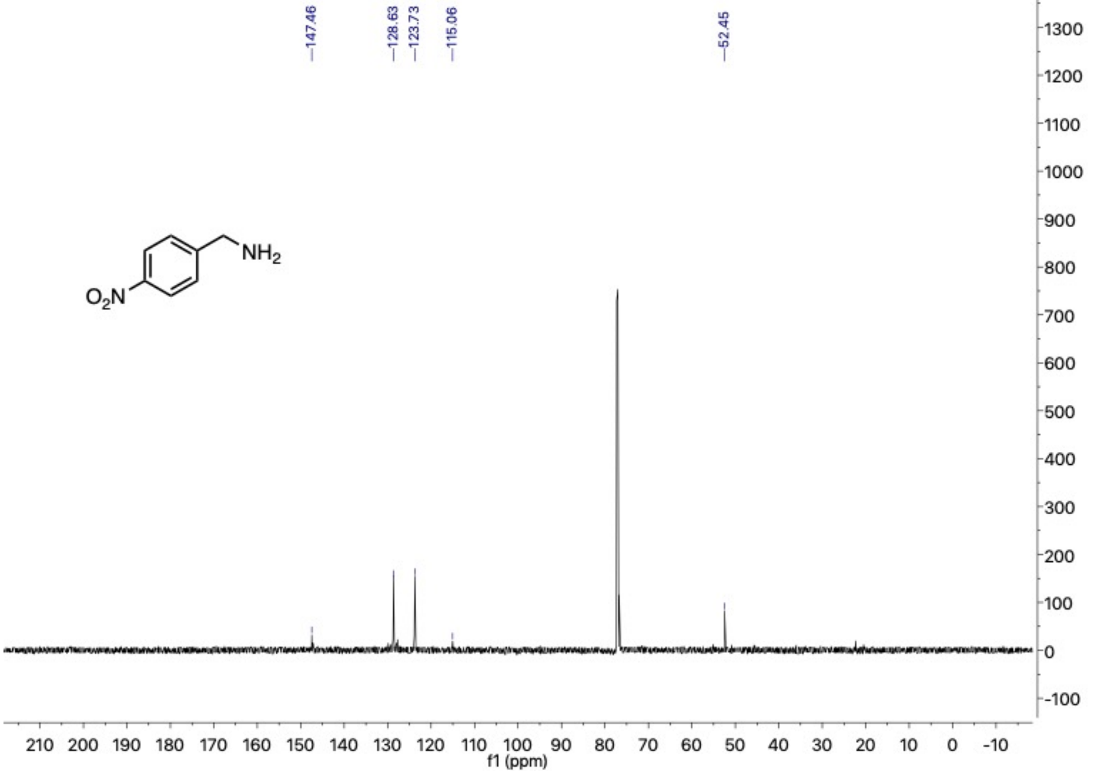

147.46
128.63
123.73
115.06
52.45
NH2
O2N
1300
1200
1100
1000
900
800
700
600
500
400
300
200
100
0
−100
210 200 190 180 170 160 150 140 130 120 110 100 90 80 70 60 50 40 30 20 10 0 −10
f1 (ppm)

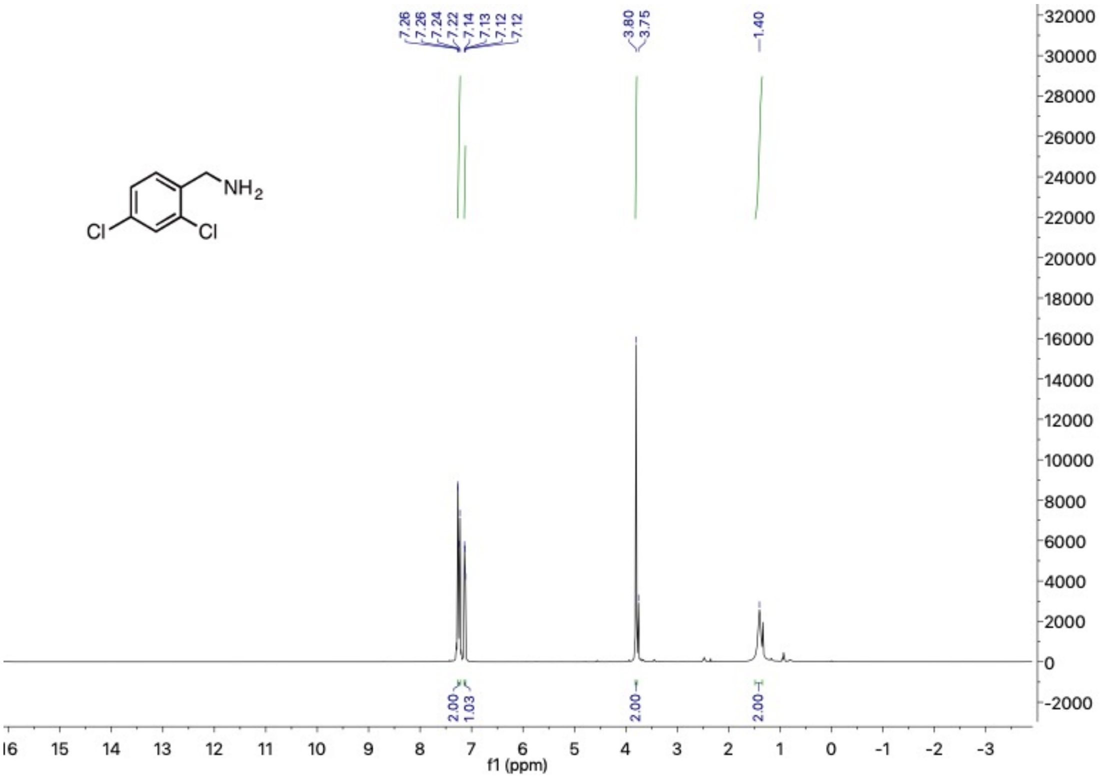
7.26
7.26
7.24
7.22
7.14
7.13
7.12
7.12
3.80
3.75
1.40
NH2
Cl
Cl
2.00
1.03
2.00
2.00
16 15 14 13 12 11 10 9 8 7 6 5 4 3 2 1 0 -1 -2 -3
f1 (ppm)
32000
30000
28000
26000
24000
22000
20000
18000
16000
14000
12000
10000
8000
6000
4000
2000
0
-2000

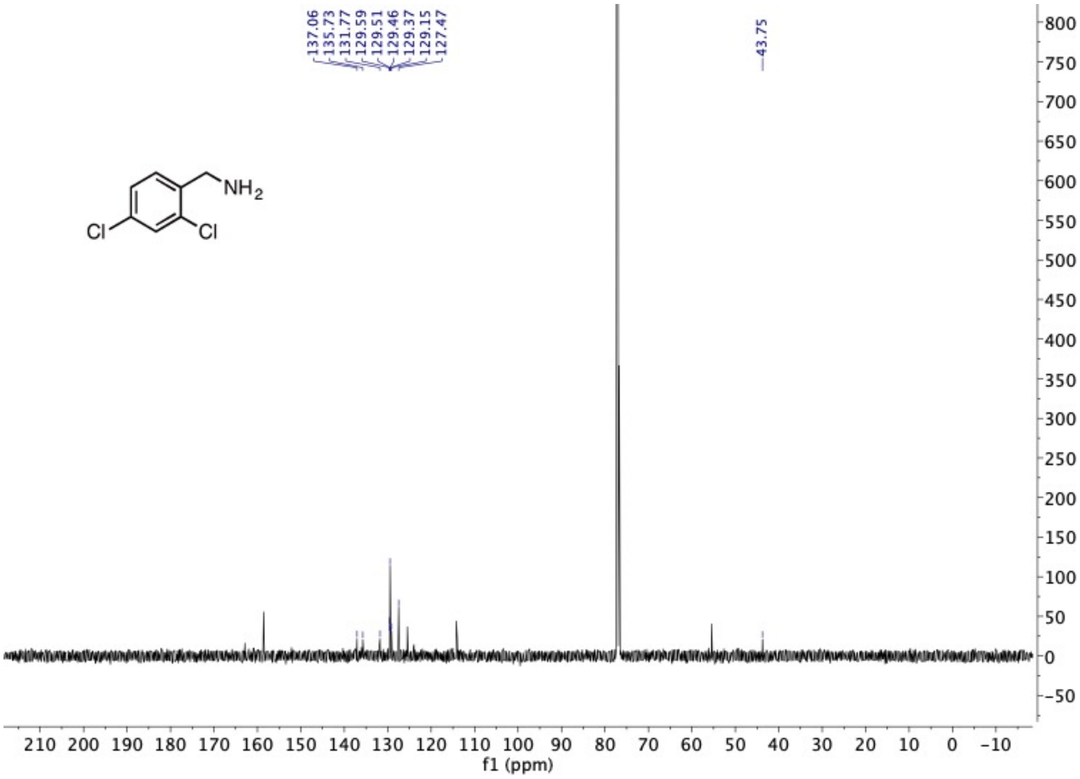
137.06
135.73
131.77
129.59
129.51
129.46
129.37
129.15
127.47
43.75
NH2
Cl
Cl
210 200 190 180 170 160 150 140 130 120 110 100 90 80 70 60 50 40 30 20 10 0 −10
f1 (ppm)
800
750
700
650
600
550
500
450
400
350
300
250
200
150
100
50
0
−50

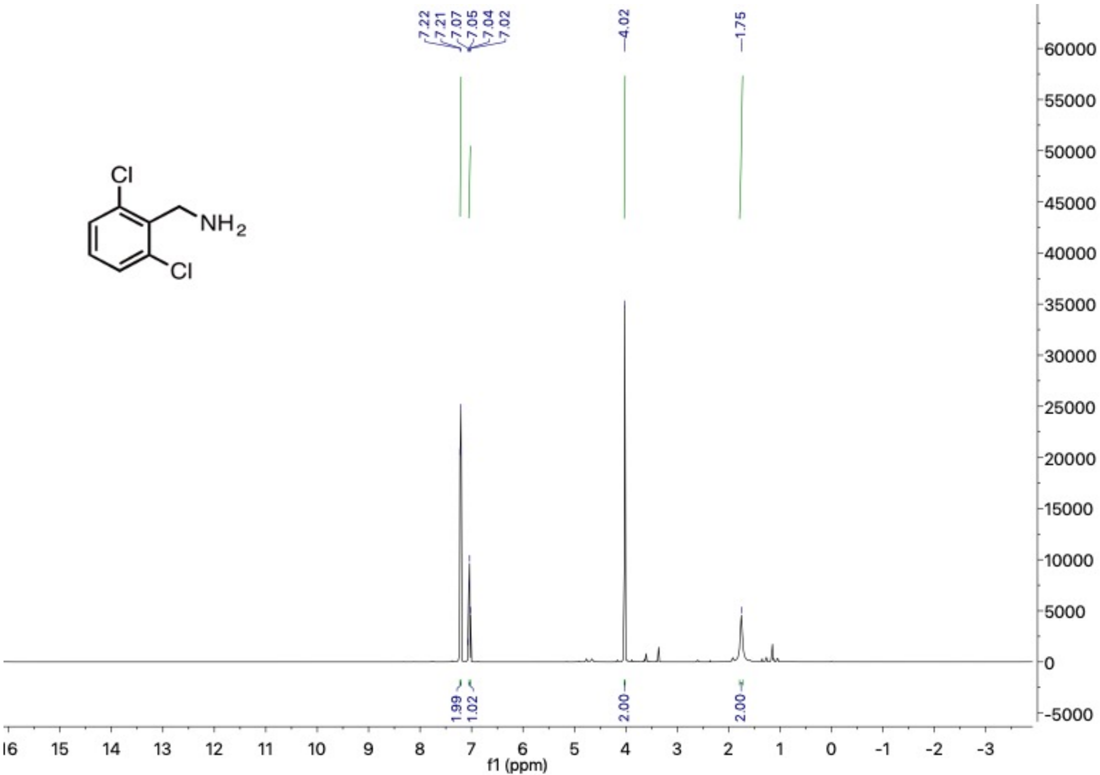
7.22
7.21
7.07
7.05
7.04
7.02
4.02
1.75
Cl
NH2
Cl
1.99
1.02
2.00
2.00
16 15 14 13 12 11 10 9 8 7 6 5 4 3 2 1 0 -1 -2 -3
f1 (ppm)
60000
55000
50000
45000
40000
35000
30000
25000
20000
15000
10000
5000
0
-5000

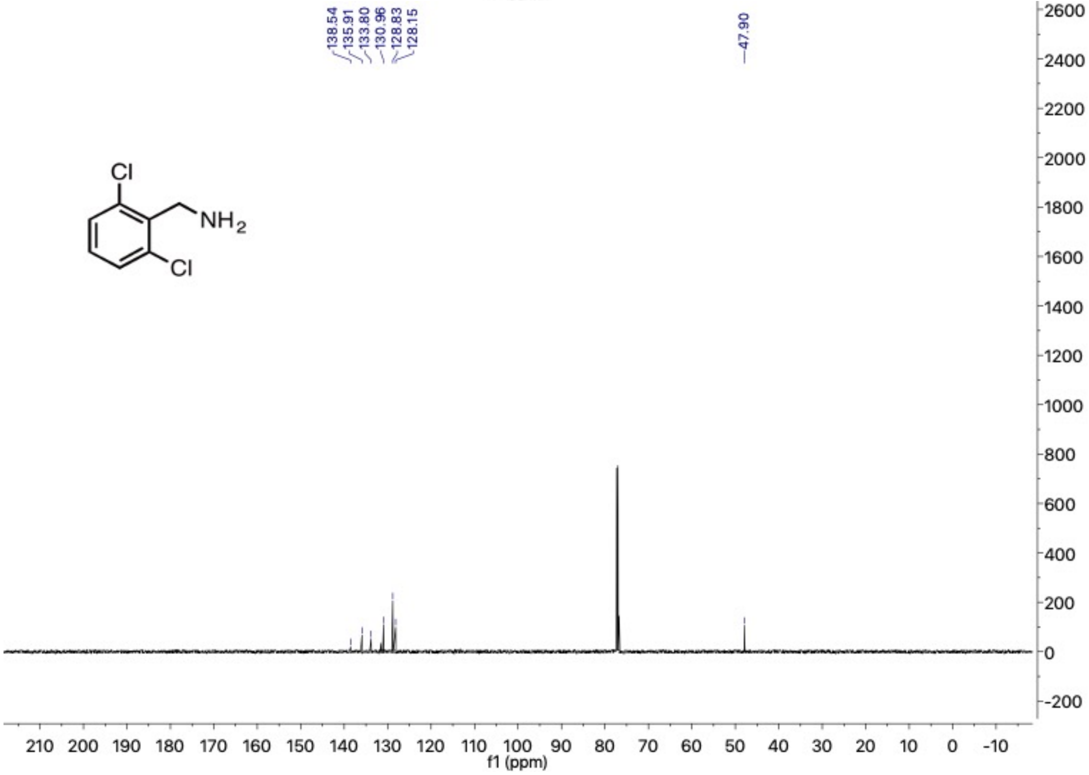
138.54
135.91
133.80
130.96
128.83
128.15
47.90
Cl
NH2
Cl
210 200 190 180 170 160 150 140 130 120 110 100 90 80 70 60 50 40 30 20 10 0 -10
f1 (ppm)
2600
2400
2200
2000
1800
1600
1400
1200
1000
800
600
400
200
0
-200

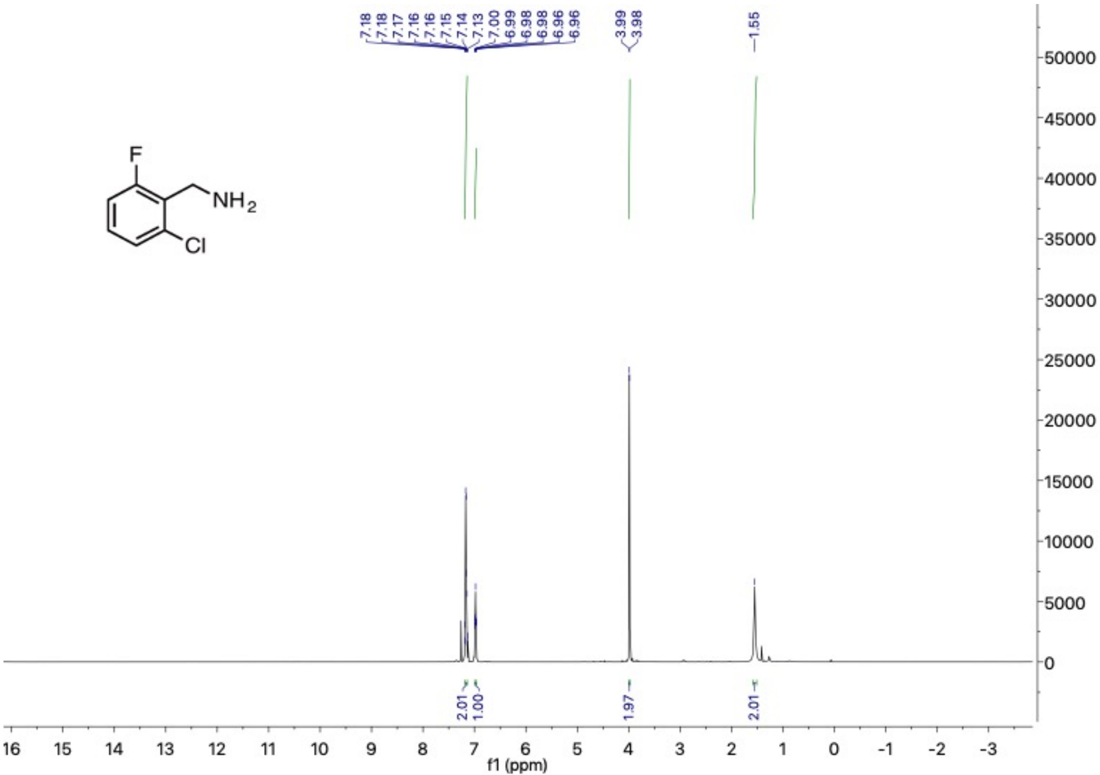
7.18
7.18
7.17
7.16
7.16
7.15
7.14
7.13
7.00
6.99
6.98
6.98
6.96
6.96
3.99
3.98
1.55
F
NH2
Cl
50000
45000
40000
35000
30000
25000
20000
15000
10000
5000
0
2.01
1.00
1.97
2.01
16 15 14 13 12 11 10 9 8 7 6 5 4 3 2 1 0 -1 -2 -3
f1 (ppm)

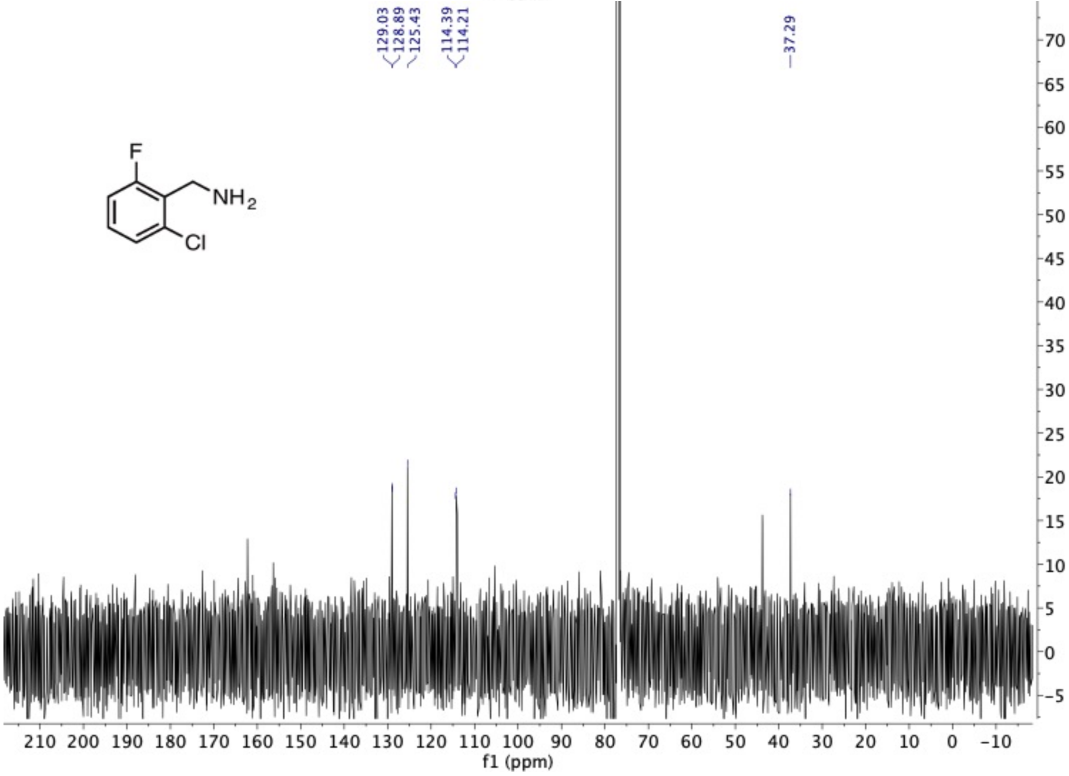
129.03
128.89
125.43
114.39
114.21
37.29
F
NH2
Cl
70
65
60
55
50
45
40
35
30
25
20
15
10
5
0
-5
210 200 190 180 170 160 150 140 130 120 110 100 90 80 70 60 50 40 30 20 10 0 −10
f1 (ppm)

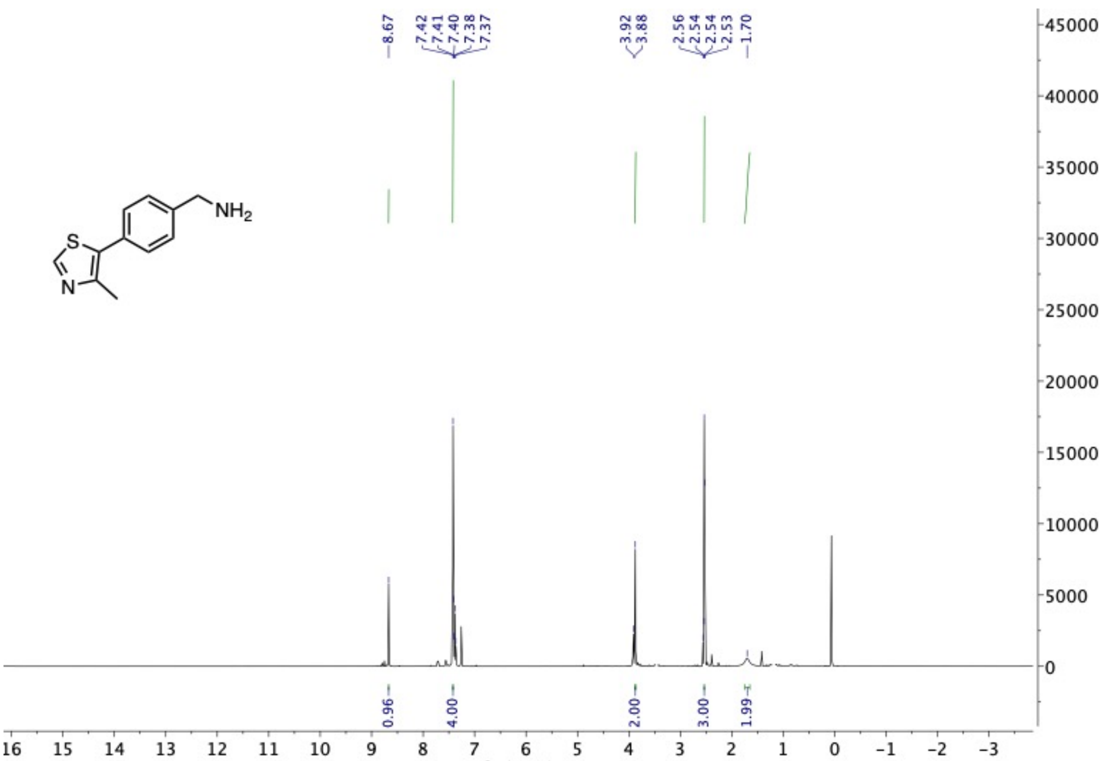
8.67
7.42
7.41
7.40
7.38
7.37
3.92
3.88
2.56
2.54
2.54
2.53
1.70
S
N
NH$_2$
0.96
4.00
2.00
3.00
1.99
16 15 14 13 12 11 10 9 8 7 6 5 4 3 2 1 0 −1 −2 −3
f1 (ppm)
45000
40000
35000
30000
25000
20000
15000
10000
5000
0

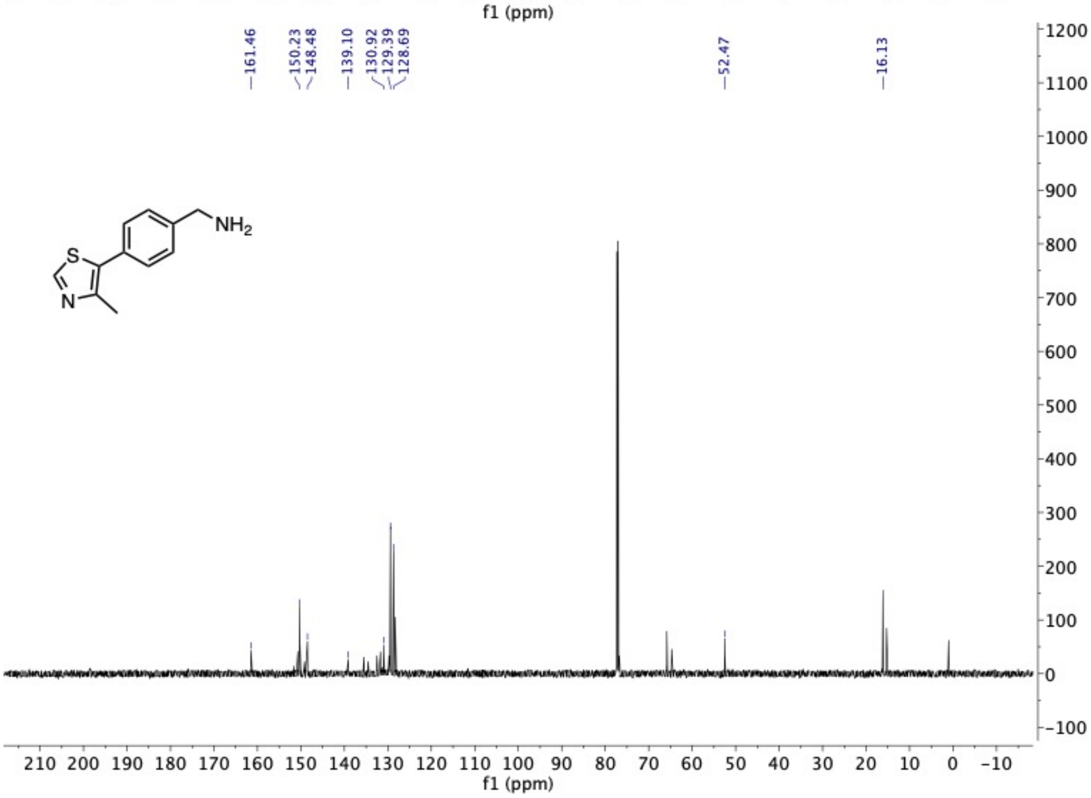
161.46
150.23
148.48
139.10
130.92
129.39
128.69
52.47
16.13
S
N
NH$_2$
210 200 190 180 170 160 150 140 130 120 110 100 90 80 70 60 50 40 30 20 10 0 −10
f1 (ppm)
1200
1100
1000
900
800
700
600
500
400
300
200
100
0
−100

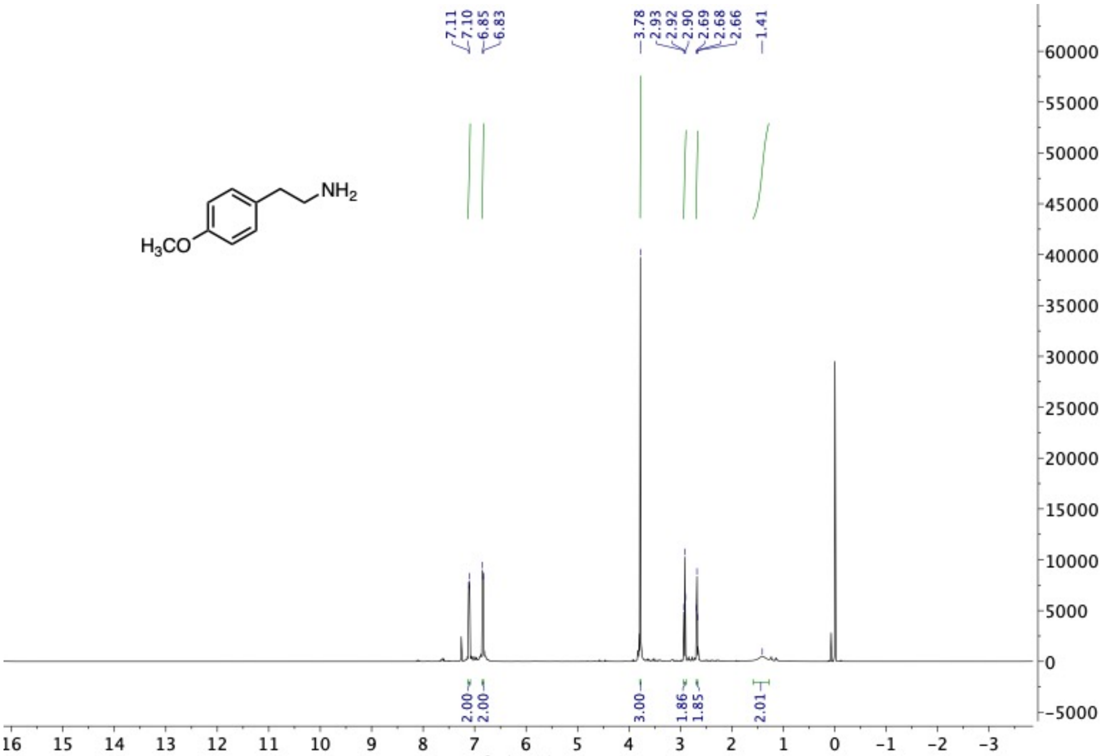
7.11
7.10
6.85
6.83
3.78
2.93
2.92
2.90
2.69
2.68
2.66
1.41
NH2
H3CO
2.00
2.00
3.00
1.86
1.85
2.01
60000
55000
50000
45000
40000
35000
30000
25000
20000
15000
10000
5000
0
−5000
16 15 14 13 12 11 10 9 8 7 6 5 4 3 2 1 0 −1 −2 −3
f1 (ppm)

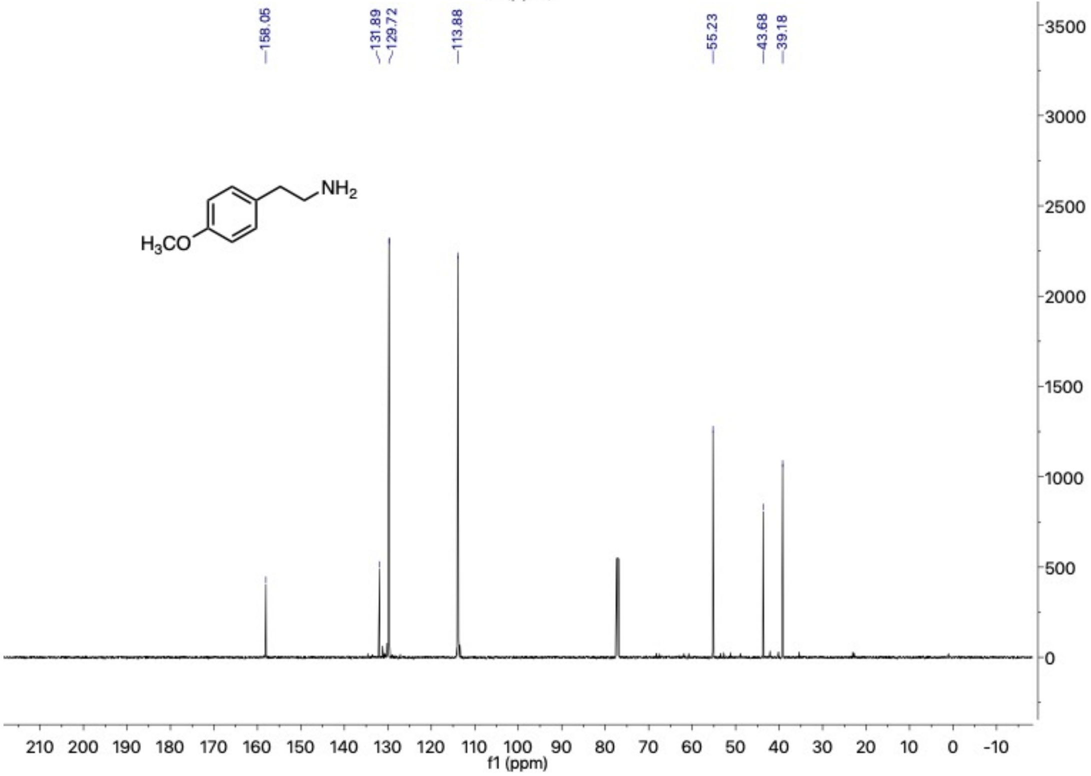
158.05
131.89
129.72
113.88
55.23
43.68
39.18
NH2
H3CO
3500
3000
2500
2000
1500
1000
500
0
210 200 190 180 170 160 150 140 130 120 110 100 90 80 70 60 50 40 30 20 10 0 −10
f1 (ppm)

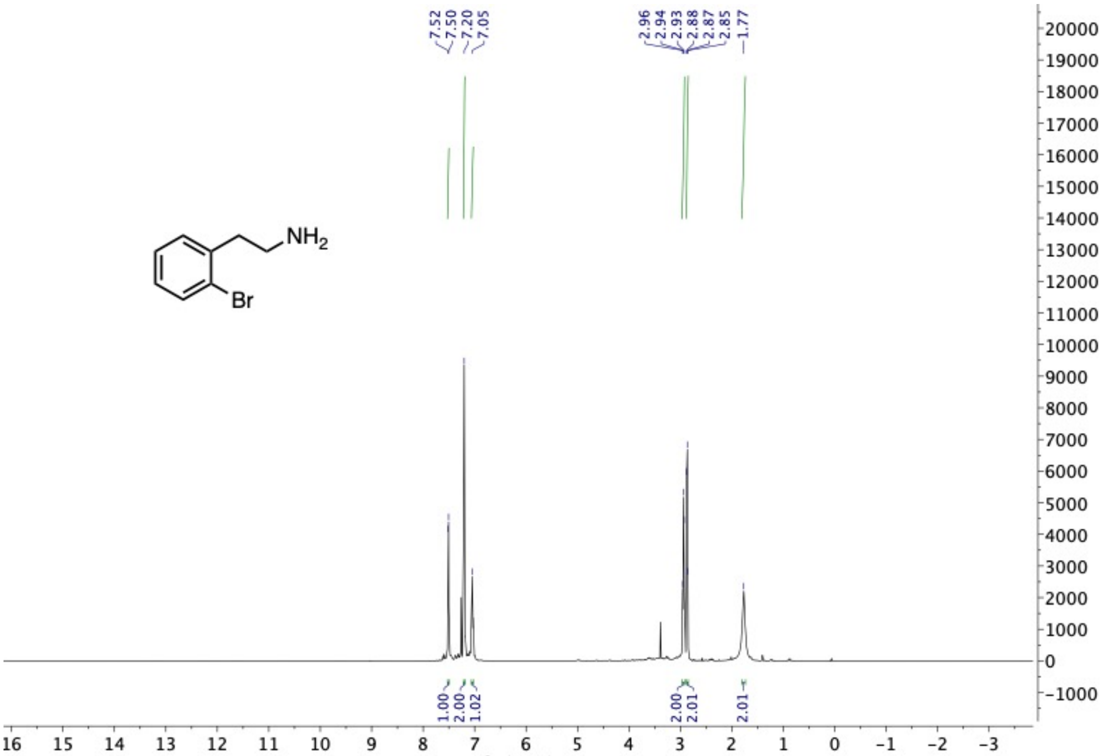

7.52
7.50
7.20
7.05
2.96
2.94
2.93
2.88
2.87
2.85
1.77
NH2
Br
1.00
2.00
1.02
2.00
2.01
2.01
f1 (ppm)
16 15 14 13 12 11 10 9 8 7 6 5 4 3 2 1 0 −1 −2 −3
20000 19000 18000 17000 16000 15000 14000 13000 12000 11000 10000 9000 8000 7000 6000 5000 4000 3000 2000 1000 0 −1000

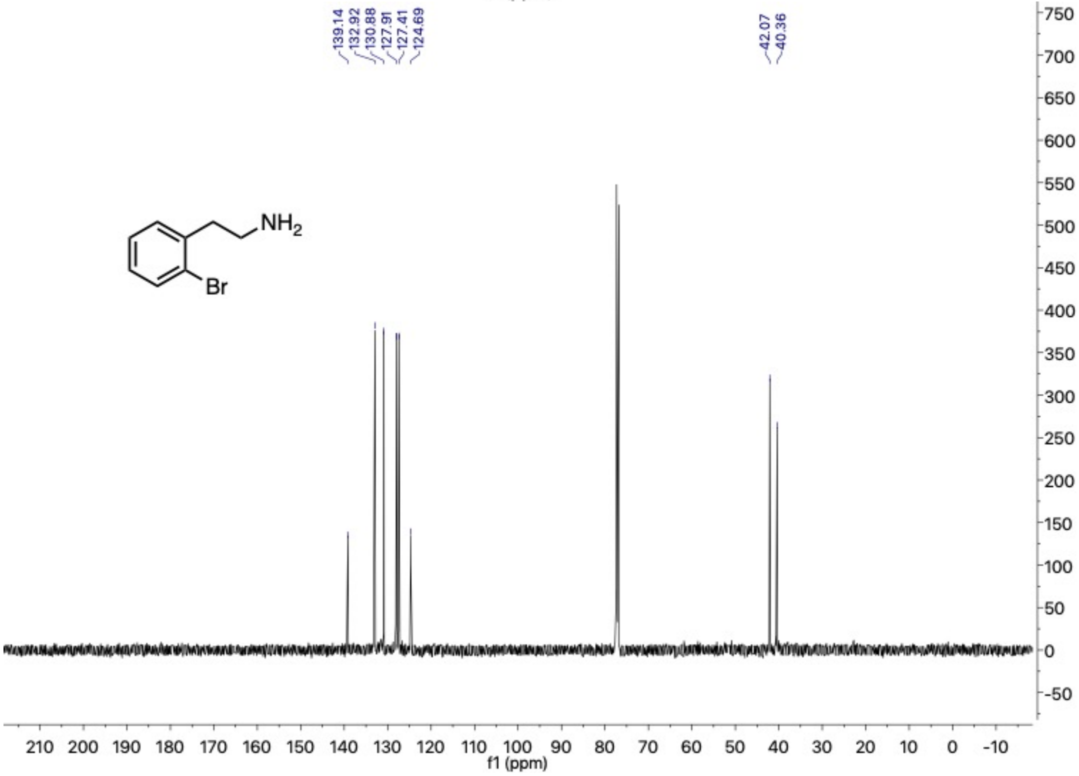

139.14
132.92
130.88
127.91
127.41
124.69
42.07
40.36
NH2
Br
f1 (ppm)
210 200 190 180 170 160 150 140 130 120 110 100 90 80 70 60 50 40 30 20 10 0 -10
750 700 650 600 550 500 450 400 350 300 250 200 150 100 50 0 -50

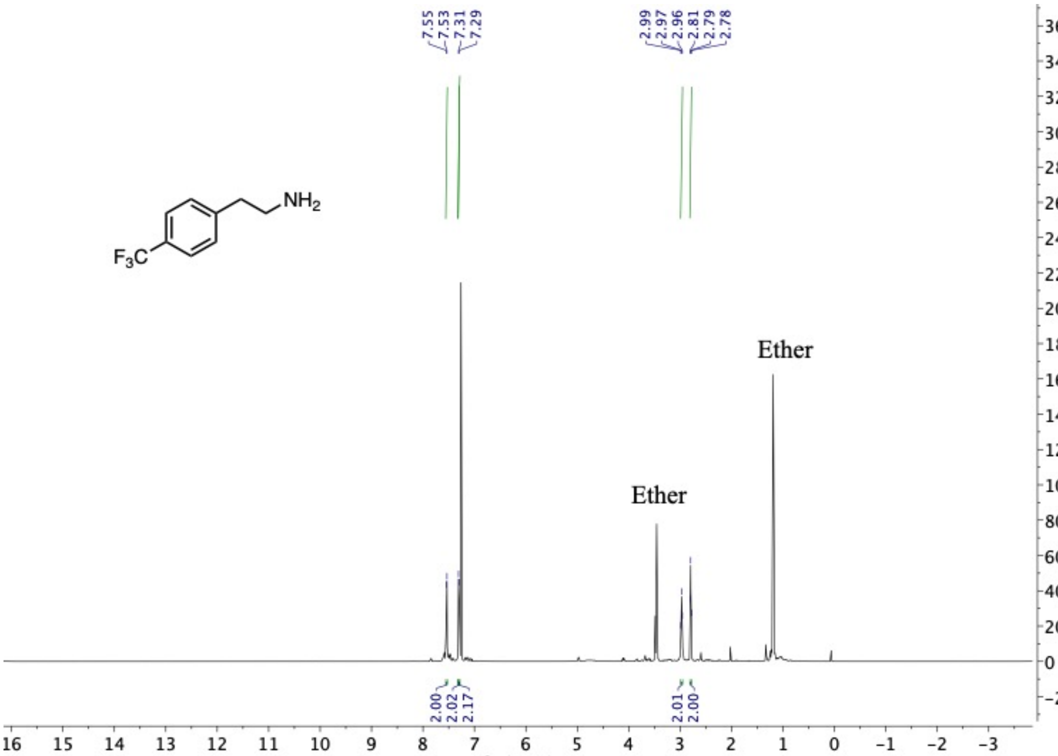
7.55
7.53
7.31
7.29
2.99
2.97
2.96
2.81
2.79
2.78
NH2
F3C
Ether
Ether
2.00
2.02
2.17
2.01
2.00
36000
34000
32000
30000
28000
26000
24000
22000
20000
18000
16000
14000
12000
10000
8000
6000
4000
2000
0
−2000
16
15
14
13
12
11
10
9
8
7
6
5
4
3
2
1
0
−1
−2
−3
f1 (ppm)

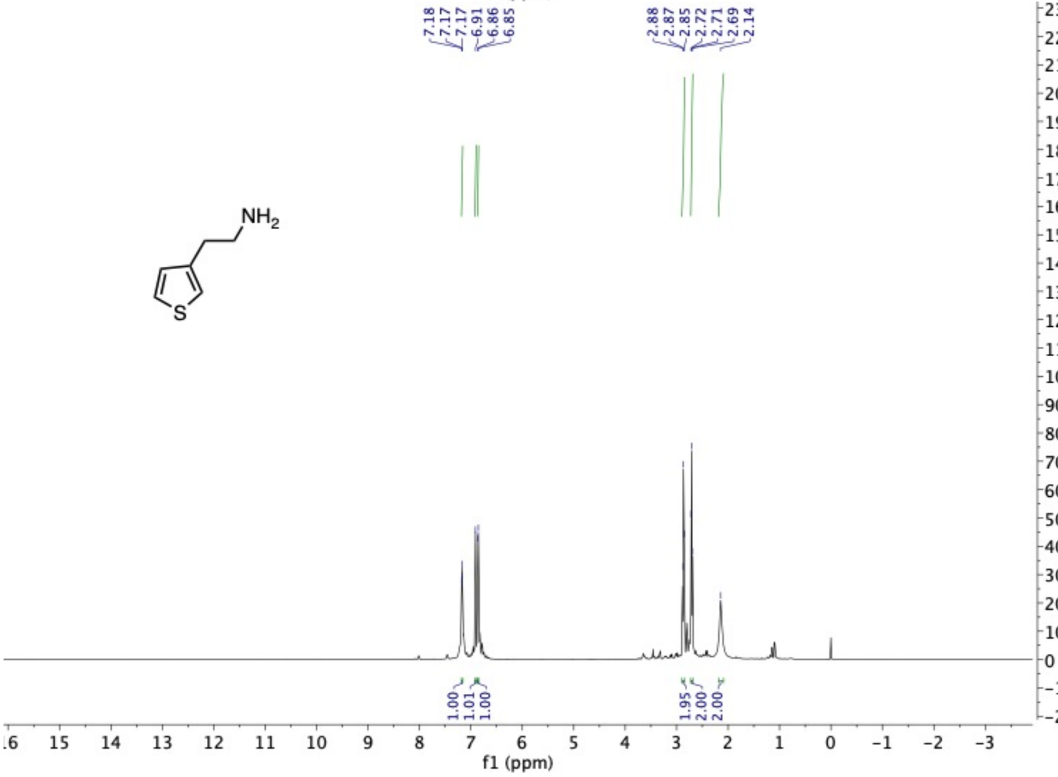
7.18
7.17
7.17
6.91
6.86
6.85
2.88
2.87
2.85
2.72
2.71
2.69
2.14
NH2
S
1.00
1.01
1.00
1.95
2.00
2.00
23000
22000
21000
20000
19000
18000
17000
16000
15000
14000
13000
12000
11000
10000
9000
8000
7000
6000
5000
4000
3000
2000
1000
0
−1000
−2000
16
15
14
13
12
11
10
9
8
7
6
5
4
3
2
1
0
−1
−2
−3
f1 (ppm)

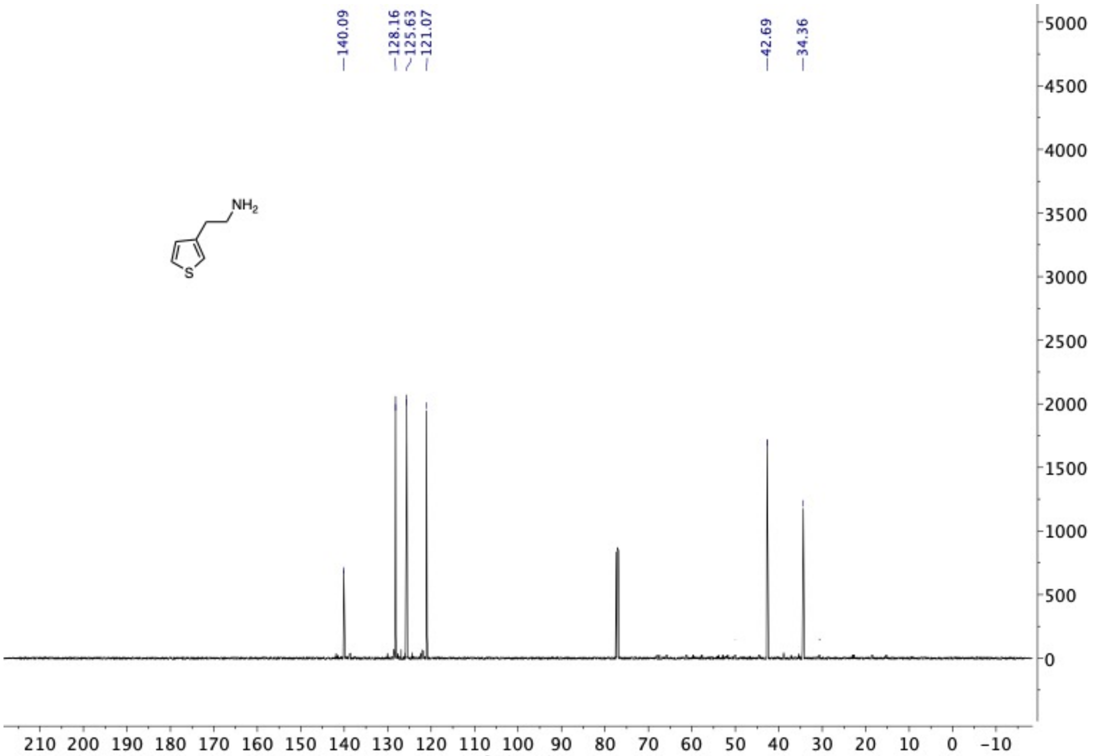

140.09
128.16
125.63
121.07
42.69
34.36
NH2
S
5000
4500
4000
3500
3000
2500
2000
1500
1000
500
0
210 200 190 180 170 160 150 140 130 120 110 100 90 80 70 60 50 40 30 20 10 0 −10
f1 (ppm)

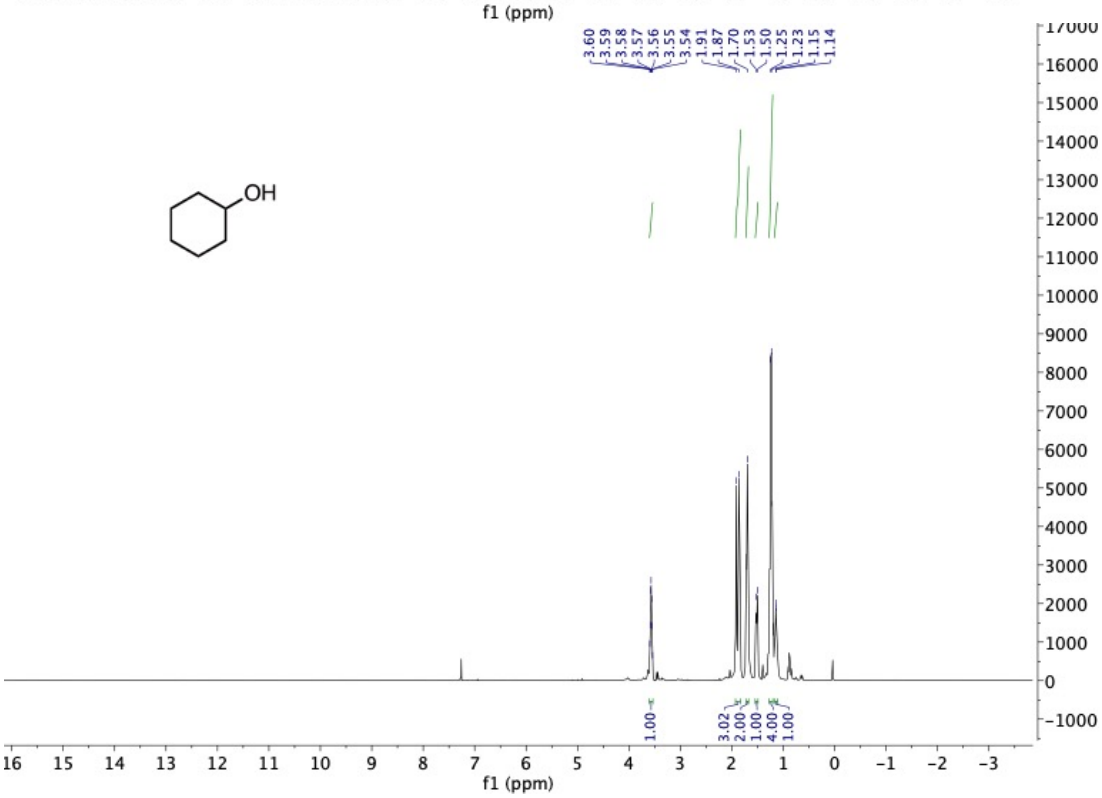

3.60
3.59
3.58
3.57
3.56
3.55
3.54
1.91
1.87
1.70
1.53
1.50
1.25
1.23
1.15
1.14
OH
17000
16000
15000
14000
13000
12000
11000
10000
9000
8000
7000
6000
5000
4000
3000
2000
1000
0
−1000
1.00
3.02
2.00
1.00
4.00
1.00
16 15 14 13 12 11 10 9 8 7 6 5 4 3 2 1 0 −1 −2 −3
f1 (ppm)

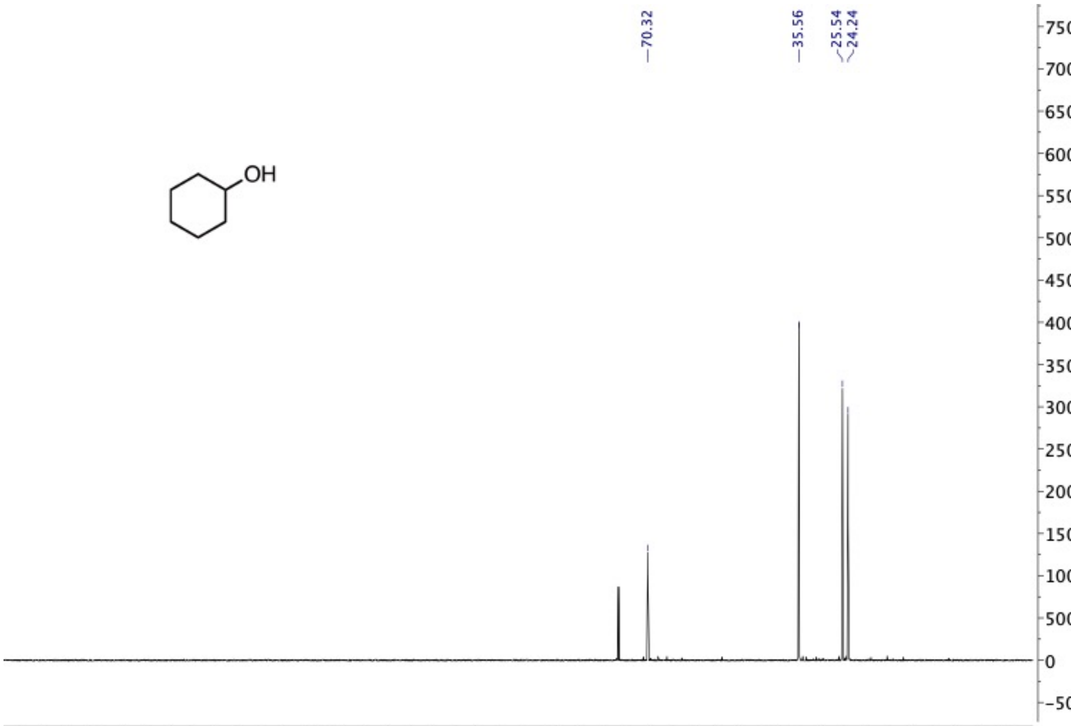
OH
70.32
35.56
25.54
24.24
7500
7000
6500
6000
5500
5000
4500
4000
3500
3000
2500
2000
1500
1000
500
0
−500
210 200 190 180 170 160 150 140 130 120 110 100 90 80 70 60 50 40 30 20 10 0 −10
f1 (ppm)

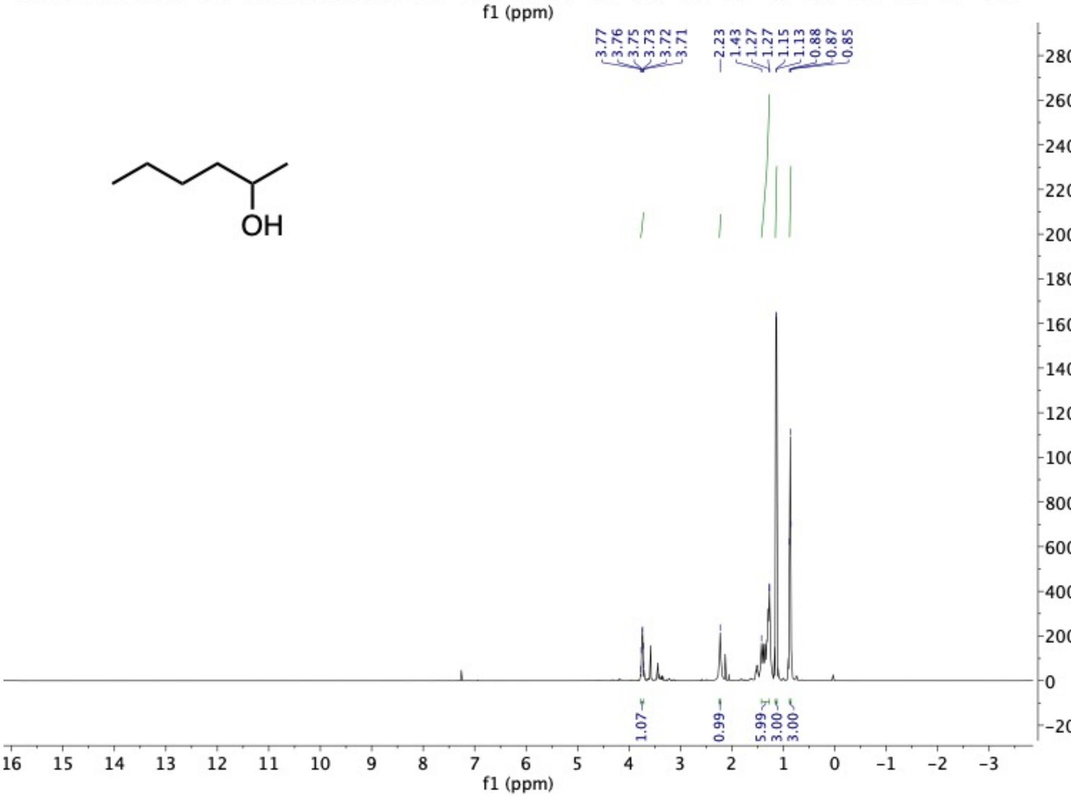
OH
3.77
3.76
3.75
3.73
3.72
3.71
2.23
1.43
1.27
1.27
1.15
1.13
0.88
0.87
0.85
1.07
0.99
5.99
3.00
3.00
28000
26000
24000
22000
20000
18000
16000
14000
12000
10000
8000
6000
4000
2000
0
−2000
16 15 14 13 12 11 10 9 8 7 6 5 4 3 2 1 0 −1 −2 −3
f1 (ppm)

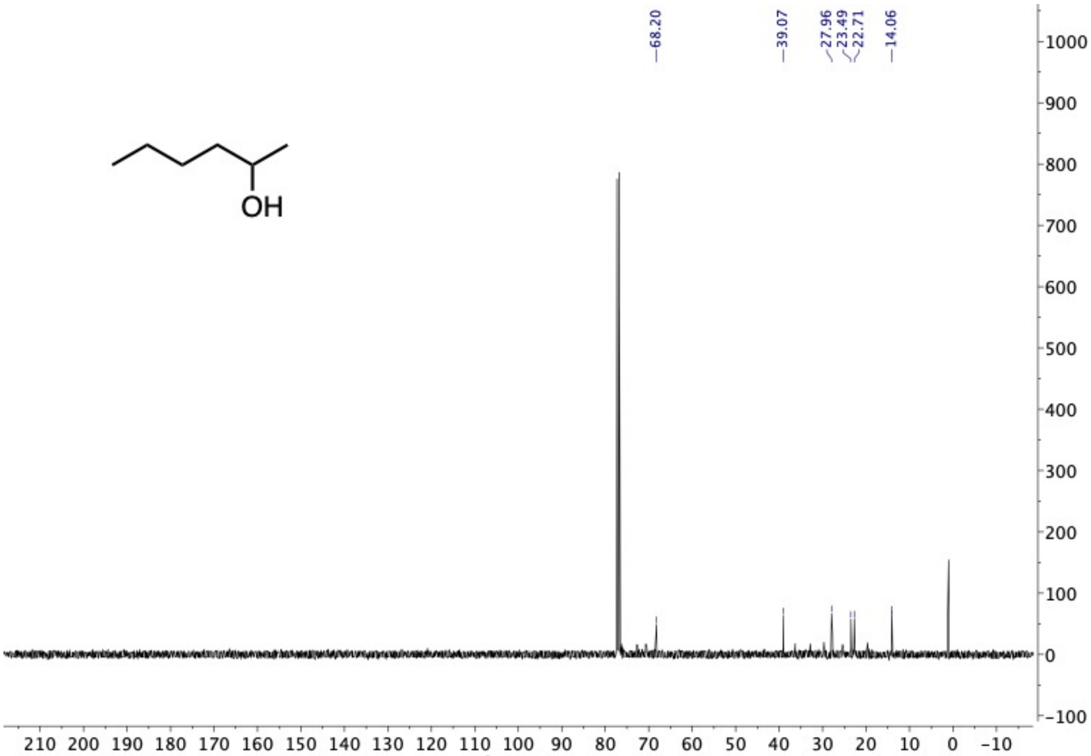

OH
68.20
39.07
27.96
23.49
22.71
14.06
1000
900
800
700
600
500
400
300
200
100
0
−100
210 200 190 180 170 160 150 140 130 120 110 100 90 80 70 60 50 40 30 20 10 0 −10
f1 (ppm)

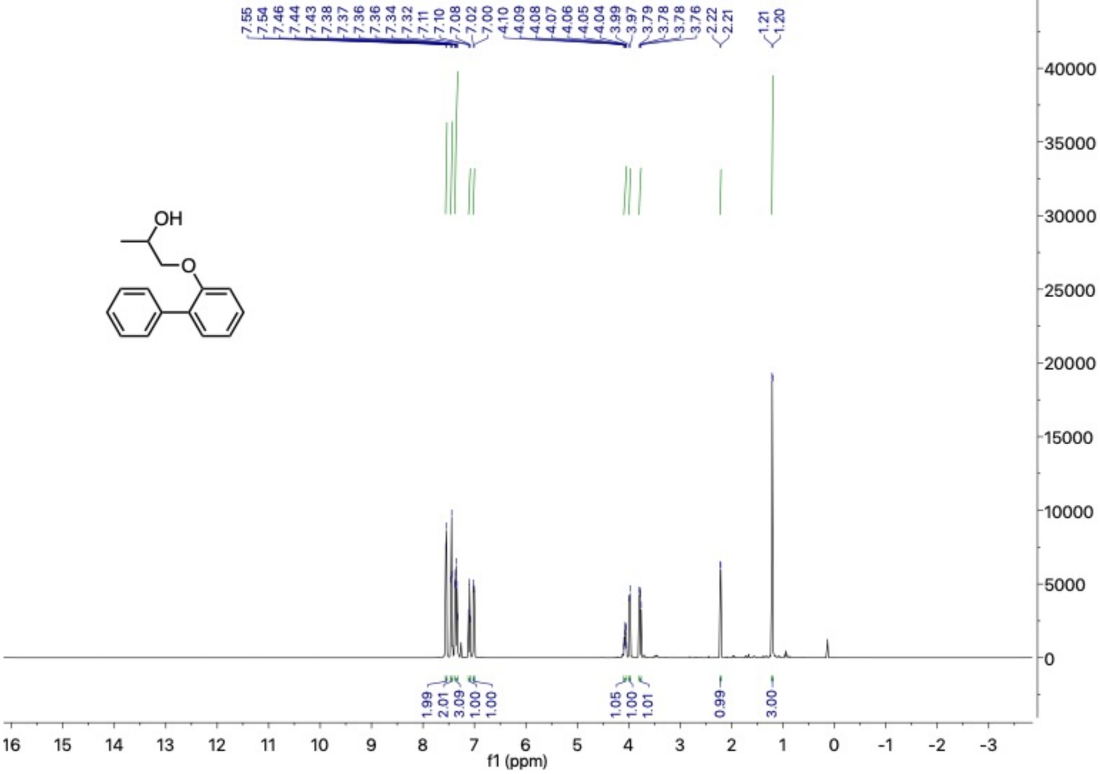

7.55
7.54
7.46
7.44
7.43
7.38
7.37
7.36
7.36
7.34
7.32
7.11
7.10
7.08
7.02
7.00
4.10
4.09
4.08
4.07
4.06
4.05
4.04
3.99
3.97
3.79
3.78
3.78
3.76
2.22
2.21
1.21
1.20
OH
O
40000
35000
30000
25000
20000
15000
10000
5000
0
1.99
2.01
3.09
1.00
1.00
1.05
1.00
1.01
0.99
3.00
16 15 14 13 12 11 10 9 8 7 6 5 4 3 2 1 0 -1 -2 -3
f1 (ppm)

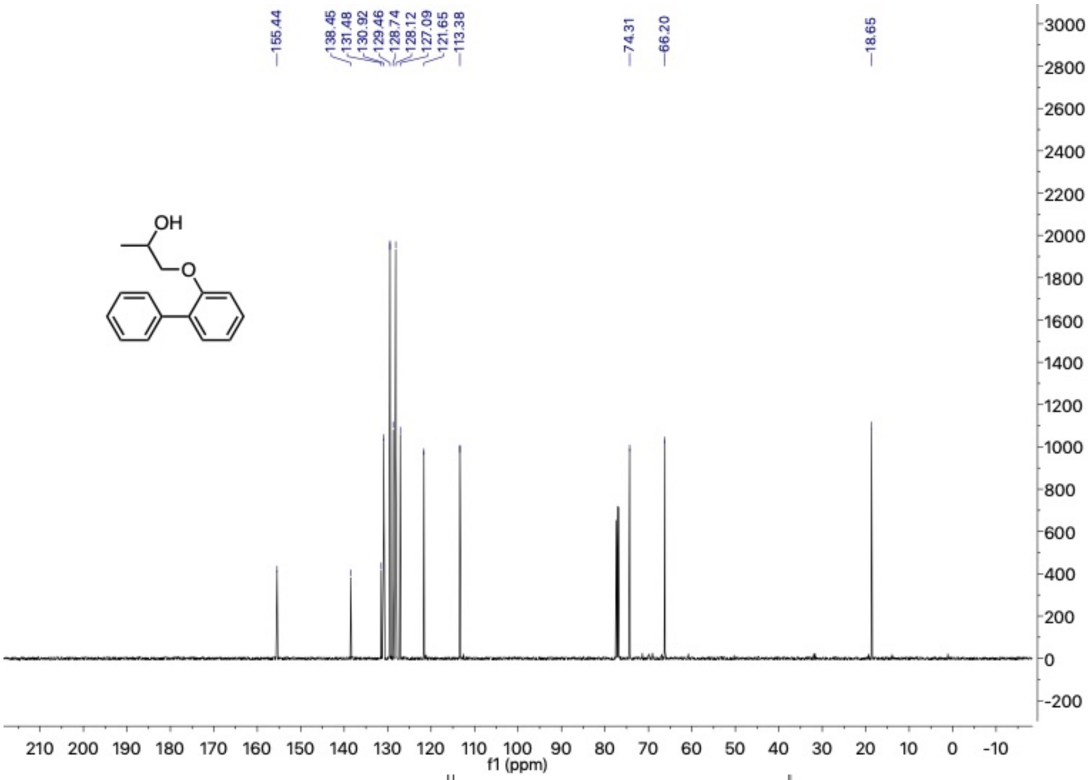
155.44
138.45
131.48
130.92
129.46
128.74
128.12
127.09
121.65
113.38
74.31
66.20
18.65
OH
O
3000
2800
2600
2400
2200
2000
1800
1600
1400
1200
1000
800
600
400
200
0
-200
210 200 190 180 170 160 150 140 130 120 110 100 90 80 70 60 50 40 30 20 10 0 -10
f1 (ppm)

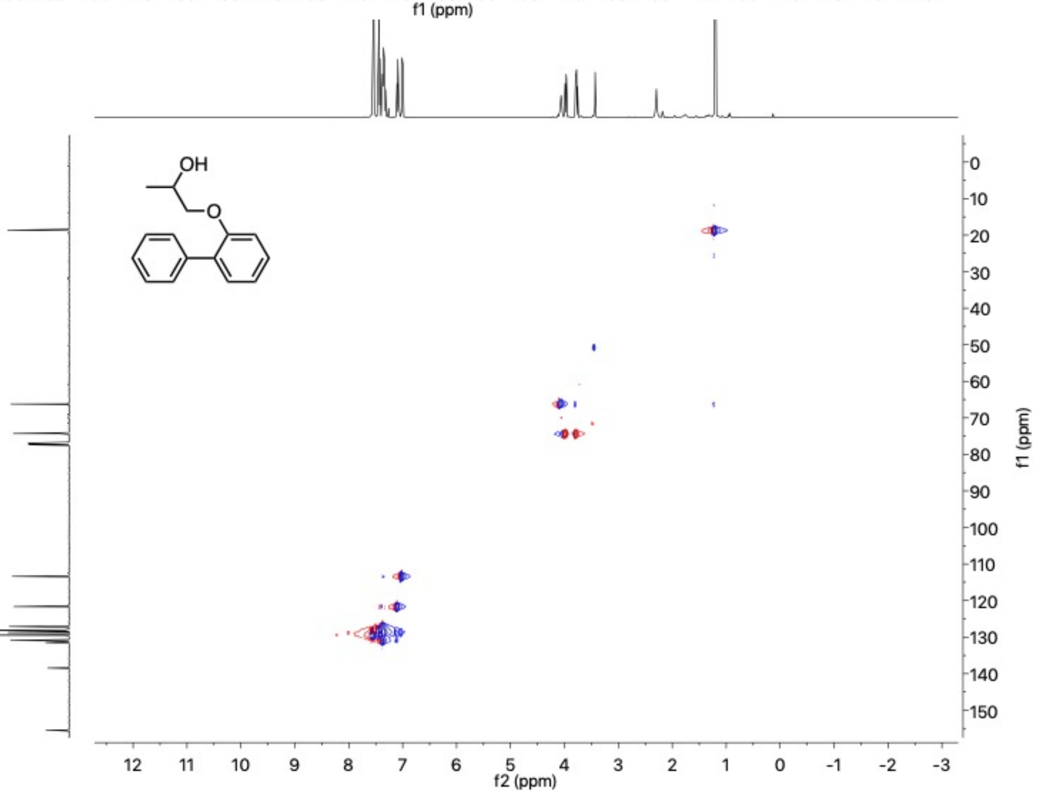
OH
O
0
10
20
30
40
50
60
70
80
90
100
110
120
130
140
150
f1 (ppm)
12 11 10 9 8 7 6 5 4 3 2 1 0 -1 -2 -3
f2 (ppm)

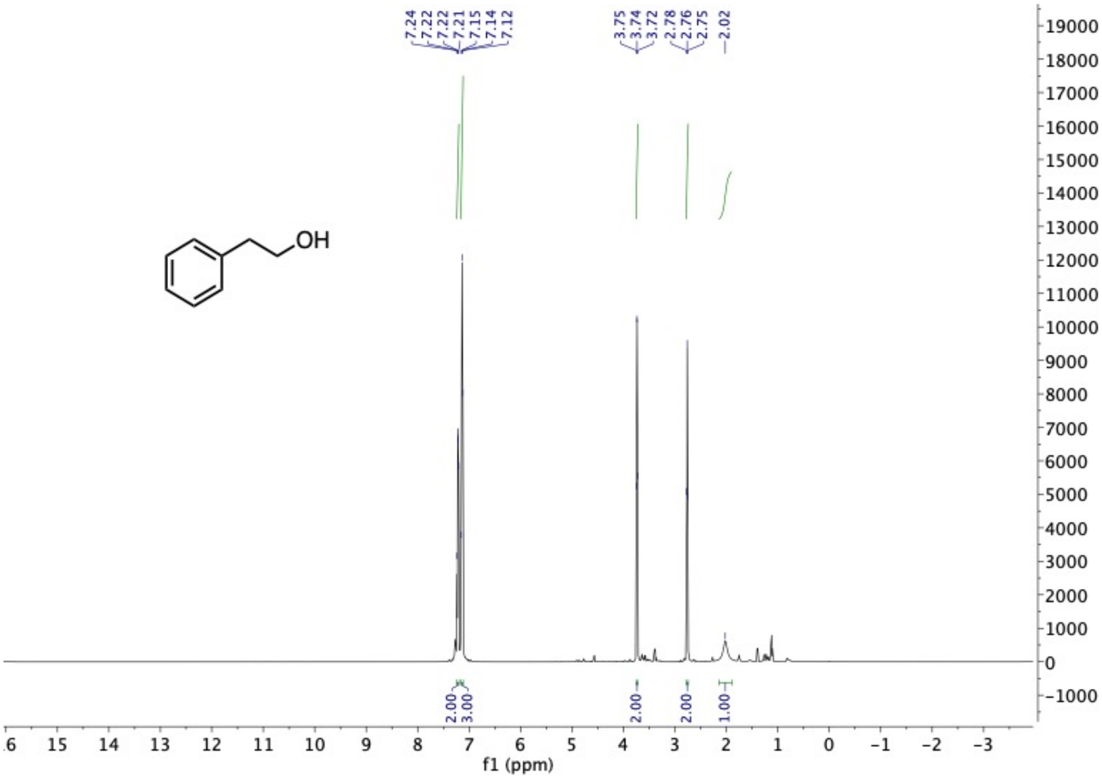
7.24
7.22
7.22
7.21
7.15
7.14
7.12
3.75
3.74
3.72
2.78
2.76
2.75
2.02
OH
2.00
3.00
2.00
2.00
1.00
19000
18000
17000
16000
15000
14000
13000
12000
11000
10000
9000
8000
7000
6000
5000
4000
3000
2000
1000
0
−1000
16 15 14 13 12 11 10 9 8 7 6 5 4 3 2 1 0 −1 −2 −3
f1 (ppm)

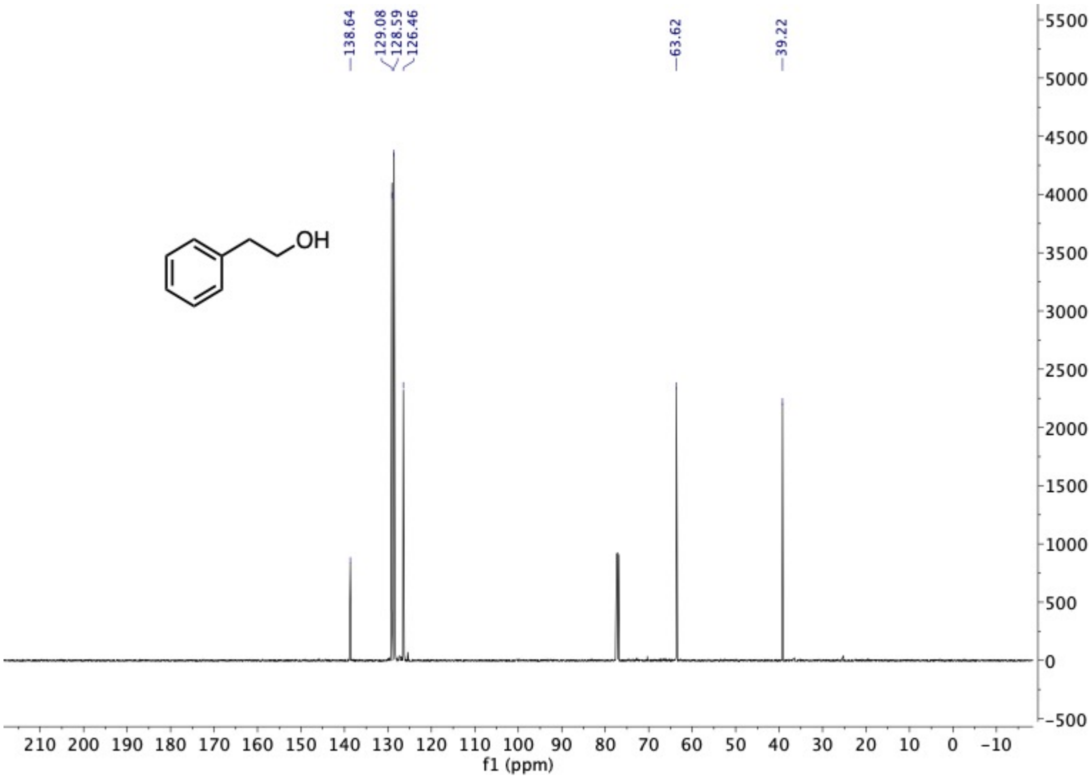
138.64
129.08
128.59
126.46
63.62
39.22
OH
5500
5000
4500
4000
3500
3000
2500
2000
1500
1000
500
0
−500
210 200 190 180 170 160 150 140 130 120 110 100 90 80 70 60 50 40 30 20 10 0 −10
f1 (ppm)

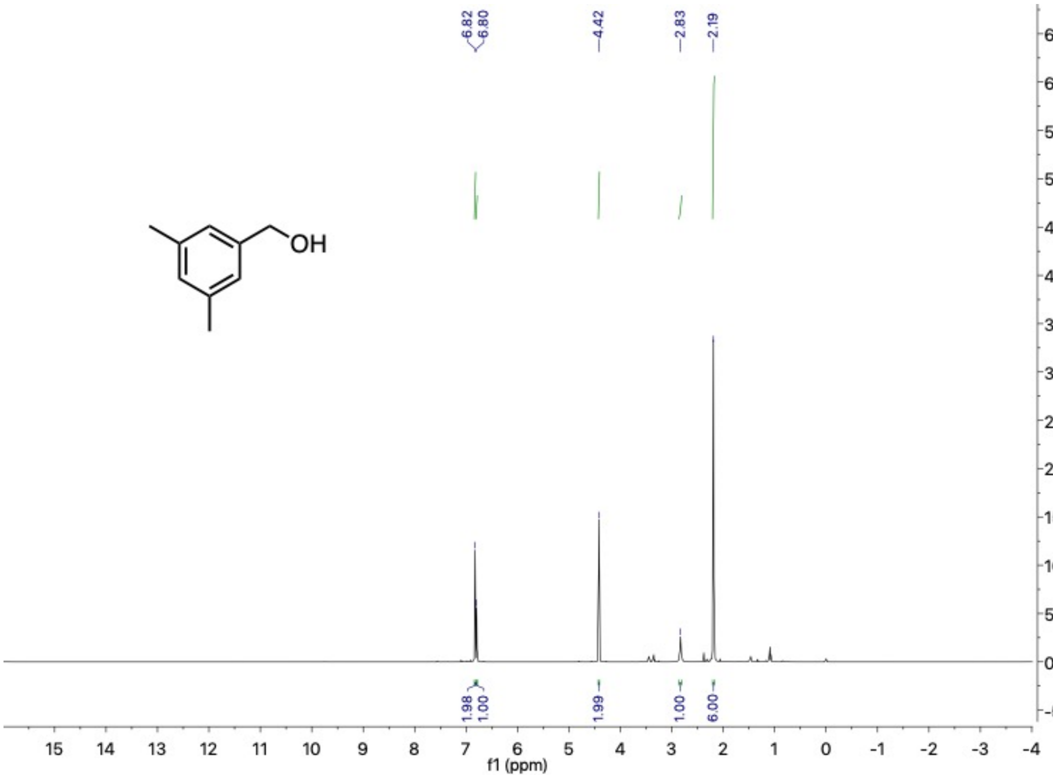
6.82
6.80
4.42
2.83
2.19
OH
1.98
1.00
1.99
1.00
6.00
65000
60000
55000
50000
45000
40000
35000
30000
25000
20000
15000
10000
5000
0
-5000
15 14 13 12 11 10 9 8 7 6 5 4 3 2 1 0 -1 -2 -3 -4
f1 (ppm)

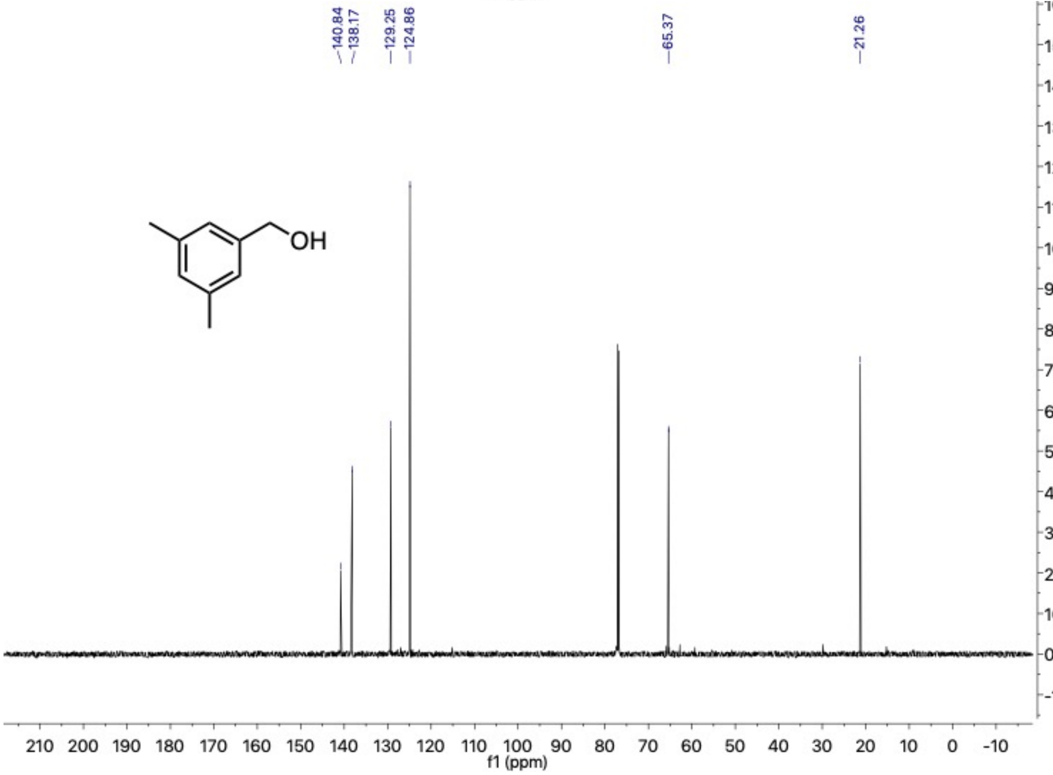
140.84
138.17
129.25
124.86
65.37
21.26
OH
1600
1500
1400
1300
1200
1100
1000
900
800
700
600
500
400
300
200
100
0
-100
210 200 190 180 170 160 150 140 130 120 110 100 90 80 70 60 50 40 30 20 10 0 -10
f1 (ppm)

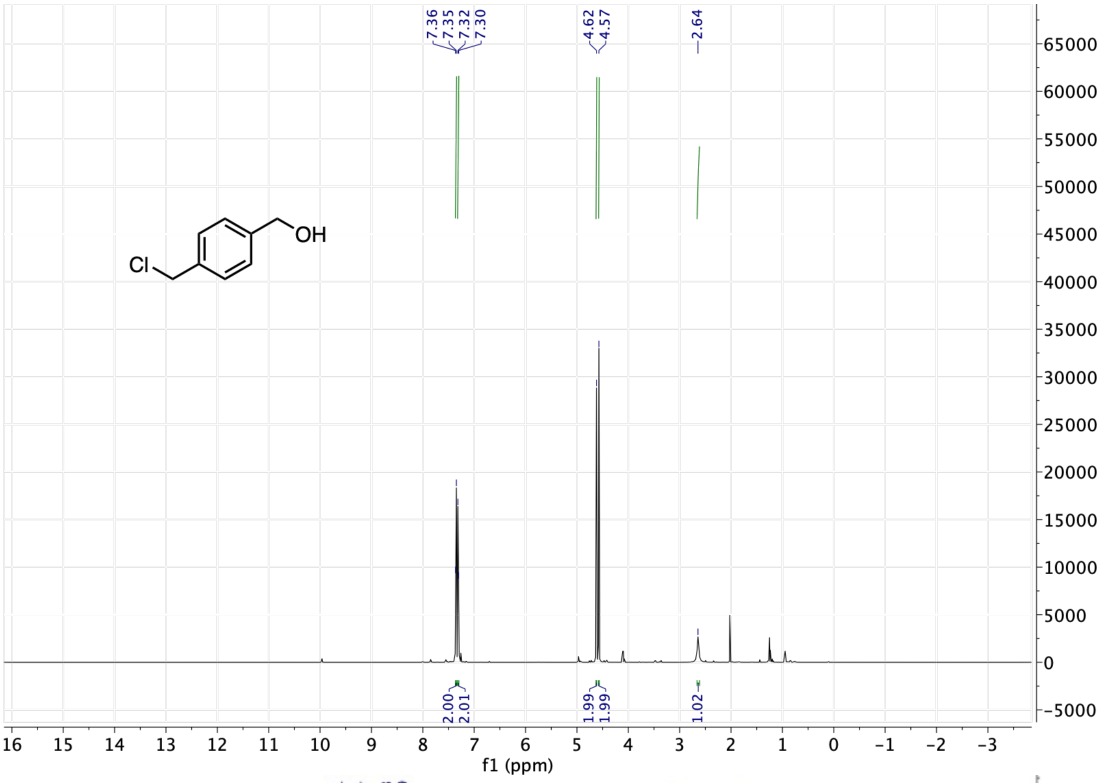
7.36
7.35
7.32
7.30
4.62
4.57
2.64
OH
Cl
2.00
2.01
1.99
1.99
1.02
65000
60000
55000
50000
45000
40000
35000
30000
25000
20000
15000
10000
5000
0
−5000
16 15 14 13 12 11 10 9 8 7 6 5 4 3 2 1 0 −1 −2 −3
f1 (ppm)

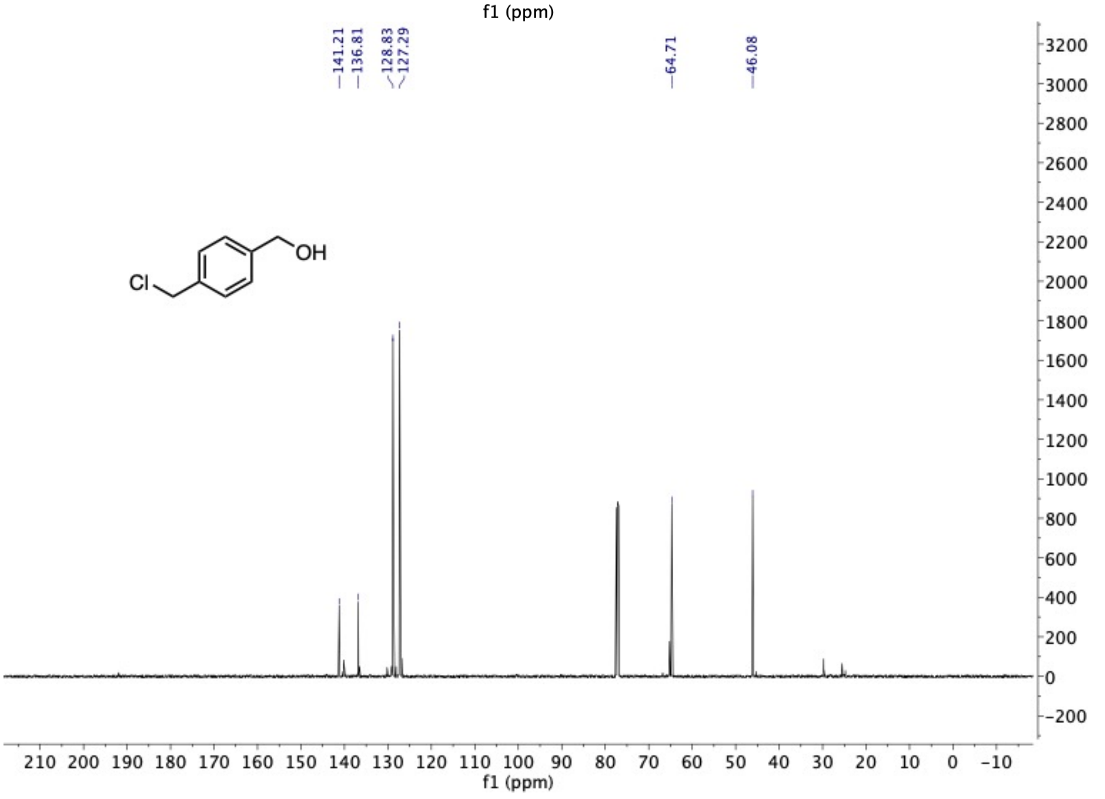
141.21
136.81
128.83
127.29
64.71
46.08
OH
Cl
3200
3000
2800
2600
2400
2200
2000
1800
1600
1400
1200
1000
800
600
400
200
0
−200
210 200 190 180 170 160 150 140 130 120 110 100 90 80 70 60 50 40 30 20 10 0 −10
f1 (ppm)

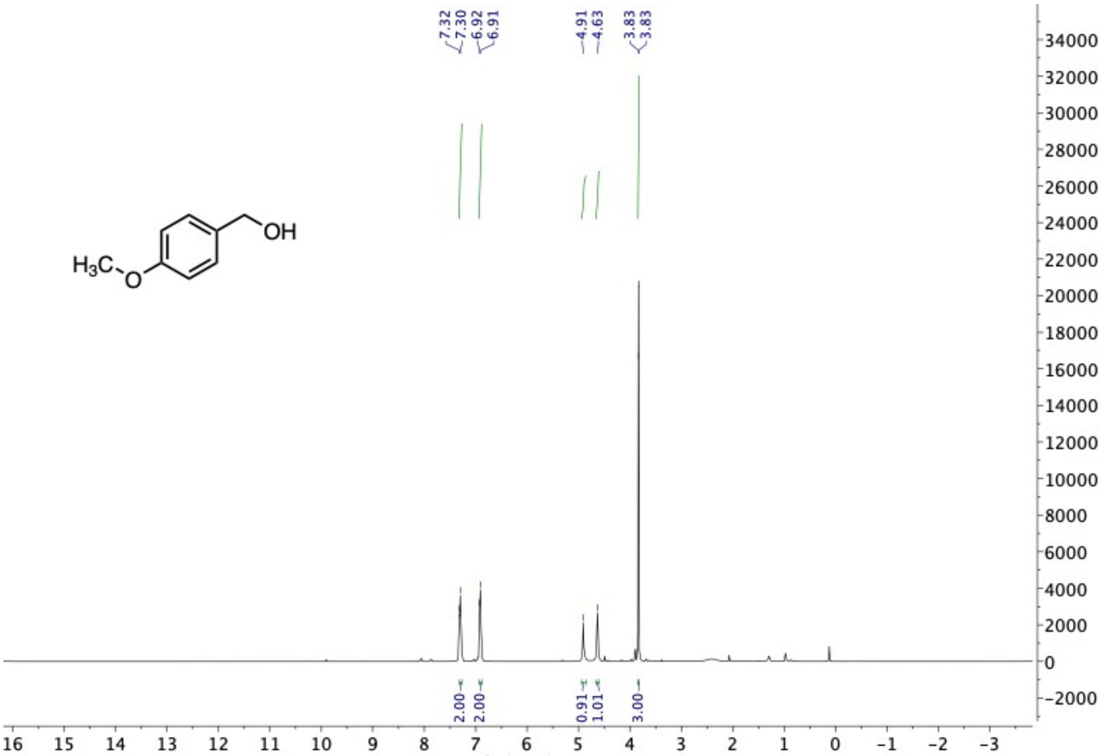
7.32
7.30
6.92
6.91
4.91
4.63
3.83
3.83
H3C
O
OH
2.00
2.00
0.91
1.01
3.00
f1 (ppm)
16 15 14 13 12 11 10 9 8 7 6 5 4 3 2 1 0 −1 −2 −3
34000 32000 30000 28000 26000 24000 22000 20000 18000 16000 14000 12000 10000 8000 6000 4000 2000 0 −2000

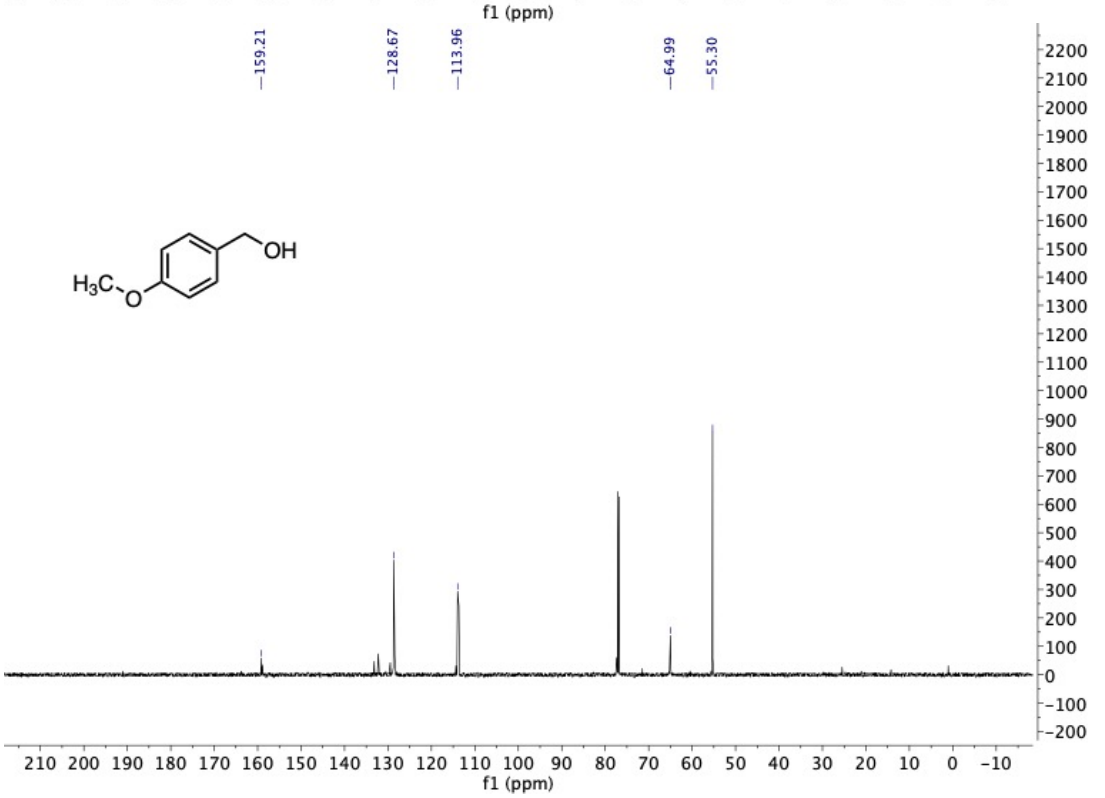
159.21
128.67
113.96
64.99
55.30
H3C
O
OH
f1 (ppm)
210 200 190 180 170 160 150 140 130 120 110 100 90 80 70 60 50 40 30 20 10 0 −10
2200 2100 2000 1900 1800 1700 1600 1500 1400 1300 1200 1100 1000 900 800 700 600 500 400 300 200 100 0 −100 −200

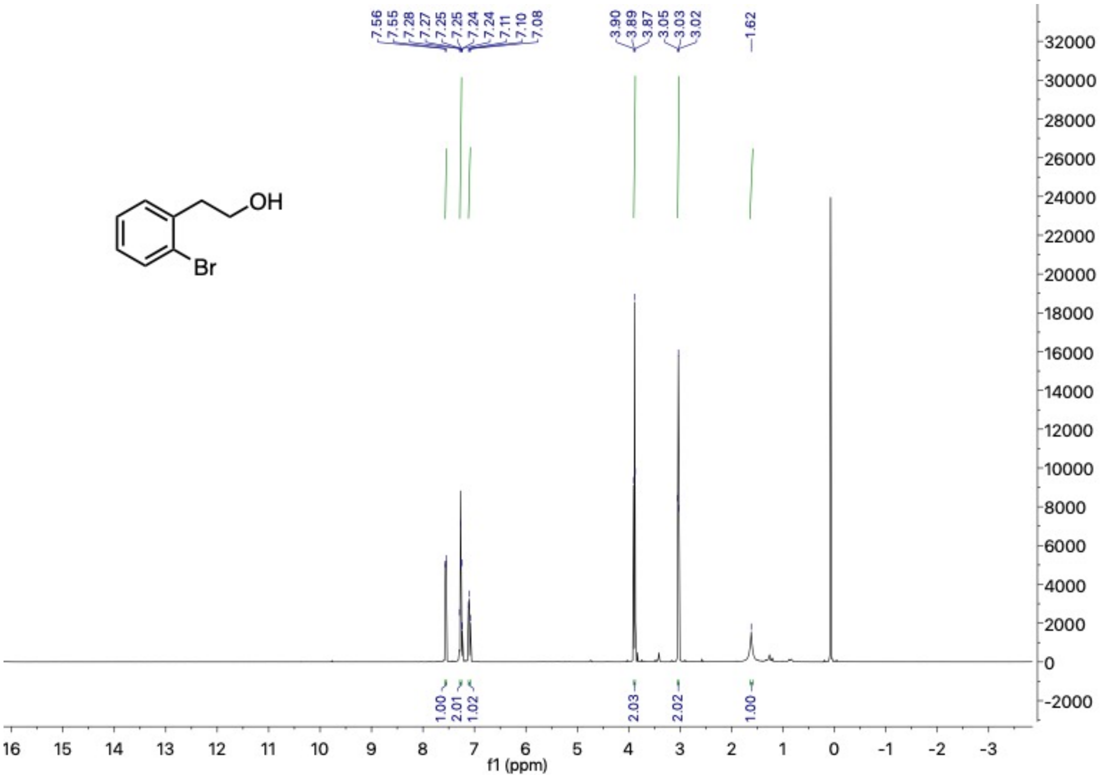
7.56
7.55
7.28
7.27
7.25
7.25
7.24
7.24
7.11
7.10
7.08
3.90
3.89
3.87
3.05
3.03
3.02
1.62
OH
Br
1.00
2.01
1.02
2.03
2.02
1.00
f1 (ppm)

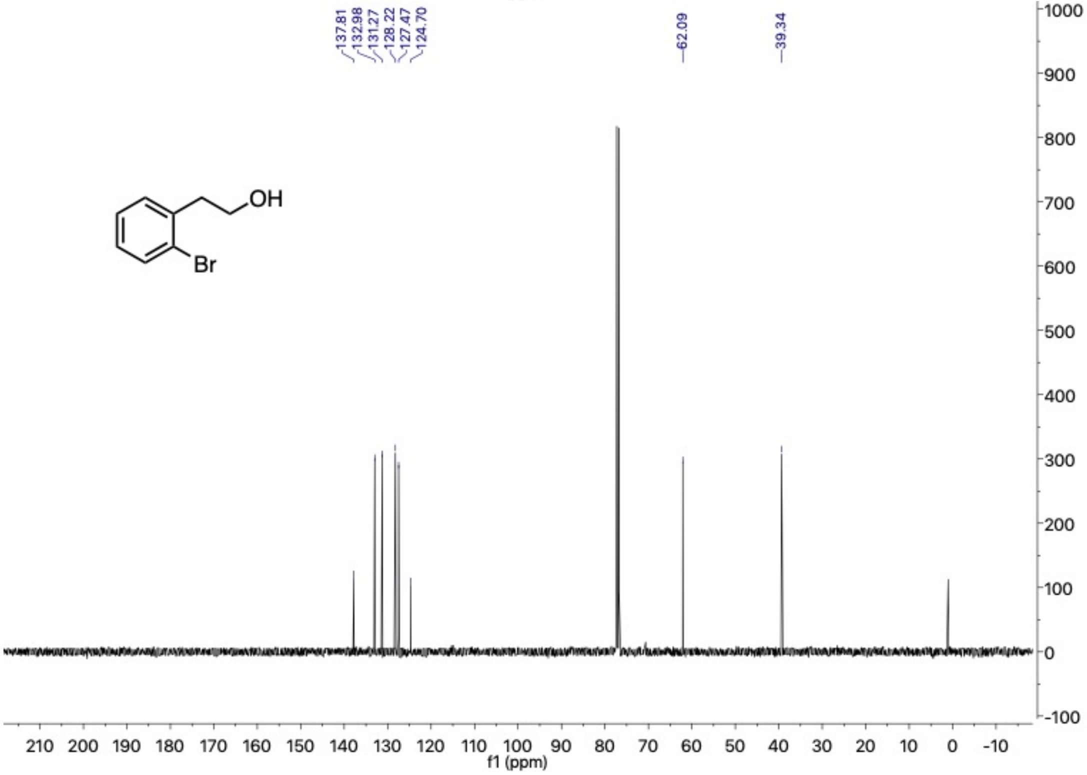
137.81
132.98
131.27
128.22
127.47
124.70
62.09
39.34
OH
Br
f1 (ppm)

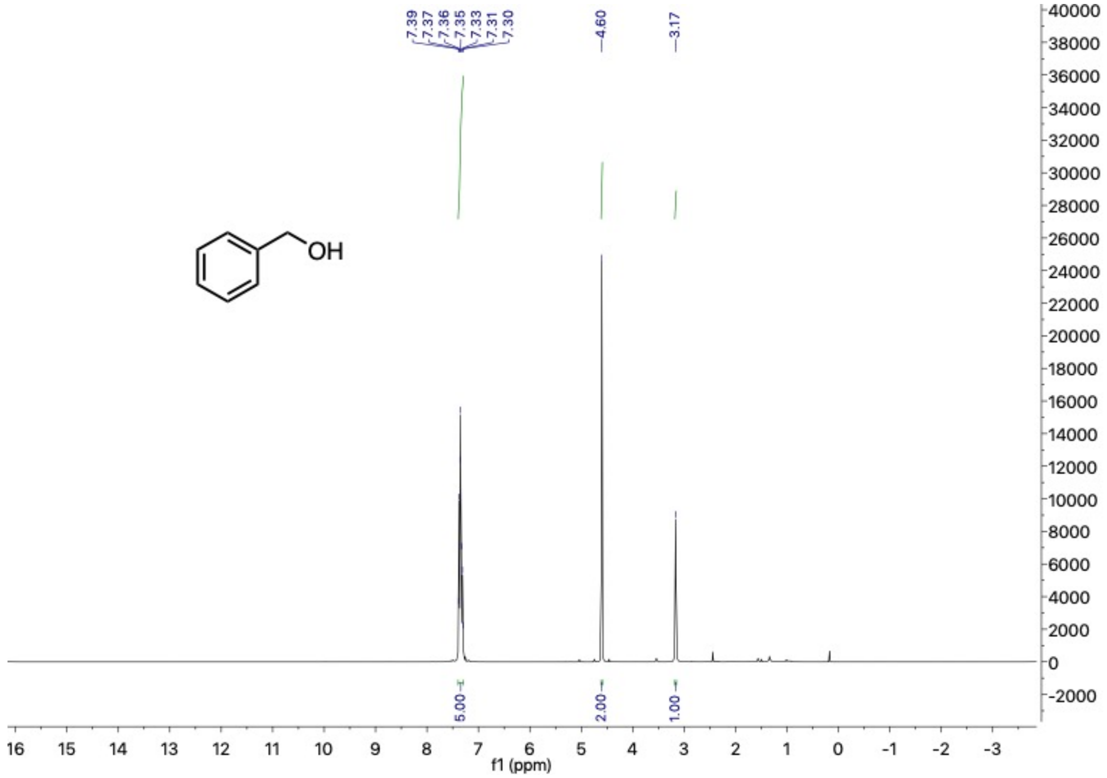
7.39
7.37
7.36
7.35
7.33
7.31
7.30
4.60
3.17
OH
5.00
2.00
1.00
40000
38000
36000
34000
32000
30000
28000
26000
24000
22000
20000
18000
16000
14000
12000
10000
8000
6000
4000
2000
0
-2000
16 15 14 13 12 11 10 9 8 7 6 5 4 3 2 1 0 -1 -2 -3
f1 (ppm)

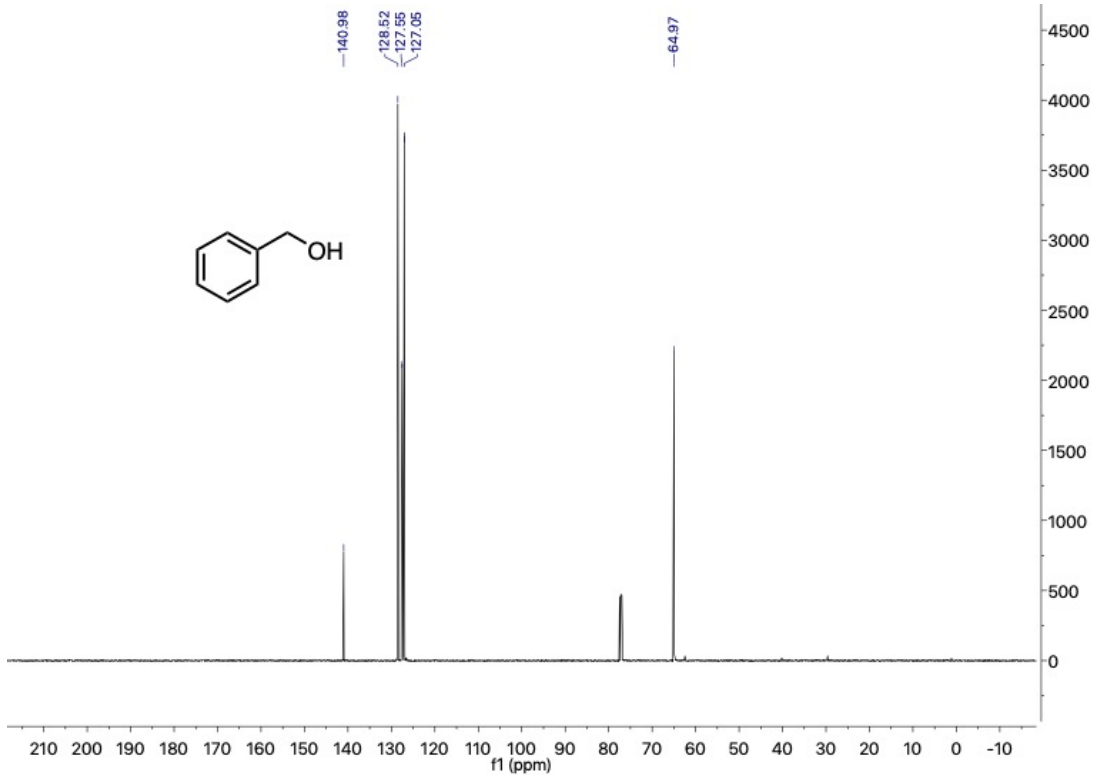
140.98
128.52
127.55
127.05
64.97
OH
4500
4000
3500
3000
2500
2000
1500
1000
500
0
210 200 190 180 170 160 150 140 130 120 110 100 90 80 70 60 50 40 30 20 10 0 -10
f1 (ppm)

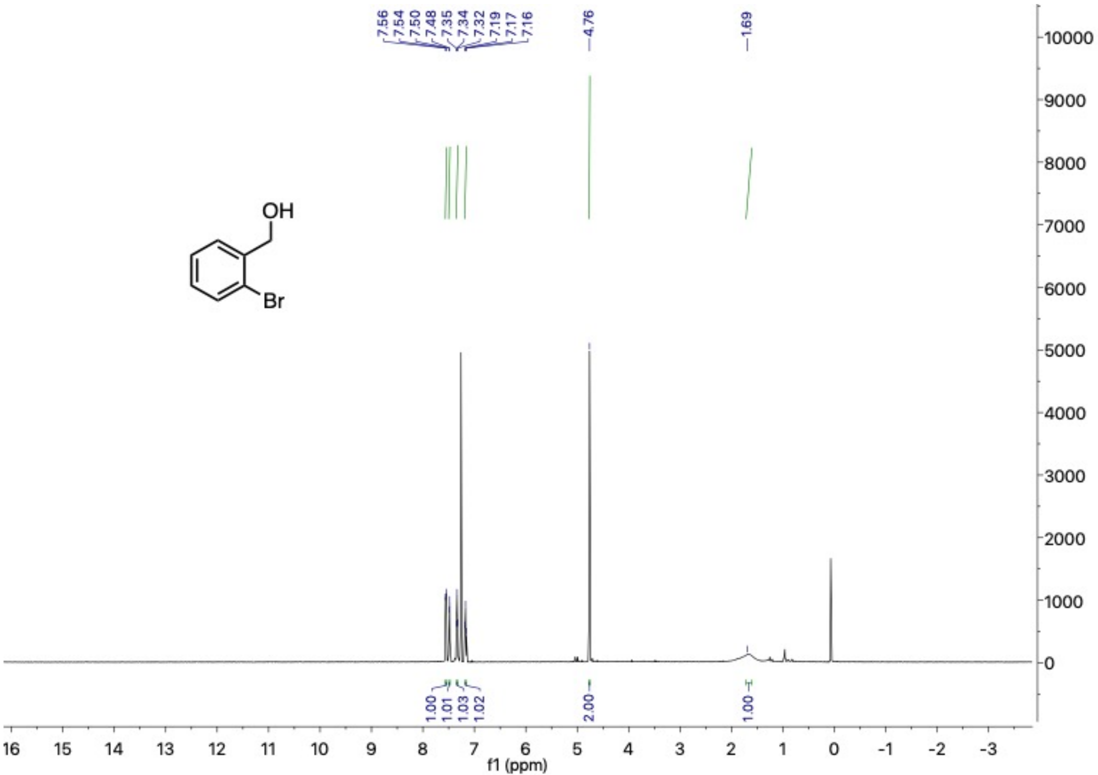
7.56
7.54
7.50
7.48
7.35
7.34
7.32
7.19
7.17
7.16
4.76
1.69
OH
Br
1.00
1.01
1.03
1.02
2.00
1.00
10000
9000
8000
7000
6000
5000
4000
3000
2000
1000
0
16 15 14 13 12 11 10 9 8 7 6 5 4 3 2 1 0 -1 -2 -3
f1 (ppm)

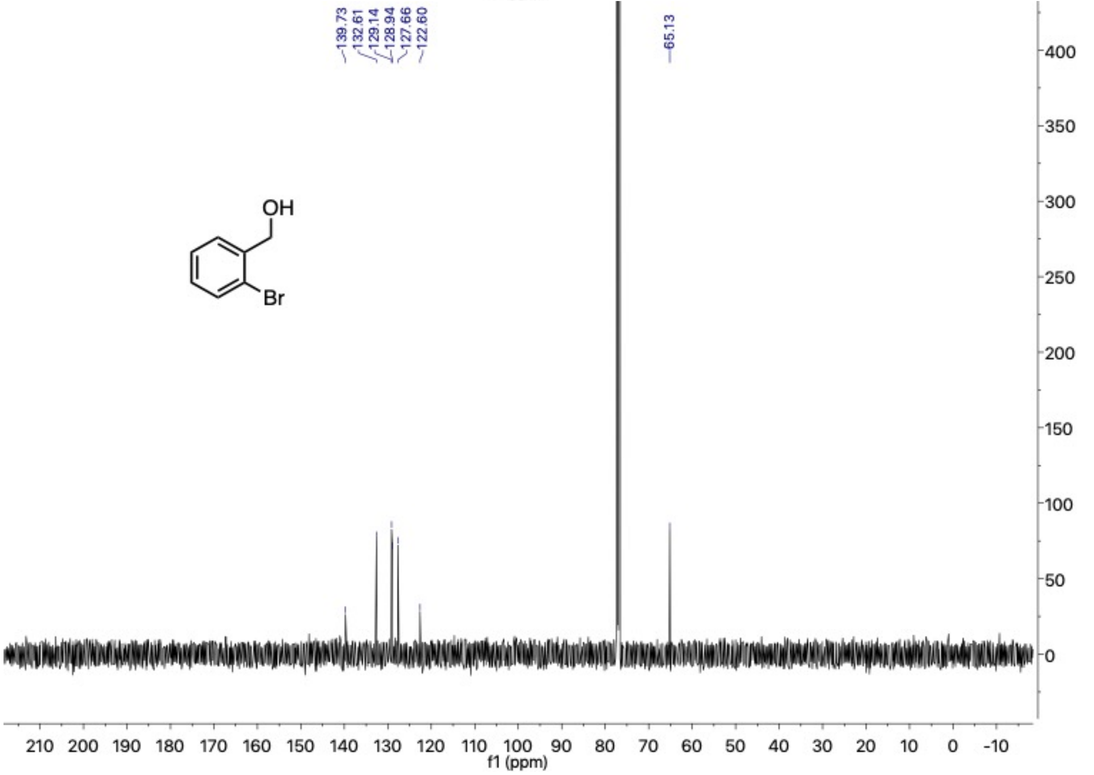
139.73
132.61
129.14
128.94
127.66
122.60
65.13
OH
Br
400
350
300
250
200
150
100
50
0
210 200 190 180 170 160 150 140 130 120 110 100 90 80 70 60 50 40 30 20 10 0 -10
f1 (ppm)

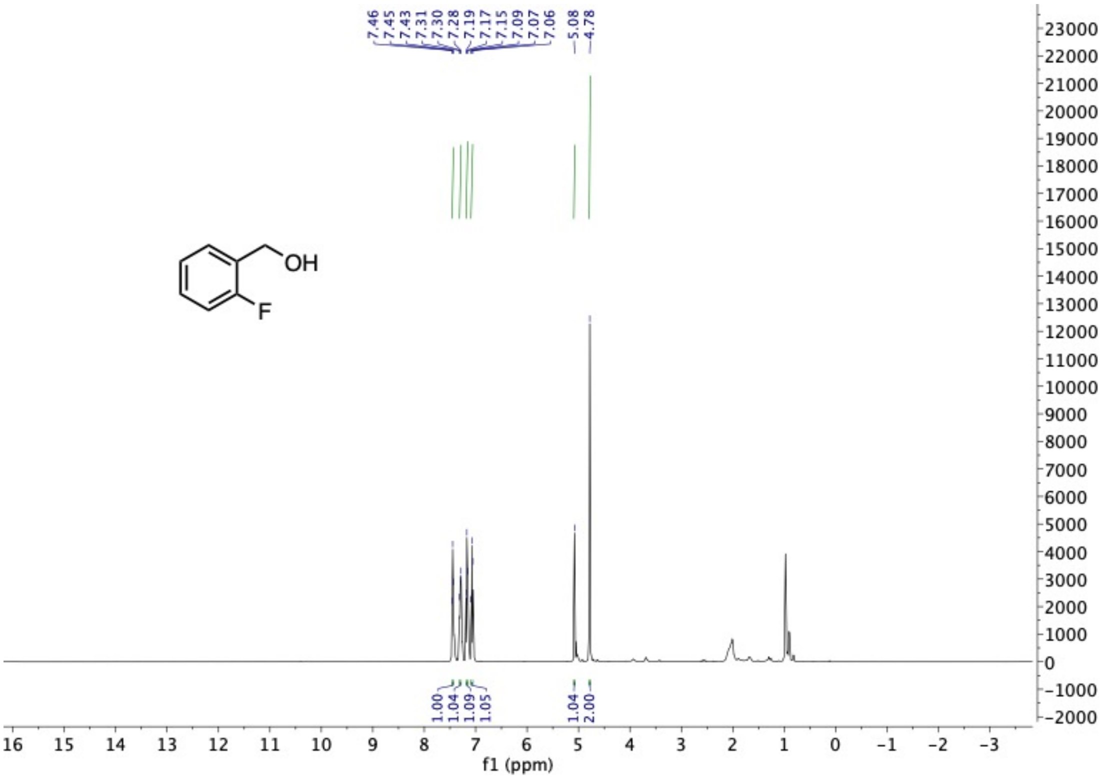
7.46
7.45
7.43
7.31
7.30
7.28
7.19
7.17
7.15
7.09
7.07
7.06
5.08
4.78
OH
F
1.00
1.04
1.09
1.05
1.04
2.00
f1 (ppm)

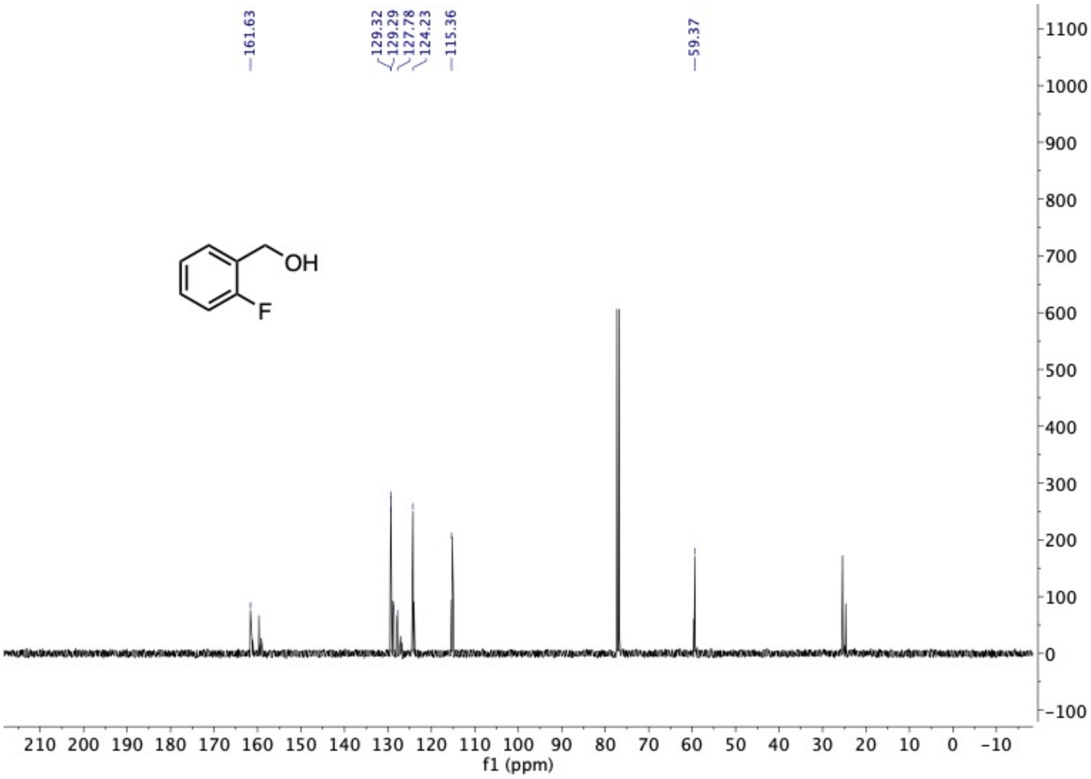
161.63
129.32
129.29
127.78
124.23
115.36
59.37
OH
F
f1 (ppm)

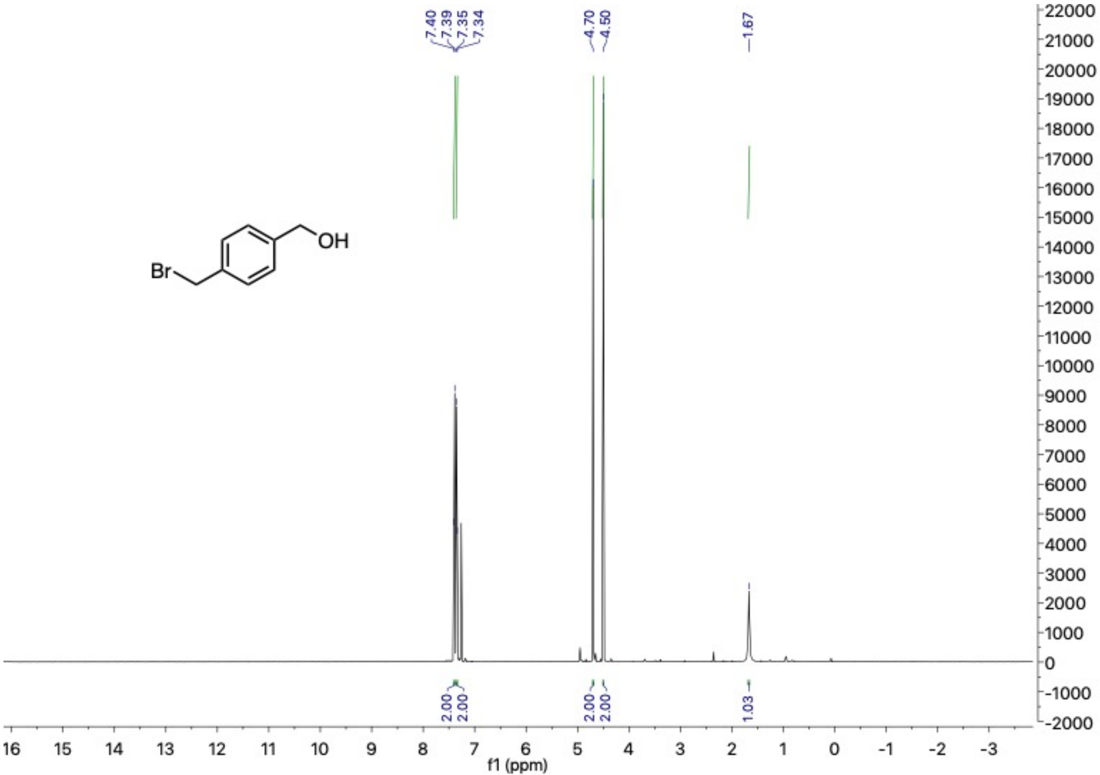
7.40
7.39
7.35
7.34
4.70
4.50
1.67
Br
OH
2.00
2.00
2.00
2.00
1.03
22000
21000
20000
19000
18000
17000
16000
15000
14000
13000
12000
11000
10000
9000
8000
7000
6000
5000
4000
3000
2000
1000
0
-1000
-2000
16 15 14 13 12 11 10 9 8 7 6 5 4 3 2 1 0 -1 -2 -3
f1 (ppm)

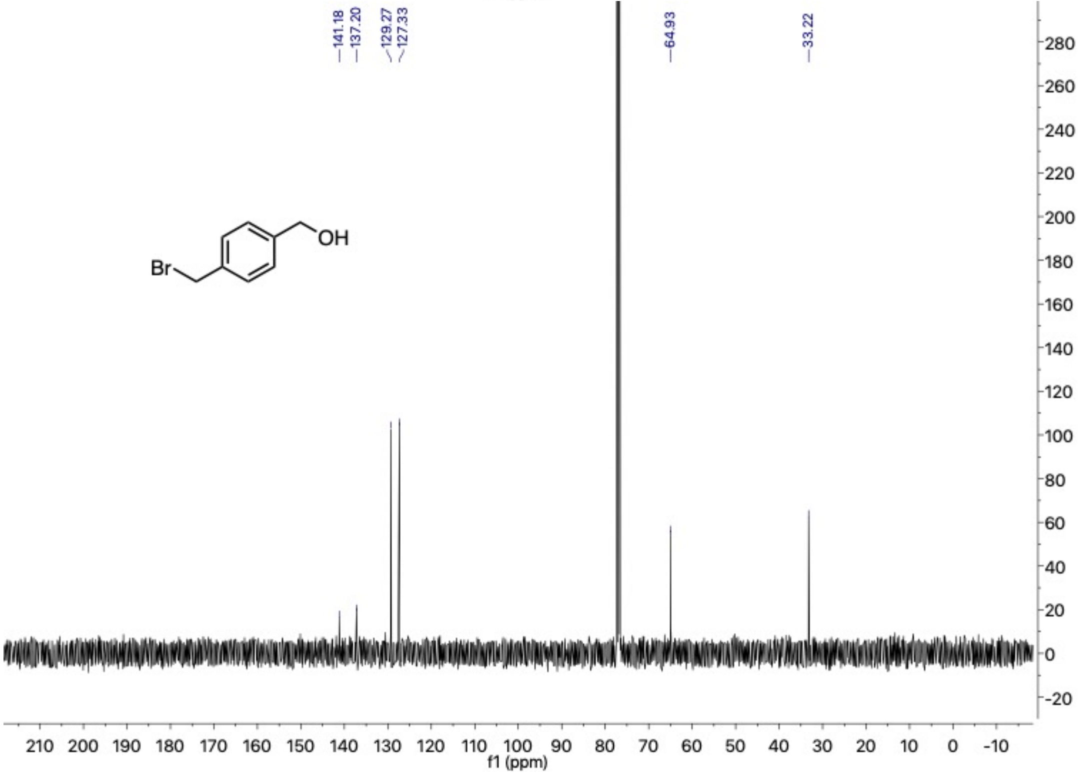
141.18
137.20
129.27
127.33
64.93
33.22
Br
OH
280
260
240
220
200
180
160
140
120
100
80
60
40
20
0
-20
210 200 190 180 170 160 150 140 130 120 110 100 90 80 70 60 50 40 30 20 10 0 -10
f1 (ppm)

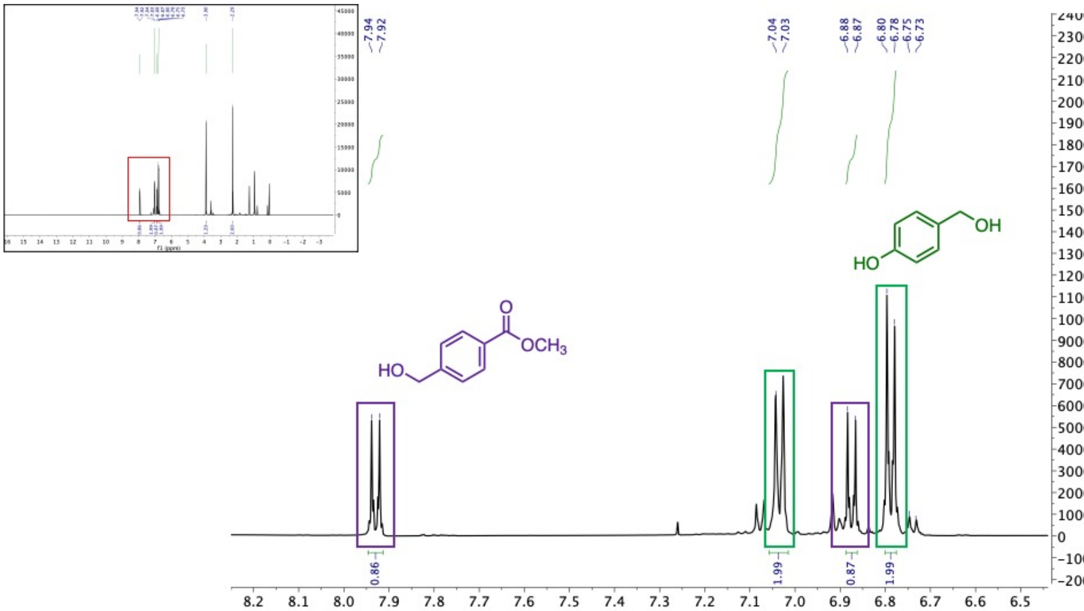

7.94
7.92
7.04
7.03
6.88
6.87
6.80
6.78
6.75
6.73
HO
OCH3
O
HO
OH
0.86
1.99
0.87
1.99
8.2
8.1
8.0
7.9
7.8
7.7
7.6
7.5
7.4
7.3
7.2
7.1
7.0
6.9
6.8
6.7
6.6
6.5
f1 (ppm)
24000
23000
22000
21000
20000
19000
18000
17000
16000
15000
14000
13000
12000
11000
10000
9000
8000
7000
6000
5000
4000
3000
2000
1000
0
-1000
-2000

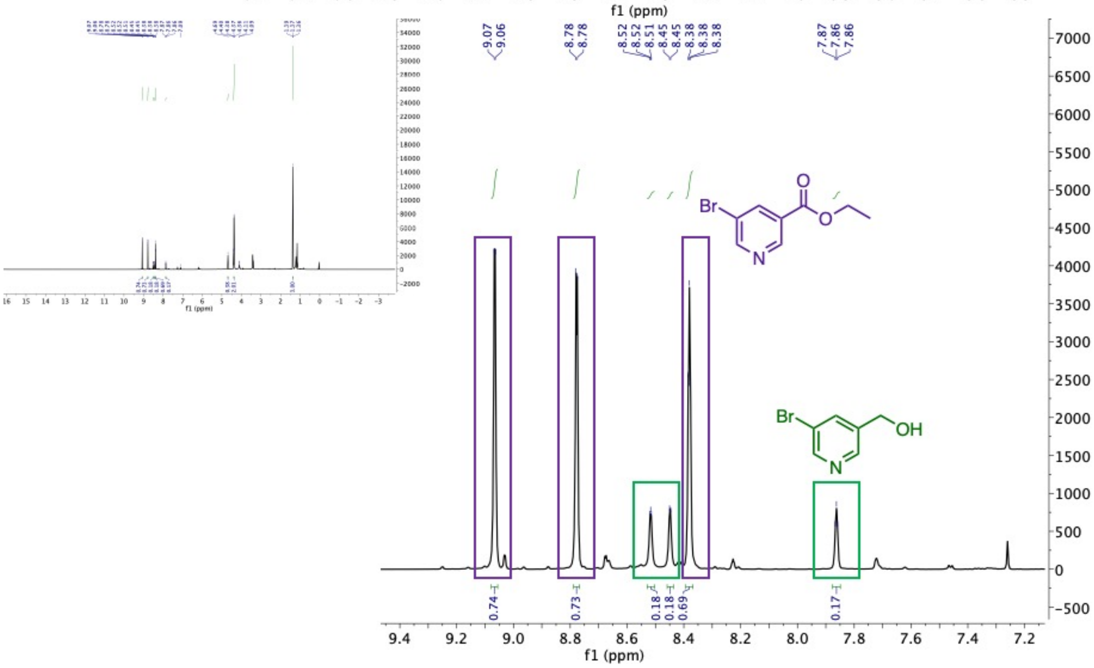

9.07
9.06
8.78
8.78
8.52
8.52
8.51
8.45
8.45
8.38
8.38
8.38
7.87
7.86
7.86
Br
O
O
N
Br
OH
N
0.74
0.73
0.18
0.18
0.69
0.17
9.4
9.2
9.0
8.8
8.6
8.4
8.2
8.0
7.8
7.6
7.4
7.2
f1 (ppm)
7000
6500
6000
5500
5000
4500
4000
3500
3000
2500
2000
1500
1000
500
0
-500

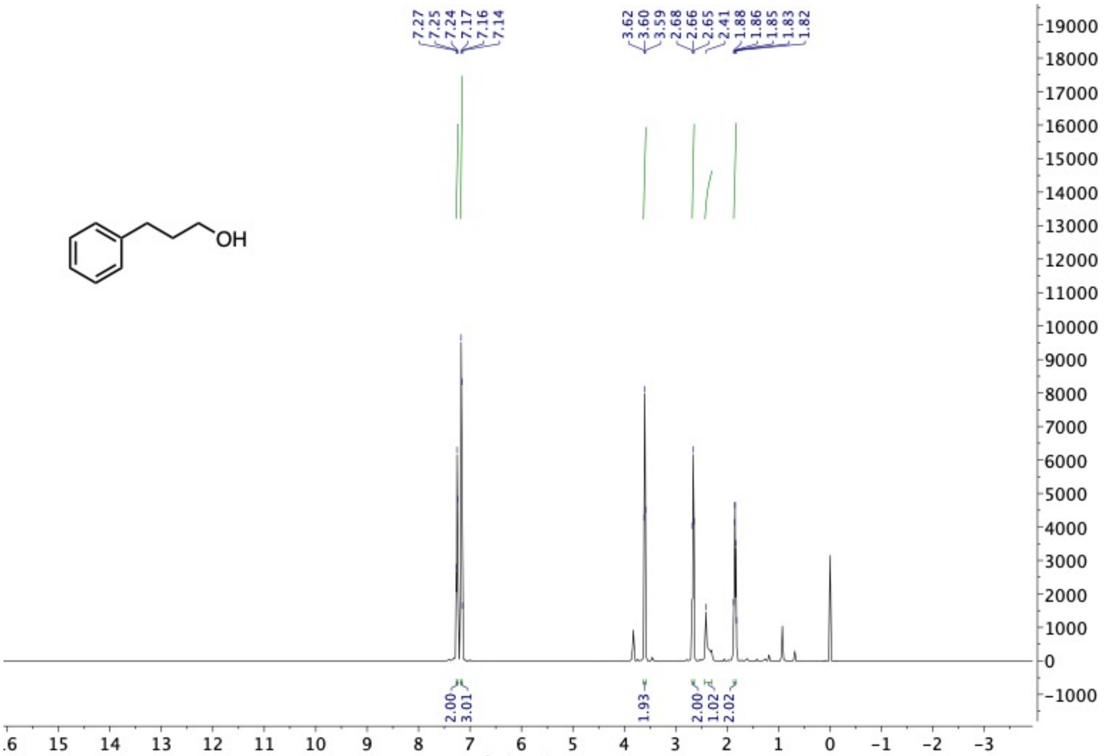
7.27
7.25
7.24
7.17
7.16
7.14
3.62
3.60
3.59
2.68
2.66
2.65
2.41
1.88
1.86
1.85
1.83
1.82
OH
2.00
3.01
1.93
2.00
1.02
2.02
f1 (ppm)

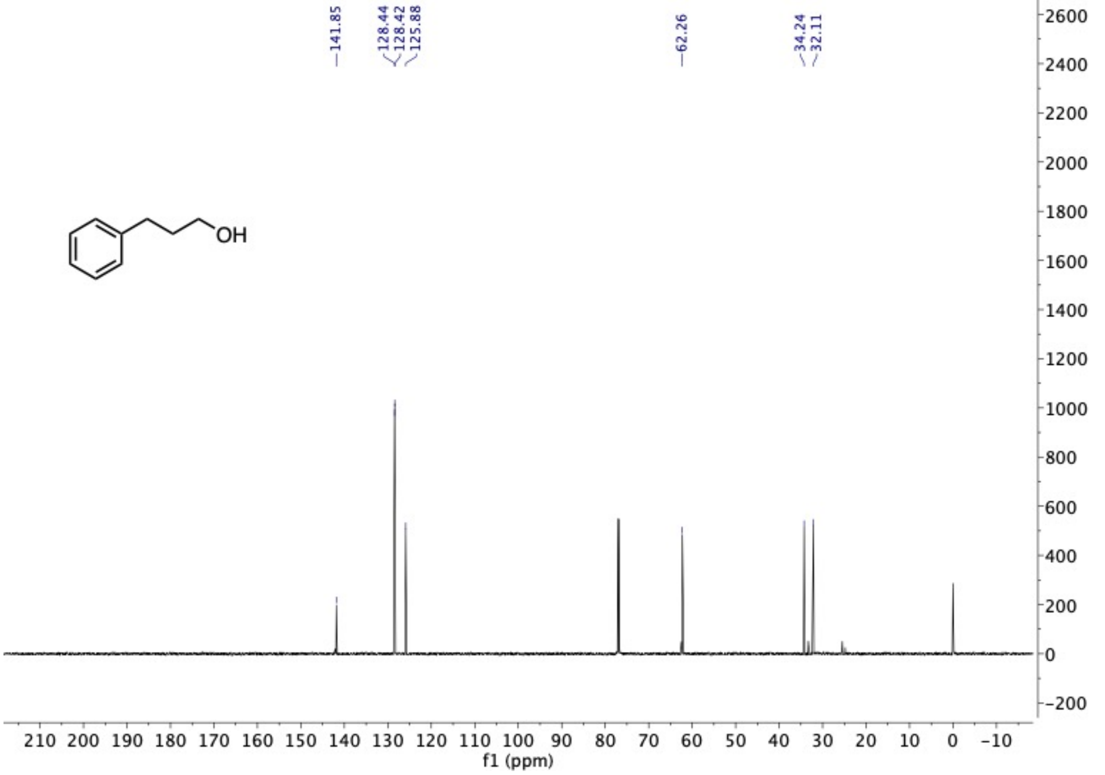
141.85
128.44
128.42
125.88
62.26
34.24
32.11
OH
f1 (ppm)

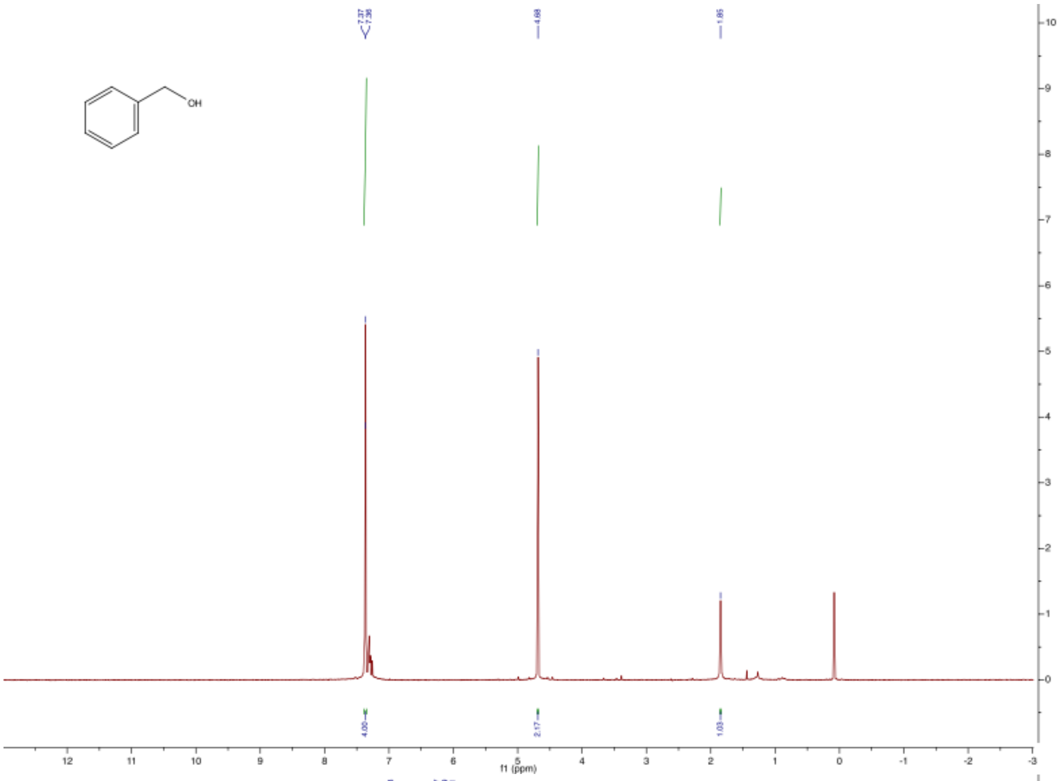
7.37
7.36
4.68
1.85
OH
4.00
2.17
1.03
f1 (ppm)
12
11
10
9
8
7
6
5
4
3
2
1
0
-1
-2
-3

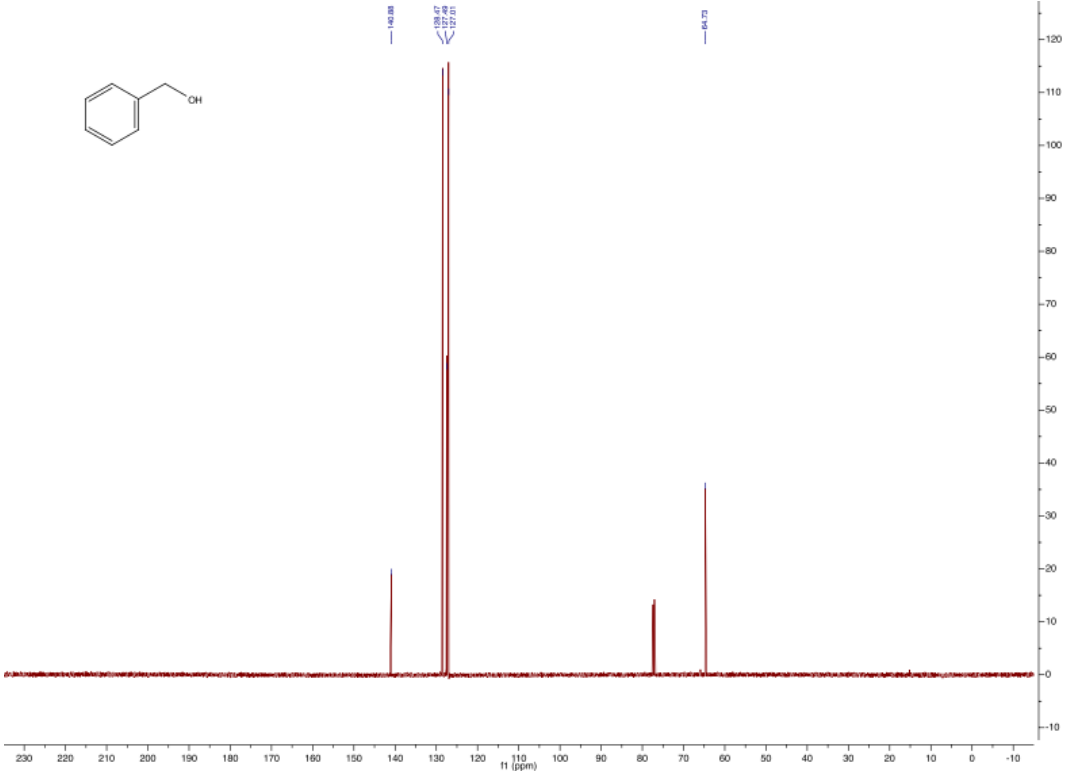
140.88
128.47
127.49
127.01
64.73
OH
f1 (ppm)
230
220
210
200
190
180
170
160
150
140
130
120
110
100
90
80
70
60
50
40
30
20
10
0
-10

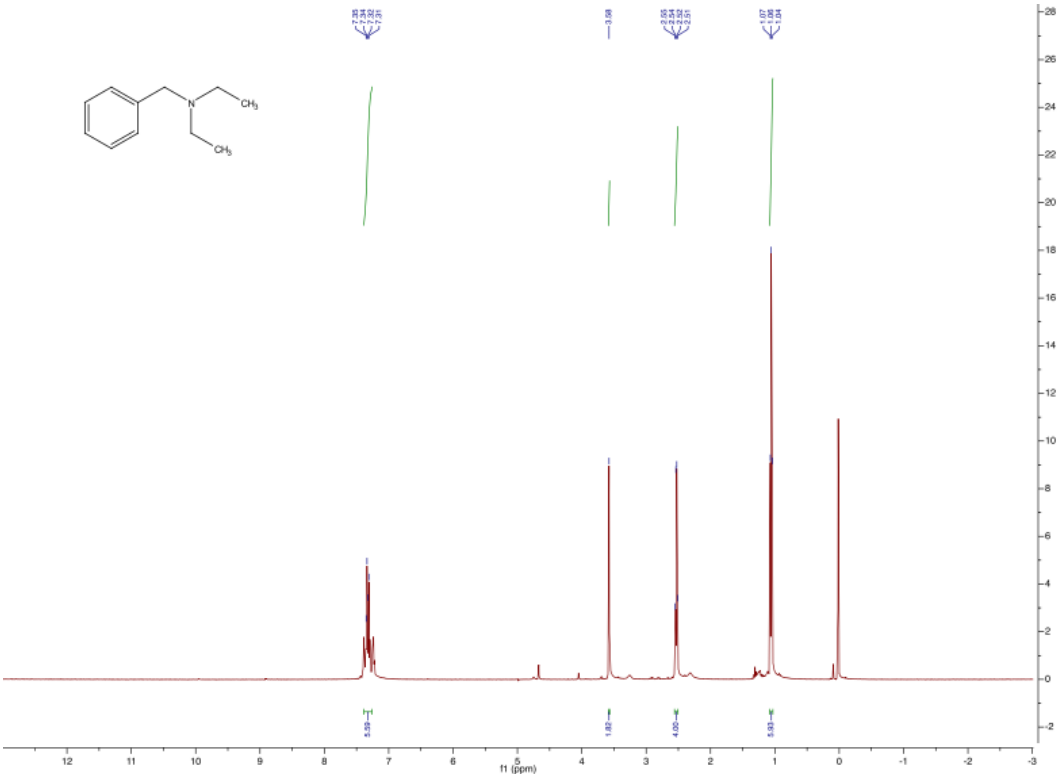

CH3
N
CH3
7.35
7.34
7.32
7.31
3.58
2.55
2.54
2.52
2.51
1.07
1.06
1.04
5.59
1.82
4.00
5.93
f1 (ppm)

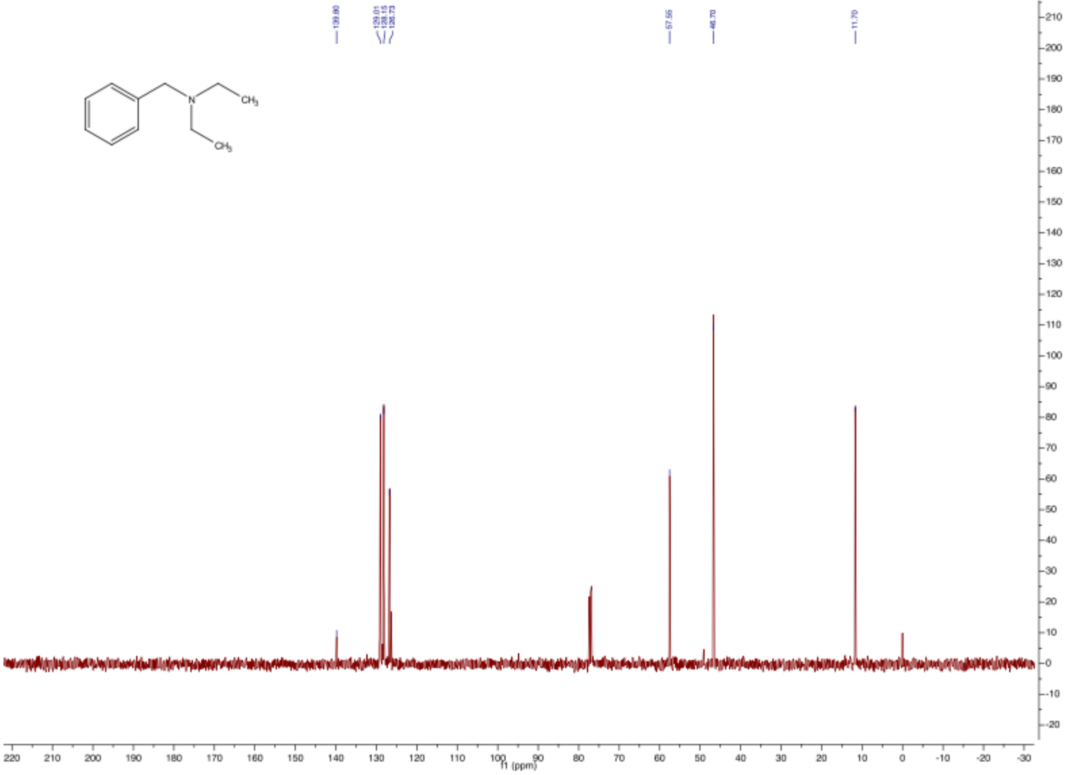

CH3
N
CH3
139.80
129.01
128.15
126.73
57.56
46.70
11.70
f1 (ppm)

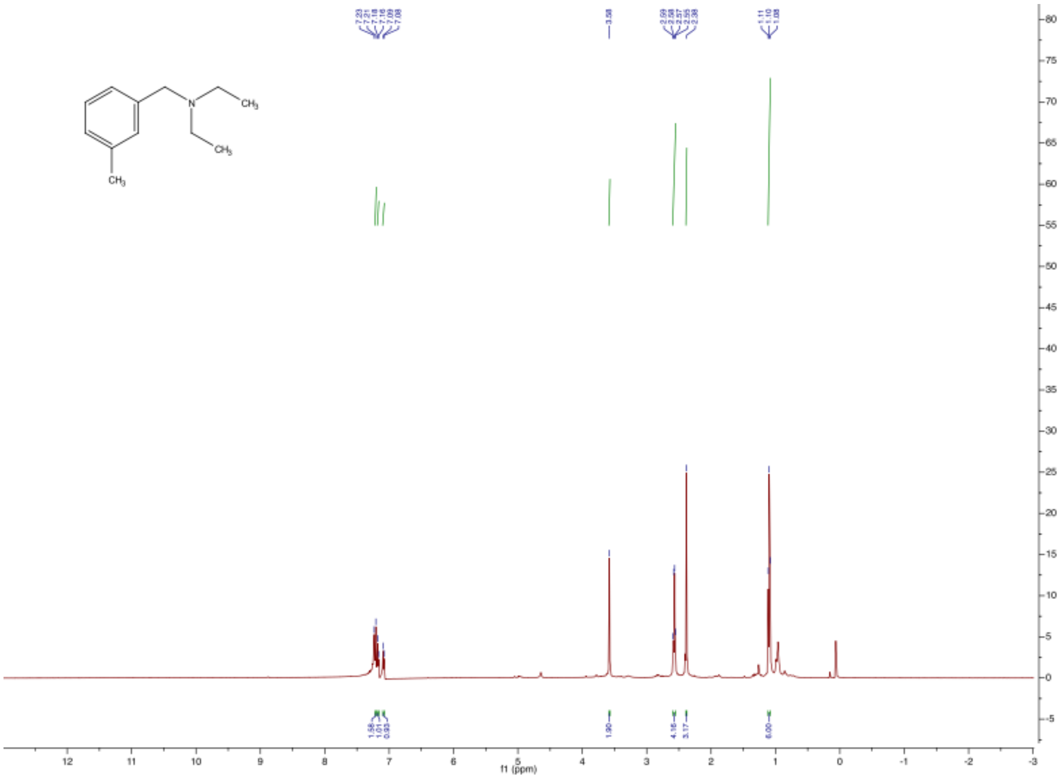
7.23
7.21
7.18
7.16
7.09
7.08
3.58
2.59
2.58
2.57
2.55
2.38
1.11
1.10
1.08
CH3
N
1.58
1.01
0.93
1.90
4.18
3.17
6.00
f1 (ppm)

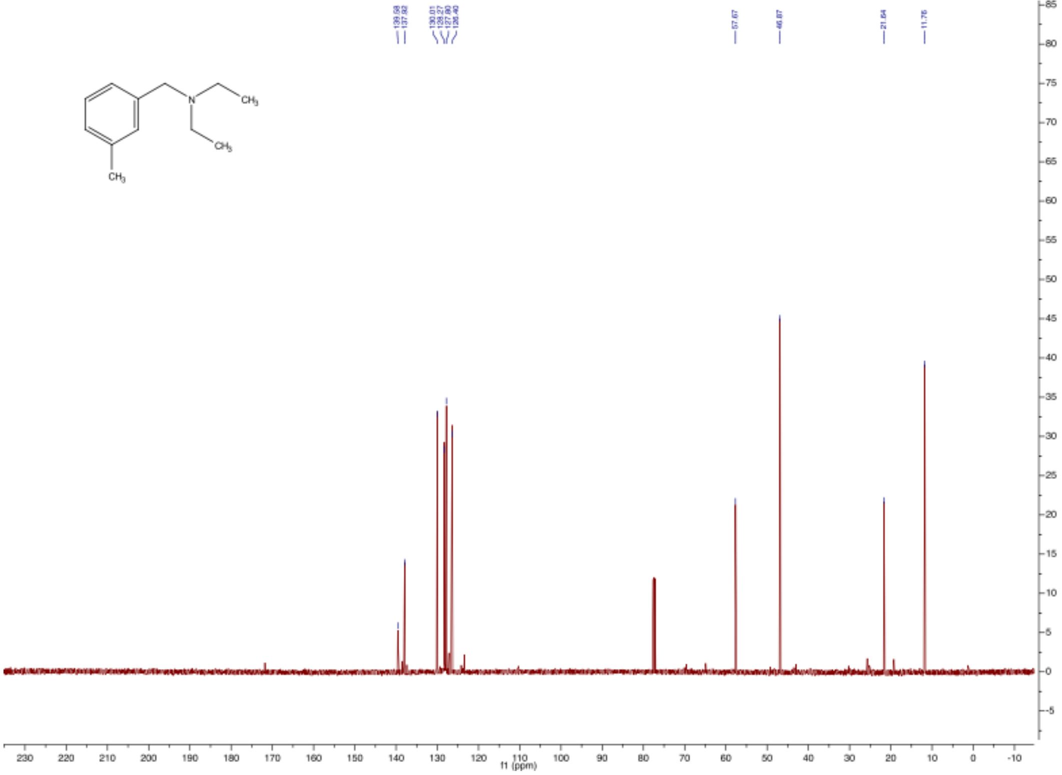
139.58
137.82
130.01
129.27
127.80
126.40
57.67
46.87
21.64
11.76
CH3
N
f1 (ppm)

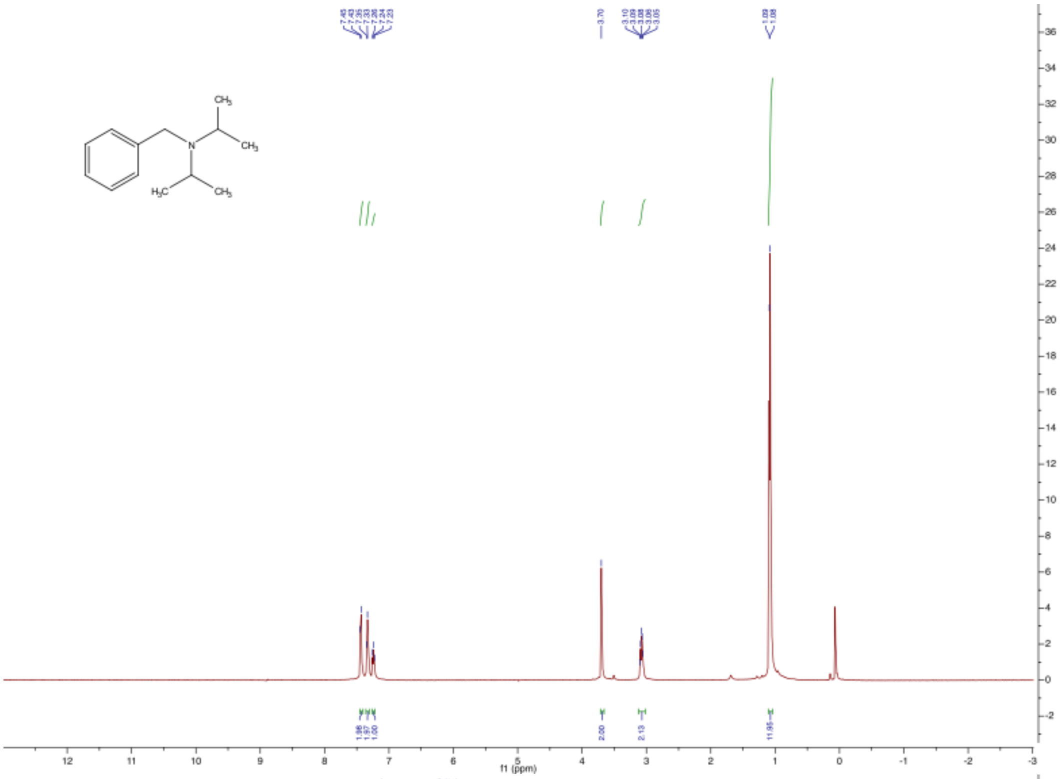
7.45
7.43
7.35
7.33
7.26
7.24
7.23
3.70
3.10
3.09
3.08
3.06
3.05
1.09
1.08
CH$_3$
CH$_3$
H$_3$C
CH$_3$
N
1.98
1.97
1.00
2.00
2.13
11.95
36
34
32
30
28
26
24
22
20
18
16
14
12
10
8
6
4
2
0
-2
12
11
10
9
8
7
6
5
4
3
2
1
0
-1
-2
-3
f1 (ppm)

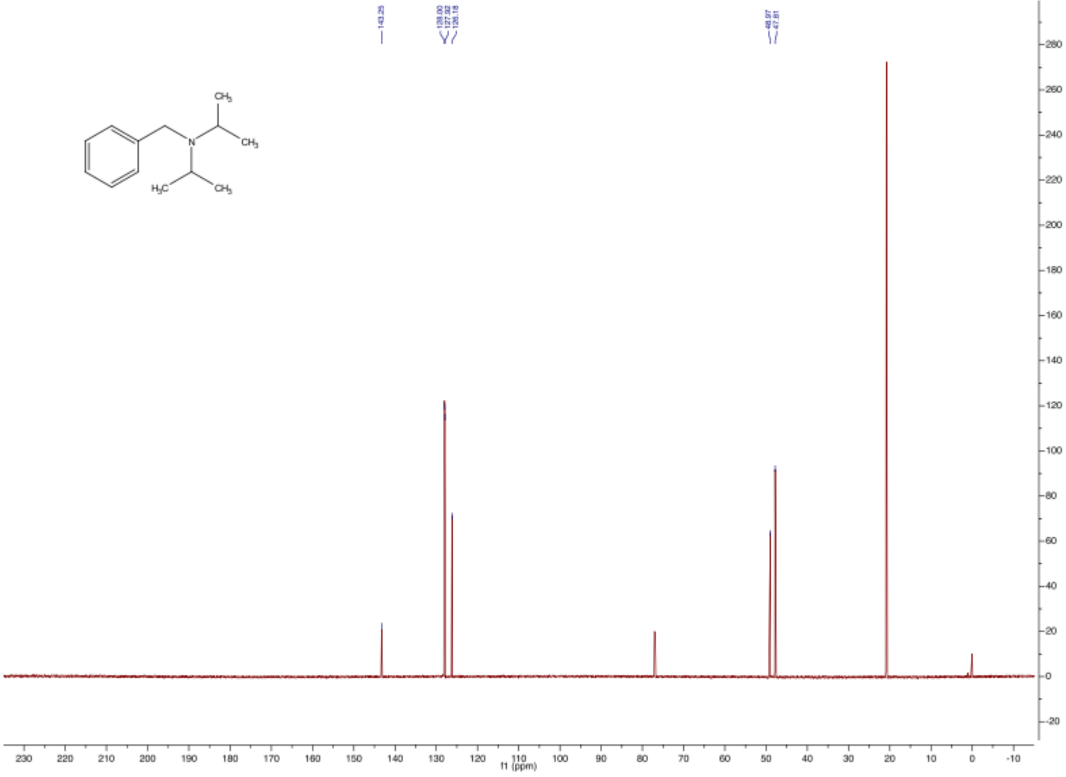
143.25
128.00
127.92
126.18
48.97
47.81
CH$_3$
CH$_3$
H$_3$C
CH$_3$
N
280
260
240
220
200
180
160
140
120
100
80
60
40
20
0
-20
230
220
210
200
190
180
170
160
150
140
130
120
110
100
90
80
70
60
50
40
30
20
10
0
-10
f1 (ppm)

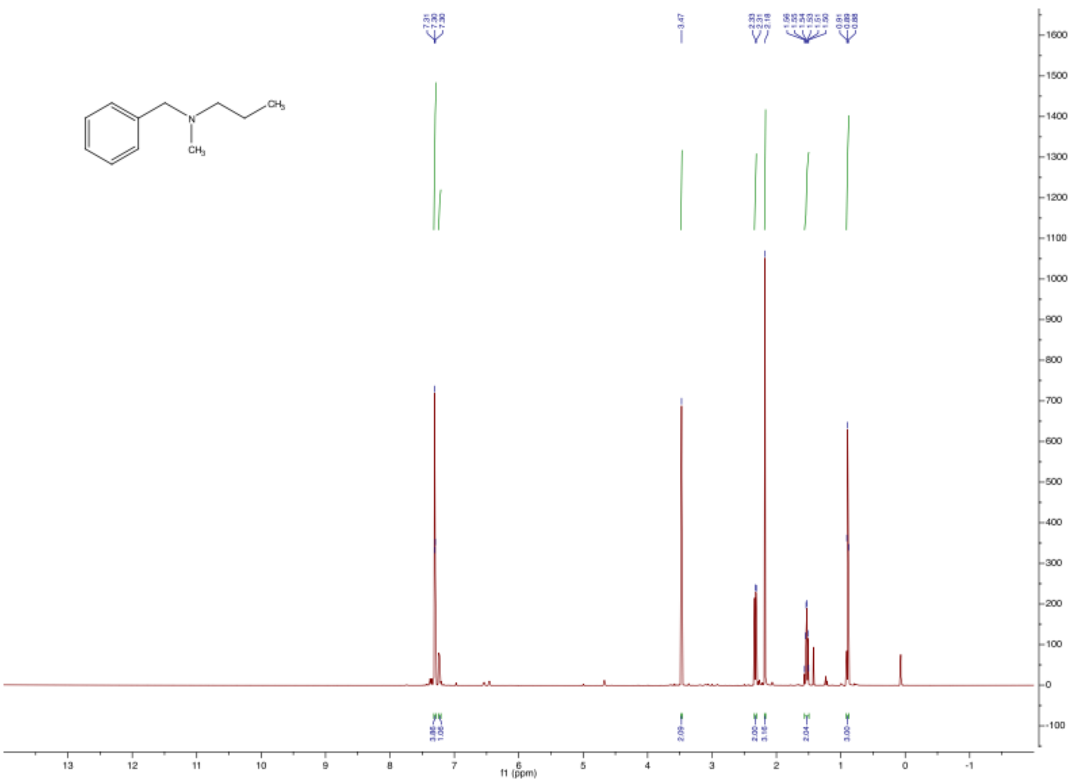
7.31
7.30
7.30
3.47
2.33
2.31
2.18
1.56
1.55
1.54
1.53
1.51
1.50
0.91
0.89
0.88
CH3
N
CH3
3.86
1.06
2.09
2.00
3.16
2.04
3.00
13
12
11
10
9
8
7
6
5
4
3
2
1
0
-1
f1 (ppm)
1600
1500
1400
1300
1200
1100
1000
900
800
700
600
500
400
300
200
100
0
-100

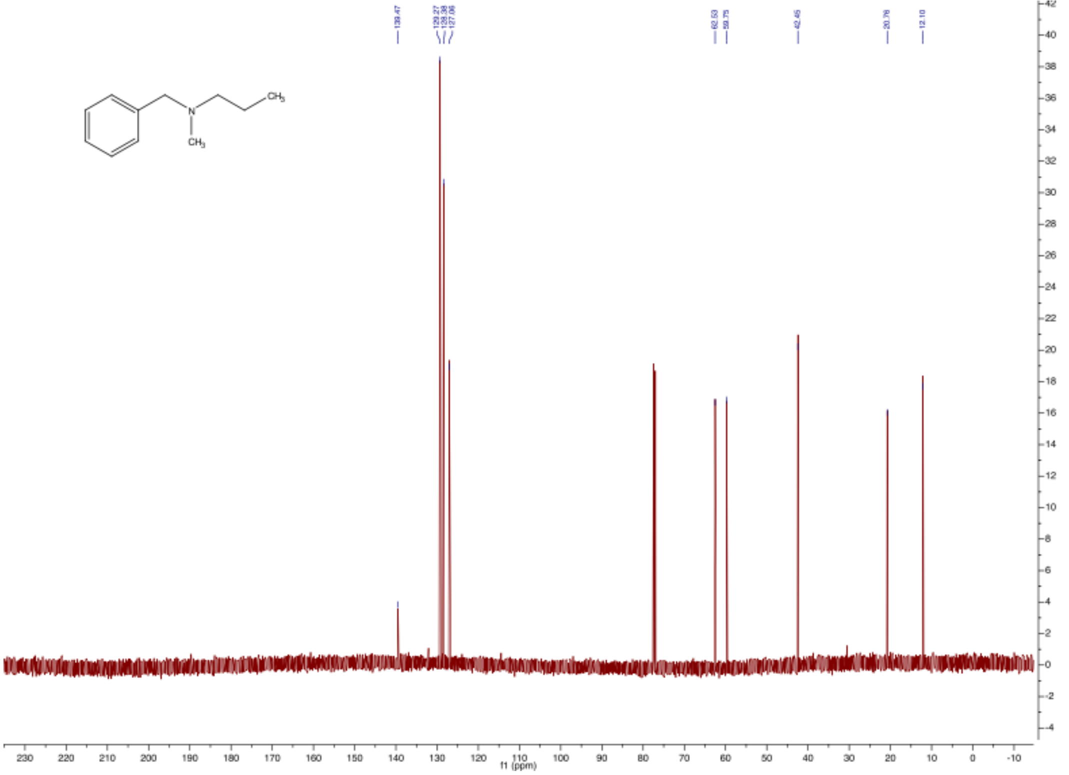
139.47
129.27
128.38
127.06
62.53
59.75
42.45
20.76
12.10
CH3
N
CH3
230
220
210
200
190
180
170
160
150
140
130
120
110
100
90
80
70
60
50
40
30
20
10
0
-10
f1 (ppm)
42
40
38
36
34
32
30
28
26
24
22
20
18
16
14
12
10
8
6
4
2
0
-2
-4

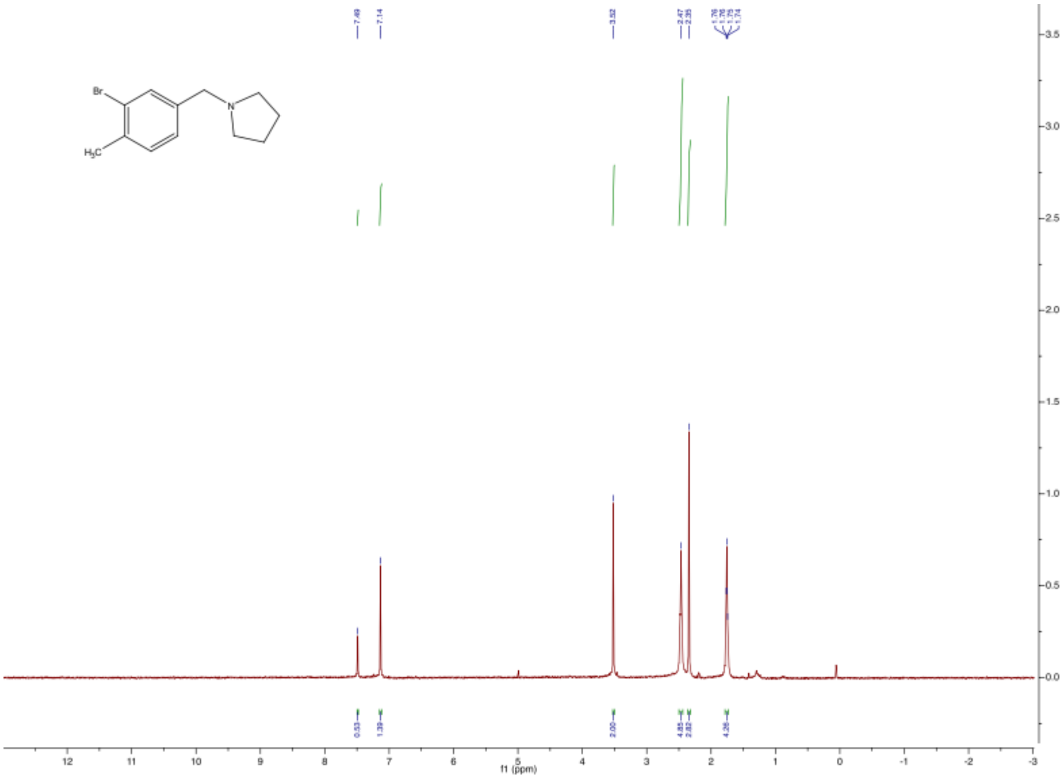
7.49
7.14
3.52
2.47
2.35
1.76
1.76
1.75
1.74
Br
N
H3C
0.53
1.39
2.00
4.85
2.82
4.26
f1 (ppm)

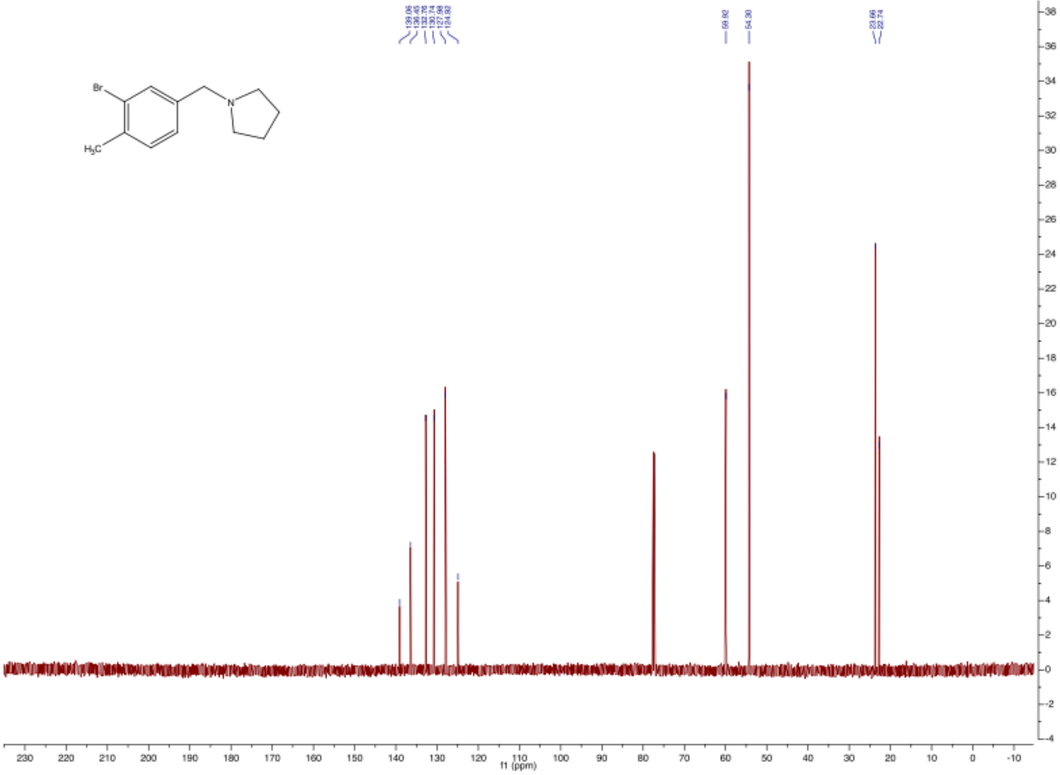
139.06
136.45
132.76
130.74
127.98
124.92
59.92
54.30
23.66
22.74
Br
N
H3C
f1 (ppm)

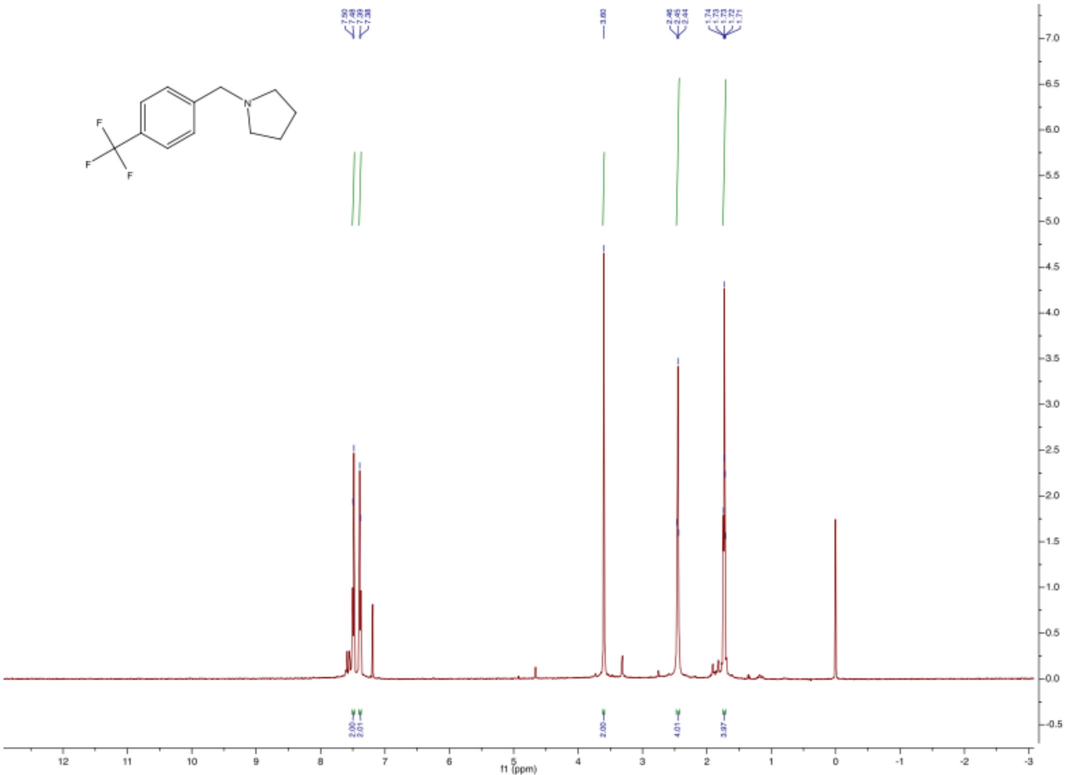
7.50
7.48
7.39
7.38
3.60
2.46
2.45
2.44
1.74
1.73
1.73
1.72
1.71
F
F
F
N
2.00
2.01
2.00
4.01
3.97
f1 (ppm)
12
11
10
9
8
7
6
5
4
3
2
1
0
-1
-2
-3
7.0
6.5
6.0
5.5
5.0
4.5
4.0
3.5
3.0
2.5
2.0
1.5
1.0
0.5
0.0
-0.5

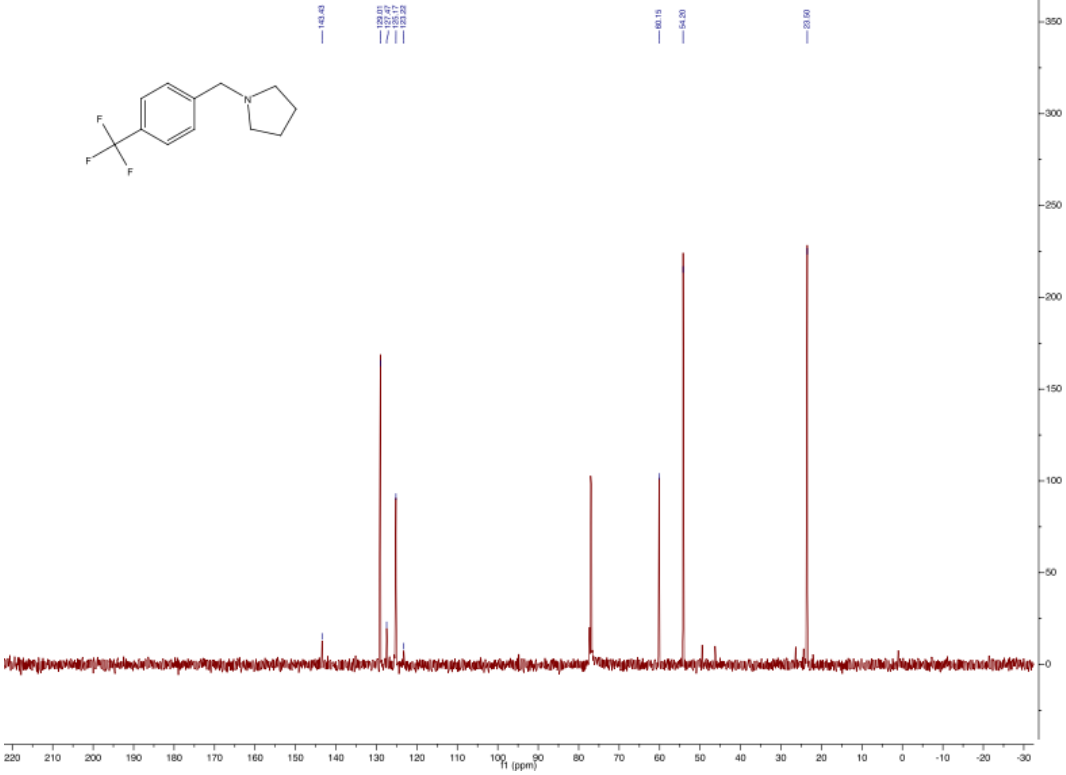
143.43
129.01
127.47
125.17
123.22
60.15
54.20
23.50
F
F
F
N
f1 (ppm)
220
210
200
190
180
170
160
150
140
130
120
110
100
90
80
70
60
50
40
30
20
10
0
-10
-20
-30
350
300
250
200
150
100
50
0

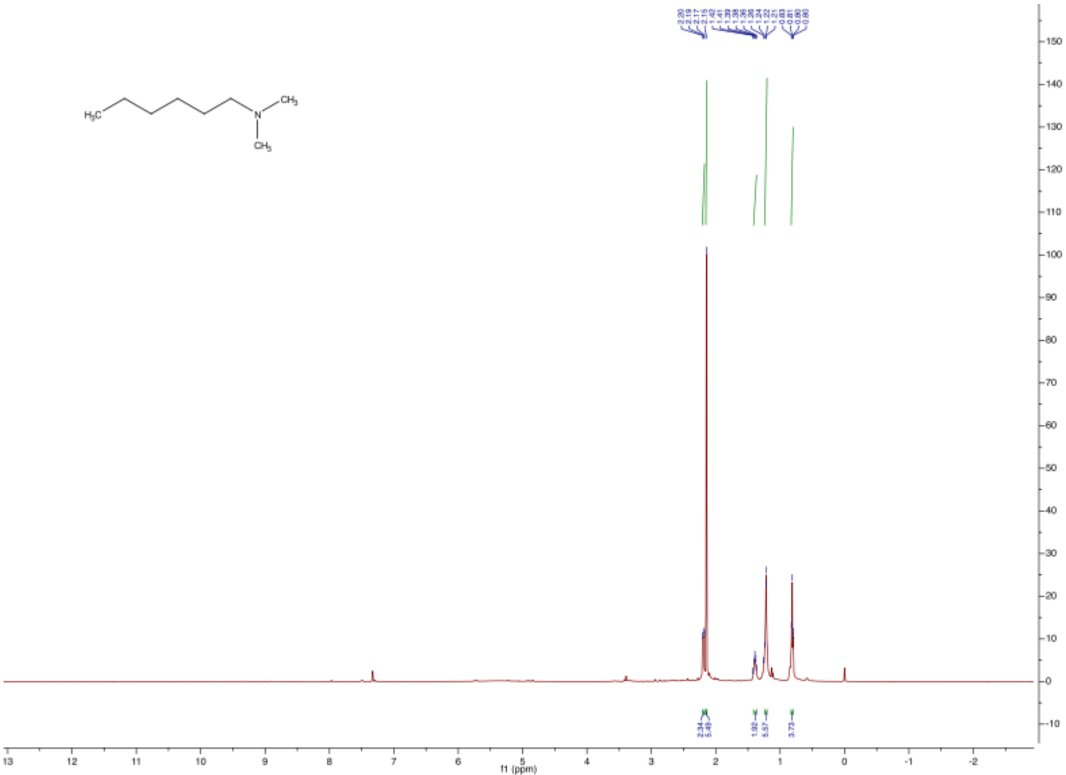

2.20
2.19
2.17
2.15
1.42
1.41
1.39
1.38
1.36
1.26
1.24
1.22
1.21
0.83
0.81
0.80
0.80
H3C
N
CH3
CH3
2.34
5.49
1.92
5.57
3.73
f1 (ppm)

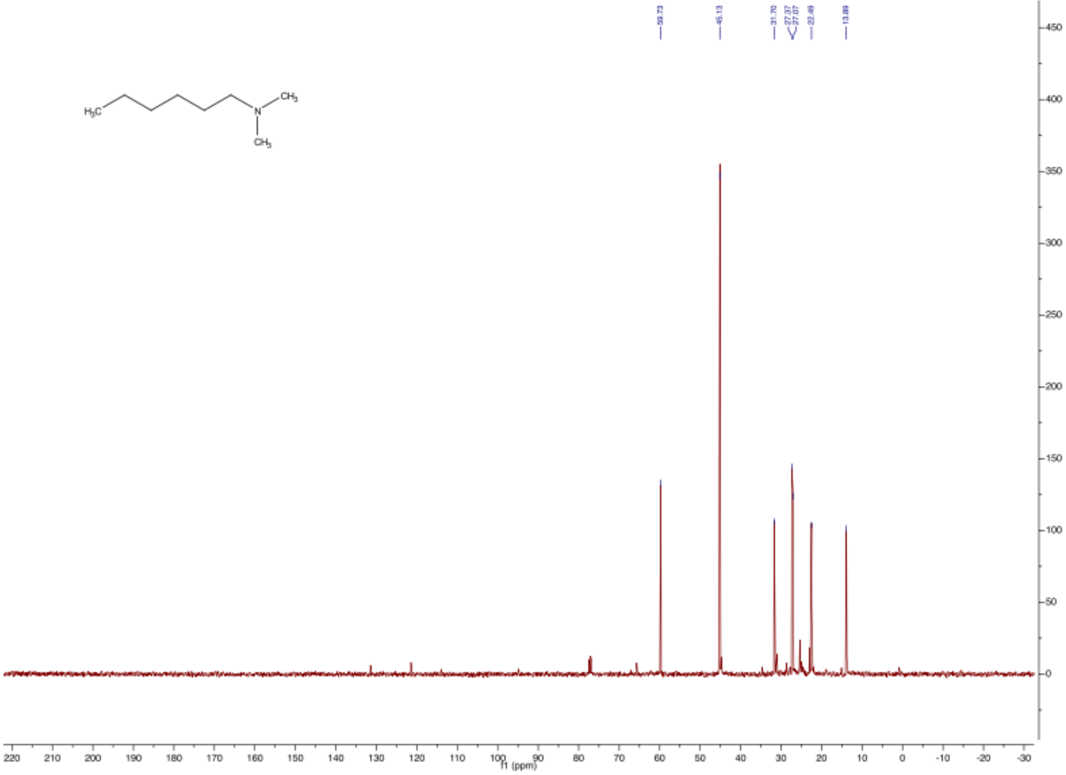

59.73
45.13
31.70
27.37
27.07
22.49
13.89
H3C
N
CH3
CH3
f1 (ppm)

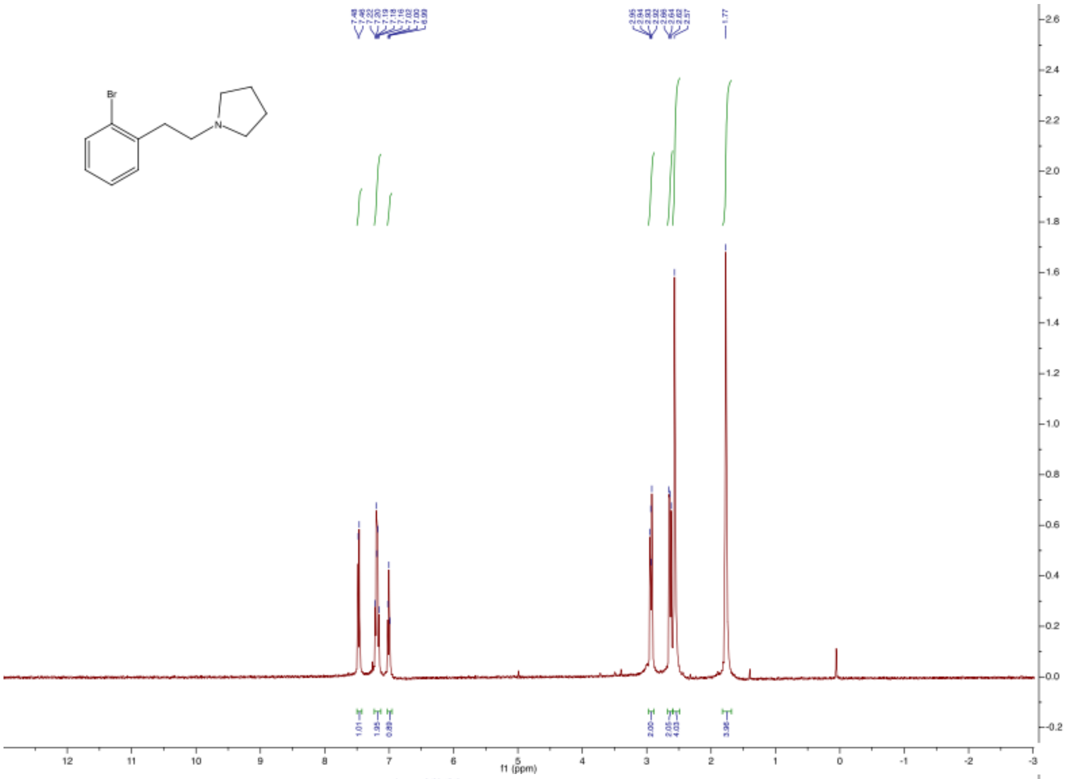
Br
N
7.48
7.46
7.22
7.20
7.19
7.18
7.16
7.02
7.00
6.99
2.95
2.94
2.93
2.92
2.66
2.64
2.62
2.57
1.77
1.01
1.95
0.89
2.00
2.05
4.03
3.96
12
11
10
9
8
7
6
5
4
3
2
1
0
-1
-2
-3
f1 (ppm)
2.6
2.4
2.2
2.0
1.8
1.6
1.4
1.2
1.0
0.8
0.6
0.4
0.2
0.0
-0.2

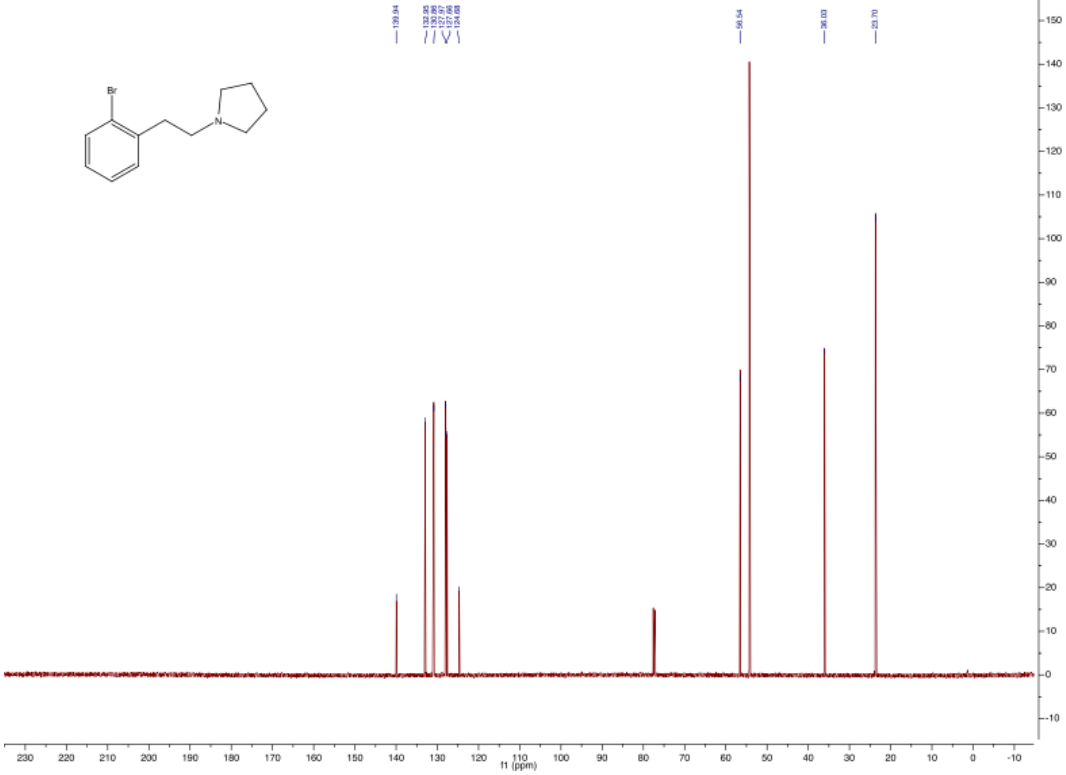
Br
N
139.94
132.93
130.86
127.97
127.66
124.68
56.54
36.03
23.70
230
220
210
200
190
180
170
160
150
140
130
120
110
100
90
80
70
60
50
40
30
20
10
0
-10
f1 (ppm)
150
140
130
120
110
100
90
80
70
60
50
40
30
20
10
0
-10

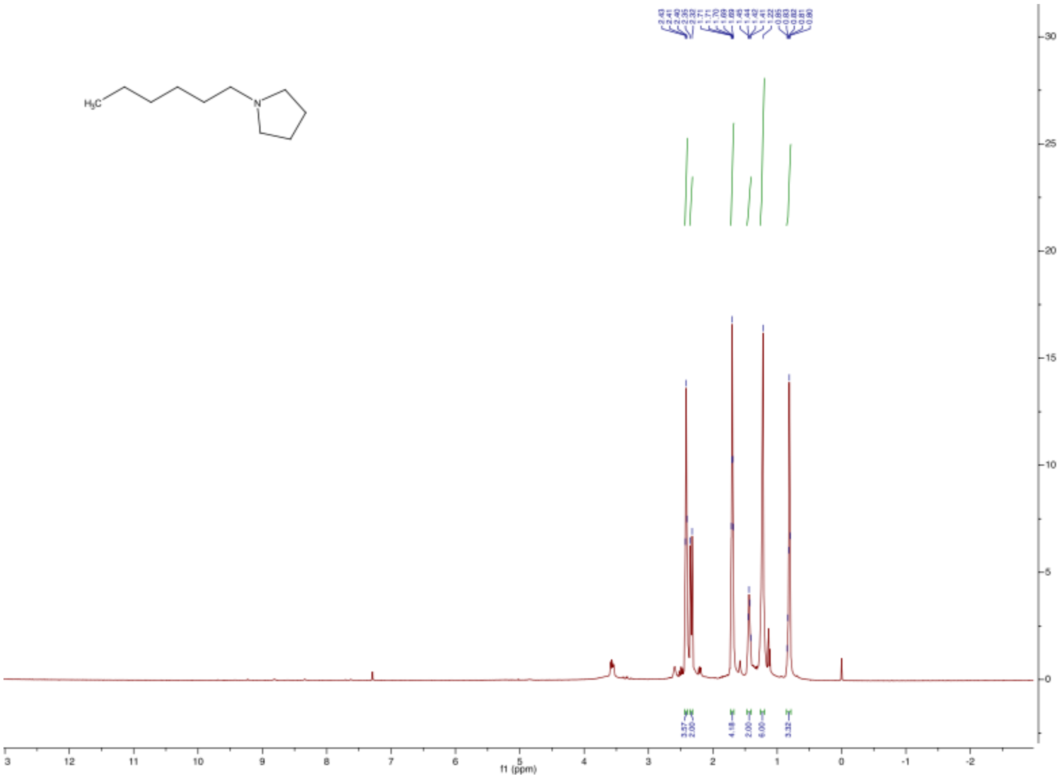
H3C
N
2.43
2.41
2.40
2.35
2.32
1.71
1.71
1.70
1.69
1.69
1.45
1.44
1.42
1.41
1.22
0.85
0.83
0.82
0.81
0.80
3.57
2.00
4.18
2.00
6.00
3.32
f1 (ppm)

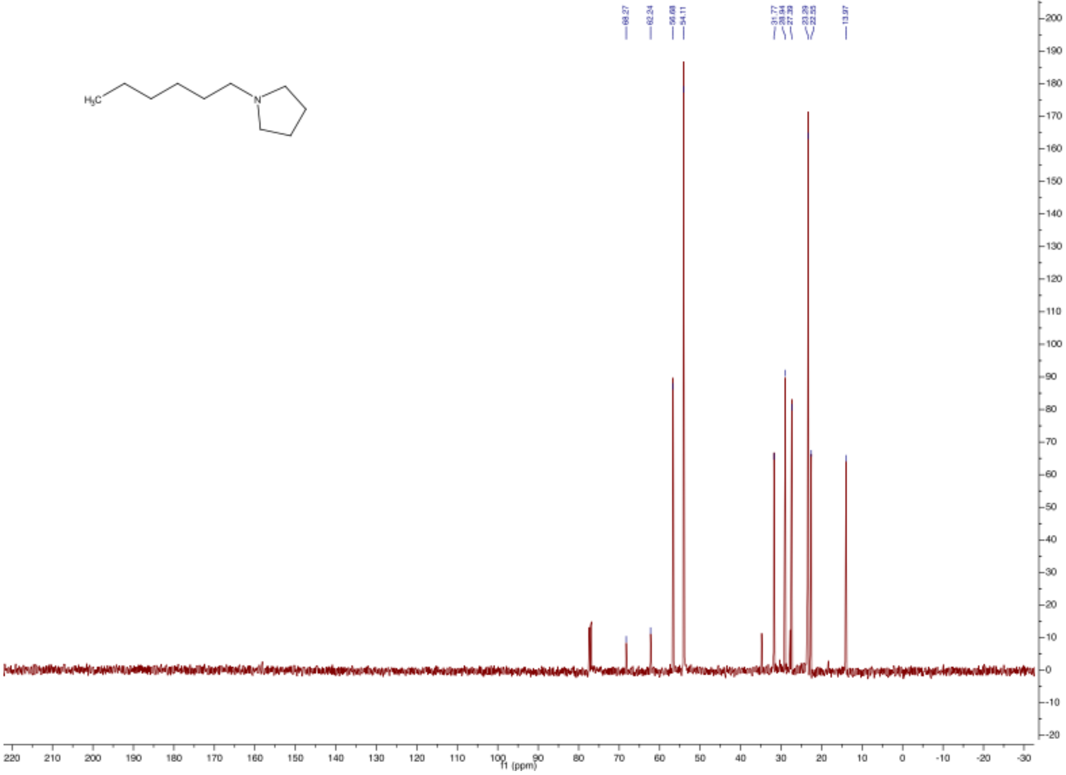
H3C
N
68.27
62.24
56.68
54.11
31.77
28.94
27.39
23.29
22.55
13.97
f1 (ppm)

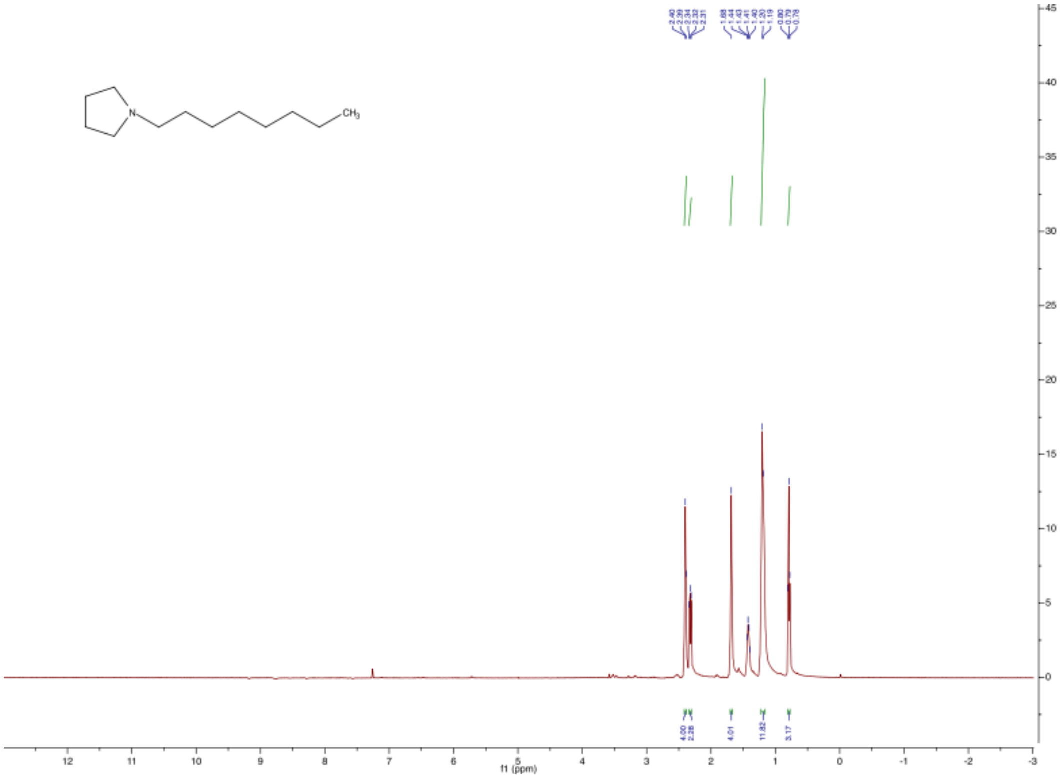
2.40
2.39
2.34
2.32
2.31
1.68
1.44
1.43
1.41
1.40
1.20
1.19
0.80
0.79
0.78
N
CH3
4.00
2.28
4.01
11.82
3.17
12
11
10
9
8
7
6
5
4
3
2
1
0
-1
-2
-3
f1 (ppm)
45
40
35
30
25
20
15
10
5
0

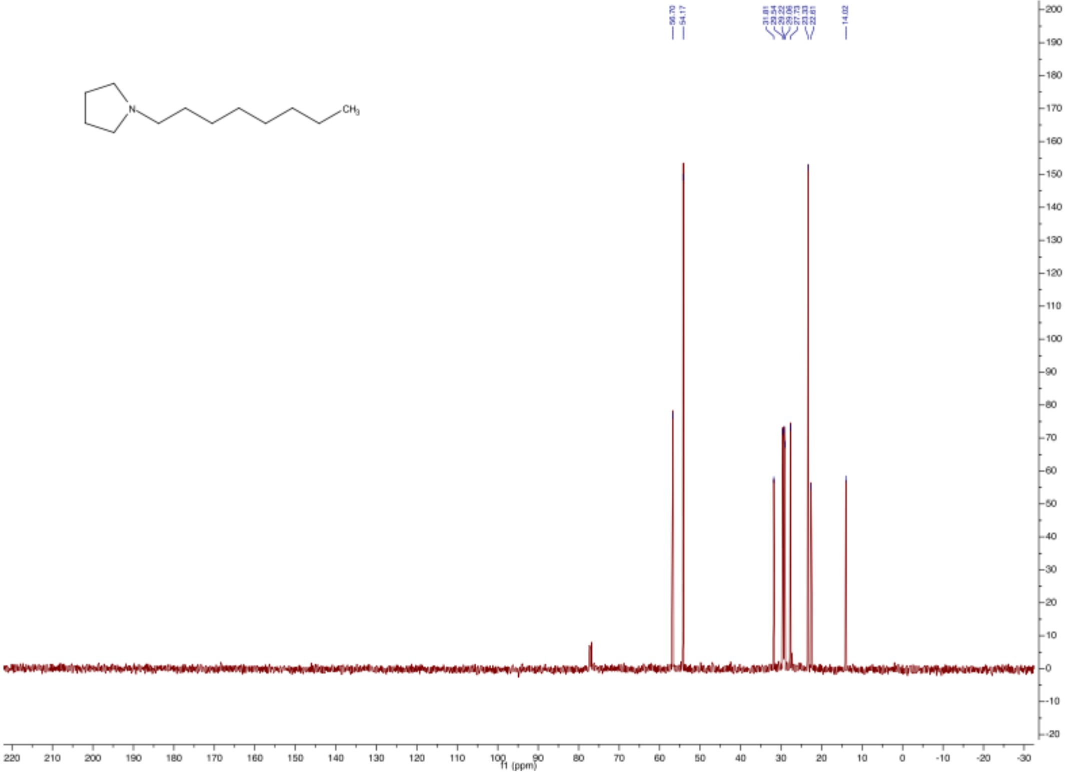
56.70
54.17
31.81
29.54
29.22
29.06
27.73
23.33
22.61
14.02
N
CH3
220
210
200
190
180
170
160
150
140
130
120
110
100
90
80
70
60
50
40
30
20
10
0
-10
-20
-30
f1 (ppm)
200
190
180
170
160
150
140
130
120
110
100
90
80
70
60
50
40
30
20
10
0
-10
-20

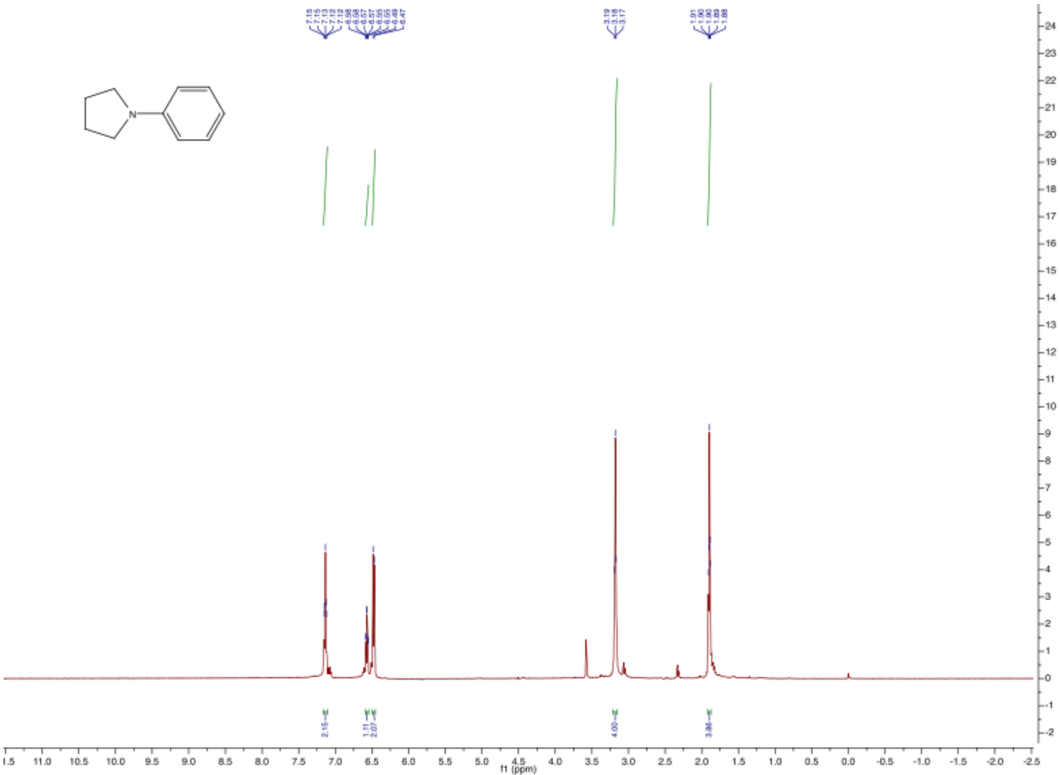
N
7.15
7.15
7.13
7.12
6.58
6.58
6.57
6.55
6.55
6.49
6.47
3.19
3.18
3.17
1.91
1.90
1.90
1.89
1.88
2.15
1.11
2.07
4.00
3.86
f1 (ppm)

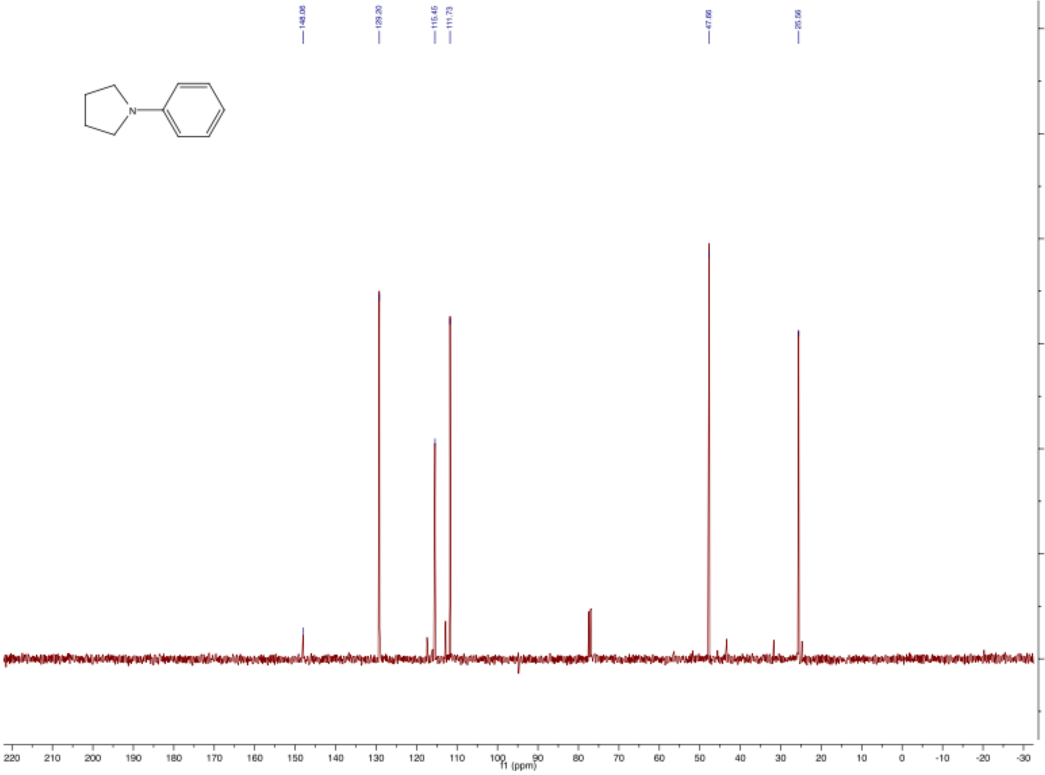
N
148.06
129.20
115.45
111.73
47.66
25.56
f1 (ppm)

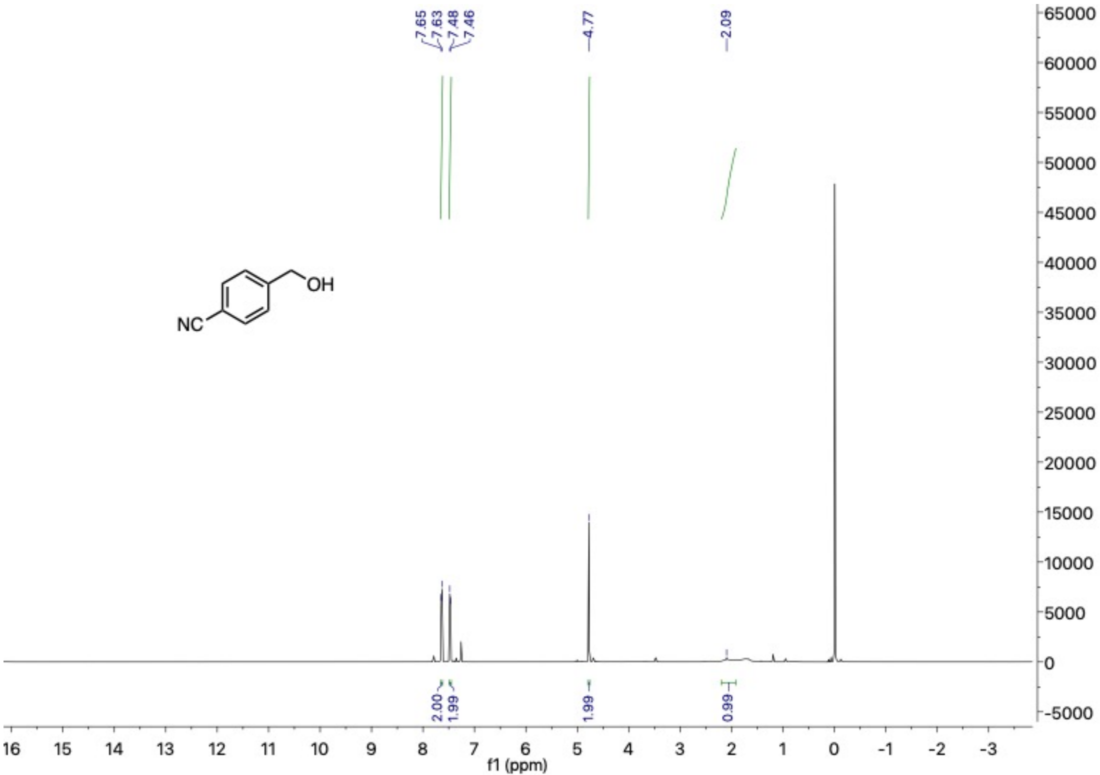
7.65
7.63
7.48
7.46
4.77
2.09
OH
NC
2.00
1.99
1.99
0.99
65000
60000
55000
50000
45000
40000
35000
30000
25000
20000
15000
10000
5000
0
-5000
16 15 14 13 12 11 10 9 8 7 6 5 4 3 2 1 0 -1 -2 -3
f1 (ppm)

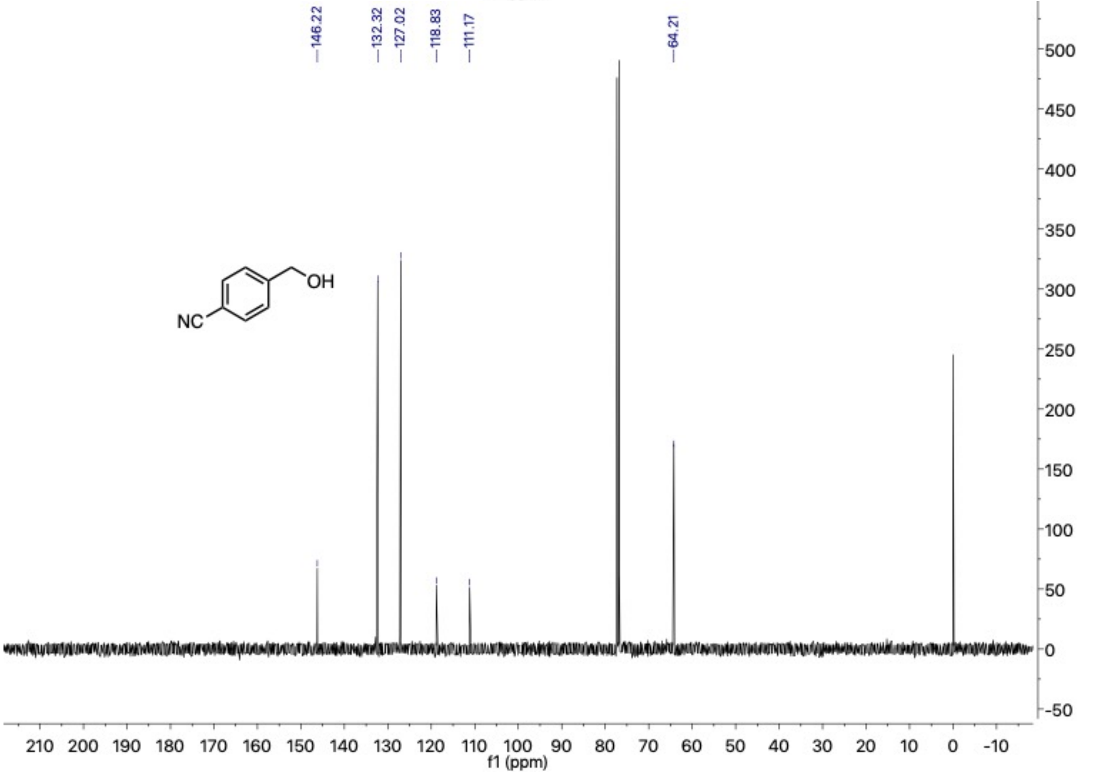
146.22
132.32
127.02
118.83
111.17
64.21
OH
NC
500
450
400
350
300
250
200
150
100
50
0
-50
210 200 190 180 170 160 150 140 130 120 110 100 90 80 70 60 50 40 30 20 10 0 -10
f1 (ppm)

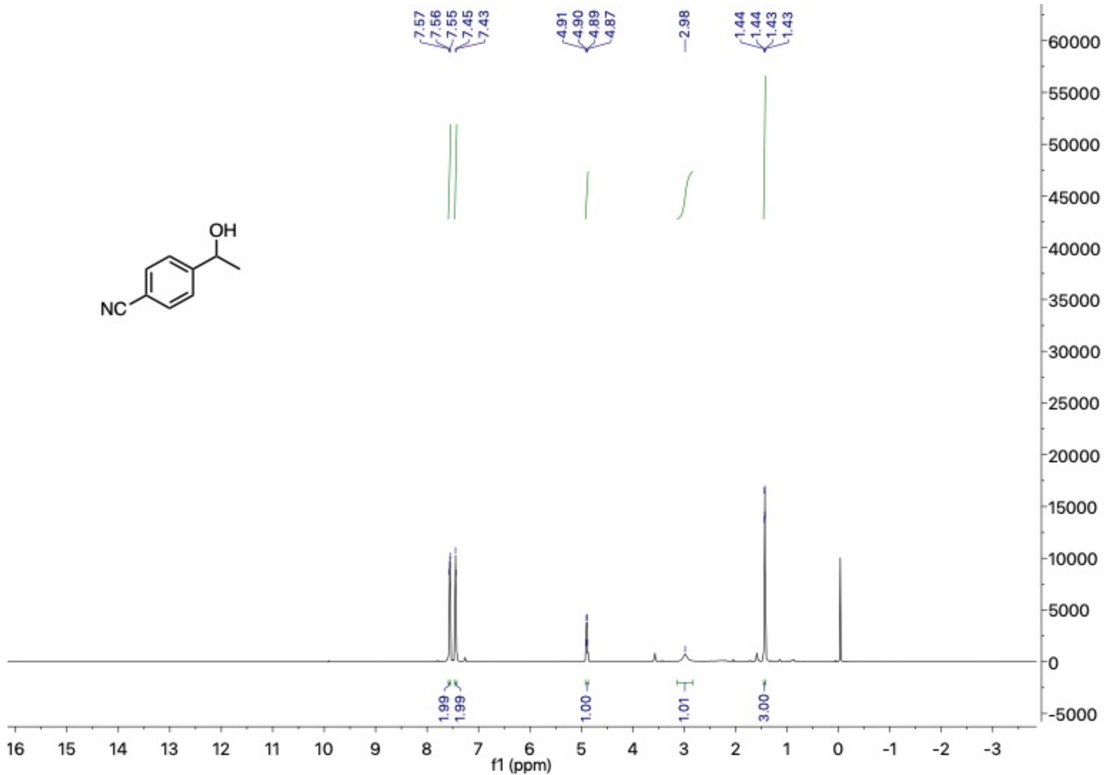
7.57
7.56
7.55
7.45
7.43
4.91
4.90
4.89
4.87
2.98
1.44
1.44
1.43
1.43
OH
NC
1.99
1.99
1.00
1.01
3.00
60000
55000
50000
45000
40000
35000
30000
25000
20000
15000
10000
5000
0
-5000
16 15 14 13 12 11 10 9 8 7 6 5 4 3 2 1 0 -1 -2 -3
f1 (ppm)

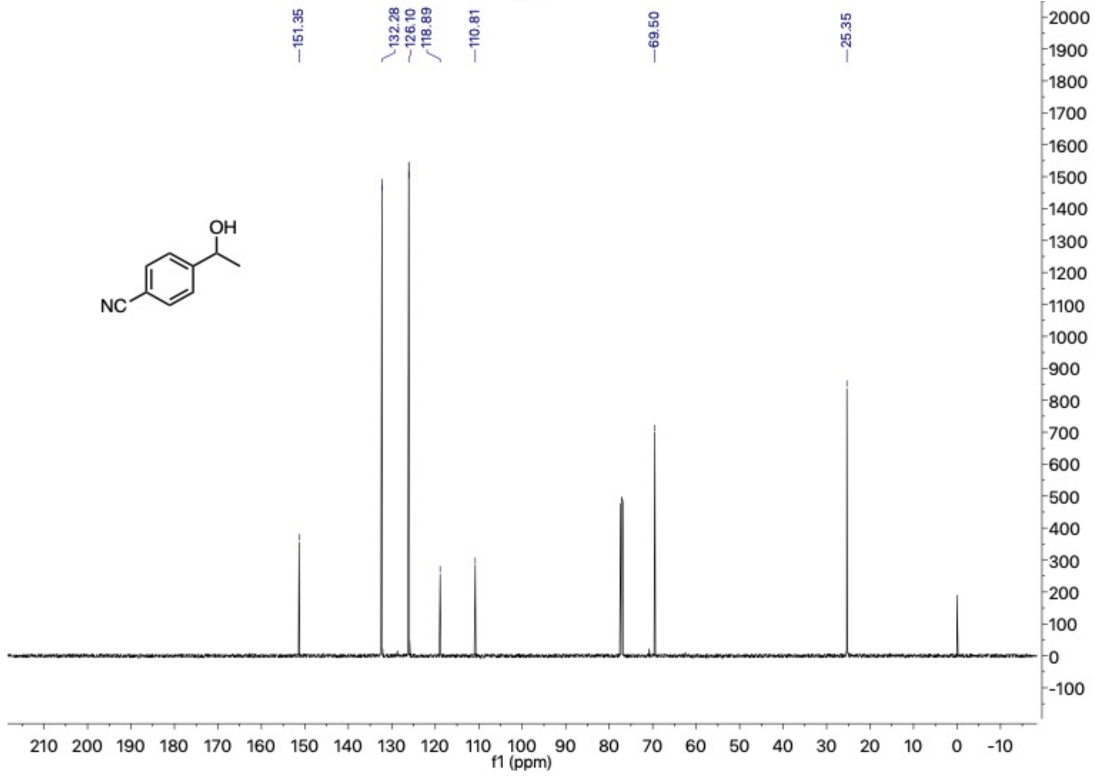
151.35
132.28
126.10
118.89
110.81
69.50
25.35
OH
NC
2000
1900
1800
1700
1600
1500
1400
1300
1200
1100
1000
900
800
700
600
500
400
300
200
100
0
-100
210 200 190 180 170 160 150 140 130 120 110 100 90 80 70 60 50 40 30 20 10 0 -10
f1 (ppm)

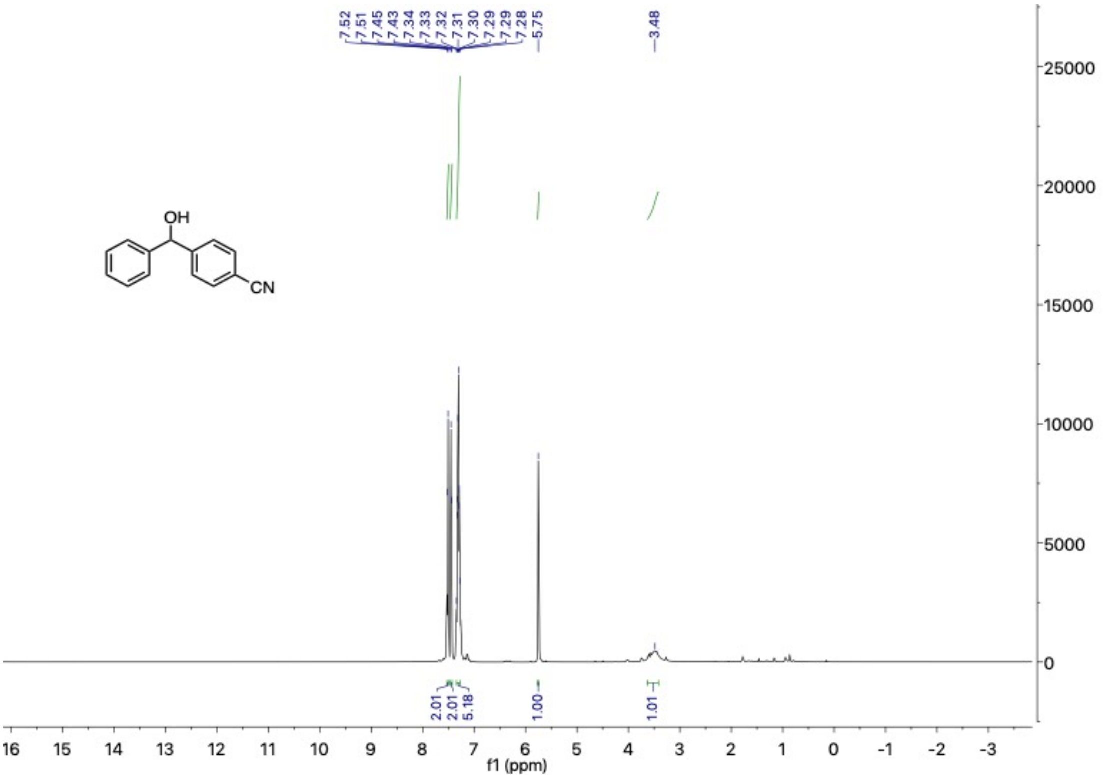
7.52
7.51
7.45
7.43
7.34
7.33
7.32
7.31
7.30
7.29
7.29
7.28
5.75
3.48
OH
CN
2.01
2.01
5.18
1.00
1.01
25000
20000
15000
10000
5000
0
16 15 14 13 12 11 10 9 8 7 6 5 4 3 2 1 0 -1 -2 -3
f1 (ppm)

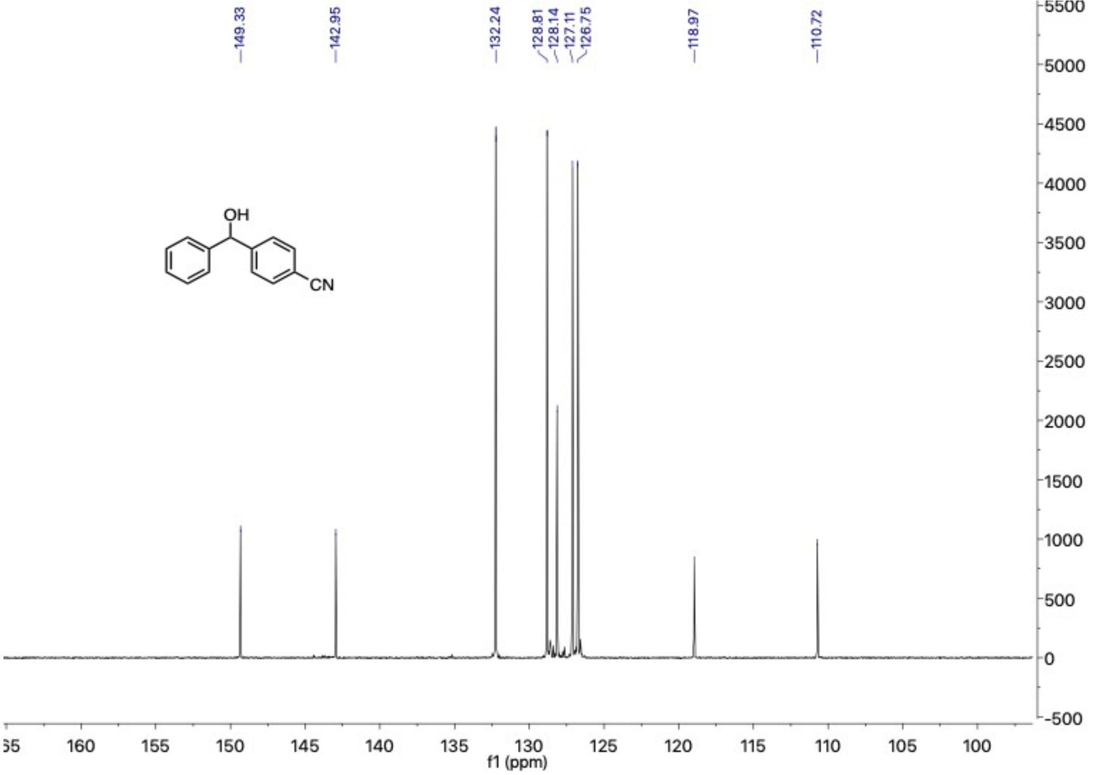
149.33
142.95
132.24
128.81
128.14
127.11
126.75
118.97
110.72
OH
CN
5500
5000
4500
4000
3500
3000
2500
2000
1500
1000
500
0
-500
65 160 155 150 145 140 135 130 125 120 115 110 105 100
f1 (ppm)

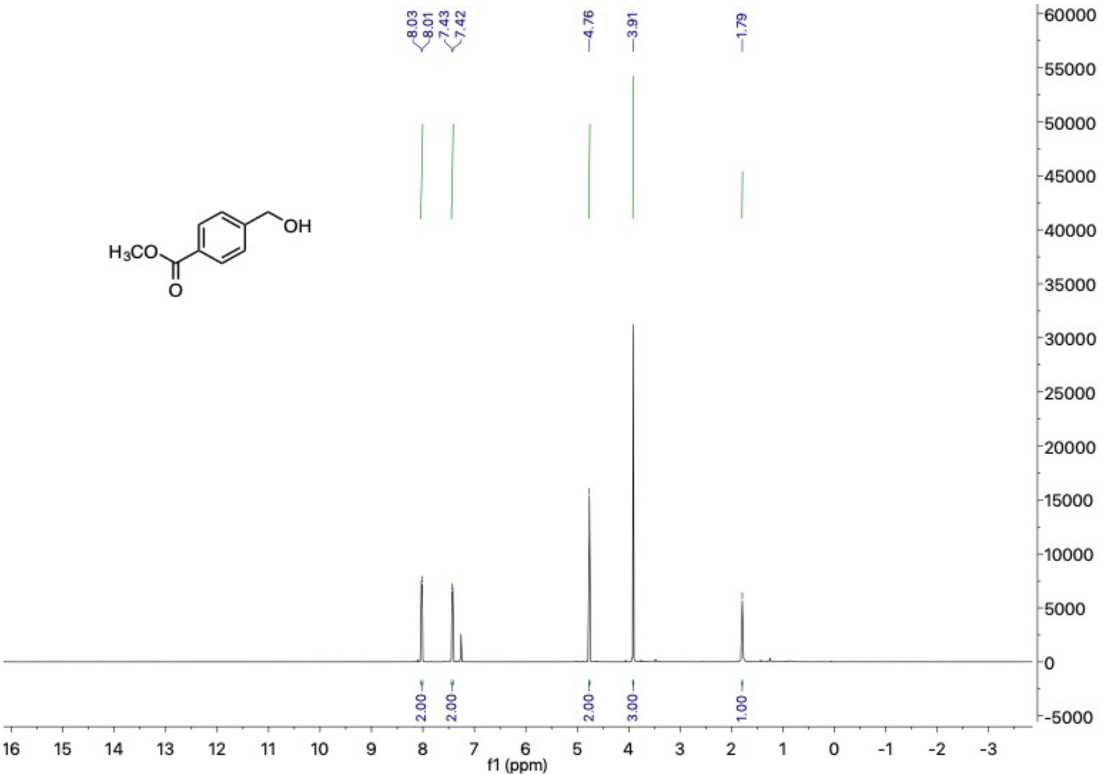
8.03
8.01
7.43
7.42
4.76
3.91
1.79
H3CO
OH
O
2.00
2.00
2.00
3.00
1.00
60000
55000
50000
45000
40000
35000
30000
25000
20000
15000
10000
5000
0
-5000
16 15 14 13 12 11 10 9 8 7 6 5 4 3 2 1 0 -1 -2 -3
f1 (ppm)

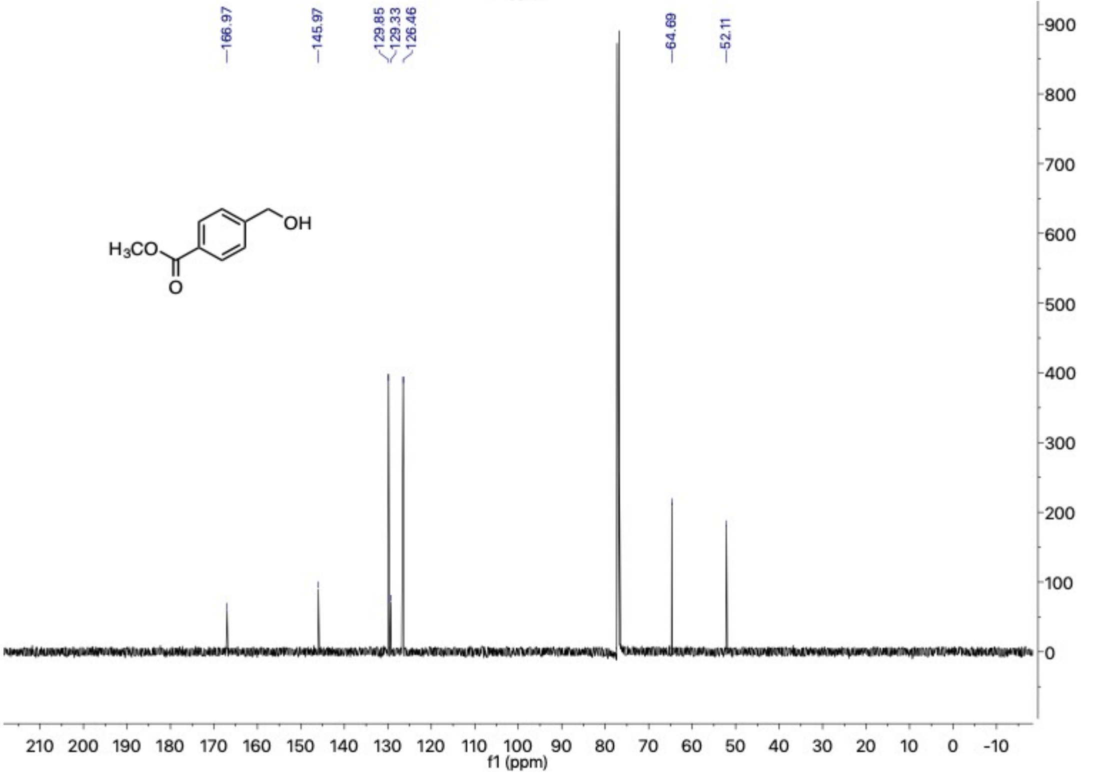
166.97
145.97
129.85
129.33
126.46
64.69
52.11
H3CO
OH
O
900
800
700
600
500
400
300
200
100
0
210 200 190 180 170 160 150 140 130 120 110 100 90 80 70 60 50 40 30 20 10 0 -10
f1 (ppm)

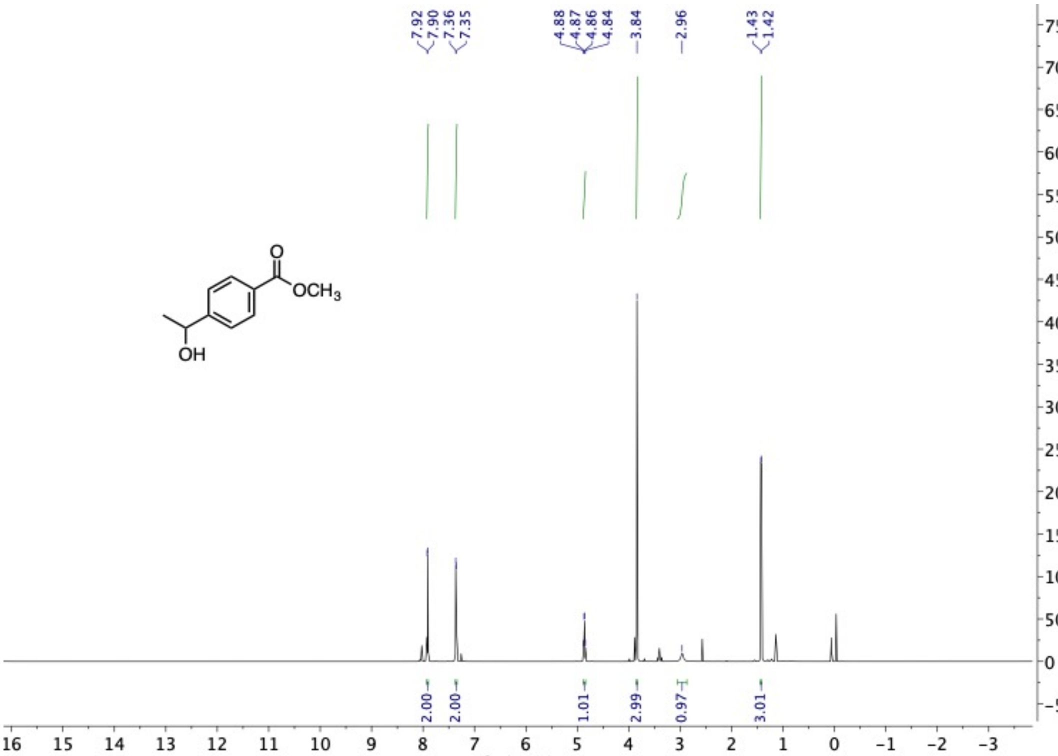
7.92
7.90
7.36
7.35
4.88
4.87
4.86
4.84
3.84
2.96
1.43
1.42
OCH3
O
OH
2.00
2.00
1.01
2.99
0.97
3.01
75000
70000
65000
60000
55000
50000
45000
40000
35000
30000
25000
20000
15000
10000
5000
0
−5000
16
15
14
13
12
11
10
9
8
7
6
5
4
3
2
1
0
−1
−2
−3
f1 (ppm)

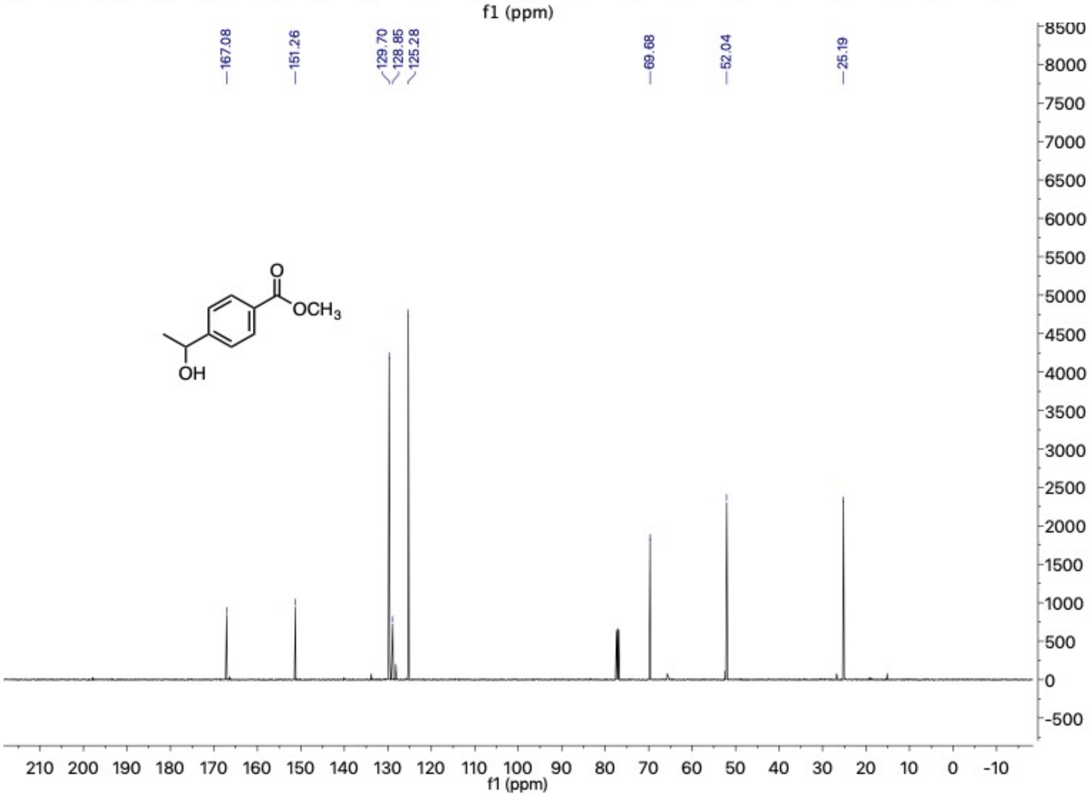
167.08
151.26
129.70
128.85
125.28
69.68
52.04
25.19
OCH3
O
OH
8500
8000
7500
7000
6500
6000
5500
5000
4500
4000
3500
3000
2500
2000
1500
1000
500
0
−500
210
200
190
180
170
160
150
140
130
120
110
100
90
80
70
60
50
40
30
20
10
0
−10
f1 (ppm)

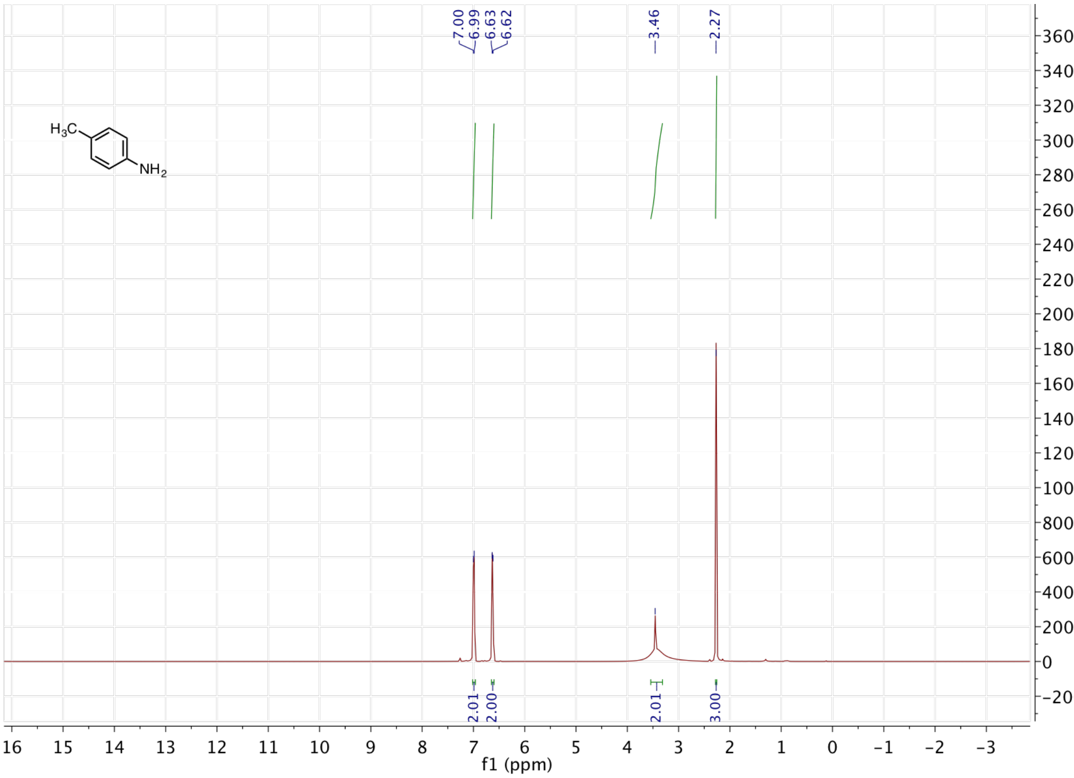
H3C
NH2
7.00
6.99
6.63
6.62
3.46
2.27
2.01
2.00
2.01
3.00
36000
34000
32000
30000
28000
26000
24000
22000
20000
18000
16000
14000
12000
10000
8000
6000
4000
2000
0
−2000
16
15
14
13
12
11
10
9
8
7
6
5
4
3
2
1
0
−1
−2
−3
f1 (ppm)

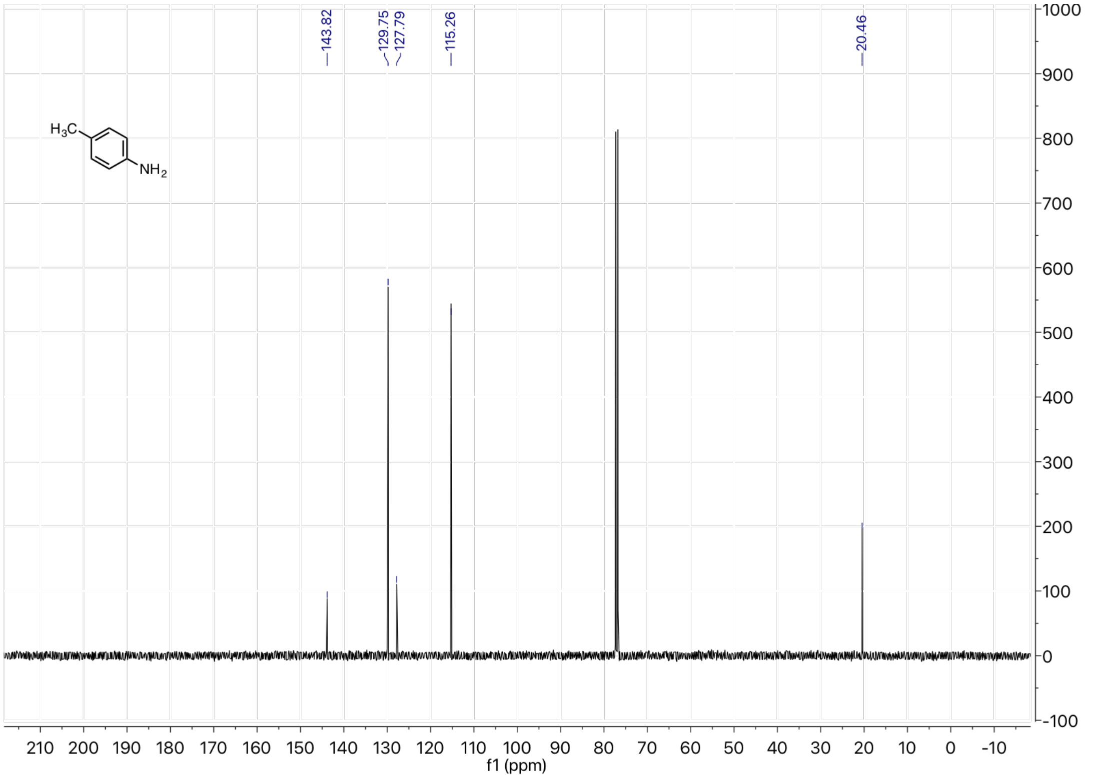
143.82
129.75
127.79
115.26
20.46
H3C
NH2
1000
900
800
700
600
500
400
300
200
100
0
-100
210 200 190 180 170 160 150 140 130 120 110 100 90 80 70 60 50 40 30 20 10 0 -10
f1 (ppm)

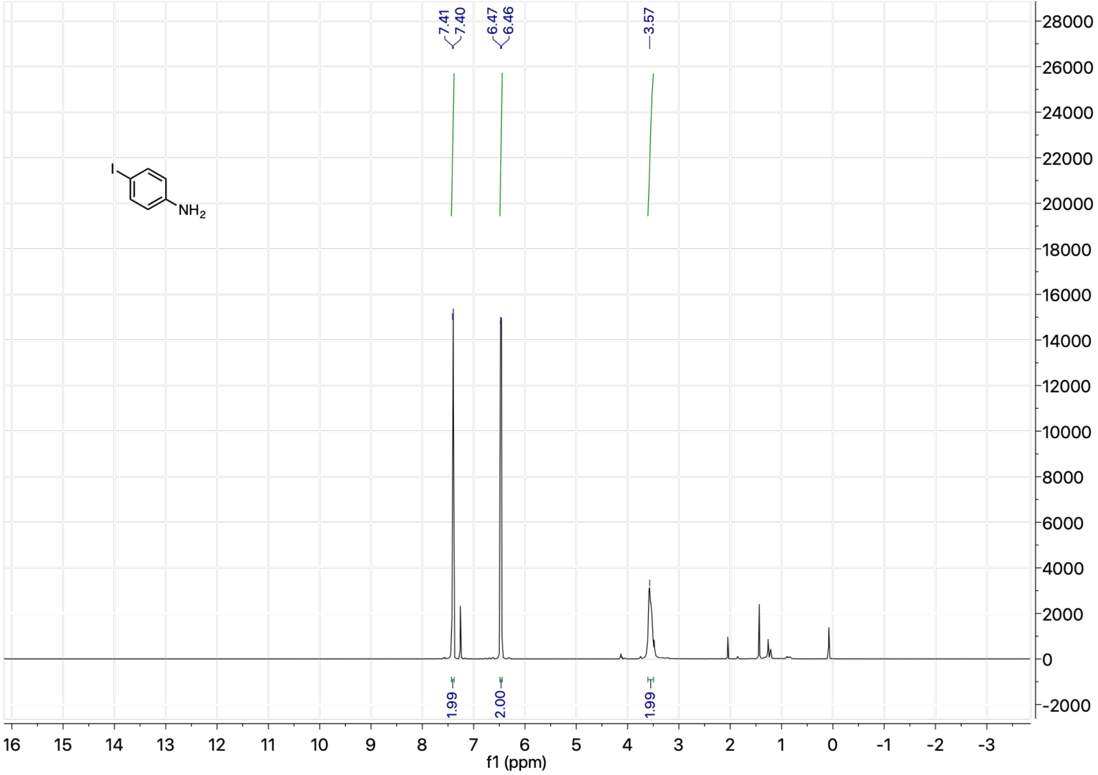
7.41
7.40
6.47
6.46
3.57
I
NH2
1.99
2.00
1.99
28000
26000
24000
22000
20000
18000
16000
14000
12000
10000
8000
6000
4000
2000
0
-2000
16 15 14 13 12 11 10 9 8 7 6 5 4 3 2 1 0 -1 -2 -3
f1 (ppm)

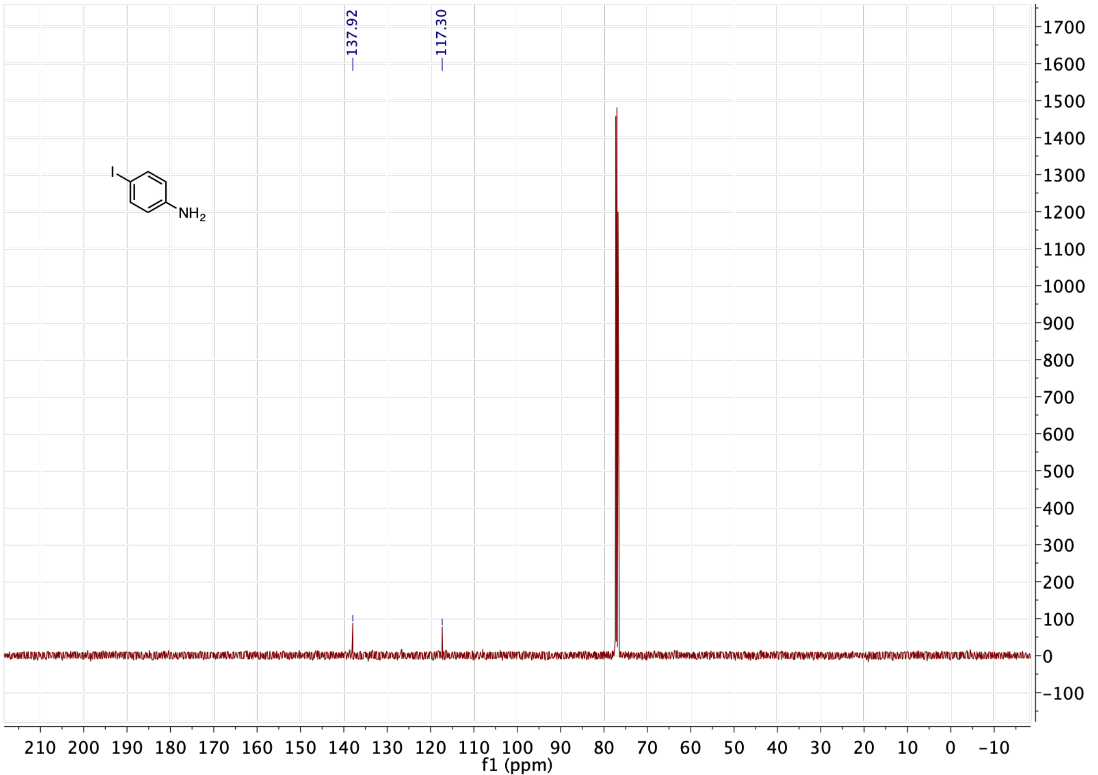
137.92
117.30
I
NH2
210 200 190 180 170 160 150 140 130 120 110 100 90 80 70 60 50 40 30 20 10 0 −10
f1 (ppm)
1700 1600 1500 1400 1300 1200 1100 1000 900 800 700 600 500 400 300 200 100 0 −100

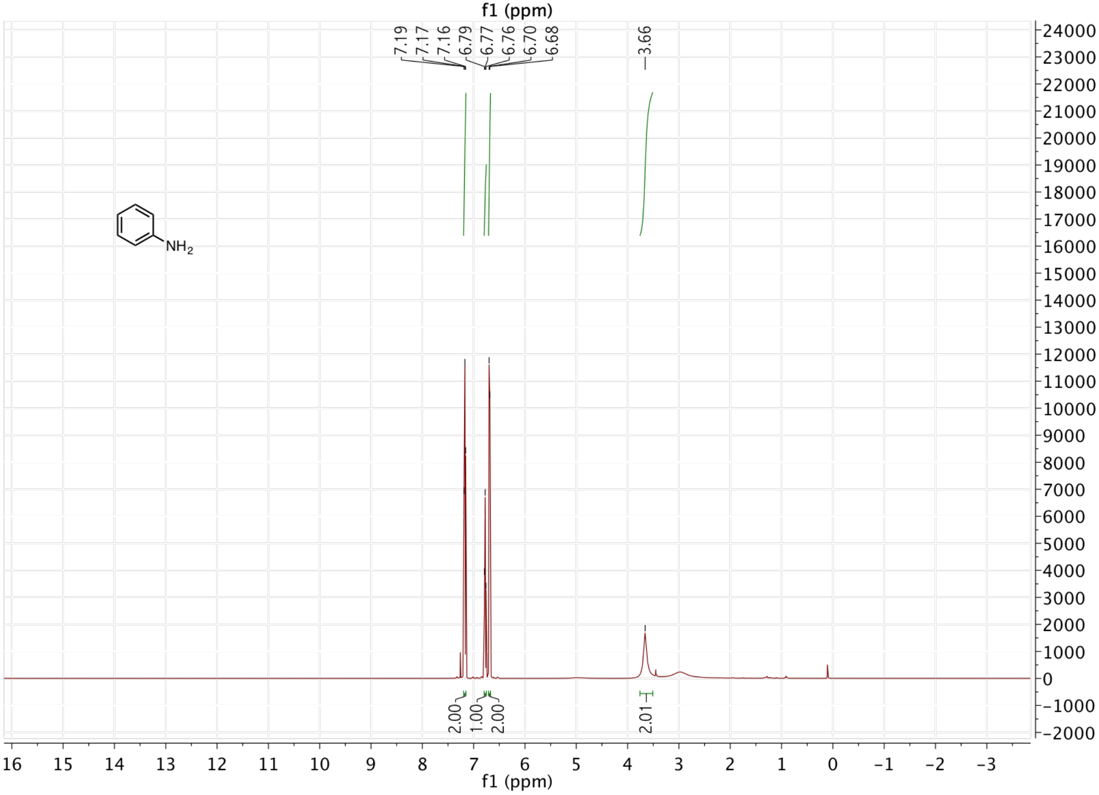
7.19
7.17
7.16
6.79
6.77
6.76
6.70
6.68
3.66
NH2
2.00
1.00
2.00
2.01
16 15 14 13 12 11 10 9 8 7 6 5 4 3 2 1 0 −1 −2 −3
f1 (ppm)
24000 23000 22000 21000 20000 19000 18000 17000 16000 15000 14000 13000 12000 11000 10000 9000 8000 7000 6000 5000 4000 3000 2000 1000 0 −1000 −2000

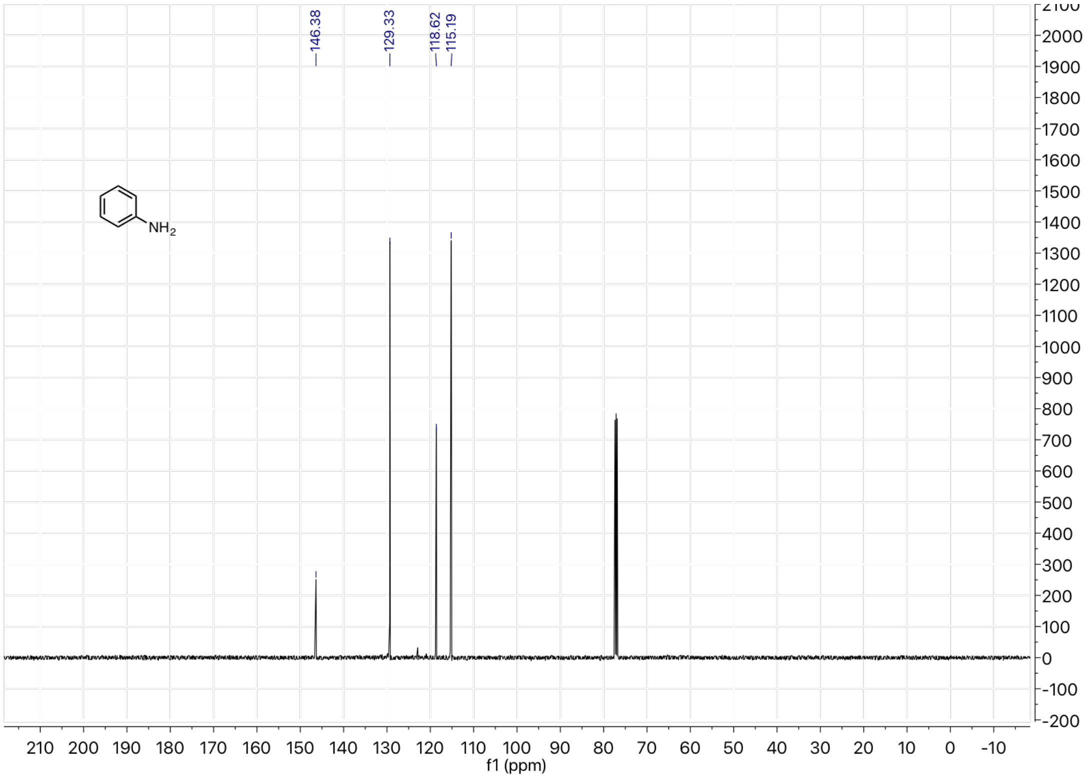
146.38
129.33
118.62
115.19
NH2
2100
2000
1900
1800
1700
1600
1500
1400
1300
1200
1100
1000
900
800
700
600
500
400
300
200
100
0
-100
-200
210 200 190 180 170 160 150 140 130 120 110 100 90 80 70 60 50 40 30 20 10 0 -10
f1 (ppm)

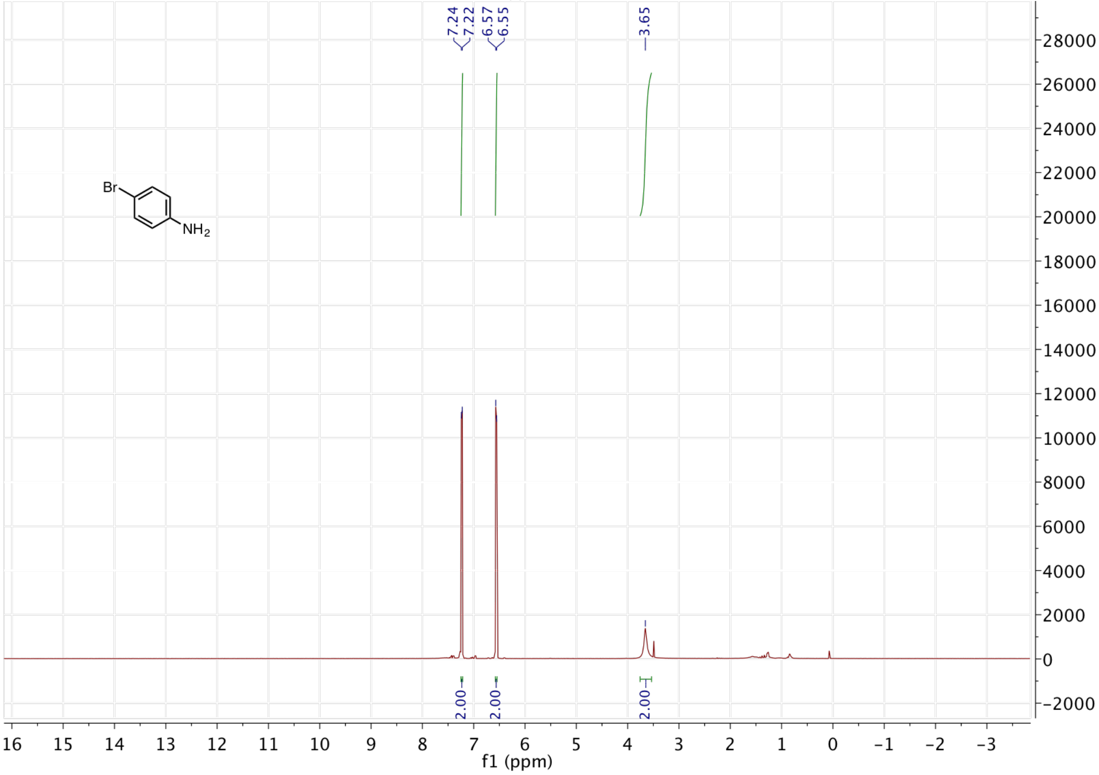
7.24
7.22
6.57
6.55
3.65
Br
NH2
28000
26000
24000
22000
20000
18000
16000
14000
12000
10000
8000
6000
4000
2000
0
-2000
2.00
2.00
2.00
16 15 14 13 12 11 10 9 8 7 6 5 4 3 2 1 0 -1 -2 -3
f1 (ppm)

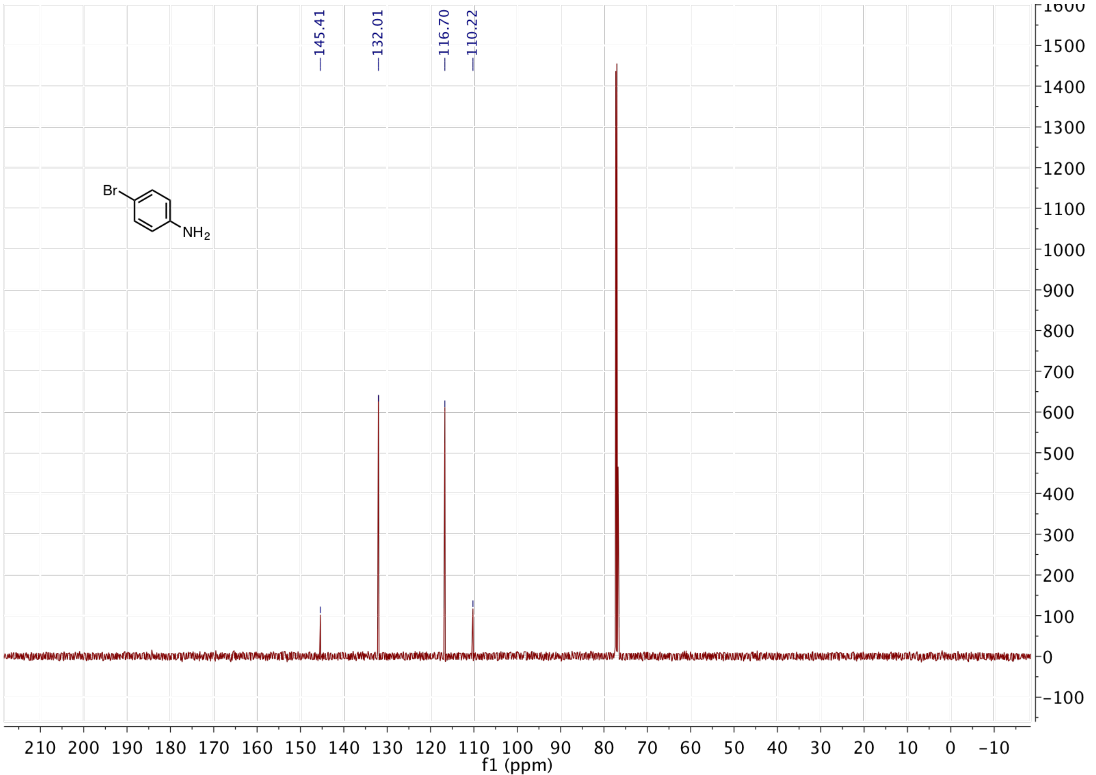

145.41
132.01
116.70
110.22
Br
NH2
1600
1500
1400
1300
1200
1100
1000
900
800
700
600
500
400
300
200
100
0
−100
210 200 190 180 170 160 150 140 130 120 110 100 90 80 70 60 50 40 30 20 10 0 −10
f1 (ppm)

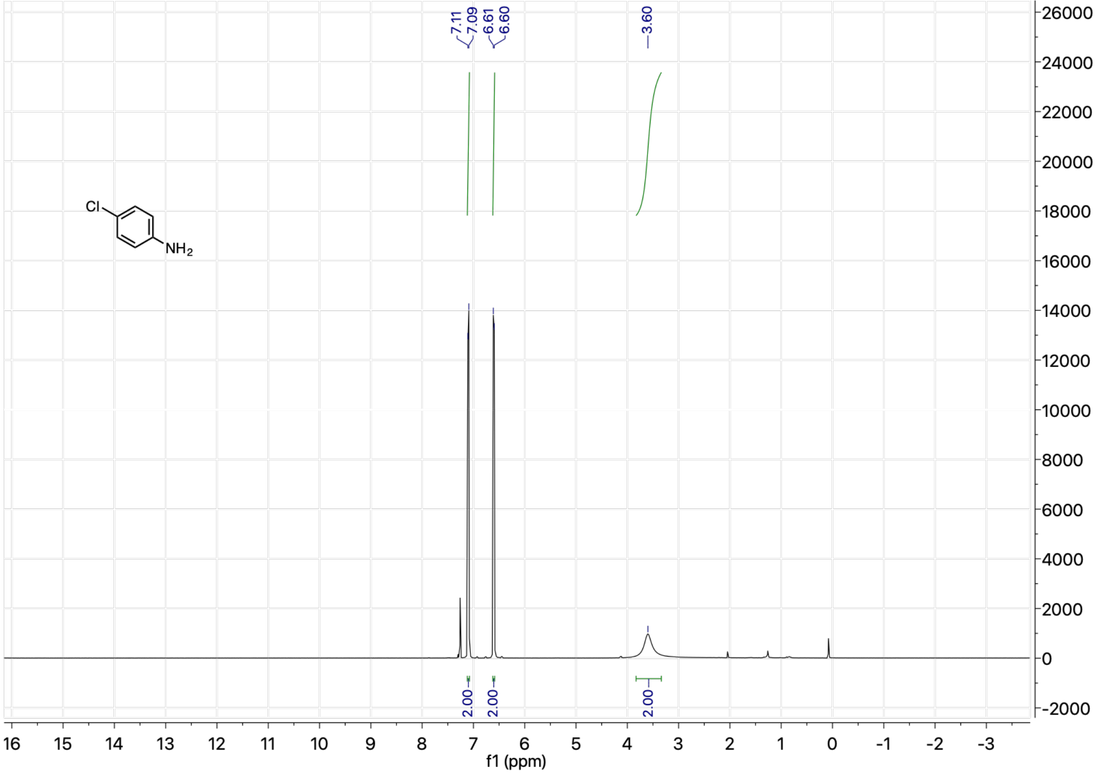

7.11
7.09
6.61
6.60
3.60
Cl
NH2
2.00
2.00
2.00
26000
24000
22000
20000
18000
16000
14000
12000
10000
8000
6000
4000
2000
0
-2000
16 15 14 13 12 11 10 9 8 7 6 5 4 3 2 1 0 -1 -2 -3
f1 (ppm)

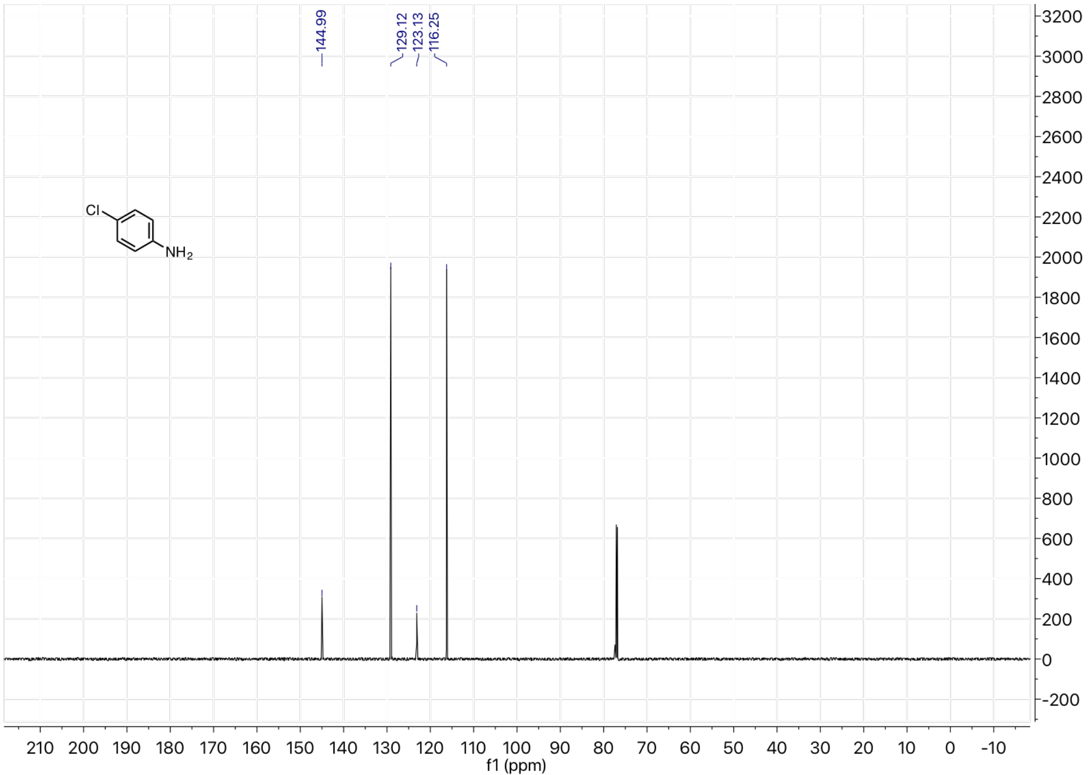

144.99
129.12
123.13
116.25
Cl
NH$_2$
3200
3000
2800
2600
2400
2200
2000
1800
1600
1400
1200
1000
800
600
400
200
0
-200
210 200 190 180 170 160 150 140 130 120 110 100 90 80 70 60 50 40 30 20 10 0 -10
f1 (ppm)

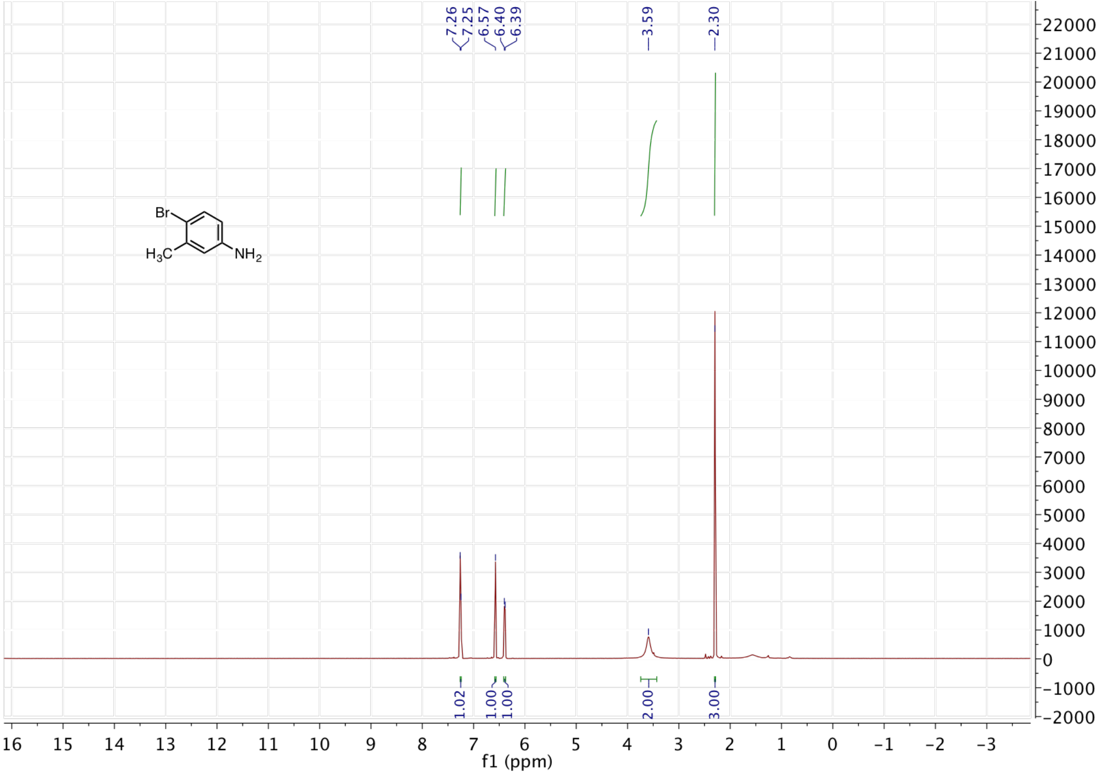

7.26
7.25
6.57
6.40
6.39
3.59
2.30
Br
H$_3$C
NH$_2$
1.02
1.00
1.00
2.00
3.00
22000
21000
20000
19000
18000
17000
16000
15000
14000
13000
12000
11000
10000
9000
8000
7000
6000
5000
4000
3000
2000
1000
0
-1000
-2000
16 15 14 13 12 11 10 9 8 7 6 5 4 3 2 1 0 -1 -2 -3
f1 (ppm)

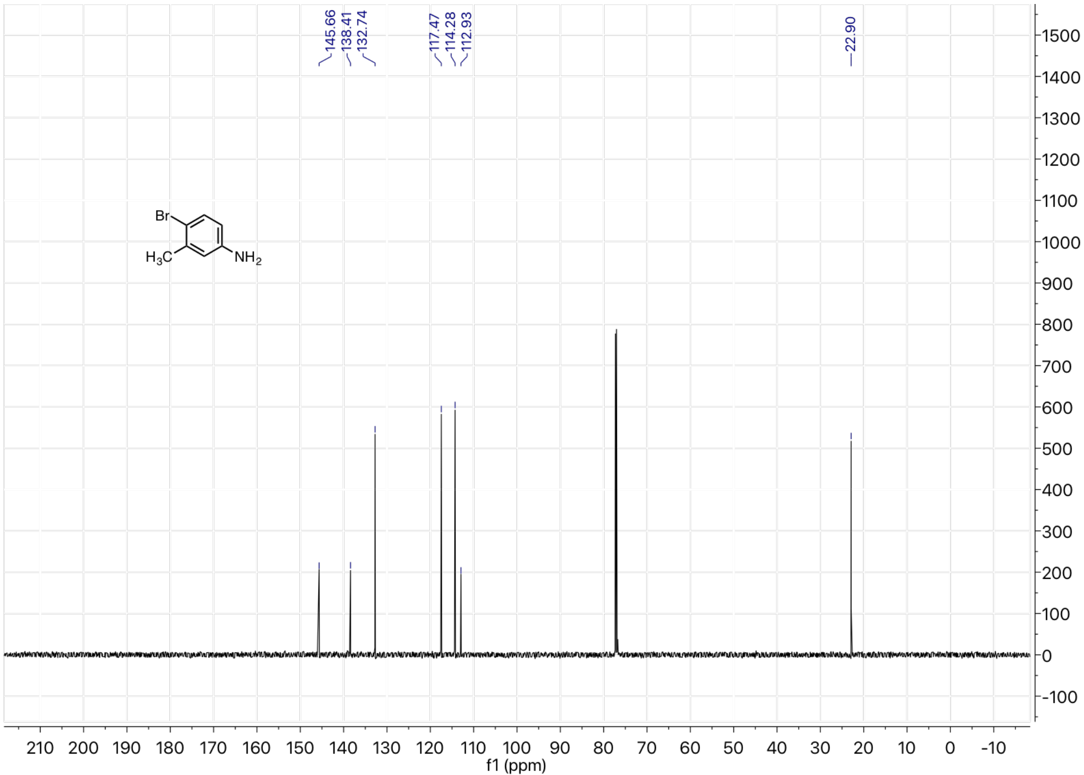

145.66
138.41
132.74
117.47
114.28
112.93
22.90
Br
H3C
NH2
1500
1400
1300
1200
1100
1000
900
800
700
600
500
400
300
200
100
0
-100
210 200 190 180 170 160 150 140 130 120 110 100 90 80 70 60 50 40 30 20 10 0 -10
f1 (ppm)

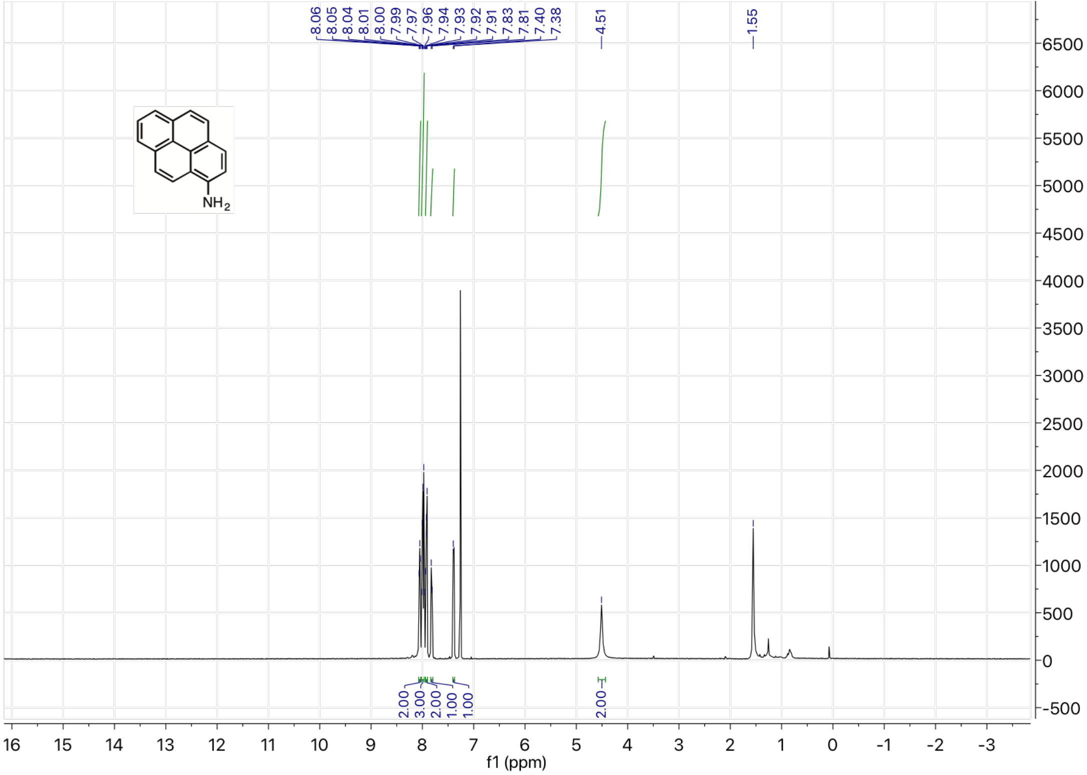

8.06
8.05
8.04
8.01
8.00
7.99
7.97
7.96
7.94
7.93
7.92
7.91
7.83
7.81
7.40
7.38
4.51
1.55
NH2
2.00
3.00
2.00
1.00
1.00
2.00
6500
6000
5500
5000
4500
4000
3500
3000
2500
2000
1500
1000
500
0
-500
16 15 14 13 12 11 10 9 8 7 6 5 4 3 2 1 0 -1 -2 -3
f1 (ppm)

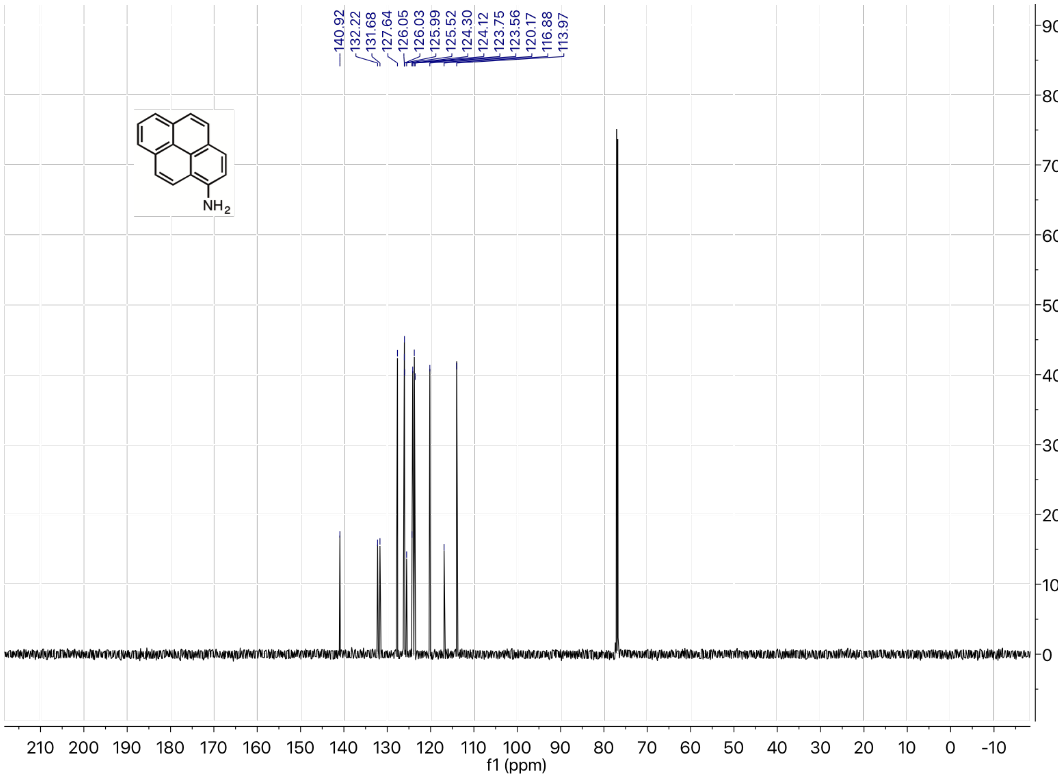
140.92
132.22
131.68
127.64
126.05
126.03
125.99
125.52
124.30
124.12
123.75
123.56
120.17
116.88
113.97
NH2
900
800
700
600
500
400
300
200
100
0
210 200 190 180 170 160 150 140 130 120 110 100 90 80 70 60 50 40 30 20 10 0 -10
f1 (ppm)

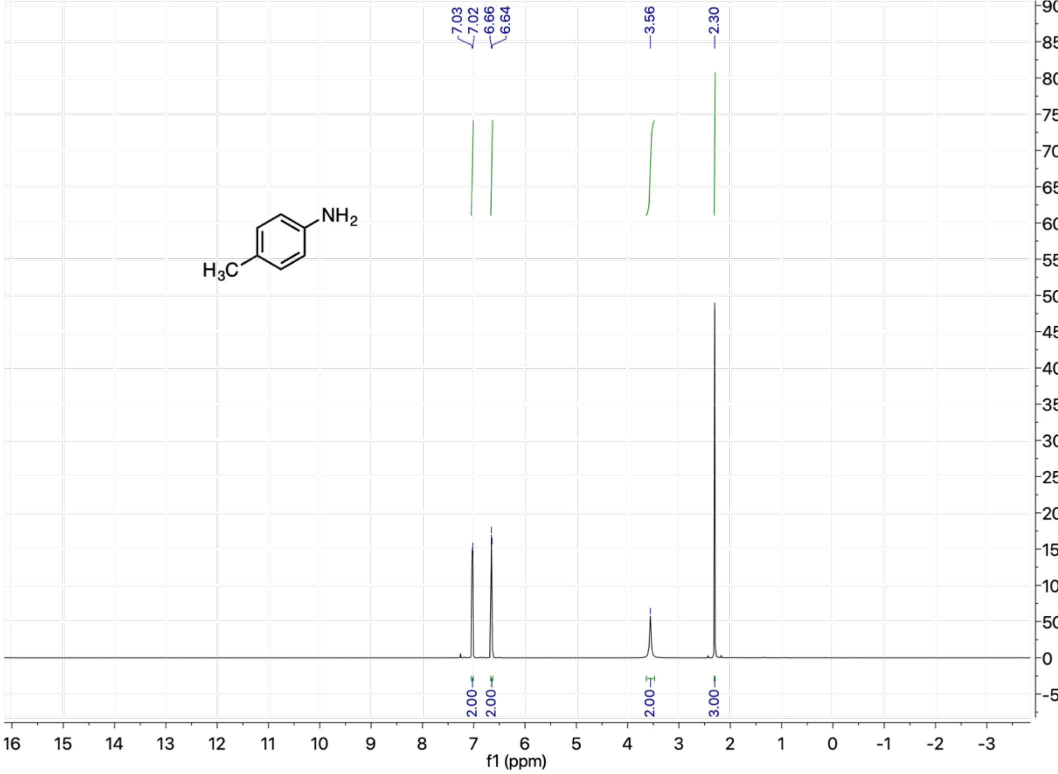
7.03
7.02
6.66
6.64
3.56
2.30
NH2
H3C
2.00
2.00
2.00
3.00
90000
85000
80000
75000
70000
65000
60000
55000
50000
45000
40000
35000
30000
25000
20000
15000
10000
5000
0
-5000
16 15 14 13 12 11 10 9 8 7 6 5 4 3 2 1 0 -1 -2 -3
f1 (ppm)

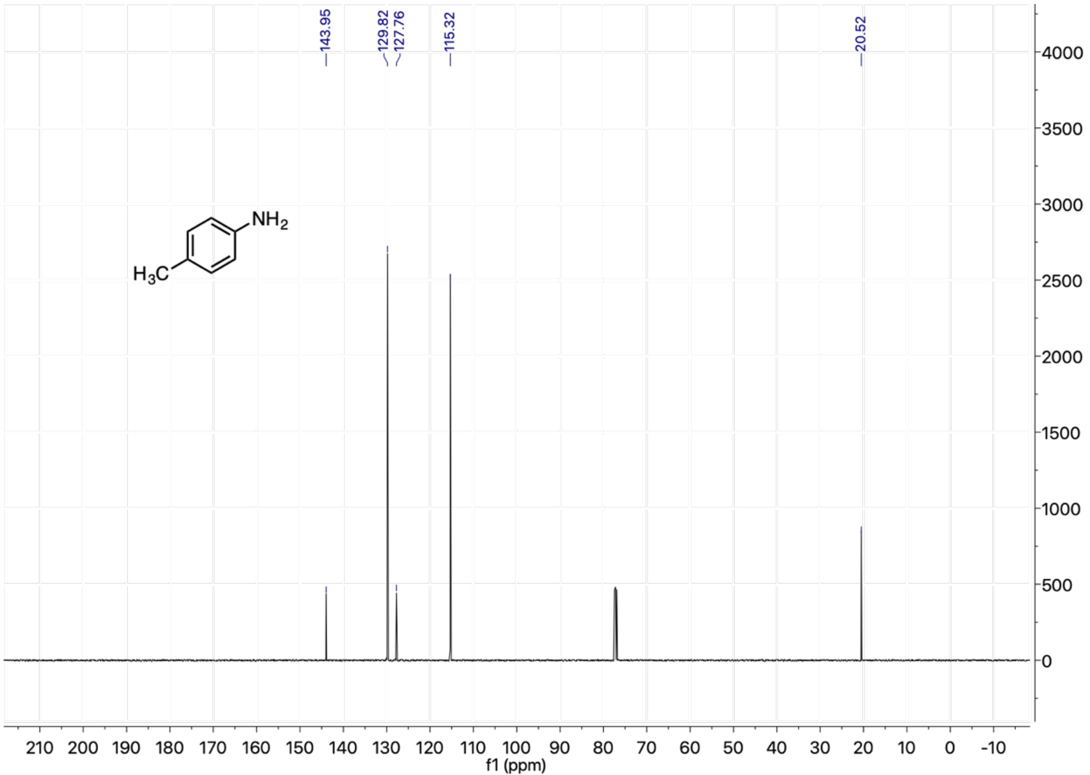
143.95
129.82
127.76
115.32
20.52
NH2
H3C
4000
3500
3000
2500
2000
1500
1000
500
0
210 200 190 180 170 160 150 140 130 120 110 100 90 80 70 60 50 40 30 20 10 0 -10
f1 (ppm)

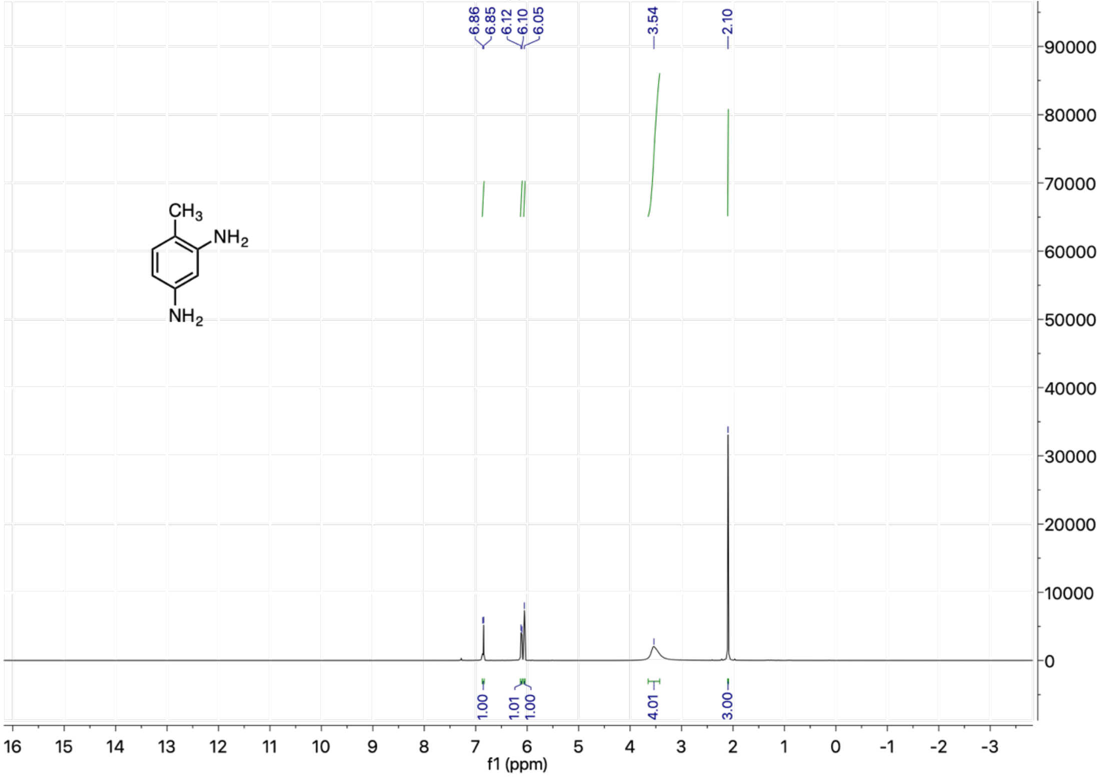
6.86
6.85
6.12
6.10
6.05
3.54
2.10
CH3
NH2
NH2
90000
80000
70000
60000
50000
40000
30000
20000
10000
0
1.00
1.01
1.00
4.01
3.00
16 15 14 13 12 11 10 9 8 7 6 5 4 3 2 1 0 -1 -2 -3
f1 (ppm)

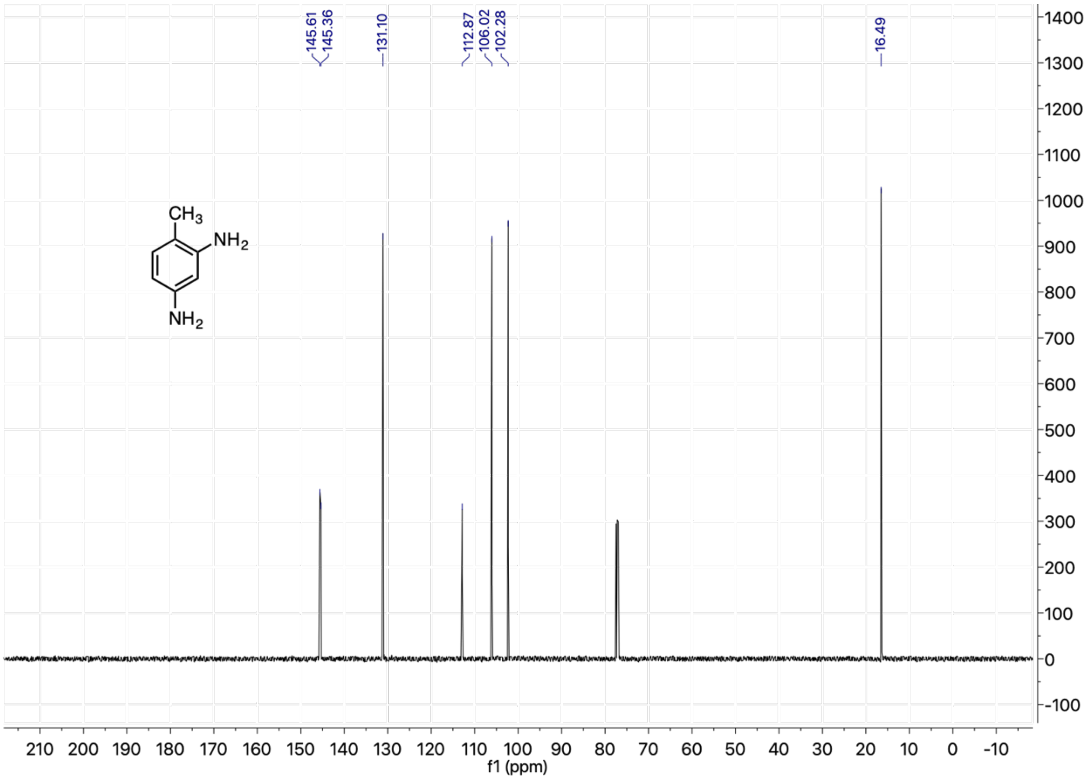
145.61
145.36
131.10
112.87
106.02
102.28
16.49
CH3
NH2
NH2
1400
1300
1200
1100
1000
900
800
700
600
500
400
300
200
100
0
-100
210 200 190 180 170 160 150 140 130 120 110 100 90 80 70 60 50 40 30 20 10 0 -10
f1 (ppm)

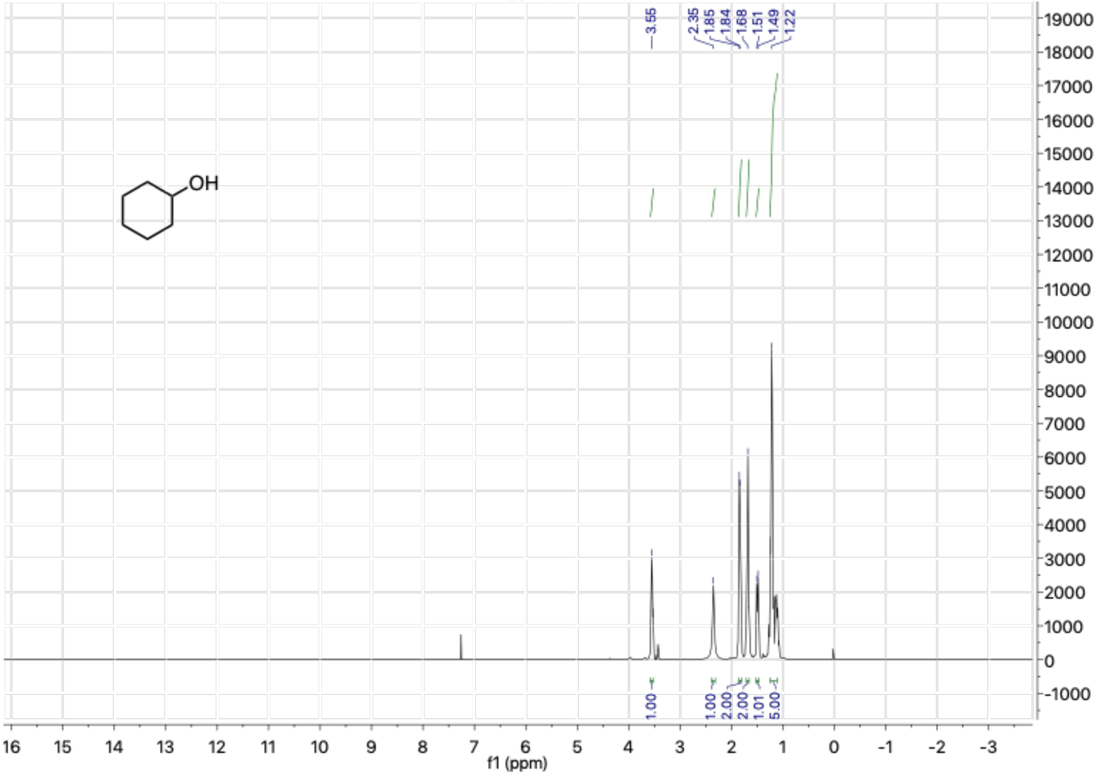
3.55
2.35
1.85
1.84
1.68
1.51
1.49
1.22
OH
1.00
1.00
2.00
2.00
1.01
5.00
19000
18000
17000
16000
15000
14000
13000
12000
11000
10000
9000
8000
7000
6000
5000
4000
3000
2000
1000
0
-1000
16 15 14 13 12 11 10 9 8 7 6 5 4 3 2 1 0 -1 -2 -3
f1 (ppm)

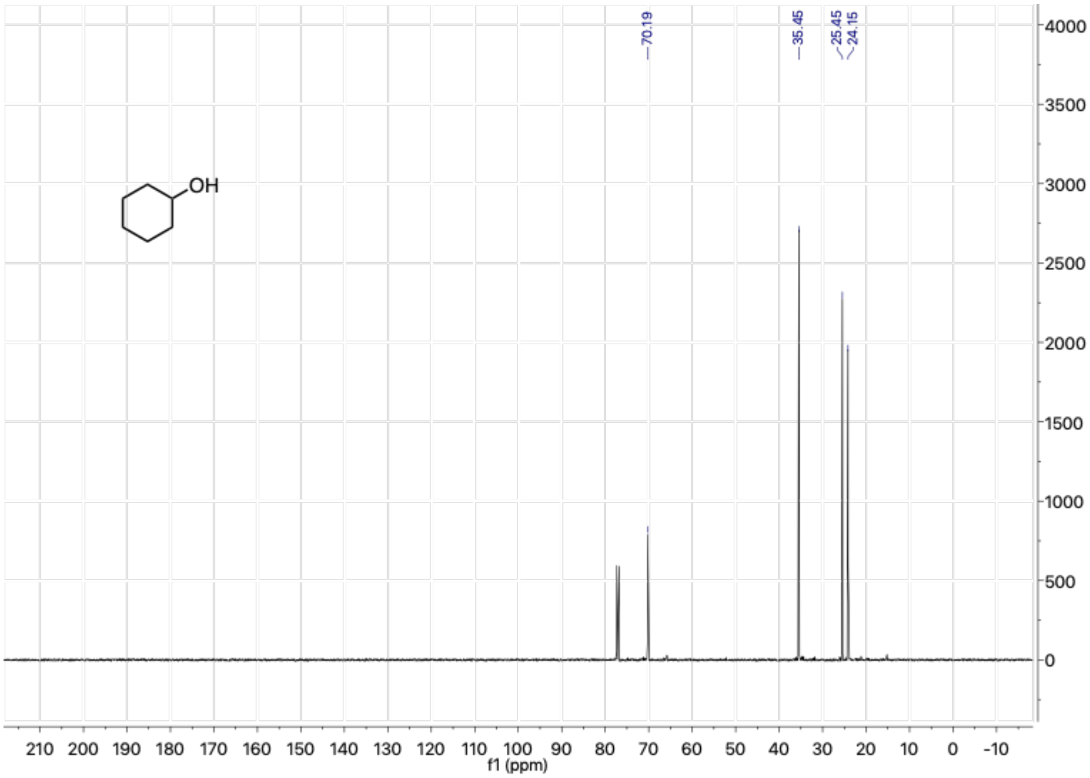
70.19
35.45
25.45
24.15
OH
4000
3500
3000
2500
2000
1500
1000
500
0
210 200 190 180 170 160 150 140 130 120 110 100 90 80 70 60 50 40 30 20 10 0 -10
f1 (ppm)

Chapter 5

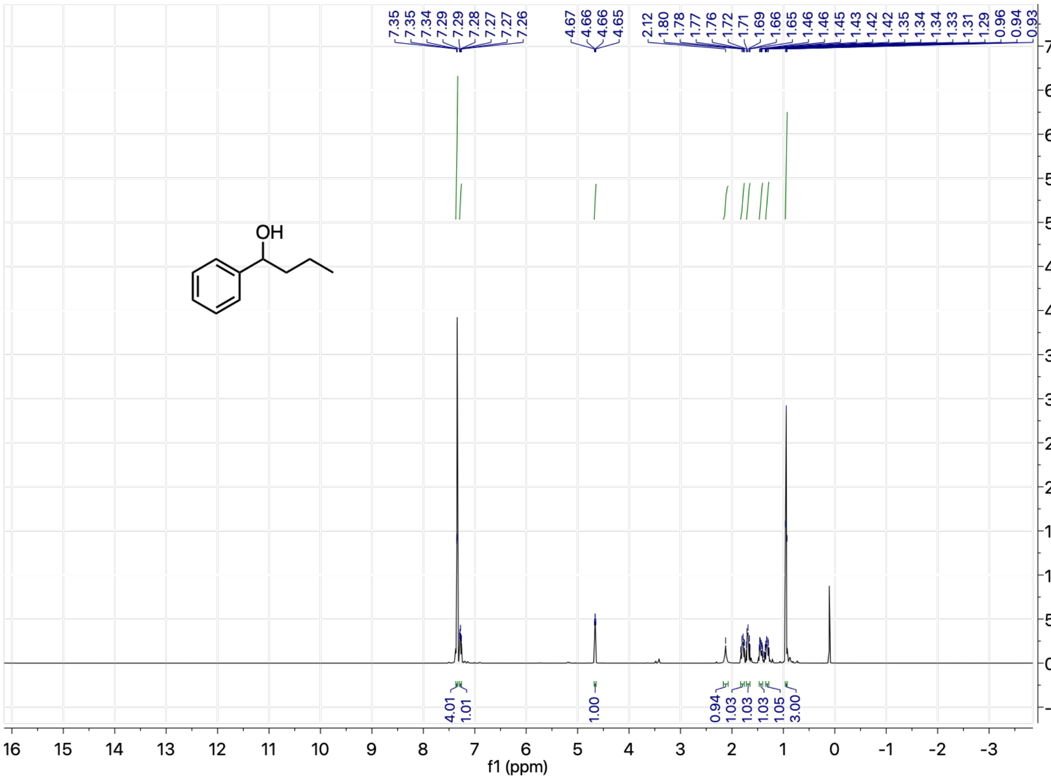
7.35
7.35
7.34
7.29
7.29
7.28
7.27
7.27
7.26
4.67
4.66
4.66
4.65
2.12
1.80
1.78
1.77
1.76
1.72
1.71
1.69
1.66
1.65
1.46
1.45
1.43
1.42
1.35
1.34
1.34
1.33
1.31
1.29
0.96
0.94
0.93
OH
4.01
1.01
1.00
0.94
1.03
1.03
1.03
1.05
3.00
70000
65000
60000
55000
50000
45000
40000
35000
30000
25000
20000
15000
10000
5000
0
-5000
16 15 14 13 12 11 10 9 8 7 6 5 4 3 2 1 0 -1 -2 -3
f1 (ppm)

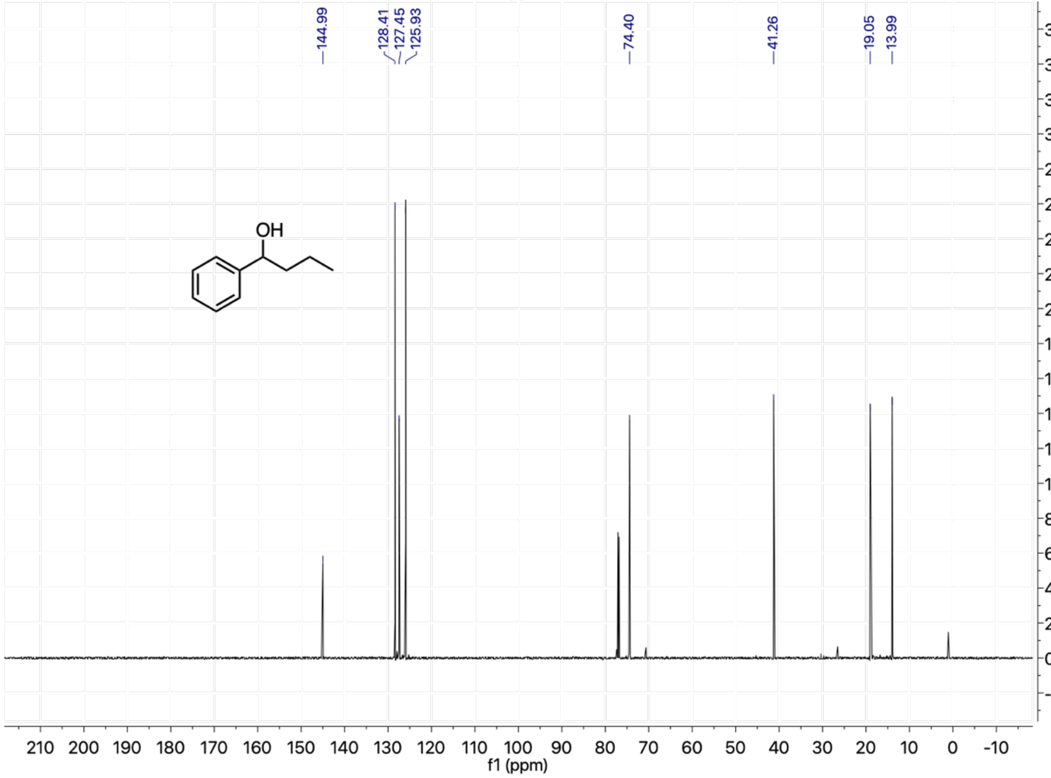
144.99
128.41
127.45
125.93
74.40
41.26
19.05
13.99
OH
3600
3400
3200
3000
2800
2600
2400
2200
2000
1800
1600
1400
1200
1000
800
600
400
200
0
-200
210 200 190 180 170 160 150 140 130 120 110 100 90 80 70 60 50 40 30 20 10 0 -10
f1 (ppm)

Bibliography

Adair, G. R. A.; Williams, J. M. J., A catalytic deracemisation of alcohols. *Chem. Commun.* **2007**, 2608-2609.

Adkins, H.; Billica, H. R., The Preparaton of Raney Nickel Catalysts and their Use Under Conditions with Those for Platinum and Palladium Catalysts. *J. Am. Chem. Soc.* **1948,** *70*, 695-698.

Agmon, N., The Grotthuss mechanism. *Chem. Phys. Lett.* **1995,** *244*, 456-462.

Akopov, G.; Yeung, M. T.; Kaner, R. B., Rediscovering the Crystal Chemistry of Borides. *Adv. Mater.* **2017,** *29*, 1604506.

Aluminum. In *Encyclopedia Britannica*.

American Mineralogist Crystal Structure Database (AMCSD)

An, J.; Work, D. N.; Kenyon, C.; Procter, D. J., Evaluating a Sodium Dispersion Reagent for the Bouveault-Blanc Reduction of Esters. *J. Org. Chem.* **2014,** *79*, 6743-6747.

Anastas, P. T.; Warner, J. C., *Green Chemistry: Theory and Practice*. Oxford University Press: UK, 1998.

Andrews, G. C., Chemoselectivity in the Reduction of Aldehydes and Ketones with Amine Boranes. *Tetrahedron Letters* **1980,** *21*, 697-700.

Andrews, G. C.; Crawford, T. C., The Synthetic Utility of Amine Borane Reagents in the Reduction of Aldehydes and Ketones. *Tetrahedron Letters* **1980,** *21*, 693-696.

Arzac, G. M.; Rojas, T. C.; Fernández, A., Boron Compounds as Stabilizers of a Complex Microstructure in a Co-B-Based Catalyst for $NaBH_4$ Hydrolysis. *ChemCatChem* **2011,** *3*, 1305-1313.

Ashby, E. C.; Cooke, B., The Mechanism of Mixed Hydride Reductions. Effects of Reagent Composition, Nature of Halogen, and Solvating Ligand on the Mechansim of Epoxide Reduction. *J. Am. Chem. Soc* **1969,** *90*, 1625-1630.

Aydin, K.; Kulakli, B. N.; Filiz, B. C.; Alligier, D.; Demirci, U. B.; Figen, A. K., Closing the hydrogen cycle with the couple sodium borohydride-methanol, via the formation of sodium tetramethoxyborate and sodium metaborate. *Int. J. Energy. Res.* **2020,** *44*, 11405-11416.

Baba, A.; Shibata, I., Dihaloindium Hydride as a Novel Reducing Agent. *Chem. Rec.* **2005,** *5*, 323-335.

Béchamp, A., *Ann. Chim. Phys.* **1854,** *42*, 186.

Bedi, D.; Brar, A.; Findlater, M., Transition metal- and solvent-free double hydroboration of nitriles. *Green Chem.* **2020,** *22*, 1125-1128.

Belisle, C. M.; Young, Y. M.; Singaram, B., Catalytic Reaction. 1. Catalytic 1,4-Hydrogenation of α,β-Unsaturated Aldehydes and Ketones Using SC-1 Nickel Boride. *Tetrahedron Lett.* **1994,** *35*, 5595-5598.

Benz, M.; Kraan, A. M. v. d.; Prins, R., Reduction of aromatic nitrocompounds with hdyrazine hydrate in the presence of an iron oxide hydroxide catalyst: II. Activity, X-ray diffraction and Mössbauer study of the iron oxide hydroxide catalyst. *Appl. Catal. A: Gen.* **1998,** *172*, 149-157.

Beygi, H.; Sajjadi, S. A., Magnetic Properties of Crystalline Nickel and Low Phosphorus Amorphous Ni 1-X P x Nanoparticles. *Mater. Chem. Phys.* **2018,** *204*, 403-409.

Bi, H. Y.; Du, M.; Pan, C. X.; Xiao, Y.; Su, G. F.; Mo, D. L., Nickel(II)-Catalyzed [5 + 1] Annulation of 2-Carbonyl-1-propargylindoles with Hydroxylamine To Synthesize Pyrazino[1,2-a]indole-2-oxides in Water. *J. Org. Chem.* **2019,** *84*, 9859-9868.

Billman, J. H.; McDowell, J. W., Reduction of Schiff Bases. III. Reduction with Dimethylamine Borane. *J. Org. Chem.* **1961,** *26*, 1437-1440.

Birkenstock, U.; Bönnemann, H.; Bogdanović, B.; Walter, D.; Wilke, G., π-Allylnickel Compounds as Homogeneous Cataly. In *Homogeneous Catalysis*, 1974; pp 250-265.

Boit, T. B.; Mehta, M. M.; Garg, N. K., Base-Mediated Meerwein-Ponndorf-Verley Reduction of Aromatic and Heterocyclic Ketones. *Org. Lett.* **2019,** *21*, 6447-6451.

Brown, C. A., Catalytic Hydrogenation. V. The Reaction of Sodium Borohydride with Aqueous Nickel Salts. P-1 Nickel Boride, a Convenient, Highly Active Nickel Hydrogenation Catalyst. *J. Org. Chem.* **1970,** *35*, 1900-1904.

Brown, C. A.; Ahuja, V. K., Catalytic hydrogenation. VI. Reaction of sodium borohydride with nickel salts in ethanol solution. P-2 Nickel, a highly convenient, new, selective hydrogenation catalyst with great sensitivity to substrate structure. *J. Org. Chem.* **1973,** *38*, 2226-2230.

Brown, H. C.; Choi, Y. M.; Narasimhan, S., Convenient procedure for the conversion of sodium borohydride into lithium borohydride in simple ether solvents. *Inorg. Chem.* **1981,** *20*, 4454-4456.

Brown, H. C.; Choi, Y. M.; Narasimhan, S., Selective Reductions. 29. A Simple Technique to Achieve an Enhanced Rate of Reduction of Representative Organic Compounds by Borane-Dimethyl Sulfide *J. Org. Chem.* **1982,** *47*, 3153-3163.

Brown, H. C.; Choi, Y. M.; Narasimhan, S., A Simple Technique to Achieve an Enhanced Rate of Reduction of Representative Organic Compounds by Borane-Dimethyl Sulfide. *J. Org. Chem.* **1982,** *47*, 3153-3163.

Brown, H. C.; Heim, P., Selective reductions. XVIII. Fast reaction of primary, secondary, and tertiary amides with diborane. Simple, convenient procedure for the conversion of amides to the corresponding amines. *J. Org. Chem.* **1973,** *38*, 912-916.

Brown, H. C.; Heim, P.; Yoon, N. M., Selective Reductions. XV. Reaction of diborane in tetrahydrofuran with selected organic compounds containing representative functional groups. *J. Am. Chem. Soc* **1970,** *92*, 1637-1646.

Brown, H. C.; Kim, S. C.; Krishnamurthy, S., Lithium Triethylborohydride as an Exceptionally Powerful and Selective Reducing Agent in Organic Synthesis. Exploration of the Reactions with Selected Organic Compounds Containgin Representative Functional Groups. *J. Org. Chem.* **1980,** *45*, 1-12.

Brown, H. C.; Krishnamurthy, S., Forty Years of Hydride Reductions. *Tetrahedron* **1979,** *35*, 567-607.

Brown, H. C.; Narasimhan, S., New powerful catalysts for the reduction of esters by lithium borohydride. *J. Org. Chem.* **1982,** *47*, 1604-1606.

Brown, H. C.; Narasimhan, S.; Choi, Y. M., Improved Procedure for Borane-Dimethyl Sulfide Reduction of Primary Amides to Amines. *Synthesis* **1981,** *6*, 441-442.

Brown, H. C.; Narasimhan, S.; Somayaji, V., Selective Reductions. 32. Structural Effects on the Reduction of Epoxides by Lithium Triethylborohydride. A Kinetic Study. *J. Org. Chem.* **1983,** *48*, 3091-3096.

Brown, H. C.; Rao, B. C., Hydroboration of Olefins. A Remarkably Fast Room-Temperature Addition of Diborane to Olefins. *J. Org. Chem.* **1957,** *22*, 1136-1136.

Brown, H. C.; Subba Rao, B. C., A New Powerful Reducing Agent-Sodium Borohydride in the Presence of Aluminum Chloride and Other Polyvalent Metal Halides. *J. Am. Chem. Soc* **1956,** *78*, 2582-2588.

Brown, H. C.; Subba Rao, B. C., A New Technique for the Conversion of Olefins into Organoboranes and Related Alcohols. *J. Am. Chem. Soc* **1956,** *78*, 5694-5695.

Brown, H. C.; Subba Rao, B. C., Hydroboration. III. The Reduction of Organic Compounds by Diborane, an Acid-type Reducing Agent. *J. Am. Chem. Soc* **1960,** *82*, 681-686.

Brown, H. C.; Wang, K. K.; Chandrasekharan, J., Hydroboration Kinetics. 7. Kinetics and Mechanism of the Reduction of Aldehydes and Ketones with 9-Borabicyclo[3.3.1]nonane Diemr. *J. Am. Chem. Soc.* **1983,** *105*, 2340-2343.

Brown, H. C.; Yoon, N. M., Reaction of Aluminum Hydride with Selected Organic Compounds Containing Representative Functional Groups. Comparison of the Reducing Characteristics of Lithium Aluminum Hydride and Its Derivatives. *J. Am. Chem. Soc* **1966,** *88*, 1464-1472.

Brown, H. C.; Yoon, N. M., Reaction of Diborane in Tetrahydrofuran with Styrene Oxide and Related Epoxides in the Presence of Boron Trifuloride. A Convenient Anti-Markovnikov Reductive Opening of Such Epoxides. *Chem. Commun.* **1968**, 1549-1550.

Brown, W. G., Reductions by Lithium Aluminum Hydride In *Organic Reactions*, John Wiley and Sons, Inc. : 2011; pp 469-509.

Buhrke, D.; Hildebrandt, P., Probing Structure and Reaction Dynamics of Proteins Using Time-Resolved Resonance Raman Spectroscopy. *Chem. Rev.* **2020,** *120*, 3577-3630.

Burg, A. B.; Schlesinger, H. I., Hydrides of Boron. VII. Evidence of the Transitory Existence of Borine (BH_3): Borine Carbonyl and Borine Trimethylammine. *J. Am. Chem. Soc.* **1938,** *59*, 780-787.

Cabacungan, J. C.; Ahmed, A. I.; Feeney, R. E., Amine Boranes as Alternative Reducing Agents for Reductive Alklylation of Proteins. *Anal. Biochem.* **1982,** *124*, 272-278.

Cabrita, I.; Fernandes, A. C., A novel efficient and chemoselective method for the reduction of nitriles using the system silane/oxo-rhenium complexes. *Tetrahedron* **2011,** *67*, 8183-8186.

Caddick, S.; Judd, D. B.; Lewis, A. K.; Reich, M. T.; Williams, M. R., A Generic Approach for the Catalytic Reduction of Nitriles. *Tetrahedron* **2003,** *59*, 5417-5423.

Calvino-Casilda, V.; Bañares, M. A., In situ Raman monitoring of Michael addition for the synthesis of 1-substituted imidazoles intermediates with antiviral properties. *Catalysis Today* **2012,** *187*, 191-194.

Calvino-Casilda, V.; Bañares, M. A.; LozanoDiz, E., Real-time Raman monitoring during coumarins synthesis via Pechmann condensation: A tool for controlling the preparation of pharmaceuticals. *Catalysis Today* **2010,** *155*, 279-281.

Calvino-Casilda, V.; Stawicka, K.; Trejda, M.; Ziolek, M.; Bañares, M. A., Real-Time Raman Monitoring and Control of the Catalytic Acetalization of Glycerol with Acetone over Modified Mesoporous Cellular Foams. *The Journal of Physical Chemistry C* **2014,** *118*, 10780-10791.

Cantillo, D.; Moghaddam, M. M.; Kappe, C. O., Hydrazine-Mediated Reduction of Nitro and Azide Functionalities Catalyzed by Highly Active and Reusable Magnetic Iron Oxide Nanocrystals. *J. Org. Chem.* **2013,** *78*, 4530-4542.

Cao, B.; Veith, G. M.; Neuefeind, J. C.; Adzic, R. R.; Khalifah, P. G., Mixed closed-packed cobalt molybdenum nitrides as non-noble metal electrocatalysts for the hydrogen evolution reaction. *J. Am. Chem. Soc.* **2013,** *135*, 19186-19192.

Carboni, B.; Monnier, L., Recent Developments in the Chemistry of Amine and Phosphine Boranes. *Tetrahedron* **1999,** *55*, 1197-1248.

Carenco, S.; Portehault, D.; Boissière, C.; Mézailles, N.; Sanchez, C., Nanoscaled Metal Borides and Phosphides: Recent Developments and Perspectives. *Chem. Rev.* **2013,** *113*, 7981-8065.

Casarini, M. E.; Ghelfi, F.; Libertini, E.; Pagoni, U. M.; Parsons, A. F., 1,2-Reduction of α,β-unsaturated hydrazones using dimethylamine-borane/p-toluenesulfonic acid: an easy route to allyl hydrazine. *Tetrahedron* **2002,** *58*, 7925-7932.

Cavaliere, S.; Hannauer, J.; Demirci, U. B.; Akdim, O.; Miele, P., Ex Situ Characterization of N_2H_4-, $NaBH_4$- and NH_3BH_3-Reduced Cobalt Catalysts Used in $NaBH_4$ Hydrolysis. *Catal. Today* **2011,** *170*, 3-12.

Chakraborty, U.; Reyes-Rodriguez, E.; Demeshko, S.; Meyer, F.; Wangelin, A. J. v., A Manganese Nanoseet: New Cluster Topology and Catalysis. *Angew. Chem. Int. Ed.* **2018,** *57*, 4970-4975.

Chan, H.-Y.; Nguyen, V.-H.; Wu, J.; Calvino-Casilda, V.; Bañares, M. A.; Bai, H., Real-time Raman monitoring during photocatalytic epoxidation of cyclohexene over V-Ti/MCM-41 catalysts. *Catalysts* **2015,** *5*, 518-533.

Chekin, F.; Sadeghi, S., Room Temperature Decomposition of Hydrazine Catalyzed by Nickel Oxide Nanoparticles. *Bulgarian Chemical Communications* **2015,** *47*, 714-719.

Chen, J.; Luo, Z., Single-point attack of two H_2O molecules towards a Lewis Acid site on the $GaAl_{12}$ clusters for hydrogen evolution. *ChemPhysChem* **2019,** *20*, 499-505.

Chen, X.-M.; Ma, N.; Zhang, Q.-F.; Wang, J.; Feng, X.; Wei, C.; Wang, L.-S.; Zhang, J.; Chen, X., Elucidation of the Formation Mechanisms of the Octahydrotriborate Anion ($B_3H_8^-$) through the Nucleophilicity of the B-H Bond. *J. Am. Chem. Soc.* **2018,** *140*, 6718-6726.

Choi, G.; Ziebarth, J. T.; Woodall, J. M.; Sherman, D.; Allen, C. R.; Kramer, R., Mechanism of Hydrogen Generation via Water Reaction with Aluminum Alloys. In *18th Biennial University/Government/Industry Micro/Nano Symposium*, IEEE: West Lafayette, IN, USA, 2010; pp 1-3.

Choi, Y. M.; Yoo, M.; An, D. K., A New Method of Partial and Chemoselective Reduction of Nitriles to Aldehydes by Lithium Diisobutyl-*iso*-propoxyaluminum Hydride (LDBIPA). *Bull. Korean Chem. Soc* **2010,** *31*, 473-474.

Clarke, C. J.; Tu, W. C.; Levers, O.; Brohl, A.; Hallett, J. P., Green and Sustainable Solvents in Chemical Processes. *Chem. Rev.* **2018,** *118*, 747-800.

Clary, J. W.; Rettenaier, T. J.; Snelling, R.; Byrks, W.; Banwell, J.; Wipke, W. T.; Singaram, B., Hydride as a Leaving Group in the Reaction of Pinacolborane with Halides under Ambient Grignard and Barbier Conditions. One-Pot Synthesis of Alkyl, Aryl, Heteroaryl, Vinyl, and Allyl Pinacolboronic Esters. *J. Org. Chem.* **2011,** *76*, 9602-9610.

Climent, M. J.; Corma, A.; Iborra, S.; Martí, L., Process Instensification with Bifunctional Heterogeneous Catalysts: Selective One-Pot Synthesis of 2'-Aminochalcones. *ACS Catal.* **2015,** *5*, 157-166.

Colthup, N. B.; Daly, L. H.; Wiberly, S. E., *Introduction to Infrared and Raman Spectroscopy*. Academic Press: San Diego, 1990.

Cooke, B.; Ashby, E. C.; Lott, J., Reductions Using Alkoxyaluminum Hydrides. I. Reduction of Epoxides. *J. Org. Chem.* **1968,** *33*, 1132-1136.

Corrias, A.; Ennas, G.; Licheri, G.; Marongiu, G.; Paschina, G., Amorphous Metallic Powders Prepared by Chemical Reduction of Metal Ions with Potassium Borohydride in Aqueous Solution. *Chem. Mater.* **1990,** *2*, 363-366.

Crimmins, M. T.; Jung, D. K.; Gray, J. L., Synthetic Studies on the Ginkgolides: Total Synthesis of (+/-)-Bilobalide. *J. Am. Chem. Soc.* **1993,** *115*, 3146-3155.

Crociani, L.; Rossetto, G.; Kaciulis, S.; Mezzi, A.; El-Habra, N.; Palmieri, V., Study of Magnesium Boride Films Obtained From $Mg(BH_4)_2$ by CVD. *Chem. Vap. Depos.* **2007,** *13*, 414-419.

Czernik, S.; French, R. J.; Magrini-Bair, K. A.; Chornet, E., The Production of Hydrogen by Steam Reforming of Trap Grease — Progress in Catalyst Performance *Energy & Fuels* **2004,** *18*, 1738-1743.

Dai, H.; Guan, H., Switching the Selectivity of Cobalt-Catalyzed Hydrogenation of Nitriles. *ACS Catal.* **2018,** *8*, 9125-9130.

Dallongeville, S.; Garnier, N.; Rolando, C.; Tokarski, C., Proteins in Art, Archaeology, and Paleontology: From Detection to Identification. *Chem. Rev.* **2016,** *116*, 2-79.

Demirci, U. B.; Miele, P., Cobalt-Based Catalysts for the Hydrolysis of $NaBH_4$ and NH_3BH_3. *Phys. Chem. Chem. Phys.* **2014,** *16*, 6872.

Deng, J., The Study of Ultrafine Ni-B and Ni-P Amorphous Alloy Powders as Catalysts. *J. Catal.* **1994,** *150*, 434-438.

Ding, Y.; Luo, S.; Weng, C.; An, J., Reductive Deuteration of Nitriles Using D_2O as a Deuterium Source. *J. Org. Chem.* **2019,** *84*, 15098-15105.

Dionigi, F.; Reier, T.; Pawolek, Z.; Gliech, M.; Strasser, P., Design Criteria, Operating Conditions, and Nickel-Iron Hydroxide Catalyst Materials for Selective Seawater Electrolysis. *ChemSusChem* **2016,** *9*, 962-972.

Dresp, S.; Dionigi, F.; Klingenhof, M.; Strasser, P., Direct electrolytic splitting of seawater: opportunities and challenges. *ACS Energy Lett.* **2019,** *4*, 933-942.

Ducry, L.; Roberge, D. M., Dibal-H Reduction of Methyl Butyrate into Butyraldehyde using Microreactors. *Org. Process Res. Dev.* **2008,** *12*, 163-167.

Duval, M.; Navarre, S.; Sagorin, G.; Denicourt-Nowicki, A.; Roucoux, A., Multigram Scale-up of the Selective Hydrogenation of alpha-Pinene with Ruthenium Nanoparticles in Water. *ACS Sustainable Chem. Eng.* **2020,** *8*, 5985-5993.

Eliel, E. L.; Delmonte, D. W., The Mechanism of Halide Reductons with Lithium Aluminum Hydride. VI. Reduction of Certain Bromohydrins and Epoxides. *J. Am. Chem. Soc* **1958,** *80*, 1744-1752.

Ellzey, S.E.; Mack, C. H.; Connick, W.J. Dehydration of primary amides with sodium borohydride. *J. Org. Chem.* **1967,** *32*, 846-847.

Eppinger, J.; Huang, K.-W., Formic Acid as a Hydrogen Energy Carrier. *ACS Energy Lett.* **2017,** *2*, 188-195.

Evans, D. S.; Prince, A., Thermal analysis of Ga-In-Sn system. *Metal Science* **1978,** *12*, 411-414.

Fan, L.; Liu, P. F.; Yan, X.; Gu, L.; Yang, Z. Z.; Yang, H. G.; Qiu, S.; Yao, X., Atomically isolated nickel species anchored on graphitized carbon for efficient hydrogen evolution electrocatalysis. *Nat. Commun.* **2016,** *7*, 10667.

Fan, M.-Q.; Xu, F.; Sun, L.-X., Studies on hydrogen generation characteristics of hydrolysis of te ball milling Al-based materials in pure water. *Int. J. Hydrogen Energy* **2007,** *32*, 2809-2815.

Fernandes, R.; Patel, N.; Miotello, A.; Filippi, M., Studies on Catalytic Behavior of Co–Ni–B in Hydrogen Production by Hydrolysis of $NaBH_4$. *J. Mol. Catal. Chem.* **2009,** *298*, 1-6.

Filimonov, V. O.; Dianova, L. N.; Beryozkina, T. V.; Mazur, D.; Beliaev, N. A.; Volkova, N. N.; Ilkin, V. G.; Dehaen, W.; Lebedev, A. T.; Bakulev, V. A., Water/Alkali-Catalyzed Reactions of Azides with 2-Cyanothioacetamides. Eco-Friendly Synthesis of Monocyclic and Bicyclic 1,2,3-Thiadiazole-4-carbimidamides and 5-Amino-1,2,3-triazole-4-carbothioamides. *J. Org. Chem.* **2019,** *84*, 13430-13446.

Fischer, S. A.; Gunlycke, D., Anaylsis of Correlated Dynamics in the Grotthuss Mechanism of Proton Diffusion. *J. Phys. Chem. B* **2019,** *123*, 5536-5544.

Flaniken, J. M.; Colins, C. J.; Lanz, M.; Singaram, B., Aminoborohydrides. 11. Facile Reduction of *N*-Alkyl Lactams to the Corresponding Amines Using Lithium Aminoborohydrides. *Org. Lett.* **1999,** *1*, 799-801.

Fleck, T. J.; William W. McWhorter, J.; Dekam, R. N.; Pearlman, B. A., Synthesis of N-Methyl-N-{(1S)-1-[(3R)-pyrrolidin-3-yl]ethyl}amine. *J. Org. Chem.* **2003,** *68*, 9612-9617.

Foley, N.; Jaskula, B. W. Gallium — A Smart Metal. https://pubs.usgs.gov/fs/2013/3006/pdf/fs2013-3006.pdf (accessed October 22, 2020).

Foley, N. K.; Jaskula, B. W.; Kimball, B. E.; Schulte, R. F., Gallium. In *Critical Mineral Resources of the United States — Ecomic and Environmental Geology and Prospects for Future Supply*, Schulz, K. J.; John H. DeYoung, J.; II, R. R. S.; Bradley, D. C., Eds. U.S. Geological Survey 2017; pp H1-H35.

Formenti, D.; Ferretti, F.; Scharnagl, F. K.; Beller, M., Reduction of Nitro Compounds Using 3d-Non-Noble Metal Catalysts. *Chem. Rev.* **2019,** *119*, 2611-2680.

Fountoulaki, S.; Daikopoulou, V.; Gkizis, P. L.; Tamiolakis, I.; Armatas, G. S.; Lykakis, I. N., Mechanistic Studies of the Reduction of Nitroarenes by $NaBH_4$ or Hydrosilanes Catalyzed by Supported Gold Nanoparticles. *ACS Catal.* **2014,** *4*, 3504-3511.

Fräulin, C.; Rinke, G.; Dittmeyer, R., In-Situ Laser Raman Spectroscopy Adapted to Process Conditions for Studying Cyclohexane Oxidation. *Journal of Flow Chemistry* **2013,** *3*, 87-91.

Fuchs, R.; VanderWef, C. A., Direction of Ring Opening in the Reduction of p-Substituted Styrene Oxides with Lithium Borohydride. *J. Am. Chem. Soc* **1954,** *76*, 1631-1634.

Fujiwara, K.; Yasuda, S.; Mizuta, T., Reduction of CO_2 to Trimethoxyboroxine with BH_3 in THF. *Organometallics* **2014,** *33*, 6692-6695.

Galatis, P.; Sollogoub, M.; Sinaÿ, P., *Encyclopedia of Reagents for Organic Synthesis*. John Wiley & Sons: New York, 2001.

Gandhamsetty, N.; Jeong, J.; Park, J.; Park, S.; Chang, S., Boron-Catalyzed Silylative Reduction of Nitriles in Accessing Primary Amines and Imines. *J. Org. Chem.* **2015,** *80*, 7281-7287.

Geng, J.; Jefferson, D. A.; Johnson, B. F. G., The Unusual Nanostructure of Nickel–Boron Catalyst. *Chem. Commun.* **2007**, 969-971.

Ghosh, A. K.; Krishnan, K., Chemoselective catalystic hydrogenation of alkenes by Lindlar Catalyst. *Tett. Lett.* **1998,** *39*, 947-948.

Gilmore, K.; Vukelić, S.; McQuade, D. T.; Koksch, B.; Seeberger, P. H., Continuous Reductions and Reductive Aminations Using Solid $NaBH_4$. *Org. Process Res. Dev.* **2014,** *18*, 1771-1776.

Glavee, G. N.; Klabunde, K. J.; Sorensen, C. M.; Hadjipanayis, G. C., Borohydride Reduction of Nickel and Copper Ions in Aqueous and Nonaqueous Media. Controllable Chemistry Leading to Nanoscale Metal and Metal Boride Particles. *Langmuir* **1994,** *10*, 4726-4730.

Goedde, D. M.; Girolami, G. S., A New Class of CVD Precursors to Metal Borides: $Cr(B_3H_8)_2$ and Related Octahydrotriborate Complexes. *J. Am. Chem. Soc.* **2004,** *126*, 12230-12231.

Haddenham, D.; Pasumanksy, L.; DeSoto, J.; Eagon, S.; Singaram, B., Reductions of Aliphatic and Aromatic Nitriles to Primary Amines with Diisopropylaminoborane. *J. Org. Chem.* **2009,** *74*, 1964-1970.

Han, M.; Ma, X.; Yao, S.; Ding, Y.; Yan, Z.; Adijiang, A.; Wu, Y.; Li, H.; Zhang, Y.; Lei, P.; Ling, Y.; An, J., Developement of a Modified Bouveault-Blanc Reduction for the Selective Synthesis of ɑ,ɑ-Dideuterio Alcohols. *J. Org. Chem.* **2017,** *82*, 1285-1290.

Hauser, J. L.; Amberchan, G.; Tso, M.; Manley, R.; Bustillo, K.; Cooper, J.; Golden, J. H.; Singaram, B.; Oliver, S. R. J., A Mesoporous Aluminosilicate Nanoparticle-Supported Nickel–Boron Composite for the Catalytic Reduction of Nitroarenes. *ACS Applied Nano Materials* **2019,** *2*, 1472-1483.

Hauser, J. L.; Tran, D. T.; Conley, E. T.; Saunders, J. M.; Bustillo, K. C.; Oliver, S. R. J., Plasma Treatment of Silver Impregnated Mesoporous Aluminosilicate Nanoparticles for Adsorptive Desulfurization. *Chem. Mater.* **2016,** *28*, 474-479.

He, T.; Wang, W.; Chen, W.; Chen, D.; Yang, K., Reactivity of Al-rich Alloys with Water Promoted by Liquid Al Grain Boundary Phases. *J. Mater. Science & Technology* **2017,** *33*, 397-403.

He, Y.; Qiao, M.; Hu, H.; Pei, Y.; Li, H.; Deng, J.; Fan, K., Preparation of Amorphous Ni–B Alloy: The Effect of Feeding Order, Precursor Salt, PH and Adding Rate. *Mater. Lett.* **2002,** *56*, 952-957.

Heinzman, S. W.; Ganem, B., The Mechanism of Sodium Borohydride-Cobaltous Chloride Reductions. *J. Am. Chem. Soc* **1982,** *104*, 6801-6802.

Heiss, J. D.; Argersinger, D. P.; Theodore, W. H.; Butman, J. A.; Sato, S.; Khan, O. I., Convection-Enhanced Delivery of Muscimol in Patients with Drug-Resistatn Epilepsy *Neurosurgery* **2019,** *85*, E3-E15.

Hendrickson, D. N.; Hollander, J. M.; Jolly, W. L., Core-Electron Binding Energies for Compounds of Boron, Carbon, and Chromium. *Inorg. Chem.* **1970,** *9*, 612-615.

Hill, A. J.; Nason, E. H., The Utilization of Cassia Oil for the Synthesis of Cinnamyl Alcohol. *J. Am. Chem. Soc* **1924,** *46*, 2236-2246.

Hofer, L. J. E.; Shultz, J. F.; Panson, R. D.; Anderson, R. B., The Nature of the Nickel Boride Formed by the Action of Sodium Borohydride on Nickel Salts. *Inorg. Chem.* **1964,** *3*, 1783-1785.

Homma, T.; Tamaki, A.; Nakai, H.; Osaka, T., Molecular orbital study on the reaction process of dimetylamine borane as a reductant for electroless deposition. *J. Electroanalytical Chem.* **2003,** *559*, 131-136.

Huang, T.; Gao, Q.; Liu, D.; Xu, S.; Guo, C.; Zou, J.; Wei, C., Preparation of Al-Ga-In-Sn-Bi quinary alloy and its hydrogen production via water splitting. *Int. J. Hydrogen Energy* **2015,** *40*, 2354-2362.

Huang, X.; Gao, T.; Pan, X.; Wei, D.; Ly, C.; Quin, L.; Huang, Y., A review: Feasibility of hydrogen generation from the reaction between aluminum and water for fuel cell applications. *J. Power Sources* **2013,** *229*, 133-140.

Hutchins, R. O.; Learn, K.; Nazer, B.; Pytlewski, D.; Pelter, A., Amine Boranes as Selective Reducing and Hydroborating Agents. A Review. *Organic Preparations and Procedures International* **1984,** *16*, 335-372.

Hydrogen Production: Natural Gas Reforming https://www.energy.gov/eere/fuelcells/hydrogen-production-natural-gas-reforming (accessed November 16, 2020).

Ilyukhina, A. V.; Kravchenko, O. V.; Bulychev, B. M.; Shkolnikov, E. I., Mechanochemical activation of aluminum with gallams for hydrogen evolution from water. *Int. J. Hydrogen Energy* **2010,** *35*, 1905-1910.

Inoue, K.; Sawada, A.; Shibata, I.; Baba, A., Indium(III) Chloride — Sodium Borohydride System: A Convenient Radical Reagent for an Alternative to Tributyltin Hydride System. *J. Am. Chem. Soc.* **2002,** *124*, 906-907.

Jaganyi, D.; Mzinyati, A., An ^{11}B NMR spectrscopy investigation of the mechanism of the reduction of nitriles by BH_3SMe_2. *Polyhedron* **2006,** *25*, 2730-2736.

Jayaraman, S.; Yang, Y.; Kim, D. Y.; Girolami, G. S.; Abelson, J. R., Hafnium Diboride Thin Films by Chemical Vapor Deposition from a Single Source Precursor. *J. Vac. Sci. Technol. Vac. Surf. Films* **2005,** *23*, 1619-1625.

Jensen, J. A.; Gozum, J. E.; Pollina, D. M.; Girolami, G. S., Titanium, Zirconium, and Hafnium Tetrahydroborates as "Tailored" CVD Precursors for Metal Diboride Thin Films. *J. Am. Chem. Soc.* **1988,** *110*, 1643-1644.

Kalidindi, S. B.; Vernekar, A. A.; Jagirdar, B. R., Co–Co_2B, Ni–Ni_3B and Co–Ni–B Nanocomposites Catalyzed Ammonia–Borane Methanolysis for Hydrogen Generation. *Phys. Chem. Chem. Phys.* **2009,** *11*, 770-775.

Kanth, J. V. B., Borane-Amine Complexes for Hydroboration. *Aldrichimica Acta* **2002,** *35*, 57-66.

Kher, S. S.; Spencer, J. T., Chemical Vapor Deposition Precursor Chemistry. 3. Formation and Characterization of Crystalline Nickel Boride Thin Films from the Cluster-Assisted Deposition of Polyhedral Borane Compounds. *Chem. Mater.* **1992,** *4*, 538-544.

Khurana, J. M.; Kukreja, G., Rapid Reduction of Nitriles to Primary Amines with Nickel Boride at Ambient Temperature. *Synth. Commun.* **2002,** *32*, 1265-1269.

Kikugawa, Y., Chemsitry of Amine-Boranes. XI. A Convenient Synthesis of Dimethylamine-Borane. *Chem. Pharm. Bull.* **1987,** *35*, 4988-4989.

Kim, S.; Ahn, K. H., Ate Complex from Diisobutylaluminum Hydride and *n*-Butyllithium as a Powerful and Selective Reducing Agent for the Reduction of Selected Organic Compounds Containing Various Functional Gropus. *J. Org. Chem.* **1984,** *49*, 1717-1724.

Kiran, V.; Mukherjee, J.; Jenjeti, R. N.; Sampath, S., Active guests in the MoS_2/$MsSe_2$ host lasttice: efficient hydrogen evolution using few-layer alloys of $MoS_{2(1-x)}Se_{2x}$. *Nanoscale* **2014,** *6*, 12856-12863.

Kollonitsch, J., Reductive Ring-Cleavage of Tetrahydrofurans by Diborane. *J. Am. Chem. Soc* **1961,** *83*, 1515.

Kondrat, S. A.; Shaw, G.; Freakley, S. J.; He, Q.; Hampton, J.; Edwards, J. K.; Miedziak, P. J.; Davies, T. E.; Carley, A. F.; Taylor, S. H., Physical Mixing of Metal Acetates: A Simple, Scalable Method to Produce Active Chloride Free Bimetallic Catalysts. *Chem. Sci.* **2012,** *3*, 2965.

Kreuder, A. D.; House-Knight, T.; Whitford, J.; Ponnusamy, E.; Miller, P.; Jesse, N.; Rodenborn, R.; Sayag, S.; Gebel, M.; Aped, I.; Sharfstein, I.; Manaster, E.; Ergaz, I.; Harris, A.; Grice, L. N., A Method for Assessing Greener Alternatives between Chemical Products Following the 12 Principles of Green Chemistry. *ACS Sustainable Chem. Eng.* **2017,** *5*, 2927-2935.

Kumaravel, S.; Thiruvengetam, P.; Karthick, K.; Sankar, S. S.; Kundu, S., Detection of Lignin Motifs with RuO_2-DNA as an Active Catalyst via Surface-Enhanced Raman Scattering Studies. *ACS Sustainable Chem. Eng.* **2019,** *7*, 18463-18475.

Kumarraja, M., Simple and Efficient Reduction of Nitroarenes by Hydrazine in Faujasite Zeolites. *Appl. Catal. Gen.* **2004,** *265*, 135-139.

Lane, C. F., Borane Amine Complexes *Aldrichimica Acta* **1973,** *6*, 51-59.

Lane, C. F., Reduction of Organic Compounds with Diborane. *Chem. Rev.* **1976,** *76*, 773-799.

Lane, C. F.; Myatt, H. L.; Daniels, J.; Hopps, H. B., Reduction of Aromatic Carboxylic Acids in the Presence of Trimethyl Borate. *J. Org. Chem.* **1974,** *39*, 3052-3054.

Lane, L. A.; Qian, X.; Nie, S., SERS Nanoparticles in Medicine: From Label-Free Detection to Spectroscopic Tagging. *Chem. Rev.* **2015,** *115*, 10489-529.

Larsen, J. W.; Freund, M.; Kim, K. Y.; Sidovar, M.; Stuart, J. L., Mechanism of the Carbon Catalyzed Reduction of Nitrobenzene by Hydrazine. *Carbon* **2000,** *38*, 655-661.

Lauwiner, M.; Rys, P.; Wissmann, J., Reduction of aromatic nitro compounds with hydrazine hydrate in the presence of an iron oxide hydroxide catalyst. I. The reduction of monosubstituted nitrobenzenes with hydrazine hydrate in the presence of ferrihydrite. *Appl. Catal. A: Gen.* **1998,** *172*, 141-148.

Lawrence, S. A., *Amines: Synthesis, Properties, and Application*. Cambridge University: Cambridge, 2004.

Leadbeater, N. E.; Smith, R. J., Real-Time Monitoring of Microwave-Promoted Suzuki Coupling Reactions Using in Situ Raman Spectroscopy. *Organic Letters* **2006,** *8*, 4589-4591.

Leggans, E. K.; Barker, T. J.; Duncan, K. K.; Boger, D. L., Iron(III)/$NaBH_4$-Mediated Additions to Unactivated Alkenes: Synthesis of Novel 20′-Vinblastine Analogues. *Org. Lett.* **2012,** *14*, 1428-1431.

Legrand, J.; Taleb, A.; Gota, S.; Guittet, M.-J.; Petit, C., Synthesis and XPS Characterization of Nickel Boride Nanoparticles. *Langmuir* **2002,** *18*, 4131-4137.

Lelental, M., Dimethylamine Borane as the Reducing Agent in Electroless Plating Systems. *J. Electrochem. Soc.* **1973,** *120*, 1650-1654.

Lelental, M., Effect of Amine Borane Structure on Activity in Electroless Plating. *J. Catal.* **1974,** *32*, 429-433.

Lemoine, D.; Jiang, R.; Taly, A.; Chataigneau, T.; Specht, A.; Grutter, T., Ligand-Gated Ion Channels: New Insights into Neurological Disorders and Ligand Recognition *Chem. Rev.* **2012,** *112*, 6285-6318.

Leng, Y.; Shi, L.; Du, S.; Jiang, J.; Jiang, P., A tannin-derived zirconium-containing porous hybrid for efficient Meerwein-Ponndorf-Verley reduction under mild conditions. *Green Chem.* **2020,** *22*, 180-186.

Li, H., Liquid Phase Hydrogenation of Acetonitrile to Ethylamine over the Co_B Amorphous Alloy Catalyst. *J. Catal.* **2003,** *214*, 15-25.

Lin-Vien, D.; Colthup, N. B.; Fateley, W. B.; Graselli, J. G., *The Handbook of Infrared and Raman Characteristic Frequencies of Organic Molecules*. Academic Press: Boston, 1991.

Liu, R.; Gu, S.; Du, H.; Li, C. M., Controlled syntehsis of FeP nanorod arrays as highly efficient hydrogen evolution cathode. *J. Mater. Chem. A* **2014,** *2*, 17263-17267.

Liu, Y.; Hu, X.; Huang, B.; Xie, Z., Surface Engineering of Rh Catalysts with N/S-Codoped Carbon Nanosheets toward High-Performance Hydrogen Evolution from Seawater. *ACS Sustainable Chem. Eng.* **2019,** *7*, 18835-18843.

Liu, Y.-C.; Huang, C.-Y.; CHen, Y.-W., Hydrogenation of P-Chloronitrobenzene on Ni–B Nanometal Catalysts. *J. Nanopartical Res.* **2006,** *8*, 223-234.

López-Porfiri, P.; Gorgojo, P.; Gonzalez-Miquel, M., Green Solvent Selection Guide for Biobased Organic Acid Recovery. *ACS Sustainable Chem. Eng.* **2020,** *8*, 8958-8969.

Lu, Z.; Williams, T. J., A dual site catalyst for mild, selective nitrile reduction. *Chem. Commun.* **2014,** *50*, 5391-5393.

Lund, H., *Ber. Dtsh. Chem. Ges* **1937,** *70*, 1520.

Ma, G.-L.; Dai, H.-B.; Zhuang, D.-W.; Xia, H.-J.; Wang, P., Controlled hydrogen generation by reaction of aluminum/sodium hydroxide/sodium stannate solid mixture with water. *J. Hydrogen Energy* **2012,** *37*, 5811-5816.

Ma, N.; Song, M.; Meng, Q.; Wei, C.; Zhang, G., Theoretical insight into the solvent effect on the stoichiometric reduction of carbonyl compounds by ammonia borane and N-methyl amine borane. *Int. J. Quantum Chem.* **2020,** *120*, 1-8.

Magano, J.; Dunetz, J. R., Large-Scale Carbonyl Reductions in the Pharmaceutical Industry. *Org. Process Res. Dev.* **2012,** *16*, 1156-1184.

Marrero-Alfonso, E. Y.; Beaird, A. M.; Davis, T. A.; Matthews, M. A., Hydrogen Generation from Chemical Hydrides. *Ind. Eng. Chem. Rres.* **2009,** *48*, 3703-3712.

Mason, P. E.; Uhlig, F.; Vaněk, V.; Buttersack, T.; Bauerecker, S.; Jungwirth, P., Coulomb explosion during the early stages of the reaction of alkali metals with water. *Nature Chemistry* **2015,** *7*, 250-254.

Maybury, P. C.; Mitchell, R. W.; Hawthorne, M. F., Hydrogen Adducts of Cobalt and Nickel Boride. *J. Chem. Soc. Chem. Commun.* **1974,** *14*, 534.

Maytum, H. C.; Francos, J.; Whatrup, D. J.; Williams, J. M. J., 1,4-Butanediol as a reducing agent in transfer hydrogenation reactions. *Chem. Asian J.* **2010,** *5*, 538-542.

Medders, G. R.; Paesani, F., Infrared and Raman spectroscopy of liquid water through "first-principles" many-body molecular dynamics. *Journal of chemical theory and computation* **2015,** *11*, 1145-1154.

Meerwein, H.; Schmidt, R., Ein neues Verfahren zur Reduktion von Aldehyden und Ketonen. *Liebigs Ann.* **1925,** *444*, 221-238.

Merki, D.; Fierro, S.; Vrubel, H.; Hu, X., Amorphous molybdenum sulfide films as catalysts for electrochemical hydrogen production in water. *Chem. Sci* **2011,** *2*, 1262-1267.

Mikolajska, E.; Calvino-Casilda, V.; Bañares, M. A., Real-time Raman monitoring of liquid-phase cyclohexene epoxidation over alumina-supported vanadium and phosphorous catalysts. *Applied Catalysis A: General* **2012,** *421-422*, 164-171.

Miller, A. E. G.; Biss, J. W.; Schwartzman, L. H., Reductions with Dialkylaluminum Hydrides. *J. Org. Chem.* **1959,** *24*, 627-630.

Muhammad, M. H.; Chen, X.-L.; Liu, Y.; Shi, T.; Peng, Y.; Qu, L.; Yu, B., Recyclable Cu@C_3N_4-Catalyzed Hydroxylation of Aryl Boronic Acids in Water under Visible Light: Synthesis of Phenols under Ambient Conditions and Room Temperature *ACS Sustainable Chem. Eng.* **2020,** *8*, 2682-2687.

Muñoz, J. d. M.; Alcázar, J.; Hoz, A. d. l.; Díaz-Ortiz, A., Application of flow chemistry to the reduction of nitriles to aldehdyes. *Tetrahedron Letters* **2011,** *52*, 6058-6060.

Nainan, K. C.; Ryschkewitsch, G. E., New synthesis of amine- and phosphine-boranes. *Inorg. Chem.* **1969,** *8*, 2671-2674.

Newman, M. S.; Fukunaga, T., The Reduction of Amides to Amines via Nitriles by Lithium Aluminum Hydride. *J. Am. Chem. Soc* **1960,** *82*, 693-696.

Nose, A.; Kudo, T., Reduction with Sodium Borohydride-Transition Metal Salt Systems. I. Reduction of Aromatic Nitro Compounds with the Sodium Borohydride-Nickelous Chloride System. *Chem. Pharm. Bull. (Tokyo)* **1981,** *29*, 1159-1161.

Nystrom, R. F.; Brown, W. G., Reduction of Organic Compounds by Lithium Aluminum Hydride. III. Halides, Quinones, Miscellaneous Nitrogen Compounds. *J. Am. Chem. Soc* **1948,** *70*, 3738-3740.

Nystrom, R. F.; Chaikin, S. W.; Brown, W. G., Lithium Borohydride as a Reducing Agent. *J. Am. Chem. Soc.* **1949,** *71*, 3245-3246.

Okamoto, Y.; Nitta, Y.; Imanaka, T.; Teranishi, S., Surface characterisation of nickel boride and nickel phosphide catalysts by X-ray photoelectron spectropscopy *J. Chem. Soc., Faraday Trans. 1* **1979,** *75*, 2027-2039.

Ong, D. Y.; Yen, Z.; Yoshii, A.; Imbernon, J. R.; Takita, R.; Chiba, S., Controlled Reduction of Carboxamides to Alcohols or Amines by Zinc Hydrides. *Angew. Chem. Int. Ed.* **2019,** *58*, 4992-4997.

Orimo, S.-i.; Nakamori, Y.; Eliseo, J. R.; Züttel, A.; Jensen, C. M., Complex Hydrides for Hydrogen Storage. *Chem. Rev.* **2007,** *107*, 4111-4132.

Orlandi, M.; Brenna, D.; Harms, R.; Jost, S.; Benaglia, M., Recent Developments in the Reduction of Aromatic and Aliphatic Nitro Compounds to Amines. *Org. Process Res. Dev.* **2018,** *22*, 430-445.

Osby, J. O.; Heinzman, S. W.; Ganem, B., Studies on the Mechanism of Transition-Metal-Assisted Sodium Borohydride and Lithium Aluminum Hydride Reductions. *J. Am. Chem. Soc.* **1986,** *108*, 67-72.

Ozerova, A. M.; Bulavchenko, O. A.; Komova, O. V.; Netskina, O. B.; Zaikovskii, V. I.; Odegova, G. B.; Simagina, V. I., Cobalt Boride Catalysts for Hydrogen Storage Systems Based on NH_3BH_3 and NaBH4. *Kinet. Catal.* **2012,** *53*, 511-520.

Pachauri, R. K.; Meyer, L. A., Climate Change 2014: Synthesis Report. Contribution of Working Groups, I, II, and III, to the Fifth Assessment Report of the Intergovernmental Panel on Climate Change. IPCC: 2014; pp 1-151.

Pal, S.; Kusumoto, S.; Nozaki, K., Dehydrogenation of Dimethylamine-Borane Catalyzed by Half-Sandwich Ir and Rh Complexes: Mechanism and the Role of Cp* Noninnocence. *Organometallics* **2018,** *37*, 906-914.

Pan, X.; Xu, Y.-J., Efficient Thermal-and Photocatalyst of Pd Nanoparticles on TiO_2 Achieved by an Oxygen Vacancies Promoted Synthesis Strategy. *ACS Appl. Mater. Interfaces* **2014,** *6*, 1879-1886.

Pasto, D. J.; Cumbo, C. C.; Hickman, J., Transfer Reactions Involving Boron. VIII. The Stereochemistry and Mechanism of the Reduction of Epoxides with Borane-d_3-Tetrahydrofuran. *J. Am. Chem. Soc* **1966,** *88*, 22012207.

Pasumansky, L.; Goralski, C. T.; Singaram, B., Lithium Aminoborohydrides: Powerful, Selective, Air-Stable Reducing Agents. *Org. Process Res. Dev.* **2006,** *10*, 959-970.

Pasumanksy, L.; Haddenham, D.; Clary, J. W.; Fisher, G. B.; Goralski, C. T.; Singaram, B., Lithium Aminoborohydrides 16. Synthesis and Reactions of Monomeric and Dimeric Aminoboranes. *J. Org. Chem.* **2008,** *73*, 1898-1905.

Patel, N.; Fernandes, R.; Edla, R.; Lihitkar, P. B.; Kothari, D. C.; Miotello, A., Superior Hydrogen Production Rate by Catalytic Hydrolysis of Ammonia Borane Using Co-B Nanoparticles Supported over Mesoporous Silica Particles. *Catal. Commun.* **2012,** *23*, 39-42.

Patelli, N.; Calizzi, M.; Migliori, A.; Morandi, V.; Pasquini, L., Hydrogen Desorption Below 150 °C in MgH_2-TiH_2 Composite Nanoparticles: Equilibrium and Kinetic Properties. *J. Phys. Chem. C.* **2017,** *121*, 11166-11177.

Patil, A.; Hatch, G.; Michaud, C.; Brotman, M.; Regunathan, P.; Tallon, R.; Andrew, R.; Murphy, S.; Murphy, S.; Undesser, P.; Redden, K. *Aluminum Fact Sheet*; Water Quality Association: Illinois, USA, 2013.

Patil, N. M.; Sasaki, T.; Bhanage, B. M., Immobilized ruthenium metal-containing ionic liquid-catalyzed dehydrogenation of dimethylamine borane complex for the reduction of olefins and nitroarenes. *RSC Adv.* **2016,** *6*, 52347-52352.

Paul, R.; Buisson, P.; Joseph, N., Catalytic Activity of Nickel Borides. *Ind. Eng. Chem.* **1952,** *44*, 1006-1010.

Pavlic, A. A.; Adkins, H., Preparation of a Raney Nickel Catalyst. *J. Am. Chem. Soc.* **1946,** *68*, 1471-1471.

Pereira de Oliveira, L.; Rocha, D. P.; Reis de Araujo, W.; Abarza Muñoz, R. A.; Longo Cesar Paixão, T. R.; Oliveira Salles, M., Forensics in hand: new trends in forensic devices (2013–2017). *Analytical Methods* **2018,** *10*, 5135-5163.

Petkar, D. R.; Kadu, B. S.; Chikate, R. C., Highly Efficient and Chemoselective Transfer Hydrogenation of Nitroarenes at Room Temperature over Magnetically Separable Fe–Ni Bimetallic Nanoparticles. *RSC Adv.* **2014,** *4*, 8004.

Piña, S.; Cedillo, D. M.; Tamez, C.; Izquierdo, N.; Parsons, J. G.; Gutierrez, J. J., Reduction of nitrobenzene derivatives using sodium borohydride and transistion metal sulfides *Tet. Lett.* **2014,** *55*, 5468-5470.

Plevachuk, Y.; Sklyarchuk, V.; Eckert, S.; Gerbeth, G.; Novakovic, R., Thermophysical Properties of the Liquid Ga-In-Sn Eutectic Alloy. *J. Chem. Eng. Data* **2014,** *59*, 757-763.

Pogorelić, I.; Filipan-Litvić, M.; Merkaš, S.; Ljubić, G.; Cepanec, I.; Litvić, M., Rapid, Efficient and Selective Reduction of Aromatic Nitro Compounds with Sodium Borohydride and Raney Nickel. *J. Mol. Catal. Chem.* **2007,** *274*, 2020-207.

Ponndorf, W. Z., The reversible exchange of oxygen between aldehydes or ketones on the one hand and primary or secondary alcohols on the other hand. *Angew. Chem.* **1926,** *39*, 138-143.

Potyen, M.; Josyula, K. V. B.; Schuck, M.; Lu, S.; Gao, P.; Hewitt, C., Borane-THF: New Solutions with Improved Thermal Properties and Stability. *Org. Process Res. Dev.* **2007,** *11*, 210-214.

Prasanth, C. P.; Joseph, E.; Abhijith, A.; Nair, D. S.; Ibnusaud, I.; Raskatov, J.; Singaram, B., Stablization of $NaBH_4$ in Methanol Using a Catalytic Amount of NaOMe. Reduction of Esters and Lactones at Room Temperature without Solvent-Induced Loss of Hydride. *J. Org. Chem.* **2018,** *83*, 1431-1440.

Prathap, K. J.; Wu, Q.; Olsson, R. T.; Dinér, P., Catalytic Reductions and Tandem Reactions of Nitro Compounds Using in Situ Prepared Nickel Boride Catalyst in Nanocellulose Solution. *Org. Lett.* **2017,** *19*, 4746-4749.

Rahman, A.; Jonnalagadda, S. B., Swift and Selective Reduction of Nitroaromatics to Aromatic Amines with Ni–Boride–Silica Catalysts System at Low Temperature. *Catal. Lett.* **2008,** *123*, 264-268.

Rai, R. K.; Mahata, A.; Mukhopadhyay, S.; Gupta, S.; Li, P.-Z.; Nguyen, K. T.; Zhao, Y.; Pathak, B.; Singh, S. K., Room-Temperature Chemoselective Reduction of Nitro Groups Using Non-Noble Metal Nanocatalysts in Water. *Inorg. Chem.* **2014,** *53*, 2904-2909.

Ramachandran, P. V.; Kulkarni, A. S.; Zhao, Y.; Mei, J., Amine-boranes bearing borane-incompatible functionalities: application to selective amine protection and surface functionalization. *Chem. Commun.* **2016,** *52*, 11885-11888.

Ramya, K.; Dhathathreyan, K. S.; Sreenivas, J.; Kumar, S.; Narasimhan, S., Hydrogen production by alcoholysis of sodium borohydride. *Int. J. Energy Res.* **2013,** *37*, 1889-1895.

Raney Nickel. https://cameochemicals.noaa.gov/chemical/4024 (accessed September 30, 2020).

Rao, C. N.; Hoz, S., Photostimulated Reduction of Nitriles by SmI_2. *J. Org. Chem.* **2012,** *77*, 4029-4034.

Reber, A. R.; Khanna, S. N.; Roach, P. J.; Woodward, W. H.; Castleman, A. W., Reactivity of aluminum cluster anions with water: Origins of reactivity and mechanisms for H_2 release. *J. Phys. Chem. A* **2010,** *114*, 6071-6081.

Rice, G. W.; Woodin, R. L., Zirconium Borohydride as a Zirconium Boride Precursor. *J. Am. Ceram. Soc.* **1988,** *71*, C-1818-C-183.

Roach, P. J.; Woodward, W. H.; Castleman, A. W.; Reber, A. C.; Khanna, S. N., Complementary Active sites cause size-selective reactivity of aluminum cluster anions with water. *Science* **2009,** *323*, 492-495.

Roger, I.; Shipman, M. A.; Symes, M. D., Earth-abundant catalysts for electrochemical and photochemical water splitting. *Nature* **2017,** *1*, 1-13.

Saavedra, J. Z.; Resendez, A.; Rovira, A.; Eagon, S.; Haddenham, D.; Singaram, B., Reaction of $InCl_3$ with Various Reducing Agents: $InCl_3$-$NaBH_4$-Mediated Reduction of Aromatic and Aliphatic Nitriles to Primary Amines. *J. Org. Chem.* **2012,** *77*, 221-228.

Saldan, I., Decomposition and Formation of Magnesium Borohydride. *Int. J. Hydrog. Energy* **2016,** *41*, 11201-11224.

Salunkhe, A. M.; Burkhardt, E. R., N,N-Diethylaniline Borane, an Efficient Reducing Agent for Reduction of Representative Functional Groups. *Tetrahedron Letters* **1997,** *38*, 1519-1522.

Sanderson, K., It's Not Easy Being Green. *Nature* **2011,** *469*, 18-20.

Schaeffer, G. W.; Anderson, E. R., The Preparation of Trimethylamine-borine, N-Trimethylborazole and N-Dimethylaminoborine. *J. Am. Chem. Soc.* **1949,** *71*, 2143-2145.

Schaefer, Z. L.; Ke, X.; Schiffer, P.; Schaak, R. E., Direct Solution Synthesis, Reaction Pathway Studies, and Structural Characterization of Crystalline Ni_3B Nanoparticles. *J. Phys. Chem. C* **2008,** *112*, 19846-19851.

Schlesinger, H. I.; Brown, H. C., Metallo Borohydrides. III. Lithium Borohydride. *J. Am. Chem. Soc.* **1940,** *62*, 3429-3435.

Schlesinger, H. I.; Brown, H. C.; Finholt, A. E., The Preparation of Sodium Borohydride by the High Temperature Reaction of Sodium Hydride with Borate Esters. *J. Am. Chem. Soc* **1965,** *75*, 205-209.

Schlesinger, H. I.; Brown, H. C.; Finholt, A. E.; Gilbreath, J. R.; Hoekstra, H. R.; Hyde, E. K., Sodium Borohydride, Its Hydrolysis and Its Use as a Reducing Agent and in the Generation of Hydrogen. *J. Am. Chem. Soc.* **1953,** *75*, 215-219.

Schmink, J. R.; Holcomb, J. L.; Leadbeater, N. E., Use of Raman spectroscopy as an in situ tool to obtain kinetic data for organic transformations. *Chemistry* **2008,** *14*, 9943-50.

Schouwink, P.; D'Anna, V.; Ley, M. B.; Daku, L. M. L.; Richter, B.; Jensen, T. R.; Hagemann, H.; Černy, R., Bimetallic Borohydrides in the System $M(BH_4)_2$-KBH_4 (M=Mg, Mn): On the Structural Diversity. *J. Phys. Chem. C.* **2012,** *116*, 10829-10840.

Schreifels, J., X-Ray Photoelectron Spectroscopy of Nickel Boride Catalysts: Correlation of Surface States with Reaction Products in the Hydrogenation of Acrylonitrile. *J. Catal.* **1980,** *65*, 195-206.

Schreifels, J. A.; Maybury, P. C.; Swartz, W. E., Comparison of the Activity and Lifetime of Raney Nickel and Nickel Boride in the Hydrogenation of Various Functional Groups. *J. Org. Chem.* **1981,** *46*, 1263-1269.

Sheldon, R. A., Metrics of Green Chemistry and Sustainability: Past, Present, and Future. *ACS Sustainable Chem. Eng.* **2018,** *6*, 32-48.

Sherif El-Eskandarany, M., The history and necessity of mechanical alloying. In *Mechanical Alloying*, William Andrew: Oxford, UK, 2015; pp 13-47.

Shimojo, F.; Ohmura, S.; Kalia, R. K.; Nakano, A.; Vashishta, P., Molecular dynamics and simulations of rapid hydrogen production from water using aluminum clusters as catalyzsers. *Phys. Rev. Lett.* **2010,** *104*, 126102.

Shrestha, R.; Dorn, S. C. M.; Weix, D. J., Nickel-Catalyzed Reductive Conjugate Addition to Enones via Allylnickel Intermediates. *J. Am. Chem. Soc* **2013,** *135*, 751-762.

Sikirzhytskaya, A.; Sikirzhytski, V.; Lednev, I. K., Determining Gender by Raman Spectroscopy of a Bloodstain. *Anal. Chem.* **2017,** *89*, 1486-1492.

Simmons, B. J.; Hoffmann, M.; Hwang, J.; Jackl, M. K.; Garg, N. K., Nickel-Catalyzed Reduction of Secondary and Tertiary Amides. *Org. Lett.* **2017,** *19*, 1910-1913.

Singh, C.; Goyal, A.; Singhal, S., Nickel-doped cobalt ferrite nanoparticles: efficient catalysts for the reduction of nitroaromatic compounds and photo-oxidative degredation of toxic dyes. *Nanoscale* **2014,** *6*, 7959-7970.

Singh, S. P.; Mukherjee, S.; Galindo, L. H.; So, P. T. C.; Dasari, R. R.; Khan, U. Z.; Kannan, R.; Upendran, A.; Kang, J. W., Evaluation of accuracy dependence of Raman spectroscopic models on the ratio of calibration and validation points for non-invasive glucose sensing. *Anal. Bioanal. Chem.* **2018,** *410*, 6469-6475.

Smith, A. M.; Whyman, R., Review of Methods for the Catalytic Hydrogenation of Carboxamides. *Chem. Rev.* **2014,** *114*, 5477-5510.

Snelling, R.; Saavedra, J. Z.; Bayrasy, P.; Abdollahian, Y.; Singaram, B., Binary reducing agents containing dichloroindium hydride for the selective, partical, or tandem reductions of bifunctional compounds consisting of halo-nitriles, halo-esters and halo-carboxylic acids. *Org. Chem. Front.* **2015,** *2*, 133-140.

Staubitz, A.; Robertson, A. P. M.; Sloan, M. E.; Manners, I., Amine- and Phosphine-Borane Adducts: New Interest in Old Molecules. *Chem. Rev.* **2010,** *110*, 4023-4078.

Stone, P.; Thompson, H., Vibrational band intensity of the hydroxyl group in phenols. *Spectrochimica Acta* **1957,** *10*, 17-20.

Strachan, J.; Barnett, C.; Masters, A. F.; Maschmeyer, T., 4-Nitrophenol Reduction: Probing the Putative Mechanism of the Model Reaction. *ACS Catalysis* **2020**, 5516-5521.

Sun, S.; Quan, Z.; Wang, X., Selective reduction of nitro-compounds to primary amines by nickel-catalyzed hydrosilylative reduction. *RSC Adv.* **2015,** *5*, 84574-84577.

Sun, Y.; Liu, C.; Grauer, D. C.; Yano, J.; Long, J. R.; Yang, P.; Chang, C. J., Electrodeposited cobalt-sulfide catalyst for electrochemical and photoelectrochemical hydrogen generation from water. *J. Am. Chem. Soc.* **2013,** *135*, 17699-17702.

Szostak, M.; Sautier, B.; Spain, M.; Procter, D. J., Electron Transfer Reduction of Nitriles Using SmI2-Et3N-H2O: Synthetic Utility and Mechanism. *Org. Lett.* **2014,** *16*, 1092-1095.

Tamelen, E. E. V.; Dewey, R. S.; Lease, M. F.; Pirkle, W. H., Selectivity and Mechanism of Diimide Reductions. *J. Am. Chem. Soc* **1961,** *83*, 4302.

Taylor, M. D.; Grant, L. R.; Sands, C. A., A Convenient Preparation of Pyridine-Borane. *J. Am. Chem. Soc* **1955,** *77*, 1506-1507.

Terrier, F., Rate and Equilibrium Studies in Jackson-Meisenheimer Complexes. *Chem. Rev.* **1982,** *82*, 77-152.

Thomas, S.; Collins, C. J.; Cuzens, J. R.; Spiciarich, D.; Goralski, C. T.; Singaram, B., Aminoborohydrides. 12. Novel Tandem S_nAr Amination-Reduction Reactions of 2-Halobenzonitriels with Lithium *N,N*-Dialkylaminoborohydrides. *J. Org. Chem.* **2001,** *66*, 1999-2004.

Tomkins, P.; Gebauer-Henke, E.; Leitner, W.; Müller, T. E., Concurrent Hydrogenation of Aromatic and Nitro Groups over Carbon-Supported Ruthenium Catalysts. *ACS Catal.* **2015,** *5*, 203-209.

Tran, P. D.; Chiam, S. Y.; Boix, P. P.; Ren, Y.; Pramana, S. S.; Fize, J.; Artero, V.; J., B., Novel cobalt/nickel-tungsten-sulfide catalysts for electrocatalytic hydrogen generation from water. *Energy Environ. Sci.* **2013,** *6*, 2452-2459.

Tyndall, S.; Wong, K. F.; VanAlstine-Parris, M. A., Insight into the Mechanism of the Pechmann Condensation Reaction Using NMR. *J. Org. Chem.* **2015,** *80*, 8951-8953.

United States Environmental Protection Agency. Facts and figures about materials, waste and recycling. https://www.epa.gov/facts-and-figures-about-materials-waste-and-recycling/aluminum-material-specific-data (accessed March 30, 2020).

Vandenabeele, P.; H.G.M., W.; Moens, L., A Decade of Raman Spectroscopy in Art and Archeology. *Chem. Rev.* **2007,** *107*, 675-686.

Vashishta, P.; Shimojo, F.; Ohmura, S.; Shimamura, K.; Mou, W.; Kalia, R. K.; Nakano, A., Rapid hydrogen production from water using aluminum nanoclusters: A quantum molecular dynamics simulation study. *Solid State Ionics* **2014,** *262*, 908-910.

Verley, A., The exchange of functional groups between two molecules: The passage of ketones to alcohols and the reverse. *Bull. Soc. Chim. Fr.* **1925,** *37*, 871-874.

Vernekar, A. A.; Patil, S.; Bhat, C.; Tilve, S. G., Magnetically Recoverable Catalytic Co–Co2B Nanocomposites for the Chemoselective Reduction of Aromatic Nitro Compounds. *RSC Adv.* **2013,** *3*, 13243.

Vogt, P. F.; Gerulis, J. J., Amines, Aromatic. In *Ullmann's Encyclopedia of Industrial Chemistry*, Wiley-VCH Verlag GmbH & Co.: Weinheim, Germany, 2000.

Vrubel, H.; Hu, X., Molybdenum boride and carbide catalyze hydrogen evolution in both acidic and basic solutions. *Angew. Chem. Int. Ed.* **2012,** *51*, 12703-12706.

Waals, D. v. d.; Pettman, A.; Williams, J. M. J., Copper-catalysed reductive amination of nitriles and organic-group reductions using dimethylamine borane. *RSC Adv.* **2014,** *4*, 51845-51849.

Walrafen, G.; Pugh, E., Raman combinations and stretching overtones from water, heavy water, and NaCl in water at shifts to ca. 7000 cm^{-1}. *Journal of solution chemistry* **2004,** *33*, 81-97.

Wang, Q.; Domen, K., Particulate photocatalysts for light-driven water spilitting: mechansim, challenges, and design strategies. *Chem. Rev.* **2020,** *120*, 919-985.

Wang, W.; Chen, D. M.; Yang, K., Investigation on microstructure and hydrogen generation performance of Al-rich alloys. *Int. J. Hydrogen Energy* **2010,** *35*, 12011-12019.

Wang, X.; Yao, W.; Zhou, D.; Fan, H., Theoretical study on the mechanism for NH_3BH_3 reduction of ketones and imines. *Molecular Physics* **2013,** *111*, 3014-3024.

Wang, Y.; Yan, B.; Chen, L., SERS tags: novel optical nanoprobes for bioanalysis. *Chem. Rev.* **2013,** *113* (3), 1391-428.

Wang, Z., Béchamp Reduction. In *Comprehensive Organic Name Reactions and Reagents*, Wang, Z., Ed. 2010.

Wang, Z.; Zong, S.; Wu, L.; Zhu, D.; Cui, Y., SERS-Activated Platforms for Immunoassay: Probes, Encoding Methods, and Applications. *Chem. Rev.* **2017,** *117*, 7910-7963.

White, S. S.; Kelly, H. C., On the Morpholine Borane Reduction of Acetone. *J. Am. Chem. Soc.* **1968,** *90*, 2009-2011.

White, S. S.; Kelly, H. C., Kinetics and Mechanism of the Morpholine-Borane Reduction of Methyl Alkyl Ketones. *J. Am. Chem. Soc.* **1970,** *92*, 4203-4209.

Winterfeldt, E., Applications of Diisobutylaluminum Hydride (DIBAH) and Triisobutylaluminum (TIBA) as Reducing Agents in Organic Synthesis. *Synthesis* **1975**, 617-630.

Wübbolt, S.; Oestreich, M., Exhaustive Chemoselective Reduction of Nitriles by Catalytic Hydrosilylation Involving Cooperative Si-H Bond Activation. *Synlett* **2017,** *28*, 2411-2414.

Xie, L.-Y.; Peng, S.; Liu, F.; Liu, Y.-F.; Sun, M.; Tang, Z.-L.; Jiang, S.; Cao, Z.; He, W.-m., Clean Preparation of Quinolin-2-yl Substituted Ureas in Water. *ACS Sustainable Chem. Eng.* **2019,** *7*, 7193-7199.

Xu, S.; Zhao, X.; Liu, J., Liquid metal activated aluminum-water reaction for direct hydrogen generation at room temperature. *Renewable and Sustainable Energy Rev.* **2018,** *92*, 17-37.

Yan, W.; Chen, B.; Mahurin, S. M.; Schwartz, V.; Mullins, D. R.; Lupini, A. R.; Pennycook, S. J.; Dai, S.; Overbury, S. H., Preparation and Comparison of Supported Gold Nanocatalysts on Anatase, Brookite, Rutile, and P25 Polymorphs of TiO_2 for Catalytic Oxidation of CO. *J. Phys. Chem. B* **2005,** *109*, 10676-10685.

Yang, C.; Jr., C. U. P., Reductions of Organic Functional Groups Using $NaBH_4$ or $NaBH_4$/LiCl in Diglyme at 125 to 162 °C. *Synthetic Communications* **1998,** *28*, 2027-2041.

Yang, L.; Dong, T.; Revankar, H. M.; Zhang, C.-P., Recent progress on fluorination in aqueous media. *Green Chem.* **2017,** *19*, 3951-3992.

Yang, X.; Fox, T.; Berke, H., Ammonia borane as a metal free reductant for ketones and aldehydes: a mechanistic study. *Tetrahedron* **2011,** *67*, 7121-7127.

Yao, K.; Li, T.; Zhao, C.; Lu, W.; Zhao, S.; Wang, J., Au_3Pd_1 Nanodendrites with Hyperbranched Architectures: Green Synthesis at Room Temperature and Highly Selective Hydrogenation for 4-Nitrophenylacetylene. *ACS Sustainable Chem. Eng.* **2020,** *8*, 14914-14925.

Yao, W.; He, L.; Han, D.; Zhong, A., Sodium Triethylborohydride-Catalyzed Controlled Reduction of Unactivated Amides to Secondary or Tertiary Amines. *J. Org. Chem.* **2019,** *84*, 14627-14635.

Yin, B.-L.; Cai, C.-B.; Lai, J.-Q.; Zhang, Z.-R.; Huang, L.; Xu, L.-W.; Jiang, H.-F., Sodium Borohydride-Nickel Chloride-Methanol Catalytic System for Regioselctive Reduction of Electron-Rich Conjugated Dienes and Reductive Cleavage of Allyl Esters Involving π-Allylnickel Intermediate. *Adv. Synth. Catal.* **2011,** *353*, 3319-3324.

Ying, C.; Bei, L.; Huihu, W.; Shijie, D., Effect of preparation parameters and alloy elements on HER performance at 0 °C in water. *Rare Metal Materials and Engineering* **2017,** *46*, 2428-2432.

Yoon, N. M.; Gyoung, Y. S., Reaction of Diisobutylaluminum Hydride with Selected Organic Compounds Containing Representative Functional Groups. *J. Org. Chem.* **1985,** *50*, 2443-2450.

Yoshida, S.; Yamashita, H.; Funabiki, T.; Yonezawa, T., Catalysis by Amorphous Metal Alloys. Part 1.—Hydrogenation of Olefins over Amorphous Ni–P and Ni–B Alloys. *J. Chem. Soc. Faraday Trans. 1 Phys. Chem. Condens. Phases* **1984,** *80*, 1435.

Yu, H.; Peng, F.; Tan, J.; Hu, X.; Wang, H.; Yang, J.; Zheng, W., Selective catalysis of the aerobic oxidation of cyclohexane in the liquid phase by carbon nanotubes. *Angewandte Chemie* **2011,** *123*, 4064-4068.

Yu, L.; Zhu, Q.; Song, S.; McElhenny, B.; Wang, D.; Wu, C.; Qin, Z.; Bao, J.; Yu, Y.; Chen, S.; Ren, Z., Non-noble metal-nitride based electrocatalysts for high-performance alkaline seawater electrolysis. *Nat. Commun.* **2019,** *10*, 1-10.

Yurderi, M.; Bulut, A.; Zahmakiran, M.; Gülcan, M.; Özkar, S., Ruthenium(0) nanoparticles stabilized by metal-organic framework (ZIF-8): Highly efficient catalyst for the dehydrogenation of dimethylamine-borane and transfer hydrogenation of unsaturated hydrocarbons using dimethylamine-borane as hydrogen source. *Applied Catal. B: Environ.* **2014,** *160-161*, 534-541.

Zakharkin, L. I.; Khorlina, I. M., *Zh. Obshch. Khim.* **1964,** *34*, 1029.

Zeng, H.; Wang, Z.; Li, C.-J., Two-in-One Strategy for Palladium-Catalyzed C-H Functionalization in Water. *Angew. Chem., Int. Ed.* **2019,** *58*, 2859-2863.

Zerecero-Silva, P.; Jimenez-Solar, I.; Crestani, M. G.; Arévalo, A.; Barrios-Francisco, R.; García, J. J., Catalytic Hydrogenation of Aromatic Nitriles and Dinitriles with Nickel Compounds. *Appl. Catal., A* **2009,** *363*, 230-234.

Zhang, C.; Lu, J.; Li, M.; Wang, Y.; Zhang, Z.; Chen, H.; Wang, F., Transfer hydrogenation of nitroarenes with hdyrazine at near-room temperature catalyzed by a MoO_2 catalyst. *Green Chem.* **2016,** *18*, 2435-2442.

Zhang, J.; Cai, Y.; Lu, G.; Cai, C., Facile and Selective Hydrogenolysis of β-O-4 Linkages in Lignin Catalyzed by Pd–Ni Bimetallic Nanoparticles Supported on ZrO_2. *Green Chem.* **2016,** *18*, 6229-6235.

Zhang, J.; Lu, G.; Cai, C., Chemoselective Transfer Hydrogenation of Nitroarenes by Highly Dispersed Ni-Co BMNPs. *Catal. Commun.* **2016,** *84*, 25-29.

Zhang, J.-W.; Lu, G.-P.; Cai, C., Chemoselective transfer hydrogenation of nitroarenes by highly dispersed Ni-Co BMNPs. *Catal. Commun.* **2016,** *84*, 25-29.

Zhang, Y.; Luo, M.; Yang, Y.; Li, Y.; Guo, S., Advanced multifunctional electrocatalyst for energy conversion. *ACS Energy Lett.* **2019,** *4*, 1672-1680.

Zhao, Z.; Yang, H.; Li, Y.; Guo, X., Cobalt-Modified Molybdenum Carbide as an Efficient Catalyst for Chemoselective Reduction of Aromatic Nitro Compounds. *Green Chem.* **2014,** *16*, 1274-1281.

Zheng, J.; Zhao, Y.; Xi, H.; Li, C., Seawater splitting for hydrogen evolution by robust electrocatalysts from secondary M (M= Cr, Fe, Co, Ni, Mo) incorporated Pt. *RSC Adv.* **2018,** *8*, 9423-9429.

Zhu, Y.; Ouyang, L.; Zhong, H.; Liu, J.; Wang, H.; Shao, H.; Huang, Z.; Zhu, M., Efficient Synthesis of Sodium Borohydride: Balancing Reducing Agents with Intrinsic Hydrogen Source in Hydrated Borax. *ACS Sustainable Chem. Eng.* **2020,** *8*, 13449-13458.

Ziebarth, J. T.; Woodall, J. M.; Kramer, R. A.; Choi, G., Liquid phase-enabled reactions of Al-Ga and Al-Ga-In-Sn alloys wtih water. *Int. J. Hydrogen Energy* **2011,** *36*, 5271-5279.

Zong, C.; Xu, M.; Xu, L. J.; Wei, T.; Ma, X.; Zheng, X. S.; Hu, R.; Ren, B., Surface-Enhanced Raman Spectroscopy for Bioanalysis: Reliability and Challenges. *Chem. Rev.* **2018,** *118*, 4946-4980.